



XXII SIMPÓSIO BRASILEIRO DE QUÍMICA TEÓRICA

BOOK OF ABSTRACTS

Welcome to the event XXII Brazilian Symposium on Theoretical Chemistry

The XXII Brazilian Symposium on Theoretical Chemistry (SBQT) will take place in the city of Niterói, at Sala Nelson Pereira dos Santos, from October 23 to 26, 2023. The XXII SBQT will promote the face-to-face meeting of the Theoretical and Computational Chemistry community, after the 2021 virtual event, which is why the motto will be “Chega de Saudade”, also to celebrate one of the symbols of Rio de Janeiro, the Bossa Nova.

The event will feature an extensive program, including plenary conferences, invited lectures and short communications by Brazilian researchers and guests from abroad, in addition to the traditional presentation in the form of panels. As always, our event will also be diversified from the point of view of the topics addressed, essentially covering the entire spectrum of research lines developed by researchers in the area, including, for example, topics such as quantum mechanics, statistical mechanics, molecular modeling, liquid systems, solids and interfaces, reactions in the gas phase, development of algorithms, among others, and encompassing numerous applications.

The SBQT, the biggest event in the area in Latin America, will continue to be a unique opportunity to promote and disseminate knowledge, create collaborations and share experiences and the latest advances in Theoretical and Computational Chemistry in Brazil, in addition to contributing to closer relationships with experimental chemistry.

Chega de Saudade. Welcome everyone!

National Organizing Committee

- José Walkimar de Mesquita Carneiro - Universidade Federal Fluminense
- Paulo Augusto Netz - Universidade Federal do Rio Grande do Sul
- Breno Rodrigues Lamaghore Galvão - Centro Federal de Educação Tecnológica (CEFET-MG)
- Daniel Francisco Scalabrin Machado -Universidade de Brasília
- Julio Cosme Santos da Silva - Universidade Federal de Alagoas
- Leonardo Baptista - Universidade do Estado do Rio de Janeiro
- Rodrigo do Monte Gester - Universidade Federal do Sul e Sudeste do Pará
- Vivian Vanessa França - Universidade Estadual Paulista

Local Organizing Committee

- José Walkimar de Mesquita Carneiro - Universidade Federal Fluminense
- Ana Carolina Ferreira de Albuquerque - Universidade Federal Fluminense
- Ednilson Orestes - Universidade Federal Fluminense
- Fernando Martins dos Santos Junior - Universidade Federal Fluminense
- Karine Nascimento de Andrade - Universidade Federal Fluminense
- Luciano Tavares Costa - Universidade Federal Fluminense
- MAURICIO T DE M CRUZ - Universidade do Estado do Rio de Janeiro
- Milena Diniz Lessa - Universidade Federal Fluminense
- Rodolfo - Universidade Federal Fluminense

Scientific Committee

- Alfredo Mayall Simas - Universidade Federal de Pernambuco
- Hélio Anderson Duarte - Universidade Federal de Minas Gerais
- Marco Antonio Chaer Nascimento - Universidade Federal do Rio de Janeiro
- Sylvio Roberto Accioly Canuto - Universidade de São Paulo
- Wagner Batista de Almeida - Universidade Federal Fluminense

NOTA EXPLICATIVA

Os resumos do SBQT 2023 foram baixados diretamente do site do evento (<https://eventos.galoa.com.br/sbqt-2023/page/2248-inicio>) em dezembro de 2023 por meio de um *bot* escrito em Python. O programa foi desenvolvido pelo doutorando do Programa de Pós Graduação em Engenharia de Defesa (PGED) do Instituto Militar de Engenharia (IME) Rubens Caio de Souza.

Todos os resumos do Simpósio disponíveis puderam ser baixados.

Para qualquer acréscimo ou correção a este documento, basta entrar contato.

Aproveitem para conhecer o melhor da Química Teórica Brasileira em 2023!

Cordialmente,

Itamar Borges Jr.

Dep. Química – Instituto Militar de Engenharia (IME)

itamar@ime.eb.br

Multiscale investigation of the structural basis for photoacclimation in the cryptophyte alga PC577 and PE545 antenna complexes

Renato D. Cunha (PG)^{1,2} and Carles E. Curutchet (PQ)^{1,2*}

renatodias@ub.edu; carles.curutchet@ub.edu

¹ Departament de Farmàcia i Tecnologia Farmacèutica, i Fisicoquímica, Facultat de Farmàcia i Ciències de l'Alimentació, Universitat de Barcelona (UB), 08028 Barcelona, Spain;

² Institut de Química Teòrica i Computacional (IQT-CUB), Universitat de Barcelona (UB), 08028 Barcelona, Spain

Palavras Chave: QM/MM polarizable, cryptophyte algae, photoacclimation, BOMD, multiscale.

INTRODUCTION

Pigment-protein antenna complexes perform a key task in photosynthesis, collecting sunlight and transporting the energy to the reaction centers.[1] Photoacclimation allows cryptophyte algae to adapt to varying sunlight intensity by changing the concentration of phycobiliprotein antenna proteins. However, recently a new mechanism has been observed that leads to shifts in the antennae absorption spectra. Evidence based on spectroscopy and X-ray crystallography on *H. pacifica* PC577 (Figure 1) and *P. Sulcata* PE545 (Figure 1) antennae suggests that this mechanism involves the change of one of the tetrapyrroles bilin chromophores, rather than a change in protein sequence or structure.[2]

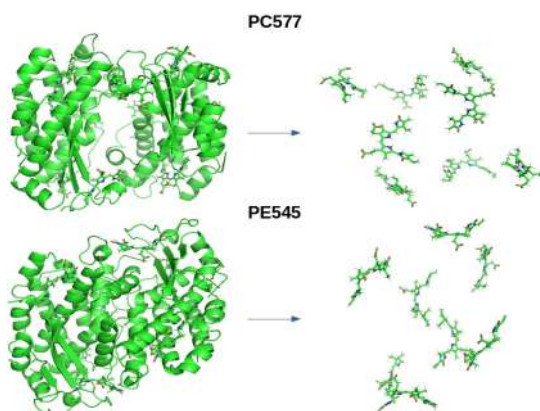


Fig. 1: PC577 and PE545 and the 8 associated chromophores.

METHODS

In this study, we investigate the structural basis for this mechanism using multiscale computational methods.[3] We report classical molecular dynamics simulations for PC577 and PE545 and their single b subunits for the native complexes as well as several variants with mutated pigments. The trajectories were then used to start multiple DFT-based QM/MM Born-Oppenheimer molecular dynamic (BOMD) simulations, later processed to estimate the bilin transition energies and electronic couplings using polarizable QM/MM calculations. Excitonic absorption spectra were then computed using the Full Cumulant Expansion formalism.[4]

RESULTS

For the standard complexes, the MD-BOMD method shows excellent agreement compared to experimental spectra. In Figure 2 we report the simulated spectra compared to the experimental one. When we exchange the PCB₁₅₈ for a DBV we can observe a small blue shift of the two bands compared to the absorption of the standard complex. Instead, when we exchange the PCB₈₂ there's a significant displacement of intensity from the red edge to the center of the spectra leading to a single broad band. The experimental absorbance spectra [2] showed a small blue shift in the high energy band.

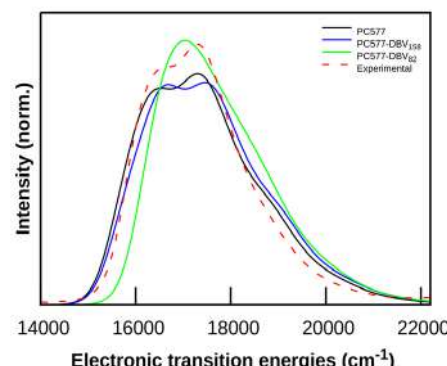


Fig. 2: Absorption spectra of PC577 variants simulated using our protocol compared to the experimental spectrum.

CONCLUSION

The preliminary results showed very reasonable absorption spectra in comparison with the experimental. The calculation with the mutated chromophores is being run to determine which chromophore the protein makes the change to acclimation.

REFERENCES

- [1] C. Curutchet, B. Mennucci, Chem. Rev. 2017, 117, 294.
- [2] L. C. Spangler et al. ACS Cent. Sci. 2022, 8, 340.
- [3] M. Corbella et al. ChemPhotoChem 2019, 3(9), 945.
- [4] L. Cupellini et al. J Phys Chem B 2020, 124, 8610.

FUNDING

PREDocs- UB fellowship funded by the University of Barcelona (Ref. 2020-88), and State Research Agency/Spanish Ministry of Science and Innovation (AEI / 10.13039/501100011033, grants MDM-2017-0767 and PID2020-115812GB-I00).

Toward Benchmark-quality Ab Initio Predictions for 3d Transition Metal Electrocatalysts - A comparison of CCSD(T) and ph-AFQMC

Hagen Neugebauer (PG),¹ Hung Vuong (PG),² John Weber (PG),² Richard Friesner (PQ),² James Shee (PQ),^{3*} Andreas Hansen (PQ)^{1*}

hagen@thch.uni-bonn.de; hansen@thch.uni-bonn.de

¹Mulliken Center for Theoretical Chemistry, Universität Bonn, Beringstr. 4, D-53115 Bonn, Germany; ²Department of Chemistry, Columbia University, 3000 Broadway, New York, NY, 10027; ³Department of Chemistry, University of California, Berkeley, California 94720, United States

Keywords: Ionization potentials, Transition metal complexes, Multireference diagnostics, Coupled cluster methods, Auxiliary field QMC

INTRODUCTION

Electron transfers involving transition metal (TM) catalysts are ubiquitous in chemistry, but are difficult to model accurately using approximate quantum chemical methods due to the often significant dynamic and static electron correlation. In contrast to thermochemical predictions for large-gap, open-shell TM complexes, for which local coupled cluster methods have been successfully applied (e.g. ROST61¹), the adequacy of the "gold standard", single-reference (SR) CCSD(T), for more challenging electronic structures is unclear. In the absence of experimental values from the gas phase, we attempt to generate near-exact auxiliary field Quantum Monte Carlo (ph-AFQMC²) reference values in a relatively small basis set to assess the accuracy of CCSD(T) for ionization potentials (IPs). We compose a set of 28 complexes relevant to homogeneous 3d electrocatalysis, classify them into subgroups based on the degree of multi-reference (MR) character in the involved states, and evaluate various coupled cluster protocols.

METHODS

The 28 complexes in the 3dTMOV³ IP test set:

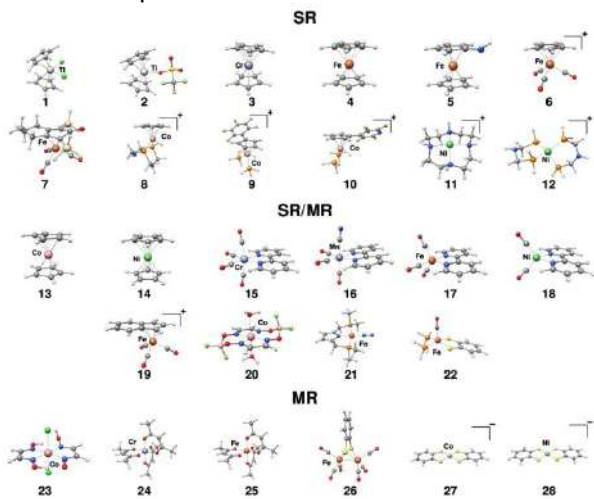


Fig. 1: Three subsets of 3dTMOV based on the degree of MR character present in the involved states.

RESULTS

Assessment of CCSD(T) protocols:

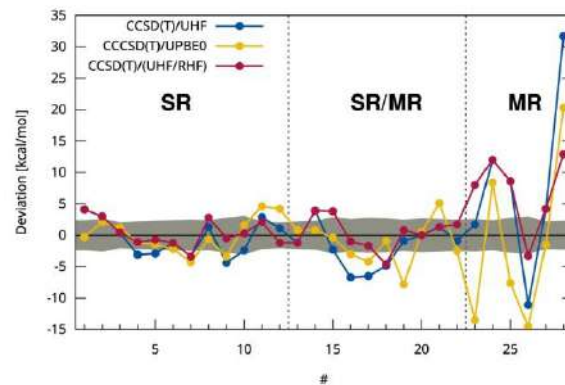


Fig. 2: Deviations of CCSD(T) with different orbitals vs. ph-AFQMC (UHF/RHF indicates RHF for singlet states).

CONCLUSIONS

- One valuable application of ph-AFQMC is to produce reference values for transition metal thermochemistry. While challenging, we demonstrate that this is possible for MR systems.
- Quantitative metrics based on symmetry breaking can delineate regimes inside of which appropriately-performed CCSD(T) can produce < 2 kcal/mol accuracy, and outside of which all SR CCSD(T) protocols tested can be expected to fail.
- Large, orbital-dependent triples contribution for complexes with triflate and F atoms, bipyridine, N₂ (triple bond), many in MR subset → opportunity to assess alternate and develop further approximate triples models.

REFERENCES

- L. R. Mauer, M. Bursch, S. Grimme, **AH**, JCTC, 2021, 17, 6134–6151.
- J. Shee, J. L. Weber, D. R. Reichman, R. A. Friesner, S. Zhang, JCP, 2023, 158, 140901.
- H. Neugebauer, H. T. Vuong, J. L. Weber, R. A. Friesner, J. Shee, **AH**, JCTC, 2023, submitted.

ACKNOWLEDGEMENTS

National Institutes of Health, German Science Foundation 1927/16-1, Department of Energy DE-AC05-00OR22725, National Science Foundation XSEDE ACI-1548562 and ID COL151.



Analise teórica da interação H₂S···SO₂

Isaac O. M. Magalhães (IC)¹, Benedito J. C. Cabral (PQ)², João B. L. Martins (PQ)^{1*}.

isaac.magalhaes@aluno.unb.br; lopes@unb.br

¹Universidade de Brasília, Instituto de Química, Laboratório de Química Computacional, Brasília, DF, 70910900, Brasil;

²BioSI-Biosystems and Integrative Sciences Institute and Departamento de Química e Bioquímica, Faculdade de Ciências, Universidade de Lisboa, 1749-016 Lisboa, Portugal

Palavras Chave: *Interação intermolecular, dímero H₂S-SO₂, CCSD(T)*

INTRODUÇÃO

O estudo da interação entre SO₂ e H₂S tem um papel importante na área ambiental, devido ao envolvimento destas moléculas na formação de compostos de enxofre que contribuem para a poluição atmosférica e o efeito estufa. Além disso, o estudo das propriedades espectroscópicas dessas moléculas pode auxiliar no entendimento da presença de enxofre em exoplanetas.^{1,2}

A química teórica e computacional é uma área de pesquisa bastante explorada para o estudo das interações intermoleculares envolvidas na formação do complexo SO₂···H₂S. Métodos *Ab initio*, como a teoria das perturbações, são úteis para calcular as propriedades moleculares e as energias de interação entre as moléculas.^{3,4}

Os resultados obtidos a partir dos cálculos teóricos podem fornecer informações valiosas para a interpretação dos dados experimentais de espectroscopias de infravermelho, ultravioleta e ressonância magnética nuclear. Além disso, a compreensão detalhada destas interações intermoleculares pode ser útil para aplicações e desenvolvimento na área ambiental.

MÉTODOS

Para este estudo, foram utilizadas as metodologias de cálculo de maior precisão energética e geométrica, incluindo MP2 (Teoria das Perturbações de *Møller-Plesset*), CCSD (Cluster Acoplado) e CCSD(T) (Correção Triplo Acoplada). As funções de base aug-cc-pVDZ (pVDZ), aug-cc-pVTZ (pVTZ), aug-cc-pVQZ (pVQZ) e aug-cc-pV5Z (pV5Z) (conjuntos de base consistentes em correlação de *Dunning* - duplo, triplo, quádruplo e quíntuplo-zeta) foram empregadas para obter maior precisão nos cálculos moleculares. Aumentou-se a precisão energética e geométrica utilizando-se funções difusas, associando-se o prefixo "aug" a elas. O erro de sobreposição de conjunto de base (BSSE), proposto por Boys e Bernardi, foi aplicado para corrigir a energia de interação calculadas. A análise e geração de imagens foram realizadas usando programas como VMD (*Visual Molecular Dynamics*) e MultiWFN (*Multifunctional Wavefunction Analyzer*).

A modelagem dos sistemas moleculares foi realizada com o software GaussView e os cálculos referidos foram executados com o pacote Gaussian16. Para cálculos CCSD(T) foi usado o programa CFOUR (*Coupled-Cluster techniques for Computational Chemistry*).^{5,6,7,8}

RESULTADOS

Foram utilizadas dez diferentes configurações geométricas como ponto de partida para investigar a interação SO₂···H₂S em níveis MP2, CCSD e CCSD(T) com as funções de base pVDZ, pVTZ, pVQZ e pV5Z (esta última apenas em nível MP2 devido ao seu alto custo computacional). Os resultados convergiram para uma única estrutura padrão, indicando a presença de um único mínimo para as funções de base utilizadas. Os valores energéticos obtidos para a interação foram consistentes entre as diferentes funções de base ao compararmos com a distância de interação S···S, como apresentado na Tabela 1.

Tabela 1. Energias de interação por distância de interação para o complexo H₂S···SO₂ nas metodologias estudadas.

		r(S···S) Å	ΔE(int) kcal mol ⁻¹
MP2	pVDZ	3,458	-3,34
	pVTZ	3,414	-3,23
	pVQZ	3,386	-3,17
	pV5Z	3,382	-3,10
CCSD	pVDZ	3,485	-3,07
	pVTZ	3,499	-2,71
	pVQZ	3,480	-2,60
CCSD(T)	pVDZ	3,463	-3,32
	pVTZ	3,454	-3,04
	pVQZ	3,427	-2,95

Para os cálculos MP2, observa-se que a distância de interação S-S diminui com o aumento da precisão da base usada, enquanto a energia de interação aumenta ligeiramente. Isso pode ser explicado por uma melhor descrição das interações de repulsão com bases mais precisas.^{9,10,11,12}

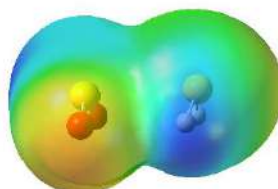


Já para os cálculos CCSD, a distância de interação S-S é maior para a base pVTZ do que para a base pVDZ, o que é consistente com a energia de interação, que é menos negativa para a base pVTZ. Essa diferença pode ser devida a uma melhor descrição das interações de dispersão com a base pVTZ.

Nos cálculos CCSD(T), a distância de interação S-S é menor do que nos cálculos MP2 e CCSD, e a energia de interação é mais negativa do que nos cálculos MP2 e CCSD. Isso sugere que a correção de triplas adicionada ao CCSD melhora a descrição das interações de dispersão, permitindo que as moléculas se aproximem mais.

Na Figura 1, podemos observar o comportamento da densidade eletrônica da interação.

Fig. 2 – Mapa de Superfície de Potencial Eletrostático do complexo H₂S···SO₂ para MP2/pVQZ.



Verificamos dessa forma como o oxigênio presente na interação se torna mais eletronegativo e com o comportamento oposto temos a eletropositividade do enxofre.

Os valores apresentados na Tabela 2, mostram como se comporta as funções de base para o complexo estudado, de acordo com os seus erros estimados usando o método de Counterpoise.

Tabela 2. Resultados das energias corrigidas com Counterpoise e seus respectivos dados de BSSE para o complexo H₂S···SO₂ nas metodologias estudadas.

		BSSE [kcal mol ⁻¹]	Corrected [kcal mol ⁻¹]
MP2	pVDZ	0,98	-2,37
	pVTZ	0,48	-2,76
	pVQZ	0,23	-2,95
	pV5Z	0,12	-3,00
CCSD	pVDZ	0,93	-2,15
	pVTZ	0,38	-2,34
	pVQZ	0,16	-2,46
CCSD(T)	pVDZ	1,06	-2,27
	pVTZ	0,45	-2,60
	pVQZ	0,18	-2,78

Os resultados apresentam uma tendência do erro de superposição de base no complexo H₂S···SO₂, s para as funções de base utilizadas, nos três níveis estudados.

CONCLUSÕES

A análise das interações de Van der Waals pode ser feita com base em duas principais características: energia de interação e distância de interação S-S. De maneira geral, esperamos que uma energia de interação mais negativa esteja associada a uma distância de interação mais curta. Tal comportamento foi observado na maioria das funções de base apresentadas na Tabela 1. Foi observado um comportamento extrapolativo para os valores de CCSD(T), para uma base mais robusta, possibilitando assim melhor caracterização da interação proposta para estudo. Como percebido com certa clareza as funções e metodologias sugeridas aqui, gera bons resultados para o caso da interação S···S.

REFERÊNCIAS

- ¹A. G. Clarke and M. Radojevic, *Atmospheric Environment*, 1967, vol. 21, no. 5, pp. 1115–1123.
- ²K. Sendt and B. S. Haynes, *J Phys Chem A*, 2005, vol. 109, no. 36, pp. 8180–8186.
- ³P. L. M. Plummer, *JOURNAL OF MOLECULAR STRUCTURE-THEOCHEM*, 1994, vol. 113, pp. 119–133.
- ⁴K. H. Lemke, *Journal of Chemical Physics*, 2017, vol. 146, no. 23.
- ⁵T. A. Ford, *J Mol Struct*, 2009, vol. 924–926, no. C, pp. 466–472.
- ⁶P. Salvador, M. Duran, and J. J. Dannenberg, *Journal of Physical Chemistry A*, 2002, vol. 106, no. 29, pp. 6883–6889.
- ⁷M. Mentel and E. J. Baerends, *J Chem Theory Comput*, 2014, vol. 10, no. 1, pp. 252–267.
- ⁸S. F. Boys and F. Bernardi, *Mol Phys*, 1970, vol. 19, no. 4, pp. 553–566.
- ⁹R. E. Bumgarner, D. J. Pauley, and S. G. Kukolich, *J Chem Phys*, 1987, vol. 87, no. 7, pp. 3749–3752.
- ¹⁰Y. Drozdova, in *2014 IEEE Asia-Pacific Conference on Applied Electromagnetics (APACE)*, 2014, IEEE, pp. xxxvii–xxxvii.
- ¹¹S. G. Kukolich and D. J. Pauley, *J Chem Phys*, 1990, vol. 93, no. 1, pp. 871–872.
- ¹²K. Matsumura, F. J. Lovas, and R. D. Suenram, *J Chem Phys*, 1989, vol. 91, no. 10, pp. 5887–5894.

AGRADECIMENTOS

CNPq, CAPES, FAPERJ e FAPDF.

Thermodynamic properties of liquid propellant mixtures of hydrazine computed via Molecular Dynamics.

Juliana J. F. S. Rêgo (PG),¹ Itamar Borges Jr. (PQ),^{1,2} Jakler Nichele (PQ).^{1,2*}

fernandes.juliana@ime.eb.br; jakler@ime.eb.br

¹ Department of Defense Engineering, Military Institute of Engineering, Rio de Janeiro, RJ, 22290-270, Brazil.

² Department of Chemical Engineering, Military Institute of Engineering, Rio de Janeiro, RJ, 22290-270, Brazil.

Palavras Chave: Molecular Dynamics, Thermodynamic Properties, Liquid Propellants, Chemical Mixtures, Hydrazine.

INTRODUCTION

Liquid propellants are energetic materials used in various industries, with a major focus in the aerospace and defense sectors [1,2,3]. Hydrazine (N_2H_4) is one of the most used liquid propellants whose properties are well described in the literature [4]. However, when such substance is used combined with others, the availability of thermodynamic data is limited. Molecular simulations are especially useful to compute thermodynamic properties, in addition to experimental methods. Here, Molecular Dynamics (MD) was combined with the post-processing technique Multistate Bennett Acceptance Ratio (MBAR) [4,5,6,7,8] to compute the thermal expansion coefficient (α_P), isothermal compressibility (χ_T), isobaric and isochoric heat capacities (C_P and C_V), Joule-Thompson coefficient (μ_{JT}), and the speed of sound (c_{sound}), for each pure substance and propellant mixtures. The results are useful for the design and optimization of rocket motors.

METHODS

This study investigated mixtures of hydrazine simulated with the following 7 substances: Ar, CH_3OH , CO, H_2O , N_2 , NH_3 , MMH (mono-methylhydrazine) and UDMH (1,1-dimethylhydrazine). These mixtures were investigated to measure important thermodynamic properties not found due to the limited data present in the literature [9]. To expand the scope of the study, the same mixtures used in Elts et al. (2012) work were employed. The simulations were performed using the LAMMPS software, employing Lennard-Jones potentials and the OPLS force field, in the NPT ensemble for 500 molecules, with a temperature range of 250 K to 500 K and a fixed pressure of 10 atm. The results were compared to results obtained with classical mixing rules [10].

RESULTS

Figure 1 presents representative results of the density vs. concentration for $T = 300$ K and $P = 10$ atm. The concentration of the second element added to hydrazine is varied from 10 to 90% (molar basis). Figure 2 presents results of α_P , for a pressure of 10 atm, in the temperature range of 250-500 K, with a fixed concentration of 50/50% for the elements in the mixture.

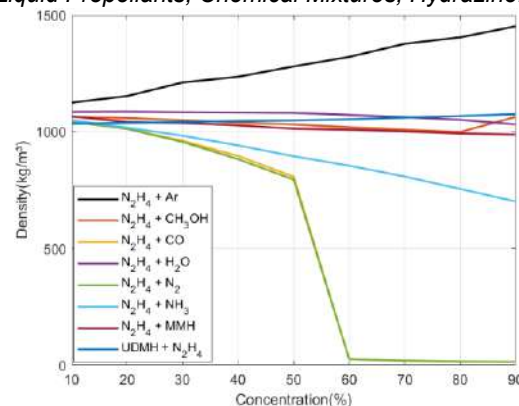


Figure 1 - Density of propellant mixtures with hydrazine as the main component.

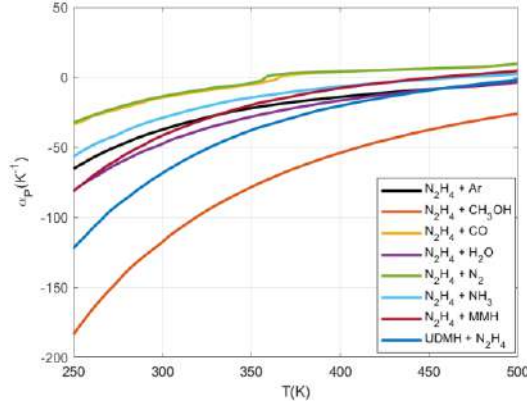


Figure 2 - Thermal expansion coefficient of propellant mixtures with hydrazine.

CONCLUSION

It was observed that the mixtures exhibited similar behaviors to each other under the given conditions, except for those that underwent phase changes. The comparison of the results with those obtained with the law of chemical proportion for mixtures demonstrated that the behavior and magnitude of the density values are similar to those obtained by the MD simulations. Ongoing investigations are focusing on the validity of the mixing rules for the other properties.

REFERENCES

- ¹CLARK, J.D., Ignition!. Rutgers Uni. Press, 1 ed. 2017.
- ²KLINGENBERG, G., AIAA. 175. 1998.
- ³SUTTON, G. P., Hist. of Liq. Rocket. Prop. AIAA. 2006.
- ⁴PATIL, K.C.; RATTAN, T.M. Inorg. Hydraz. Wiley & S. 2014.
- ⁵KAMBERAJ, H., Mol. Dyn. in Sim. Stat. Phys. Springer, 2020.
- ⁶STONE, A. J. et al. NATO ASI Se. 135. Springer Neth. 1984.
- ⁷NICHELE, J., et al., J. of Supercritical Fluids. 135. 225. 2017.
- ⁸AIMOLI, C.G., et al., Fluid Phase Equilibria. 368. 80. 2014.
- ⁹ELTS, E., et al., Fluid Phase Equilibria. 322-323. 79-91 p. 2012.
- ¹⁰SMITH, J.M. et al., Introd. à Term. Da Eng. Quím. 7ed. LTC.2007.

ACKNOWLEDGEMENTS

The authors thank the support of the Brazilian Army and the Brazilian agencies CAPES, CNPq, and FAPERJ.

Properties of agrochemicals for the development of sensors

Giovana Magnani (IC)¹, Sara S. Portela (IC)¹, Yasmin da Silva (IC)¹, Antonio D. S. G. Lima (PG)², Renato D. Cunha (PG)^{3,4}, Leonardo M. Carneiro (PG)¹, Diégo U. Melo (PG)¹, Carles Curutchet (PQ)^{3,4}, Mateus R. Lage (PQ)^{2,5}, Ednilson Orestes (PQ)^{1,6}, Paula Homem-de-Mello (PQ)^{1*}

paula.mello@ufabc.edu.br

¹Centro de Ciências Naturais e Humanas, Universidade Federal do ABC (UFABC), Santo André/SP; ²Centro de Ciências de Imperatriz, Universidade Federal do Maranhão, Imperatriz/MA; ³Departament de Farmàcia i Tecnologia Farmacèutica, i Físicoquímica, Facultat de Farmàcia i Ciències de l'Alimentació, Universitat de Barcelona (UB), Barcelona, Spain; ⁴Institut de Química Teòrica i Computacional (IQTCUB), Universitat de Barcelona (UB), 08028 Barcelona, Spain; ⁵Centro de Ciências de Balsas, Universidade Federal do Maranhão, Balsas/MA; ⁶Departamento de Ciências Exatas, Escola de Engenharia Industrial Metalúrgica de Volta Redonda, Universidade Federal Fluminense (UFF), Volta Redonda/RJ.

Keywords: Agrochemicals, Sensors, Porphyrins, Electronic properties, Log P.

INTRODUCTION

Agrochemicals are overused in Brazil, with severe consequences for the environment. The proposition of simple and accessible sensors is paramount to preserving water quality. On the other hand, porphyrins can be used in optical, voltammetric, or amperometric sensors for different compounds.¹ In this work, the most used agrochemicals (fungicides, herbicides, and insecticides) in Brazil, particularly in the region of the Balsas and Tocantins rivers, were evaluated from the point of view of their structural and electronic properties to subsequently design sensors based on porphyrins for their detection in water. Thus, based on simulations for different agrochemicals, porphyrin structures were proposed that could perform a specific interaction with each subgroup of agrochemicals.

METHODS

B3LYP functional and 6-311G(d,p) basis set were employed to optimize the geometries and calculate the vibrational frequencies for the selected agrochemicals: 13 fungicides, 18 insecticides, and 16 herbicides. Then, different electronic properties and reactivity indexes were obtained, such as energies and map of HOMO and LUMO, hardness, dipole moment, partial atomic charges and electrostatic potential surfaces, among others. The *n*-octanol-water partition coefficients (logP) were calculated with the implicit solvation model in the MST scheme² and compared to the empirically estimated logP's. Based on the geometry and all these properties, the compounds were compared to the analytes already known for porphyrin sensors. In the preliminary studies of the interaction of agrochemicals with porphyrins, the ω B97X-D³ functional was used.

RESULTS

Fig. 1 presents some of the results for an agrochemical, the chlorothalonil, with its interaction with the porphyrin, as proposed. We compared the obtained data, like reactivity indices, partial atomic charges, and electrostatic potential surface, with

those of compounds from ref [1]. In preliminary studies, the electronic absorption spectrum of porphyrin undergoes remarkable changes, indicating the possibility of its use as a colorimetric sensor. Additionally, the logP's obtained were compared, indicating a better agreement of the logP obtained from PubChem (ChEMBL) with the MST strategy.

Dipole moment (D)	29,2	
LUMO (eV)	-3,24	
HOMO (eV)	-8,11	
Δ HL (eV)	4,87	
logP ALOGPS	3,98	
logP Pubchem	2,90	
logP MST	3,04	

Figure 1 – Selected properties calculated for chlorothalonil fungicide and one of the structures obtained for the aggregate with the zinc porphyrin.

CONCLUSIONS AND PERSPECTIVE

The initial analyses for the 47 agrochemicals showed that the calculated properties are suitable for sensor design. In future studies, molecular dynamics will be performed for a better evaluation of the agrochemical-porphyrin interaction and the selectivity of the interaction in aqueous solution.

REFERENCES

¹R Paolesse et al. Chemical Reviews, 2016, 117, 2517.

²WJ Zamora et al. J. Phys. Chem. B, 2017, 121, 9868.

³J-D Chai and M. Head-Gordon, PCCP., 2008, 10, 6615.

ACKNOWLEDGEMENT

FAPESP (22/01833-5 e 22/01785-0), CNPq, CAPES, PREDOCS (UB 2020-88), State Research Agency / Spanish Ministry of Science and Innovation (AEI / 10.13039 / 501100011033, MDM-2017-0767 and PID2020-115812GB-I00)

On the Energetic Nature of Hydrogen-bond red-shift: An application of the IQA force constant partitioning method.

Leonardo J. Duarte (PQ),^{1*} Roy E. Bruns (PQ),² Atualpa A.C. Braga (PQ).¹

ljduarte@iq.usp.br

¹Chemistry Institute, University of São Paulo, São Paulo, SP, 05508-900, Brazil.; ²Chemistry Institute, University of Campinas, Campinas, SP, 13083-970, Brazil.

Palavras Chave: QTAIM, Hydrogen bond, Redshift, Force constants, IQA.

INTRODUCTION

The red-shift of the X-H (X = F, O, N) stretch is notable evidence of the existence of a hydrogen-bonded system. Upon the formation of the hydrogen bond, electronic density is transferred from the acceptor moiety of the complex to the donor hydrogen atom, causing an elongation of the X-H bond and a reduction of the force constant. Within the orbital paradigm of chemistry, the red-shift is caused by the donation of electrons from base to the σ^* orbital of the X-H bond. The population increase in the anti-bonding orbital is, therefore, responsible for the decrease in the force constant.

In this work, we present a description of the H-bond red-shift in terms of the molecular electronic density using the Quantum Theory of Atoms in Molecules formalism of the Interacting Quantum Atoms (IQA) energy decomposition scheme.

METHODS

All molecules and complexes had their geometries optimized at the B3LYP/aug-cc-pVTZ levels of theory using GAUSSIAN16¹ software. The wavefunction of each system was integrated using AIMAll² software yielding the QTAIM/IQA parameters need to compute the force constants. The use of B3LYP is justified since the calculation of IQA quantities is restricted to a few DFT functionals.

A numerical method is utilized to compute the infrared frequency of molecules and complexes. Starting from the equilibrium geometry of the system, distorted geometries are generated by displacing each atom in the positive and negative directions of each Cartesian axes. For each geometry, the IQA components are obtained. The data recovered from the calculations are used to calculate numerical second derivatives and construct the Hessian matrix. The elements of such a matrix is given by:

$$h_{i,j} = \sum_{k=1}^{N^2} \frac{\partial^2 E_{IQA}^k}{\partial \sigma_i \partial \sigma_j} \quad (1)$$

where E_{IQA}^k is one of the N^2 IQA terms, with N being the number of atoms in the system.

The vibrational frequencies are determined by diagonalizing the mass-weighted Hessian. IQA contributions to the eigenvalues are also obtained

from the partitioning showed in (1). This method is detailed in a previous publication from the authors³.

RESULTS

Two types of H-bonded complexes are shown in this abstract. One type consists of complexes where the donor molecule is H_2O , another consists of complexes where the HF molecule is the H donor.

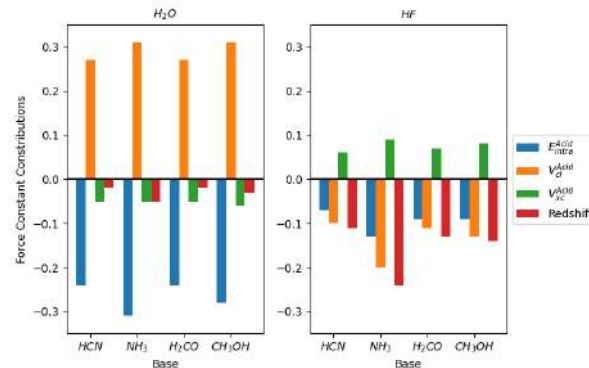


Figure 1: IQA contributions to the redshift. In blue: Intratomic energy variation; Orange: Coulomb; Green: Exchange-correlation. Red: Total variation, i.e. redshift.

The variation in IQA contributions for each system is showed in Figure 1. Note that the sum of all variations equals the redshift. The variations in the IQA contribution are calculated by subtracting the eigenvalue contribution to the X-H stretch in the complex from the value in the monomer.

CONCLUSIONS

The results show that the red-shift energetic origins are different for each acid. When H_2O act as H donor, the red-shift is mostly determined by the Intratomic and exchange-correlation, whereas the red-shift of the F-H stretch is caused primarily by the Coulomb contribution. The H acceptor molecule modulates the amount of variation in the above-mentioned cases. The better the acceptor the greater is the variation in the IQA contributions.

REFERENCES

- (1) Frisch, M. J.; Trucks, G. W.; et al. Gaussian16 Revision C.01, 2016. (2) Todd A. Keith. AIMAll, 2019. (3) Duarte, L. J.; Bruns, Roy. E. *J. Phys. Chem. A* **2022**, 126 (48), 8945–8954.

ACKNOWLEDGMENTS

LJD thanks FAPESP for the postdoctoral fellowship #2022/09260-1 and the Institute of Chemistry of both UNICAMP and USP.



Grupo Heme como catalisador da hidrogenação molecular de CO₂: Uma exploração computacional

Franciscarlos Soares (PG),¹ Égil Sá (PQ).^{1,2*}

prof.franciscarlos@gmail.com; egil.sa@ufpi.edu.br

¹Laboratório de Química Teórica, Universidade Federal do Piauí, Teresina, Piauí 64049-550, Brasil.

²Coordenação de Ciências Biológicas, Universidade Federal do Delta do Parnaíba, Parnaíba, Piauí 64202-020, Brasil.

Palavras-Chave: Utilização de CO₂, DFT, hidrogenação, nova química organometálica.

INTRODUÇÃO

Um grande esforço vem sendo feito para desenvolver reações para utilização do CO₂, sendo uma delas a sua hidrogenação direta resultando em formato/ácido fórmico. Vários catalisadores organometálicos homogêneos baseado em metais nobres foram desenvolvidos para este processo.¹ Tem havido um esforço para transladar a química feita com metais nobre para metais abundantes, e nesse contexto, para a reação de hidrogenação direta de CO₂, foram preparados alguns catalisadores, como por exemplo o [Fe^{II}(H)(η²-H₂)(PP₃^{Ph})]⁺, que mostrou altas taxas de reatividade.² Porfirinas de ferro (Heme) são geralmente usadas em outra reação de utilização do CO₂, a redução eletroquímica,⁴ mas não existem estudos sobre a hidrogenação direta usando porfirinas como catalisadores, que é o que este trabalho busca avaliar.

MÉTODOS

A abordagem do nosso problema se dá pela modelização da superfície de energia potencial da reação de hidrogenação direta do CO₂ catalisada por Heme, que já foi previamente discutido na literatura⁵ para esta reação. A modelização, nos estados singlete e triplete, foi feita baseado na Teoria Funcional da Densidade, através do funcional M06 e do conjunto de funções de bases XXXX para o ferro e XXXX para todos os demais. Correções dispersão de Grimme e correções do solvente foram também consideradas.

RESULTADOS

A **Figura 1** mostra a superfície de energia potência associada ao mecanismo da reação mostrada no **Esquema 1**. O mecanismo inicia pela coordenação da molécula de H₂ ao centro ácido do grupo Heme, seguido por sua cisão heterolítica promovida pelo co-catalisador básico (NEt₃), formando o intermediário Fe3, que tem um hidreto coordenado ao centro metálico. Este hidreto é transferido ao carbono do CO₂, via ataque nucleofílico (Fe5), seguido pela liberação do formato e a coordenação de uma nova molécula de H₂.

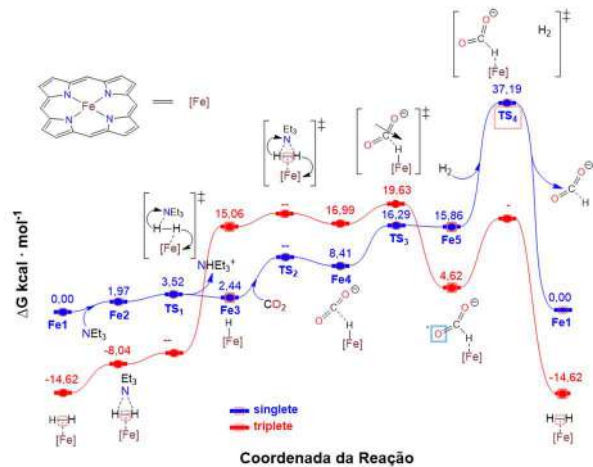


Figura 1: Mecanismo geral da hidrogenação direta do CO₂ catalisada por Heme.

A reação é exergônica (-14,6 kcal/mol) e apresenta uma pequena barreira energética (42.2 kcal/mol), o que é similar com o comportamento cinético e termodinâmico mostrado por outros catalisadores de Ferro⁵ com boa atividade experimental.²

CONCLUSÕES

O grupo Heme pode ser utilizado como catalisador para a reação de hidrogenação direta do CO₂ dado ao comportamento cinético e termodinâmico similar a outros sistemas catalíticos sabidamente efetivos.

REFERÊNCIAS

1. L. Roy, B. Mondal, S. Ye Dalton Trans., 2020, vol. 49, pg. 16608.
2. C. Ziebart, C. Federsel, P. Anbarasan, R. Jackstell, W. Baumann, A. Spannenberg and M. Beller, J. Am. Chem. Soc., 2012, vol. 134, pg. 20701.
3. B. Mondal, F. Neese, S. Ye Inorg. Chem., 2015, vol. 54 pg. 7192.
4. G. F. Manbeck, E. Fujita J. Porphyrins Phthalocyanines 2015; vol. 19, pg. 1.
5. B. Mondal, F. Neese, S. Ye Inorg. Chem., 2015, vol. 54 pg. 7192.

AGRADECIMENTOS

F. Soares agradece a Secretaria de Educação do Governo do Maranhão pela licença capacitação. Agradecemos ao CENAPAD-Unicamp pelo tempo computacional.

Investigação Computacional das Propriedades de Clusters $\text{Ni}_m\text{Pd}_{n-m}$

Tiago M. de Souza (PG),^{1*} Lucas B. Pena (IC),¹ Juarez L. F. Da Silva(PQ)², Breno R. L. Galvão(PQ).¹

tiagomendesdesouza@yahoo.com

¹ Centro Federal de Educação Tecnológica de Minas Gerais, CEFET-MG, Av. Amazonas 5253, 30421-169, Belo Horizonte, MG, Brasil; ² Instituto de Química de São Carlos, Universidade de São Paulo, P.O. Box 780, 13560-970, São Carlos, SP, Brasil

Palavras Chave: níquel, paládio, nanoliga, catálise, hidrogênio

INTRODUÇÃO

O H_2 gerado a partir da água vem chamando atenção como uma alternativa aos combustíveis fósseis, contudo, os materiais atualmente utilizados no processo de catálise desta reação como Au e Pd são muito caros, o que é um obstáculo à produção desse gás em larga escala.^{1,2} Afin de reduzir os elevados custos desse processo, vem se buscando ligas de metais abundantes, como Ni, com metais nobres.² Tendo em conta que os materiais baseados em Ni e nanoclusters de Pd são prováveis catalisadores em reações de evolução de oxigênio,³ e que há relevante dissociação da água em superfícies de Ni metálico,⁴ o presente trabalho pretende elucidar as propriedades eletrônicas e estruturais de nanoligas de Ni e Pd de 13 átomos, com o intuito de, posteriormente, avaliar as propriedades de clusters de 27 e 41 átomos, bem como verificar as correlações entre as mesmas.

MÉTODOS

Neste trabalho, executamos cálculos a nível DFT, com o uso do método *projector augmented wave* e *funcional PBE*, em pacote computacional VASP.⁵ Inicialmente foram realizados testes de convergência com geometrias de clusters Ni_{13} e Pd_{13} encontradas na literatura.^{6,7,8} Após esses testes, as geometrias de mais baixa energia de cada elemento (denominadas estruturas pais) foram selecionadas para gerar as geometrias das ligas. Após a geração de todas as possíveis permutações, foram selecionadas, utilizando o algoritmo k-means,⁹ 30 estruturas para realização de cálculos de triagem, com energia de corte de 341 eV. Ao final desses cálculos iniciais, 15 estruturas foram selecionadas novamente usando o método k-means, e considerando uma maior energia de corte de 438 eV.

RESULTADOS

Clusters de composições intermediárias possuem as menores E_{exc} . Além disso, as geometrias mais estáveis de cada composição apresentaram momento magnético total, m_t , praticamente constante até o $n=10$. Notamos, ainda, que entre as estruturas de menor energia as ligas Ni_5Pd_8 e Ni_7Pd_6 apresentam menor gap global, E_{gap} .

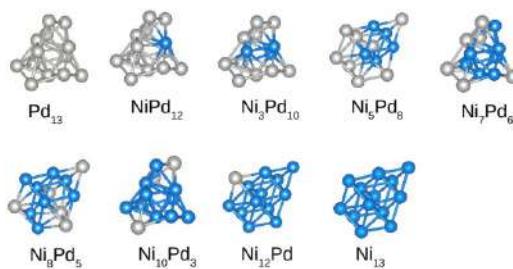


Figura 1:Estruturas de mais baixa energia dos clusters de 13 átomos.

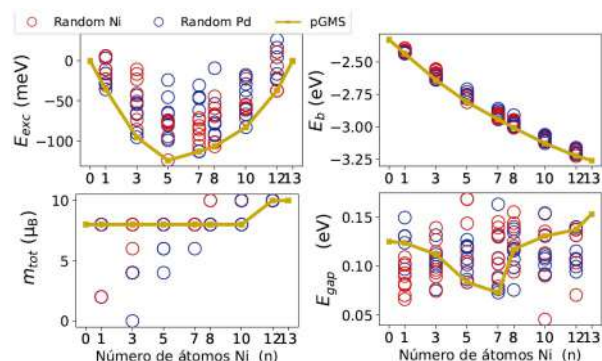


Figura 2: Propriedades eletrônicas dos clusters de 13 átomos: momento magnético total (m_t), energia de excesso (E_{exc}), energia de ligação (E_b), Gap HOMO-LUMO (E_{gap}).

CONCLUSÕES

As propriedades das partículas variam muito com a geometria. Se considerarmos apenas as geometrias mais estáveis, vemos que composições intermediárias tendem a ter os menores valores de E_{exc} e E_{gap} .

REFERÊNCIAS

1. J. Wang et al., *J. Alloys Compd.*, 2020, 819, 153346
2. J. Zhang et al., *Angew. Chem.*, 2016, 128, 6814
3. A. Munir et al., *ChemSusChem*, 2019, 12, 1517
4. L. Zhu et al., *J. Phys. Chem. C*, 2020, 124, 25835
5. G. Kresse, J. Furthmüller, *Phys. Rev. B*, 1996, 54, 11169
6. A. Chaves et al., *Phys. Chem. Chem. Phys.*, 2017, 19, 15484
7. Y. Liu et al., *Eur. Phys. J. D*, 2011, 61, 389
8. P. Nava et al., *Phys. Chem. Chem. Phys.*, 2003, 5, 3372
9. L.R. da Silva et al., *Comput. Mater. Sci.*, 2022, 215, 111805

AGRADECIMENTOS

CINE, CAPES, FAPEMIG (APQ-00597-22).



Ruthenium, Platinum and Palladium fcc Nanoparticles for Hydrogen Production and Storage

Marietjie J. Ungerer (PhD)¹, Nora H. de Leeuw (R)²

UngererMJ@cardiff.ac.uk; N.H.deLeeuw@leeds.ac.uk

¹School of Chemistry, Cardiff University, Park Place, Cardiff, CF11 3AT, UK

²School of Chemistry, Faculty of Engineering and Physical Sciences, University of Leeds, Leeds LS2 9JT, UK

Keywords: (Ruthenium, Hydrogen, Storage, fcc, Platinum)

INTRODUCTION

Hydrogen is a major sustainable energy vector, which is set to play a leading role in attaining a net zero carbon economy. More recently, global research efforts have shifted towards storing hydrogen in condensed phases.¹ One example is liquid organic hydrogen carriers (LOHC) being used for reversible hydrogen storage and transport. Various catalysts have been used for both the hydrogenation and dehydrogenation reactions, including precious Pt, Pd and Ru metals.² The dominant phase of the bulk Ru metal is hexagonal close-packed (*hcp*), which has been studied extensively. However, significantly less attention has been paid to the face-centered cubic (*fcc*) phases, which have been observed in nanoparticles.

METHODS

Electronic structure techniques based on the density functional theory (DFT) with long-range dispersion corrections [DFT-D2, DFT-D3 and DFT-D3-(BJ)] were used to calculate fundamental properties of the catalysts, e.g. the lattice parameters, surface energies and work functions of the (001), (011) and (111) surfaces of Ru, Pd and Pt in the *fcc* phase, induced magnetisation the electronic structures, work functions, the chemical bonding and electron transfer occurring during the adsorption of hydrogen.^{3,4} Investigate systematically the magnetic moments of two different morphologies and various sizes of Ru nano-dots in the *fcc* phase. To confirm the results obtained by the plane-wave DFT methodologies, additional atom-centered DFT calculations were carried out on the smallest nano-dots to establish accurate spin-splitting energetics.

RESULTS

When investigating the surface properties of the three metals, the DFT-D2 method generally underestimated the lattice parameters by up to 2.2% for Pt and 2.8% for Ru. The surface energies followed the observed trend (111) < (001) < (011) for both Ru and Pd with all three methods, which is comparable to experimental data. For Pt the same trend was observed with DFT-D2 and DFT-D3(BJ), but it deviated to Pt (111) < Pt (011) < Pt (001) for the DFT-D3 method. DFT-D2 overestimated the surface energies for all three Miller Indexes. The best correlation for the surface energies was obtained

with the DFT-D3 and DFT-D3(BJ) methods, both of which have deviate by less than 15% deviation for all surfaces with respect to experiment. The work function followed the trend of Φ (111) < Φ (001) < Φ (011) for all three metals and calculated by all three methods. Five different types of Ru, Pd and Pt nanoparticles were considered, including icosahedral, decahedral, cuboctahedral, cubic and spherical particles of different sizes. The bulk, surface and nanoparticle calculations showed that the DFT-D2 method for Pt overestimated the exchange-correlation, leading to higher energy values that can be contributed erroneously to a more stable structure. The calculations showed that as soon as the surface-to-bulk ratio > 1, the energy per atom resembles bulk energy values.

CONCLUSIONS

The Wulff morphology of all three metal types showed that the (111) surface is the dominant surface but that the (001) and (011) surfaces are also expressed in the particle morphologies. For the Ru₁₃ nano-dots of different morphologies (icosahedral and cubic), it was seen that the spin-polarised calculations led to the more stable structure, which was not the case for the icosahedral Ru₅₅ and cubic Ru₆₃ structures. Surprisingly, we found that in most cases of Ru nano-dots, the high spin electronic structures had the most favourable energies and were hence the most stable.

REFERENCES

- 1 G. Petitpas, S. Aceves, Hydrogen Storage Technology: Materials and Applications, (CRC Press 2013).
- 2 P.M. Modisha, C.N.M. Ouma, R. Garidzirai, P. Wasserscheid, D. Besserabov, Energy Fuels 33, 2778 (2019)
- 3 Ungerer, M.J.; De Leeuw, N.H., Computational Insights into Ru, Pd and Pt fcc Nano-Catalysts from Density Functional Theory Calculations: The Influence of Long-Range Dispersion Corrections, Catalysts 2022, 12(10), 1287.
- 4 Ungerer, M.J.; De Leeuw, N.H., A DFT Study of Ruthenium fcc Nano-Dots: Size-Dependent Induced Magnetic Moments, Nanomaterials 2023, 13(6), 1118.

ACKNOWLEDGMENTS

This research was undertaken using the Supercomputing Facilities at Cardiff University, UK, operated by ARCCA on behalf of Supercomputing Wales (SCW) projects, which is part-funded by the European Regional Development Fund (ERDF) via Welsh Government. This work used the Isambard 2 UK National Tier-2 HPC Service operated by GW4 and the UK Met Office.

Investigação teórica da relevância do anel 1,2,4-trioxano na atividade leishmanicida da artemisinina e derivados.

Marcos Daniel G Pizon (IC),¹ Antonio Florêncio de Figueiredo (PQ),² Heriberto Rodrigues Bitencourt (PQ),³ José Ciríaco Pinheiro (PQ).^{4*}

marcos.pizon@icen.ufpa.br; ciriaco@ufpa.br, antonio.florencio@ifpa.edu.br, heriberto.ufpa@gmail.com

¹Universidade Federal do Pará, Instituto de ciências exatas e naturais; ²Laboratório de Química Teórica e Computacional, UFPA, Belém, PA; ³IFPA Castanhal, PA; ⁴Laboratório de Síntese Orgânica, UFPA, Belém, PA.

Palavras-Chave: Artemisinina e derivados, Relevância do anel 1,2,4-trioxano, Atividade leishmanicida

INTRODUÇÃO

A Leishmaniose é causada por três (3) espécies diferentes de *Leishmania* patogênica aos humanos: *L. donovani*; *L. tropica*; *L. braziliensis*¹. Neste trabalho, artemisinina e derivados com atividade contra *L. donovani* são investigados com o potencial eletrostático molecular (*molecular electrostatic potential, MEP*) e com a interação ligante-receptor para identificar características estruturais necessárias às atividades biológicas e prováveis interações com um receptor em um processo biológico, visando compreender o papel do anel 1,2,4-trioxano na atividade leishmanicida.

MÉTODOS

Na Figura 1 são mostradas as estruturas 2D dos compostos investigados (**1**, **2**, **3**). Inicialmente, a estrutura cristalográfica da artemisinina², foi completamente otimizada no nível B3LYP/6-31**. Os resultados obtidos reproduziram adequadamente o anel 1,2,4-trioxano (**1**, **2**), quando comparados aos dados experimentais na conformação mais estável da molécula. Com a geometria otimizada, as estruturas dos derivados foram construídas, otimizadas e calculados o potencial eletrostático molecular (*Molecular Electrostatic Potential, MEP*) e a interação com o heme. O heme consiste do Fe no centro da protoporfirina e para a descrição mais real do ambiente biológico na intenção ligante-heme, o resíduo de histidina foi deixado ligado ao Fe²⁺. O heme foi obtido do complexo 1A6M-RSCB-PDB³, o qual contém somente a cadeia A.

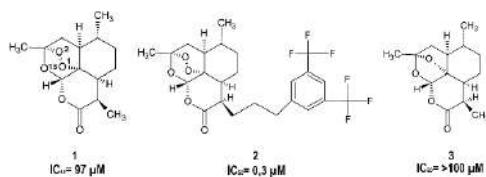


Fig 1. Estruturas-2D da artemisina (1) e derivados (2,3)

RESULTADOS

Na Figura 2, são mostradas as estruturas 2D (a), os mapas de MEP (b) e as interações com a heme dos compostos 1, 2 e 3 (c). Na região colorida em vermelho, amarelo e verde, com MEP (b) negativo nas faixas: -119,9 a -15,80 kcal/mol (1) e -112,3 a -53,65 kcal/mol (2) destaca-se o anel 1,2,4-

trioxano (**1**, **2**), indicando sua importância em um possível ataque eletrofílico por um alvo biológico. Para o derivado **3** o MEP negativo situa-se na faixa -107,9 a -13,37 kcal/mol. Além disso, a inexistência do anel 1,2,4-trioxano nesse derivado evidencia a diminuição da densidade eletrônica na região importante à atividade leishmanicida e, consequentemente, leva à inatividade de **3**. A interação de cada ligante (**1**, **2** e **3**) com o heme (Fe²⁺) é mostrada na Fig 2 (c). Para os compostos **1** e **2**, essa interação ocorre nas distâncias dO₁Fe= 2,61, dFeO₂=3,70 Å e dFeO₁=2,54, FeO₂=3,37 Å, respectivamente, evidenciando preferencialmente a aproximação Fe²⁺ e O₁. No derivado **3**, a inexistência do anel 1,2,4-trioxano condiciona-o a aproximação do O com o Fe²⁺, dFeO=3,20 Å, impossibilitando a interação necessária à existência da atividade leishmanicida do **3**.

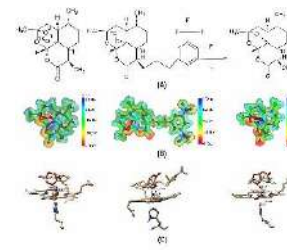


Figura 2. Estrutura 2D, mapas de MEP e interação com o heme dos compostos 1, 2 e 3

CONCLUSÕES

A investigação dos compostos através do MEP evidenciou a importância do anel 1,2,4-trioxano à atividade leishmanicida.

A investigação ligante-heme possibilitou identificar as interações específicas entre o anel 1,2,4-trioxano e o Fe²⁺ do heme.

O substituinte, -(CH₂)₃-C₆H₄(3,5-CF₃), em **2**, possibilita melhor orientação no encaixe do ligante ao heme e a melhora substancial da atividade leishmanicida em relação à artemisinina (**1**).

REFERÊNCIAS

- ¹J. Carvalho, et al, JCTN, 2011, 8, 1.
- ²M. Ortalli, et al, EJMC, 2019, 170, 126.
- ³J. Vojtechovsky, et al, BJ, 1999, 27, 2153.

AGRADECIMENTOS

LQTC, UFPA.



Propriedades eletrônicas para EuF obtidas com o CASSCF(6,6) + PT2

Luiz Cunha de Miranda (PG),¹ Nelson Henrique Morgan (PQ)²

luizcunhabrv@yahoo.com.br; nhmorgen@unicamp.br

¹*Instituto de Química, Universidade Estadual de Campinas, Campinas, Brasil*

²*Instituto de Química, Universidade Estadual de Campinas, Campinas, Brasil*

Palavras Chave: Oscilador anarmônico, Molécula diatômica, Energia de dissociação, Propriedades eletrônicas.

INTRODUÇÃO

A estrutura eletrônica dos elementos lantanídeos representa um desafio considerável para o trabalho experimental e teórico.¹ A análise das curvas da superfície de energia potencial (SEP) permite obter algumas propriedades eletrônicas e moleculares. Nesse resumo apresentamos numa abordagem simples resultados para a molécula diatômica EuF no estado fundamental. O estudo foi feito considerando-se o formalismo do potencial anarmônico. Foram utilizados cálculos de estrutura eletrônica no nível CASSCF(6,6) com a adição de correlação eletrônica dinâmica no nível PT2. Os resultados obtidos são próximos aos valores experimentais.

MÉTODOS

As propriedades eletrônicas (comprimento de ligação, frequência vibracional, constante de força e energias de dissociação de EuF) foram obtidas com os métodos HF, MP2, B3LYP, CASSCF(6,6) e CASPT2(6,6). O conjunto de base DZP-DKH de Jorge e co-autores² foi adaptado para pseudopotencial de Stuttgart RSC1997 ECP. As SEPs foram construídas usando varredura de 0,8 a 4,0 Å em intervalos de 0,1 Å. Calcula-se a energia potencial - $V(R)$, em função do comprimento de ligação R , posteriormente ajustado pelo polinômio de ordem n , como descrito pela Eq. (1):

$$V(R) = \frac{1}{R - R_e} \sum_{n=0}^{10} C_n (R - R_e)^n \quad (1)$$

No mínimo da primeira derivada deste polinômio obteve-se o R_{eq} . A constante de força k associada à ligação química deste sistema é dada pela segunda derivada, como mostra a Eq. (2), e a partir

$$k = \left(\frac{\partial^2 V(R)}{\partial R^2} \right)_{R=R_e} \quad (2)$$

desse valor se obteve a frequência vibracional (ν) – Eq. (3), onde μ é a massa reduzida do sistema.

$$\nu = \frac{1}{2\pi} \sqrt{\frac{k}{\mu}} \quad (3)$$

RESULTADOS

As Figs. 1a e b mostram as SEPs dos métodos mono e multiconfiguracionais, respectivamente. E na Tabela 1 estão os dados das constantes espectroscópicas obtidas a partir dessas SEPs e seus respectivos valores experimentais. Todos os cálculos foram feitos com o programa Gaussian16.

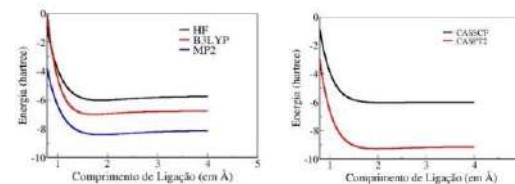


Figura 1. (a) SEPs de EuF nos níveis HF, B3LYP e MP2 e (b) CASSCF e CASPT2.

Tabela 1. Propriedades Eletrônicas para EuF.

Nível	R_e (Å)	u (cm ⁻¹)	$k/10^{-6}$ (mDyne/Å)	ZPE (hartree)	D_e (kJ/mol)	D_0 (kJ/mol)
HF	1,923	778,359	6,028	0,002	859,589	859,591
B3LYP	1,885	914,126	8,314	0,002	875,657	875,659
MP2	1,923	755,969	5,687	0,002	862,084	862,086
CASSCF(6,6)	1,997	326,403	1,000	0,001	606,720	606,721
CASPT2(6,6)	1,971	605,074	3,643	0,001	527,78	527,79
Experimental	1,977 ³	606 ³	3,65 ³	-	-	528,00 ⁴

CONCLUSÕES

O método multiconfiguracional CASSCF(6,6) com correlação dinâmica PT2 apresentou valores próximos dos registrados na literatura, como era de se esperar, visto que introduz apropriadamente os efeitos de correlação eletrônica.

REFERÊNCIAS

- M. Dulick, E. Murad; R. F. Barrow, *J. of Chem. Phys.*, **1986**, 85, 385.
- F. E. Jorge, A. Canal Neto, G.G. Camiletti, S.F. Machado J. *Chem. Phys.* **2009**, 130, 064108.
- I. Gotkis, I. *J. of Chem. Phys.*, **1991**, 95, 6086.
- J. Dean. *Lange's Handbook of Chemistry*, **1999**, 15, 4.

AGRADECIMENTOS

Os autores agradecem a infraestrutura computacional do IQ/Unicamp e o apoio financeiro da FAPESP e CNPq.

Influence of connector type on akamptisomerism and light absorption spectra in BODIPY-Porphyrin systems

Karine N. de Andrade (PG),¹ Natalia M. Raffaeli (IC),¹ Patrick L. L. Rocha (IC),¹ Rodolfo G. Fiorot (PQ)^{1*}
karineandrade@id.uff.br; rodolfofiorot@id.uff.br

¹Department of Organic Chemistry, Chemistry Institute, UFF, Outeiro de São João Batista, 24020-141, Niterói, RJ, Brazil
Keywords: Bond Angle Inversion, Chromophore, Isomerism, Photosensitizers, TD-DFT

INTRODUCTION

Boron dipyrromethene, BODIPY, is a well-known organic chromophore commonly used in porphyrin rational substitutions. The presence of different connectors in the BODIPY-porphyrin system can give rise to intramolecular charge transfer (ICT) porphyrin—BODIPY, making these systems highly versatile as photosensitizers.¹ Perturbations in the electronic structure can impact the ICT and the resulting light absorption spectra. Recently, a phenomenon known as bond angle inversion (BAI), or akamptisomerism, has been discovered in porphyrin with B–O–B bridges.² This isomerism leads to a change in the pseudo-plane of the porphyrin molecule in akamptisomers, potentially affecting their light absorption spectra. Herein, we investigated the influence of the BODIPY(BO)-porphyrin(Po) connector on akamptisomerism and its effect on the electronic structure for the isomers pairs. To achieve this, we selected two different connectors: ethyne (**A**), which allows for direct π conjugation, and pentane (**B**), which involves non-covalent interactions (NCI) in the BODIPY-porphyrin scaffold (Fig. 1).

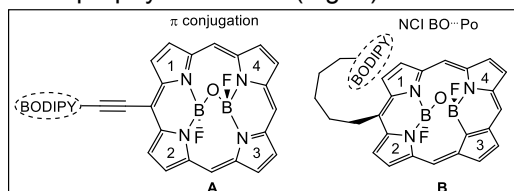


Fig. 1: Evaluated BODIPY-porphyrins systems.

METHODS

We employed the DFT-B3LYP-D3/6-31+G(d,p) and TD-CAM-B3LYP/6-31+G(d,p) methods to explore the BAI and absorption profile, respectively, simulating 80 excited states (*singlets*) for each system at G09 software.

RESULTS

While system **A** exhibits a linear configuration, system **B** adopts a C-shape, allowing for NCI between BO and Po. The BAI passes by a TS with a linear B–O–B bridge, in which the oxygen atom changes from sp^3 (minimum-energy point) to sp (TS) hybridization (Fig. 2), with energy barriers of $\Delta G^\ddagger = 26.3$ (**A**) and 26.8 (**B**) kcal mol⁻¹. These BAI barriers classify both systems as akamptisomers, forming isoenergetic isomers t_1 and t_2 .

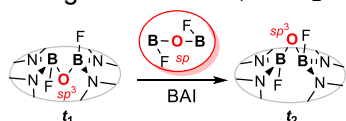


Fig. 2: Bond angle inversion (BAI) processes.

We analyzed the UV-Vis spectra (Fig. 3) to study the photophysical properties of the akamptisomer pairs t_1 and t_2 of **A** and **B**. We also included the non-substituted porphyrin with a B–O–B bridge (Po_{BOB}, black curve) for comparison. In both cases, we observed a redshift compared to Po_{BOB}, indicating ICT mainly from the porphyrin to BODIPY. In case **A**, the ICT occurred along the π bond, as evidenced by the density of states of the frontier Kohn-Sham orbitals in Fig. 3. This led to a significant red shift of approximately 84 nm for the Soret band. However, in case **B**, the absorption bands are similar to the reference system. In case **A**, the direct BODIPY-porphyrin conjugation resulted in enhanced absorption in the light region (Q band region) due to increased permissiveness.

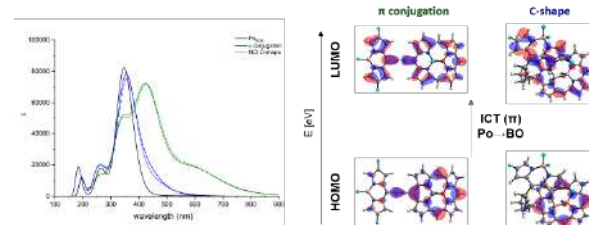


Fig. 3: Light absorption spectra and frontier Kohn-Sham orbitals for t_1 **A** (blue) and **B** (green) systems.

The akamptisomers t_1 and t_2 exhibited similar electronic structure for both connectors, suggesting that the BAI process does not significantly affect the absorption profile with only one *meso* BODIPY substitution. Akamptisomers showing substantial differences in the photophysical properties can be potentially utilized as photoswitches. Therefore, we expect to explore *meso* and β substitutions that can generate such distinct profiles, as push-pull devices or the insertion of chromophores into the porphyrin framework.

CONCLUSIONS

This research provided insights into the relationship between the BODIPY-porphyrin connector, akamptisomerism, and the resulting electronic structure. The direct π conjugation has more influence on electronic structure, resulting in a large redshift and strong ICT. This connector will be explored in the design of new BODIPY-porphyrin akamptisomers, particularly for the design of new photoswitches.

REFERENCES

- S. Cinear, et al, Dyes Pigm., **2022**, 206, 110573.
- P. J. Canfield, et al, Nat. Chem., **2018**, 10, 615.

ACKNOWLEDGES

CNPq, CAPES, FAPERJ and LoboC-UFRJ.

Corroles versus porphyrins as binucleating ligands of diboron complexes: stereochemistry and bond angle inversion exploration

Patrick L. L. Rocha (IC),¹ Natalia M. Raffaeli (IC),¹ Karine N. Andrade (PG)¹, Rodolfo G. Fiorot (PQ)^{1*}

patrickllr@id.uff.br; rodolfofiorot@id.uff.br

¹Department of Organic Chemistry, Chemistry Institute, Universidade Federal Fluminense (UFF), Outeiro de São João Batista, 24020-141, Niterói, RJ, Brazil

Keywords: Akamptisomerism, DFT, Tetrapyrroles

INTRODUCTION

Porphyrins and ring-contracted analogues, such as corroles, offer remarkable redox chemistry and unique coordination properties, acting as Lewis-base scaffolds for various complexes.¹ These macrocycles can form diboron complexes reacting with $\text{BF}_3\text{-OEt}_2$ in basic media, which can then undergo hydrolysis reactions. These complexes have diverging stereochemistry — *cisoid* corroles and *transoid* porphyrins (Fig. 1).² Moreover, Canfield and co-workers have reported a new form of isomerism in porphyrins, known as akamptisomerism, resulting from the bond angle inversion (BAI) of (FB)—O—(BF) *transoid* linkages. This unique isomerism can lead to isolable isomers, with an energy barrier of $22.5 \text{ kcal mol}^{-1}$.³ Despite structural similarities, the BAI has not yet been identified in corroles. Herein, we aim to elucidate the stereochemical preferences (*transoid* x *cisoid*) observed in corrole and porphyrin diboron complexes, as well as to investigate the viability of the BAI for alternative (Y_1B)—O—(BY_2) moieties.

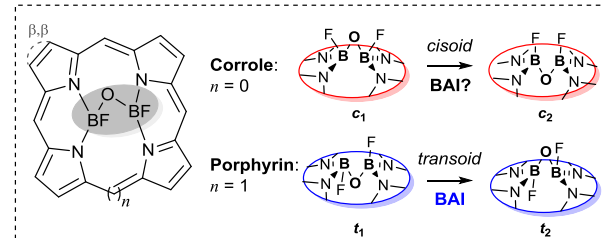


Fig. 1: Stereochemistry of diboron complexes — n refers to the number of meso-carbons.

MATERIALS AND METHODS

All gas phase geometry optimizations, characterizations by vibrational frequency, and estimations of thermal correction parameters were realized through DFT calculations at the B3LYP-D3/6-31+G(d,p) level. More refined electronic energy was calculated through single-point energies (SPE) with the def2-QZVP basis set.

RESULTADOS

Our calculations showed that the *cisoid* c_1 stereoisomer is $14.8 \text{ kcal mol}^{-1}$ (Gibbs free energy) more stable for the corrole than its *transoid* counterpart. In agreement with experimental findings, the opposite was identified for porphyrin, in which the *transoid* stereoisomer is favorable by $6.6 \text{ kcal mol}^{-1}$.² We attribute this to the smaller cavity areas of corroles (7.70 \AA^2) as

measured by the $\text{N}\cdots\text{N}$ distances in the bonded structure), which favor the boron “out-of-plane” *cisoid* c_1 arrangement of the boron. In porphyrin, the larger area (8.15 \AA^2) can accommodate one boron in the cavity, making the *transoid* configuration more stable than the strained *cisoid* one. Regarding the BAI process of β,β -benzyl-substituted, it only occurs through the *transoid* configuration in porphyrin ($22.5 \text{ kcal mol}^{-1}$), while the barrier is prohibitive in corroles (45 kcal mol^{-1}). The *cisoid* BAI in both systems does not occur because the c_2 is not a minimum energy point in the PES. Due to that, we replaced the (Y_1B)—O—(BY_2) moieties (see Table 1) aiming to promote the *cisoid* stereoisomer through noncovalent interactions within the Y linkages.

Table 1. Relative Gibbs Free Energies (kcal mol^{-1}) of the *cisoid* c_1 corrole and porphyrine diboron complex relative to the *transoid* t_1 stereoisomer for (Y_1B)—O—(BY_2).

Entry	Y	$\Delta G_{(\text{Corroles})}$	$\Delta G_{(\text{Porphyrine})}$
1	$\text{Y}_1=\text{Y}_2=\text{F}$	-14.8	6.6
2	$\text{Y}_1=\text{Y}_2=\text{OH}$	-16.1	4.8
3	$\text{Y}_1=\text{Y}_2=\text{Ph}$	-25.1	0.2
4	$\text{Y}_1=(\text{NH}_2), \text{Y}_2=(\text{COOH})$	-21.9	2.6
5	$\text{Y}_1=(\text{N}(\text{CH}_3)_2), \text{Y}_2=(\text{COOH})$	-21.1	4.5
6	$\text{Y}_1=\text{Y}_2=(\text{C}_6\text{Ph})$	---	10.0

Our results indicate that the presence of noncovalent interactions $\text{Y}_1\cdots\text{Y}_2$ in entries 2–5 promotes the stability of the *cisoid* c_1 over the *transoid*. For $\text{Y}_1=(\text{NH}_2)$, $\text{Y}_2=(\text{COOH})$ (entry 4), we report a new form of “out-of-plane” isomerism, not classifiable by *amplo* and *parvo* stereodescriptors.³

CONCLUSIONS

A consistent justification for experimental stereochemical preferences was reported. The role of noncovalent interactions is yet to be measured, as well as its effect on akamptisomerism phenomena.

REFERENCES

- J. Mack, Chemical Reviews, 2016, vol. 117 pg. 3444-3478
- P. J. Brothers, Inorganic Chemistry, vol. 50 pg. 12374-12386
- P. J. Canfield et al, Nature, 2018, vol. 10 pg. 615-624

ACKNOWLEDGEMENTS

CNPq, CAPES, FAPERJ, and LoboC-UFRJ (NACAD).



Determinação de constantes de velocidade do mecanismo de oxidação do gás metano na troposfera por meio de redes neurais artificiais

Vitor Roberto de Oliveira (IC),^{1*} Emilio Borges (PQ).¹

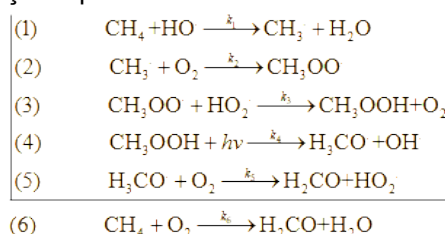
vitor.roberto@ufv.br

¹Departamento de Química – Universidade Federal de Viçosa –Viçosa, Minas Gerais

Palavras Chave: Redes Neurais Artificiais, Problemas Inversos, Metano, Química Ambiental.

INTRODUÇÃO

A oxidação do metano é um processo de grande interesse ambiental por se tratar de um gás que contribui para o efeito estufa além de levar à produção de metanal, um precursor para formação de monóxido de carbono¹. O mecanismo dessa reação envolve as seguintes equações químicas:



A obtenção de constantes de velocidade para todas as etapas de um mecanismo radicalar, a partir das concentrações experimentais de apenas uma das espécies envolvidas no processo, pode ser abordada como um *problema inverso* utilizando-se um algoritmo numérico apropriado, capaz de regularizar o problema que é naturalmente mal-colocado². O presente resumo relata a obtenção de todas as constantes de velocidade para o mecanismo anterior utilizando uma rede neural artificial de Hopfield para abordar o problema inverso correlato².

MÉTODOS

Cada etapa do mecanismo cinético anterior pode ser modelada numericamente como um sistema não linear do tipo $K(f)=g$ em que g , f e K representam, respectivamente, as concentrações do produto, as constantes de velocidade a serem invertidas e o modelo diferencial obtido pela lei da ação das massas. A abordagem consiste em encontrar as constantes de velocidade f a partir das concentrações g , utilizando-se o modelo diferencial K . Esse processo foi realizado utilizando-se um algoritmo baseado em redes neurais do tipo Hopfield que tem se mostrado bastante eficaz no tratamento de vários problemas inversos mal-colocados envolvendo processos cinéticos³.

RESULTADOS

Para iniciar o procedimento foi utilizada a constante experimental k_1 , de valor $6,18 \times 10^{-15} \text{ cm}^3 \text{ molecule}^{-1} \text{ s}^{-1}$ a 298K ¹. A partir dessa constante, foram obtidas as concentrações experimentais das espécies produzidas na primeira etapa. Essas concentrações foram utilizadas para construir a função objetivo na rede de Hopfield que obteve a constante de velocidade para a segunda reação do mecanismo. Essa segunda constante foi usada para gerar as concentrações das espécies da terceira etapa que foram inseridas na rede de Hopfield para obter a terceira constante e assim, sucessivamente, até que todas as constantes de velocidade fossem determinadas. As constantes de velocidade obtidas em $\text{cm}^3 \text{ molecule}^{-1} \text{ s}^{-1}$ foram $k_2=6,770 \times 10^{-15}$, $k_3=6,951 \times 10^{-15}$, $k_4=6,861 \times 10^{-15}$, $k_5=6,661 \times 10^{-15}$, $k_6=1,010 \times 10^{-14}$. Essas constantes reproduzem as concentrações das espécies no mecanismo de oxidação do metano com um erro médio de 1,4%, o que mostra a validade química das mesmas.

CONCLUSÕES

O método aqui utilizado obteve valores para constantes de velocidade que não podem ser facilmente encontradas na literatura, para reações de difícil monitoramento. O algoritmo também levou a uma boa reproduzibilidade das concentrações já que o erro médio foi de 1,4%. A eficácia desta rede neural para este tipo de problema é evidente, mostrando potencial para a determinação de vários parâmetros cinéticos para outros mecanismos químicos radicalares.

REFERÊNCIAS

- ¹ B. Pitts, J. Pitts, Chemistry of the Upper and Lower Atmosphere, 2000. pg 182.
- ² E. Borges, Problemas Diretos e Inversos em Dinâmica Molecular, Espectroscopia Vibracional, Cinética Química e Espalhamento Quântico, 2008. pg 83.
- ³ M. M. J. Junior, S. A. Fernandes, E. Borges, B. E. L. Baêta, F. A. Rodrigues, Molecular Catalysis, 2022, vol. 518. pg 112079.

AGRADECIMENTOS

À Universidade Federal de Viçosa.

Detection of nerve agents using fluorescent probes

Bruno Gabriel Motta Rodrigues (IC),¹ Itamar Borges Jr. (PQ),^{*1,2}

bruno.rodrigues@ime.eb.br; itamar@ime.eb.br

¹ Department of Chemical Engineering, Military Institute of Engineering, Rio de Janeiro, RJ, 22290-270, Brazil.

² Department of Defense Engineering, Military Institute of Engineering, Rio de Janeiro, RJ, 22290-270, Brazil.

Palavras Chave: Nerve Agents, DFT, B3LYP, Fluorescence, Quenching, Single Point Energy, Geometry Optimization

INTRODUCTION

Nerve agents are highly toxic chemical warfare agents that can be absorbed through skin, inhalation, and ingestion. For their detection, gas chromatography, Raman spectrometry, and enzymatic bio-sensing are usually employed.^[1,2] Another approach for detecting them is using fluorescent sensors. They are promising devices due to the combination of high sensitivity, operational simplicity, low cost, and real-time response.

METHODS

We investigated the fluorescence spectra of recently synthesized sensors, named NMU-1^[2] and HBQ (10-hydroxybenzo[h]quinoline).^[1] They were developed in three forms: neutral molecule, hydrolyzed by the acetylcholinesterase (AChE), and bonded to diethyl chlorophosphosphate (DCP), an organophosphate simulant.

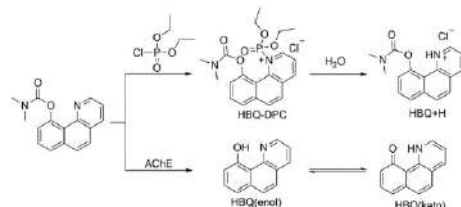


Figure 1 – Reaction schemes of HBQ with AChE and DCP.

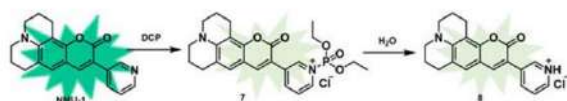


Figure 2 – Reaction scheme of NMU-1 with DCP (NMU-DCP) and subsequent hydrolysis (NMU-H).

Initial geometries were built using Avogadro and afterward optimized with the DFT/B3LYP//def2-TZVP method. The aqueous environment was simulated employing the CPCM solvation model implemented in Orca. CAMB3LYP TD-DFT single-point calculations were carried out for the ground state and the first singlet excited

state. Once the Hessians of both states were obtained, and the Orca ESD module was used to simulate the fluorescence spectra of these compounds.

RESULTS

Figure 3 presents the computed fluorescence spectra of HBQ, HBQ-DPC, and HBQ-Keto as a function of the transition energy. Figure 4 shows the simulated fluorescence spectra for NMU-1 and NMU-H.

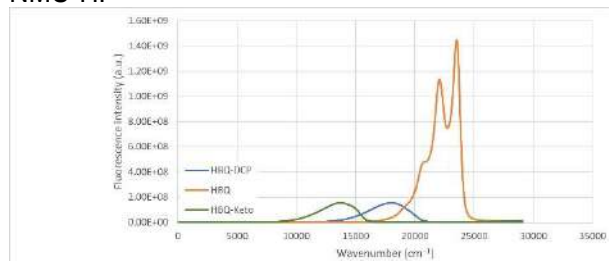


Figure 3 – Fluorescence of HBQ and other derivatives

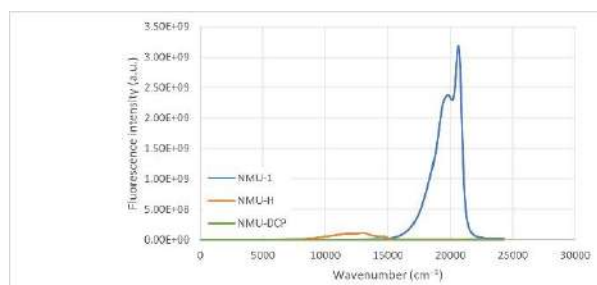


Figure 4 – Fluorescence of NMU-1 and other derivatives

CONCLUSION

We found a prominent change in the emission spectrum for the NMU-1 and HBQ sensors, characterizing the fluorescence quenching used for detection.^[3] The different positions of the maxima of the fluorescence bands are useful for fast detection based on the concentration of the species. Furthermore, the maximum emission peak of NMU-1 (20000 cm^{-1})^[2] and HBQ-H ($20000\text{--}24000\text{ cm}^{-1}$)^[1] are very close to the experimental data obtained in aqueous solution.

REFERENCES

¹Wenqi, M. et al., J. of Hazardous Materials.410.124811.2017

²Zhang, L. et al., Spectrochimica Acta. 275. 121171.2022

³Weert, M. van der et al., J. of Molecular Structure.998.144-150.2011

ACKNOWLEDGEMENTS

The authors thank the support of the Brazilian Army and the Brazilian agencies CAPES, CNPq, and FAPERJ.

Estudo teórico da artemisinina e seus derivados com atividade contra câncer de mama

Gustavo N. R. Alves (IC),^{1*} José C. Pinheiro (PQ)^{1,2}, Antônio F. De Figueiredo (PQ)³, Heriberto R. Bitencourt (PQ)⁴

gustavoalves@icen.ufpa.br; ciriaco@ufpa.br

¹Laboratório de Química Teórica e Computacional, UFPA, Belém, PA; ²Instituto Amazônia dos Saberes, São Luis, MA; ³IFPA, Castanhal, PA; ⁴Laboratório de Síntese Orgânica, UFPA, Belém, PA

Palavras-chave: Artemisinina. MEP, Docking Molecular, interação ligante-receptor, Câncer de mama.

INTRODUÇÃO

Câncer é a denominação para um grupo de doenças caracterizadas pelo crescimento e multiplicação descontrolados de células anormais, capazes de invadir estruturas próximas e se espalharem em diversas regiões do organismo.¹ Neste trabalho, artemisinina (Fig 1) e seus derivados^{2,3} (**1-3**) com atividade contra câncer de mama, são estudadas utilizando potencial eletroestático molecular (*Molecular E electrostatic Potential, MEP*) e docking molecular.

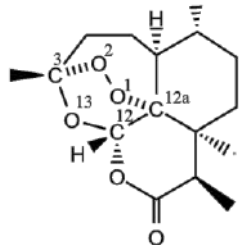


Fig 1. Estrutura base da artemisinina

MÉTODOS

O ponto de partida foi a construção das estruturas a partir da cristalografia da artemisinina⁴ e otimização completa com o programa Gaussian 98. A comparação da geometria teórica da artemisinina, na conformação mais estável, com os dados experimentais indicou o método B3LYP/6-31G** para o desenvolvimento da pesquisa. Mapas de MEP e o estudo da interação ligante-receptor (transferrina)⁵ foram construídos e analisados.

RESULTADOS

Na Fig 2 são mostrados as estruturas 2D, Os mapas de MEP e os complexos ligante-transferrina da artemisinina (**1**, $IC_{50} = 87,6 \mu M$) e derivados **2** ($IC_{50} = 28,8 \mu M$) e **3** ($IC_{50} = 2,1 \mu M$). Preliminarmente essa figura mostra os mapas de MEP mostram que a região de MEP mais negativo da artemisinina e seus derivados situa-se no anel 1,2,4-trioxano (Fig 1) da molécula, com os MEPS nas faixas -131,1 a aproximadamente maior que -0,2630 kcal.mol⁻¹ (mais ativos) e -133,6 a aproximadamente maior que -6.714kcal.mol⁻¹ (menos ativos); essa região é suscetível a ataques eletrofílicos. A interação dos compostos **1,2** e **3**

(Fig 2) mostra que a região da artemisinina e derivados interagem com a transferrina (Fe^{2+}) na região do anel 1,2,4-trioxano, com as distâncias entre FeO_1 e FeO_2 iguais a 2,24 e 2,61, 2,66 e 2,88, 3,52 e 4,40 Å para os compostos **1,2** e **3**, respectivamente. Como pode ser noticiado, verifica-se uma maior interação $Fe^{2+}O_1$, comparado ao $Fe^{2+}O_2$, em todos os compostos, e sua diminuição com o aumento da atividade biológica do composto.

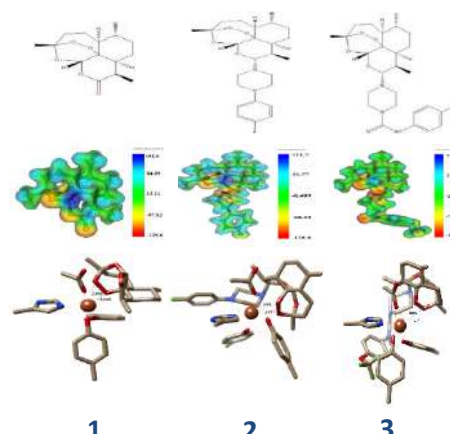


Fig 2. Estrutura 2D, Mapas de MEP (kcal/mol) e Docking Molecular da artemisinina, e derivados **2** e **3**.

CONCLUSÕES

Os mapas de MEP indicam a região do anel 1,2,4-trioxano como a região suscetível a ataque eletrofílico. Em adição a interação ligante-transferrina evidencia que os compostos mais ativos apresentam maiores distâncias $Fe^{2+}O_1$.

REFERÊNCIAS

- National Cancer Institute. Chemotherapy to Treat Cancer. 2015. Disponível: <https://www.cancer.gov/about-cancer/understanding/what-is-cancer> acessado em 10 de setembro de 2022
- HU, Yanping et al. BMCL 29, 1138-1142, 2019.
- LI, Shu et al. BMCL 28, 13, 2275-2278, 2018.
- J. N. Lisgarten, B. S. Potter, C. Bantuzeko et al. JCC 28, 539 – 543, 1998
- BARBOSA, Jardel P. et al. JSCS, 76, 9, 1263-1282, 2011.

AGRADECIMENTOS

LQTC e UFPA



Computation insights into sustainable catalysis: A UK Catalysis Hub perspective

Matthew G Quesne (PhD)^{1,2*}, C. Richard A. Catlow (PhD)^{1,2*}

QuesneM@cardiff.ac.uk; CatlowR@cardiff.ac.uk

¹Cardiff Catalysis Institute, School of Chemistry, Cardiff University, Cardiff CF10 3AT, UK; ²UK Catalysis Hub, Research Complex at Harwell, Rutherford Appleton Lab, Harwell, Oxfordshire OX11 0FA, UK

Keywords: Sustainable Catalysis, Circular Economy, Computational Chemistry, Density Functional theory, Molecular Dynamics, Quantum Mechanics/Molecular Mechanics

INTRODUCTION

The UK Catalysis Hub is a pinioning research program funded since 2013 by the Engineering and Physical Sciences Research Council (EPSRC). It is based in the research council in Harwell, which is home to the Diamond synchrotron facility as well as the UK's largest neutron source. The program co-ordinates projects from 25 different Universities and explores all aspects of catalytic science. This presentation will give a deep dive into the computational component of the Hub's programme with a specific focus on: (1) catalyst design for the circular economy and (2) using modelling to bridge the traditional divide between Homogeneous and Heterogeneous Catalysis.

METHODS

Quantum mechanical techniques can offer crucial insights into the reaction mechanisms catalyzed by (i) enzymatic biocatalysts,^{1,2} (ii) homogenous catalysts^{3,4} and (iii) heterogenous catalytic materials^{5,6}. Moreover, when such techniques are combined with classical molecular dynamics, hybrid QM/MM cluster models can be constructed that act as relatively computationally inexpensive methods for studying large catalysts from microporous and mesoporous materials⁷ to heterogenous nanocatalysts⁸ and are often especially useful during the study of enzymatic reaction mechanisms.⁹

RESULTS

This talk will highlight the ways in which the modern computational techniques discussed above are able to compliment other aspects of catalytic science in aiding the transition to more sustainable chemistry. A focus will be given to several recent Hub projects as well as the implementation of state-of-the art multiscale techniques to study the active site of complex materials (Figure 1). A common theme throughout this presentation will be the importance of combining the best aspects of heterogenous and homogenous catalysis in order to revolutionise the chemical space available for catalyst design. There will also be an overview as to how Harwell facilities enable fine scale detail of *in-operando* catalysis to be studied and how such insights feed into more reliable *in-silico* models.

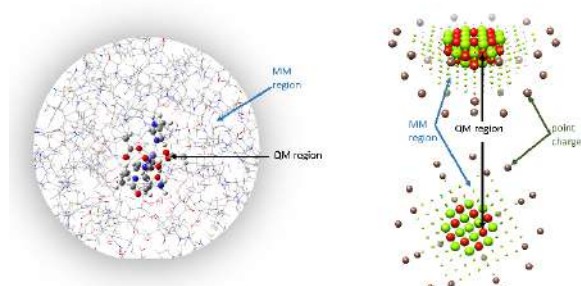


Figure 1. QM/MM model setup for biocatalysts (left) and ionic heterogeneous catalysts (right).

CONCLUSIONS

This talk will highlight how multiple state-of-the-art computational techniques are being applied to study a diverse range of novel catalytic project throughout UK institutions, with a key focus on applications for sustainable chemistry.

REFERENCES

- ¹ S.P. de Visser, M.G. Quesne, B. Martin, P. Comba and U. Ryde, *Chem Commun*, 2014, **50**, 262–282.
- ² M. Ortmayer, F.J. Hardy, M.G. Quesne, K. Fisher, C. Levy, D.J. Heyes, C.R.A. Catlow, S.P. de Visser, S.E. Rigby, S. Hay and A.P. Green, 2021. *JACS Au*, **1**, 913-918.
- ³ H. M. Neu, T. Yang, R.A. Baglia, T.H. Yosca, M.T. Green, M.G. Quesne, S.P. de Visser and D.P. Goldberg, *J Am Chem Soc*, 2014, **136**, 13845–13852.
- ⁴ S. Sahu, M.G. Quesne, C.G. Davies, M. Dürr, I. Ivanović-Burmazović, M.A. Siegler, G.N.L. Jameson, S.P. de Visser and D.P. Goldberg, *JACS*, 2014, **136**, 13542-13545.
- ⁵ A. Roldan, N.H. de Leeuw, C.R.A. Catlow, M.G. Quesne and F. Silveri, *PCCP*, 2019, **21**, 5335–5343.
- ⁶ M. G. Quesne, A. Roldan, N. H. De Leeuw and C. R. A. Catlow, *PCCP*, 2018, **20**, 6905–6916.
- ⁷ L. Negahdar, A.M. Beale, N.E. Omori, M.G. Quesne, M.D. Frogley, F. Cacho-Nerin, W. Jones, S.W.T. Price and C.R.A. Catlow, *ACS Catal*, 2021, **11**, 13091–13101.
- ⁸ Z. Xie, Y. Sui, J. Buckeridge, C.R.A. Catlow, T.W. Keal, P. Sherwood, A. Walsh, D.O Scanlon, S.M. Woodley, and A.A. Sokol, 2017, *Physica Status Solidi*, **214**, 1600445
- ⁹ M. G. Quesne, T. Borowski and S. P. de Visser, *Chemistry—A European Journal*, 2015, **22**, 2562.

ACKNOWLEDGMENTS

Computing facilities for this work were provided by ARCCA at Cardiff University, HPC Wales, and through our membership of the U.K.'s Materials Chemistry Consortium (MCC). The U.K. Catalysis Hub is thanked for resources and support. This work also used the Cirrus UK National Tier-2 HPC Service at EPCC (<http://www.cirrus.ac.uk>) funded by the University of Edinburgh and EPSRC (EP/ P020267/1). Catalysis Hub Consortium is funded by EPSRC (grants EP/R026815/1, EP/K014854/1, and EP/M013219/1). The MCC is funded by EPSRC (EP/F067496).

Ketonisation of Carboxylic Acids over ZrO_2 -based catalysts for Biomass Valorisation: The Role of Surface Acid-Base Sites

Maicon Delarmelina (PQ)^{1,2*}, Gunjan Deshmukh (PQ)^{2,3}, Haresh Manyar (PQ)^{2,3}, C. Richard A. Catlow (PQ)^{1,2}

DelarmelinaM@cardiff.ac.uk.

¹School of Chemistry, Cardiff University, Cardiff, CF10 3AT, United Kingdom; ²UK Catalysis Hub, Research Complex at Harwell, STFC Rutherford Appleton Laboratory, Didcot, OX11 0FA, United Kingdom; ³School of Chemistry and Chemical Engineering, Queen's University Belfast, Belfast, BT9 5AG, United Kingdom.

Palavras-chave: Zirconia, Carboxylic Acid, Ketonisation, Enolisation, DFT.

INTRODUCTION

Production of liquid fuels from biomass by the Hydrothermal Liquefaction process (HTL) has gained increasing industrial and academic attention due to its advantages to conventional pyrolysis.¹ The aqueous phase formed during HTL of biomass is rich in carboxylic acids, which can potentially be used for the production of biofuels. However, these molecules require chemical upgrading for improving their physicochemical properties prior to their use as fuels. Ketonisation is an important approach for the initial upgrading of carboxylic acids, leading to the reduction of their oxygen content, and increasing their stability and energy efficiency.² In this context, acid–base bifunctional catalysts are particularly desirable as they can be easily modified in order to optimise their activity and selectivity.³ Here, we investigate how sulfation and doping of zirconia catalysts influence the ketonisation of carboxylic acids.

METHODS

All calculations were performed using the VASP package within the framework of periodic density functional theory and at RPBE-D3+U ($U_{\text{Ti}(d)} = 4.0$ eV) level. Brillouin zone sampling was performed using the Monkhorst–Pack scheme with a k-point grid of $5 \times 5 \times 1$ together with a Gaussian smearing broadening of 0.02 eV. Calculated energy barriers were computed by CI-NEB and IDM approaches.

RESULTS

The two key steps of the β -ketoacid ketonisation mechanism of acetic acid were investigated here: enolisation and C-C coupling steps. The most favourable energy profiles over pristine c- ZrO_2 (111) and t- ZrO_2 (101) surfaces, as well as over Ca-, Y-doped c- ZrO_2 (111), and sulfated t- ZrO_2 (101) are shown in Figure 1.

Reduction of enolisation barrier was computed on Ca- and Y-doped c- ZrO_2 (111), whilst sulfation led to an increase of the energy barrier for this step. Additionally, sulfation led a significant reduction of the energy barrier of the C-C coupling step, but only small changes were computed for the doped systems.

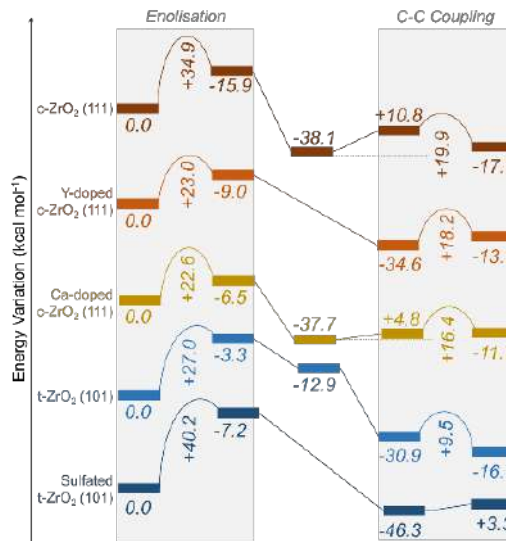


Figure 1. Energy profile for ketonisation of acetic acid.

The origin of these changes is discussed based on the modification of the strength of acid/basic surface sites, their interaction with reactants/intermediates, and the resulting effect over transition state structures and computed energy barriers. Furthermore, these results are used to rationalise distinct conversion rates and selectivities observed experimentally for these catalysts.

CONCLUSIONS

Tuning of the acidity and basicity of the surface sites of zirconia can be used as a powerful tool for modifying the energy profile of ketonisation reactions and improving the conversion rate and selectivity of this process. Our results provide design principles for the preparation of more efficient catalysts for the chemical upgrading of carboxylic acids into biofuels.

REFERENCES

- ¹B. Hao *et al.* Green Chem., **2021**, *23*, 1562. ²J. Watson *et al.* Prog. Energy Combust. Sci. **2020**, *77*, 100819; D. L.-Perez, *et al.* Bioresour. Technol. **2022**, *343*, 126084. ³Boekaerts, B. F. Sels, Appl. Catal. B: Environm. **2021**, *283*, 119607.

ACKNOWLEDGEMENT

The UK Catalysis Hub, EPSRC, MCC, Supercomputing Wales, HPC Cirrus, and HPC Archer2.

Benchmark Between Molecular Docking and SAPT Calculations in Biological Systems: Interaction of Opioid Receptors and Ligands.

Vinícius S. Donnici (MSc)¹, Daniel F. S. Machado (R)^{1*}, Guilherme D. R. Matos 3 (R)^{1*}

vinicius.donnici@gmail.com; daniel.scalabrin@unb.br guilhermedrmatos@gmail.com;

¹University of Brasília, Chemistry Institute, Complex Systems Modeling Laboratory

Keywords: Opioids, Benchmark, Symmetry-Adapted Perturbation Theory, Molecular Docking

INTRODUCTION

In theoretical chemistry calculations, it is important to obtain a good balance between the computational cost and the accuracy of the methods used. Molecular docking calculations, despite having a low computational cost, have a low accuracy in their results. To evaluate the performance of simpler models, it is often interesting to use other methods, such as SAPT quantum calculations, for benchmarking purposes.

METHODS

In this work, the opioid systems MOR (PDB 8F7R), KOR (PDB 8F7W) and DOR (PDB 8F7S) were minimized by the program GROMACS using AmberFF14sb force fields. Molecular docking was then performed using the program DOCK6, where energy footprints – per-residue interaction energy measurements – were calculated from the result. From the graph of the interaction energy between the receptor residues with the ligand, residue-ligand pairs were selected to perform SAPT calculations. The calculations were performed using the jun-cc-pvdz basis set in SAPTO and FI/SAPTO. The SAPT electrostatic interaction energies were compared to the electrostatic energies from docking, and the SAPT dispersion interaction energies were compared to the van der Waals energies from docking.

RESULTS

Figure 1: Dispersion Energy Plot

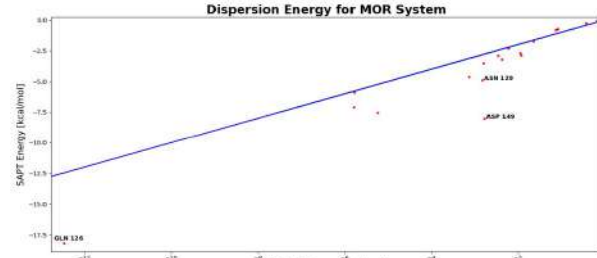
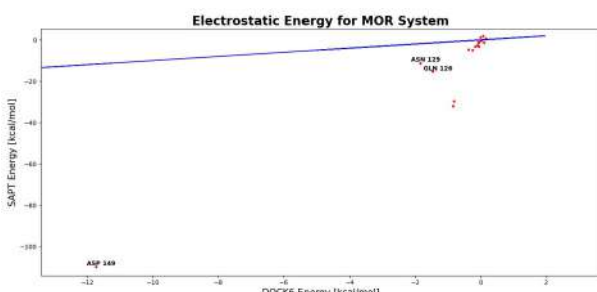


Figure 2: Electrostatic Energy Plot



In the graphs, the blue line represents ideality, where the molecular docking energy values, both electrostatic and dispersion, should be equal to the values obtained by SAPT/FISAPT quantum calculations. However, it is possible to observe a discrepancy between the values obtained by docking and SAPT calculations in both graphs. The behavior of electrostatic energies in docking shows that for some residues there is a considerable accuracy in the calculations, with some deviations, but for residues such as glutamate 126 and aspartate 149, both negatively charged residues, there is a discrepancy of values of up to 5.71 kcal/mol.

In the graphs comparing electrostatic energies, it is visible that there is a greater escape from ideality for most of the residues studied. The greatest energy disparity found was for the aspartate residue 149, negatively charged residue, where the difference between the energy found by SAPT/FISAPT and by molecular docking is approximately 98.08 kcal/mol.

CONCLUSIONS

Electrically charged residues, especially anionic residues, showed a greater escape from ideality, compared to neutral residues.

The future perspectives of the work include the adaptation of molecular dockings performed by DOCK6 through multigrids, which will be configured according to the trend line equation observed in the energy comparisons.

Future work will also include the reason why some residues calculated by molecular docking show an energy higher than expected by SAPT/FISAPT.

REFERENCES

1. "Psi4 1.4: Open-Source Software for High-Throughput Quantum Chemistry", D. G. A. Smith, L. A. et al., *J. Chem. Phys.* (2020). DOI: 10.1063/5.0006002
2. "DOCK 6: Impact Of New Features and Current Docking Performance.", Alle WJ, et al., *J. Comput. Chem.* (2015) Jun 5;36(15):1132-56. DOI: 10.1002/jcc.23905. PMID: 25914306. PMCID: PMC4469538
3. "Structures of the Entire Human Opioid Receptor Family.", Wang, Y., et al., *J. Cell.* (2023), Vol 186, Issue 2, p. 413-427-e17. DOI: 10.1016/j.cell.2023.12.026

ACKNOWLEDGMENTS

Thanks to CNPQ and FAP-DF for funding the project. To the University of Brasília for providing the study space. To SBQT for providing the presentation space.

Optoelectronic properties of star-shaped 1,3,5-triazine-core derivatives for organic solar cells

Nathália M. P. Rosa (PG),¹ Itamar Borges Jr. (PQ).^{1*}

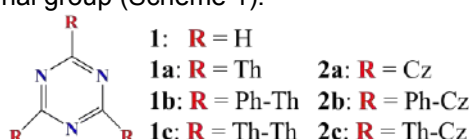
nathalia.rosa@ime.eb.br; itamar@ime.eb.br

¹Departamento de Química, Instituto Militar de Engenharia (IME), Rio de Janeiro, RJ 22290-270, Brazil

Keywords: triazine; organic solar cells; dye-sensitized solar cells; photovoltaics. DFT studies;

INTRODUCTION

The 1,3,5-triazine molecule is an organic heterocyclic compound used as a building block in organic light-emitting diodes (OLEDs),^{1a} dye-sensitized solar cells (DSSCs)^{1b} and organic solar cells (OSCs).^{1c} The π -electron deficiency of the 1,3,5-triazine (TZ) core allows its use as an electron acceptor (A), and when bonded to an electron donor (D), can induce significant amounts of charge transfer from the donor (D) to the accepting (A) portion.^{2,3} Substituents such as carbazole (Cz), thiophene (Th) and phenyl (Ph) bonded to the TZ core have gained attention as important components in multiple optoelectronic and photovoltaic applications.⁴ In this work, we investigated a series of star-shaped D–A molecules with 1,3,5-triazine as a acceptor core. Phenyl and thiophene groups were employed as terminal groups and/or π bridges, and carbazole as terminal group (Scheme 1).



Scheme 1. Investigated molecules. (Ph -phenyl; Th – thiophene; Cz – carbazole)

METHODS

Geometry optimization and harmonic frequency calculations were performed for all molecules using the B3LYP//6-31+G(d,p) method. Electronic vertical transitions employing TD-DFT were performed using the CAM-B3LYP functional and the basis set. All calculations were carried out in the gas phase and employed the Gaussian09 package.

RESULTS

The results show that the HOMO orbitals are located mainly in the aromatic end groups and in the conjugated π bridge fragment with minor contributions from the triazine nucleus. On the other hand, LUMOs reside mainly in the triazine core, with minor contributions from terminal groups and π -bridge fragments (Figure 1). This behavior suggests the possibility of intramolecular charge transfer. Figure 2 shows the energies of the HOMO and LUMO orbitals of all molecules studied. The energy of the LUMOs of all molecules is above the

CB (conduction band) of TiO₂, and the LUMO orbitals of PC₆₁BM and ITIC (typical acceptors for OSCs), suggesting an effective injection of electrons.

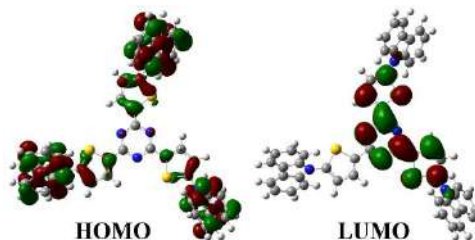


Figure 1. Electron density distribution of frontier molecular orbitals of 2c.

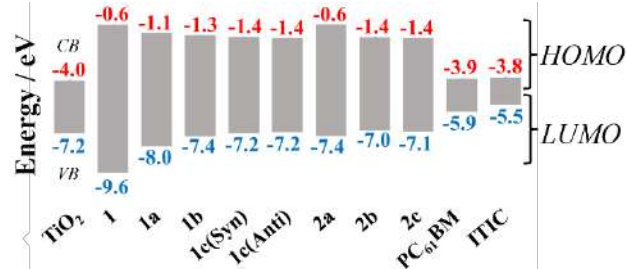


Figure 2. HOMO (red values) and LUMO (blue values) energies of the investigated systems. (CB is conduction band and VB is valence band for TiO₂).

CONCLUSION

The results obtained so far suggest that charge transfer is possible for all molecules, as the LUMO of all dyes is above the CB of TiO₂, favoring charge transfer from the dyes to the CB. In addition, the molecules may present interesting characteristics for application in OSCs, since the LUMO of all molecules is above the LUMO of typical acceptors.

REFERENCES

- ¹ (a) N. Gupta, M.R. Nagar, Anamika, P. Gautam, B. Maiti, J.H. Jou, and B.K. Kuila, ACS Appl Polym Mater, 2022, 5, 130–140. (b) H. Zhang, X.F. Zang, Y.P. Hong, and Z.E. Chen, Synth Met, 2021, 280, 1–7. (c) S.Y. Shiao, C.H. Chang, W.J. Chen, H.J. Wang, R.J. Jeng, and R.H. Lee, Dyes and Pigments, 2015, 115, 35–49.
- ² V. V. M., S. Pola, and P. Chetti, Spectrochim Acta A Mol Biomol Spectrosc, 2021, 245, 1–13.
- ³ R. Jin, Comptes Rendus Chimie, 2015, 18(9), 954–959.
- ⁴ (a) P. Zassowski, P. Ledwon, A. Kurowska, A.P. Herman, M. Lapkowski, V. Cherpak, Z. Hotra, P. Turyk, K. Ivaniuk, P. Stakhira, G. Sych, D. Volyniuk, and J.V. Grazulevicius, Dyes and Pigments, 2018, 149, 804–811. (b) V. Dávila Cerón, L.A. Illicachi, and B. Insuasty, Molecules, 2023, 28(1), 1–36.

ACKNOWLEDGMENTS

CNPq, CAPES, FAPERJ

Precisão dos Funcionais Duplo-Híbrido na Determinação das Frequências Experimentais dos Isômeros Neutros C_nH_2 ($n = 2, 3, 4$ e 6)

Lenin J. D. Soto (PQ),^{1*} Ricardo R. Oliveira (PQ),¹ Enio F. da Silveira (PQ),² Marco A. C. Nascimento (PQ).¹

lenin@iq.ufrj.br

¹Universidade Federal do Rio de Janeiro, Instituto de Química, Cidade Universitária, CT Bloco A sala 412, Rio de Janeiro, RJ 21949-900, Brasil; ²Pontifícia Universidade Católica do Rio de Janeiro, Departamento de Física, Rio de Janeiro, RJ 22451-900, Brasil.

Palavras Chave: C_nH_2 , Frequência, Anarmonicidade, DFT, MIS.

INTRODUÇÃO

Hidrocarbonetos insaturados são detectados na combustão de hidrocarbonetos e na fuligem. No espaço sideral, a molécula *ciclo-C₃H₂* (*c-C₃H₂*) foi a primeira molécula orgânica cíclica observada na nuvem molecular Taurus (TMC-1).[1]

O meio interestelar (MIS) consiste de gás e poeira entre as estrelas, representando 20 – 30 % da massa da galáxia. Devido às condições particulares de temperatura, densidade e radiação no MIS, as espécies moleculares não estão em equilíbrio termodinâmico, razão pela qual sua identificação envolve a análise de espectros complexos que são obtidos em diversos comprimentos de onda.[2]

Visando facilitar a interpretação dos espectros observados, testamos a precisão de diferentes abordagens computacionais para a determinação de frequências harmônicas (ω) e anarmônicas (v) dos isômeros neutros C_nH_2 ($n = 2, 3, 4$ e 6).

MÉTODOS

Usando principalmente um método com correlação explícita, F12-CCSD(T), com uma base especial de orbitais, cc-pVTZ-F12, além do conjunto de base auxiliar complementar, cc-pVTZ-F12-CABS, calculamos a geometria de mínima energia e os valores de ω dos hidrocarbonetos mostrados na Fig. 1.

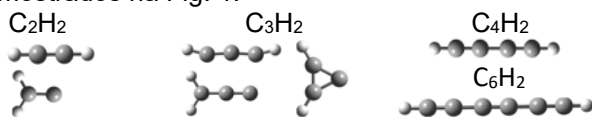


Fig. 1. Isômeros neutros C_nH_2 ($n = 2, 3, 4$ e 6). CCSD(T)/cc-pVTZ para o *t*-C₆H₂.

Adicionalmente, ω e v foram calculados com nove métodos de funcional da densidade duplo-híbrido: B2PLYP, B2PLYPD, B2PLYPD3, mPW2PLYP, mPW2PLYPD2, DSDPBEP86, DSDPBEP86D2, PBE0DH e PBEQIDH, com o conjunto base aug-cc-pVTZ. A anarmonicidade foi determinada com o método DVPT2.

Para os cálculos F12 o programa ORCA 5.0.3 foi empregado enquanto os resultados DFT foram obtidos com o programa G16 vA.03.

RESULTADOS

A partir das 43 frequências experimentais dos isômeros C_nH_2 foi obtido um erro médio absoluto (EMA) de $\sim 35 \text{ cm}^{-1}$ para a grandeza ω usando os métodos F12 e CCSD(T).

Na Fig. 2 é mostrado o EMA das grandezas ω e v determinado com diferentes funcionais. Todas as metodologias DFT apresentam valores de EMA superiores a 37 cm^{-1} e na maioria dos casos EMA (ω) \sim EMA (v).

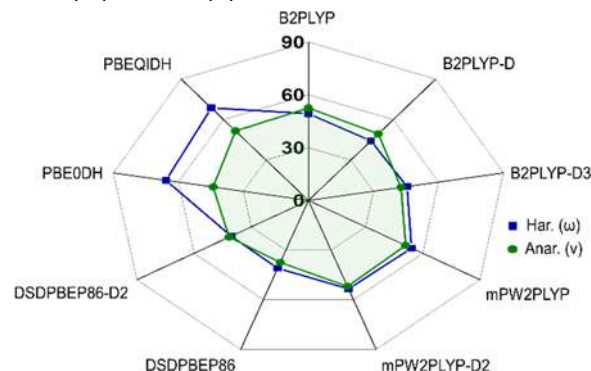


Fig. 2. Valores do EMA (cm^{-1}) de ω e v usando funcionais duplo-híbrido dos isômeros mostrados na Fig. 1.

CONCLUSÕES

Foram comparados os valores de ω e v obtidos com nove funcionais duplo-híbrido com as frequências experimentais para sete isômeros da família C_nH_2 .

Os resultados mostraram que nenhum dos funcionais empregados fornece frequências em bom acordo com as experimentais, mesmo com a inclusão da correção anarmônica.

Por outro lado, a menor discrepância entre a frequência experimental resulta do método de função de onda sem correção anarmônica.

REFERÊNCIAS

- 1 P. Thaddeus, J.M. Vrtilek, C.A. Gottlieb, *Astrophys. J.*, 1985, 299, L63–L66.
- 2 S. Hayakawa, M. Takahashi, K. Arakawa, N. Morishita, *J. Chem. Phys.*, 1999, 110, 2745–2748.

AGRADECIMENTOS

Este trabalho foi apoiado por CAPES. Os autores agradecem ao CNPq, FAPERJ e LNCC/MCTI.

Revisiting Rotational Isomerism of Organic Compounds

Daniela Rodrigues Silva (PhD)^{1*}, Célia Fonseca Guerra (R)¹, Matheus P. Freitas (R)², F. Matthias Bickelhaupt (R)^{1,3,4}
d.rodrigues.silva@vu.nl

¹ Department of Chemistry and Pharmaceutical Sciences, Amsterdam Institute of Molecular and Life Sciences (AIMMS), Vrije Universiteit Amsterdam, De Boelelaan 1083, 1081 HV Amsterdam, The Netherlands

² Department of Chemistry, Institute of Natural Sciences, Federal University of Lavras, 37200-900 Lavras, Minas Gerais, Brazil

³ Institute of Molecules and Materials, Radboud University, Heyendaalseweg 135, 6525 AJ Nijmegen, The Netherlands

⁴ Department of Chemical Sciences, University of Johannesburg, Auckland Park, Johannesburg 2006, South Africa

Keywords: Density functional theory, Kohn-Sham molecular orbital theory, energy decomposition analysis

INTRODUCTION

A firm grasp of the driving forces behind conformational isomerism is crucial for the rational design of molecules with tailor-made properties. To properly elucidate the physical mechanism at play, one must take into account the geometrical relaxations that occur in response to a conformational change, which can otherwise hide the original causal factors.¹ With this in mind, we reinvestigate the rotational isomerism around the C–C bond in archetypal organic compounds within the framework of Kohn-Sham molecular orbital (KS-MO) theory.

METHODS

We investigate the origin of the conformational preferences in the $\text{XH}_2\text{C}-\text{CH}_2\text{X}^2$, $\text{XH}_2\text{C}-\text{CH}_2\text{OH}^3$, and $\text{XH}_2\text{C}-\text{CHO}^4$ ($\text{X} = \text{F}, \text{Cl}, \text{Br}, \text{I}$) model systems at ZORA-BP86-D3(BJ)/QZ4P. The Activation Strain Model (ASM) along with the matching, canonical Energy Decomposition Analysis (EDA)⁵ as a function of the rotation around the C–C bond are employed to unravel the causal physical factors underlying the conformational trends.

RESULTS

Our bonding analyses reveal that overall rotational energy profiles are always set by steric repulsion between occupied–occupied orbitals. The latter favors the less steric crowded *anti* conformation (1, Fig. 1). However, the conformational preferences can be shifted to *gauche*, leading to the so-called *gauche* effect, if one of the two requirements are met: i) if the relative steric repulsion is too weak and thus easily counteracted by subtle attractive interactions (e.g., hyperconjugation²) (1→2, Fig. 1); or ii) if stronger intramolecular interactions take place (e.g., hydrogen bonding³) (1→3, Fig. 1).

In contrast to currently accepted model, we show that hyperconjugation always favors *gauche*. The reason why this subtle interaction manifests in the *gauche* effect is because the steric $\text{X}\cdots\text{X}$ repulsion between fluorine atoms is small enough to not overrule the *gauche* preference set by

hyperconjugation. We highlight that the origin of steric repulsion is not electrostatic repulsion between electron charge clouds, on the contrary, electrostatic interactions favor steric crowding.⁴

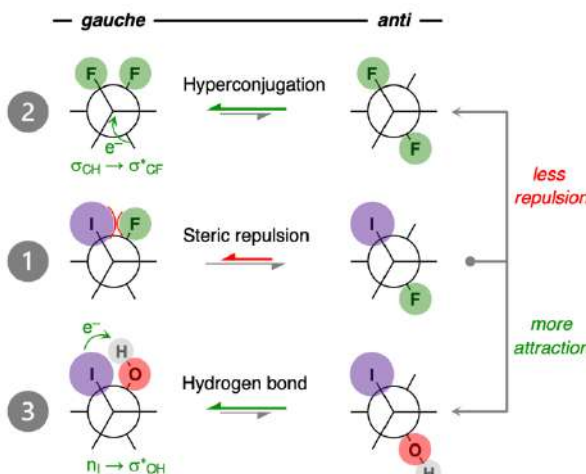


Figure 1. Conformational preferences of 1,2-disubstituted ethanes.

CONCLUSIONS

Our analyses lead to a novel, fundamentally revisited picture of the physical mechanisms behind well-known conformational effects in organic chemistry.

REFERENCES

- 1 F. M. Bickelhaupt, E. J. Baerends, *Angew. Chem.* **2003**, *115*, 4315; *Angew. Chem. Int. Ed.* **2003**, *42*, 4183.
- 2 D. Rodrigues Silva, L. de Azevedo Santos, T. A. Hamlin, C. Fonseca Guerra, M. P. Freitas, F. M. Bickelhaupt, *ChemPhysChem* **2021**, *22*, 641.
- 3 F. A. Martins, L. de Azevedo Santos, D. Rodrigues Silva, C. Fonseca Guerra, F. M. Bickelhaupt, M. P. Freitas, *J. Org. Chem.* **2022**, *87*, 11625.
- 4 D. Rodrigues Silva, L. de Azevedo Santos, T. A. Hamlin, F. M. Bickelhaupt, M. P. Freitas, C. Fonseca Guerra, *Phys. Chem. Chem. Phys.* **2021**, *23*, 20883.
- 5 T. A. Hamlin, P. Vermeeren, C. Fonseca Guerra, F. M. Bickelhaupt, in *Complementary Bonding Analysis* (Ed.: S. Grabowsky) De Gruyter, Berlin, **2021**, pp. 199–212.

ACKNOWLEDGMENTS

The support of NWO, CNPq, CAPES, and FAPEMIG is gratefully acknowledged.

Investigação teórica sobre as propriedades ópticas lineares e não lineares do cristal DAPSH.

Renato Medeiros (PG),^{1,4,5*} Clodoaldo Valverde (PQ),^{1,2} Leandro R. Franco (PQ),³ Francisco A. P. Osório (PQ),^{4,5} Marcos A. Castro (PQ),⁴ Tertius L. Fonseca (PQ).⁴

renato_medeiros@discente.ufg.br

¹Campus de Ciências Exatas e Tecnológicas, Universidade Estadual de Goiás, Anápolis-GO, 75001-970, Brazil;

²Universidade Paulista, Goiânia-GO, 74845-090, Brazil; ³Department of Engineering and Physics, Karlstad University, 65188 Karlstad, Sweden; ⁴Instituto de Física, Universidade Federal de Goiás, Goiânia-GO, 74690-900, Brazil; ⁵Pontifícia Universidade Católica de Goiás, Goiânia-GO, 74605-010, Brazil.

Palavras Chave: *DAST, DAPSH, Susceptibilidade, Momento de dipolo, Índice de Refração.*

INTRODUÇÃO

Neste estudo, avaliamos o momento dipolar, a polarizabilidade linear e as hiperpolarizabilidades de primeira e segunda ordem do cristal DAPSH utilizando um esquema de polarização iterativa¹. Os resultados teóricos foram comparados com dados experimentais disponíveis.

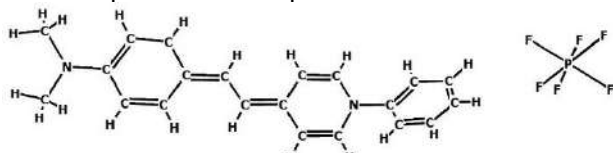


Figura 1: Estrutura do composto DAPSH ($C_{21}H_{21}F_6N_2P$)

MÉTODOS

O método é utilizado até que o momento de dipolo alcance a convergência, como podemos ver na Figura 2 a seguir.

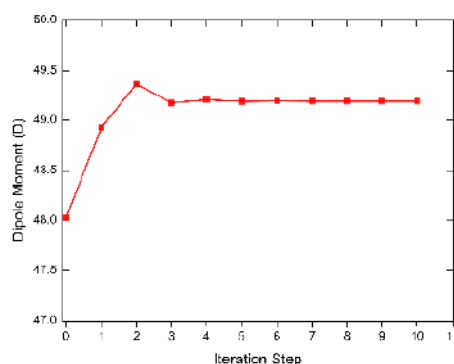


Figura 2: Convergência do momento de dipolo de acordo com os passos de iteração.

Foram calculados o momento dipolar total, a polarizabilidade linear média e as hiperpolarizabilidades de primeira e segunda ordem relacionadas à geração de segunda harmônica, ao efeito dc-Kerr e ao índice de refração dependente da intensidade (IDRI). Também foram estimadas a hiperpolarizabilidade média de segunda ordem e as suscetibilidades linear, de segunda ordem e de terceira ordem, além do índice de refração. Os cálculos foram realizados com o uso do método CAM-B3LYP/6-311++G(d,p) no pacote Gaussian16.

RESULTADOS

O resultado do momento dipolar total do cristal DAPSH obtido foi de 49,2 D. Foram calculadas as polarizabilidades lineares estáticas e dinâmicas, tanto isoladas quanto incorporadas ao ambiente, na faixa de frequência de $\omega = 0.0239$. Observou-se que os efeitos de polarização do ambiente diminuem a polarizabilidade da unidade assimétrica. O índice de refração do cristal foi calculado para $\lambda = 1907 \text{ nm}$, $n = 1,5$. Os resultados da primeira hiperpolarizabilidade (β) para sistema cristalino foram 252,99, estático, e 214,97 para 1907 nm, ambos em $(\times 10^{-30} \text{ esu})$. Esses resultados indicam que o efeito do campo de polarização diminui a primeira hiperpolarizabilidade. Os resultados para a segunda hiperpolarizabilidade média, $\langle \gamma(-\omega; \omega, \omega, \omega) \rangle$, são $461,00 \times 10^{-36} \text{ esu}$, estático, e $465,31 \times 10^{-36} \text{ esu}$ para 1550 nm para o cristal, resultando em aumentos em torno de 6% em relação aos valores da molécula isolada. Os resultados para a susceptibilidade não linear de terceira ordem no ambiente cristalino, $\langle \chi^{(3)}(-\omega; \omega, \omega, -\omega) \rangle$, são $0,91 \times 10^{-20} \text{ m}^2/\text{V}^2$ para o caso estático e $1,16 \times 10^{-20} \text{ m}^2/\text{V}^2$ para 1907 nm. Valores significativos em comparação com os resultados obtidos para outros cristais orgânicos, como derivados de chalcona³.

CONCLUSÕES

Este trabalho⁴ forneceu uma primeira estimativa das susceptibilidades macroscópicas. Para a segunda hiperpolarizabilidade, os efeitos de polarização têm um impacto negligenciável, mas o resultado estimado para a susceptibilidade de terceira ordem é significativo em comparação com os resultados para outros cristais orgânicos.

REFERÊNCIAS

¹ Fonseca, T. L., et al., J. Chem. Phys., 2010, 133, 144103.

² Figi, H. et al. J. Opt. Soc. Am. B, 2008, 25, 1786.

³ Brandao, I. et al., J. Chem. Phys., 2021, 154, 094501.

⁴ Valverde, C. et al. Sci Rep 2023, 13, 8616.

AGRADECIMENTOS

PPGF-IF/UFG, CNPq, CAPES e FAPEG (PRONEX) (Brasil), LaMCAD/UFG, SNIC no Centro Nacional de Supercomputação da Universidade de Linköping (NSC)



Hydrogenation of CO₂ to Methanol Using Ruthenium-Triphos Catalyst: Complete Free Energy Profile and Microkinetic Analysis

Ellen V. D'Alessandro (PG),^{1*} Josefredo R. Pliego Jr. (PQ).¹

dalessandroellen@gmail.com

¹Natural Science Departament - São João del-Rei Federal University (UFSJ)

Keywords: CO₂, Methanol, Ru-Triphos, TS, DFT.

INTRODUCTION

In 2022, the atmospheric concentration of carbon dioxide surpassed 419 ppm, contributing to global warming and ocean acidification¹. Therefore, efforts are needed to reduce CO₂ levels. Catalytic hydrogenation of CO₂ to methanol is particularly promising, offering environmental and economic benefits. However, its high thermodynamic stability is a challenge due to its low reactivity. Efficient catalyst development is crucial for CO₂ conversion. In 1995, the first homogeneous metal-catalyzed hydrogenation of CO₂ to methanol was achieved using Ru clusters in the presence of halide anions at high temperature and pressure. An important advance was achieved in 2015 using the Ru-Triphos catalyst at 140 °C, p_{H₂} = 60 bar and p_{CO₂} = 20 bar.² Previous theoretical calculations were not able to explain quantitatively the experiments. In the present report, we described in detail the mechanism and kinetics of the catalytic cycle of CO₂ conversion to methanol using Ru-Triphos, passing through all the possible steps, intermediates and transition states, considering the solvent effect. A detailed microkinetic analysis was also done.

METHODOLOGY

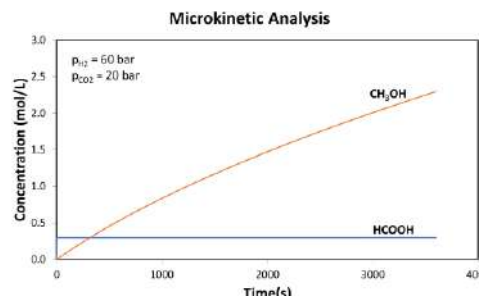
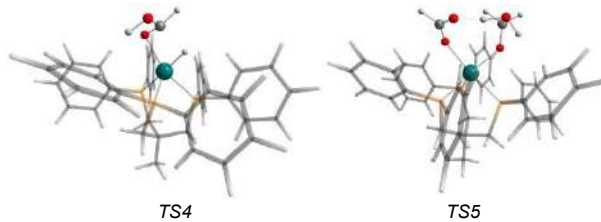
Geometry optimizations and harmonic frequencies calculations were performed with PBE functional with RI and dispersion correction D3BJ. The mdef2-SVP basis set was used for nitrogen and oxygen, and def2-SVP for the remaining atoms. For the Ru atom, the Stuttgart-Dresden ECP was used to the core electrons. Aiming to obtain more accurate electronic energies on the optimized structures, single point calculations were done with the ωB97M-V functional and mdef2-TZVPP basis set was used for nitrogen and oxygen, def2-TZVPP for the remaining atoms. The SMD model was used to obtain the solvation free energy of THF solvent. All the calculations were done with the ORCA 5 program. Microkinetic calculations were done with the Kintecus program.

$$G_{\text{sol}} = (E_{\text{el}} + G_{\text{n}} + 1.89 \text{ kcal mol}^{-1}) + \Delta G_{\text{solv}}$$

RESULTS

The detailed mechanism of hydrogenation of CO₂ to methanol with Ru-Triphos in THF solution has been obtained. The reaction proceed through many steps, including the formation of formic acid and acetaldehyde. Several steps need a catalyst

for proton transfer process, and the HCOOH generated in the partial reduction of CO₂ is acting as the catalyst (stationary concentration of 0.3 mol/L). Two transition states are critical in the reaction, the hydride transfer to formic acid (TS4), and the formation of formaldehyde with releasing of water (TS5). Despite the low barriers of the transition states, a stable complex of the catalyst with methanol product raises the overall ΔG[‡] to 28 kcal mol⁻¹, leading to a very slow kinetics at room temperature. However, at 140 °C, p_{H₂} = 60 bar and p_{CO₂} = 20 bar, the complete conversion to methanol was predicted by the microkinetic analysis presented below.



CONCLUSIONS

The complete reaction mechanism and free energy profile for conversion of CO₂ to methanol catalyzed by Ru-Triphos complex has been calculated by a reliable DFT method. The microkinetic analysis has predicted that the rate of methanol formation in the experimental conditions is in agreement with the experimental observations. Thus, we have explained quantitatively this reaction system.

REFERENCES

¹ Laboratory, G. M. Earth System Research Laboratories. Trends in atmospheric CO₂. <https://gml.noaa.gov/ccgg/trends/> (2023).

² Wesselbaum, S. et al.. Chem. Sci. 6, 693–704 (2015).

ACKNOWLEDGMENT

The authors thank the agencies CNPq, FAPEMIG and CAPES for the support.



A theoretical evaluation of the redox activity on ATCUN and XH metallic peptides

André L. P. de Melo* (PG)¹, Maurício Domingues Coutinho Neto (PQ)¹

melo.andre@ufabc.edu.br; mauricio.neto@ufabc.edu.br

¹ABCsim - CCNH, Universidade Federal do ABC, Santo André – SP - Brasil

Keywords: DFT, Peptides, Copper, Nickel, Redox

INTRODUCTION

Peptides are elements of great importance for modern catalysis, given the wide range of possible amino acid combinations. Modifications in its sequence lead to geometric and redox profile changes, thus suggesting a potential modulation of its electrochemical behavior. Here we perform a theoretical study of metal complexes involving the peptide motifs ATCUN¹ (Amino-terminal-copper-nickel-binding) and XH (Amino-terminal-histidine-binding).

METHODS

The creation of peptide complexes was performed by combining SMILES (Simplified Molecular Input Line Entry System) strings and openBabel², with its gen3D algorithm, which uses the built-in OBBBuilder API to generate three-dimensional structures from 0D to 2D structures. Each target peptide structure is composed of string fragments that are then concatenated into the final desired molecule. Initial structures were first pre-optimized with the semi-empirical GFN2-xTB³ method and later optimized with the DFT method, where the ORCA⁴ package was employed. Regarding the DFT calculations, a combination of the PBE (Perdew-Burke-Ernzerhof) functional, belonging to the generalized gradient approximation class and the range-separated WB97x-D3 (developed by Head-Gordon et al) was used, both with Becke-Johnson dispersion corrections. As for the bases employed, 6-31G(d,p) and tzvp (triple zeta valence potential) were assigned to each functional, respectively. By our preliminary analysis, the combination proved to be cost-effective and exhibited good agreement with experimental results for this type of system. The protocol used here was validated by the PBE0/def2-tzvp method, as well as the cc-DLPNO/def2-tzvp method. Fukui coefficients calculations were performed from the Hirshfeld charges of the system.

RESULTS

The reduction potential data obtained for ATCUN ($\text{Cu}^{3+}/\text{Cu}^{2+}$) and XH ($\text{Cu}^{2+}/\text{Cu}^+$) complexes after the optimization steps are displayed in the following tables.

Peptide-Complex	Calc. Redox Potential(mV)	Exp. Red. Pot. (mV)	Variation
Cu-GGH	1049	1068	19
Cu-KGH	1176	1051	-125
Cu-GKH	1168	1057	111
Cu-KKH	1172	1017	-155
Cu-GHK	-854	-830	24

Table 1. Copper peptides reduction potentials.

Peptide-complex	Calc. Redox potential (mV)	Exp. Redox. Potential (mV)	Variation
Ni-GGH	1308	1087	-221
Ni-KGH	1356	1097	-259
Ni-GKH	970	1097	127
Ni-KKH	1280	1077	-203
Ni-GHK	-1057	-	-

Table 2. Nickel peptides reduction potentials.

In this way, a variation of a maximum of 259mV is obtained in relation to the experimental result. The results obtained here were validated for both nickel and copper complexes for a given reference molecule belonging to each motif, whose peptides of choice were GGH and GHK.

CONCLUSIONS

The redox potential values calculated with the proposed protocol show good agreement with experimental data. In addition, the method employed also responded correctly to the variation of the selected motif, displaying a negative sign of redox potential for the XH motif and a positive sign for the ATCUN motif.

REFERENCES

- ¹ Acc. Chem. Res. 1997, 30, 3, 123–130
- ² J. Cheminform. 2011, 3, 33
- ³ J. Chem. Theory Comput. 2019, 15, 3, 1652–1671
- ⁴ J. Chem. Phys. 2020, 152, 224108

ACKNOWLEDGEMENTS

This study was financed in part by the Coordenação de Aperfeiçoamento de Pessoal de Nível Superior - Brasil (CAPES) - Finance Code 001



Variational Transition State Theory Rate Constants of the Hydrogen Abstraction Reaction $H + H_2SiO \rightarrow SiOH + H_2$

Edson F. V. de Carvalho (PQ),¹ Filipe Gustavo Kano (PG),² Luiz Fernando de Araújo Ferrão (PQ),²
Francisco B. C. Machado (PQ),² Orlando Roberto-Neto (PQ)^{3*}

*orlando@ieav.cta.br

¹Departamento de Física, Universidade Federal do Maranhão, 65085-580, São Luís, Maranhão, Brazil

²Departamento de Química, Instituto Tecnológico da Aeronáutica, 12228-900, José dos Campos, São Paulo, Brazil

³Divisão de Aerotermodinâmica e Hipersônica, Instituto de Estudos Avançados, São José dos Campos, 12228-001, São Paulo, Brazil

Palavras-Chave: $H + H_2SiO$; Density Functional Theory; CCSD(T); Thermochemistry; Rate constants.

INTRODUÇÃO

Silane (SiH_4) is widely used as a precursor of silicon atoms to produce a variety of films in photovoltaic panels, development of photo sensors, manufacturing of electronic devices, and is also employed as an additive to fuels in aerospace vehicles [1]. One of the less studied elementary reactions of the mechanism of silane oxidation is the abstraction reaction of H_2SiO by a hydrogen atom, i.e., $H + H_2SiO \rightarrow HSiO + H_2$ (R1). A study of combustion models with methods of collision limit analysis (CVL) for (R1) shows a large discrepancy in the experimental determination of the enthalpy of formation of H_2SiO [2]. In reason of the lack of experimental and theoretical thermochemical data for (R1) [2,3], in this investigation the DFT, CCSD(T), and variational transition state theory with multidimensional tunneling corrections (VTST/MT) methods are employed to compute accurate electronic structures, reaction paths, and rate constants of (R1). Also, we have carried out calculations of the kinetic isotope effect (KIE) for k^{R1}/k^{R2} and k^{R1}/k^{R3} involving the reaction paths $D + H_2SiO \rightarrow HSiO + DH$ (R2) and $H + D_2SiO \rightarrow DSiO + DH$ (R3).

MÉTODOS

The equilibrium geometries and harmonic vibrational frequencies of the stationary states (i.e., reactants, products, and saddle point) of the reaction paths are computed employing various levels of theory, as the M06-2X and ω B97-X-D DFT (density functional theory), and the coupled-cluster with single-double and perturbative triples corrections (CCSD(T)) with the correlation consistent aug-cc-pVnZ basis set and the CBS limit. The rate constants calculations were carried out with the VTST-IOC method improved with the multidimensional tunneling corrections zero-curvature tunneling (ZCT), small-curvature tunneling (SCT), large-curvature tunneling (LCT), and microcanonically optimized multidimensional tunneling (μ OMT) approximations [4].

RESULTADOS

The T_1 diagnostic values computed by the CCSD/aug-cc-pVQZ method show that for all doublet species, the multireference character of the wave functions is within the recommended limit

of 0.044. Calculations with the M062-X, ω B97X-D, and CCSD(T) methods with the aug-cc-pVTZ basis set, and with the CBS_{T-Q} approach give values for the barrier height (V^\ddagger) and energy reaction (ΔE) in excellent agreement, and the computed average values with unsigned uncertainty are equal to 4.46 ± 0.18 (V^\ddagger) and 21.72 ± 0.68 kcal.mol⁻¹ (ΔE). The best convergence of adiabatic-vibrational reaction path was found by using the ω B97X-D/aug-cc-pVTZ method, with high-level corrections of electronic energies and vibrational frequencies carried out with the CCSD(T)/aug-cc-pV5Z and CCSD(T)/aug-cc-pVTZ methods. The CVT/ μ OMT rate constants at the temperature range of 1000 – 2500 K agree with empirical data [2]. VTST/MT calculations predict normal KIE (equal or larger than 1) converging to 1 at high temperatures.

CONCLUSÕES

There is an excellent agreement among the DFT and CCSD(T) methods in the calculations of electronic barrier height and reaction energy with average values, and unsigned uncertainty, of 4.46 ± 0.18 (V^\ddagger) and 21.72 ± 0.68 kcal.mol⁻¹ (ΔE). The ω B97-X-D DFT employed in building the low-level $H + H_2SiO \rightarrow HSiO + H_2$ reaction path gives barrier height (4.74 kcal.mol⁻¹) and reaction energy (-22.13 kcal.mol⁻¹) which are in excellent agreement with the best electronic energy calculations. For k^{R1}/k^{R2} and k^{R1}/k^{R3} , CVT/ μ OMT rate constants predict normal KIE converging to 1 at high temperatures. Calculations of the rate constants in function of temperature could be used to improve models of global combustion of $H_2/O_2/SiH_4$ systems.

REFERÊNCIAS

- ¹B. Hidding, M. Pfitzner, D. Simone, C. Bruno, C. Acta Astronautica 2008, 63, 379-388.
- ²K. P. Chatelian, R. Mével, D. A. Lacoste, Combustion and flames 2020, 217, 346-358.
- ³M. Zachariah, W. Tsang, J. Phys. Chem. 1995, 99, 5308-5318.
- ⁴A. Fernández-Ramos, B. A. Ellingson, B. C. Garrett, D. G. Truhlar. Variational Transition State Theory with Multidimensional Tunneling. In Reviews in Computational Chemistry; Ed.: K. B. Lipkowitz, T. R. Cundari, Wiley-VCH, Hoboken, N. Jersey, 2007, Vol. 2, pp. 125-232.

AGRADECIMENTOS

CNPq, FAPEMA, FAPESP

Push-pull substituents in akamptisomeric porphyrins in the design of photoswitch devices

Natalia Marques Raffaeli (IC),¹ Patrick de Lima Rocha (IC),¹ Karine Nascimento de Andrade (PG),¹ Rodolfo Goetze Fiorot (PQ).^{1*}

nataliamarques@id.uff.br; rodolfofiorot@id.uff.br

¹ Instituto de Química, Universidade Federal Fluminense, Niterói, RJ, Brasil.

Keywords: Bond angle inversion, DFT, Isomerism, Molecular machine, TD-DFT

INTRODUCTION

Molecular photoswitches experience a transformation into stable states with distinct properties when exposed to light. Recently, a novel form of isomerism called akamptisomerism¹, which involves the bond angle inversion (BAI) of a strained (F)B–O–B(F) bridge anchored in porphyrin macrocycles, has been discovered. For isolatable isomers to exist, the BAI barrier should be higher than 20 kcal mol⁻¹. During this process, the pseudo-plane of the porphyrin pyrrole rings is altered, thereby potentially influencing their electronic properties and enabling the design of photoswitch devices. Push-pull systems, which consist of donor and acceptor groups interconnected by a π system to allow intramolecular charge transfer (ICT), have been extensively investigated in the literature.³ This is due to the essential role played by the ICT phenomena in various molecular motors and photosensitizers. Herein, we evaluate two types of push-pull systems (Fig. 1) with anchored B–O–B bridges to explore their effect on the BAI and photophysical profile of the individual akamptisomers.

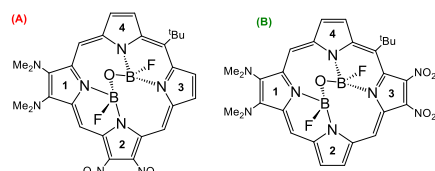


Fig 1. Structure of the evaluated porphyrins: (A) ring **1–2** and (B) ring **1–3**.

METHODS

For the investigation of the bond angle inversion and their photophysical properties, DFT calculations were employed using the B3LYPD3/6-31+G(d,p)¹ method in geometry optimization and frequency calculations, along with TD-DFT calculations using the CAM-B3LYP/6-31+G(d,p)² method to simulate the UV-Vis absorption spectra.

RESULTS

The two systems showed a barrier of $\Delta G^\ddagger = 24.9$ (**A**) and 21.5 (**B**) kcal mol⁻¹. During the BAI, the B–O–B bridge passes by a transition state characterized by a linear arrangement. The observed values indicate that each system is capable of producing isolatable akamptisomers, leading to the formation of isoenergetic isomers *t*₁ and *t*₂ — figure 2.

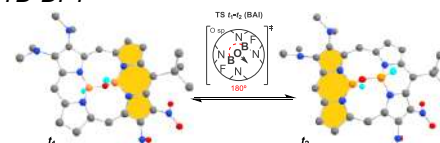


Fig 2. Process of BAI *t*₁ → *t*₂. Changes in the porphyrin pseudo-plane are highlighted in yellow.

The photophysical properties of the akamptisomeric pairs (*t*₁/*t*₂) were examined by simulation of their UV-Vis absorption spectra (Fig. 3). A redshift was observed in the two systems when compared to a non-substituted porphyrin with a B–O–B bridge (black curve). In terms of the absorption difference between akamptisomers *t*₁/*t*₂, we observed a maximum displacement of $\lambda = 28$ nm and 54 nm, for system A (push-pull **1–2**) and B (push-pull **1–3**), respectively. Therefore, the insertion of the donor and acceptor groups in the β,β-pyrrole at alternate positions (ring **1–3**) enhances the differentiation in absorption between the akamptisomeric isomers. This can be explained by the occurrence of ICT taking place in different pseudo-planes in **B**, whereas in **A**, the delocalization occurs within the same pseudo-plane. Thus, this evidence supports the presence of a push-pull effect, as ICT decreases the energy of the molecule's boundary orbitals, resulting in a bathochromic shift.

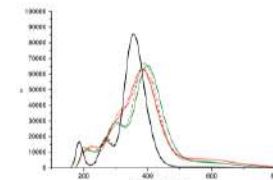


Fig 3. Theoretical UV/Vis spectra for **A** (red), **B** (green) and non-substituted porphyrin (black).

CONCLUSIONS

The two systems were classified as akamptisomers, since the barriers for the BAI are higher than 20 kcal mol⁻¹. Modifying alternative pseudo-planes resulted in a more substantial difference between the photophysical profiles of the akamptisomer pairs. Further modifications will be explored to enhance their suitability for the photoswitch application, with greater differentiation between the photophysical profile.

REFERENCES

¹Nature Chemistry, 2018, v. 10, p. 615-624; ²Molecules, 2021, v. 26, p. 71760; ³RSC Adv, 2014, v.4, 58826.

ACKNOWLEDGMENTS

CNPq, CAPES, FAPERJ, and LoboC NACAD (a22006).



Molecular Dynamics Hygroscopic Study of Biogenic Aerosols from the Amazon Rainforest

Emanuel F. D. Mancio (PG),^{1*} Kaline Coutinho (PQ).¹

Categories: Researcher (PQ), Graduate Student (PG).

emanuelmancio@usp.br; kaline@if.usp.br

¹*Instituto de Física, Universidade de São Paulo, São Paulo – SP – Brasil*

Keywords: *Aerosols, Organic Biogenic Molecules, Water Effect, Molecular Dynamics, Hygroscopy.*

INTRODUCTION

In recent decades, the human expansion on the Amazon region has significantly changed the dynamics of land use and occupation. This has led to an increase in concentration of aerosols particles and greenhouse gases in the atmosphere. And, although, climate change has been greatly studied, the role of biogenic aerosol particles in the atmosphere is quite lacking in scientific investigations.

Aerosol particles have a crucial role in the hydrological cycle, as they are precursors of cloud condensation nuclei (CCN), which, with water vapor, form cloud droplets. And, more than 60% of the aerosol particles from the Amazon rainforest can act as CCN. Because of aerosol particles diversity, there is a need for studies that can inform the characteristics of these particles in an aqueous environment to better understand their effect in climate phenomena. Furthermore, understanding their hygroscopic properties, mainly the surface attributes, can enhance the comprehension on the life cycle of the clouds.

METHODS

In this project, we are conducting theoretical study of molecular modeling, using quantum calculations and classical computer simulations, of natural biogenic molecules, sulfuric acid (H_2SO_4) and its ions bisulphate (HSO_4^-) and sulphate (SO_4^{2-}), in the presence of water. Firstly, we calculated electronic properties of isolated and solvated molecules. Then, we analyzed its interaction with other molecules in the environment under thermodynamic conditions analogous to cloud drops and also of water vapor. Some combinations of biogenic molecules presents spontaneous aggregation and formation of nanoparticles. The dynamics, and geometry and surface properties of these nanoparticles were studied and discussed depending on its composition and the influence of humidity.

RESULTS

Our vapor simulations, figure 1, show that in less than 50 ns, some sulfuric acid molecules will

capture enough water molecules to deprotonate¹ to bisulphate ion and after that the aggregate grows by a factor of 11. Furthermore, the second deprotonation of H_2SO_4 , the sulphate ion, that does not occur in the atmosphere², interestingly is less hygroscopic than HSO_4^- .

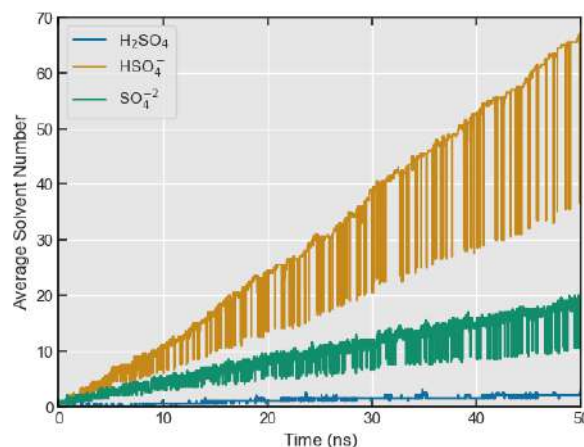


Figure 1 - Temporal evolution of average number of molecules of water around biogenic ones, taken from vapor simulations.

CONCLUSIONS

We conclude that the deprotonation of biogenic molecules enhances its hygroscopic properties, therefore being crucial to the formation of aerosol particles. Also, this process rapidly occurs in the atmosphere for sulfuric acid.

REFERENCES

- V. Loukonen, T. Kurtén, I. Ortega, H. Vehkamäki, A. Padua, K. Sellegrí, M. Kulmala, ACP, 2010, 10(10) 4961.
- T. Ishiyama, A. Morita, T. Miyamae, PCCP, 2011, 13(47) 20965

ACKNOWLEDGMENTS

This study was financed by Brazilian funding agencies FAPESP (grants 2021/09016-3 and 2022/01284-1), CAPES and CNPq.



Experimental and theoretical study of nitro compounds to aromatic alcohol: a sustainable biocatalytic transformation from Amazonian fungi

Neidy S. S. dos Santos (PG),¹ Sávio G. Fonseca (PG),² Franco F. Almeida (PG),¹ Ezequiel de A. Belo (PQ),³ Marcelo R. S. Siqueira (PQ),⁴ Ednilson dos S. Niculau (PQ),⁵ Sebastião da C. Silva (PQ),⁶ Darlisson A. Santos (PQ),⁷ Patrício F. Provasi (PQ),⁸ Tarciso S. de Andrade-Filho (PQ),⁹ Antonio R. Cunha (PQ),¹⁰ Rodrigo do M. Gester (PQ).^{11*}

neidysamara@gmail.com; gester@unifesspa.edu.br*

¹Programa de Pós-Graduação em Química, Universidade Federal do Sul e Sudeste do Pará, Marabá-PA, Brazil;

²Programa de Pós-Graduação em Química de Produtos Naturais, Universidade Federal do Rio de Janeiro, Rio de Janeiro-RJ, Brazil;

³Faculdade de Engenharia Mecânica, Universidade Federal do Pará, Tucuruí-PA, Brazil;

⁴Curso de Física, Universidade Federal do Amapá, Macapá-AP, Brazil;

⁵Centro de Ciências Integradas/Química, Universidade Federal do Norte do Tocantins, Araguaína-TO, Brazil;

⁶Faculdade de Química, Universidade Federal do Sul e Sudeste do Pará, Marabá-PA, Brazil;

⁷Departamento de Química Fundamental, Universidade Federal de Pernambuco, Recife-PE, Brazil;

⁸Department of Physics, IMIT, Northeastern University, CONICET, Argentina;

⁹Faculdade de Física, Universidade Federal do Sul e Sudeste do Pará, Marabá-PA, Brazil;

¹⁰Universidade Federal do Maranhão, Maranhão-MA, Brazil;

¹¹Instituto de Física, Universidade de São Paulo, São Paulo-SP, Brazil.

Palavras-chave: DFT, Solvent effects, NLO, Biotransformation.

INTRODUCTION

The potential of natural products with potential applications in fields such as biology, pharmacology and materials science has attracted significant attention in contemporary scientific research. Therefore, this study focuses on the biotransformation of 1-nitro-2-phenylethane (1N2PE) from *Aniba canellilla* into 2-phenylethanol (2PE) using fungal species obtained from the Brazilian Amazon region. Our main objective was to examine how the biotransformation impacted the structural, electronic, spectroscopic and nonlinear optical properties of the compounds.¹

METHODS

The 1N2PE compound was obtained from *Aniba canellilla* oil for the 2PE biotransformation reaction, using the fungi: *Aspergillus flavus*, *Colletotrichum* sp., *Lasiodiplodia caatinguensis* and *Rigidoporus lineatus*. After purification of the compounds the experimental infrared spectra. The structures were optimized in the ground and excited states using the Gaussian 09², via Density Functional Theory (DFT), using the M06-2X/6-311++G(d,p) method.^{3,4} To model the solvent implicit and explicit, two methods were employed, the Integral Equations Formalism - Polarizable Continuous Model (IEF-PCM) and the Electrostatic Medium Solvent Configuration (ASEC). The classical Monte Carlo simulations and the generation of the liquid environment were performed using the DICE⁵ code, using the optimized parameters of all atoms for liquid simulations (OPLS-AA). The calculations aimed to obtain the infrared, Raman, UV-visible, emission and projected state density spectra, as well as non-linear optical properties, reactivity parameters and electronic excitations.

RESULTS

The bioconversion reaction described involves replacing a nitro group (NO_2) with a hydroxyl group (OH) in chromophores. Experimental and theoretical vibrational analysis revealed charge transfer effects in the studied compounds. The solvent influenced their molecular conformations and vibrational spectra, mainly in the donor and acceptor groups. The solvent reduced the response of 1N2PE but improved the optical parameters of 2PE, which exhibited a low refractive index and significantly higher first hyperpolarizability (42.79 a.u.) compared to urea.

CONCLUSIONS

Bioconversion transforms the compound from electrophilic to nucleophilic, affecting its molecular reactivity. PCM reduces bathochromic shift, while ASEC amplifies hypsochromic shift, but both methods indicate mild solvent effects. The refractive index increases in both gas and solvent from 1N2PE to 2PE, where 2PE exhibits approximately twice the first hyperpolarizability (β) compared to 1N2PE, making it intriguing for optoelectronics.

REFERENCES

- 1 F. F. Almeida, et al. Chem. Phys. Lett., 2022, v. 804, p. 139867.
- 2 M. J. Frisch, et al. Gaussian. Inc., Wallingford CT, 2013.
- 3 A. Raiol, et al. J. Mol. Liq., 2021, v. 340, p. 116887.
- 4 S. Fonseca, et al. J. Mol. Model., 2022, v. 28, p. 85.
- 5 H. M. Cezar, et al. J. Chem. Inf. Model., 2020, v. 60, n. 7, p. 3472-88.

ACKNOWLEDGMENT

CAPES, CNPq, FAPESPA, CONICET, LCC/UNIFESSPA.



Some “Simple” Problems About Atoms and Molecules

Alejandro Lopez Castillo (PQ)^{1*}

*alcastil@ufscar.br

¹Departamento de Química – UFSCar – São Carlos SP

Keywords: *intrinsic angular momentum; second solution; separability; dimensionality; fundamental forces*

INTRODUCTION

We will deal with general aspects of atoms and molecules (**A&M**), considering some problems reasonably understood and others less so.

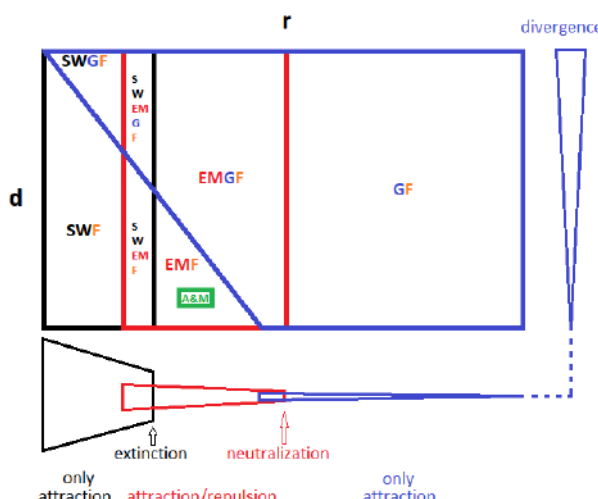
We will discuss some symmetry and dimensionality aspects of the H and H_2^+ and their implications for **A&M** problems. We will deal with the relevance of the one-electron effective potential approximation in **A&M** and its relation with its quasi-separability. We will discuss some particularities of **A&M** concerning other physical systems. We will also compare some properties of the fundamental forces (weak (WF), strong (SF), electromagnetic (EMF), and gravitational (GF)) and show that the **EMF** has special characteristics responsible for everything we will discuss in this work.

METHODS

We will use exact and numerical methods to solve the Schrödinger equation (SE), including self-adjoint transformation, second solution, dimensionality, and separability. We will use basic and pragmatic results that permeate the literature in the area.

RESULTS

We discuss some results that are usually ignored because they are supposedly “known” [1,2,3,4]. We will combine some of these results and make some extensions and discussions, still under development, for **A&M** systems considering the fundamental forces [5].



Many aspects of **A&M** are well understood. However, we believe it would be pertinent to ask the following questions:

- 1) Would it be worthwhile to discuss classical aspects of quantum mechanics? For example, how to treat the first derivative term of SE [1];
- 2) Although the SE is not, in principle, relativistic, could it predict an intrinsic angular momentum of the type $\hbar/2$? For example, as that obtained through a self-adjoint transformation [1];
- 3) How special is the **EMF** compared to other fundamental forces? For example, see the behavior of this force in the diagram above (density (d) versus the effective range of fundamental forces (r)) [5];
- 4) Are there other solutions, in addition to those commonly used, relevant to describing **A&M**? The second solution of SE could be one possible [2];
- 5) Could other dimensions, in addition to 3D, be relevant for the electronic description of **A&M**? Some results for the H_2^+ might indicate such relevance [3].
- 6) Is it essential to understand why certain approximations describe **A&M** (n-bodies) with enormous accuracy? This is important compared to the difficulties of describing other n-body problems [4];
- 7) Are **A&M** systems separable? **A&M** separability can be evaluated when compared to other systems [4];
- 8) Would the usual procedures in quantum chemistry be able to “extract” from SE “all” electronic states of **A&M**? There are some states that could not be obtained in these ways [4].

CONCLUSIONS

We can conclude that there is no guarantee that all the essential ingredients for describing atoms and molecules are being considered (in the literature). However, the importance of this needs to be better understood.

REFERENCES

- ¹A. López-Castillo, Theo.Chem.Acc.,2020,139,51.
- ²E. Flauzino & A. López-Castillo, Int.J.Theo.Phys.,2023,62,80.
- ³A. López-Castillo, Comp.Theo.Chem.,2021,1205,113438.
- ⁴A. López-Castillo, Theo.Chem.Acc.,2020,139,149.
- ⁵A. López-Castillo, in preparation.

ACKNOWLEDGMENT

FAPESP – 2019/12501-0, CAPES – 001, Fundación Carolina.

DFT calculation of new N-heterocycles as potential corrosion inhibitors.

Raquel Leal Silvério (PG)^{1*}, Diego Pereira Sangi (PQ)², Lilian Weitzel Coelho Paes (PQ)³, Elivelton Alves Ferreira (PQ)².

raquelsilverio@id.uff.br; dpsangi@id.uff.br; lilianweitzel@id.uff.br; eliveltonalves@id.uff.br

¹Programa de Pós-Graduação em Engenharia Metalúrgica (PPGEM), Universidade Federal Fluminense, Volta Redonda, Rio de Janeiro, Brazil; ² Instituto de Ciências Exatas, Universidade Federal Fluminense, Volta Redonda, Rio de Janeiro, Brazil; ³Departamento de Ciências Exatas, Escola de Engenharia Industrial e Metalurgia de Volta Redonda, Volta Redonda, Rio de Janeiro, Brazil.

Key Words: Density Functional Theory, N-Heterocycles, Corrosion, Organic Corrosion Inhibitors.

INTRODUCTION

Corrosion is one of the problems that has a great economic impact. Several approaches are therefore employed to reduce the corrosion process of mild steel and one of these approaches is the use of corrosion inhibitor. A number of heterocyclic compounds have been reported to be effective inhibitors^{1,2}. In this way, N-heterocycles compounds 2-(nitromethylene)-1,3-oxazinane (G04) and 2-(nitromethylene)hexahydropyrimidine (G07) are proposed for the first time as corrosion inhibitors. In this work, a computational study of molecular properties is presented, using Density Functional Theory (DFT).

METHOD

The full molecular geometry optimization of the G04 and G07 molecules was carried out by employing the density functional theory at B3LYP level and 6-311G(d,p) basis set with Gaussian 09 software. Frequency calculations were performed with the optimized geometries to validate the minimum stationary point of the potential energy surface. The UCA-FUKUI software package³ was used to calculate the condensed-to-atom Fukui indices.

RESULTS

The optimized structures obtained by DFT calculations of the studied inhibitors are shown in Figure 1.

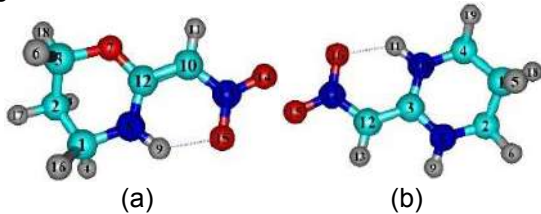


Figure 1: Optimized structures of (a) G04 (b) G07

The HOMO–LUMO gap are very crucial for studying reactivity and stability of structures. From table 1, it is notice that no significant difference between their energy gap (ΔE). The MEP explains the distribution of charge in molecule. The figure 2 shows the maps of the electrostatic potential distribution. As it can be seen the region around oxygen atoms shows the most negative potential region (red). The HOMO is

delocalized over the N13-C10-C12 for G04 and N14-C12-C3 for G07. The LUMO are characterized by π^* -antibonding orbital.

Table 1: Quantum Chemical parameters for studied compounds: B3LYP/6-311G(d,p)

	G04	G07
LUMO (eV)	-1,59	-1,11
HOMO (eV)	-6,40	-5,90
ΔE (eV)	4,81	4,79
μ (Debye)	8.53	8.79
η	2,40	2,39
ΔN	0,62	0,73

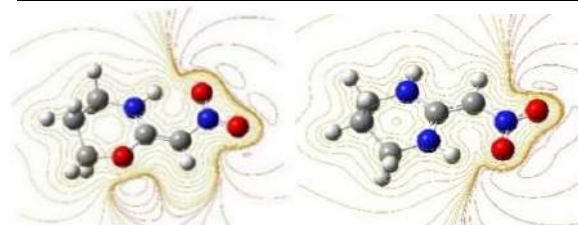


Figure 2: Molecular electrostatic potential of G04 (left) and G07 (right).

The calculated Fukui indices of the two molecules show that C10 and C12 participate in the electrophilic attack for G04 and G07 respectively. On the other hand, O15 are the more susceptible sites for a nucleophilic attack for both G04 and G07.

CONCLUSION

In present study global and local reactivities of G04 and G07 were explore in order to elucidate their electronic structures and predict their efficiency toward corrosion inhibition using DFT calculation. The results suggested that the G04 and G07 inhibitors have abilities to interact with the iron surface. The inhibition efficiency follows the order G07>G04.

REFERENCE

- 1 D Verma, Ebano et al., Materials Advances, 2021, v.2, p.3806.
- 2 S. Costa et al., Chem Eng Commun, 2018, p.1165.
- 3 J. Sánchez-Márquez et al., J. Mol. Model, v20, p. 2492.

ACKNOWLEDGMENT

PPGEM/UFF, FAPERJ and CAPES.



Investigação teórica sobre o mecanismo de síntese do ADN.

Letícia Marques de Souza Vetrano de Queiroz (PG),¹ Gabriel Freire Sanzovo Fernandes (PQ),¹ Luiz Fernando de Araújo Ferrão (PQ).^{1*}

vetrano@ita.br; ferrao@ita.br

¹Departamento de Química (CTE-Q), Instituto Tecnológico de Aeronáutica (ITA), 12228-900, São José dos Campos, SP, Brasil.

Palavras Chave: ADN, Mecanismo, Síntese, DFT, Propelentes.

INTRODUÇÃO

Perclorato de amônio (AP) é, atualmente, o agente oxidante mais utilizado em propelentes sólidos compósitos de motores foguetes. Apesar de sua eficiência, é também, altamente prejudicial ao meio ambiente, uma vez que sua decomposição libera compostos clorados na atmosfera.¹ Neste sentido, nota-se um aumento do interesse sobre a produção do agente oxidante Dinitramida de Amônio (ADN): um composto químico altamente energético, capaz de gerar maior impulso específico em comparação ao AP e livre de halogênios.^{1,2} A rota de síntese do ADN mais utilizada envolve a nitração do íon sulfamato em meio aquoso, na proporção 2:1 (2 NO₂⁺ para 1 NH₂SO₃⁻), produzindo ácido dinitramídico (HDN), que, posteriormente, reage com amônio (NH₄⁺) para produzir o ADN. Quando sintetizado, o ADN apresenta diversos tamanhos e formas, promovendo um comportamento mecânico inadequado ao propelente.² Dessa forma, visando um melhor planejamento da rota de síntese, o presente trabalho se estuda por meio da química quântica molecular possíveis caminhos reacionais para síntese do ADN.

MÉTODOS

Para a caracterização da superfície de energia potencial da reação de nitração do sulfamato, os estados estacionários (reagentes, produtos, e pontos de sela), barreiras adiabáticas e caminhos de mínima energia de cada etapa do mecanismo foram investigados pela teoria do funcional da densidade (DFT) dentro da aproximação HMGGA, M06-2X, combinado com uma base dupla zeta polarizada (def2-SVP). Esses cálculos foram realizados em fase gasosa por meio do software Gaussian 09.

RESULTADOS

A adsorção (SS1) do íon nitrônio (NO₂⁺) pelo íon sulfamato (NH₂SO₃⁻) foi caracterizada partindo de 8 geometrias iniciais, variando os ângulos α e β (Figura 1), os quais formaram 4 mínimos com estruturas distintas (SS1(A-D)), obtidos na proporção: 1:1:4:2. Cinco caminhos reacionais foram propostos, dos quais 2 são referentes à nitração e à dimerização, respectivamente, do mínimo com maior proporção de formação –

SS1(C). Os outros 3 caminhos reacionais propostos, são referentes a 1- do mínimo de maior energia, SS1(A), em direção ao SS1(C), 2- por meio do SS1(B) formando nitroamina e convergindo à rota obtida com o SS1(C) e 3- por meio do SS1(D) em direção à rota do SS1(C).

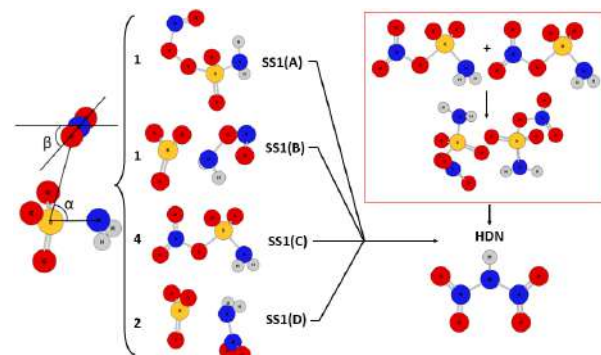


Figura 1. Esquema simplificado representando a adsorção do NO₂⁺ pelo íon sulfamato para formação de HDN. As rotas dos SS1(A), SS1(B) e SS1(D) convergem para a rota do SS1(C). Destacado em vermelho, representa-se o esquema de dimerização do SS1(C) para formação de HDN.

CONCLUSÕES

No presente trabalho, foram estudados possíveis caminhos reacionais da nitração do íon sulfamato pelo íon nitrônio. Na primeira etapa da reação, notou-se que a seção de choque entre os pares de íons apresenta um papel importante com respeito a formação do SS1 e à proporção de formação destes, sugerindo os caminhos reacionais envolvendo uma segunda nitração e dimerização. É importante ressaltar que, diferentemente da reação convencional para produção de ADN, na qual ocorrem duas nitrações, o caminho de dimerização apresentou uma proporção de 1:1 de NO₂⁺ e NH₂SO₃⁻.

REFERÊNCIAS

- ¹ F. Chen, et al., DT, 2023, v.19 163-195.
² M. Y. Nagamachi, et al., JATM, 2009, 1. 153-160.

AGRADECIMENTOS

O presente trabalho foi realizado com apoio da Coordenação de Aperfeiçoamento de Pessoal de Nível Superior - Brasil (CAPES) - Código de Financiamento 001.

Triaryliminophosphorane-thiourea: Design of a highly enantioselective organocatalyst for the addition of nitromethane to enone

Virginia C. Rufino (PG),¹ Josefredo R. Pliego Jr. (PQ).^{1*}

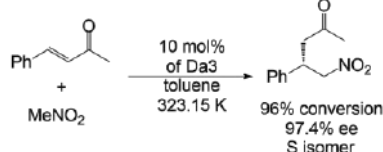
virginiacamila12@gmail.com; pliego@ufs.edu.br

¹Departamento de Ciências Naturais (DCNat), Universidade Federal de São João del-Rei – UFSJ

Keywords: Theoretical design, Triaryliminophosphorane-thiourea, Michael addition, Enantioselectivity, Reactivity.

INTRODUCTION

First proposed in 2013 by Dixon and coauthors,¹ triaryliminophosphorane-thiourea is a class of bifunctional organocatalysts, which combine a strongly basic group, triaryliminophosphorane, with a hydrogen bond donor group. Offering considerable reactivity as well as good to high enantiomeric excess, these catalysts have been successfully applied in both Mannich, aldol and Michael reactions.² Inspired by the potential of this new class of organocatalysts, we conducted the rational design of a new organosuperbase (Da3) for the Michael addition of nitromethane to 4-phenylbut-3-en-2-one in toluene solution, whose outstanding performance is presented below.



Scheme 1. Michael addition of nitromethane to 4-phenylbut-3-en-2-one catalyzed by Da3.

METHODOLOGY

Geometry optimizations and harmonic vibrational frequency calculations were performed at X3LYP/def2-SVP level of theory. Single-point energy calculations were performed at M06-2X/def2-TZVPP level of theory. To obtain the solvation free energy, single-point calculations were done at SMD/X3LYP/def2-SVP level of theory, using toluene as the solvent. A detailed microkinetic analysis (Kintecus program) was done using the complete free energy profile.

RESULTS

Taking the Dixon's catalyst (Da0) as a prototype structure, the main requirement for designing a new catalyst is to conduct an effective and enantioselective lowering in the ΔG^\ddagger of the carbon-carbon bond formation step in the Michael addition. Having determined the ΔG^\ddagger values for the main transition states (TSs) we conducted specific structural modifications, until obtaining a

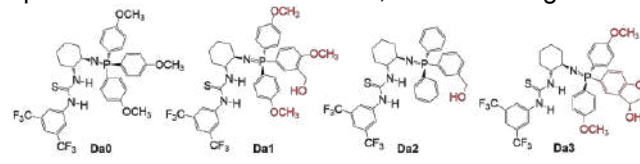


Figure 1. Catalysts structures investigated in this work.

structure with the best performance for the reaction, Da3 (Figure 1).

Next, we investigated the complete reaction mechanism for the Michael addition. The first step, the deprotonation of nitromethane, has a relatively low ΔG^\ddagger , 16.5 kcal mol⁻¹. The two main TSs for the carbon-carbon bond formation step, TS2si and TS1re, has a ΔG^\ddagger value of 22.8 and 25.7 kcal mol⁻¹, respectively. The final step, regarding the formation of the final product, has ΔG^\ddagger values for the TSs from 21.2 kcal mol⁻¹. In terms of free energy, the new catalyst proposed by us proves to be effective. Another important quantity is the enantiomeric excess (ee), which at room temperature has a calculated value of 98.2% (reaction time of 5 days, 60% conversion). On the other hand, if the reaction is conducted at 323.15K, the reaction time is reduced for 1 day, the conversion increases to 96% and there is a minimal effect on the value of ee, which becomes 97.4%. (Figure 2)

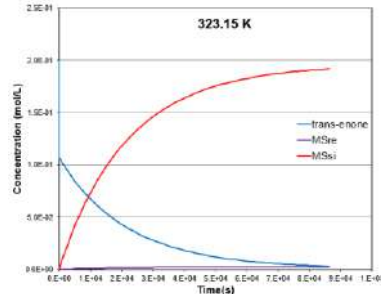


Figure 2. Microkinetic modeling for the Michael addition catalyzed by Da3 at 50 °C.

CONCLUSIONS

In conclusion, in this work we have designed a new catalyst for the Michael addition. We have investigated the complete reaction mechanism, free energy profile and done a detailed microkinetic analysis. Our results indicate that this new catalyst considerably outperforms the original Dixon's catalyst.

REFERENCES

- 1 M. G. Núñez, A. J. M. Farley, D. J. Dixon, *J. Am. Chem. Soc.* **2013**, 135, 16348.
- 2 M. Formica, D. Rozsar, G. Su, A. J. M. Farley, D. J. Dixon, *Acc. Chem. Res.* **2020**, 53, 2235.

ACKNOWLEDGMENTS

CNPq, CAPES, FAPEMIG



Enhancing performance and advancing methodology: A benchmark study using the custom dp4+ tool

Lucas Haidar Martorano (PG),¹ Alessandra Leda Valverde (PQ),¹ Ariel Marcelo Sarotti (PQ),² Fernando Martins dos Santos Junior.¹

lucashm@id.uff.br/fernando_martins@id.uff.br

¹Department of Organic Chemistry, Chemistry Institute, Fluminense Federal University (UFF), Niterói, RJ, Brazil.

²Department of Organic Chemistry, Rosario Chemistry Institute (IQUIR), Rosario Nacional University (UNR), Rosário, Argentina.

Keywords: Benchmark, DP4+, NMR.

INTRODUCTION

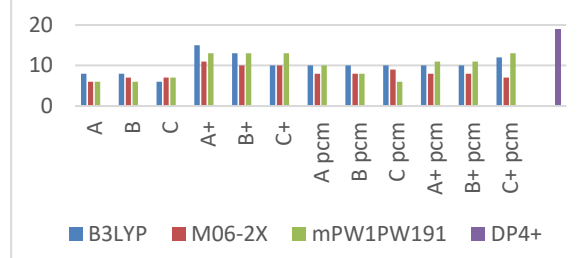
In the early 20th century, structural elucidation was limited to organic synthesis.¹ However, advancements in spectroscopic techniques and molecular modeling have become powerful tools for determining molecule structures.² Despite the combination of these techniques, the issue of structural reassignment still exists.² To address this, novel tools like DP4 and DP4+ have been developed for structural elucidation using NMR. These tools compare experimental NMR data with potential structures using advanced algorithms, providing the most likely structural assignment.² However, it's important to note that these tools have been misused in several documented cases.³ Misuse usually happens when they are applied outside their intended theory levels, which compromises the reliability of the results.³ To solve this problem, Sarotti's group developed a customized DP4+ tool that can be used at any theory level.⁴ In this scenario, through an innovative approach involving theoretical calculations based on 36 distinct levels of theory commonly used in NMR calculations, 36 new customized DP4+ tools have been developed.^{2,4} To evaluate and validate the new DP4+ tools, we selected 18 diverse molecules with known and fully assigned ¹H and ¹³C NMR spectra, and the tools were ranked based on their respective results. These advancements significantly improve the precision and reliability of structural determination in NMR studies.

METHODOLOGY

The NMR chemical shift calculations were performed using the Gauge Included Atomic Orbitals-Hybrid Density Functional Theory (GIAO-HDFT) method at 36 levels of theory. Geometry optimization employed three functionals (B3LYP, mPW1PW91, and M06-2X), while NMR calculations utilized three different functionals (B3PW91, ωB97X-D, and PBE0). Two basis sets (6-31G* and 6-31+G*) were used and were computed gas phase and solution (IEFPCM, solvent: chloroform). All calculation were performed using the Gaussian 09 software package.⁵

RESULTS AND DISCUSSION

To facilitate the discussion, we created a simplified scoring system similar to DP4+:
DP4+ probability >= 95%: 3 points;
DP4+ probability >= 50%: 1 point;
DP4+ probability < 50%: 0 points.



Index: OPT: B3LYP – blue; M06-2X – red; mPW1W1 – green. NMR: A – B3PW91; B – ωB97X-D; C – PBE0. Diffuse - +; solvent – pcm.

All the tools have been successfully developed. So far, calculations have been conducted on four molecules. It is evident that the levels utilizing the 6-31+G* basis function in the gas phase have demonstrated notable performance. Among these levels, the B3PW91/6-31+G*/B3LYP/6-31+G* combination has shown the most favorable results, indicating its superiority in accurately predicting the molecular structures.

CONCLUSIONS

Despite the limited number of molecules used in the analysis, it is evident that the obtained results closely resemble those of the best theory level found in the original DP4+ tool. It is worth noting that this slight discrepancy might be attributed to the variations in the number of molecules utilized during the development of the new tools. Nevertheless, a remarkable achievement was made with the development of 36 new DP4+ tools.

REFERENCES

- K. C. Nicolau, S. A. Snyder, Tetrahedron Lett. 2006, 47, 7353-7356.
- Costa et al. Org. Chem. Front. 2021, 8, 2019-2058.
- M. O. Marcarino, S. Cicetti, M. M. Zanardi, A. M. Sarotti, Nat. Prod. Rep. 2022, 39, 58-76.
- M. M. Zanardi, A. M. Sarotti, J. Org. Chem. 2021, 86, 8544-8548.
- D. J. Tantillo, Chemical Shift Repository with Coupling Constants Added Too, <http://cheshirenmr.info/index.htm>, 2019.
- Frisch et al. Gaussian 09; Gaussian Inc.: Wallingford, CT, 2009

ACKNOWLEDGEMENTS

To the funding agencies CNPq, CAPES and FAPERJ, for the financial support.

Quantum Computing and Chemistry: a case study

Caio M. Porto (PhD)¹, Rene A. N. Silva (R)¹, Nelson H. Morgan (R)^{1*}

c145568@dac.unicamp.br; nome@unicamp.br; nhmorgan@unicamp.br

¹Universidade Estadual de Campinas - Unicamp

Keywords: Quantum Computing, VQE, UCCSD

INTRODUCTION

Quantum computing holds the promise of completely changing the theoretical and computational Chemistry field. It could accelerate current calculations and make possible what today is inaccessible with much higher precision. Quantum calculations are performed in quantum qubits, for which an analogy can be a group of calcium atoms in the ground state and/or excited state. Qubits not only can exist in two states, 0 and 1, but they can be in a superposition of both states at the same time and can be entangled. The most impactful barrier for full quantum calculations is the errors introduced by decoherence. Due to these errors, currently we are at the noisy intermediate-scale quantum (NISQ) era. The most promising candidate algorithm in the near future is the variational quantum eigensolver (VQE). Our objective was to study the different parts of the VQE algorithm and understand their importance, and how and to which system size can computational chemists employ them currently and in the near future.

METHODS

All the calculations were performed using the Qiskit package from IBM. The VQE method requires an ansatz and a classical optimizer. The ansatz was constructed through the unitary coupled cluster method, using single and double excitations. The simultaneous perturbation stochastic approximation (SPSA) was chosen as the classical optimizer and the Jordan-Wigner mapper as the fermion to qubit mapper. The initial point was taken as the Hartree-Fock result. Since a HF point should be relatively close to the CCSD, it is possible to avoid traveling barren portions of the potential energy surface (PES) or avoiding unwanted local results. The molecules studied were H₂, HLi and He₂.

RESULTS

The most important parameter to evaluate the possibility of running a desired calculation is the depth of the circuit. For the H₂ molecule, using the STO-3G, 3-21G and 6-31G basis sets the circuit has 134, 1022, and 8678 single qubit rotation gates and 56, 768 and 14616 double qubit CNOT gates, respectively. The circuit for the STO-3G basis can be seen in Fig. 1a. Considering the coherence time and the time necessary to perform a gate, 6-31G would not be feasible in the vast majority of commercially available quantum computers.

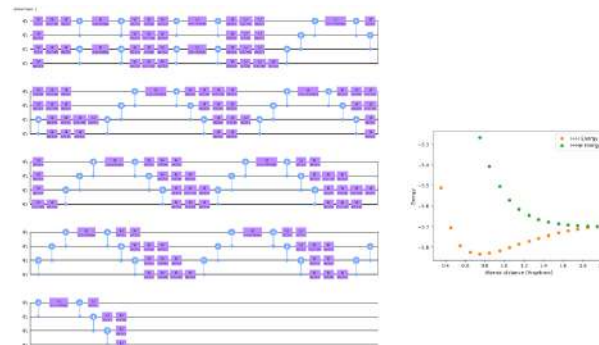


Figure 1. a) Quantum circuit for the UCCSD ansatz of the H₂ molecule calculated using VQE at the STO-3G level, and b) dissociation curve for the H₂ and He₂ molecules calculated using VQE, UCCSD and at the 3-21G level.

Therefore, we have calculated, using a quantum computer simulator, the dissociation curves for the H₂ and He₂ (Fig. 1b) molecules with the 3-21G basis set, and HLi with STO-3G basis set. The variational result is essentially the same as the exact results, calculated by diagonalizing the ansatz matrix. The reason is that the quantum computer simulator does not generate noise, which would be a significant source of error. There are many strategies to mitigate those errors and the next steps of the work is to run these calculations on available quantum computers.

CONCLUSIONS

Quantum computers have been an intense area of development, with quick leap forwards. At the same time, for quantum chemistry calculations, practical applications are still in the future. Nevertheless, given the rate of improvements (IBM has announced a 400 qubit QC), it is probably much closer than we anticipate. The biggest limitation are decoherence errors, which limit the circuit depth, and other source of errors not touched here, which require mitigation techniques. The next steps are using available quantum computers to perform the present calculations and applying mitigation techniques.

REFERENCES

- 1) Bauer, B., Bravyi, S., Motta, M., & Chan, G. K. L. (2020) Chemical Reviews, 120(22), 12685-12717.
- 2) Qiskit contributors. (2023). Qiskit: An Open-source Framework for Quantum Computing. doi:10.5281/zenodo.2573505

ACKNOWLEDGMENTS

The authors would like to thank CNPq, Fapesp (2021/11039-1) and the Institute of Chemistry for the computational infrastructure.

Modelagem Computacional do Mecanismo de Ação da Enzima Trans-sialidase do Parasita *Trypanosoma cruzi*

Jhonatan D. B. Alves (PG),^{1*} Juliana A. B. da Silva (PQ),² Maria Carolina P. Lima (PQ).³

Jhonatan.deivs@ufpe.br; juliana.bsilva@ufpe.br

¹Programa de Pós-Graduação em Química, Departamento de Química, Universidade Federal Rural de Pernambuco, Recife-PE; ²Núcleo Interdisciplinar de Ciências Exatas e da Natureza, CAA, Universidade Federal de Pernambuco, Caruaru-PE; ³Department of Medicinal Chemistry, University of Utah, Salt Lake City, Utah, United States of America.

Palavras-chave: Modelagem Computacional, QM/MM, *Trypanosoma cruzi* Trans-Sialidase, Sialil-lactose

INTRODUÇÃO

Trypanosoma cruzi (T. cruzi ou Tc) é o protozoário parasita unicelular causador da doença de Chagas. A *Trypanosoma cruzi* Trans-Sialidase (TcTS), uma enzima pertencente ao *Trypanosoma cruzi*, é um exemplo de um importante catalisador biológico para o desenvolvimento da doença causada por esse parasita. O substrato essencial para TcTS é o ácido siálico (SA). A enzima TcTS remove uma unidade SA, inicialmente ligada a um glicosídeo presente na superfície da célula hospedeira, transferindo o SA para outro glicosídeo na superfície das células do parasita, o que permite que o parasita passe despercebido em nosso sistema imunológico. Neste trabalho, foi investigado o mecanismo alternativo de ação da TcTS proposto por Oliveira et al.¹, envolvendo um intermediário ternário formado pelo doador e receptor que se ligam à enzima simultaneamente usando método de dinâmica molecular (DM), docking e QM/MM.

MÉTODOS

Os métodos e programas utilizados neste trabalho foram: para a modelagem das estruturas moleculares, pdb4amber e SwissModel/ H++; para as simulações de DM, foram utilizados os campos de Força AMBER ff14SB e GLYCAM_06j-1 (para carboidratos), e os programas Ambertools e sander; o Docking Molecular foi realizado com o programa Dock 4.0 e os cálculos de QM/MM com Ambertools, sander, umbrella sampling.

RESULTADOS

O uso do docking possibilitou verificar se a formação do complexo ternário (TcTS, SLT e uma lactose) é possível. Em posse do resultado da DM, foram avaliados os resultados de RMSD (Figura 1) e RMSF correspondente ao complexo ternário e o gráfico de energia potencial (Figura 2), obtido dos cálculos QM/MM.

A partir de simulações DM mais longas, nossos resultados corroboraram com àqueles obtidos por Oliveira et al.¹, que encontraram evidências de que, após a ligação do doador (α -2,3-sialil-lactose), ocorre um rearranjo estrutural que abre

uma segunda cavidade capaz de conter a unidade acceptora, permitindo um mecanismo direto sem a necessidade da saída do doador para a transferência. Ou seja, o mecanismo da reação entre a TcTS e o ácido siálico não pode seguir o modelo ping-pong, bastante citado na literatura, sendo necessária a elaboração de um mecanismo diferente, que não necessita que a lactose ligada ao ácido siálico saia do sítio ativo da enzima TcTS.

Figura 1. Docking e RMSD do complexo ternário.

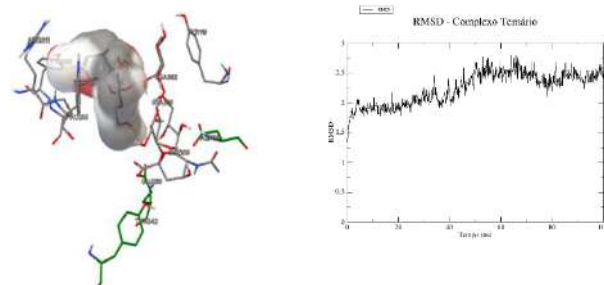
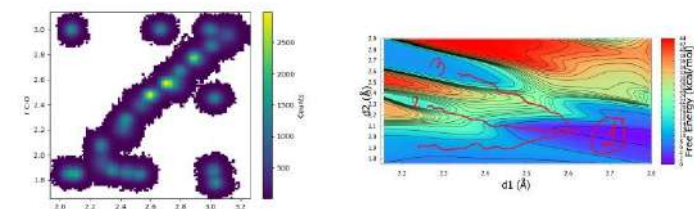


Figura 2. Histograma e PMF da reação



CONCLUSÕES

Nossos resultados sugerem que o mecanismo da reação entre a TcTS e o ácido siálico não segue o modelo ping-pong, sendo necessária a elaboração de um mecanismo diferente, que não necessita que a lactose ligada ao ácido siálico saia do sítio ativo da enzima TcTS.

REFERÊNCIAS

- ¹ Oliveira, I. A., A. S. Gonçalves, J. L. Neves, M. von Itzstein, A. R. Todeschini. 2014. Evidence of Ternary Complex Formation in *Trypanosoma cruzi* trans-Sialidase Catalysis. The Journal of Biological Chemistry 289: 423–436, doi: 10.1074/jbc.M112.399303.

AGRADECIMENTOS

FACEPE, UFRPE, CNPq.



Investigação Teórica do Complexo Hidrazina Borano como uma Alternativa a Hidrazina: O Sistema Reacional $N_2H_4BH_3 + H$

Augusto R. Rodrigues (PG),¹ Rene F. K. Spada (PQ).^{1*}

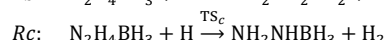
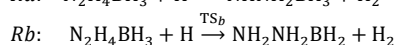
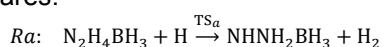
augustoarr@ita.br; rfkspada@ita.br

¹Departamento de Física, Instituto Tecnológico de Aeronáutica, São José dos Campos, 12.228-900 São Paulo, Brasil

Palavras Chave: Complexo hidrazina borano, *Ab initio*, DFT, Teoria do estado de transição

INTRODUÇÃO

O complexo hidrazina borano ($N_2H_4BH_3$) surge como uma alternativa promissora à hidrazina (N_2H_4) como propelente aeroespacial devido a sua provável maior densidade de energia e menor toxicidade. Este estudo investiga três reações elementares:



que envolvem a abstração de hidrogênio da $N_2H_4BH_3$, importantes na previsão das propriedades energéticas da molécula.

MÉTODOS

Os cálculos das propriedades termoquímicas foram realizados otimizando a geometria dos pontos estacionários e obtendo as energias do ponto zero (ZPE) das frequências harmônicas. Esses resultados foram obtidos usando a teoria de perturbação de Møller-Plesset (MP2) e os funcionais de densidade (DFT) M06-2X, ω B97X e ω B97X-D3, com conjuntos base cc-pVDZ, cc-pVTZ, def2-SVP e def2-TZVP.

Com base nas geometrias otimizadas pelo DFT ω B97X-D3, foram realizados cálculos usando a teoria *Couple-Cluster* com excitações simples, duplas e triplas conectadas (CCSD(T)). Para obter resultados mais precisos usou-se a aproximação de orbital natural localizado (DLPNO) e a extrapolação para o limite do conjunto base completo (CBS), utilizando aug-cc-pVY_Z (Y=T,Q). As propriedades energéticas calculadas incluíram energia de reação eletrônica (ΔE), altura da barreira clássica (V^\ddagger), altura da barreira adiabática vibracional ($\Delta V_a^{G,\ddagger}$), entalpia da reação a 0 K (ΔH_0^0), energia livre de Gibbs (ΔG) e ΔG^\ddagger . Para verificar a conectividade dos reagentes, estados de transição e produtos, foram realizados cálculos da coordenada intrínseca da reação (IRC). Além disso, foram calculadas cargas atômicas usando o método de análise de população natural (NPA) e usadas as teorias do estado de transição (TST) e do estado de transição variacional (CVT) para obter os coeficientes de velocidade. Os resultados foram ajustados em uma equação de Arrhenius modificada e comparados com dados pré-

existentes para avaliar o comportamento da molécula em diferentes faixas de temperatura.

RESULTADOS

Os resultados de melhor precisão foram obtidos com a abordagem CCSD(T)/CBS// ω B97X-D3/def2-TZVP, que mostrou a reação Rb, com a abstração de hidrogênio do grupo borano, apresentando a menor barreira adiabática (4,0 kcal/mol), seguida pela reação Rc (8,6 kcal/mol) com a abstração no grupo central da amina, e a maior barreira foi obtida para a abstração de hidrogênio do grupo amina na extremidade da molécula na reação Ra (10,9 kcal/mol). As reações são exotérmicas, e os valores de ΔG indicaram suas espontaneidades. A reação Rb teve os maiores coeficientes de velocidade (350K: $1,4 \times 10^{-13} \text{ cm}^3 \cdot \text{molécula}^{-1} \cdot \text{s}^{-1}$), mostrando ser a reação predominante em ambientes onde a reação $N_2H_4BH_3 + H$ ocorre. Os coeficientes ajustados na equação de Arrhenius mostraram que a molécula $N_2H_4BH_3$ possui uma estabilidade cinética melhor do que a N_2H_4 em temperaturas abaixo de 650K.

CONCLUSÕES

O estudo fornece dados valiosos sobre as propriedades termoquímicas e cinéticas do complexo hidrazina borano e seu potencial como uma alternativa de maior densidade energética e mais segura do que a hidrazina abaixo de 650K, temperatura de manuseio por operadores humanos.

REFERÊNCIAS

- T. Hugle, M. F. Kuhnel, D. Lentz, Hydrazine borane: a promising hydrogen storage material, *J. Am. Chem. Soc.* 131 (2009) 7444-7446.
- F. Neese, The ORCA program system. *WIREs Comput. Mol. Sci.* 2: 73-78, 2012.
- D. Ferro-Costas, D. G. Truhlar, A. Fernández-Ramos, Pilgrim: A thermal rate constant calculator and a chemical kinetics simulator, *Comput. Phys. Commun.* 256 (2020) 107457.
- D. Ferro-Costas, M. N. D. Cordeiro, D. G. Truhlar, A. Fernández-Ramos, Q2DTor: A program to treat torsional anharmonicity through coupled pair torsions in flexible molecules, *Comput. Phys. Commun.* 232 (2018) 190205.

AGRADECIMENTOS

Agradecemos o apoio da Fundação de Amparo à Pesquisa do Estado de São Paulo (FAPESP) [nº 2019/07671-4] e do Conselho Nacional de Desenvolvimento Científico e Tecnológico (CNPq) [nº 307846/2021-0, 423423/2021-5 e 405562/2022-5].

Estabilidade do ânion trifluormetil complexado com K⁺(18-coroa-6) e implicações para reações S_NAr: Predições teóricas

Gabryelle C. Marçal Salgado (PG),¹ Josefredo R. Pliego Jr. (PQ).^{1*}

gabryellecarvalhomarcalsalgado@gmail.com, * pliego@ufs.edu.br

¹Universidade Federal de São João del-Rei, Campus Dom Bosco, Departamento de Ciências Naturais (DCNAT), Praça Dom Helvécio, 74 – Bairro Dom Bosco, São João del-Rei – MG, CEP 36301-160.

Palavras Chave: (ânion trifluormetil, éter coroa, trifluormetilação, dissociação, substituição nucleofílica aromática).

INTRODUÇÃO

A inserção do ânion trifluormetil, CF_3^- , em moléculas orgânicas (trifluormetilação) pode afetar suas propriedades físico-químicas e assim potencializar sua eficácia como fármacos e agroquímicos.^{1,2} Durante muitos anos, acreditou-se na existência do CF_3^- somente de forma transitória em fase condensada.³ Porém, em 2015, ele foi caracterizado como ânion livre complexado a macrocíclicos.⁴ Este trabalho visa modelar a estabilidade química do CF_3^- de forma a avaliarmos seu potencial uso em reações S_NAr.

MÉTODOS

Os cálculos teóricos foram realizados no programa Orca 5 utilizando o nível ω B97X-D3/def2-SVP para otimização de geometria, frequências harmônicas e efeito do solvente (SMD). Cálculo de energia no ponto em nível ω B97M-V/def2-TZVPP.

RESULTADOS

Uma possível rota para inserir o grupo trifluormetil em compostos orgânicos é por meio da formação do complexo entre KCF_3 e o éter coroa (18C6), $KCF_3(18C6)$ (MS2). O poliéster macrocíclico estabiliza o par iônico complexando com o potássio, e enfraquece a ligação entre $K^+ - CF_3^-$, permitindo que o CF_3^- seja um nucleófilo reativo. Porém, apesar do interesse do complexo MS2 como nucleófilo em reações de substituição nucleofílica aromática (S_NAr), há a possibilidade da espécie MS2 dissociar, como demonstrado na Figura 1. Desse modo, deve-se conhecer esse

processo para verificar se a dissociação do ânion compete com a trifluormetilação. No mecanismo da Figura 1, inicialmente o complexo $KCF_3(18C6)$ se dissocia, formando um difluorcarbono livre, com um ΔG^\ddagger de 21,7 kcal mol⁻¹. O produto formado por $KF(18C6)$ e a molécula de CF_2 estão a 16,7 kcal mol⁻¹ acima dos reagentes. Estando em solução, outro complexo $KCF_3(18C6)$ pode reagir com o difluorcarbono resultante da dissociação e formar o intermediário MS2b, termodinamicamente estável em -29,5 kcal mol⁻¹. Em seguida, o ânion em MS2b também pode dissociar via TSb, liberando CF_2CF_2 e $KF(18C6)$, com uma barreira de energia livre de 16,9 kcal mol⁻¹. Os produtos estão com ΔG levemente acima de MS2b. A análise sugere que o ânion $CF_2CF_3^-$ complexado (MS2b) seja o produto final.

CONCLUSÕES

O ânion trifluormetil complexado com $K^+(18C6)$ se dissocia com $\Delta G^\ddagger = 21,7$ kcal mol⁻¹. Assim, para que a trifluormetilação S_NAr aconteça com o complexo $KCF_3(18C6)$, deve-se escolher um substrato que tenha ΔG^\ddagger que seja menor do que a energia livre de ativação para dissociação do $KCF_3(18C6)$.

REFERÊNCIAS

- ¹Shah, P.;Westwell, A.D.; *J.Enz.Inhib.Med.Chem.* **2007**, 22, 527-540. ²Cho,E.J. et.al.; *Sci.* **2010**, 328, 1679-1681. ³Prakash, G.K.S. et al.; *Angew.Chem.Int.Ed.* **2014**, 53, 11575-11578. ⁴Lishchynskyi, A. et.al.; *Angew. Chem. Int. Ed.* **2015**, 54, 15289-15293.

AGRADECIMENTOS

CNPq, CAPES e FAPEMIG.

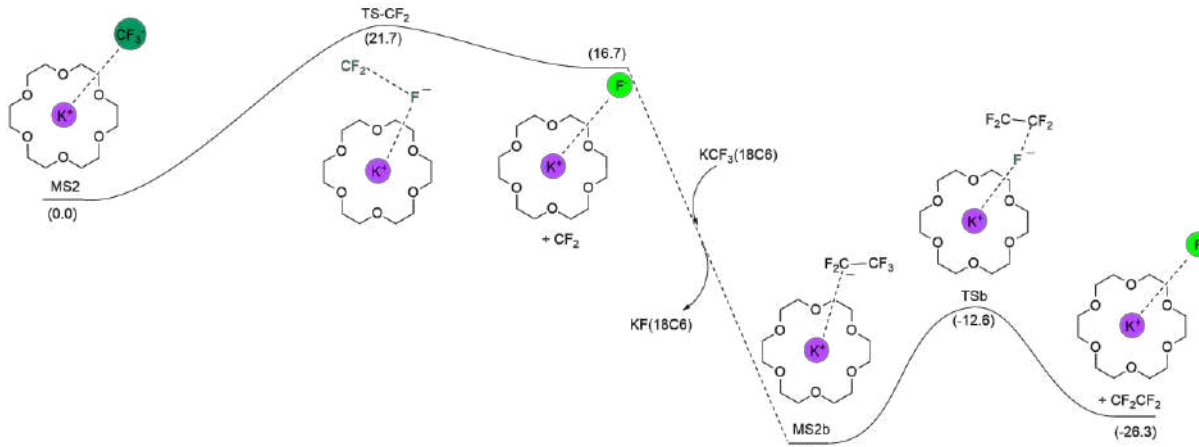


Figura 1. Comportamento do complexo $KCF_3(18C6)$ em solução de tolueno.

Modeling the cellular uptake of functionalized carbon nanohorns loaded with cisplatin through a breast cancer cell membrane

Eduardo R. Almeida (PG)^{1*}, Priscila V. S. Z. Capriles (PQ)², Hélio F. Dos Santos (PQ)³, Fabien Picaud (PQ)⁴.

eduardoe.r.a@hotmail.com

^{1,3}Núcleo de Estudos em Química Computacional (NEQC), Departamento de Química, Instituto de Ciências Exatas, Universidade Federal de Juiz de Fora (UFJF), Campus Universitário, Martelos, Juiz de Fora, MG, 36036-330, Brazil.

²Grupo de Modelagem Computacional Aplicada (GMCA), Programa de Pós-graduação em Modelagem Computacional (PGMC), Departamento de Ciência da Computação, Instituto de Ciências Exatas, Universidade Federal de Juiz de Fora (UFJF), Campus Universitário, Martelos, Juiz de Fora, MG, 36036-330, Brazil.

⁴Laboratoire de Nanomédecine, Imagerie et Thérapeutiques, EA 4662, Centre Hospitalier Universitaire de Besançon, Université de Franche-Comté (UFC), 16 route de Gray, 25030 Besançon cedex, France.

Keywords: Cisplatin, Carbon nanohorn, Cell membrane, Permeation, Molecular dynamics.

INTRODUCTION

Chemically modified carbon nanohorns (CNH) have been considered promising cisplatin (cddp) nanovectors for treating cancers, including breast cancer, due to their biocompatibility and ability to adhere on the surface of malignant cells, thereby reducing the drug dissipation and the side effects of conventional formulations.^{1,2} Since the cellular uptake of CNH has not been clarified at the molecular level, this work involves the analysis of the transmembrane transport of these nanocarriers of cddp through a breast cancer cell membrane using molecular dynamics simulations.

METHODS

Three CNH models were built: oxidized model (CNHox), covalently functionalized model (CNHfcov), and noncovalently functionalized model (CNHf-ncov) using experimental data.^{3,4} The inclusion complexes were built based on the cddp encapsulation: 3cddp@CNHox, 3cddp@CNHfcov, and 3cddp@CNHf-ncov. A membrane model (C_memb) of a breast cancer cell was also built using the CHARMM-GUI website. The interaction between nanoformulations and the C_memb was analyzed using steered molecular dynamics (DM) simulations and the umbrella sampling method.

RESULTS

The simulations unveiled the transmembrane transport mechanism of the nanocarriers, which we divided in four stages (Fig.1): (i) approach, (ii) insertion, (iii) permeation, and (iv) internalization. The potentials of mean force (PMF) (Fig.2) demonstrated that permeation events of these nanovectors through a membrane are highly unfavorable with free energy barriers of ~55 kcal mol⁻¹ despite the low structural disturbance of the membrane. Conversely, the adsorption of CNH on the C_memb, which was characterized by a potential well of about -6.8 kcal mol⁻¹, was the spontaneous step of this mechanism.

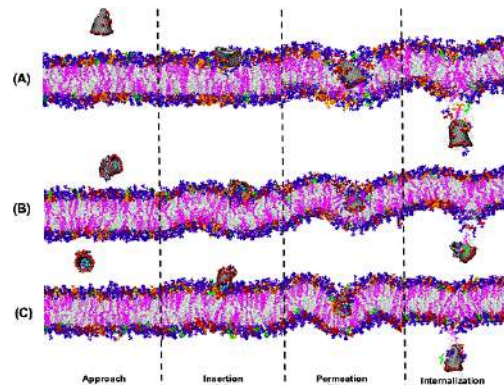


Fig.1 Interaction mechanism of the inclusion complexes through the membrane (C_memb).

Our study reinforces the biomedical applications of CNHs as non-disruptive nanovectors of cddp for cell membranes, which may potentially accumulate on the surface of cancer cells.

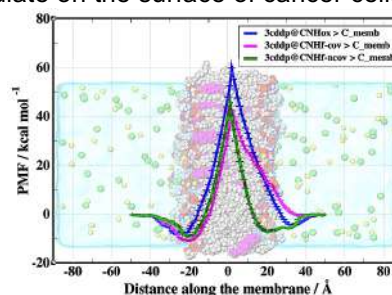


Fig.2 PMF referring to the transmembrane transport of the inclusion complexes.

CONCLUSIONS

The most likely cddp delivery mechanism should involve the adsorption and retention of CNH on the surface of cancer cells, allowing the loaded cddp to be slowly released and transported through the cell membrane.

REFERENCES

- K. Ajima, et al. ACS Nano, 2008, 2, 1057-2064.
- M. Curcio, et al. J. Carbon Research, 2021, 7, 1-18.
- B. Hifni, et al. ACS Appl. Biom. Mater., 2020, 3, 6790-6801.
- C. Gao, et al. J. Colloid Interface Sci., 2022, 628, 273-286.

ACKNOWLEDGEMENTS

CAPES, FAPEMIG, UFJF, UFC.

A molecular dynamics approach to spermine and spermidine SI-PPCs interactions with heparin and DNA

Frederico Henrique do C. Ferreira (UR)¹, Nicholas P. Farrell (R)², Luiz Antônio Sodré Costa (R)^{1*}

frederico.h@outlook.com; lrcosta@gmail.com

¹ NEQC – Departamento de Química – Universidade Federal de Juiz de Fora, Juiz de Fora, MG - Brasil.

² Department of Chemistry, Virginia Commonwealth University, Richmond, VA 23284-2006, USA

Keywords: SI-PPCs, DNA, Heparan Sulphate, Molecular Dynamics.

INTRODUCTION

Cancer stands as the second leading cause of deaths among the realm of non-communicable diseases globally. Consequently, it remains a prominent focal point of extensive research endeavours, with the goal of discovering novel and efficacious therapies to combat its various associated conditions. Initially, cisplatin emerged as the inaugural and soon became an extensively prescribed drug for this ailment, paving the way for subsequent direct analogues such as carboplatin and oxaliplatin, which received widespread approval for clinical usage^{1,2}. The mechanism of action employed by these prodrugs originated a non-analogous entity named BBR3464, which introduced the concept of noncovalent interactions. This breakthrough led to the emergence of Substitution-Inert Polynuclear Platinum Complexes (SI-PPCs), comprising a class of compounds which interacts with phosphate and sulphate groups via their PtN₄ centres through hydrogen interactions. One notable exemplar of this novel category is TriplatinNC, which has demonstrated efficacy against certain cancer subtypes.² The aim of this project is to evaluate the substitution of simple diamine ligand chains to both spermine and spermidine in the interaction with biomolecules such as DNA and Heparan Sulphate as shown in Figure 1. The analysis was based on molecular dynamics simulations of the systems.

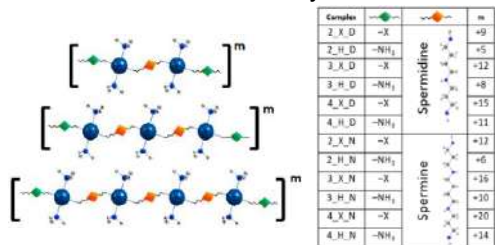


Figure 1. Systematic notations given to the metal complexes according to both the linking and terminal chains and the number of metal centres.

METHODS

The metal complexes structures were optimized in BHandH/6-31+G(d,p) and structural parameters were obtained via VFFDT toolkit. Several MD simulations were performed comprising the studied species employing all GAFF, ff14SB and bsc1 force-fields. The simulations were 200ns long preceded by alternating heating and equilibrium steps of 50K until 310K. Calculations

and analysis were conducted by AMBER 12 software package.

RESULTS

The interaction energies were all favourable for both the systems comprising DNA and heparin. The higher the number of Pt centres the lower the energy. Terminal amine chains also accounted for more thermodynamically stable interactions along with higher SASA decrease. Complexes 2_X_N and 3_X_D were above average in all parameters considered in this analysis. The number of cyclic structures among phosphates/sulphates and PtN₄ motifs were higher among the 2/3-centred complexes whether the number of ‘simple’ H-bonds were substantially higher among the 4 centred ones.

COMPLEX	ΔE_{HEP}	ΔE_{DNA}	%SASA _{HEP}	%SASA _{DNA}
2_H_D	-70.87	-63.39	5.31	2.65
2_H_N	-76.13	-81.61	6.63	3.00
2_X_D	-184.15	-137.14	14.46	4.74
2_X_N	-238.49	-199.21	14.87	16.50
3_H_D	-93.62	-91.73	9.07	3.60
3_H_N	-152.18	-140.1	11.56	4.99
3_X_D	-225.17	-187.18	16.00	7.57
3_X_N	-316.44	-43.76	22.41	7.76
4_H_D	-158.72	-152.91	12.79	5.49
4_H_N	-181.5	-155.75	17.14	5.94
4_X_D	-249.26	-46.29	16.59	6.62
4_X_N	-333.33	-327.65	23.27	9.81

Table 1 – Summary of interaction energy means (ΔE) for the SI-PPCs with both Heparin and DNA and their respective percentage decrease (%SASA) in the SASA of the biomolecules. Values in bold indicate they are above the average; energy values are reported in kcal mol⁻¹ and SASA in Å².

CONCLUSIONS

The simulations agreed with published results in the literature. The complexes reduced the solvent accessible surface area on both biomolecules indicating a possible decrease on their biological roles, which is supported by the thermodynamic favoured interaction energies with all SI-PPCs.

REFERENCES

- 1 N. P. Farrell, Drugs Future 2012, 37 795–806.
- 2 Harris, A. L.; Ryan, J. J.; Farrell, N. P. Mol. Pharm. 2006, 69, 666-672.
- 3 N. P. Farrell, Chem. Soc. Rev. 2015, 44, 8773-8785.

ACKNOWLEDGMENTS

CNPq, UFJF, EULER-CeMEAI/USP



Application of the Quantum Variational Monte Carlo method with explicit correlation function in the calculation of ionization energies of the N₂ molecule.

Josué de Jesus Oliveira Araújo (PG),¹ Rogério Custodio (PQ).^{1*}

j203713@dac.unicamp.br; roger@iqm.unicamp.br

¹Institute of chemistry, UNICAMP. Rua Josué de Castro Sn, cidade universitária, Campinas-SP.

Keywords: Ionization, Energy, Quantum Monte Carlo, Correlation.

INTRODUCTION

The ionization potential represents the energy required to remove an electron from a neutral atom or molecule, and it is a fundamental measure of the stability of chemical systems¹. This information is of enormous utility, providing valuable insights for understanding the structure and properties of materials. The objective of the present study is to evaluate the calculation of this property using the Quantum Variational Monte Carlo method for the N₂ molecule.

METHODS

The Hartree-Fock wave functions used were obtained with double-zeta (DZ) Slater basis functions and at the Hartree-Fock limit (LHF). Explicit correlation functions of the Boys² type with 9 parameters were optimized for N₂ using the simplex method and employed in the calculation of ionization energies. The different ionization energies were obtained by taking the difference between the neutral system's energy and the energy after removing one electron from the system (E(0)) and ionized (E(+))³:

$$EI = E(+) - E(0)$$

RESULTS

The results obtained are summarized in Table 1..

Table 1: Single ionization energies, in eV, for the orbitals of N₂ using the DZ and LHF basis sets. Absolute errors are shown in parentheses..

Orbital	DZ	LHF	Exp ⁴
1σ	411.2 (1.3)	411.5(1.6)	409.9
2σ(g)	40.68 (3.39)	37.60(1.56)	37.29
2σ(u)	18.99(0.39)	19.23(0.63)	18.60
1π	15.86(-0.93)	15.77(-1.02)	16.789
3σ(g)	14.26(-1.24)	16.88(1.39)	15.497

The values in parentheses represent the difference between the calculated values and the reference experimental data. Interestingly, the errors obtained for the core ionization are relatively close to the valence results, even without any relativistic corrections. This suggests that somehow, the optimization of explicit correlation parameters leads to error cancellation

that is compatible with the effects produced by relativistic effects. Furthermore, it is observed that the results using the DZ Slater basis functions show deviations relatively close to the calculations with functions at the Hartree-Fock limit. The largest deviation was observed for the orbital 2σ(g) with DZ functions, while the calculations for the orbital 2σ(u) showed the smallest deviation from the experimental data, both for DZ and LHF calculations. The average absolute error for the DZ calculations is 1.45 eV, while the LHF calculations have an average absolute error of 1.32 eV. This result indicates that although the results may exhibit significant differences at the Hartree-Fock level, the inclusion of explicit correlation makes the two calculation levels practically equivalent. Using explicit correlation functions with a larger number of parameters is possible, but the time required for optimization and the quality of the results do not justify their use, even though they may introduce some improvement.

CONCLUSIONS

Indeed, the Quantum Variational Monte Carlo method with explicit correlation proves to be a straightforward alternative for calculating ionization energies of the N₂ molecule, exhibiting excellent performance even under limited calculation conditions such as using the DZ Slater basis. However, to draw more general conclusions, other systems are being evaluated and studied.

REFERENCES

- ¹ P. K. Ghosh, Introduction to Photoelectron Spectroscopy; John Wiley and Sons: New York, 1983.
- ² W. M. C. Foulkes, L. Mitas, R. J. Needs, G. Rajagopal, Rev. Mod. Phys. 73, 33 (2001).
- ³ K. E. Schmidt, and J. W. Moskowitz, "Correlated Monte Carlo wave functions for the atoms He through Ne," The Journal of chemical physics 93.6 (1990): 4172-4178.
- ⁴ K. Siegbahn, ESCA applied to free molecules, 1969.

ACKNOWLEDGMENTS

CAPES, FAPESP, UNICAMP

Exploring axial chirality and determining absolute configuration of a novel atropoisomeric bis-phenylpropene lignamide from *Matternichia princeps* using DFT calculations and spectroscopic methods.

Ana Carolina F. de Albuquerque (PQ),^{*1} Thiago A. de M. Brito (PG),² Marcelo S. da Silva (PQ),² Josean F. Tavares (PQ),² Lucas da S. Abreu (PQ),¹ Fernando M. dos Santos Jr (PQ).¹

acfalbuquerque@id.uff.br

¹Institute of Chemistry, Fluminense Federal University, Niterói, Rio de Janeiro, Brazil; ²Postgraduate Program in Natural and Synthetic Bioactive Products, Federal University of Paraíba, João Pessoa, Brazil.

Keywords: TD-DFT, ECD, chirality, natural products, absolute configuration.

INTRODUCTION

In a recent comprehensive phytochemical investigation of the *Matternichia princeps* species, a plant commonly found in the Brazilian Atlantic Forest, we successfully isolated a novel atropoisomeric bis-phenylpropene lignanamide (Fig. 1). The structure of this compound was elucidated through 1D and 2D Nuclear Magnetic Resonance (NMR) studies, revealing a symmetrical arrangement with duplicated NMR signals, suggesting the presence of axial chirality. The primary objective of our study was to confirm the existence of axial chirality using DFT calculations. Additionally, we aimed to determine the absolute configuration of this newly isolated natural product by comparing quantum-mechanical (QM) calculated and experimental electronic circular dichroism (ECD) data.

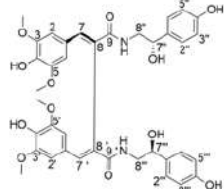


Fig. 1. Structure of the novel bis-phenylpropene lignamide, isolated from *Matternichia princeps*.

METHODS

To confirm the presence of atropisomerism in the structure of the isolated compound, we conducted DFT calculations, using B3LYP/6-31G(d) level of theory, on the free energy barrier as a function of rotation around the C7-C8-C8'-C7' dihedral angle. Confirming the atropisomerism, the next step was to determine the absolute configuration of the isolated natural product. For this, for each of the eight possible stereoisomers of the isolated compound, randomized conformational searches were performed in the Spartan'18 software package.¹ The more significant conformations were selected for geometry optimizations at gas phase, using B3LYP/6-31G(d). ECD spectra were simulated using CAM-B3LYP/TZVP, using PCM (methanol). The final ECD spectra were generated based on

the Boltzmann statistics of the selected conformers and plotted against experimental spectrum. All QM calculations were performed using Gaussian 16 software package.²

RESULTS

The calculated relative free energy value of 29.04 kcal.mol⁻¹ confirms the presence of axial chirality (Fig. 2) in the isolated compound.

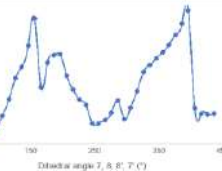


Fig. 2. Calculated energy levels (in kcal.mol⁻¹) for the conformers of the isolated compound.

The good agreement obtained by comparison of experimental ECD spectra with the corresponding calculated spectra for the (7'S,7''S,8aS) stereoisomer (Fig. 3) confirmed the absolute stereochemical configuration of the natural product.

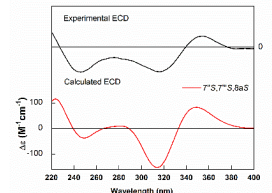


Fig. 3. Comparison between the experimental (in black) and calculated (in red) ECD spectra.

CONCLUSIONS

Through DFT calculations, the presence of axial chirality was confirmed. Moreover, based on calculated and experimental ECD spectroscopy, it was possible to determine the absolute configuration of the isolated natural product.

REFERENCES

¹Spartan'14 Wavefunction, Inc. Irvine, CA

²Gaussian 16, Gaussian, Inc. Wallingford, CT

ACKNOWLEDGMENTS

CAPES, CNPq and NACAD-UFRJ supercomputer.

Predição da hidrólise dos elementos de terras raras e a coordenação com sulfato.

Alexandre C. Bertoli (PQ),^{1*} Luciano T. Costa (PQ),¹ Hélio A. Duarte (PQ),² Wagner B. Almeida (PQ).¹

bertolialexandre@yahoo.com.br

¹Instituto de Química – Universidade Federal Fluminense; ²Departamento de Química – Universidade Federal de Minas Gerais.

Palavras-Chave: DFT, Hidrólise, Terras Raras, Drenagem ácida de minas.

INTRODUÇÃO

Medições espectroscópicas revelaram que, ao contrário do comportamento de pequenos complexos quelantes, as moléculas de água coordenadas aos Elementos de Terras Raras (REE), aumentam a afinidade e a estabilidade do pH de seus complexos.¹ Perante essa descoberta, avaliamos a hidrólise dos REE, considerando a 1^a, 2^a e 3^a hidrólise, expandindo a discussão para a coordenação com sulfato mediante a presença dos REE na drenagem ácida de minas.

MÉTODOS

As geometrias foram otimizadas empregando o funcional de troca-correlação (XC) PBE com os conjuntos de base def2-TZVP. Para os REE, os elétrons do núcleo interno foram substituídos por ECP, e os elétrons tratados com def-TZVP. As correções D3 e RI foram aplicadas para acelerar os cálculos. Além disso, corrigimos os cálculos para efeitos relativísticos usando a aproximação regular de ordem zero (ZORA). Ao longo dos cálculos, foram utilizados critérios rígidos de convergência do SCF e grades de integração aumentadas (Grid6). As frequências vibracionais na aproximação harmônica foram calculadas para garantir que as geometrias otimizadas da fase gasosa sejam mínimos verdadeiros na superfície de energia potencial. A influência do ambiente solvente (fase aquosa, constante dielétrica $\epsilon = 80,4$) também foi considerada no Modelo de Solvatação Baseado na Densidade (SMD). Todos os cálculos foram realizados usando o pacote do programa de química quântica ORCA versão 5.0.3.²

RESULTADOS

A hidrólise dos REE, com a consequente alteração na ionização dos elétrons f, reproduz curvas em padrões zigue-zague característicos. Tal fato é causado por mudanças no número de interações de troca e emparelhamento. Além disso, as mudanças no momento angular orbital total dos elétrons levam à oscilação da energia de ionização.³ Variações bruscas de energia livre foram observadas na 1^a hidrólise Sm (29,5 kcal.mol⁻¹) - Eu 15,6 (kcal.mol⁻¹), na 3^a hidrólise Eu

(33,9 kcal.mol⁻¹) - Gd (22,4 kcal.mol⁻¹), e na reação com sulfato entre Eu (-30,1 kcal.mol⁻¹) - Gd (-46,0 kcal.mol⁻¹). O $[\text{Eu}(\text{H}_2\text{O})]^{3+}$ e o $[\text{Gd}(\text{H}_2\text{O})]^{3+}$ têm a configuração eletrônica $[4f\ 6\ 5d\ 0\ 6s\ 0]$ e $[4f\ 7\ 5d\ 0\ 6s\ 0]$, respectivamente. Os elétrons adicionados nas reações preenchem os orbitais f e s do Eu e Gd, respectivamente, reduzindo a variação da energia livre e estabilizando as espécies.

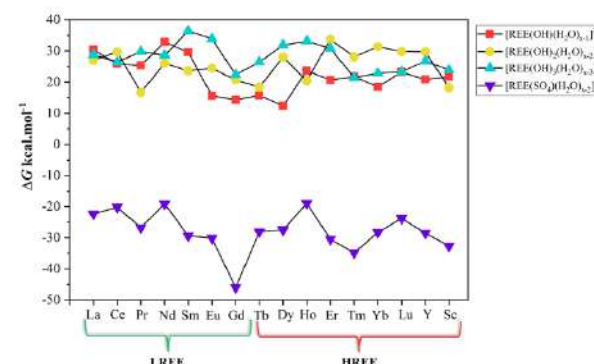


Figura 1: Variação da energia livre (ΔG_{aq}) dos REE em fase aquosa após as etapas de hidrólise e coordenação ao sulfato.

CONCLUSÕES

Os REE são separados em dois grupos designados como REE leves (LREE) (La-Gd), favorecendo a coordenação à 9 moléculas de H_2O , e os posteriores (Tb-Lu, Sc e Y), coordenados a 8 H_2O , classificados como pesado (HREE). Destaca-se que os REE do meio da série (Sm, Eu, Gd, Tb e Dy), estão em um equilíbrio entre 8 e 9 moléculas de água na esfera de coordenação. Assim, podem apresentar números de coordenação não inteiros e flutuações entre as geometrias.

REFERÊNCIAS

- Mattocks, J. A.; Cotruvo, J. A.; Deblonde, G. J.-P.; Chem. Sci. 2022, 13, 6054.
- Silva, G. C.; Bertoli, A. C.; Duarte, H. A.; Ladeira, A. C. Q.; J. Environ. Chem. Eng. 2022, 10, 108715.
- Lang, P. F.; Smith, B. C.; J. Chem. Educ. 2010, 87, 875.

AGRADECIMENTOS

FAPERJ and FAPEMIG. Based Mineral High-Performance Materials and Processes Network–RENOVAMin (Proc. RED-00102-16).

Absorption Spectra of p-Nitroaniline Derivatives: Charge Transfer Effects and the Role of Substituents using Hammett's Theory

Matheus Máximo Canadas Costa (PG)¹, Itamar Borges Jr (PQ)^{1*}

matheusmaximocanadas@hotmail.com; itamar@ime.eb.br

¹ Department of Chemistry, Military Institute of Engineering (IME), Rio de Janeiro, RJ, 22290-270, Brazil.

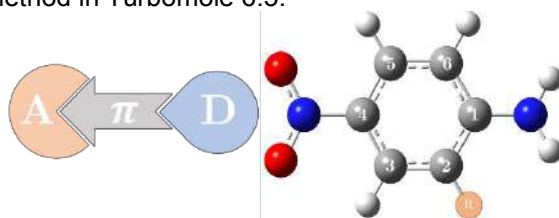
Keywords: *P*-nitroaniline, Absorption, Hammett's Substituent Theory; ADC(2) Ab Initio Wave Functions; Intramolecular Charge Transfer.

INTRODUCTION

The push-pull *p*-nitroaniline (*p*NA) is a structurally simple compound with strong solvatochromism and characteristic optical properties.^[1-4] Despite the interest in *p*NA, the influence of substituents on its molecular properties, such as the HOMO-LUMO energy gap and charge transfer (CT) effects, remains unknown. Furthermore, understanding the impact of substituents is crucial for gaining insights into the electronic properties of push-pull compounds. For this purpose, we used Hammett's theory,^[5] which quantifies the electron-donating and the electron-acceptor power of the substituents.

METHODS

The following substituents inserted at position 2 (Scheme 1) of *p*NA were studied, namely, the electron-withdrawing groups (EWGs) Br, CCl₃, CF₃, Cl, CN, COOH, F, NO₂, and SO₂H, and the electron-donor groups (EDGs) C₆H₅, CCH, CH₃, NH₂, OCH₃, and OH. Machine-learning Hammett's constants (σ_m , σ_m^0 , σ_R , σ_I) recently computed by our group were used.^[6] Geometries were optimized using the DFT/CAM-B3LYP//def2-TZVPD method. Gas phase vertical singlet excitations were computed using the RI-ADC(2)//def2-TZVPD method in Turbomole 6.5.



Scheme 1 – *p*NA. R indicates the substituent.

RESULTS

Figure 1 shows the natural transition orbitals (NTO) with the transition amplitudes λ_i , oscillator strengths (f), and charge transfer (CT) values of the brightest states in the first and second bands of the absorption electronic spectra.

Figure 2 illustrates the correlation between the σ_R Hammett constant, which describes resonance effects, and the HOMO-LUMO energy gap. Substituents indicated in red in the plot redshifted the absorption spectra, while blue substituents blueshifted it.

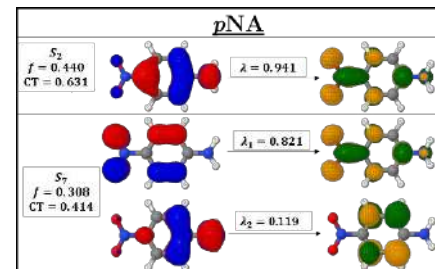


Figure 1 – The brightest state of the first and second bands.

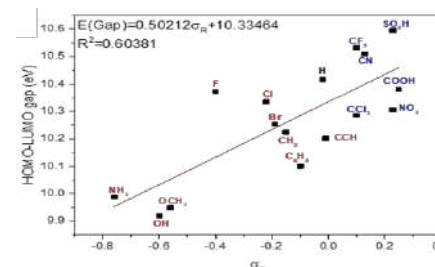


Figure 2 – The HOMO-LUMO energy gap correlation with the σ_R constants.

CONCLUSIONS

We found that EDGs redshifted the electronic absorption spectra and increased charge transfer effects. In contrast, EWGs decreased charge transfer effects and blueshifted the spectra, except for halogens, which caused a slight redshift.

Hammett's constants and the HOMO-LUMO gap correlations reveal smaller energy gaps for EDGs and larger ones for EWGs. In particular, we found that strong EDGs in *p*NA, namely, OH, OCH₃, and *p*NA-NH₂ are potential candidates for low-gap materials for applications in organic electronic devices.

REFERENCES

- 1 M.H. Cardenuto, K. Coutinho, B.J.C. Cabral, S. Canuto, *Advances in Quantum Chemistry*, 2015, DOI:10.1016/bs.aq.2015.03.006.
- 2 M. Hidalgo, R. Rivelino, S. Canuto, *Journal of Chemical Theory and Computation*, 2014, DOI:10.1021/ct401081e.
- 3 A. V. Sanches, L. R. Marques, A. C. Borin, R. A. Ando, *Physical Chemistry Chemical Physics*, 2022, DOI:10.1039/D2CP04401C.
- 4 A. A. I. ABED-ELMAGEED, *Optical Materials*, 2020, DOI:10.1016/j.optmat.2020.110378
- 5 L. P. Hammett, *Journal of the American Chemical Society*, 1937, DOI:10.1021/ja01280a022.
- 6 G. Monteiro-de-Castro, J.C. Duarte, I.Borges., *Journal of Organic Chemistry*, 2023, DOI:10.26434/chemrxiv-2023-5g6gp.

ACKNOWLEDGEMENTS

The authors thank the support for this research by the Brazilian agencies FAPERJ, CNPq and CAPES.

Applications of machine learning to chemistry: new Hammett's constants, sensitivity of energetic materials and organic photovoltaics

Itamar Borges Jr. (PQ),^{1*} Julio Cesar Duarte (PQ),² Gabriel Monteiro-de-Castro (PG)¹

itamar@ime.eb.br

¹ Dep. de Química, Instituto Militar de Engenharia (IME), Rio de Janeiro, RJ 22290-270, Brazil

² Dep. de Engenharia de Computação, Instituto Militar de Engenharia (IME), Rio de Janeiro, RJ 22290-270, Brazil

Keywords: Machine Learning/Artificial Intelligence, Substituent Effect, Energetic Materials, Organic Photovoltaics

INTRODUCTION

Machine learning (ML) and Artificial Intelligence (AI) techniques have been applied successfully to a large variety of problems in chemistry, physics, and materials science.¹ In this work, we present and discuss recent applications of ML in our group to different chemistry problems, namely: (i) determination of a new set of different kinds of Hammett's σ constants for investigating the substituent effect,² (ii) evaluation of the impact sensitivity of energetic materials³ and, (iii) materials for organic electronics.⁴ Hammett's theory is widely used to investigate quantitatively the substituent in chemistry. The sensitivity of the explosives is a critical issue even in civilian applications (e.g., airbags), and investigating new organic materials for developing flexible and cheap solar cells, as well as other organic electronic devices, is especially important.

METHODS

Different ML algorithms and theoretical approaches were tested and used to investigate those problems. To obtain new Hammett's σ constants for meta- and para-substituted benzoic acid derivatives, we tested different types of quantum chemical atomic charges to determine 219 new σ values, including 92 previously unknown. For 53 nitroaromatic explosives, we used atomic electric multipoles to rationalize the molecular origin of their sensitivity to impact. Considering that diketopyrrolopyrrole (DPP) systems have promising applications in different organic electronic devices, we studied the effect of 20 different substituents in DPP derivatives using Hammett's theory. Other applications of ML to chemistry are underway and will be presented at the Symposium.

RESULTS

When light falls on DPP, which can be used as a donor material in a solar cell, it creates a bound electron-hole pair (exciton) that should dissociate to produce an electric current. Practical applications in this field should look for materials with low exciton binding energies (E_{bind}). Employing our ML Hammett's constants, and an ML clustering algorithm, we identified average

values of both E_{bind} and σ constants that can indicate properties for developing potential materials for applications – see Fig. 1.

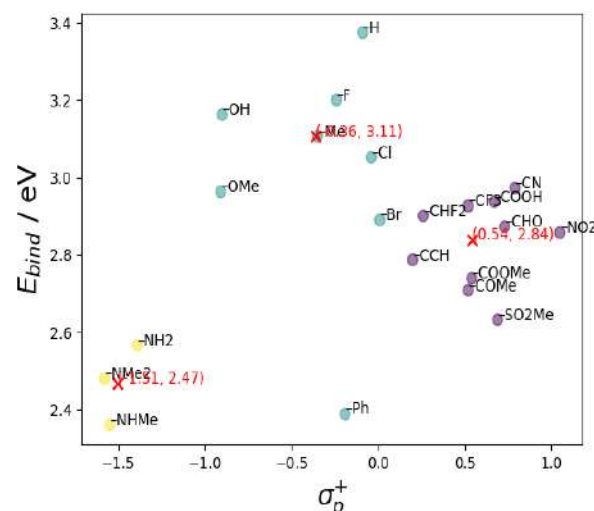


Figure 1. E_{bind} values σ_p^+ for different substituents.

For the nitroaromatic explosives, we found that the most important properties contributing to the impact sensitivity given by h_{50} (cm) are the electron delocalization in the ring atoms and the total polarization of the nitro groups. Interestingly, we found that these properties, as well other two (the total charge of the nitro groups and their number), affect the sensitivity differently depending on the h_{50} value: for the most sensitive explosives ($h_{50} \lesssim 50$ cm), the four properties contribute to reducing it, whereas for highly insensitive explosives ($h_{50} \gtrsim 200$ cm) all of them contribute to increasing it. Explosives with intermediate sensitivities ($50 \text{ cm} \lesssim h_{50} \lesssim 100$ cm) to properties contribute to increasing h_{50} , while two others contribute to reducing it.

We thank FAPERJ, CNPq and CAPES for support of this research.

1. (a) Dral, P. O., *J. Phys. Chem. Lett.* **2020**, 11, 2336; (b) Aspuru-Guzik et al, *Nature Rev. Mat.* **2022**, 4, 761
2. Monteiro-de-Castro, G.; Duarte, J. C.; Borges, I., Jr., *J. Org. Chem (JOC)* **2023**. DOI: [10.1021/acs.joc.3c00410](https://doi.org/10.1021/acs.joc.3c00410)
3. Duarte, J. C.; da Rocha, R. D.; Borges, I., *Physical Chemistry Chemical Physics* **2023**, 25 (9), 6877-6890.
4. Monteiro-de-Castro, G.; Borges Jr, I., A H. *Journal of Computational Chemistry* **2023**. DOI: 10.1002/JCC.2719

Benchmarking electronic structure methods for the cobalt porphyrin

Souza, J. R. (PG)^{*1}; Moraes, M. M. (PG)²; Aoto, Y. A. (PQ)²; Homem-de-Mello, P. (PQ)¹

jhonathan.souza@ufabc.edu.br

¹ Centro de Ciências Naturais e Humanas, Universidade Federal do ABC, Santo André, São Paulo, Brazil.

² Centro de Matemática, Computação e Cognição, Universidade Federal do ABC, Santo André, São Paulo, Brazil.

Keywords: Benchmarking, Electronic Structure, Excited-states, TDDFT, NEVPT2

INTRODUCTION

Electronic structure of porphyrins presents very interesting properties for the photochemistry application.^{1,2} Thus, calculations on the absorption spectrum of cobalt(II) porphyrin, using several density functionals (DFT) and multireference n-electron valence perturbation (NEVPT) theories are described. From this, the lowest-energy states of doublet and quartet spin multiplicities, the excited states that originate the Q and B bands of porphyrins, some higher-energy $\pi-\pi^*$ excitations and charge-transfer states, HOMO-LUMO gaps, and ionization potentials are investigated.

METHODS

Geometry optimization were done using TPSSh functional and def2-TZVP basis set, as implemented in ORCA software. BP86, B3LYP, TPSSh, OLYP, M06-L, PBE0, M06, CAM-B3LYP, ω B97X functionals were employed for TDDFT calculation of fifty vertical excitations for Co(II) porphyrin. TDA (default in Orca software) also was employed. Multireference calculations have been performed at the state specific NEVPT2 level of theory, together with cc-pVDZ-DK basis set and the active space of 15 electrons and 11 orbitals.

RESULTS

Figure 1: States energy diagram calculated by different DFT functionals.

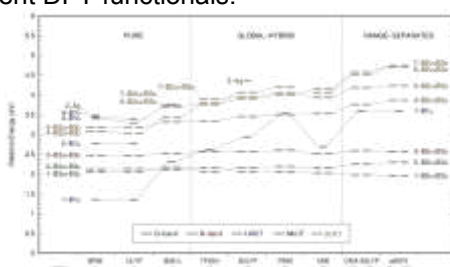


Figure 2: Alpha MOs energy diagram calculated by different DFT functionals.

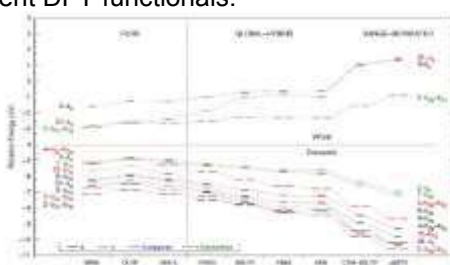
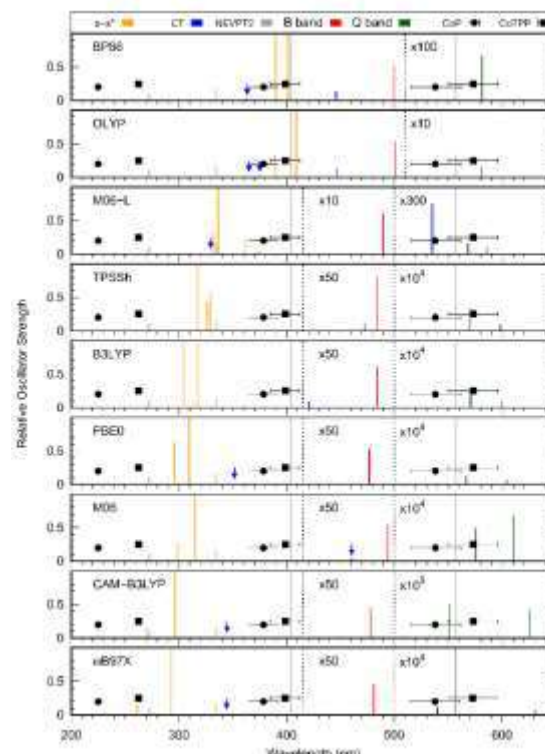


Figure 3: Absorption spectra calculated by means of TDDFT functionals and NEVPT2 method.



CONCLUSIONS

The difference between energy levels and orders depending on the methodology shows the difficulty to elucidate the electronic structure of this compound. Our results indicate that the main characteristics of porphyrins UV-Vis spectra, namely Q and B bands, depend exclusively on the macrocycle molecular orbitals. Among the methods employed here, NEVPT accurately predicts both bands, while for DFT, pure functionals are the most accurate to predict Q band, followed by the hybrid functionals. Range-separated functionals predicted Q-band partially in the expected energy range, but the band split is the largest when compared to other functionals.

REFERENCES

1. J. Mack et al., *J. Porph. Phthal.*, 2014, 18, 630-641.
2. J. M. Lopes et al., *Spectrochim. Acta*, 2019, 215, 327-333.

ACKNOWLEDGEMENTS

CAPES, FAPESP (#2018/25576-6, #2018/14629-1), UFABC



Complete basis set extrapolations of self-consistent field energies provided by new relativistic prolapse-free basis sets

Roberto Luiz A. Haiduke (PQ),^{1*} Julielson dos Santos Sousa (PG)¹

haiduke@iqsc.usp.br

¹Departamento de Química e Física Molecular, Instituto de Química de São Carlos, Universidade de São Paulo, Av. Trabalhador São-Carlense, 400, CP 780, 13560-970 – São Carlos, SP, Brasil

Keywords: CBS extrapolation, Relativistic Gaussian basis sets, SCF energies, Variational prolapse.

INTRODUCTION

Strategies for attaining accurate energies are now widespread in electronic structure studies. In general, these techniques are based on extrapolation equations that provide estimates of self-consistent field (SCF) and correlation energies at the complete basis set (CBS) limit. However, although such CBS extrapolations are quite common in non-relativistic investigations, there are specific difficulties with this respect in relativistic quantum chemistry calculations. For example, the variational prolapse affects the proper description of inner core electrons by basis sets and causes the obtaining of energies that may be lower than the exact values in the worst-case scenario.¹ Nevertheless, the absolute energies are not reliable even in less severe variational prolapse situations. Therefore, CBS extrapolations of basis sets with variational prolapse are frequently doomed to provide unrealistically low absolute electronic energies. Since 2006, new research has shown that it is really possible to design prolapse-free basis sets that remain compact as well by means of a polynomial version of the Dirac-Fock method (p-GCDF).² Hence, a quadruple-zeta quality set (RPF-4Z) was firstly developed.³ Recently, primitive sets were generated⁴ to provide even smaller relativistic prolapse-free basis sets of double- and triple-zeta quality (RPF-2Z and RPF-3Z, respectively), which is a work still in progress. Here, we investigate the capability of the RPF-XZ family of basis sets in providing accurate CBS estimates of SCF energies in relativistic calculations respecting the Dirac-Fock limit.

METHODS

The Dirac-Fock-Coulomb (DFC) calculations have been done within the DIRAC 23 package.⁵ The default Gaussian model is chosen for the finite-nucleus representation. The small component integrals (SS|SS) are fully considered in the calculations to a proper comparison with reference results from numerical methods.⁶ The small component functions are generated from the large ones by default kinetic balance conditions. Two customary power law equations were considered in the CBS extrapolations done here to provide DFC energy values at this limit (E_{CBS}),⁷

$$E_{SCF}(X) = E_{CBS} + AX^{-3} \quad \text{or}$$

$$E_{SCF}(X) = E_{CBS} + A(X + \frac{1}{2})^{-4},$$

where X is the basis set cardinal number (X = 2, 3, and 4 for the RPF-XZ family) and A is a parameter. Hence, these CBS estimates require at least two DFC calculations. Alkaline earth metals, noble gases up to Radon and small molecules (HF, N₂, H₂O, H₂S, and BH₃) are considered in this study.

RESULTS

Here, we investigated two approaches to test the power law CBS extrapolations. First, we evaluate linear regressions done by using DFC results from the three RPF-XZ sets. The coefficients of determination (R^2) were considered. Next, we used only the DFC values from pairs of sets to evaluate E_{CBS} : [1] RPF-2Z and RPF-3Z (2Z,3Z), and [2] RPF-3Z and RPF-4Z (3Z,4Z).

The linear regressions showed excellent R^2 values, which are always larger than 0.92, with E_{CBS} results from intercepts deviating at most by 3.5 mHartree from reference data.⁵

Next, the E_{CBS} values from the (2Z,3Z) pair present errors smaller than 4.5 mHartree, while those from the (3Z,4Z) pair show only deviations up to 2.2 mHartree.

CONCLUSIONS

The power law extrapolations are adequate for describing SCF energies from the RPF-XZ sets. Thus, the new prolapse-free family of relativistic basis sets discussed here is able of providing very accurate CBS extrapolations of DFC energies compared to reference numerical data.

REFERENCES

- ¹ H. Tatewaki, Y. Mochizuki, TCA, 2003, 109, 40.
- ² R.L.A. Haiduke, A.B.F. da Silva, JCC, 2006, 27, 61.
- ³ T.Q. Teodoro, A.B.F. da Silva, R.L.A. Haiduke, JCTC, 2014, 10, 3800.
- ⁴ E.F. Gusmão, R.L.A. Haiduke, JCC, 2022, 43, 1901.
- ⁵ T. Saue *et al.*, JCP, 2020, 152, 204104.
- ⁶ (a) L. Visscher, K.G. Dyall, At. Data Nuc. Data Tables, 1997, 67, 207; (b) J. Anderson, B. Sundahl, R. Harrison, G. Beylkin, JCP, 2019, 151, 234112.
- ⁷ (a) T. Helgaker, W. Klopper, H. Koch, J. Noga, JCP, 1997, 106, 9639; (b) J.M.L. Martin, CPL, 1996, 259, 669.

AKNOWLEDGEMENTS

CAPES (88887.658222/2021-00), CNPq (306763/2021-4), and FAPESP (2022/05138-0).

Hammett's Analysis of Substituent Effects in Functionalized Diketopyrrolopyrrole (DPP) Systems

Gabriel Monteiro-de-Castro (PG),¹ Itamar Borges Jr.(PQ).^{1*}

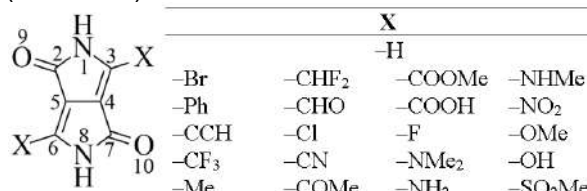
gabriel.castro@ime.eb.br; itamar@ime.eb.br

¹ Departamento de Química, Instituto Militar de Engenharia (IME), Rio de Janeiro, RJ, 22290-270, Brazil.

Keywords: Diketopyrrolopyrrole; Organic photovoltaics; Hammett's theory; Substituent effects; Optoelectronics.

INTRODUCTION

Diketopyrrolopyrrole (DPP) has drawn much attention due to its potential in optoelectronic applications, showing that it can broaden the absorption spectra and increase intra-charge transfer (ICT), especially in organic photovoltaics (OPV).¹ DPP-based materials have strong absorption and emission ability, excellent thermo- and photostability, good charge mobility, and significant Stokes shift.² Binding substituent groups to a DPP core is easily achievable^{2b} and provides changes in the optical and charge transport properties.³ We studied the substituent effects using Hammett's theory (HT), which furnishes constants (σ) that quantify the ability of the substituent to donate or withdraw electrons.⁴ HT has been shown to have a wide range of chemical applications.⁵ We focused here on employing HT to DPP-X systems and investigated the correlation between different σ and different opto- and electrochemical properties of these systems (Scheme 1).



Scheme 1. Investigated DPP-based systems.

METHODS

Our machine-Learning (ML)-based σ constants were used.⁶ B3LYP-D3/Def2-TZVP geometry optimization and vibrational frequency calculations were carried out on different monomers of mono-(DPP-X₁) and di-substituted (DPP-X₂) DPP-X derivatives. Gas-phase CAM-B3LYP/Def2-TZVP TDDFT excited state vertical calculations were also done. All calculations were employed ORCA 5.0.1.

RESULTS

We computed essential parameters for evaluating photovoltaic systems such as the power conversion efficiency (PCE) and the open-circuit voltage (V_{OC}). According to our results, the values of V_{OC} can be directly related to the different σ constants; the best results are in Figure 1.⁷ It is seen that larger σ values, corresponding to electron-withdrawing substituents lead to larger

values of V_{OC} . The PCE is a function, among other parameters, of V_{OC} . The correlation between the ML-based σ and the PCE values for a DPP-based OPV device can be used for designing new donor and acceptor materials for OPVs by allowing the selection of the most promising substituents.

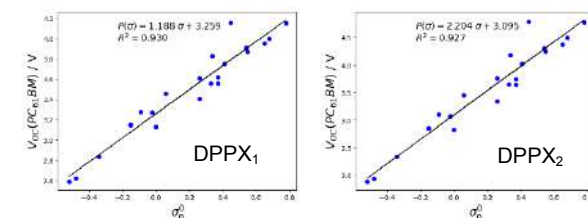


Figure 1. Best correlations V_{OC} and ML-based Hammett's constants.

Presently, we are working on similar properties of extended DPP-X polymers as well as investigating DPP-X stacking systems in the framework of HT. These results will be presented at the Symposium.

CONCLUSIONS

We found relevant correlations of OPV with different types of Hammett's constants. In particular, higher the values of σ constants correlate with the higher the values of PCE and V_{OC} , which shows a way of developing new materials with promising properties.

REFERENCES

- R. Jin, X. Zhang, W. Xiao and A. Irfan, *Theor. Chem. Acc.*, 2018, 137, 145.
- (a) D. C. Young, M. Tasior, A. D. Laurent, Ł. Dobrzycki, M. K. Cyrański, N. Tkachenko, D. Jacquemin and D. T. Gryko, *J. Mater. Chem. C Mater.*, 2020, 8, 7708-7717; (b) W. Li, L. Wang, H. Tang and D. Cao, *Dyes and Pigments*, 2019, 162, 934-950.
- J. Dhar, D. P. Karothu and S. Patil, *Chemical Communications*, 2015, 51, 97-100.
- (a) L. P. Hammett, *Chem. Rev.*, 1935, 17, 125-136; (b) L. P. Hammett, *J. Chem. Phys.*, 1937, 4, 613-617.
- A. Jezuita, K. Ejsmont and H. Szatłowicz, *Struct. Chem.*, 2021, 32, 179-203.
- G. Monteiro-de-Castro, J. C. Duarte, I. Borges Jr., *J. Org. Chem.*, 2023, DOI: 10.1021/acs.joc.3c00410.
- G. Monteiro-de-Castro, I. Borges Jr., *J. Comp. Chem.*, 2023, DOI: 10.1002/jcc.27195

ACKNOWLEDGMENTS

CNPq, FAPERJ, and CAPES.



Cálculos de Química Quântica Computacional: Auxiliando na Detecção de Cianopoliínos Presentes no Meio Interestelar

ANDERS, Gilberto (PG),¹ SILVA FILHO, Eloi Alves (PQ).^{1*}

prof.gilberto.anders@gmail.com; eloisilv@gmail.com

¹Departamento de Química, Universidade Federal do Espírito Santo

Palavras-Chave: Astroquímica Teórica, Meio Interestelar, Cianopoliínos, Química Quântica Computacional, Constante Rotacional.

INTRODUÇÃO

A composição química do Meio Interestelar (MIE) é de interesse dos astroquímicos. O MIE constitui cerca de 10% da matéria do universo observável, e é caracterizado por baixas densidades e temperaturas.¹ A Astroquímica começou em 1963 com a detecção do radical OH, e desde então mais de 200 moléculas foram detectadas no MIE². Avanços na radioastronomia impulsionaram a Astroquímica e estudos têm se concentrado na distribuição da matéria e na presença de moléculas como "traçadores" de gases. Algumas espécies químicas do MIE têm um papel importante em reações químicas na Terra. A identificação de espécies químicas no MIE geralmente envolve comparação de espectros com moléculas conhecidas em laboratório. Em alguns casos, previsões teóricas e cálculos *ab initio* e semiempírico são usados³. As constantes rotacionais são parâmetros espectroscópicos importantes e podem ser obtidas por cálculos de Química Quântica Computacional⁴. As espécies químicas estudadas nesse trabalho pertencem a um grupo chamado de Cianopoliínos, cuja fórmula geral é HC_nN (com n = 3, 5, 7...). Os cinco primeiros Cianopoliínos da série já foram identificados no MIE (HC₃N, HC₅N, HC₇N, HC₉N, HC₁₁N). Os outros quatro Cianopoliínos estudados ainda não foram identificados no MIE (HC₁₃N, HC₁₅N, HC₁₇N e HC₁₉N). Cálculos de Química Quântica Computacional podem ser utilizados para auxiliar na detecção desses e de outros Cianopoliínos ainda não identificados no MIE.

MÉTODOS

As geometrias dos nove Cianopoliínos foram otimizadas no nível de teoria DFT/B3LYP/6-311G++(df,pd), com o software GAMESS-US⁵. Para fins de comparação entre métodos teóricos, também foi utilizado o método semiempírico PM7, com o software MOPAC-2016⁶. Os nove Cianopoliínos estudados foram separados em dois conjuntos. Cinco dessas moléculas (que compuseram o "conjunto de correlação"), foram usadas para propor modelos de correlação, relacionando constantes rotacionais teóricas e

experimentais, com propriedades moleculares teóricas, especificamente: massa da molécula; momento de inércia; e comprimento entre os átomos das duas extremidades de cada molécula. As outras quatro moléculas (que compuseram o "conjunto de teste"), foram usadas para verificar a validade dos modelos de correlação propostos.

RESULTADOS

De acordo com os resultados obtidos, existe uma alta correlação entre a constante rotacional com: o comprimento molecular; o momento de inércia; e a massa da molécula.

A correlação entre a constante rotacional com o comprimento da molécula, com o momento de inércia, e com a massa da molécula, foram obtidos, respectivamente, R² = 1, R² = 1 e R² = 0,9999.

CONCLUSÕES

Neste trabalho os nove primeiros membros da família de Cianopoliínos foram estudados por meio de cálculos de Química Quântica Computacional (*ab initio* e semiempírico).

Os resultados mostraram que a partir das constantes rotacionais calculadas, foi obtida uma alta correlação com o comprimento molecular, momento de inércia e massa da molécula.

Espera-se que essa correlação se estenda às espécies de maiores massas dessa família de moléculas, e que possa auxiliar na possível detecção dessa e de outras espécies químicas similares no espaço interestelar.

REFERÊNCIAS

- ¹ MACIEL, W. J., 2002.
- ² WOON, D. E.; HERBST, E., 2009, vol. 185, pg. 273-288.
- ³ BRYCE, M.R., 2021.
- ⁴ TRABELSI, T.; et al., 2023, pg. 10, 949:55, 2023.
- ⁵ SCHMIDT, M.W., et al., 1993, 14, 1347-1363.
- ⁶ STEWART, J.J.P., 2016.

AGRADECIMENTOS

À CAPES, CNPq, FAPES e UFES.

IntRotPy: A Fast Routine for Calculation of the Thermodynamic Data from the Internal Rotation Motion.

Mateus Fernandes Venâncio (PQ)¹

mateus.venancio@ufba.br¹

¹Departamento de Físico-Química, Instituto de Química, Universidade Federal da Bahia, Salvador, Brasil.

Palavras Chave: Internal rotation, Statistical Thermodynamics, Density Functional Theory, Python.

INTRODUCTION

Internal rotation is a fundamental molecular motion that is often neglected in calculating thermodynamic properties. This work presents a Python code that calculates thermodynamic data from the potential energy surface (PES) of a dihedral angle.

METHODS

Our code calculates the eigenvalues for the internal rotation from a PES using a code developed in Python. The PES data are fitted as a Fourier series. The Hamiltonian matrix is then constructed as a circulant determinant due to the periodicity of the internal rotation movement. The eigenvalues are then calculated, and the partition function is obtained and used to compute the macroscopic thermodynamic data. The implementation follows the protocol developed in our previous work¹.

RESULTS

Our preliminary data were obtained for simple systems such as H₂O₂, C₂H₆, and C₂H₅OH. We will present here the simpler case: hydrogen peroxide. Figure 1 presents the PES for the rotation of the HOOH dihedral.

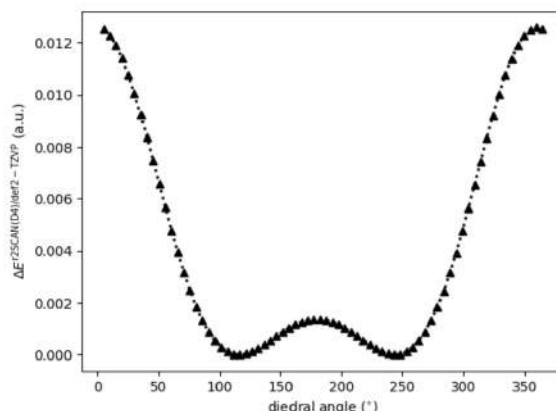


Figure 1. PES for H₂O₂ at the r2-SCAN(D4)/def2-TZVP level of theory.

The absolute values of entropy are shown in Table 1. It is possible to observe that the entropy value obtained from routine calculations which use the harmonic oscillator (OH) and the Rigid Rotor (RR) approximations are less than 1 cal mol⁻¹ K⁻¹ below the experimental value. Using the entropy

value from our code it is possible to increase the prediction to an excellent agreement with experimental data within the experimental deviation.

Table 1. Absolute entropy (in cal mol⁻¹ K⁻¹) for H₂O₂ at r2-SCAN(D4)/def2-TZVP.

Motion	S (cal mol ⁻¹ K ⁻¹)
Translational	36.49
Rotational	16.64
Vibrational	1.27
Total (OH + RR)	54.40
Internal rotation	1.37
Total	55.77
Experimental ²	55.79 ± 0.12

The entropy increase in other species (C₂H₆ and C₂H₅OH) is also observed. The first species has its entropy increased from 54.37 (OH + RR) to 54.64 cal mol⁻¹ K⁻¹ (expt. 54.86 ± 0.12 cal mol⁻¹ K⁻¹)³ and the increase in ethanol value is from 64.46 to 66.52 (expt. 66.53 cal mol⁻¹ K⁻¹)⁴.

Now, we are testing the code for other systems and different computational methods in order to evaluate the influence of the PES on the thermodynamic data.

CONCLUSIONS

Our results agreed with the investigated molecules' experimental standard gas phase entropy. This program allows the acquisition of molecular properties at a low computational cost at relatively fast calculations.

REFERENCES

- ¹Venâncio, M.F.; Dos Santos, H.F.; De Almeida, W.B.;
- ²Giguère, P.A., Liu, I.D., Dugdale, J.S., Morrison, J.A., Canadian Journal of Chemistry, 32 (2) 1954
- ³Kemp, J.D., Pitzer, K.S., J. Am. Chem. Soc., 59 (2) 1937.
- ⁴Gurvich, L.V.; Veyts, I. V.; Alcock, C. B., Thermodynamic Properties of Individual Substances, Fourth Edition, Hemisphere Pub. Co., New York, 1989

ACKNOWLEDGEMENTS

The author acknowledges Prof. Tiago Vinicius Alves (UFBA) for the valuable discussions and Prof. Willian Ricardo Rocha (UFMG) for permitting the utilization of his computational resources.

Unraveling the interaction of a 5-halouracil series with silver nanoparticles through SERS and DFT calculations.

Antonio Morais Neto (PG)¹, Paula Homem-de-Mello (PQ)¹, Mónica Benicia Mamián-López (PQ)¹

antonio.morais@ufabc.edu.br

¹Centro de Ciências Naturais e Humanas, UFABC, Santo André.

Keywords: SERS, biosensors, plasmonics, RNA, DFT

INTRODUCTION

The DNA and RNA bases and their derivates are widely studied and applied in diverse bio-related areas. Among them, the 5-halouracils, 5-XU (uracil with a halogen substituent at the C5 position) have come to attention recently due to their mutagenic activity and as antitumor agents or biomarkers.¹ Besides, they have a high affinity for nanostructured noble metals, allowing studying them through surface-enhanced Raman spectroscopy, SERS.¹ Understanding the nature of these interactions and the factors tuning them allows the optimization of plasmonic-based biosensors. Computational simulations based on Density Functional Theory (DFT) are essential for a deepening comprehension of how the activated sites of molecules behave in the presence of metallic surfaces and their impact on SERS spectra.² This work compares the DFT-calculated SERS spectra of a 5-XU (X= F, Cl, Br) series on a silver cluster (Ag_{20}) to the corresponding experimental SERS spectra. The results shown here are on the path to optimizing biosensing methodologies based on plasmonic materials.

METHODS

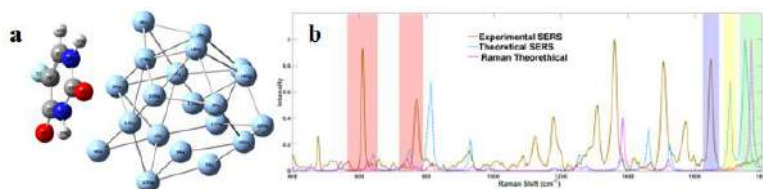
The three 5-XU compounds were optimized in gas phase and on the Ag_{20} cluster, following the strategy and structure proposed by Seuret-Hernández *et al.* (2022).³ The protocol was adapted to include dispersion correction by using WB97XD functional. The DFT simulations were performed in Gaussian09 software, and LANL2DZ basis set. Vibrational calculations were performed to ensure that the structures were a minimum and to obtain Raman and SERS spectra. The experimental SERS spectra were acquired in a Renishaw InVia confocal Raman microscope ($\lambda_0=532\text{nm}$, 20x objective lens).

RESULTS

Various characteristic vibrational modes were identified by comparing the 5-XU series' experimental and theoretical SERS spectra (Fig

1). The interactions Ag---O=C and Ag---H-C=C can be described by vibrational modes below 400 cm^{-1} , which is not feasible for the experimental approach. However, intense bands were found in the $600\text{-}800\text{ cm}^{-1}$ region (pyrimidine ring deformation and ring breathing), highlighted in red, and in $1500\text{-}1800\text{ cm}^{-1}$ (C=O and C=C stretching), highlighted in blue (experimental), highlighted yellow, and green (theoretical). So, the adsorbed structure obtained (Fig. 1a) and the analysis of the theoretical spectra indicated that the bands in the region $1700\text{-}1800\text{ cm}^{-1}$ could guide the definition of the interaction site, that is, the adsorption through C=O of 5-FU on AgNPs. This behavior is also observed for 5-CIU and 5-BrU as well but in different orientations.

Figure 1 - (a) Optimized Structure 5-FU- Ag_{20} cluster; **(b)** Experimental and theoretical SERS for 5-FU-AgNP and theoretical Raman spectrum for 5-FU.



CONCLUSION

From DFT calculations, it's possible to understand the preferential interaction between 5-halouracil and the AgNPs due to the intensification of the vibrational modes in $1700\text{-}1800\text{ cm}^{-1}$. Moreover, even though the adsorption site is the same for all the halouracils, the orientation is different. This will be explored in more detail in further experimental works.

REFERENCES

¹Dobrowoloski, J.C. *et al*, J. Phys. Chem. A, 2005, 109, 2167.

²Muniz-Miranda, M. *et al*, Molecules, 2023, 28, 573.

³Seuret-Hernández, H. Y *et al*, J. Mol. Graphs. Model., 2022, 115, 108234.

ACKNOWLEDGMENTS

UFABC, Central Experimentais Multiusuário (CEM-SA) CAPES, CNPq, FINEP, and LEM-USP.

Theoretical calculation of pKa of indirubin: unexpected high acidity explains its easy deprotonation followed by S_N2 reaction

Eloah P. Ávila (PD),^{1*} Josefredo R. Pliego Jr. (PQ),² Ana Flávia S. Fuzaro (PG),¹ Gabriela L. P. Suhett (IC),¹ Richard M. Grazul (PQ),¹ Mauro V. de Almeida (PQ)¹

*eloahavila@ice.ufif.br

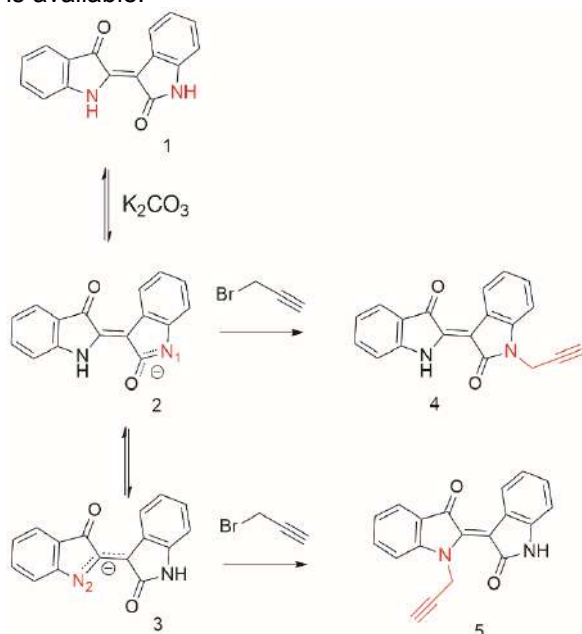
¹Chemistry Department, Federal University of Juiz de Fora (UFJF)

²Natural Science Department, Federal University São João del-Rei (UFSJ)

Keywords: Indirubin, DFT,

INTRODUCTION

Indirubin (**1**) is a bioactive alkaloid and a promising prototype for new drugs. The insertion of triazole ring derivatives to its skeleton may delineate a new approach to solving problems related to its low bioavailability and improved biological properties. A strategy to incorporate triazole requires an initial propargylation of indirubin (Scheme 1). Recently, we have found that a moderate K₂CO₃ base is able to deprotonate Indirubin in DMSO, and the corresponding anion can be alkylated via S_N2 reaction as presented in the Scheme 1. However, this easy deprotonation is intriguing, because normal amides and amines have pKa values around 25 and 30, respectively, in DMSO solution.¹ This unexpected property of indirubin prompted us to investigate its pKa in DMSO solution by theoretical calculations, because no experimental data is available.



Scheme 1: Deprotonation of indirubin in two positions, followed by S_N2 reaction.

METHODOLOGY

Geometry optimizations and frequency calculations were performed at PCM/B3LYP/6-31G(d,p) level of theory in DMSO solution. Single point energy

and solvation calculations were done at ωB97X-D/6-311G+(d,p) level using the PCM model in DMSO, with atomic cavities defined by the Bondi radii and scale factor of 1.35. These cavities have a good performance for pKa calculation in DMSO.² The pKa of the HA acid was determined by the proton exchange scheme, though the equations:



$$pK_a(\text{HA}) = pK_a(\text{HB}) + \frac{\Delta G_{pe}}{1.364}$$

Where HB is the anchor species, with available pKa.

RESULTS

The calculations of the pKa of indirubin in the N1 and N2 positions, using H₂O, CH₃COOH and CH₃CONH₂ species as anchor, are presented in the Table 1.

Table 1: Calculated pKa values

Position	Anchor species	pKa (DMSO)
N1	H ₂ O	16.4
N2	H ₂ O	19.3
N1	CH ₃ COOH	18.0
N2	CH ₃ COOH	20.9
N1	CH₃CONH₂	14.9
N2	CH₃CONH₂	17.8

The results in Table 1 shows a range of 3 pKa units, depending on the anchor species. We consider that acetamide is the best anchor because is most similar to indirubin. Thus, our best estimate indicates pKa values in N1 and N2 position as being 14.9 and 17.8 units, respectively.

CONCLUSIONS

The present results show that the pKa values of indirubin at N1 and N2 positions in DMSO solution are indeed much smaller than the corresponding amides and amines, explaining its deprotonation by K₂CO₃.

REFERENCES

- ¹F. G. Bordwell, *Acc. Chem. Res.*, 1988, **21**, 456.
- ²G. I. Almerindo, D. W. Tondo and J. R. Pliego Jr, *J. Phys. Chem. A*, 2004, **108**, 166.

ACKNOWLEDGMENT

FAPEMIG, CNPq and CAPES for the support.



O Método da Equalização da Eletronegatividade na Derivação de Cargas: Aplicações em Dinâmica e Termodinâmica de Líquidos Iônicos

Jonathan B. Brum (PG),¹ Cauê T. O. G. Costa (PQ),¹ Luciano T. Costa (PQ)^{1*}.

jonathanbrito@id.uff.br; ltcosta@id.uff.br.

¹Instituto de Química – Universidade Federal Fluminense

DFT, EEM, Eletronegatividade, Líquidos Iônicos, Físico-Química.

INTRODUÇÃO

Os líquidos iônicos são amplamente estudados na literatura por possuírem propriedades físico-químicas únicas, sendo aplicados como solventes em síntese, catálise e dispositivos eletroquímicos. Para o estudo das propriedades desses compostos puros e suas misturas, modelos não polarizáveis e polarizáveis tem sido explorados ao longo de décadas. Como são espécies formadas em grande parte por cátions orgânicos e ânions inorgânicos ou orgânicos, estes possibilitam uma combinação superior a 10^8 espécies, das quais se estima apenas menos de 10^3 até então investigadas.¹ Neste trabalho, explorou-se a utilização do Método da Equalização da Eletronegatividade (EEM²), aplicado a Teoria do Funcional da Densidade (DFT) e método semiempírico *xTB*³, bem como o pacote de dinâmica molecular (GROMACS⁴), combinado com o kit de ferramentas quântica Psi4⁵ para o cálculo de diversas propriedades de íons isolados. Além disso foram desenvolvidas rotinas em Python com o objetivo de gerar automatização, organização e assim facilitar a análise dos resultados.

MÉTODOS

Uma base de dados contendo 161 cátions e 65 ânions, todos de líquidos iônicos, foi utilizada. Os sistemas, em sua forma isolada em fase gás, tiveram suas geometrias otimizadas, com posterior cálculo de frequência e análise populacional para obtenção de propriedades eletrônicas, elétricas, entre outras (como energia de ionização, afinidade eletrônica, diferença entre HOMO e LUMO e etc.), realizados pelo software *xTB*. Paralelamente a isso, otimizações das geometrias no nível de teoria B3LYP/aug-cc-pVTZ tal como o cálculo do potencial eletrostático dos íons isolados foram realizadas utilizando o kit de cálculos quânticos Psi4 aliada ao pacote de dinâmica molecular GROMACS, seguindo o protocolo do *Alexandria Chemical Toolkit*⁶. Atualmente estão sendo realizados cálculos de *singlepoint* e otimização para as combinações de N cátions e N ânions em diferentes posições e aproximações de íon e contra-íon que estarão concluídos até o evento. Tais sistemas serão analisados em comparação com bancos de dados presentes na literatura, como também serão utilizados modelos estatísticos de modo a comparar as propriedades *singlepoint* como

também a distribuição de cargas entre os íons isolados e os potenciais eletrostáticos.

RESULTADOS

Tendo em vista o volume molecular presente nos líquidos iônicos, o banco de dados possuiu ênfase em cátions derivados de ciclos nitrogenados, aromáticos ou não, como também estruturas iônicas menores. Os cátions de alto volume molecular a serem otimizados foram em sua grande maioria derivados imidazolio, pirrolidinio, piridinio e morfolinio, enquanto os de baixo volume molecular amônio, sulfônio, fosfônio e guanidinio. Os ânions foram derivados de sulfonato, amida, fosfato além de diversos haletos. Foram realizados cálculos de 13 propriedades *singlepoint* para todas as 226 estruturas. Além disso foram gerados 82 superfícies de potenciais eletrostáticos, com foco nas estruturas mais comuns na literatura.

CONCLUSÕES

Foi possível estimar as propriedades eletrônicas e elétricas, bem como estruturais e termodinâmicas dos íons investigados. Em perspectiva futura deseja-se gerar uma série de descritores quânticos para futuras aplicações de modo a explorar as combinações de cátions e ânions e dessa forma alcançar a melhor descrição do ambiente químico desses sistemas iônicos pouco explorados, servindo assim de *dataset* para aplicações de modelos de Aprendizado de Máquina e parametrização de campos de força polarizável para simulações de Dinâmica Molecular.

REFERÊNCIAS

- 1 R. Vekariya, Journal of Molecular Liquids, 2016, 227. 44-60.
- 2 W. Mortier et al. Journal of the American Chemical Society. 1985, 107. 829–835.
- 3 S. Spicher, S. Grimme, Angewandte Chemie, 2020, 132. 15795–15803.
- 4 H. Bekker et al. Physics computing, 1993, 92. 252-256.
- 5 D. Smith et al. The Journal of Chemical Physics, 2020, 152. 184108.
- 6 M. Ghahremanpour et al. Scientific Data, 2018, 5. 180062.

AGRADECIMENTOS

Ao órgão de fomento CAPES; Ao Grupo de Modelagem Molecular e Simulação Computacional pelo uso de suas instalações.



Estudo teórico e cinético das principais etapas do mecanismo de reação do HPA criseno com radicais nitrato na atmosfera.

Renan Santos Serpa (IC),¹ Camilla Alves Neves Leite (IC),² Tadeu Leonardo Soares e Silva (PQ).^{1*}

Tadeu.leonardo@fat.uerj.br

¹Universidade do Estado do Rio de Janeiro- Faculdade de Tecnologia- Laboratório de Química Computacional da Faculdade de Tecnologia. Avenida Dr Omar Dibo Calixto Afrange km 304 (Pólo Industrial), no sentido RJ-SP.
Palavras Chave: (Criseno, HPA, DFT, Radical, Nitrato).

INTRODUÇÃO

HPAs (Hidrocarbonetos policíclicos aromáticos) são conhecidos mundialmente pelos seus potenciais efeitos mutagênicos e carcinogênicos e são emitidos ao meio ambiente principalmente pela via de processos de combustão de motores a diesel. A USEPA (Agência de Proteção Ambiental dos Estados Unidos), definiu 16 HPAs como poluentes prioritários e um deles é o criseno.

O criseno é um dos HPAs mais tóxicos e cancerígenos e não se sabe ainda o mecanismo para a reação com o radical nitrato, sendo assim o escolhido para estudo¹.

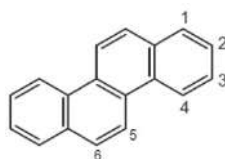
O radical nitrato, é formado na atmosfera durante a noite pela reação de ozônio com moléculas NOx, e sofre decomposição sob a luz solar².

Neste projeto, investigou-se de forma teórica a adição do radical nitrato com o objetivo de posteriormente comparar as constantes de velocidade calculadas teoricamente, com as obtidas experimentalmente, e propor um mecanismo reacional para esta reação.

MÉTODOS

Inicialmente foram otimizadas as geometrias dos reagentes criseno e NO₃, e dos estados de transição (TS), em nível DFT, com os funcionais BHandHLYP e M062X com as bases 6-311++G(d,p) e cc-pVDZ, no programa Gaussian 16³. Cada ponto de sela possuiu uma frequência imaginária, posteriormente sendo confirmadas pelo cálculo de coordenada intrínseca de reação (IRC).

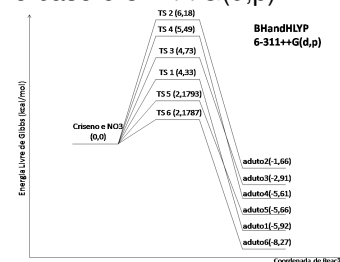
Abaixo temos as posições de ataque no HPA criseno.



As constantes de velocidade foram calculadas utilizando a seguinte equação: $k = (kb^*T/h) \exp(-\Delta G^*/RT)$ em que kb é a constante de Boltzman, h é a constante de Planck, T é 298,15 K, R é a constante dos gases e ΔG é a energia de ativação de Gibbs. Constante calculada para o estado padrão de 1mol/L.

RESULTADOS

A seguir temos o perfil de energia livre de Gibbs, com a coordenada de reação, para a adição de radicais nitrato no HPA criseno, em BHandHLYP e base 6-311++G(d,p).



A seguir a tabela com as constantes de velocidade calculadas teoricamente em cm³/(molécula*s). Os valores experimentais são de 10¹¹ e 10¹² cm³/(molécula*s).

	BHandHLYP/ 6-311++G(d,p)	BHandHLYP/ cc-pVDZ	M062X/ 6-311++G(d,p)	M062X/ cc-pVDZ
Maior barreira	3,07.10 ⁻¹³	9,81.10 ⁻¹⁴	2,02.10 ⁻¹²	1,34.10 ⁻¹³
Menor barreira	2,62.10 ⁻¹⁰	5,20.10 ⁻¹¹	1,68.10 ⁻⁹	9,55.10 ⁻¹¹

CONCLUSÕES

A reação de adição de radicais nitrato e o criseno, pode apresentar 6 adutos diferentes. A partir dos resultados, foi possível calcular a constante de velocidade da reação elementar da adição do radical nitrato no criseno, com posterior comparação com resultados experimentais e assim propiciar a elucidação do mecanismo reacional. Os resultados foram muito satisfatórios.

REFERÊNCIAS

- Silva, T. L. S.; Cruz, B.S.S.; Correa, S.M. **Estudo teórico-experimental das emissões de hidrocarbonetos policíclicos aromáticos E derivados de motores diesel.**
- ZHAO, NAN; SHI, XIANGLI; XU, FEI et al. **Theoretical investigation on the mechanism of NO₃ radical-initiated atmospheric reactions of phenanthrene.** Journal of Molecular Structure, v. 1139, p. 275-281, 2017.

- ³Gaussian. Expanding the limits of computational chemistry. Disponível em: <<http://gaussian.com>>. Acesso em: 31 ago. 2019.

AGRADECIMENTOS

Ao CNPq pelas bolsas de iniciação científica.
SABALCORE COMPUTING INC.

Modelos de Formação de Glicolaldeído no Meio Interestelar (ISM)

Hemilly Oliveira Souza (PG)^{1*}, Glauco F. Bauerfeldt (PQ)¹, Neubi Francisco Xavier Jr. (PQ)²

hemillyoliveirasouza@gmail.com

¹ Universidade Federal Rural do Rio de Janeiro, Brasil; ² University of Surrey, England.

Palavras Chave: Glicolaldeído, Astroquímica, Silicato

INTRODUÇÃO

Descobertas recentes de compostos essenciais à vida, a exemplo do carbono,¹ fósforo,² aminoácidos³ e açúcares⁴ em ambiente astroquímico, tem incentivado a comunidade científica a buscar os caminhos que possam desvendar os mistérios sobre a origem da vida. O Glicolaldeído - GLA (HCOCH_2OH) é considerado o membro mais simples da classe dos monossacarídeos. Devido a sua abundância no meio interestelar (ISM), vários estudos teóricos foram propostos para investigar a síntese de GLA em fase gasosa e em superfícies, especialmente em silicato cósmico amorfo.⁵ Porém, estudos recentes têm demonstrado a vasta abundância de silicatos cristalinos no ISM, ressaltando a necessidade de novos estudos nessas superfícies.⁶ Neste trabalho, reportamos um estudo teórico das propriedades cinéticas e termodinâmicas de reações elementares que leva a síntese do GLA em fase gasosa e em superfície de silicato cristalino (forsterita) no ISM.

MÉTODOS

Para a fase gasosa, cinco reações elementares foram investigadas (Tabela 1) em nível CCSD(T)/M06-2X/aug-cc-pVTZ+ZPE. Os coeficientes de velocidade foram calculados com o programa KCVT em uma faixa de temperatura entre 50 e 500 K. Para o estudo em superfície, o slab periódico foi montado assumindo energia de corte de 90 Ry e pontos k (3.3.1). Cálculos teóricos foram realizados no programa QUANTUM ESPRESSO, usando DFT com a aproximação de gradiente generalizado (GGA), adotando o funcional PBE com USPP. Atingindo o modelo de superfície e determinando o modo de adsorção de menor energia, caminhos de reação foram obtidos através de cálculos CI-NEB.

RESULTADOS

O estudo conformacional revelou a conformação *cis* de GLA como a de menor energia. Os resultados apresentados na Tabela 1 e confirmados pelas constantes de velocidade, sugerem que R3, R4 e R5 são os canais mais prováveis para a formação de GLA.

A rota R5 foi investigada em superfície de silicato cristalino e os modos favoráveis de energia de

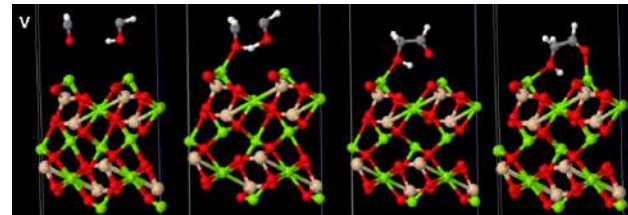
adsorção de H_2CO e HCOH revelaram cinco caminhos reacionais, partindo de reagentes fisisorvidos e/ou quimisorvidos.

Tabela 1. Diferenças de energia (ΔE° , kcal/mol) e barreiras ($V^\#$, kcal/mol) de reação obtidas em nível CCSD(T)/aug-cc-pVTZ//M06-2X/aug-cc-pVTZ+ZPE.

	Reação	ΔE°	$V^\#$
R1	$\text{CO} + \text{CH}_3\text{OH} \rightarrow \text{HOCH}_2\text{CHO}$	0,75	86,1
R2	$\text{H}_2\text{O} + \text{CH}_2\text{CO} \rightarrow \text{HOCH}_2\text{CHO}$	-5,25	77,1
R3	$\text{HCO} + \text{CH}_2\text{OH} \rightarrow \text{HOCH}_2\text{CHO}$	-78,9	-
R4	$\text{OH} + \text{CH}_2\text{CHO} \rightarrow \text{HOCH}_2\text{CHO}$	-85,3	-
R5	$\text{H}_2\text{CO} + \text{HCOH} \rightarrow \text{HOCH}_2\text{CHO}$	-73,2	10,1

Os resultados sugerem três rotas que levaram a formação de GLA, sendo que a rota V apresentou a formação de GLA fortemente adsorvida à superfície, com $E_{\text{ads}} = -205,03$ kcal/mol, partindo de reagentes fisisorvidos na superfície (Figura 1).

Figura 1. Caminho reacional da rota V para a síntese de Glicolaldeído



CONCLUSÕES

O presente estudo suporta a síntese de GLA em fase gasosa e em superfície no ISM por meio de reação entre H_2CO e HCOH , com baixas barreiras energéticas. A rota inédita de formação de GLA em silicato cristalino de forsterita revela uma nova possibilidade de síntese astroquímica desse composto, portanto com profundas implicações na química pré-biótica.

REFERÊNCIAS

- ¹O. Berné *et al.*, Nature, 2023, p. 1-3
- ²F. Postberg *et al.*, Nature, 2023, v. 618, p. 489-493
- ³S. Iglesias-Groth *et al.*, MNRAS, 2023, v. 523, p. 2876–288
- ⁴Y. Furukawa *et al.*, PNAS, 2019, v. 116, n. 49, p. 24440-24445.
- ⁵F. Kemper *et al.*, ApJ, 2004, v. 609, p. 826
- ⁶DO-DUY *et al.*, MNRAS, 2020, v. 493, p. 4463-4517

AGRADECIMENTOS

À FAPERJ, CAPES e LNCC-SINAPAD – Santos Dumont (sdumont-chamadas/paper220119).



KINETICS OF ENVIRONMENTAL BIOCOMPLEXITY: EXPERIMENTS, QUANTUM CHEMISTRY AND MACHINE LEARNING

Flávio Olimpio Sanches-Neto (PQ),^{1,2,3*} Kleber Carlos Mundin (PQ),¹ Valter Henrique Carvalho-Silva (PQ).^{1,2}

flavio.neto@ifg.edu.br

¹ Instituto de Química, Universidade de Brasília, Caixa Postal 4478, Brasília 70904-970, Brazil;

² Modeling of Physical and Chemical Transformations Division, Theoretical and Structural Chemistry Group, Goiás State University, Anápolis 75132-903, Brazil;

³ Instituto Federal de Educação, Ciência e Tecnologia de Goiás, Valparaíso de Goiás, GO, 72876-601, Brazil.

Keywords: *Machine learning, Reaction rate constant, deformed-Transition State Theory.*

INTRODUCTION

Micro-pollutants of emerging concern have imposed a major technological challenge: pesticides, drugs, and other anthropogenic substances are increasingly found in aquatic and atmospheric environments and even in water supplies, being related to adverse effects on biota and human health [1-2]. Overcoming this challenge requires understanding the behavior of these species in the environment and developing technologies that minimize their dissemination. Theoretical chemical kinetics, combined with machine learning, can be useful for understanding and predicting the behavior of emerging micro-pollutants in the environment [3-5]. This can help develop more effective technologies to minimize their dissemination and negative impacts. With this knowledge, it is possible to optimize processes for the degradation of organic pollutants, making them more efficient and economical.

METHODS

Viable alternatives applied in this thesis include the use of radical-based oxidation processes using both experimental – via the competition kinetics method – and theoretical protocols – blend of kinetic, quantum chemistry, and machine learning calculations.

In this study, the *deformed-Transition State Theory* was used to compute the values of the reaction rate constant. Gaussian 16 software was employed to perform quantum chemistry calculations. Machine learning models were used to train the data, including XGBoost, Random Forest, and MLP.

RESULTS

In a first study, the mechanisms, kinetics, and an evaluation of the toxicity of picloram degradation – a pesticide widely used in the world - initiated by OH radicals indicate that: i) two favorable pathways occur by addition to the pyridine ring, ii) picloram and the majority of degradation products are estimated as harmful; however, ii) these compounds can suffer photolysis by sunlight.

However, the competition kinetic method and the quantum chemistry description make the degradation analyses a formidable enterprise, considering the costs of ad hoc instrumental equipments and dedicated computational efforts. To overcome the demanding conventional procedures, we developed a free and user-friendly web application (www.pysirc.com.br) based on holistic machine learning combined with molecular fingerprints models that permits the compilation of kinetic parameters and mechanistic interpretation of radical-based oxidation attacks according to the OECD principles. Machine learning algorithms were implemented, and all models provided high goodness-of-fit for radical-based degradation in aquatic and atmospheric environments. The models were interpreted using the SHAP (SHapley Additive exPlanations) method: the results showed that the model developed made the prediction based on a reasonable understanding of how electron-withdrawing/donating groups interfere in the reactivity of the radicals.

CONCLUSIONS

We argue that our models and web interface can stimulate and expand the application and interpretation of kinetic research on contaminants in water and air treatment units based on advanced oxidative technologies. By providing an accessible and user-friendly platform, researchers and practitioners can easily apply our models to their own data, facilitating the development of more effective and efficient treatment strategies for emerging micro-pollutants.

REFERENCES

- ¹ MEI, Qiong et al, CEJ, 2019, 373, 668-676.
- ² WILKINSON, John L. et al., PNAS, 2022, 119, 2113947119.
- ³ SANCHES-NETO, Flávio O. et al., Chemosphere, 2021, 278, 130401.
- ⁴ SANCHES-NETO, Flávio O. et al., ES&T, 2021, 55, 12437-12448.
- ⁵ SANCHES-NETO, Flávio O. et al., Atmos. Environ., 2022, 275, 119019.

ACKNOWLEDGMENT

We would like to express our gratitude to IFG, UEG, CAPES, and FAPEG for the support provided in this study.

Alkylation of Amines with Alkyl Bromides: Explaining the low selectivity

Luis F. Resende (PG),¹ Josefredo R. Pliego Jr. (PQ).^{1*}

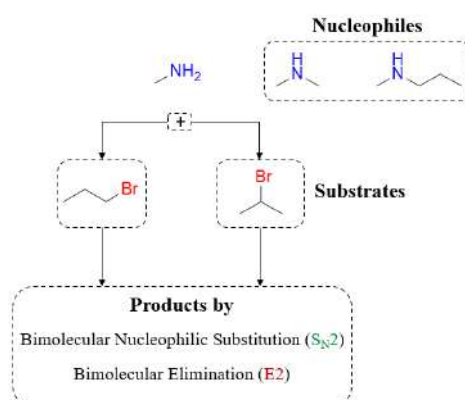
Luis.f.q.resende@gmail.com; pliego@ufsj.edu.br

¹Departamento de Ciências Naturais (DCNat), Universidade Federal de São João del-Rei (UFSJ), São João del-Rei, Minas Gerais, Brasil CEP 36301-160.

Keywords: S_N2 , $E2$, Solvent effects, Free energy profile.

INTRODUCTION

Simple aliphatic amines represent an important class of organic compounds whose applications are extensive. One of the most conceptually simple and traditional methods for obtaining alkylamines is the S_N2 N-alkylation with alkyl halides to generate higher alkylated aliphatic amines. However, it is widely recognized that such reactions have major disadvantages in terms of selectivity, being difficult to limit the reaction to the monoalkylation.¹ In this work, we have investigated the free energy profile for N-alkylation of simple amines with alkyl bromides to better understanding this limited selectivity.



Scheme 1: Relationship between nucleophiles and substrates investigated, as well as the chemoselectivity of the reactions.

METHODS

Geometry optimizations were done with the X3LYP functional and the def2-SVP basis set. Diffuse functions (ma-def2-SVP) were included for the N and Br atoms. The optimizations have included the solvent effect (acetonitrile) via CPCM method. Single point energy calculations were done with the wB97X-D3/ma-def2-TZVPP level of theory. The solvation free energy was calculated by SMD/X3LYP method. The free energy in solution was obtained by: $G_{sol} = E_{ele} + G_{vrt} + \Delta G_{solv}$. Standard state of 1 mol L⁻¹ and 25°C.

RESULTS

The free energy profile for the reaction of each nucleophile and substrate was determined. Figure 1 presents the results for methylamine reaction with 1-bromopropane. The results have indicated that all reactions have high

chemoselectivity for S_N2 versus $E2$ competition, with the formation of resulting S_N2 ion pairs being the main reaction products. As the substrate changes from primary to secondary bromide, the elimination pathways become more competitive (reduction of 1.3 and 3.3 kcal mol⁻¹ for TS-E2anti e TS-E2syn, respectively, for methylamine). An important finding is that the dimethylamine ($\Delta G_{sol}^\ddagger = 24.9$ kcal mol⁻¹) is more reactive than methylamine ($\Delta G_{sol}^\ddagger = 25.6$ kcal mol⁻¹) towards S_N2 reaction with 1-bromopropane. This fact indicates that as the monoalkylation takes place, the following alkylation becomes more feasible, generating dialkylated product. Thus, a mixture of products is formed even using one equivalent of the alkylating agent. A possibility to induces selectivity would be designing nanostructured environment able to better stabilize the transition state for monoalkylation.²

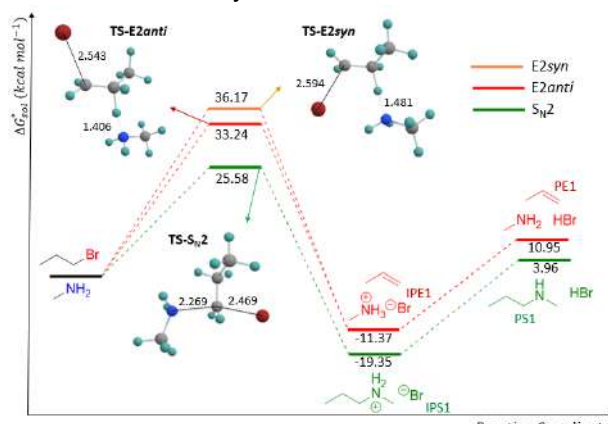


Figure 1: Free energy profile in solution for the reaction between methanamine and 1-bromopropane.

CONCLUSIONS

The free energy profiles in solution indicates that the highest reactivity is obtained with dimethylamine. Thus, more substitution on the amine increases its reactivity, decreasing the selectivity of the alkylation and generating mono and dialkylated products.

REFERENCES

- S. Bhattacharyya, U. Pathak, S. Mathur, S. Vishnoi and R. Jain, *RSC Advances*, 2014, **4**, 18229.
- J. R. Pliego Jr, *Phys. Chem. Chem. Phys.*, 2011, **13**, 779.

ACKNOWLEDGMENT

CNPq, FAPEMIG and CAPES.

Decision trees for coordination chirality in metal complexes

Gabriel H. L. Munguba (R)^{1*}, Mateus F. da Silva (UR)¹, Frederico T. Silva (R)¹, Gabriel A. Urquiza-Carvalho (R)¹, Alfredo M. Simas (R)¹
gabriel.munquba@ufpe.br

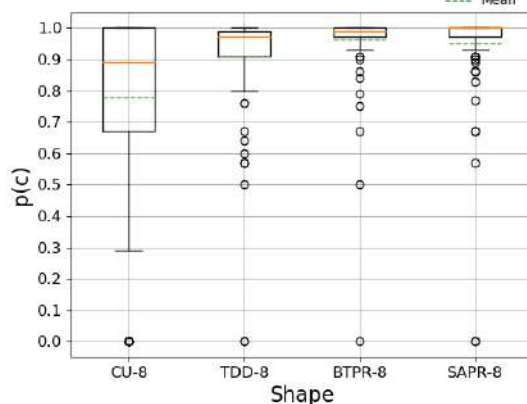
¹ Departamento de Química Fundamental, Universidade Federal de Pernambuco, Recife, PE, Brazil

Keywords: chiral lanthanide complexes, chiral-at-metal probabilities, decision trees, coordination compounds.

INTRODUCTION

Molecular chirality is widely present in nature and plays a crucial role in essential biochemical processes. Chiral coordination complexes are compelling due to their unique electromagnetic responses, with f-block metal elements showing superior chiroptical properties compared to carbon atoms. For instance, among hundreds of potential generic formulas for an eight-coordinated complex with mono- and/or bi-dentate ligands (CN-8), the likelihood of obtaining a random chiral-at-metal stereoisomer is remarkably high for most of them. The boxplots below illustrate this probability for the most common CN-8 coordination polyhedral shapes (CP), many exhibiting values above 90%, considering only permutational factors. Regions inside the rectangles cover half of all formulas.

Figure 1 – Boxplots for the most common CN-8 polyhedral shapes illustrating the chiral-at-metal probabilities.



METHODS

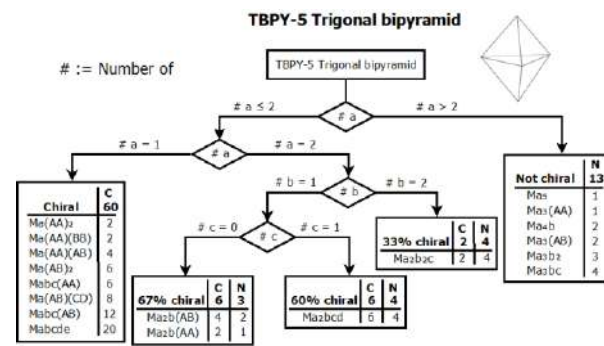
Polya's method and Haigh's approach were used to determine the number of chiral stereoisomers in coordination polyhedra with different shapes and ligand arrangements, as introduced by Silva *et al.* (2018)¹. The probability of whether a coordination compound structure of a particular shape is chiral becomes a function of the particular generic molecular formula, and of the symmetry elements of the point group of its coordination polyhedron.

RESULTS

The decision trees indicate that the primary factor impacting the probability of a coordination complex being chiral-at-metal is the maximum number of identical monodentate ligands, "# a". Indeed, lower

"# a" promote a higher chance for chirality due to the implied diversity of other ligand types. Additionally, bidentate ligands, both symmetric AA and asymmetric AB, also contribute to higher chiral probabilities by triggering helicoidal arrangements around the metal center. For this abstract, we show a very simple example: the decision tree for the trigonal bipyramidal shape geometry (TBPY-5).

Figure 2 – Decision tree for the trigonal bipyramidal (TBPY-5) shape of coordination polyhedron.



Based on the flowchart, it can be inferred that a TBPY-5 metal complex is incapable of exhibiting metal-centered chirality if the condition "# a > 2" is fulfilled. But, if the alternative condition "# a ≤ 2" is met, further assessments are necessary. In particular, if the condition "# a = 1" is satisfied, any coordination complex represented by the generic formulas on the leftmost terminal node is expected to display chirality at the metal center.

CONCLUSIONS

We introduce a robust mathematical framework to determine the probability of coordination chirality in metal complexes, based on their generic chemical formula and polyhedral shape. Our novel decision trees reveal a relevant finding: a substantial number of crystallographic structures of lanthanide complexes are likely to display chirality at the metal center, a characteristic that is frequently disregarded. Remarkably, this relevant property is indeed rarely recognized, notwithstanding its significant technological implications.

REFERENCE

¹ F. T. Silva, S. L. S. Lins, A. M. Simas, *Inorg. Chem.* 2018, 57, 17, 10557–10567.

ACKNOWLEDGMENTS

CNPq, FACEPE, CAPES and PRONEX.

Inclusion of paraoxon, parathion, and methyl parathion into α -cyclodextrin: a GFN2-xTB multi-equilibrium quantum study.

Jonathan Campos Marcelino¹, Carolina Lúcia Cardoso Ribeiro¹, Gleicy Teixeira¹, Erick Ferreira Lacerda¹, Cleber Paulo Andrade Anconi^{1*}

jonathan.marcelino@ifsudestemg.edu.br; cleberanconi@ufa.br

¹Laboratório de Química Fundamental (LQF), Department of Chemistry, Institute of Natural Sciences, University of Lavras, Lavras-MG, 37200-900, Brazil

Keywords: CD-based host–guest systems, GFN2-xTB semiempirical method, Binding constant, UD-APARM, Pesticides

INTRODUCTION

Cyclodextrins (CDs) comprise a family of cyclic oligosaccharides produced by an enzymatic process. They can accommodate guest molecules in their cavities to form inclusion compounds. This property makes CDs suitable for application in environmental protection. These compounds have been shown to efficient as a pesticide complexing agent. The knowledge of host–guest binding constants is important, as it generally controls the efficiency of remediation process¹.

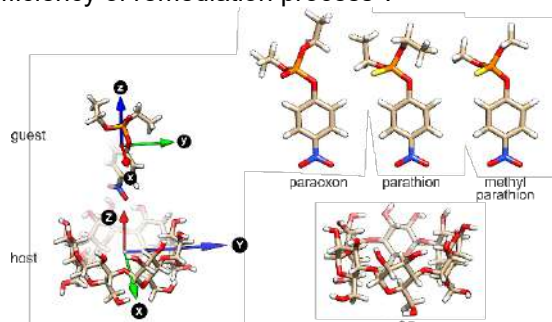


Fig. 1 Right, UD-APARM axes of inertia for individual molecules in a supramolecular system formed with a CD (host) and a guest to evaluate the relative position and rotation. Left, pesticides and α -CD structure.

METHODS

- Each system was studied considering more than 792 possible inclusion positions.
- The UD-APARM program was used to build these systems².
- The GFN2-xTB method was employed to obtain theoretical data³.
- After optimizations and determination of free Gibbs energy, in condensed phase, log K values were obtained for the inclusion compounds PRX@ α -CD, PTN@ α -CD and MPTN@ α -CD.

RESULTS

Pesticide	Systems	Log of binding constant			Error
		K _{xTB}	K _{EXP} ⁴	Adjusted	
PRX	16	4.20	1.92	1.95	2%
MPTN	10	4.49	2.28	2.22	3%
PTN	06	5.10	2.77	2.79	1%

Table 1. Equilibrium constants obtained by the semiempirical method GFN2-xTB ($\log K_{xTB}$)

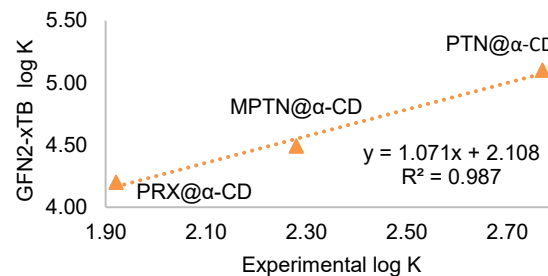


Fig. 2 - Linear correlation between experimental and theoretical binding constants for including PRX, MPTN, and PTN pesticides with α -CD.

CONCLUSIONS

The small error associated with adjusted data attests to the robustness of the UD-APARM/GFN2-xTB implementation in association with the ALPB continuum solvent model that gives valuable information if the searching protocol identified the representative supramolecular arrangements in a multi-equilibrium scope for CD-based systems.⁵

REFERENCES

- 1 Landy, D.; Mallard, I.; Ponchel, A.; Monflier, E.; Fourmentin, S. Remediation technologies using cyclodextrins: an overview. *Environmental Chemistry Letters* **2012**, *10* (3), 225-237. Review. DOI: 10.1007/s10311-011-0351-1.
- 2 Anconi, C. P. A. Relative Position and Relative Rotation in Supramolecular Systems through the Analysis of the Principal Axes of Inertia: Ferrocene/Cucurbit 7 uril and Ferrocenyl Azide/beta-Cyclodextrin Case Studies. *Acs Omega* **2020**, *5* (10), 5013-5025. DOI: 10.1021/acsomega.9b03914.
- 3 Bannwarth, C.; Ehler, S.; Grimme, S. GFN2-xTB-An Accurate and Broadly Parametrized Self-Consistent Tight-Binding Quantum Chemical Method with Multipole Electrostatics and Density-Dependent Dispersion Contributions. *Journal of Chemical Theory and Computation* **2019**, *15* (3), 1652-1671. DOI: 10.1021/acs.jctc.8b01176.
- 4 Kamiya, M.; Mitsuhashi, S.; Makino, M. CATALYTIC PROPERTIES OF CYCLODEXTRINS ON THE HYDROLYSIS OF PARATHION AND PARAOXON IN AQUATIC MEDIUM CONTAINING HUMIC ACIDS. *Chemosphere* **1992**, *25* (12), 1783-1796. DOI: 10.1016/0045-6535(92)90019-n.
- 5 Marcelino, J. C.; Ribeiro, C. L. C.; Teixeira, G.; Lacerda, E. F.; Anconi, C. P. A. Inclusion of paraoxon, parathion, and methyl parathion into α -cyclodextrin: a GFN2-xTB multi-equilibrium quantum study. *Journal of Inclusion Phenomena and Macrocyclic Chemistry* **2023**. DOI:10.1007/s10847-023-01192-3.

ACKNOWLEDGMENTS

The authors thank Professor Hélio Ferreira dos Santos, the Laboratório Central de Computação Científica (LCC) of UFLA for providing additional computing resources. Furthermore, professor Cleber Paulo Andrade Anconi also thanks the Fundação de Amparo à Pesquisa do Estado de Minas Gerais (FAPEMIG) for supporting the Laboratório de Química Fundamental (LQF), where the research was conducted.

Reatividade e Estabilidade de Clusters de $(\text{TiO}_2)_n$, $n = 1 - 8$.

Letícia C. S. Faria (PG),¹ Gabriel F. S. Fernandes (PQ),¹ Leonardo T. Ueno (PQ),¹ Luiz F. A. Ferrão (PQ).^{1*}
leticiacarolaine@ita.br; ferrao@ita.br

¹ Instituto Tecnológico de Aeronáutica (ITA), Divisão de Ciências Fundamentais, Departamento de Física, Departamento de Química, 12228-900, São José dos Campos, SP, Brasil.

Palavras-Chave: Clusters, Função estabilidade, Índices de reatividade, DFT Conceitual.

INTRODUÇÃO

A busca por moléculas/clusters com elevada estabilidade é de grande interesse no desenvolvimento de nanodispositivos.¹ Hoje em dia, clusters com poucos átomos, e propriedades magnéticas e eletrônicas altamente ajustáveis podem ser sintetizados em escala laboratorial.¹ Como parte do objetivo de desenvolver clusters de TiO₂ como photocatalisadores para redução de CO₂, o presente estudo faz uma prospecção sobre as propriedades de pequenos aglomerados de dióxido de titânio. Para isso, comparamos suas estabilidades e reatividades por meio de índices obtidos a partir de suas funções de onda / densidades eletrônicas, considerando a função estabilidade (ϵ^3) e índice de reatividade ($\Delta\omega^\pm$),^{2,3} e os relacionando com as energias de adsorção de CO₂.

MÉTODOS

A função estabilidade ϵ^3 é utilizada para ranquear a estabilidade de espécies químicas, se baseando em parâmetros moleculares derivados da estrutura eletrônica, que se divide em descritores cinéticos e termodinâmicos. Para clusters, o ϵ^3 é capaz de identificar números mágicos em concordância com resultados experimentais.² Os descritores cinéticos são: potencial de ionização (E_I) e energia de excitação eletrônica (T_e), o descritor termodinâmico é a variação da energia livre de atomização (ΔG_{atom}). A função é expressa da seguinte forma:

$$\epsilon^3 = |E_I| \times |T_e| \times |\Delta G_{atom}|$$

O índice de eletrofilicidade relativa ($\Delta\omega^\pm$), estima a capacidade de uma molécula em atuar como um eletrófilo por meio de um balanço entre a capacidade da molécula em doar ou receber elétrons. Os cálculos foram realizados usando o método DFT na aproximação B3LYP com o conjunto base de Pople 6-31G(d). Os parâmetros de estabilidade foram comparados com a energia de adsorção (E_{ADS}) de CO₂ nos $(\text{TiO}_2)_n$.

RESULTADOS

Conforme mostrado na Figura 1a, os índices de estabilidade e reatividade apresentaram comportamentos complementares, sendo que os aglomerados com $n=2$, 4 e 7 devem corresponder

a números mágicos, ou seja, sistemas com elevada estabilidade e baixa reatividade. Na Figura 1b verifica-se que as energias de adsorção de CO₂ acompanham a estabilidade, com exceção do aglomerado mais estável ($n=7$).

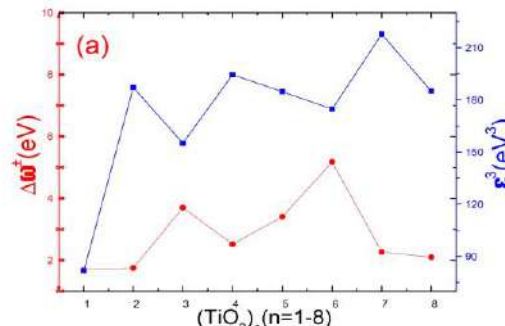


Figura 1a: Estabilidade e reatividade dos clusters de TiO₂ estudados.

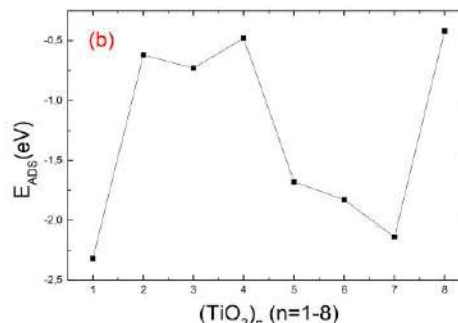


Figura 1b: Energia de adsorção do CO₂ nos clusters de TiO₂ estudados.

CONCLUSÕES

Observa-se que os parâmetros de estabilidade e reatividade demonstram certa concordância com as energias de adsorção. As próximas etapas envolvem avaliar a aparente discordância no caso do $(\text{TiO}_2)_7$, em especial através de estudos acerca da estabilidade local dos clusters.

REFERÊNCIAS

- ¹ P. Jena, A. Castleman, PNAS, 2006, 103, 10560 –10569.
- ² G. F. S. Fernandes *et al.*, J. Phys. Chem. A, 2020, 124, 454-463.
- ³ T.-H. Wang *et al.*, J. Phys. Chem. C, 2011, 115, 9344-9360.

AGRADECIMENTOS

O presente trabalho foi realizado com apoio da Coordenação de Aperfeiçoamento de Pessoal de Nível Superior - Brasil (CAPES) - Código de Financiamento 001.

Morphogenesis in Synthetic Chemical Cells

Leonardo Silva-Dias (PG) & Alejandro Lopez-Castillo (PQ).

leonardosilvadias@estudante.ufscar.br

Chemistry Department, Federal University of São Carlos, São Carlos, São Paulo 13 565-905, Brazil.

Key words: Symmetry breaking, chemical and physical differentiation, active droplets, self-organization in chemistry.

INTRODUCTION

The earliest theoretical description of morphogenesis was proposed by Alan M. Turing in his seminal 1952 article.[1] In this paper, Turing presents a model that is particularly applicable for a heterogeneous ring of discrete compartments, i.e., cells.[2] Even though, this model is relevant in biology it cannot be used for making predictions in this context due to the difficulties of comparison of experiment and theory.[2-3] To overcome this problem, researchers reported an experimental reaction-diffusion system for testing Turing's theory of morphogenesis. Such a system is formed by synthetic "cells", i.e., aqueous droplets containing the Belousov-Zhabotinsky (BZ) chemical reactants, stabilized by surfactant in dispersed oil.[2] The main point in such a construction is that most of the chemical species in the BZ reaction are polar, remaining trapped in the cells. However, less polar intermediates can diffuse through the oil medium, acting as chemical signals.[2] Considering the experimental setup exposed previously and the general theory of chemically active droplets [4], we present in this work a continuous heterogeneous model for describing morphogenesis and the emergence of spatiotemporal structures.[3] Through the 2D calculations, we find the six spatiotemporal structures predicted by Turing in 1952 and experimentally observed, in a 1D array of droplets. Moreover, under Turing instability, with a determined chemical wavelength, our model undergoes morphogenesis.[3]

MODEL

The Model proposed is the following [3]:

$$F[\phi] = \int d^2r \left[-\frac{\beta}{2}(\phi - \psi)^2 + \frac{\alpha}{4}(\phi - \psi)^4 + \frac{k}{2}|\nabla\phi|^2 \right]$$

$$\frac{\partial\phi}{\partial t} = \eta k(-a + u) + \nabla \cdot \left(m\nabla \frac{\delta F[\phi]}{\delta\phi} \right)$$

$$\frac{\partial u}{\partial t} = f(u, v) - c_2u + d_2w_2 + (D_u^{(P)}\frac{\phi}{\Phi} + D_u^{(N)}(1 - \frac{\phi}{\Phi}))\nabla^2 u$$

$$\frac{\partial v}{\partial t} = g(u, v) - c_1v + d_1w_1 + (D_v^{(P)}\frac{\phi}{\Phi} + D_v^{(N)}(1 - \frac{\phi}{\Phi}))\nabla^2 v$$

$$\frac{\partial w_1}{\partial t} = (c_1v - d_1w_1)\Theta(r) + (D_{w_1}^{(P)}\frac{\phi}{\Phi} + D_{w_1}^{(N)}(1 - \frac{\phi}{\Phi}))\nabla^2 w_1$$

$$\frac{\partial w_2}{\partial t} = (c_2u - d_2w_2)\Theta(r) + (D_{w_2}^{(P)}\frac{\phi}{\Phi} + D_{w_2}^{(N)}(1 - \frac{\phi}{\Phi}))\nabla^2 w_2.$$

with,

$$f(u, v) = k_1a - (k_4 + k_3b)u + k_2u^2v$$

$$g(u, v) = k_3bu - k_2u^2v$$

RESULTS

We obtained the six spatiotemporal states predicted by Turing, see Fig. 1, and observed morphogenesis under Turing instability, see Fig 2.

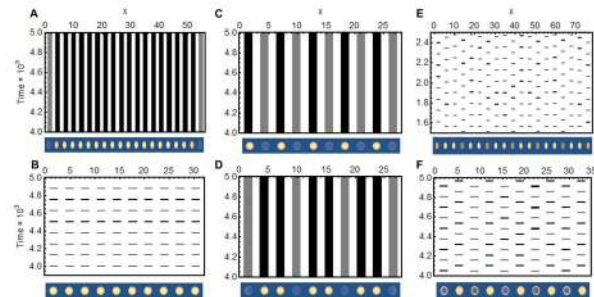


Fig.1: Space-time plots exposing the six cases predicted by Turing.

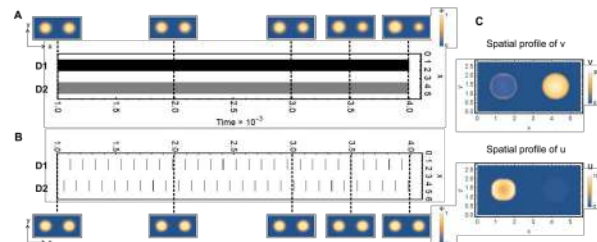


Fig.2: A) Morphogenesis. B) Oscillatory behavior does not induce morphogenesis. C) Spatial profile of the chemicals.

CONCLUSION

Through the proposed model, we have precisely shown that morphogenesis of these nonbiological cells follows a well-defined sequence of events: emergence of Turing patterns creating local asymmetries of the chemical processes, i.e., chemical differentiation, propagation of a significant difference of the osmotic pressure between the synthetic cells, generation of flows of solvent from the cell with lower osmotic pressure to the cell of higher osmotic pressure, and shape variation, i.e., physical morphogenesis.[3]

REFERENCES

- [1] Turing, A. M. Philos. Trans. R. Soc. Lond. **237**, 37 (1952).
- [2] Tompkins, N.; Li, N.; Girabawee, C.; Heymann, M.; Ermentrout, G. B.; Epstein, I. R.; Fraden, S. Proc. Natl. Acad. Sci. U. S. A. **12**, 4397 (2014).
- [3] Silva-Dias, L; Lopez-Castillo, A. J. Phys. Chem. Lett. **13.1**, 296 (2022).
- [4] Weber, C. A.; Zwicker, D.; Jülicher, F.; Lee, C. F. Rep. Prog. Phys. **82**, 064601 (2019).

ACKNOWLEDGMENTS

FAPESP, Grants 2019/12501-0 and 2019/23205-3, & CAPES, finance code 001.

Estudo Cinético das reações de combustão dos isômeros (Z) e (E) do buten-2-oato em baixas temperaturas.

Leandro da S Pereira (PG),^{1*} Glauco F Bauerfeldt (PQ),¹ Leonardo Baptista (PQ)².

leandroifr@gmail.com

¹Universidade Federal Rural do Rio de Janeiro. BR-465, Km 7 Seropédica-Rio de Janeiro; ²Universidade do Estado do Rio de Janeiro. Avenida Dr Omar Dibo Calixto Afrange, s/n, Rod. Pres. Dutra, km 303.

Palavras Chave: Ésteres, Combustão, Baixas temperaturas, DFT.

INTRODUÇÃO

As moléculas de ésteres metílicos estão na composição do biodiesel e de lubrificantes para serem usados nos motores à compressão. O uso desses produtos acarretam numa diminuição no consumo de combustíveis derivados do petróleo, porém, isso não cessa as emissões de poluentes.¹

A LTC (Low Temperature Combustion) busca diminuir as emissões de NOx e fuligem por realizar o processo de combustão a temperaturas mais baixas. Essa técnica faz uso de sistemas EGR (Exhaust Gas Recirculation), de máquina de compressão rápida e adição de oxidantes fortes, como por exemplo O₃ dentro da câmara de combustão.²

Devido o problema da emissões de NOx e fuligem e viabilizar o uso de um éster leve como um combustível sintético e/ou aditivo, este trabalho tem como objetivo o estudo termodinâmico e cinético da reação de ozonólise em baixas temperaturas dos isômeros (Z) e (E) do buten-2-enoato de metila.

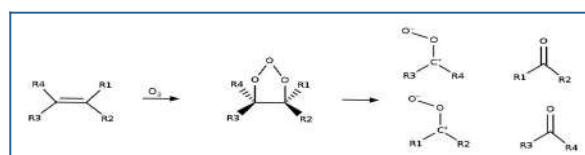
MÉTODOS

Foi feita uma análise conformacional nos isômeros E (crotonato de metila) e Z ((Z)-2-buteno-2-oato de metila). As conformações foram obtidos a partir na mudança dos ângulos diedros das moléculas.

As geometrias de todas espécies participantes do mecanismo foram otimizadas em nível M08-HX/aug-cc-pvtz.

As propriedades termodinâmicas foram calculadas a 298 K e 1 atm, considerando as aproximações do oscilador harmônico e rotor rígido. Os coeficientes de velocidade foram obtidos via Teoria do Estado de Transição (TST) convencional e variacional, na faixa de temperaturas de 270 a 820 K e a 1 atm.

Abaixo segue as etapas do mecanismo de Criegee estudada neste trabalho.



RESULTADOS

No total, foram obtidas sete conformações distintas, sendo quatro (E) e três (Z). Os isômeros de menor energia relativa se encontram na Figura 1.

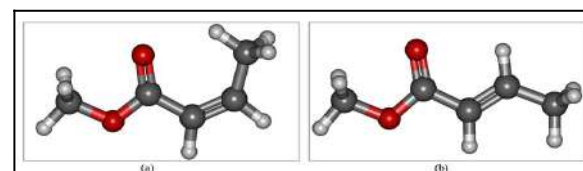


Figura 1. Estruturas de menor energia. Estrutura (a) isômero (Z), estrutura (b) isômero (E). M08-HX/aug-cc-pvtz

As geometrias dos estados de transição obtidas a partir das conformações de menor energia de cada isômero se encontram na Figura 2.

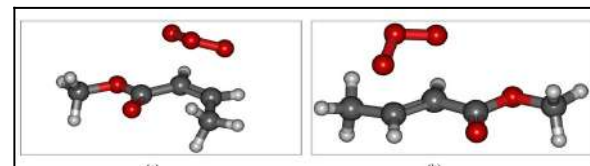


Figura 2. Estruturas de transição dos isômeros de menor energia. Estrutura (a) isômero (Z), estrutura (b) isômero (E). M08-HX/aug-cc-pvtz.

Os valores dos coeficientes de velocidade para reações de O₃ com os isômeros de menor energia foram 9.43X10⁻¹⁸ cm³/(molécula . s), para o isômero (Z), e 1.87X10⁻¹⁸ cm³/(molécula . s), para o isômero E, a 320 K e a 1 atm. Grosjean et al. (1993) relatou um coeficiente de velocidade (4,39 ± 0,29)X10⁻¹⁸ cm³/(molécula . s) a 291 K e a 1 atm.

CONCLUSÕES

Os resultados indicam que há relativa concordância com o resultado obtido na literatura. Atualmente estão sendo feitos cálculos para refinar os resultados.

REFERÊNCIAS

- ¹ Kerenkan, A. E. et al. Catal. Sci. Technol, 2016.
² Imtenan, S. et al. Energy Conversion and Management, 2014.

AGRADECIMENTOS

Agradecemos a CNPq, CAPES e FAPERJ.

Stability and Aromaticity in Chemically Modified (ma,nz ; $m=5,7/n=5-7$) Periacenes

Luan Gabriel Fonseca dos Santos (PG),¹ Julio Cesar Verli Chagas (PG),¹ Luiz Fernando de Araújo Ferrão (PQ),¹ Francisco Bolívar Correto Machado (PQ),^{1*}

fmachado@ita.br

¹Departamento de Química / Instituto Tecnológico de Aeronáutica

Palavras Chave: Polycyclic aromatic hydrocarbons, Electronic Structure, Organic semiconductors, Delocalization.

INTRODUCTION

Polycyclic aromatic hydrocarbons (PAH's) have been receiving attention in different scientific areas, since it can be used in several fields, especially as organic semiconductors. However, the description of their electronic properties poses challenges because they exhibit an open-shell character in their ground state¹. A possible alternative to decrease the high reactivity consists in modifying the structure by replacing carbon atoms/rings by other elements. Using this strategy, the present work investigates the stability and aromaticity of (ma,nz ; $m=5,7;n=5-7$) modified periacenes, by replacing the carbon periacene rings by boron and nitrogen rings. In the ma,nz configuration, a and z corresponds to armchair and zigzag ends.

METHODS

Figure 1 displays the two pristine systems, in addition to the seven hybrid models proposed. Considering all the mentioned sizes configurations, for each type of modification, a total of 54 different structures were generated.

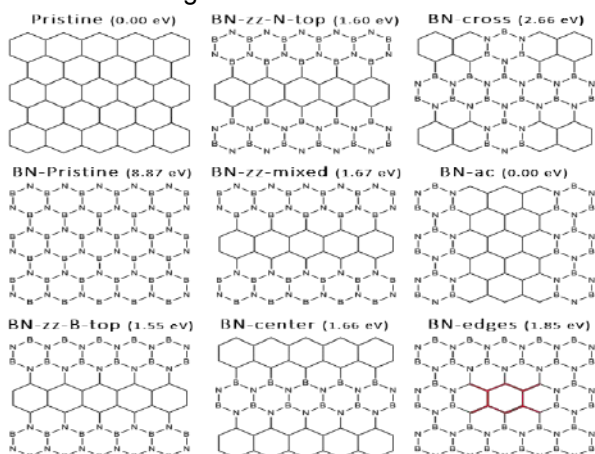


Figure 1: Illustration of the schematic ($5a,5z$) structures and their respective S-T splitting values, at MRCI level. The red lines indicate a substituted-like benzene, in the core of the BN-edges structure.

The geometry optimization for all structures were carried out through the Density Functional Theory (DFT), on a ω B97xD/6-31G* level, in the unrestricted version. Single-point calculations were performed with MCSCF, CASPT2, MRCI and MR-AQCC methods, to calculate the vertical singlet-triplet (S-T) splitting. For the stability, aromaticity,

radical character and charge transfer analysis, some other descriptors were used, such as the Fractional Occupation Number Weighted Electron Density (FOD)² and the Harmonic Oscillator Model of Aromaticity (HOMA index)³.

RESULTS

Compared to the pristine periacenes, the values of the S-T splitting significantly increase, especially when BN-rings were added on the zigzag borders, indicating an increase in stability. However, it is not the case for the BN-ac structures, in which the BN-rings are added on the armchair. The stability analysis observed via the S-T splitting were also observed by the FOD results, meaning that the numbers of fractional occupancy are smaller for all the proposed hybrid structures. As expected, it was also verified that the general aromaticity, indicated by the HOMA index, increases for the structures that presented higher S-T splitting values and lower values of unpaired electrons (N_{FOD}). The BN-pristine presents a S-T splitting around 7 eV (at MR-AQCC level) and a N_{FOD} close to zero, demonstrating its elevated closed-shell character.

CONCLUSIONS

Most of the proposed modifications increase the S-T splitting, decreases the number of fractional occupancy and increases general HOMA indexes, compared to the pristine periacenes. Therefore, the substitution of carbon rings by BN-rings is a way to generate more stable structures, with a S-T splitting in the visible range, which open the possibility to applications as organic semiconductors. Special attention needs to be taken when analyzing the ($5a,5z$) BN-edges structure, which has a substituted-like benzene ring in its core. This formation can be seen as four CH_2 connections, which diminishes the delocalization of π electrons in the center ring, turning the structure less stable than those with a smaller number of BN-rings.

REFERENCES

1. M. PITOŇÁK, et al., JCTC, 2008, 4. 1829-1834.
2. T. M. KRYGOWSKI, et al., Chem. Rev., 2001, 101. 1385-1420.
3. C. GRIMME, et al., Chem. Eur. J., 2017, 23. 6150-6164.

ACKNOWLEDGEMENTS

CAPES, CNPq, FAPESP.

Mechanisms Gold Nanoalloys Stabilization Through Ab Initio Calculations and Data Mining Tools

Lucas B. Pena (IC),^{1*} Lucas R. Da Silva (IC),² Breno R. L. Galvão (PQ)¹, Juarez L. F. Da Silva (PQ)²

lucas.bernardesp205@gmail.com

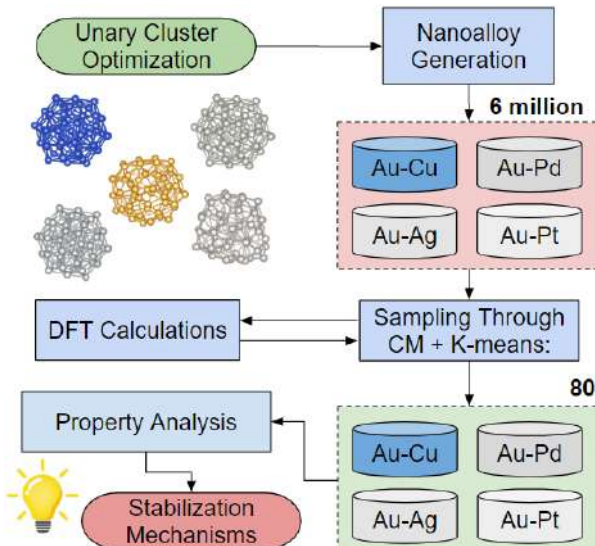
¹Centro Federal de Educação Tecnológica de Minas Gerais, Av. Amazonas 5253, Belo Horizonte, MG, Brasil, 30421-169; ²Instituto de Química de São Carlos, Universidade de São Paulo, PO Box 780, São Carlos, SP, Brasil, 13566-590.

Keywords: Nanocluster, Nanoalloy, K-Means, DFT.

INTRODUCTION

Metallic nanoclusters have emerged as a promising material due to their unique properties, resulting from quantum confinement effects, which depend on size, geometry and composition.^[1] Among these, gold nanoparticles stand out for their remarkable stability, biocompatibility, and infrared fluorescence. Exploiting these attributes, numerous applications have been envisioned, including biosensors, drug carriers^[2] and potential catalysts for CO₂ conversion and H₂ production.^[3] While pure gold clusters of 55 atoms have been previously synthesized in the laboratory,^[4] exploring gold nanoalloys could provide valuable insights to guide future research.

METHODOLOGY



The total energy of the systems was determined through ab initio calculations using the PBE-D3 method^[5,6] as implemented in the VASP software,^[7] employing the projector-augmented wave (PAW) approach.^[8] Initial configurations were proposed based on literature geometries for unary systems of each element. From these, a vast number of structures were generated through random and design-principles oriented permutations, resulting in a total of 6 million nanoalloy structures. The studied compositions were fixed as Au_(55-x)TM_x, where TM = Cu, Pd, Ag, Pt, and x = 6, 13, 20, 28, 35, 42, 49, with permutations achieved by replacing gold atoms with TM in the Au₅₅ cluster geometry and vice

versa. For structure sampling, the Coulomb Matrix molecular descriptor and the k-means grouping algorithm were utilized to select the most representative alloys per composition.^[9] Throughout this process, 2450 DFT-level geometric optimization calculations were performed, yielding the most stable structures, whose properties were analyzed for the understanding of the stabilization mechanisms.

RESULTS

The decreasing order of stability for the nanoalloy systems was Au-Cu, Au-Pd, Au-Ag, with Au-Pt being entirely unfavorable for any structure. The preferred structure for the unary (and alloy) Cu₅₅, Pd₅₅ and Ag₅₅ clusters was the symmetrical icosahedral geometry, while the amorphous structures of the unary Au₅₅ and Pt₅₅ showed lower stability. The most stable structures for the Au-Cu and Au-Pd exhibited core-shell conformations, with gold atoms on the surface. In the case of the Au-Ag system, the preferred design was an onion-like, with a central gold atom and an intermediate layer of silver atoms.

CONCLUSIONS

- The results corroborate the mechanism of alloy stabilization through charge transfer with the formation of an anionic surface and cationic core.
- Alloy stability is related to an increase in the difference of electronegativity between the metallic elements and compaction effects which reduces strain.
- The preference of gold atoms on the surface can be explained by its lower surface energy.

REFERENCES

- ¹ S. Maity, D. Bain, A. Patra, *Nanoscale*, 2019, 11, 22685.
- ² P. Yu, et al. *Part. & Part. Sys.* 2014, 32, 142.
- ³ X. Cai, et al. *ACS Catalysis*, 2022, 10638.
- ⁴ Z. Wang, R. Palmer, *Nano Lett.* 2022, 12, 5510.
- ⁵ J. Perdew, et al. *Phys. Rev. Lett.* 1996, 77, 3865.
- ⁶ S. Grimme, et al. *J. Chem. Phys.* 2010, 132, 154104.
- ⁷ G. Kresse, J. Hafner, *Phys. Rev.* 1993, B 48, 13115.
- ⁸ G. Kresse, D. Joubert, *Phys. Rev.* 1999, B 48, 13115.
- ⁹ F. Orlando, et al. *J. Chem. Infor. Mod.* 2021, 61 (7), 3411.

ACKNOWLEDGMENTS

CNPq (311508-2021-9), CINE, CAPES, FAPEMIG (APQ-00597-22), FAPESP (2017/11631 – 2; 2018/21401 – 7).

Polarização de novos conjuntos relativísticos de funções de base Gaussianas sem prolapo variacional de qualidade duplo- e triplo- ζ : elementos dos blocos s e p

Julielson dos Santos Sousa (PG),^{1*} Eriosvaldo Florentino Gusmão (PQ),¹ Prof. Dr. Roberto Luiz Andrade Haiduke (PQ)¹

julielson@usp.br; eriosvaldo.gusmao@alumni.usp.br; haiduke@iqsc.usp.br

¹ Departamento de Química e Física Molecular, Instituto de Química de São Carlos, USP, São Carlos, SP.

Palavras Chave: (*Cálculos multi-referenciais, Funções de polarização, Duplo- ζ , Triplo- ζ*).

INTRODUÇÃO

Em 1926, Dirac discutiu que os cálculos das propriedades de sistemas quânticos, como átomos e moléculas, seriam problemas de matemática aplicada [1]. A partir dessa premissa, ele formalizou a combinação da relatividade especial com a teoria quântica, estabelecendo assim a base da nova mecânica quântica. Quando aplicada ao tratamento de estrutura eletrônica com conjuntos de funções de base, a equação de Dirac apresenta desafios específicos. Um deles corresponde ao prolapo variacional [2], um problema normalmente associado à uma descrição deficiente da região mais próxima do núcleo que pode resultar em energias incorretamente inferiores aos valores exatos. O objetivo deste trabalho é atuar no desenvolvimento de novos conjuntos de base sem prolapo variacional, RPF-2Z e RPF-3Z.

MÉTODOS

Complementação dos conjuntos de funções Gaussianas primitivas através da adição de funções de correlação/polarização (C/P) escolhidas por meio de cálculos multi-referenciais de interação de configurações com excitações simples e duplas (MR-CISD) do espaço de valência dos átomos ou moléculas do tipo MH, estas últimas somente para hidrogênio e metais alcalinos. Um tratamento aproximado foi usado para tratar as integrais de repulsão intereletrônica entre funções do tipo *small* (SS|SS), que são geradas por meio de condições de balanço cinético. Os conjuntos de base foram sempre usados na forma descontraída. O programa computacional empregado foi o DIRAC 22 [3].

RESULTADOS

Primeiramente, o estudo envolveu a seleção do número adequado de funções a serem adicionadas aos conjuntos relativísticos sem prolapo variacional de funções primitivas Gaussianas de tamanhos pequeno e médio [4], ou seja, funções C/P para os blocos s e p dos seis primeiros períodos. Realizamos cálculos MR-CISD durante a incrementação do conjunto de base para escolher as funções C/P que resultam nas maiores reduções de energia. Assim, uma função d foi escolhida para compor o conjunto RPF-2Z dos átomos do bloco p. Esta função

possui expoente idêntico à de uma das funções s já disponíveis para os sub-blocos 2d e 3d (estratégia que visa reduzir o número de funções *small* geradas por meio do balanço cinético). Para o conjunto RPF-2Z dos elementos dos sub-blocos 4p, 5p e 6p, a função d adicionada é mais difusa que aquelas já presentes nas primitivas destes átomos. Por sua vez, para compor o conjunto triplo- ζ dos sub-blocos 2p e 3p, RPF-3Z, foram escolhidas duas funções C/P do tipo d (com expoentes idênticos às funções s) e uma f (com expoente análogo à uma função do tipo p). Para os elementos dos sub-blocos 4p, 5p e 6p, que já possuem orbitais d ocupados, foi selecionada mais uma função d difusa e uma função f para a base RPF-3Z.

Os elementos do bloco s são mais complicados e conjuntos C/P requerem funções difusas do tipo p, além de funções d e f. Por sua vez, elementos deste bloco que possuem orbitais vazios de novas simetrias com energia próxima aos seus orbitais de valência exigem que um número significativo de funções p (Li e Be), d (K e Ca) ou f (Cs e Ba) seja considerado. Isto tudo foi analisado e permitiu obter os conjuntos RPF-2Z e RPF-3Z finais, que estão sendo avaliados em cálculos moleculares.

CONCLUSÕES

Neste estudo, funções de correlação/polarização foram adicionadas a partir de resultados de cálculos MR-CISD, de forma a prover conjuntos de qualidade duplo- e triplo- ζ sem prolapo variacional (RPF-2Z e RPF-3Z).

REFERÊNCIAS

- [1] P.A.M. Dirac, Proceedings of the Royal Society of London. Series A, 1926, 112, 661.
- [2] K. Fægri Jr., Theor. Chem. Acc., 2001, 105, 252.
- [3] DIRAC, a relativistic ab initio electronic structure program, Release DIRAC22 (2022), written by L. Visscher et al.
- [4] (a) E.F. Gusmão, R.L.A. Haiduke, J. Comput. Chem., 2022, 43, 1901. (b) E.F. Gusmão, R.L.A. Haiduke, J. Comput. Chem., 2023, submetido para publicação.

AGRADECIMENTOS

Os autores agradecem ao IQSC-USP, CAPES (88887.658222/2021-00), CNPq(306763/2021-4) e FAPESP (2022/05138-0).

Interaction between transition metal complexes derived from flavonoid ligands and DNA nitrogenous bases

Ricardo F. Maierhoffer de Carvalho (IC),¹ Jadson C. Belchior (PQ),² Leonardo A. de Souza (PQ).^{1*}

rmaierhffer@gmail.com; leonardosouza@ppqg.uerj.br

¹Universidade do Estado do Rio de Janeiro, ²Universidade Federal de Minas Gerais

Keywords: Metal complexes; Nitrogenous bases; Molecular stability; DFT; Cancer

INTRODUCTION

Flavonoids are polyphenolic compounds that can be extracted from fruits, vegetables, seeds and tea leaves.¹ In addition to their antioxidant, antiviral and anti-inflammatory activities, flavonoids have been used in design studies of new cancer drugs. Despite the positive results reported in the literature, the interaction mechanisms of metal complexes derived from flavonoid ligands with DNA are still not elucidated.¹ In this work, calculations of the density functional theory (DFT) of electronic structure of adducts between the nitrogenous bases (BN) Guanine (GUA) and Adenine (ADE) with complexes of the Metal-Catechin type in aqueous medium were performed.

METHODS

Initially, calculations were performed to optimize the geometry and vibrational harmonic frequencies of the models of isolated complexes in the gas phase. Then, the structures of complex-GUA and complex-ADE interactions were modeled and optimized. Electronic structure calculations were performed using the Gaussian 09 package, employing the B3LYP and M06-2X functionals combined with the 6-311G(d,p) and 6-311+G(d,p) basis set to C, H, O and N, and the LANL2DZ effective core potential (ECP) for Zn(II), Cu(II) and Fe(II) ions. The thermodynamic parameters in the aqueous phase of the interactions between the complexes and the nitrogenous bases were corrected using the PCM and SMD approaches.

RESULTS

Twenty-one complex-BN interaction structures have been optimized. Octahedral and tetrahedral geometries were thought of, and water molecules were used to complete the metal coordination sphere. Figure 1 shows some of the complexes-GUA geometries calculated at the M06-2X/LANL2DZ/6-311G(d,p) level. Our results revealed that the guanine molecule monodentately coordinated the metal ions through its N7 atom. Possibly, a very similar to the interaction of cisplatin and DNA. Table 1 shows that the Zn(II)-Catechin-GUA interaction is the most thermodynamically favorable. The interaction between the Fe(II)-Catechin complex and the adenine molecule can also be highlighted as energetically more favorable.

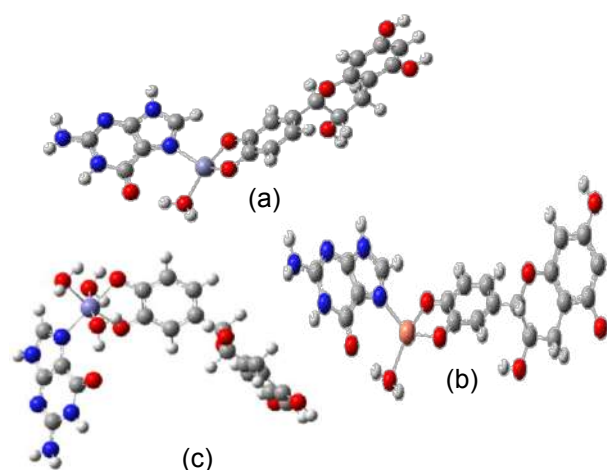


Figure 1. Optimized geometries of M-Catechin-GUA interactions.

Table 1. Energetic and thermodynamic parameters (kcal mol⁻¹) of some M-Catechin-BN adducts.

Structures	ΔE_F	ΔH_F	ΔG_F	$T\Delta S$
Zn(II)-Catechin-GUA	-372 (14.8) [12.1]	-40.9 (11.1) [8.4]	-59.3 (-7.2) (-9.9)	18.4 (18.4) [18.4]
Zn(II)-Catechin-ADE	-36.3 (18.1) [15.5]	-40.3 (14.1) [11.5]	-58.5 (-4.1) [-6.6]	18.2 (18.2) [18.2]
Cu(II)-Catechin-GUA	-35.5 (-12.4) [-13.5]	-35.9 (-12.9) [-14.0]	-34.5 (-11.5) [-12.5]	-1.44 (-1.44) [-1.44]
Fe(II)-Catechin-GUA	-37.5 (-12.6) [-8.9]	-37.7 (-12.8) [-9.12]	-34.9 (-9.9) [-6.3]	-5.77 (-5.77) [-5.77]
Fe(II)-Catechin-ADE	-42.1 (-15.4) [-10.8]	-42.4 (-15.8) [-11.2]	-38.2 (-11.6) [-7.1]	-4.14 (-4.14) [4.14]

Values in parentheses and square brackets were calculated with PCM and SMD, respectively.

CONCLUSIONS

Possibly, metal complexes derived from flavonoid ligands may interact covalently with DNA.

REFERENCES

- ¹E. Jabeen et al. Inorg. Chim. Acta, 2019, 496, 119048.

ACKNOWLEDGEMENTS

To my parents and FAPERJ for financial support (E-26/211.911/2021) from the NEQULT-UERJ research group.



Stability of Ag₂CrO₄ Surfaces by Ab Initio Thermodynamics

Augusto Facundes da Silva (PG),^{1*} Miguel A. San-Miguel (PQ).¹

facundes.as@gmail.com

¹Department of Physical Chemistry, Unicamp

Key-words: Silver Chromate, Density Functional Theory, Thermodynamics, Surface Stability

INTRODUCTION

Silver chromate (Ag₂CrO₄) is one of the silver-based oxides widely studied due to its excellent photocatalytic activity in the degradation of organic matter. This property relies on forming reactive oxygen species (ROS) on the material's surface, which occurs through the interaction of photogenerated electrons and holes with atmospheric water and oxygen molecules. In this context, it is crucial to have a comprehensive understanding of the surface physics and chemistry of the semiconductor. This understanding not only helps elucidate the fundamental physical and chemical aspects of the structures but also aids in comprehending ROS formation and, consequently, the origins of its photocatalytic activity. To achieve this goal, the present study utilized Density Functional Theory (DFT) combined with thermodynamic formalism (known as ab initio thermodynamics¹) to calculate quantum-mechanical based quantities at finite temperatures and pressures. This approach allows for the investigation of environmental effects on solid phases. It was employed to analyze the stability of surface structures experimentally observed by the group² in terms of its surface Gibbs free energy.

METHODS

The mathematical formalism was developed by adapting previous descriptions¹ to the specific system under study. The DFT total energies were calculated using the VASP software, employing the PBE-GGA functional. Surface models derived from a bulk Ag₂CrO₄ structure were optimized in terms of *k*-points and cut-off energy before being relaxed. Surface models by means of non-symmetric and stoichiometric slabs were created using the in-house Pymatgen software³.

RESULTS

The Gibbs surface free energy (γ) for the Ag₂CrO₄ crystal was derived as a function of temperature, oxygen pressure (both defined by the oxygen chemical potential μ_0), and silver content (defined by the silver chemical potential μ_{Ag}), being expressed as

$$\gamma(T, P) = \frac{1}{A} [\Gamma(T, P) - \mu_{\text{Ag}}(T, P)N_{\text{Ag,Cr}} - \mu_0(T, P)N_{\text{O,Cr}}]$$

where

$$\Gamma(T, P) = G^{\text{slab}}(T, P, N_{\text{Ag}}, N_{\text{Cr}}, N_0) - N_{\text{Cr}}g_{\text{Ag}_2\text{CrO}_4}^{\text{bulk}}(T, P)$$

$$N_{\text{Ag,Cr}} = N_{\text{Ag}} - 2N_{\text{Cr}} \\ N_{\text{O,Cr}} = N_0 - 4N_{\text{Cr}}$$

with A as the slab surface area, and N_i as the number of atoms of the species i .

As an approximation, the pressure and the Helmholtz free energy contributions to the Gibbs free energy of the solid phase were considered as negligible. Therefore, the Γ term can be approximated as

$$\Gamma(T, P) \approx E^{\text{slab}} - N_{\text{Cr}}E_{\text{Ag}_2\text{CrO}_4}^{\text{bulk}}$$

where the term E^i is the total energy of the structure i , which can be computed using DFT. Furthermore, the oxygen chemical potential (μ_0) was defined based on statistical mechanics formalisms², and the silver chemical potential (μ_{Ag}) was varied respecting the physically permitted values of the function $\mu_{\text{Ag}}(T, P)$.

The model is currently being applied to various terminations of the (001), (010), (100), (011), (110), (101), and (111) surfaces of Ag₂CrO₄ and validated by comparing the calculated surface energies obtained from the model with the previously reported and purely DFT-based surface total energies (at 0 K)² of some terminations for the (001), (100), and (010) surfaces.

CONCLUSIONS

The Ag₂CrO₄ surface models were developed and are being studied using the derived thermodynamical formalism, aiming to investigate the stability under different environmental conditions.

REFERENCES

1. Rogal, K. Reuter. Educational Notes RTO-EN-AVT-142, Paper 2. Neuilly-sur-Seine, France: RTO, 2007. Available from: <http://www.rto.nato.int/abstracts.asp>.
2. M. Assis, C. et al. Applied Surface Science 2021, 545.
3. Ong, S. P. et al. Computational Materials Science, 2013, 68, 314–319.

ACKNOWLEDGES

This work is supported by CNPq (grant 131853/2022-8), FAPESP (2016/23891-6, and 2017/26105-4), and Centro de Desenvolvimento de Materiais Funcionais (CDMF/CEPID/FAPESP 2013/07296-2).



Simulações espectroscópicas de fulerenos hidrogenados

Ricardo R. Oliveira (PQ),^{1*} Germán Molpeceres (PQ),² Ricardo Montserrat (PG),¹ Felipe Fantuzzi (PQ),³ Alexandre B. Rocha (PQ)¹ e Johannes Kästner (PQ).⁴

rrodrigues.iq@gmail.com

¹ Departamento de Físico-Química, Instituto de Química, Universidade Federal do Rio de Janeiro, Rio de Janeiro, Brasil

² Department of Astronomy, Graduate School of Science, The University of Tokyo, Tokyo 113 0033, Japan

³ School of Chemistry and Forensic Science, University of Kent, Canterbury CT2 7NH, UK

⁴ Institute for Theoretical Chemistry, University of Stuttgart, Stuttgart, Germany

Palavras Chave: fulereno, espectroscopia, hidrogenação, astroquímica, DFT

INTRODUÇÃO

A presença do fulereno (C_{60}) no meio interestelar (*interstellar medium*, ISM) foi proposta a partir de duas bandas de absorção (9632 Å e 9577 Å) relativas ao espectro eletrônico da espécie ionizada (C_{60}^+). Essas transições estão na região do infravermelho próximo e fazem parte do conjunto das bandas interestelares difusas (*diffuse interstellar bands*, DIBs). Devido a presença de uma grande quantidade de átomos de hidrogênio no ISM, é esperado que fulerenos hidrogenados e seus cátions, $C_{60}H_n^{+q}$, sejam formados. Em particular, o $C_{60}H_4$ já foi detectado em laboratório junto com o $C_{60}H_{18}$ e $C_{60}H_{36}$.^{1,2} Dessa forma, o objetivo do presente trabalho é a simulação de propriedades estruturais e espectroscópicas de fulerenos hidrogenados com a composição $C_{60}H_n^{+q}$ ($n=0-4$, $q=0,+1$) para auxiliar na detecção dos mesmos.

MÉTODOS

As estruturas dos isômeros de baixa energia foram geradas a partir da rotina de obtenção de sítios de protonação implementada a rotina *Conformer-Rotamer Ensemble Sampling Tool* (CREST) acoplado ao programa *extended tight-binding* (xtb) em nível GFN2-xTB. As geometrias foram refinadas realizando cálculos de otimização de geometria e frequências vibracionais para a simulação do espectro na região do infravermelho e também para o cálculo do potencial de ionização (PI) e afinidade por prótons (AP). Esses cálculos foram realizados em nível DFT com o funcional B3LYP e a base def2-TZVP. A partir das geometrias otimizadas, cálculos de transição vertical em nível TDDFT utilizando o funcional $r^2\text{SCAN}$ foram realizados com 300 estados para a simulação do espectro de absorção com a mesma base. Todos os cálculos *tight-binding* e DFT foram realizados nos programas xtb 6.4 e ORCA 5.0, respectivamente.

RESULTADOS

Os resultados dos cálculos de PI e AP estão na Tabela 1. É possível observar que todas as espécies hidrogenadas apresentam PI menor e AP maior do que o C_{60} .

Tabela 1 – PI e AP obtidos em nível B3LYP/def2-TZVP.

Espécie	PI (eV)	AP (kJ mol ⁻¹)
C_{60}	7,33	864
$C_{60}H$	6,60	946
$C_{60}H_2$	7,03	889
$C_{60}H_3$	6,40	915
$C_{60}H_4$	6,81	-

Na Figura 1 estão presentes as estruturas de mínimo global obtidas nesse trabalho.

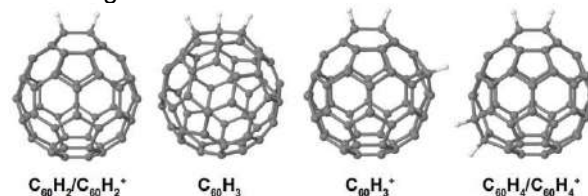


Figura 1 – Estruturas de mínimo global.

Vários isômeros apresentaram transições eletrônicas na região do infravermelho próximo. Algumas dessas transições estão destacadas na Tabela 2.

Tabela 2 – Transições eletrônicas na região do infravermelho próximo obtidas em nível $r^2\text{SCAN}/\text{def2-TZVP}$.

Espécie	λ (nm)	E (eV)
$C_{60}H_2^+$	3873; 3832; 3144; 1778	0,32; 0,32; 0,39; 0,70
$C_{60}H_3$	1155; 1020	1,07; 1,22
$C_{60}H_3^+$	1272; 1168; 1103	0,97; 1,06; 1,12
$C_{60}H_4^+$	3436; 3087; 1899; 1661	0,36; 0,40; 0,65; 0,75

CONCLUSÕES

Diversos derivados do C_{60} apresentam transições eletrônicas na região do infravermelho próximo e são candidatos à detecção astronômica.

REFERÊNCIAS

¹ Y. Zhang, S. Kwok e S. Sadjadi, J Phys Conf Ser, 2016, 728 052004.

² Y. Zhang, S. Sadjadi, C. Hsia e S. Kwok, Astrophys. J., 2017, 845, 76.

AGRADECIMENTOS

RRO agradece ao CNPq, a CAPES e a FAPERJ (JCNE, N° DO PROCESSO E-26/200.249/2023). Agradece também ao LNCC por fornecer recursos computacionais via supercomputador SDumont.

Simulação do espectro de absorção do benzeno: do discreto ao contínuo, da fase gás ao sólido molecular

Ricardo M. A. Silva (PG)*,¹ Ricardo R. de Oliveira Junior (PQ),¹ Alexandre B. da Rocha (PQ).¹

rmontserrat98@gmail.com

¹Instituto de Química, Universidade Federal do Rio de Janeiro, Brasil.

Palavras Chave: Agregado molecular, TDDFT, Espectroscopia teórica, Benzeno.

INTRODUÇÃO

Os agregados moleculares são sistemas que despertam interesse em aplicações envolvendo suas propriedades fotofísicas. As estruturas dos agregados estão relacionadas às mudanças observadas na absorção e na emissão destas substâncias quando comparadas com o monômero em fase gasosa. Neste sentido, o presente trabalho investiga os efeitos da agregação molecular no espectro de absorção do benzeno, explorando transições eletrônicas até a região do contínuo.

MÉTODOS

O Quantum Espresso¹ (v. 7.0) foi empregado para os cálculos de TDDFT com base de ondas planas (PW) e funcional PBE. Um pseudopontencial *ultrasoft* foi usado (energia corte de 60 Ry para a função de onda e 480 Ry para densidade). Os espectros do sólido e do monômero, dímeros e tetrâmero extraídos do cristal de benzeno foram gerados. Por fim, o espectro para o monômero foi obtido com o Gaussian 09,² em nível ω B97XD/6-31+G(d) e com bases de Kaufmann para a representação do contínuo. Funcionais GGA, meta-GGA e híbridos ainda serão testados. Empregou-se protocolo baseado em funções quadraticamente integráveis (L^2).³

RESULTADOS

Os espectros de absorção gerados com a base de ondas planas são mostrados na Figura 1. A linha vertical indica o primeiro potencial de ionização do benzeno (9,24 eV). Observa-se que a transição $\pi \rightarrow \pi^*$ mais intensa é deslocada para o vermelho no sólido, o que está de acordo com o resultado experimental.⁴ O tetrâmero, cuja estrutura é a junção dos dímeros 1 e 2, apresenta um espectro mais suave do que os dois dímeros.

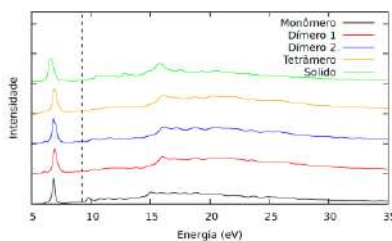


Figura 1: espectros de absorção em nível PBE/PW.

A Figura 2 mostra a região abaixo do potencial de ionização para os dímeros. Nota-se a presença de transições proibidas por simetria para o grupo de ponto D_{6h} por volta de 5 eV para o dímero 2 (paralelo), sugerindo que a quebra de

simetria leva essas excitações a serem permitidas. Observa-se também que o dímero 1 ("T" distorcido) exibe deslocamento hipsocrômico para a transição mais intensa.

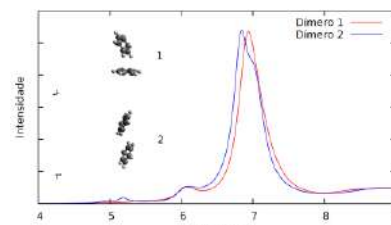


Figura 2: espectros de absorção em nível PBE/PW para os dímeros.

Por fim, comparou-se o método baseado em ondas planas com a continuação analítica empregando funções L^2 para o monômero (Figura 3). Observa-se que a região até 15 eV é melhor descrita com a base de ondas planas. Após esta energia, observa-se uma curva mais suave, corretamente descrita pelo método com base L^2 . Apesar de a base de ondas planas ser naturalmente adequada para a descrição de estados do contínuo, nota-se que a base de funções gaussianas também foi capaz de descrever satisfatoriamente o espectro.

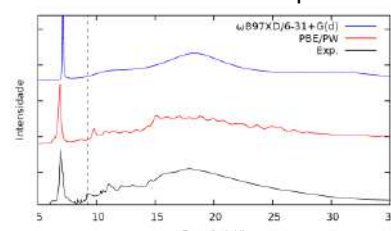


Figura 3: comparação entre espectros com metodologias distintas.

CONCLUSÕES

O efeito da agregação pode ser observado nos espectros. Foi possível também validar os resultados encontrados com base de ondas planas frente ao resultado experimental e em relação ao cálculo com base de funções L^2 .

REFERÊNCIAS

- ¹P. Gianozzi, et al, J. Chem. Phys., 2020, vol. 152.
- ²J. Hiscock, et al, Gaussian 09, Wallingford, CT, 2009.
- ³B. N. C. Tenorio et al, Prog. Theor. Chem. Phys., 2021, vol. 33.
- ⁴U. Killat, J. Phys. C: Solid State Phys., 1974, vol. 7, pg. 2396.

AGRADECIMENTOS

CAPES, LNCC, UFRJ.

Análise teórica da estabilização de derivados benzoxazólicos

Ana Júlia Ferrugini Souza (IC),¹ Diego Pereira Sangi (PQ),¹ Julliane Yoneda (PQ).¹

anajfs@id.uff.br; jullianeyoneda@id.uff.br

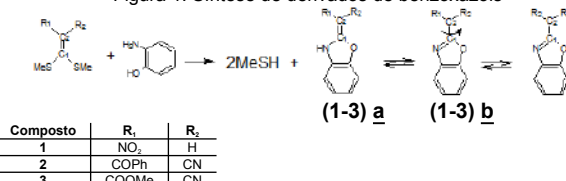
¹Instituto de Ciências Exatas, Universidade Federal Fluminense, Volta Redonda- RJ.

Palavras Chave: Modelagem Molecular, Derivados Benzoxazólicos, Barreira Rotacional.

INTRODUÇÃO

Os benzoxazóis são compostos orgânicos de extrema importância, tendo em vista a potencial atividade biológica dos mesmos.¹ Os derivados benzoxazólicos (**1-3**) podem ser facilmente obtidos pela reação de dupla substituição vinílica entre etenoditioacetais polarizados e 2-aminofenóis, como mostra a Figura 1.¹

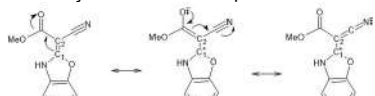
Figura 1: Síntese de derivados de benzoxazóis



Composto	R ₁	R ₂
1	NO ₂	H
2	COPh	CN
3	COOMe	CN

Dois isômeros são possíveis nestas transformações. Na primeira estrutura (**a**), o composto é estabilizado pela deslocalização do par de elétrons π presente entre os átomos C₁ e C₂, como exemplificado na Figura 2. Outra possível estrutura (**b**), é estabilizada pelo caráter aromático do anel devido aos elétrons π presentes entre os átomos N e C₁.

Figura 2: Deslocalização dos elétrons π presentes no composto **3a**



Dados experimentais de Ressonância Magnética Nuclear (RMN) para os produtos destas reações indicam a existência de apenas um produto em cada reação, estando a ligação dupla dentro do anel em **1**, e fora do anel em **2** e **3**. O presente trabalho tem por objetivo avaliar, via Modelagem Molecular, este resultado experimental, a partir da investigação das diferenças de estabilização das estruturas **a** e **b** dos derivados **1-3**.

MÉTODOS

O estudo foi realizado com o programa Spartan'10(Wavefunction, Inc.). Primeiramente, foi feita a análise conformacional de cada possível produto (formas **a** e **b**, Figura 1) utilizando o método AM1. A estrutura do confórmero de menor energia foi otimizada com o método B3LYP/6-311+G**, e a partir da geometria otimizada, foi possível obter a estrutura mais estável através da comparação da energia dos compostos nas formas **a** e **b**. Por fim, calculou-se para os produtos em que a estrutura **a** é a mais estável, o perfil energético, pela rotação do diedro N-C₁-C₂-R₂, de 30 em 30 graus, com o método PM3.

RESULTADOS

Através dos cálculos de energia, foi possível observar que o composto **1** é melhor estabilizado pela aromaticidade (estrutura **1b**). Por outro lado, a ressonância com os substituintes fora do sistema cíclico estabiliza melhor os compostos **2** e **3**, resultando nas estruturas **2a** e **3a** (Tabela 1).

Tabela 1: Energia dos derivados benzoxazólicos nas formas **a** e **b**

Composto	Energia (kcal/mol)		ΔE (kcal/mol)
	a	b	
1	-403937,37	-403938,54	1,17
2	-549633,07	-549620,56	12,51
3	-476504,57	-476498,48	6,09

Dados da literatura indicam que para que a interconversão entre dois confórmeros seja lenta o suficiente para que eles existam como compostos diferentes, a barreira de energia deve ser maior que 24 kcal/mol.² Ou seja, para barreiras menores que 24 kcal/mol, existe livre rotação. As barreiras de energia foram calculadas para os compostos **2a** e **3a**, e apresentaram valores inferiores ao valor de referência (Tabela 2). Isso demonstra que as estruturas avaliadas, devem possuir uma deslocalização dos elétrons π , resultando em um caráter parcial de ligação simples para a ligação C₁=C₂, que pode apresentar livre rotação, justificando a observação experimental da existência de apenas um produto reacional, uma vez que os compostos **2a** e **3a** poderiam existir na forma de dois diastereoisômeros (E e Z) caso a ligação C₁=C₂ fosse rígida.

Tabela 2: Barreira rotacional para os derivados na forma **a**

Composto	Barreira rotacional (kcal/mol)
2a	22,04
3a	22,47

CONCLUSÕES

O estudo realizado permitiu compreender e justificar a formação preferencial dos isômeros **1b**, **2a** e **3a** observados experimentalmente, e poderá ser utilizado para previsão de produtos em futuras sínteses de derivados benzoxazólicos.

REFERÊNCIAS

- ¹Sangi, D.P. et. al. "Benzoxazoles as novel herbicidal agents". Pest. Manag. Sci., 75: 262-269, 2019.
²Warren, J. et. al. Organic Chemistry, 2nd ed. Oxford University Press, 2012.

AGRADECIMENTOS

PIBIC/UFRJ, FAPERJ.

Carbon dioxide capture through functionalized graphenes with alkaline earth metal oxides

Gabriel L. Salomon (IC),¹ Umar L. Rezende (PG),² Jadson C. Belchior (PQ),² Leonardo A. De Souza (PQ).^{1,*}

gabrielsalomon13@gmail.com; leonardosouza@ppgq.uerj.br

¹Universidade do Estado do Rio de Janeiro; ²Universidade Federal de Minas Gerais

Keywords: Functionalized graphenes; Carbon dioxide; Greenhouse effect; Adsorption thermodynamics; DFT

INTRODUCTION

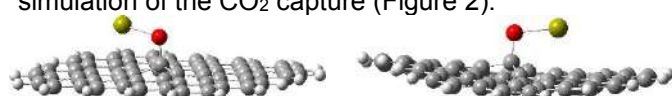
The emission of greenhouse gases has caused severe climate changes on the planet. Studies have shown that properly functionalized carbon nanostructures can form materials capable of capturing carbon dioxide gas (CO_2) and converting it into renewable energy.¹ According to the literature, these adsorbent nanocomposites can be used in the constitution of potential filters in automobile exhaust systems and in materials for the internal lining of calcination furnaces at mining companies.² In this work, electronic structure DFT calculations were performed to simulate CO_2 capture through its reaction with the surface of pristine (PG) and Stone-Wales defective (SWG) graphenes functionalized with calcium oxide.

METHODS

Graphene models functionalized with calcium oxide (PG-CaO and SWG-CaO) were optimized and their vibrational frequencies calculated through the B97D functional combined with the 6-31g(d,p) basis function. We consider different functionalization sites on the surface of PG and SWG. Then, relaxed scan calculations were performed to simulate the potential energy surface (SEP) of the reaction between the CO₂ molecule and the PG-CaO and SWG-CaO models. The thermodynamic barrier for formation of the reaction product was estimated in the gaseous phase. All calculations were performed using the Gaussian 09 package.

RESULTS

Three PG12-CaO and six SWG12-CaO structures were optimized with different arrangements for the position of the oxide on the graphene surface. Figure 1 shows the most thermodynamically stable geometries. In both structures, CaO was observed interacting with the edges of the graphene models. Figure 1a shows the structure used during the simulation of the CO₂ capture (Figure 2).



(a) PG-CaO (b) SWG-CaO
Figure 1. Optimized geometries of the graphene models functionalized with calcium oxide

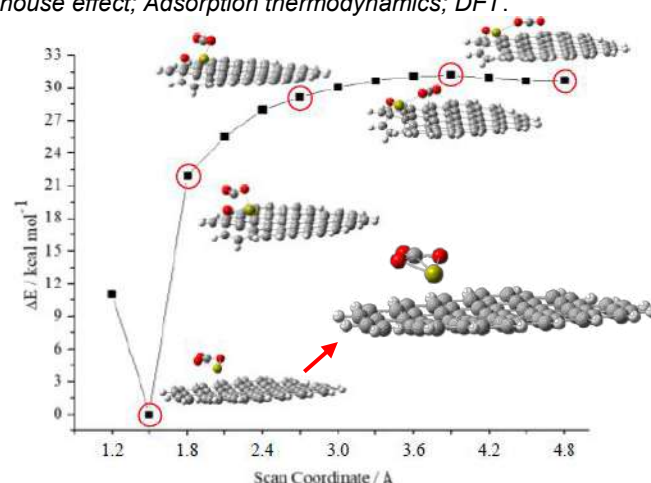


Figure 2. Scan curve of the simulation of the reaction between CO₂ and PG12-CaO.

The reaction result was the formation of calcium carbonate, which adsorbed on the graphene surface, named CaCO₃#PG. The final product formed by simulating the reaction with PG-CaO is only 2.12 kcal mol⁻¹ thermodynamically more favorable than the result obtained with the SWG-CaO model (Table 1).

Table 1. Relative thermodynamic parameters (kcal/mol⁻¹) of CaCO₃ formation on the surface of graphene models.

Structures	$\Delta H_{\text{Relative}}$	$\Delta G_{\text{Relative}}$
CaCO ₃ #PG	0	0
CaCO ₃ #SWG	0.85	2.12

CONCLUSIONS

Our DFT calculations demonstrated that the capture of the CO₂ molecule in the form of carbonate on the surface of graphenes is thermodynamically favorable. Electronic properties are being investigated in order to estimate the electrical potential or capacitance of nanostructures as potential constituents in renewable energy devices.

REFERENCES

- ² Cabrera-Sanfelix, P. J. Phys. Chem. A, 2019, 113, 493

ACKNOWLEDGEMENTS

To FAPERJ for the financial support (E-26/211.911/2021) of the research group NEQuLT – UERJ.

Molecular modeling of inclusion compounds formed by Pt(IV) prodrugs and cyclodextrins

Larissa P. N. M. Pinto (PG),¹ Jadson C. Belchior (PQ),² Diego F. Paschoal (PQ),³ Leonardo A. De Souza (PQ).^{1*}

lpn.machado@gmail.com; leonardosouza@ppgq.uerj.br

¹Universidade do Estado do Rio de Janeiro; ²Universidade Federal de Minas Gerais; ³Universidade Federal do Rio de Janeiro.

Keywords: Cyclodextrin; Pt(IV) complexes; DFT; Solubility; Cancer.

INTRODUCTION

Pt(IV) complexes have been presented as an alternative to Pt(II) complexes in cancer chemotherapy. Studying the stability and solubility of these compounds, isolated or combined with other drugs, and even in the form of inclusion compounds are of fundamental importance, since such properties are related to the transport and activation step of the complexes in the intracellular environment.¹ In this work, density functional theory (DFT) calculations were performed to investigate of the structural and electronic properties, spectroscopic characterization and thermodynamic parameters of formation of inclusion compounds constituted by Pt(IV) complexes and the cyclodextrin molecule (CD).

METHODS

Initially, rigid scan calculations were performed simulating the encapsulation of the Pt(IV) prodrug in the β-CD cavity. The geometries corresponding to the minima of the potential energy curve (ECP) were optimized and characterized as equilibrium structures through the calculation of vibrational harmonic frequencies. Calculations were performed at four theoretical levels combining the B3LYP and M06-2X functionals with the 6-31G(d,p) and def2-SVP basis set and the LANL2DZ pseudopotential for the Pt atom. Thermodynamic parameters and electronic properties of inclusion compound models were analyzed. All calculations were performed using the Gaussian 09 package.

RESULTS

Among the seventeen inclusion compound models involving the Pt(IV) complex (Figure 1a), the four DFT theoretical levels employed revealed ten structures thermodynamically stable in an aqueous medium. Figure 1b shows the geometry of the most stable inclusion compound according to the PCM implicit solvation approach ($\Delta G_F = -15 \text{ kcal mol}^{-1}$). Table 1 shows the trend of energy values for the four most stable inclusion compounds (14–17) studied. These data were obtained at the M06-2X/LANL2DZ/def2-SVP level. HOMO-LUMO Gap for this inclusion compound demonstrates a greater contribution from the Pt(IV) complex.

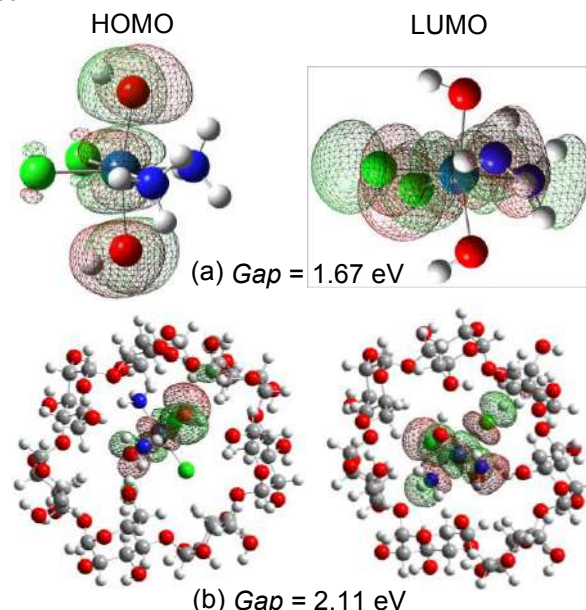


Figure 1. Structures of the Pt(IV) complex (a) and its inclusion compound Pt(IV)@β-CD (b). HOMO-LUMO were calculated at PBE/LANL2DZ/def2-SVP level.

Table 1. Thermodynamic parameters (kcal mol^{-1}) of the inclusion compounds.

	ΔE_F	ΔE_F^{PCM}	ΔH_F	ΔG_F	$T\Delta S$
14	-50.2	-34.4	-47.1 [-31.2]	-27.8 [-11.9]	-19.3
15	-63.1	-41.8	-59.8 [-38.5]	-36.3 [-15.0]	-23.5
16	-59	-42.6	-56.5 [-40.1]	-34.9 [-18.5]	-21.6
17	-54.7	-37.6	-51.6 [-34.5]	-31.5 [-14.4]	-20.1

CONCLUSION

The formation of Pt(IV)@β-CD inclusion compounds may be energetically favorable and enhance the solubility of Pt(IV) complexes.

REFERENCES

¹Davis, M. E. et al. Nat. Rev. Drug. Discov. 2004, 12, 1023.

ACKNOWLEDGEMENTS

To FAPERJ for the doctoral scholarship (E-26/204.106/2022) and for the financial support (E-26/211.911/2021) of the research group NEQuIT – UERJ.

Hydrolysis of Hafnium(IV) and Zirconium(IV): A theoretical quantum approach.

Pedro Augusto de Andrade Novaes (PhD)¹, Hélio Anderson Duarte (R)²

pedroaugusto29@hotmail.com; helioaduarte@gmail.com

¹Universidade Federal de Minas Gerais

Keywords: Hydrolysis; Hafnium; Zirconium

INTRODUCTION

Zirconium finds numerous applications, such as in nuclear reactors, artificial gemstones, ceramics, and cosmetics, among others¹. Hafnium and zirconium are classified as hard metals, and their cations exhibit a pronounced oxophilic nature with very similar strong Lewis acid characteristics. Understanding the internal and external coordination can provide insight into the strength and selectivity of metal transfer during liquid-liquid extraction, aiding in the development of novel extraction reagents and processes².

The behavior of Zr(IV) and Hf(IV) in aqueous solution is important in this context. The aqua complexes and their hydrolysis are investigated by quantum mechanical methods providing information about the structures and thermodynamics. The hydrolyses were modeled according to scheme 1.

- I. $[M(H_2O)_8]^{4+} + H_2O \rightarrow [M(H_2O)_7(OH)]^{3+} + H_3O^+$
- II. $[M(H_2O)_7(OH)]^{3+} + H_2O \rightarrow [M(H_2O)_7(O)]^{2+} + H_3O^+$
- III. $[M(H_2O)_7(OH)]^{3+} + H_2O \rightarrow [M(H_2O)_6(OH)_2]^{4+} + H_3O^+$

Scheme 1. Hydrolysis reaction (M = Hf, Zr).

METHODS

The geometries were optimized at the DFT level using the PBE XC functional with the def2-TZVPPD basis set. For zirconium and hafnium, 28 and 60 electrons from the inner-shell core, respectively, were replaced by an effective core potential (ECP), and the SMD model was used to describe an implicit solvent. Empirical dispersion corrections from Grimme (D3) were applied. Vibrational frequencies at the harmonic approximation have been calculated to ensure that the optimized geometries represent true minima on the potential energy surface (PES). All calculations were performed using the software ORCA 5.0.3².

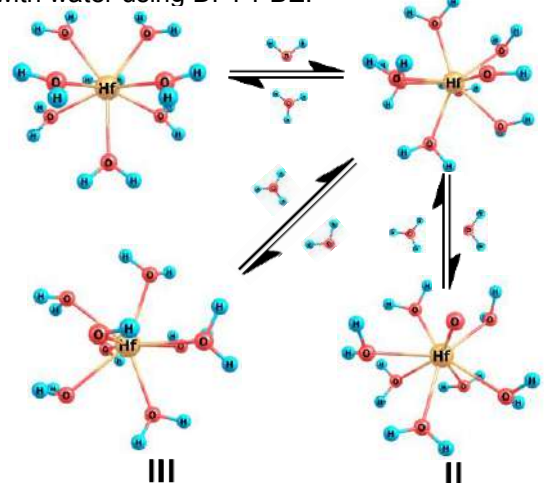
RESULTS

The thermodynamic parameters of the reactions proposed in scheme 1 are described in Table 1. The optimized structures of the reactions performed using PBE are depicted in Figure 1. The thermodynamic parameters indicate that reactions I, II, and III are endergonic for both Hf and Zr. We can also observe that the estimated free energies using different XC functionals follow the same tendency.

Table 1. Thermodynamic Parameters for reactions I, II, and III with Hf.

Reaction	Thermodynamic Parameters (kcal/mol) at 273.15 K				ΔH			
	PBE	PBE0	PBE D3	B3LYP	PBE	PBE0	PBE D3	B3LYP
I	1,98	4,57	5,33	4,80	2,65	5,18	5,60	5,32
II	22,34	27,62	26,85	26,83	25,41	29,91	30,17	29,49
III	10,64	12,63	14,85	13,45	12,62	14,57	17,17	15,31

Figure 1. Optimized structures of Hf coordinated with water using DFT PBE.



CONCLUSIONS

The coordination of Zr and Hf with water is discussed in detail. They prefer to coordinate 8 water molecules. The ΔG of hydrolysis will be compared with the available experimental data. The coordination of SO₄²⁻ with Zr and Hf ions will be presented.

REFERENCES

- ¹ Kraš, A., & Milošev, I. (2023). The Aqueous Chemistry of Zirconium as a Basis for Better Understanding the Formation of Zirconium Conversion Coatings: Updated Thermodynamic Data. *Journal of The Electrochemical Society*, 170(2), 021508.
- ² BERTOLI, A. C. et al. Unveiling the Zirconium and Hafnium Speciation in Fluoride-Nitric Acid Solutions by Paper Spray Ionization Mass Spectrometry Combined with DFT Calculations. *European Journal of Inorganic Chemistry*, v. 2021, n. 12, p. 1175–1185, 26 mar. 2021
- ³ NEESE, F. Software update: The ORCA program system—Version 5.0. *Wiley Interdisciplinary Reviews: Computational Molecular Science*, v. 12, n. 5, 1 set. 2022.

ACKNOWLEDGMENTS

CNPq, CAPES, FAPEMIG.



Simulação dinâmica molecular das interações entre hidroxiapatita e um peptídeo derivado da estaterina.

Carolina Ruis Ferrari (PG),¹ Tiago Espinosa de Oliveira (PQ),² Marília Afonso Rabelo Buzalaf (PQ)¹, Paulo Augusto Netz (PQ).^{3*}

netz@iq.ufrgs.br

¹Departamento de Ciências Biológicas, Escola de Odontologia de Bauru, USP, Bauru, SP

²Departamento de Farmacociências, UFCSPA, Porto Alegre, RS

³Departamento de Físico-Química, Instituto de Química, UFRGS, Porto Alegre, RS

Palavras Chave: hidroxiapatita, estaterina, dinâmica molecular, esmalte dentário

INTRODUÇÃO

A chamada película adquirida atua como uma barreira contra a desmineralização do esmalte dentário. Dentre as proteínas constituintes da camada basal da película adquirida encontra-se a estaterina. A compreensão detalhada das interações desta proteína com a hidroxiapatita, principal componente mineral do esmalte dentário, é um ponto de partida promissor para se obter, otimizar e aprimorar substâncias peptídicas com potencial emprego em produtos odontológicos. Para esta finalidade, foram realizadas extensas simulações de dinâmica molecular envolvendo hidroxiapatita e um peptídeo derivado da estaterina.

MÉTODOS

A estrutura da estaterina (62 resíduos) foi obtida do banco UniProt (P02802), sua estrutura secundária foi predita usando Alpha-Fold¹ e somente 15 resíduos relevantes da porção N-terminal foram considerados. O preparo e a fosforilação de duas serinas foi realizado com CHARMM-GUI². A superfície de hidroxiapatita (face 001) foi modelada com o campo de forças INTERFACE³. Foram consideradas duas orientações iniciais (A) resíduos neutros e negativos voltados para a superfície e (B) resíduos positivos voltados para a superfície. Os sistemas foram simulados (1 μ s cada sistema) usando GROMACS⁴ e as trajetórias foram analisadas em relação a aspectos estruturais (RMSD, Rg, H-Bonds), dinâmicos e termodinâmicos (energia livre de interação usando MM/GBSA)⁵.

RESULTADOS

Em todas as simulações, o peptídeo, na presença de superfície de HAP, migrou e passou a interagir com a superfície. A alteração conformacional no peptídeo foi moderada (Figura 1a) no entanto a interação com a superfície torna o peptídeo menos enovelado (Figura 1b) e envolve a formação de ligações de hidrogênio (Figura 1c). A energia livre de interação é favorável em todos os sistemas (Figura 1d). A orientação inicial com resíduos positivos direcionados à superfície (orientação B, acima, em verde nas figuras)

resulta interações mais acentuadas que no sistema com orientação inicial A (em vermelho nas figuras).

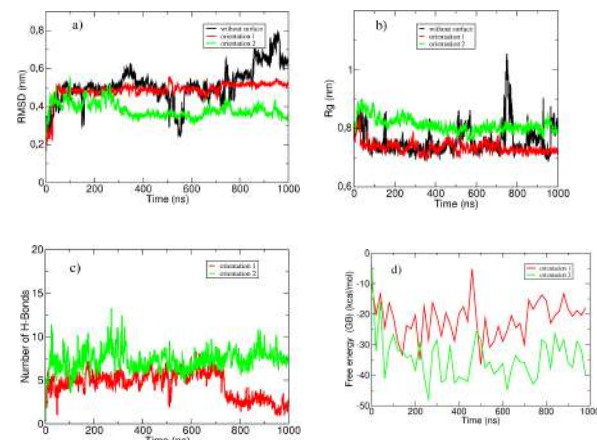


Figura 1. a) Desvio médio quadrático (RMSD), b) Raio de giro, c) ligações de Hidrogênio com a superfície e d) Energia Livre de Intereração. Em preto: peptídeo isolado. Vermelho: orientação A, verde: orientação B.

A monitoração das distâncias entre os resíduos de peptídeos e a superfície mostraram que os resíduos negativos são importantes no ancoramento do peptídeo, no entanto, o peptídeo se reorienta maximizando as interações de resíduos positivamente carregados com a superfície de hidroxiapatita, corroborando resultados da literatura⁶.

CONCLUSÕES

Usando simulações de dinâmica molecular foi possível mapear o padrão de interações entre um peptídeo derivado da estaterina e a hidroxiapatita, o que representa uma etapa importante no desenho racional de peptídeos protetores contra o desgaste dentário.

REFERÊNCIAS

- 1 Jumper J, et al. Nature. 2021;596(7873):583-589.
- 2 Jo S, et al. J Comput Chem. 2008;29(11):1859-1865.
- 3 Heinz H, et al. Langmuir. 2013;29(6):1754-65.
- 4 Abraham, M. J. et al. SoftwareX. Volumes 1–2, 2015;19–25.
- 5 Valdés-Tresanco, M.S., et al. Journal of chemical theory and computation (2021) 17, 6281–6291.
- 6 Makrodimitris, K., D. et al. JACS (2007) 129:13713-13722

AGRADECIMENTOS

CNPq, CAPES, Centro de Supercomputação UFRGS (CESUP)

Stochastic closed Frank model in two dimensions: chiral symmetry breaking over bounded surfaces

José Cândido de Souza Filho (PQ),^{1*} Alejandro López-Castillo (PQ),²
jcsfilho@uem.br; alcastil@ufscar.br

1 Dep. de Ciências, Universidade Estadual de Maringá (UEM), Goioerê, PR, 87360-000, Brasil (professor); Chemistry Department, Universidade Federal de São Carlos (UFSCar), São Carlos, SP, 13565-905 Brazil (post doctoral). **2** Chemistry Department, Universidade Federal de São Carlos (UFSCar), São Carlos, SP, 13565-905 Brazil (professor).

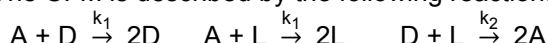
Key words: Homochirality; Chiral-symmetry-breaking; Stochastic-method; Ehrenfest-urn-model; Neighborhood-size.

INTRODUCTION

Systems far from equilibrium can be brought to homochiral states, producing enantiomeric purity D(L), by the process of chiral symmetry breaking^{1,2}. Frank's model was the first to form asymmetric homochiral states from an almost racemic mixture. In this work, the Closed Frank model³ (CFM) will be explored from a stochastic point of view, in two dimensions^{4,5}. From a racemic mixture, the influence of the neighborhood size (NS) of the reaction on the reach of global homochirality (GH) as well as on the time to reach it was studied.

METHOD

The CFM is described by the following reactions:



The stochastic simulation of the CFM was carried out by the Practical Stochastic Method^{6,7} through Monte Carlo steps: **1** - Matrix M (N, N) is filled randomly by D, L, and A particles, and the neighborhood⁸ is defined: (n_n, n_n) cells; **2** - Two cells are drawn; **3** - Establish the neighborhood around the cell 1; **4** - If the cell 2 belongs to the neighborhood then the reactions can take place; **5** - If cell 1 contains a particle D(L) and cell 2 a particle A, then the reaction $D(L)+A \rightarrow 2D(L)$ occurs; **6** - If cell 1 contains D(L) and cell 2 is empty, then D(L) diffuses. The same procedure for $D+L \rightarrow 2A$. In other cases, nothing occurs.

RESULTS

The time to reach the GH (arbitrary units) was obtained for different relative NS (Fig.1). Fifty simulations were performed for each NS.

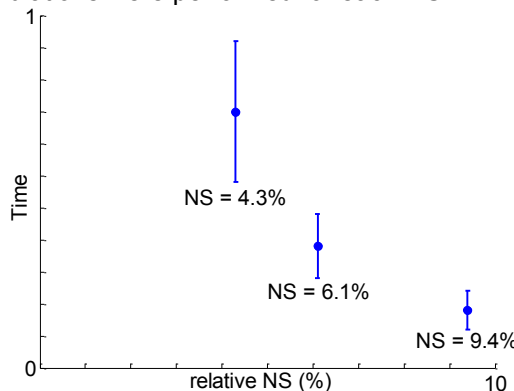


Fig. 1: Time to reach GH as a function of relative NS; relative NS = $(2n_n+1)^2/N^2$.

The GH starts to be reached for relative NS from 1% (Fig.2). For smaller sizes, there is the

formation of homochiral clusters (HC) which asymptotically reach a final aspect (Fig.3).

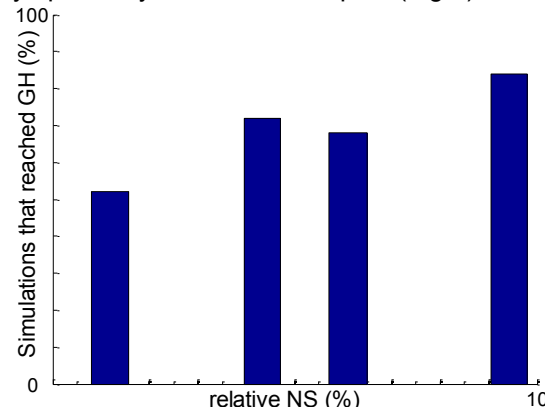


Fig. 2: Simulations that reached the GH.

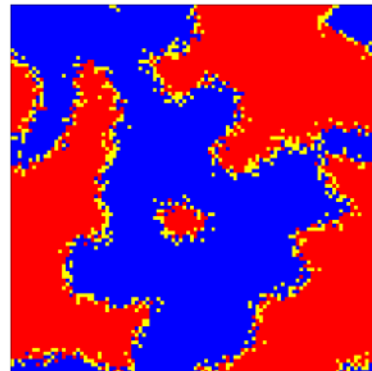


Fig. 3: Examples of Homochiral clusters (final aspect): red (D); blue (L); yellow (A). relative NS = 0.5%.

CONCLUSIONS

There is a minimum relative NS to reach GH, and the time to reach it increases as this value decreases. When GH is not reached, HC form and asymptotically reach a final aspect.

REFERENCES

- 1- Kondepudi & Prigogine, Modern Thermodynamics: From Heat Engines to Dissipative Structures, Wiley-Blackwell, 2014.
- 2- López-Castillo, A. Chirality (2022), 34(1), 104-113.
- 3- Jafarpour, F., Biancalani, T., & Goldenfeld, Phys. Rev. E (2017), 95(3), 032407.
- 4- Liu, H., Li, H., He, Y., Cheng, P., Zhang, Y. Q., Feng, B., & Chen. Nature Comm. (2023), 14(1), 2100.
- 5- Gillet, J., Rongy, L., & De Decker, Y. PCCP (2022), 24(42), 26144-26155
- 6- Silva-Dias, L., & López-Castillo, A. Quim. Nova (2015), 38, 1232-1236.
- 7- López-Castillo, A., & Souza-Filho, J.C. Quim. Nova (2007), 30, 1759-1762
- 8- Souza Filho, J. C., & López-Castillo, A. (2021). The role of the diffusion process in bimolecular reactions with neighborhood. Int. J. Chem. Kin53(4), 492-503.

ACKNOWLEDGMENTS

FAPESP – 2019/12501-0, CAPES – 001. JCSF: DCI/UEM and DQ/UFSCar for supporting the postdoctoral project.

Complex Build 1.1.0: From Lanthanides to Scandium and Yttrium with New Functionalities for Advanced Complex Design

Gabriel, H. L. Munguba (R)¹, Gabriel A. Urquiza-Carvalho (R)¹, Frederico T. Silva (R)¹, Alfredo M. Simas* (R)¹

gabriel.munguba@ufpe.br; simas@ufpe.br

¹ Departamento de Química Fundamental, Universidade Federal de Pernambuco, Recife, PE, Brazil

Keywords: Complex Build, rare-earth complexes, coordination polyhedra, stereoisomerism, coordination compounds.

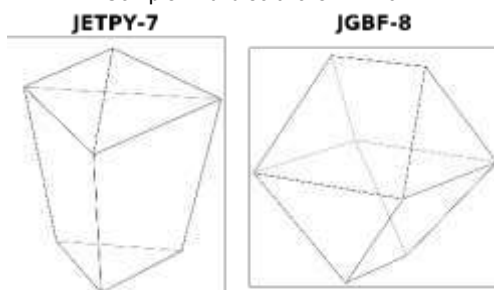
INTRODUCTION

Complex Build¹, a novel algorithm and software for the precise generation of starting structures in computational chemistry, accounting for full stereochemical control, coordination chirality, and optimal ligand positioning for metallic centers with higher coordination numbers, particularly targeting lanthanides is now extended to include scandium and yttrium, as well as new shapes of coordination polyhedra together with their sphericities.

METHODS

Scandium(III) and yttrium(III) coordination bond lengths were parametrized for the most important coordinating atoms from more than 250 good crystallographic structures that were collected from the Cambridge Structure Database (CCDC). For this version, the following new shape geometries were added: elongated trigonal pyramid (JETPY-7) and the gyrobifastigium (JGBF-8).

Figure 1 – New shapes of coordination polyhedra added to the Complex Build software v.1.1.0.



Tables with the stereoisomer codes and random coordination ratios for all conceivable complex generic formulas with mono- and/or bi-dentate ligands were derived from Polya's and Haigh's enumeration method².

RESULTS

Scandium and yttrium can now be selected from the periodic table widget as metal centers for coordination complex assembling, as illustrated in Figure 2. Complex Build can now calculate the sphericities φ of a coordination compound ellipsoid, either for the first coordination shell or for the whole molecule. The respective envelopes and principal axes (a , b and c) are also displayable, as well as coordination polyhedron area A_p (\AA^2) and volume V_p (\AA^3).

Figure 2 – The Periodic Table widget of the Complex Build Software displaying the availability of scandium and yttrium as metal centers

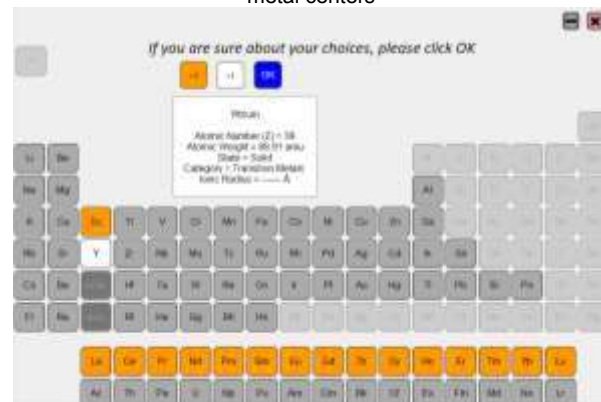
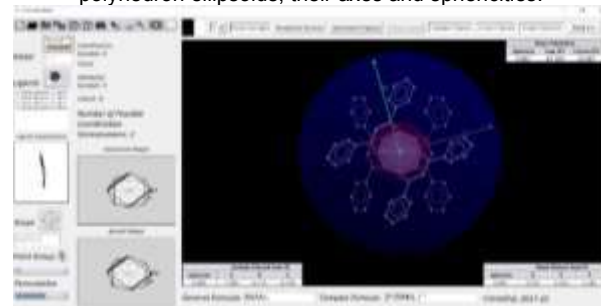


Figure 3 – Coordination compound $[\text{Y(DBM)}_4]^-$. Complex and polyhedron ellipsoids, their axes and sphericities.



CONCLUSIONS

Complex Build, version 1.1.0, introduces significant enhancements and new features, offering researchers an even more powerful and versatile tool for advanced metal complex design. Scandium and Yttrium are now available metal centers, along with the newly added JGBF-8 and JETPY-7 shapes of coordination polyhedra. Sphericities and values for the principal moments of inertia and principal axes of inertia are also shown.

To download the software, access video tutorials, and find more information, please visit: <https://complexbuild.sparkle.pro.br/>.

REFERENCES

¹ G. H. L. Munguba, G. A. Urquiza-Carvalho, F. T. Silva, A. M. Simas, *Sci Rep*, 2021, 11, 21493.

² F. T. Silva, S. L. S. Lins, A. M. Simas, *Inorg. Chem.* 2018, 57, 17, 10557–10567.

ACKNOWLEDGMENTS

CNPq, FACEPE, CAPES and PRONEX.

Thermodynamic analysis of the formation of metal complexes derived from flavonoid ligands with potential antitumor activity

Alejandro F. Santos (IC),¹ Jadson C. Belchior (PQ),² Leonardo A. de Souza (PQ).^{1*}

alejandro.fsantz@gmail.com; leonardosouza@ppgq.uerj.br

¹Universidade do Estado do Rio de Janeiro; ²Universidade Federal de Minas Gerais

Keywords: Metal complexes of flavonoids; thermodynamic parameters; molecular stability; DFT; Cancer.

INTRODUCTION

Recent studies have revealed that flavonoids, widely known for their antioxidant and anticancer properties, may be part of the composition of anticancer drugs.¹ However, many flavonoids are poorly soluble in water and difficult to separate from a sample of tea leaves, for example.¹ A solution to increase the solubility of flavonoids in aqueous media to enhance their biological activity is the complexation with transition metal ions with a low oxidation state.¹ In this work, it was performed density functional theory (DFT) calculations to analyze the electronic and thermodynamic properties of Zn(II), Fe(II), and Cu(II) complexes with the flavonoid ligands kaempferol and quercetin, named M-flavonoid.

METHODS

The geometry optimization and the harmonic vibrational frequencies calculations of the complexes were performed using the B3LYP functional combined with the 6-311G(d,p) and 6-311+G(d,p) basis set to C, H and O, and the LANL2DZ effective core potential (ECP) for Zn(II), Cu(II) and Fe(II) ions. All calculations were performed using the GAUSSIAN09 package. The energetic and thermodynamic parameters of complexes formation in aqueous media were estimated using the PCM approach.

RESULTS

Table 1. Thermodynamic parameters (kcal mol⁻¹) of the metallic complexes studied.

Structures	ΔE_F	ΔH_F	ΔG_F
Zn(II)-kaempferol	-190.7 (-22.5)	-191.8 (-23.6)	-199.4 (-31.1)
Fe(II)-kaempferol	-203.6 (-33.0)	-203.9 (-33.2)	-206.5 (-35.8)
Cu(II)-kaempferol	-202.5 (-31.6)	-203.2 (-32.3)	-211.1 (-40.2)
Zn(II)-quercetin	-337.4 (-38.4)	-338.0 (-39.1)	-341.9 (-42.9)
Fe(II)-quercetin	-356.3 (-51.2)	-353.7 (-48.6)	-361.2 (-56.1)
Cu(II)-quercetin	-350.8 (-50.9)	-352.7 (-52.8)	-380.6 (-80.7)

*Values in parentheses were calculated with PCM.

*Values highlighted in red were calculated with the base set 6-311G(d,p).

Thirty-six molecular structures were optimized. We considered octahedral and tetrahedral geometries with water molecules to complete the metal coordination sphere. Our previous results demonstrated that the five-membered ring formed between the bidentate quercetin ligand and the metal is more stable in the Zn(II)-quercetin, Fe(II)-quercetin and Cu-quercetin (Figure 1). In general, the B3LYP/LANL2DZ/6-311+G(d,p) level revealed more thermodynamically stable geometries (Table 1) compared to the structures optimized with the 6-311G(d,p) basis set. Analyzing the energy parameters corrected with the solvent effect (PCM-water), the molecular stability of the optimized complexes is maintained in aqueous medium.

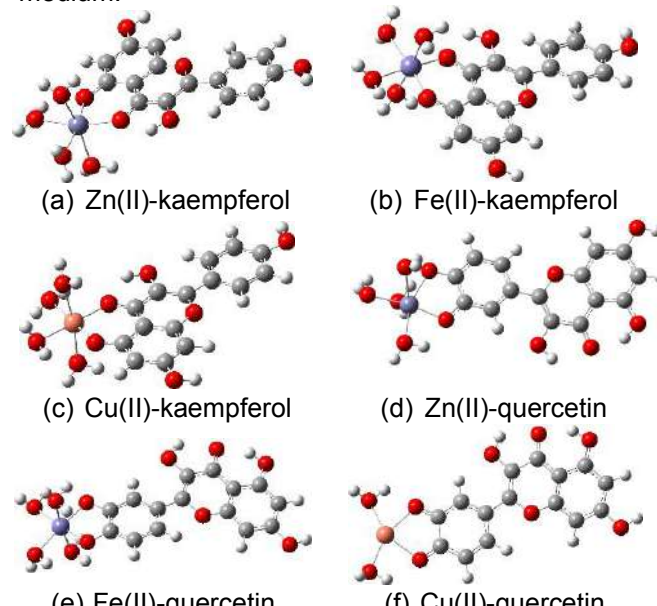


Figure 1. Optimized geometries of M-flavonoid complexes.

CONCLUSIONS

Metal complexes with flavonoid ligands can be stable and can increase the bioavailability of the molecule in an aqueous medium.

REFERENCES

- ¹ M. Šimunková et al. J. Mol. Liq., 2022, 359, 119230.

ACKNOWLEDGEMENTS

To CNPq for the undergraduate scholarship and to FAPERJ for the financial support (E-26/211.911/2021) of the research group NEQuLT – UERJ.

UD-APARM, a robust tool to PES exploration: the chiral recognition of fenchone and camphor by α -CD through GFN2-xTB as a study case

Cleber Paulo Andrada Anconi (R)^{1*}

cleberanconi@ufla.br; cleberanconi@ufla.br

¹Laboratório de Química Fundamental (LQF), Department of Chemistry, Institute of Natural Sciences, University of Lavras, Lavras-MG, 37200-900, Brazil

Keywords: Chiral Recognition, Cyclodextrin, GFN-xTB, UD-APARM

INTRODUCTION

Since chirality is crucial in life science, chiral recognition by cyclodextrins (CDs) corresponds to an important field of research¹, in which practical applications are related to separation techniques.² In terms of theoretical investigation, such studies pose a significant challenge mainly due to the accuracy of a theoretical method required to differentiate small binding constants relative to chiral guests into CDs. The bottleneck consists of adequately exploring the Potential Energy Surface (PES) of a given method in which the UD-APARM software can be employed. This work applied our previous approach³ to investigate the complex formed by fenchone and camphor with α -cyclodextrin with the aid of the UD-APARM software.

METHODS

For 1:1 systems, 2,160 starting arrangements for each guest/CD pair, comprising the association of the fenchone and camphor (Fig. 1) and α -CD, were obtained through UD-APARM⁴ and submitted to optimization and frequency calculations with the GFN2-xTB method⁵ with subsequent evaluation of the solvation energy with the ALPB⁶ continuum approach.

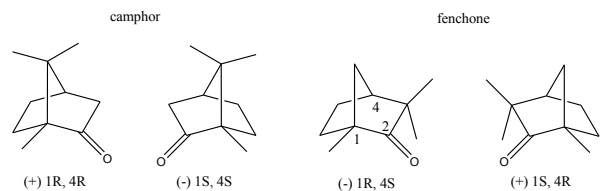


Fig. 1 Molecules investigated herein that form 1:1 and 2:1 host-guest systems with α -CD

Afterward, with UD-APARM, the most favorable 1:1 systems were used to construct a 2:1 (host/guest) association (288 arrangements for each of 18 stable arrangements identified previously for 1:1) to estimate the 2:1 binding constants in the scope of the multi-equilibrium approach. Within this work, UD-APARM constructed, automatically and on a reproducible basis, 13,824 supramolecular starting systems ($2,160 \times 4 + 288 \times 18$).

RESULTS

Through the optimization and frequency evaluation of unprecedented 13,824 CD-based systems at the GFN2-xTB semiempirical level of theory, the binding constants for the formation of the inclusion of camphor and fenchone guests into α -CD were evaluated (Table 1)

Table 1. Log of the binding constants evaluated at 300.6 K at GFN2-xTB (ALPB) level of theory along with experimental data.

guest	1:1 host-guest		2:1 host-guest	
	xTB	Expt. ⁷	xTB	Expt. ⁷
(+)-fenchone	0.90	2.74	5.06	6.51
(-)-fenchone	0.23	2.72	4.10	5.83
(+)-camphor	1.42	-	4.65	9.32
(-)-camphor	2.02	-	7.18	8.93

From the investigation of 8,640 1:1 supramolecular associations, only 37 (0.43%) were identified, with $\Delta G_{\text{water}} < 0$ being 18 (0.21%) non-equivalent supramolecular systems. According to Table 1, binding constants are smaller than experimental data. For 1:2 systems, the (+) camphor data does not fit the experimental trend.

CONCLUSIONS

If we exclude the data for (+) camphor, a linear correlation with $R^2=0.9902$ is obtained for 1:2 systems. The applicability of the UD-APARM was illustrated, considering the small associations effectively employed to obtain the theoretical data.

REFERENCES

- 1 M. Rekharsky and Y. Inoue, *J. Am. Chem. Soc.*, 2000, **122**, 4418–4435.
- 2 S. Wang, L. Li, Y. Xiao and Y. Wang, *TrAC Trends Anal. Chem.*, 2019, **121**, 115691.
- 3 C. P. A. Anconi and L. C. A. Souza, *Comput. Theor. Chem.*, 2022, **1217**, 113916.
- 4 C. P. A. Anconi, *ACS Omega*, 2020, **5**, 5013–5025.
- 5 S. Grimme, C. Bannwarth and P. Shushkov, *J. Chem. Theory Comput.*, 2017, **13**, 1989–2009.
- 6 S. Ehlert, M. Stahn, S. Spicher and S. Grimme, *J. Chem. Theory Comput.*, 2021, **17**, 4250–4261.
- 7 M. Nowakowski and A. Ejchart, 2014, 337–342.

ACKNOWLEDGMENTS

The author thanks Professor Hélio F. S. dos Santos for accessing the NEQC, LCC/UFLA, and FAPEMIG for supporting the Laboratório de Química Fundamental (LQF).



Proline containing lipopeptide modelling with Hybrid Particle-field: From parameter optimization to investigating experimental data

Pedro Tendrih Sodré (PhD)^{1,2}, Manuel Carrer (PhD)², Henrique Musseli Cezar (PhD)², Michele Cascella (R)^{2*}, Mauricio Domingues Coutinho-Neto (R)^{1*}

t.sodre@ufabc.edu.br; michele.cascella@kjemi.uio.no ; mauricio.neto@ufabc.edu.br

¹UFABC - ABCSM, ²UiO - Hylleraas Centre

Keywords: Auto differentiation, Molecular Dynamics, Hybrid Particle-Field, Small-Angle X-rays, metainference

INTRODUCTION

Experimental and molecular dynamics investigations suggest that proline (PRO) containing lipopeptides aggregates provide a tailored chemical environment to improve aldol reaction catalysis and glyphosate detection.^{1,2} In this work, differentiable Molecular Dynamics³ and metainference hybrid particle-field analyses were carried out using -HyMD, a differentiable version of HyMD,^{4,5} to examine the structural properties of the self-assembly of PRWGC₁₈ (PRO containing) lipopeptides.^{1,2} HyMD implements Hamiltonian hybrid Particle-Field (HhPF) molecular dynamics⁶ that uses a coarse grain representation of the system together with a particle field representation of the intermolecular interactions. HhPF allows for much larger time and length scales than what is attainable with all-atom MD. All non-bonding parameters were predicted using a target function and designed autodiff method that reproduces all-atom MD properties as previously described in the literature.³ Small angle experimental SAXS data for the system was used along the metainference approach⁸ to construct a theoretical picture of the self-assemble aggregates. We were able to offer a microscopic perspective of how concentration and pH interact, which is consistent with the Cryo-TEM images shown in the experimental data. We were able to replicate the emergence of oblate structures in equilibrium with smaller, spherical objects when pH is raised. Additionally, we were also able to quantify the appearance of larger aggregates, which is associated with improved catalysis, as the quantity of lipopeptide rises.

METHODS

Differential Molecular Dynamics were run with the HyMD^{3,4,6} package at constant pressure⁵ to obtain the χ matrix.

These parameters were used to run non bias and metainference⁷ biased simulations towards Small-Angle X-rays (SAXS) data⁸

RESULTS

Force-field parameters were obtained targeting the radial distribution function (rdf) of proline containing lipopeptides using -HyMD. Coupling

the HhPF to metainference bias produces SAXS spectra in excellent agreement with the experiment, allowing for the investigation at molecular level of the effects of pH and concentration onto the aggregation. Elongated oblate structures in equilibrium with small spheres are observed with the increase on the pH, and the aggregation number increases with the concentration.

CONCLUSIONS

By employing differentiable HyMD, we were able to obtain model parameters that reproduce the atomistic rdf at the coarse grain detail. However, all-atom structures are not capable of reproducing experimental SAXS data, probably due to poor sampling times. The soft HhPF model is easily driven to the correct structural ensemble by coupling it to metainference. For the pH, oblate elongated structures are seen with small spheres, while for the concentration, we observe that the aggregation number increases with the addition of lipopeptides. For biosensor applications, the elongated structures are seen at Cryo-TEM⁴, whereas for catalysis the concentration relates to the catalytic efficiency³.

REFERENCES

- ¹Soares, B.M., PCCP, 2021, 23, 10953-10963
- ²Gerbelli, B.B., *Nanoscale Adv.*, 2022, 4, 3592-3599
- ³Thaler, S., Zavadlav, J. *Nat Commun*, 2021, 12, 6884
- ⁴Ledum, M.; Sen, S.; Li, X.; Carrer, M.; Feng Y.; Cascella, M.; Bore, S. L. *J. Chem. Theory Comput.* 2023, 19, 2939-2952
- ⁵Ledum, M.; Carrer, M.; Sen, S.; Li, X.; Cascella, M.; Bore, S. L. *Journal of Open Source Software (JOSS)* 2023, 8(84), 2475-9066, 4149
- ⁶Bore, S. L.; Cascella, M. *J. Chem. Phys.* 2020, 153, 094106
- ⁷Bonomi, M., *Sci. Adv.*, 2016, 2, 1501177
- ⁸Paissoni, C. *J. Appl. Cryst.*, 2019, 52, 394-402

ACKNOWLEDGMENTS

CAPES, FAPESP, CNPq, NFR

This study was financed in part by the Coordenação de Aperfeiçoamento de Pessoal de Nível Superior – Brasil (CAPES) – Finance Code 001.

This work has received support by the Research Council of Norway through the CoE Hylleraas Centre for Quantum Molecular Sciences (Grant No. 262695) and the Norwegian Supercomputing Program (NOTUR) (Grant No. NN4654K).

Intermolecular Interactions According to Molecular Orbital Theory

Lucas de Azevedo Santos (PhD),^{1*} Teodorico C. Ramalho (R),² F. Matthias Bickelhaupt (R).^{1,3,4}

I.deazevedosantos@vu.nl.

¹Department of Chemistry and Pharmaceutical Sciences, Amsterdam Institute for Molecular and Life Sciences (AIMMS), Vrije Universiteit Amsterdam, De Boelelaan 1108, 1081 HZ Amsterdam (The Netherlands).

²Department of Chemistry, Institute of Natural Sciences, Universidade Federal de Lavras, CEP 37200-900, Lavras-MG (Brazil).

³Institute for Molecules and Materials, Radboud University Nijmegen Heyendaalseweg 135, 6525 AJ Nijmegen (The Netherlands).

⁴Department of Chemical Sciences, University of Johannesburg Auckland Park, Johannesburg 2006 (South Africa).

Keywords: Bond theory, Density functional theory, Intermolecular interactions, Molecular orbital theory.

INTRODUCTION

Pnictogen (PnB), chalcogen (ChB), halogen (XB), and hydrogen (HB) bonds are intermolecular interactions of the type $D_m Z \cdots A$, where $Z = \text{Pn, Ch, X, H}$.^{1,2,3} These intermolecular interactions play a crucial role in chemical reactivity, supramolecular materials, and drug design.⁴ Typically, the σ -hole model is invoked to rationalize the unexpected attraction between two partially negatively charged atoms and the geometry of these intermolecular interactions.⁵ This model posits that the $D_m Z \cdots A$ complexes are bound and linear due to a Coulombic attraction between a positive electrostatic potential on the molecular surface of the bond donor ($D_m Z$) and the negative, point charge-like bond acceptor (A^-).

METHODS

Herein, we explain how and why the σ -hole model is physically flawed, and we provide a sound bonding mechanism that covers the causal factors underlying the directionality and stability of $D_m Z \cdots A^-$ complexes ($Z = \text{Pn, Ch, X; D, A} = \text{F, Cl, Br}$) at ZORA-M06/QZ4P level, based on quantitative Kohn-Sham molecular orbital (KS-MO) theory, using our activation strain model and canonical energy decomposition analysis.⁶

RESULTS

We show how the treatment of atoms and molecules according to the σ -hole model is oversimplified and unphysical.³ Not the Coulombic interactions, but the steric Pauli repulsion with the lone-pair orbitals of Z is the driving force preventing the bending of the bond acceptor A^- away from $D-Z \cdots A^-$ linearity (Figure 1). In fact, the Coulombic interactions favor (not oppose) bending.

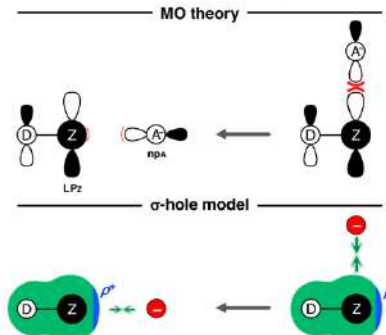


Figure 1. MO theory versus the σ -hole model.

The cohesion in these interactions furthermore receives a major contribution from HOMO–LUMO orbital interactions, stemming from the charge transfer from an occupied np atomic orbital of A^- into the empty σ^* $D-Z$ antibonding orbital of $D_m Z$.

CONCLUSIONS

Therefore, we suggest abandoning the term non-covalent interactions for such bonds and instead using the designation intermolecular covalent interactions (ICI).

REFERENCES

- 1 L. de Azevedo Santos, T. A. Hamlin, T. C. Ramalho, F. M. Bickelhaupt, *Phys. Chem. Chem. Phys.* **2021**, 23, 13842.
- 2 L. de Azevedo Santos, S. C. C. van der Lubbe, T. A. Hamlin, T. C. Ramalho, F.M. Bickelhaupt, *ChemistryOpen* **2021**, 10, 391.
- 3 L. de Azevedo Santos, T. C. Ramalho, T. A. Hamlin, F. M. Bickelhaupt, *Chem. Eur. J.* **2023**, 29, e202203791.
- 4 S. Benz, A. I. Poblador-Bahamonde, N. Low-Ders, S. Matile, *Angew. Chem. Int. Ed.* **2018**, 130, 5506.
- 5 J. S. Murray, P. Politzer, *ChemPhysChem* **2021**, 22, 120.
- 6 T. A. Hamlin, P. Vermeeren, C. Fonseca Guerra, F. M. Bickelhaupt, in *Complementary Bonding Analyses* (Ed.: S. Grabowski), De Gruyter, Berlin, 2021, pp. 199–212.

AGRADECIMENTOS

We thank the Netherlands Organization for Scientific Research (NWO), and the Brazilian agencies CAPES and FAPEMIG for all financial support.



Alto Potencial da Superfície δ -FeOOH (001) Pura e Dopada com Nb na Adsorção e Degradação de um Agente Neurotóxico

Viviane S. Vaiss (PQ),¹ Teodorico C. Ramalho (PQ),² Paulo T. B. Campos (PG).^{2*}

vaissviviane@gmail.com; paulotadashi02@gmail.com

¹Instituto de Química, Universidade Federal Fluminense, Campos de Valonginho s/n, Centro, Niterói, 24020-14, Rio de Janeiro, Brazil; ²Departamento de Química, Universidade Federal de Lavras, Lavras, MG, 37203-202, Brazil.

Palavras Chave: (Cálculos DFT, Agentes neurotóxicos, Tabun, Degradação, Ferroxita).

INTRODUÇÃO

Os agentes neurotóxicos são compostos organofosforados extremamente tóxicos e considerados arma química de destruição em massa¹. Eles atuam inibindo a enzima acetilcolinesterase (AChE), causando o colapso do sistema nervoso central e a morte¹.

O agente neurotóxico Soman (GD) foi sintetizado em 1944 e é mais potente que seus antecessores, Tabun e Sarin. Devido à alta toxicidade e facilidade de produção, há uma necessidade de materiais que possam remover e/ou degradar esses compostos².

A Ferroxita (δ -FeOOH) possui propriedades bifuncionais e ferromagnéticas que lhe permitem ser aplicada em diversas áreas. Apesar de seu enorme potencial, a δ -FeOOH não tem sido muito estudada³.

Neste trabalho, investigamos, a partir de cálculos baseados na Teoria do Funcional da Densidade (DFT), a remoção e a degradação do agente neurotóxico Soman através da fisssorção e quimissorção dissociativa nas superfícies (001) da δ -FeOOH pura e dopada com nióbio.

MÉTODOS

Todos os cálculos foram realizados com o pacote Quantum Espresso⁴, o qual é baseado na DFT^{5,6} com condições de contorno periódicas. O efeito de troca e correlação foi incluído com o funcional de troca e correlação do tipo GGA-PBE⁷, e as interações dos elétrons de valência com o núcleo e os elétrons do caroço foram tratadas pelo método do projetor de ondas aumentadas (PAW)⁸.

As barreiras energéticas da reação de dissociação do GD foram encontradas com o método NEB⁹.

RESULTADOS

Primeiramente, foram estudados os modos de adsorção da molécula de Soman nas superfícies (001) da δ -FeOOH pura e dopada com Nb. O modo preferencial encontrado de adsorção nas duas superfícies foi via o átomo de oxigênio fosforil (P=O). A energia de adsorção calculada foi de -6,6 kcal/mol e -43,5 kcal/mol para a adsorção nas superfícies pura e dopada, respectivamente.

Para investigar o processo de dissociação da molécula de Soman foi proposto um mecanismo baseado na inibição da AChE. Os produtos encontrados na reação de dissociação da molécula Soman nas superfícies (001) δ -FeOOH pura e dopada foram uma molécula de metilfosfonato de pinacolila carregada negativamente e uma molécula de HF adsorvida na superfície carregada positivamente.

O ΔE encontrado no processo de dissociação foi de -33,96 kcal/mol e -29,51 kcal/mol para as superfícies pura e dopada, respectivamente. Já a energia de ativação obtida foi de 16,58 kcal/mol para a reação na superfície pura e de 8,80 kcal/mol na superfície dopada.

CONCLUSÕES

A molécula de Soman adsorveu nas superfícies (001) da δ -FeOOH pura e dopada com Nb preferencialmente via o átomo de oxigênio fosforil, sendo que a adsorção na superfície Nb- δ -FeOOH foi muito mais forte do que na superfície pura. A dopagem da superfície com átomo de Nb também favoreceu a reação de dissociação da molécula, abaixando a energia de ativação da reação.

Tanto a superfície pura da δ -FeOOH quanto a superfície dopada com nióbio apresentaram grande potencial para adsorção e degradação do agente neurotóxico Soman. É provável que resultados semelhantes sejam alcançados para compostos organofosforados com uma estrutura semelhante à do Soman.

REFERÊNCIAS

- ¹R. Alvim, V. Vaiss, A. Leitão, I. Borges, RVQ, 2014, 6, 687.
- ²B. Lukey, J. Romano Jr, H. Salem, *Chemical Warfare Agents: Chemistry, Pharmacology, Toxicology and Therapeutics*, Second edition, CRC Press, Boca Raton, 2007.
- ³L. Lacerda, et al. *J. Mol. Model.*, 2021, 27, 249.
- ⁴P. Giannozzi, et al. *J. Phys. Condens. Matter*, 2009, 21, 395502.
- ⁵P. Hohenberg, W. Kohn, *Phys. Rev.*, 1964, 136, B864.
- ⁶W. Kohn, L. J. Sham, *Phys. Rev.*, 1965, 140, A1133.
- ⁷J. P. Perdew, K. Burke, M. Ernzerhof, *Phys. Rev. Lett.*, 1996, 77, 3865.
- ⁸P. E. Blöchl, *Phys. Rev. B*, 1994, 50, 17953.
- ⁹G. Henkelman, B. Uberuaga, H. Jónsson, *J. Chem. Phys.*, 2000, 113, 9901.

AGRADECIMENTOS

FAPEMIG (Processo PPM-00831-15), CNPq (Processos 307837/2014-9 e 10230/2022-5) e a University of Hradec Kralove (Faculty of Science, VT2019-2021).

A DFT study of Pd(OAc)₂ assisted C(sp²)-H bond activation

Wagner Fernandes Fogos¹, Milena Diniz Lessa¹, José Walkimar De Mesquita Carneiro.^{1*}

wagnerfogos@id.uff.br; jose_walkimar@id.uff.br

Universidade Federal Fluminense, Departamento de Química Inorgânica, Instituto de Química, Outeiro de São João Batista- Niterói, RJ - Brasil

Keywords: DFT; Heck Reaction; Activation C-H bond; functionalization; catalysis

INTRODUCTION

Activation of C-H bonds is a process that involves enhancing the reactivity of molecules through a specific factor. In synthetic organic chemistry, C-H activation is an attractive target, enabling the substitution of a C-H bond with a new bond, resulting in a highly reactive functionalized carbon atom. Coordination compounds have been applied as catalysts to facilitate specific chemical transformations, interacting with C-H bonds in a molecule and activating them for functionalization, which has proven to be a viable alternative.^{1,2} The understanding of the mechanistic aspects of directed C-H bond activation has led to the efficient design of more recent protocols for cross-coupling reactions.³ In the present study we investigated the activation of C-H bonds in 1,2,3-triazole catalyzed by palladium acetate. Activation of a C-H bond in 1,2,3-triazole is the initial step in the relevant conjugation to naphthoquinones, in a Heck -type reaction forming a C-C bond.

METHODS

The geometries of the reported species were fully optimized without any restriction. Transition structures were identified by calculation of the second order Hessian matrix. All calculations were performed using the CAM-B3LYP functional with the Def2SVP basis set. Implicit solvation effects were included using the IEFPCM solvation model, with water as the solvent.

RESULTS

Our goal was to determine the activation parameter for the first step in the coupling between 1,2,3-triazoles and 1,4-naphthoquinones, catalyzed by Pd(OAc)₂. Figure 1 shows the investigated triazoles. Figure 2 is a representation of the pathway leading to activation of the C-H bond in the triazoles by Pd(OAc)₂.

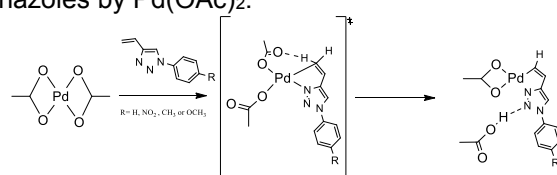


Figure 1: Activation of the C-H bond via concerted metalation for the reaction between 1,2,3-triazole and palladium acetate. After forming a pre-reactive complex where the 1,2,3-triazole coordinates to the palladium acetate via one of the basic nitrogen atoms (in contrast to coordination via the double bond), there occurs the activation of the C-H bond, via proton transfer to

one of the acetate anions, in a concerted transition structure with coordination of the double bond to the palladium center. The activation energy for this concerted step is lower than the alternative one, where activation involves firstly the coordination of the double bond to the palladium center, followed by a nucleophilic attack on the transient cationic center.

A representative energy profile diagram for C-H bond activation is shown in Figure 2.

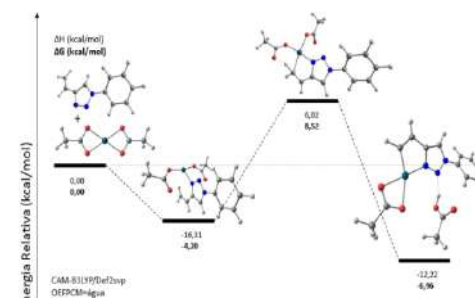


Figure 2: Energy profile of C-H bond activation

In the transition structure, the computed interatomic distances are: 1.38 Å (O-H), 1.94 Å (Pd-H), and 2.17 Å (Pd-C), indicating simultaneous interaction between all the atoms involved in the bond activation. The calculated activation energy is 12.72 kcal/mol, suggesting an energetically accessible and efficient reaction, making it a viable and cost-effective approach for organic synthesis. Effects of electron donating and electron withdrawing groups on the activation parameters were also investigated.

CONCLUSIONS

Basic nitrogen atoms of 1,2,3-triazole coordinate preferentially to a palladium cationic center, as compared to carbon-carbon double bonds. Activation energy for C(sp²)-H bond activation is only 12.7 kcal/mol, in a concerted transition structure with participation of carbon, oxygen, palladium and hydrogen atoms, indicating a fast and efficient catalysed process.

REFERENCES

- ¹ T. Dalton, T. Faber C-H Activation: Toward Sustainability and Applications. ACS Cent Sci. 2021, 7(2). 245-26.
² A. Iain. Recent Advances in C–H Activation for the Synthesis of π -Extended Materials, 2020, 2(8). 951-974.
³ H. Davies, Recent Advances in C–H Functionalization. J. Org. Chem. 2016, 81. 343–350

ACKNOWLEDGMENT

Thanks to the support given by PGQ-UFF, LMQC-UFF, CAPES, FAPERJ and CNPq.

Inclusion of the flavonoids kaempferol, luteolin, morin and quercetin into β -cyclodextrin using a multi-equilibrium quantum approach.

Gleicy Teixeira (R)¹, Erick Ferreira Lacerda (UR)¹, Cleber Paulo Andrada Anconi (R)^{1*}

gleicy.teixeira1@estudante.ufla.br; cleberanconi@ufla.br

¹Laboratório de Química Fundamental (LQF), Department of Chemistry, Institute of Natural Sciences, University of Lavras, Lavras-MG, 37200-900, Brazil

Keywords: CD-based host-guest systems, GFN2-xTB semiempirical method, Binding constant, UD-APARM, Flavonoids

INTRODUCTION

Flavonoids are molecules with antioxidant, antibacterial, anti-inflammatory and anticancer properties from the secondary metabolites of plants, present in the daily diet of the people¹. Due to their instability and hydrophobic character, research on supramolecular systems involving the inclusion of flavonoids (guests) in cyclodextrins (hosts) has been shown to be a promising field, since cyclodextrins (CDs) are a type of cyclic oligosaccharide easily absorbed by the body, managing to modulate the absorption of flavonoids².

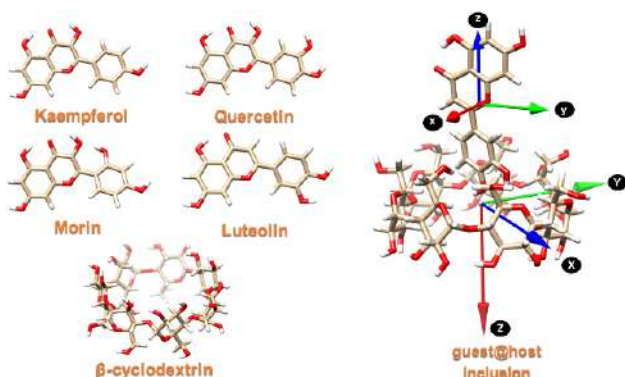


Fig. 1 Left: flavonoids and β -cyclodextrin structure. Right: UD-APARM axes of inertia for individual molecules in a supramolecular system formed with a CD (host) and a guest to evaluate the relative position and rotation.

METHODS

- Each system was studied considering more than 520 possible inclusion positions.
- The UD-APARM program was used to build these systems³.
- The GFN2-xTB method was employed to obtain theoretical data⁴.
- After optimizations and determination of free Gibbs energy, in the condensed phase, log K values were obtained for the inclusion compounds K@ β -CD, Q@ β -CD, M@ β -CD and L@ β -CD.

RESULTS

Table 1. Equilibrium constants obtained by the semiempirical method GFN2-xTB ($\log K_{\text{xtb}}$)

Flavonoid	Systems	Log of binding constant	
		xTB	Expt. ⁵
Morin	05	5.95	2.12
Quercetin	13	6.05	2.40
Luteolin	10	8.19	3.15
Kaempferol	17	6.48	3.65

CONCLUSIONS

Our previous studies addressed a linear correlation between theoretical and experimental data. The data in Table 1 indicates that the potential energy surface (PES) exploration employed must be improved with a focus on the kaempferol@ β -CD system. For the other inclusion compounds, the experimental trend was achieved.

REFERENCES

- Gu, H.-F.; Mao, X.-Y.; Du, M. *Critical Reviews in Food Science and Nutrition* **2020**, 60 (5), 810-825.
- Bai, Y.; An, N.; Chen, D.; Liu, Y.-z.; Liu, C.-p.; Yao, H.; Wang, C.; Song, X.; Tian, W. *Carbohydrate Polymers* **2020**, 231, 115714.
- Anconi, C. P. A. *Acs Omega* **2020**, 5 (10), 5013-5025.
- Bannwarth, C.; Ehler, S.; Grimme, S. *Journal of Chemical Theory and Computation* **2019**, 15 (3), 1652-1671.
- Wang, R.; Ding, B.; Liang, G. *Journal of Molecular Liquids* **2022**, 346, 117068.

ACKNOWLEDGMENTS

The authors thank Professor Hélio Ferreira dos Santos for the access to the NEQC (Núcleo de Estudos em Química Computacional, UFJF, Brazil) computer facility and also thanks the Laboratório Central de Computação Científica (LCC) of UFLA for providing additional computing resources. Furthermore, professor Cleber Paulo Andrada Anconi also thanks the Fundação de Amparo à Pesquisa do Estado de Minas Gerais (FAPEMIG) for supporting the Laboratório de Química Fundamental (LQF), where the research was conducted.

Catalytic Activity Trends in Ceria Surfaces for the Water Oxidation Reaction

Lanna E. B. Lucchetti (PhD)^{1*}, Pedro A. S. Autreto (R)¹, James M. de Almeida (R)², Mauro C. Santos(R)¹, Samira Siahrostami (R)³

lanna.emilli@ufabc.edu.br; pedro.autreto@ufabc.edu.br; james.almeida@ilum.cn pem.br;
mauro.santos@ufabc.edu.br; samira.siahrostami@ucalgary.ca

¹Centro de Ciências Naturais e Humanas (CCNH), Universidade Federal do ABC (UFABC), Santo André, SP, Brazil;

²Ilum, Centro Nacional de Pesquisa em Energia e Materiais (CNPEM), Campinas, SP, Brazil; ³Department of Chemistry, University of Calgary (UofC), Calgary, Alberta, Canada

Keywords: computational hydrogen electrode, catalysis, density functional theory, water oxidation

INTRODUCTION

Enhancing catalytic materials is of paramount importance for an environmentally sustainable future. Manipulating the exposed crystal facets can fine-tune the catalytic efficiency of metallic oxides. Herein we delve into the influence of different CeO_2 surface orientations, (100), (110), (111), (221), and (331), in the water oxidation reaction (WOR) using density functional theory (DFT) calculations and the computational hydrogen electrode (CHE) framework.

METHODS

DFT calculations have been performed with Quantum ESPRESSO. Core electrons were described with SSSP pseudopotentials, the valence electrons with plane-wave basis functions, Ce-4f states with a Hubbard parameter of $U = 5$ eV, and the exchange and correlation energy with (GGA-PBE) functionals. Following the CHE model, adsorption energies were calculated taking gaseous H_2 and H_2O as references.

RESULTS

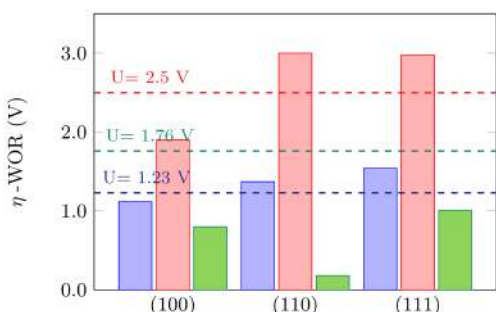


Figure 1: WOR overpotentials on CeO_2 surfaces.

Among the crystallographic planes considered, (100), (110), and (111), each promotes specific oxygen electrochemistry reactions to yield O_2 , H_2O_2 , and $\cdot\text{OH}$ formation, respectively, as indicated by the calculated overpotentials (bars) shown in Fig.1, where the catalytic activity is determined by lying below the thermodynamic

limit (dashed lines), and by the different regions they fall into the selectivity diagram shown in Fig.2.

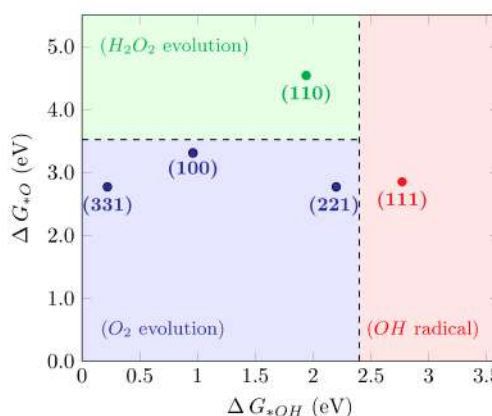


Figure 2: Selectivity diagram for the WOR on CeO_2 surfaces.

Our findings also indicate that the presence of oxygen vacancies alters the selectivity of (110) and (111) surfaces, favoring O_2 evolution.

CONCLUSIONS

CeO_2 surface orientation plays a crucial role in the catalytic activity for the WOR. This work offers a comprehensive understanding of CeO_2 's ability to catalyze the WOR through different routes.

REFERENCES

- 1 L. E. B. Lucchetti, P. A. S. Autreto, J. M. de Almeida, M. C. Santos, S. Siahrostami, React. Chem. Eng., 2023, 8, 1285-1293.
- 2 S. Siahrostami, G.-L. Li, V. Viswanathan, J. K. Nørskov, J. Phys. Chem. Lett., 2017, 8, 1157–1160.

ACKNOWLEDGMENTS

The authors thank FAPESP (2019/01925-4, 2021/14794-5, 2017/10118-0), CNPq (310045/2019-3, 429727/2018-6), CAPES, PRH/ANP, CCM-UFABC, and the University of Calgary's CFREF Program.

Efeito do encapsulamento em β -ciclodextrina sobre o comportamento fotofísico de benzopsoraleenos

Thiago F. Silva (PG),¹ Eduardo F. Franca (PQ),² Guedmiller S. Oliveira (PQ)², Antonio E. H. Machado (PQ)^{1,2*}

thfelipesilva005@gmail.com; aehmachado@gmail.com

¹Programa de Pós-Graduação em Ciências Exatas e Tecnológicas, Univ. Fed. Catalão, Av. Dr. Lamartine Pinto de Avelar, 1120 - 75704-020 Catalão, Goiás, GO; ²Instituto de Química, Univ. Fed. Uberlândia, Uberlândia, MG.

Palavras Chave: Encapsulamento, Benzopsoraleenos, β -ciclodextrina, Comportamento Fotofísico, Geração de $^1\text{O}_2$ ($^1\Delta_g$).

INTRODUÇÃO

Psoraleenos são produtos naturais derivados da cumarina. Alguns desses tem sido empregados como drogas em terapia PUVA^{1,2}. Sua ação está relacionada à habilidade em causar danos ao DNA: na ausência de luz, se intercalam a pares de bases do DNA, resultando em complexos moleculares fracos, sem efeitos biológicos significativos³. No entanto, quando expostos à radiação UVA, esses complexos dão origem a cicloadutos covalentes, fator de risco de mutagenicidade e suas consequências². Por outro lado, análogos sintéticos baseados no dibenzofurano não apresentam esse tipo de tendência². Além disso, alguns desses compostos são capazes de sensitizar a produção de oxigênio singlet com eficiência quântica apreciável¹. Por isso, quando irradiados, induzem efeitos fototóxicos^{4,5}, possuindo boa habilidade de inibir o crescimento de tumores malignos^{2,6}.

MÉTODOS

Os benzopsoraleenos tiveram suas estruturas otimizadas e estimada a energia dos dez primeiros estados excitados singlet e tripleto, usando o funcional B3LYP combinado com o conjunto de bases atômicas dgdzvp. Tanto nas otimizações como nos cálculos das energias de excitação considerou-se água e metanol como solventes, empregando o método CPCM. Os cálculos foram executados com o software Gaussian G09, rev. E.01. Na visualização dos resultados empregou-se os softwares GaussView 5, VMD e Origin.

RESULTADOS

O efeito do encapsulamento em β -ciclodextrina sobre o comportamento fotofísico de dois benzopsoraleenos, compostos (1) e (2), Figura 1, foi avaliado e confrontado com dados experimentais.

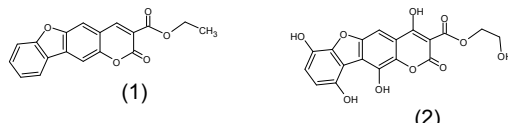


Figura 1. Representação do composto 3 – etoxicarbonil - 2H - benzofuro [3,2-e] – 1- benzopiran – 2 ona (1) e do seu análogo hidroxilado (2).

A análise dos diagramas de estados e dos orbitais moleculares envolvidos, para o composto (1) em solução, sugere a ocorrência de ISC entre o estado singleto S_1 e o estado tripleto de menor energia imediatamente adjacente corrobora os dados experimentais,^{1,7} favorecendo a população do estado T_1 e, consequentemente, as condições para a transferência de energia entre este estado e o oxigênio molecular ($^3\text{O}_2$), possibilitando a produção de oxigênio singlet ($^1\text{O}_2$ $^1\Delta_g$). O mesmo tipo de tendência é observado também para o composto (2) como para as espécies encapsuladas em β -ciclodextrina, Figura 2, sugerindo que, independente do meio, o encapsulamento não deve comprometer o comportamento fotofísico dessas espécies.

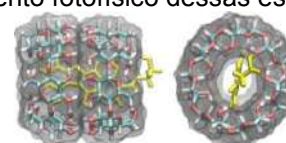


Figura 2. Representação do composto (2) encapsulado em β -ciclodextrina.

As informações obtidas sugerem que a presença de grupos OH no composto (2) não interfere na tendência de sensitização de produção de $^1\text{O}_2$ para essa espécie. Deve-se ressaltar, ainda, que o encapsulamento em β -ciclodextrina favorece a solubilização do fármaco em água, facilitando o seu transporte.

CONCLUSÕES

Os dados obtidos sugerem que o encapsulamento dos compostos (1) e (2) em β -ciclodextrina preserva o comportamento fotofísico observado para essas espécies em solução.

REFERÊNCIAS

- 1Machado et al., *J. Photochem. Photobiol.-A*, 2001, 146, 75;
- 2Oliveira et al., *Eur. J. Med. Chem.*, 2006, 41, 367;
- 3Chilin et al., *J. Med. Chem.*, 1999, 42, 2936;
- 4Potapenko, *J. Photochem. Photobiol.-B*, 1991, 9, 1;
- 5Bordin et al., *Photochem. Photobiol.*, 1992, 55, 221;
- 6Oliveira et al., *Chem. Biodivers.*, 2007, 4, 980;
- 7Maia et al., *J. Photochem. Photobiol.-A*, 2016, 326, 21.

AGRADECIMENTOS

CAPES e FAPEMIG.

Environmentally Friendly Reaction: Conversion of Methane to Methanol over Cu-MAZ activated by CO₂

Ana C. M. Tello (PQ),¹ Carlos H. F. da Cunha (PG),¹ Tássia C. P. Pereira,¹ Alejandro Lopez-Castillo (PQ),² Jose M. C. Bueno (PQ).¹

anacmora@gmail.com

¹Department of Chemical Engineering, Federal University of São Carlos, P.O. Box 676, 13565-905 São Carlos, SP, Brazil; ²Department of Chemistry, Federal University of São Carlos, P.O. Box 676, 13565-905 São Carlos, SP, Brazil

Key words: Cu-MAZ, DFT, Methane, Methanol, CO₂.

INTRODUCTION

Catalytic oxidation of CH₄ to methanol in cyclic processes over Cu/Zeolites occurs by activating of aggressive oxidants such as O₂ or elevated temperature.^{1,2} In contrast, we studied experimentally the methane oxidation over Cu-MAZ employing CO₂, a more environmentally friendly oxidant, demonstrating that CO₂ can substitute O₂ in the process.³ Theoretical studies based on DFT calculations reveal the characteristics of catalytic centers of the material and the intermediates formed during the catalytic process.

METHODS

Geometry optimizations for the 8-RM of *gem*-cage (Fig. 1a) of MAZ zeolite containing the [Cu₂(μ-O)]⁺²–MAZ, [Cu₂(μ-OH)₂]⁺²–MAZ and [Cu₃(μ-O)₃]⁺²–MAZ active species were performed and the UV-Vis spectra calculated at the B3LYP-D3/def-SVP level with Orca code. Nonetheless, first-principles molecular dynamics simulations were carried out before optimization to obtain average structures. The CO₂ activation over [Cu⁺–Cu⁺]⁺²–MAZ was studied and the *gme* cage of MAZ (Fig. 1b) was chose to be interact with the molecules of CO₂. The transition states were obtained with the Climbing Image Nudged Elastic Band method (CI–NEB) and at the PBE-D3/def-SVP level, as implemented in CP2K code.

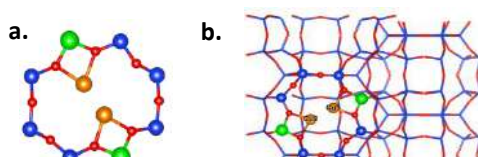


Fig. 1. Optimized structures of a. 8-MR of Cu-MAZ and b. Supercell 1x1x2 with the [Cu⁺–Cu⁺]⁺² site hosted in the 8-MR of the cage MAZ.

RESULTS

Fig. 2 shows the comparison between experimental and theoretical UV-Vis spectra for the [Cu₂(μ-OH)₂]⁺²–MAZ system. The main bands at 36.000 and 41.600 cm⁻¹ are characteristic of the paired copper monohydroxide.⁴

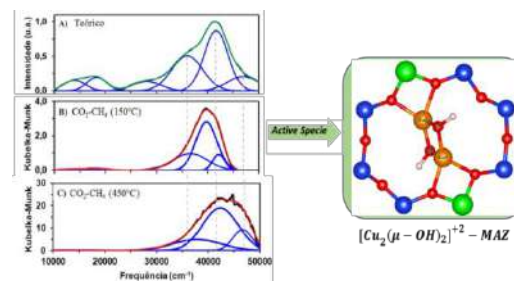


Fig. 2. Comparison of theoretical and calculated and UV-Vis spectra for determination of the active specie.

The adsorption energy of 15.753 kJ/mol calculated show weak interaction between Cu⁺ cations with the CO₂, and the energy required to reach the transition state is 142 kJ/mol. The transition state structure shows strong interaction of CO₂ with the zeolite wall (Fig 3).

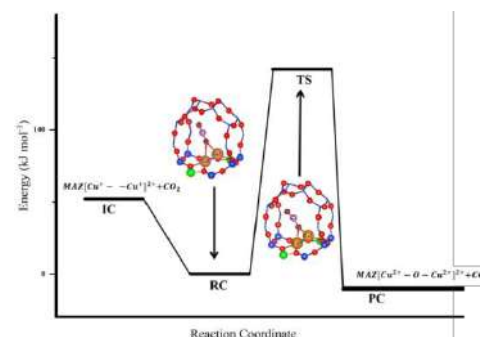


Fig. 3. Theoretical energy diagram for CO₂ activation over MAZ[Cu₂]⁺².

CONCLUSIONS

The [Cu₂(μ-OH)₂]⁺²–MAZ was identified as the main species that reacted with CH₄ when CO₂ was used as an oxidant. Cu⁺ species formed from [Cu₂(μ-OH)₂]⁺²–MAZ do not activate the CO₂ molecule, and the Cu⁺ is not reoxidized.

REFERENCES

1. M. A. Newton, et. al., *J Am Chem Soc*, 2018, 140 (32), 10090.
2. A. J. Knorpp, et. al., *ChemComm*, 2019, 55 (78), 11794.
3. J. M. Bueno, et. al., *Processo para conversão direta de metano a metanol livre de oxigênio molecular em baixas temperaturas.*, 2023. Disponível em: <http://hdl.handle.net/11449/243966>.
4. H. Li, et. al., *Chem Sci*, 2019, 10 (8), 2373.

ACKNOWLEDGMENTS

FAPESP (2022/05343-2, 2018/01258-5, and 2019/12501-0), CNPq and CAPES (001).



Estudos de modelagem molecular na busca de produtos naturais como inibidores com atividade anti-esquistossomose

Rafaela Molina de Angelo^{1*} (PG), João Henrique G. Lago (PQ)¹, Káthia Maria Honório² (PQ)

r.molina@ufabc.edu.br; kmhonorio@usp.br

¹Universidade Federal do ABC – UFABC Santo André, Brasil; ²Universidade de São Paulo – Escola de Artes, Ciências e Humanidades EACH -USP, Brasil.

Palavras Chave: Esquistossomose, Modelagem Molecular, Docking Molecular, Produtos Naturais.

INTRODUÇÃO

A esquistossomose é definida como uma das doenças parasitárias que mais afetam o homem, acometendo cerca de 240 milhões de indivíduos em escala global. Seu tratamento é feito com o uso do medicamento Praziquantel (PZQ), que apresenta algumas limitações e não confere prevenção à reinfecção. É válido ressaltar que alguns estudos^{1,2} apresentaram resultados significativos em relação a compostos com atividades inibitórias frente ao verme *Schistosoma Mansoni*. Contudo, ainda não é conhecido um alvo biológico direto para o tratamento da doença. Desta forma, é de extrema necessidade a busca por novos fármacos para essa enfermidade, assim como um melhor entendimento sobre o mecanismo de inibição dos possíveis alvos biológicos relacionados. O trabalho de De Mori *et al.*³ sugere que a enzima diidroorotato desidrogenase do *Schistosoma Mansoni* (SmDHODH) pode ser uma forte candidata a alvo dessa enfermidade. Entretanto, há um possível sítio alostérico que precisa ser melhor explorado. Assim, neste trabalho foram realizadas simulações computacionais para analisar as interações de 4 compostos isolados de produtos naturais^{1,2} (com atividade inibitória em relação ao parasita) frente ao receptor SmDHODH, assim como entender as propriedades farmacocinéticas dos compostos selecionados.

MÉTODOS

As estruturas dos compostos foram preparadas no pacote Sybyl, incluindo o cálculo das cargas MOPAC. A seguir, foram realizadas simulações de docking desses compostos com a enzima SmDHODH. Para a validação dos parâmetros escolhidos, foi realizada a etapa de redocking, na qual a função Chemscore teve melhor desempenho, com o sítio delimitado em 5 Å e o resíduo Ser53 flexibilizado. Em seguida, os servidores Achilles, FTmap e CavityPlus foram utilizados para a busca de possíveis sítios alostéricos e o mapeamento dessas cavidades para a realização do acoplamento molecular. Para a validação da escolha da SmDHODH, foi realizada a predição dos possíveis alvos biológicos que os 4 compostos poderiam interagir, usando o servidor SwissPredictTarget. Por fim, as propriedades farmacocinéticas das moléculas foram calculadas utilizando o servidor SwissADME.

RESULTADOS

Os resíduos His50, Ser53 e Arg130 presentes no sítio de ligação ortostérico da SmDHODH são os responsáveis pela estabilização do ligante cristalográfico QLA, que apresenta similaridade estrutural ao PZQ. Desta forma, as primeiras simulações de docking realizadas foram neste sítio. O composto melhor ranqueado e que apresentou 5 interações via ligação de hidrogênio, sendo 3 delas com o resíduo Arg130, foi treo-austrobailignana-6-1 (1). Os resultados das análises do FTmap e Achilles sugeriram que a cavidade que poderia ser um potencial sítio alostérico da enzima se refere à uma porção próxima às alças na região superior do receptor, assim como sugerido por outros estudos³. Desta forma, o segundo docking foi realizado nessa região (possivelmente alostérica) e o melhor ranqueado, com 5 interações via ligação de hidrogênio, também foi o composto (1). Em ambas as simulações, o composto ácido ent-caur-16-en-19-óico (3) foi o que apresentou os menores valores de energia de interação, assim como o menor número de interações. Nos estudos das propriedades farmacocinéticas, os compostos (3) e ácido 15β-senecioiloxi-ent-caur-16-en-19-óico (4) foram os únicos que tiveram o valor de log P violando a regra de Lipinski, o que poderia dificultar a chegada e atuação do inibidor no receptor. Por fim, foi realizada uma análise dos dois sítios de ligação em relação a hidrofobicidade/hidrofilicidade. O sítio 1 possui resíduos hidrofóbicos tanto na entrada da cavidade quanto no bolsão interno. Na entrada do sítio 2 existem loops que apresentam uma significativa flexibilidade na abertura e fechamento do bolsão. As alças possuem caráter hidrofílico, contudo, mais para o interior do sítio, os resíduos hidrofóbicos aparecem em maior quantidade.

CONCLUSÕES

Este estudo apresenta a enzima SmDHODH como um promissor alvo para o tratamento da esquistossomose e sugere um sítio alostérico. O composto (1) apresentou o maior número de interações via ligação de hidrogênio em ambos os sítios de ligação, assim como os melhores valores de energia, indicando uma significativa estabilização da molécula no receptor.

REFERÊNCIAS

¹Brito *et al.*, Scientific Reports, 2022, 12:19320.

²Sessa *et al.*, J. Nat. Prod., 2020, 24;83(12):3744-3750

³De Mori *et al.*, The FEBS Journal, 2021, 288, 930–944

AGRADECIMENTOS

CAPES, FAPESP, CNPq e UFABC.

Investigação teórica do potencial de ação de compostos áuricos com atividade biológica na inibição da Tioredoxina Redutase (TrxR).

Giset Y. Sánchez Delgado (PQ),^{1*} Frederico H. do C. Ferreira (PG),² Diego F. S. Paschoal (PQ),³ M. Navarro (PQ),¹ Hélio F. Dos Santos (PQ).²

gysdelgado@ice.ufjf.br

¹LAQBIQ: Laboratório de Química Bioinorgânica e Catálise; ²NEQC: Núcleo de estudos em Química Computacional,

^{1,2}Departamento de Química, Universidade Federal de Juiz de Fora, Campus Universitário Martelos, 36036-900 Juiz de Fora, MG, Brasil; ³NQTCM: Núcleo de Química Teórica e Computacional de Macaé, Polo Ajuda, Federal University of Rio de Janeiro, Campus UFRJ-Macaé, 27971-525 Macaé, RJ, Brasil.

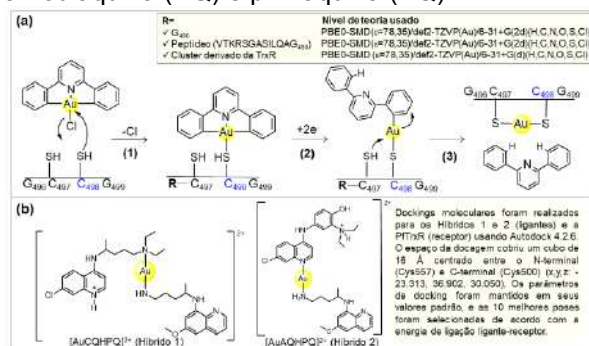
Palavras Chave: *Complexos de ouro em medicina, Tioredoxina Redutase, Câncer, Malária, DFT.*

INTRODUÇÃO

A TrxR é uma flavoenzima essencial para o crescimento celular, com a função de controlar a concentração de espécies nocivas na célula humana. Esta enzima também está presente nos parasitas da Malária (PfTrxR), sendo essencial para seu equilíbrio redox intracelular. TrxR e PfTrxR encontram-se altamente expostas em células cancerosas, e no parasita da Malária no hospedeiro humano, proporcionando um potencial alvo para a quimioterapia. Diversos compostos de ouro, por apresentarem alta afinidade por enzimas contendo grupos tióis (tais como TrxR), são fortes inibidores desta enzima e portanto, considerados promissores agentes anticâncer e antimaláricos. A estabilidade redox e a alta afinidade do ouro por tióis celulares influenciam a ação biológica nestes complexos. Ambas características foram abordadas para o complexo anticâncer $[Au^{III}(C^N C)Cl]$, na presença de modelos de TrxR (Fig 1a). Adicionalmente, técnicas de modelagem molecular foram aplicadas para obter alguns *insights* sobre a interação de complexos híbridos de ouro(I) (Fig 1b) com a PfTrxR.

MÉTODOS

Figura 1. (a) Etapas de reação estudadas para $[Au^{III}(C^N^NC)Cl]$. (b) Estruturas de híbridos de ouro(I) contendo as drogas cloroquina (CQ), amodiaquina (AQ) e primaquina (PQ).



RESULTADOS

A tendência à redução de $[Au^{III}(C^N^NC)Cl]$ aumenta após a reacção de troca Cl^-/Cys_{498} (1; Fig.

1a), evidenciando um papel primário do ligante auxiliar na estabilidade redox deste complexo de ouro(III); sendo pouco influenciado pelo ambiente enzimático da TrxR. No entanto, a forma como o carbânion ($C^N^-C^-$) é neutralizado durante a redução (2), define a espontaneidade nesta etapa. A reação final de substituição C^N^-C/Cys_{497} (3), mostrou-se dependente do estado de protonação da Cys₄₉₇. No estado protonado (-SH), a substituição com transferência de prótons simultânea é exergônica (-28,3 kcal mol⁻¹) e induz a um estado de transição tardio, com uma alta barreira de energia (38,9 kcal mol⁻¹). No entanto, quando a reação é abordada com o grupo tiol desprotonado (-S⁻), esta se mostra mais rápida com uma energia de ativação de 19,7 kcal mol⁻¹. Resultados de docking molecular indicam uma interação mais favorável entre o C-term da PfTrxR e o híbrido 1, em relação ao híbrido 2. A flexibilidade da estrutura do híbrido 1 permite-lhe adotar conformações que favorecem o contato com enzima. Estudos de dinâmica molecular estão sendo executados atualmente com o objetivo de expandir e quantificar a análise.

CONCLUSÕES

Os resultados relatam informações relevantes sobre o mecanismo redox de complexos ciclometalados de ouro(III), apoiando sua atuação como pró-drogas anticâncer. A dissimilaridade na coordenação das drogas CQ ou AQ com ouro(I) nos híbridos (Fig 1b), pode ter implicações para a inibição da PfTrxR e sua atividade antimarialária. Os achados são concordantes com os efeitos inibitórios dos compostos áuricos na inibição da enzima, observados experimentalmente.

REFERÊNCIAS

- ¹ G.Y. Sánchez Delgado et al, Inorg. Chem. 2021, 60. 3181-3195. ² G.Y. Sánchez Delgado et al, JBIC, 2018, 23. 1283-1293.
³ C.S. Pereira et al, Pharmaceuticals, 2022, 14. 1251.
⁴ G.Y. Sánchez Delgado et al, J. Inorg. Biochem. 2022, 236. 111970.

AGRADECIMENTO

CAPES (*Finance Code 001*), FAPESM/CNPq(BPD-00777/22),
SDumont/LNCC, EULER- CeMEAI/USP.



Estudo ab initio dos efeitos excitônicos nas propriedades ópticas de estruturas bidimensionais de fósforo negro (BP).

Diana M. N. Thomen (PG),¹ Andrey Chaves (PQ),² André J. C. Chaves (PQ),¹ Ivan Guilhon (PQ),¹ Marcelo Marques (PQ),¹ e Lara K. Teles(PQ).¹

diana.thomen@gta.ita.br

¹Instituto Tecnológico de Aeronáutica, São José dos Campos, Brasil;

²Universidade Federal do Ceará, Av. da Universidade, 2853 - Benfica, Fortaleza, Brasil

Palavras Chave: *Materias 2D, fosforeno, Fósforo Negro, DFT, Polaritons hiperbólicos*

INTRODUÇÃO

A obtenção do primeiro material bidimensional (2D), o grafeno, desencadeou inúmeras pesquisas envolvendo outros materiais 2D. Dentro os materiais que possuem sua estrutura em camadas, um que vem ganhando grande destaque recentemente é o fosforeno, obtido a partir do Fósforo Negro (BP). Juntamente com suas propriedades eletrônicas únicas, o fosforeno é um dos exemplos mais proeminentes de materiais anisotrópicos, considerando apenas as coordenadas no plano. Essa anisotropia é frequentemente refletida nas propriedades ópticas do material, resultando em estados plamônicos com diferentes frequências para polarizar a luz, considerando cada direção e, assim, tem-se a dispersão de um plasmon-polariton na forma hiperbólica. Polaritons hiperbólicos no plano, naturais em materiais em camadas, já foram estudados e demonstrados em MoO₃ e WTe₂, que são baseados em ressonâncias de fônon e plasmon, respectivamente. Em trabalhos experimentais recentes, foi previsto que a monocamada de BP hospeda naturalmente exciton-polaritons hiperbólicos, o que abriu uma nova perspectiva de polaritons hiperbólicos naturais no plano, baseados em excitons[1]. No entanto, a literatura ainda carece de estudos sobre esse tema, levando em consideração o ponto de vista teórico dos cálculos ab initio.

MÉTODOS

Foram estudadas 5 estruturas de fosforeno, sendo elas a monocamadas e os quatro tipos de bicamada. Todos os cálculos foram realizados usando o VASP (Vienna Ab initio Simulation Package). As estruturas de bandas foram calculadas usando os métodos DFT e HSE06. As propriedades ópticas foram obtidas usando o método GW+BSE, para que fosse possível simular a interação elétron-buraco.

RESULTADOS

A priori foram realizados cálculos de DFT e HSE para analisar o comportamento eletrônico e óptico das estruturas mencionadas. Estas análises iniciais foram compatíveis com dados encontrados na literatura. Na sequência foram realizadas as análises de função dielétrica com a presença de excitons em monocamada de fósforo negro. A partir destas foi observado fortes indícios de que o fosforeno hospeda naturalmente um exciton-polariton hiperbólico (HEP). Esses indícios ficaram evidentes ao avaliar o pico negativo nas respostas da parte real da função dielétrica, avaliando as duas direções no plano. Após isso, foram analisadas as respostas ópticas dos vários tipos de empilhamento de bicamadas e notou-se que esse efeito pode ser controlado ao trocar o tipo de empilhamento. Ainda, neste trabalho, foi avaliado outras formas de controlar este efeito, assim foi estudado o comportamento da bicamada do tipo AB com aplicação de strain na direção perpendicular ao plano, sendo que esta análise possibilitou visualizar que a aplicação de strain é capaz de mover os picos das respostas ópticas. Desta forma, foi observado também que o efeito de HEP pode ser manipulado, o que indica versatilidade em possíveis aplicações.

CONCLUSÕES

Neste trabalho foram encontrados indícios de que as estruturas de fosforeno hospedam naturalmente HEP. Os resultados obtidos abrem caminhos para estudos de sistemas anisotrópicos e suas propriedades ópticas, usando métodos matemáticos como o BSE para simular o comportamento excitônico nessas estruturas.

REFERÊNCIAS

- ¹F. Lei, et al, *Nature Communication*, 2021, 12. 5628.
²L. G. Fereira, et al, *Phys. Rev. B*, 2008, 78. 125116.

AGRADECIMENTOS

Agradecemos à CNPq pelo financiamento da pesquisa e ao ITA por ceder seu espaço.

Estudo da decomposição térmica de organofosforados

Lisandra Paulino dos Santos(PG),^{1,2*} Alexandre Rodrigues Tôrres (PQ),² Leonardo Baptista (PQ).²

autor1@seuemail.com; lisandra.santos@discentes.fat.uerj.br

¹Programa de Pós-Graduação em Química, Instituto de Química, Universidade do Estado do Rio de Janeiro

²Departamento de Química e Ambiental, Faculdade de Tecnologia, Universidade do Estado do Rio de Janeiro

Palavras Chave: organofosforados, modelo cinético, decomposição térmica, simulação numérica, microcinética.

INTRODUÇÃO

Organofosforados é uma classe de compostos amplamente utilizados no nosso dia-a-dia. São utilizados como defensivos agrícolas, retardantes de chama e até mesmo armas químicas. Devido as propriedades químicas desta família, o descarte correto destes compostos tem se mostrado complicado. Por este motivo a incineração tem sido usada para destruição destes compostos evitando assim seu descarte no meio ambiente. Por este motivo, o presente trabalho visa investigar o mecanismo proposto na literatura para decomposição térmica de organofosforados, identificar os caminhos de reação para formação de poluentes e eficiência de degradação das espécies estudadas.

MÉTODOS

A partir do modelo de Glaude¹ simular numericamente em um reator 0-D, a volume constante, a decomposição térmica do Sarin, dimetil metilfosfonato (DMMP), diisopropil metanofosfonato (DIMP) e trimetilfosfonato (TMP). Foi considerada uma faixa de temperaturas de 800 a 2000 K para a mistura de combustível metano/etano/ar, mistura 3, e uma faixa de temperatura de 800 a 1000 K para as demais misturas de combustíveis e ar. Os combustíveis estudados foram metano, etano, propano e biogás em condições estequiométricas. A segunda etapa foi a simulação de um reator contínuo em fase gasosa. A simulação foi realizada a partir do software Cantera 2.5² com a interface em linguagem Python.

RESULTADOS

Foi verificado que além da dependência com o valor da temperatura inicial, a eficiência da decomposição de algumas moléculas é influenciada pelo tipo de combustível. Sendo a molécula de TMP mais sensível a mudança de combustíveis. Um dos problemas verificados na decomposição do Sarin foi a formação de HF ao fim da reação, Tabela 1.

Além da formação de CO e CO₂, a decomposição térmica de todos compostos produziu as espécies HOPO₂, HPO₂ e HOPO como produtos da queima.

Tabela 1: Fração molar dos poluentes formados na decomposição térmica do Sarin utilizando biogás.

Temperatura (K)	HF	CO ₂	CO
800	$2,79 \times 10^{-6}$	$4,02 \times 10^{-2}$	$8,36 \times 10^{-10}$
900	$6,32 \times 10^{-5}$	$4,02 \times 10^{-2}$	$5,52 \times 10^{-7}$
1000	$1,09 \times 10^{-4}$	$4,02 \times 10^{-2}$	$6,66 \times 10^{-5}$

A análise de fluxo ao longo da simulação permite visualizar a microcinética associada à formação dos poluentes descritos.

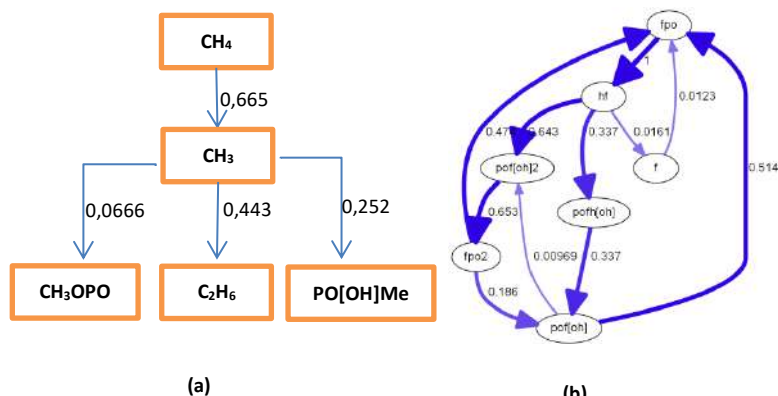


Figura 1:(a) Análise de fluxo resumida mostrando a participação do combustível;(b)Análise de fluxo da formação de HF durante a decomposição do Sarin.

A análise descrita na Figura 1 e também permite inferir como cada combustível utilizado participa do mecanismo de decomposição térmica.

CONCLUSÕES

Foi estudada a decomposição térmica de cinco organofosforados e avaliados os poluentes formados durante o processo. A decomposição dos compostos estudados depende da temperatura inicial e tipo de combustível usado. Foi levantado quais reações precisam ser revisadas e quais espécies precisam ter seus parâmetros termodinâmicos recalculados.

REFERÊNCIAS

- (1) Glaude, P. A.; Melius, C.; Pitz, W. J.; Westbrook, C. K. *Proc. Combust. Inst.* **2002**, 29 (2), 2469–2476.
- (2) Goodwin, D. G.; Speth, R. L.; Moffat, H. K.; Weber, B. W. Cantera: An Object-oriented Software Toolkit for Chemical Kinetics, Thermodynamics, and Transport Processes. <https://doi.org/10.5281/zenodo.1174508>.

AGRADECIMENTOS

Agradecemos o apoio financeiro da FAPERJ.

Estudo por Docking e por design de novo de receptores opioides δ, μ e κ visando a geração de ligantes seletivos.

Sara Gomes Sampaio (IC),¹ Guilherme Duarte Ramos Matos (R)^{1,2*}

sampaio.sara1331@outlook.com; guilhermedrmatos@gmail.com

¹Laboratório de Modelagem de Sistemas Complexos (LMSC), Instituto de Química (IQ), Universidade de Brasília (UnB);

²Department of Applied Mathematics and Statistics, Stony Brook University, EUA

Palavras Chave: Receptores opioides, Design de novo, Docking.

INTRODUÇÃO

Receptores opioides são receptores acoplados a proteínas G (GPCRs) que se destacam pela sua relação com a analgesia.¹ Os agonistas opioides, uma vez usados em excesso, causam dependência química, provocam reações adversas e podem levar até mesmo à morte. Dada a variedade de funções biológicas associadas à ativação desses receptores, propusemos usar o design de novo^{2,3} para gerar novos ligantes para os receptores δ, μ e κ (DOR, MOR e KOR, respectivamente) visando observar seletividade da interação com cada alvo.

MÉTODOS

Ligantes foram construídos no sítio de ligação das proteínas κ (PDB: 6B73), μ (PDB: 6DDE) e δ (PDB: 4N6H) usando o algoritmo de design de novo do programa DOCK 6.9.² O ensemble gerado foi, então, submetido a um experimento de cross-docking (Figura 1) e os ligantes organizados por energia.

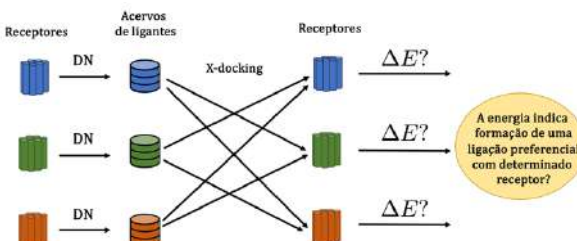


Figura 1: Esquema experimental das simulações feitas no DOCK6.

RESULTADOS

Foram geradas 2295 ligantes em potencial para a proteína κ, 2577 para a proteína μ e 2090 para a proteína δ. Resultados preliminares sugerem que o design de ligantes seletivos usando o software DOCK6 não é um problema trivial, mas que pode ser feito, devido a resultados encorajadores para a proteína κ, parcialmente ilustrados na tabela e figura abaixo.

Tabela 1 - Seletividade do ligante 5_0, 4_1 e 5_5 comparado aos receptores δ, μ e κ.

Receptor	Ligante 5_0	Ligante 4_1	Ligante 5_5
DOR (4N6H)	-53,651291	-46,204559	-49,761295
MOR (6DDE)	-53,139938	-49,765900	-52,878563
KOR (6B73)	-73,785522	-69,299500	-67,735954

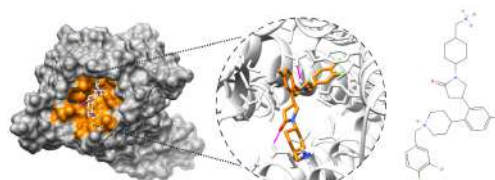


Figura 2: Ligante 5_0 junto ao receptor 6B73

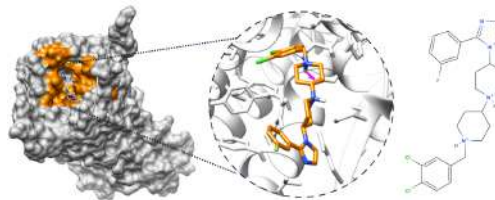


Figura 3: Ligante 4_1 junto ao receptor 6B73.

CONCLUSÕES

Resultados preliminares apontam que, a despeito da similaridade de aproximadamente 80% entre os receptores, é possível gerar ligantes seletivos, como conseguimos evidenciar bem quanto ao receptor KOR. Resultados semelhantes não foram encontrados para os receptores MOR e DOR. Planeja-se investigar a razão da seletividade no receptor KOR, a fim de traçar estratégias de design seletivo para os demais receptores.

REFERÊNCIAS

- Janecka, A.; Fichna, J.; Janecki, T. Opioid Receptors and Their Ligands. Current Topics in Medicinal Chemistry 4 (1), 1–17.
- Allen, W. J.; Balius, T. E.; Mukherjee, S.; Brozell, S. R.; Moustakas, D. T.; Lang, P. T.; Case, D. A.; Kuntz, I. D.; Rizzo, R. C. DOCK 6: Impact of New Features and Current Docking Performance. J. Comput. Chem. 2015, 36 (15), 1132–1156.
- Allen, W. J.; Fochtman, B. C.; Balius, T. E.; Rizzo, R. C. Customizable de Novo Design Strategies for DOCK: Application to HIVgp41 and Other Therapeutic Targets. Journal of Computational Chemistry 2017, 38 (30), 2641–2663.

AGRADECIMENTOS

Universidade de Brasília e Prof. Dr. Daniel Francisco Scalabrin Machado.



Cálculo da energia do estado fundamental para a interação entre o íon ferroso e a molécula de oxigênio em cavidades confinantes

Leonan Augusto Massete Perá (PG)^{1*}, Josimar Fernando da Silva (PQ)², Elso Drigo Filho (PQ)¹.

leonan.pera@unesp.br;

¹Universidade Estadual Paulista “Júlio de Mesquita Filho” (UNESP), Campus de São José do Rio Preto – Instituto de Biociências, Letras e Ciências Exatas (IBILCE).

²Instituto Federal de Educação, Ciência e Tecnologia de São Paulo (IFSP), Campus Votuporanga.

Palavras Chave: *Interação íon-dipolo induzido, Sistema confinado, Método variacional, Mecânica quântica supersimétrica.*

INTRODUÇÃO

A interação entre o íon ferroso e a molécula de oxigênio em hemoproteínas pode ser considerada como confinada devido a cavidade formada pela estrutura da macromolécula.

Soluções de sistemas confinados via Método Variacional aliado à Mecânica Quântica Supersimétrica (MQS) vem apresentando bons resultados na literatura [1,2].

Visto isso, o presente trabalho se propõe a solucionar e investigar o efeito do confinamento no sistema sob o potencial íon-dipolo induzido confinado, que mimetiza a interação de interesse e é dado por [3]

$$V(r) = -\frac{\alpha(Ze)^2}{2(4\pi\epsilon_0\epsilon)^2} \frac{1}{r^4}. \quad (1)$$

MÉTODOS

Para solucionar esse sistema de forma aproximada foi empregado o Método Variacional [4]. Os valores obtidos podem ser refinados com a minimização de parâmetros variacionais inseridos na função de onda teste.

A função de onda teste foi obtida com o uso do formalismo da MQS com a equação

$$\phi_0(r) \propto e^{-\int W_{ap}(r) dr}, \quad (2)$$

sendo $W_{ap}(r)$ uma função denominada superpotencial e que deve satisfazer uma equação do tipo Riccati [5].

O confinamento considera uma simetria esférica e para tanto inserimos no superpotencial os termos

$$\frac{1}{r_c - r} \text{ e } \frac{1}{r - r_{exc}}.$$

RESULTADOS

Como ansatz para o superpotencial usamos $W_{ap}(r) = b - \frac{b}{r^4} - \frac{1}{r - r_{exc}} + \frac{1}{r_c - r}$ e substituindo na equação (2) a função de onda teste é

$$\phi_0(r) \propto (r - r_{exc})(r_c - r)e^{-\frac{b}{3r^3} - br}, \quad (3)$$

sendo b o parâmetro variacional.

O valor de energia para o estado fundamental do sistema foi calculado para diferentes volumes de cavidades. Fixamos $r_{exc} = 4,66295 \text{ u.a.}$ e variamos o valor de r_c entre 4,9787 u.a. e 11,9589 u.a. de comprimento. A Tabela 1 apresenta alguns dos valores obtidos

Tabela 1: Autovalores de energia, em unidades atômicas, obtidos via Método Variacional para diferentes volumes de cavidades com permissividade de um meio aquoso.

Volume (u.a.)	r_c (u.a.)	Energia (u.a.)	b
101, 23	4,9787	0,002365440	0,072204
164, 29	5,2000	0,000204286	0,187239
202, 45	5,2845	-0,000066288	0,240987
337, 42	5,6441	-0,000486670	0,511587
6748, 33	11,9589	-0,000578466	2,014810

Fonte: Elaborada pelos autores

É possível observar uma variação da energia ligada à variação dos volumes de cavidade confinante, sendo que para volumes menores (confinamento drástico) a energia aumenta.

CONCLUSÕES

Verificamos que o uso dos métodos propostos é viável para solução do sistema sob o potencial íon-dipolo induzido confinado.

Observamos, com os resultados obtidos, um efeito anômalo dos valores de energia do estado fundamental para regiões com menor volume, que são positivos. Apesar desse fato, esse valor de energia é um estado ligado devido às barreiras de confinamento que mimetizam a conformação da proteína.

O modelo proposto permite obter bons resultados para a interação entre o íon-ferroso e a molécula de oxigênio que ocorre em cavidades esféricas.

REFERÊNCIAS

- SILVA, J. F. da; CARUSO, I. P.; DRIGO FILHO, E. Interaction between iron ion and dipole carbon monoxide inside spherical cavities. *The European Physical Journal D*, Springer, v. 75, n. 1, p. 1–9, 2021.
- SILVA, F. R.; DRIGO FILHO, E. Confined lennard-jones potential: A variational treatment. *Modern Physics Letters A*, World Scientific, v. 25, n. 08, p. 641–648, 2010.
- ISRAELACHVILI, J. N. *Intermolecular and surface forces*. [S.I.]: Academic press, 2011.
- SCHIFF, L. I. *Quantum mechanics*. [S.I.]: McGraw Hill press, 1968. v. 3.
- DRIGO FILHO, E. *Supersimetria aplicada à mecânica quântica: estudo da equação de Schrödinger*. [S.I.]: Editora Unesp, 2009.

AGRADECIMENTOS

LAMP agradece o suporte financeiro parcial do Conselho Nacional de Desenvolvimento Científico e Tecnológico (CNPq: 130527/2021-1).

Does Carbon Nanotubes Efficiently Adsorb Fipronil? New Insights from Theoretical Calculations.

Thales das Chagas Vieira (IC),¹ Felippo Batista de Lima (IC),¹ Henrique Cury Boaro (IC),¹ Neubi Francisco Xavier Junior (PQ),² Glauco Favilla Bauerfeldt (PQ) ^{1,*}

thalesvchagas@gmail.com; bauerfeldt@ufrj.br

¹ Departamento de Química Fundamental, Universidade Federal Rural do Rio de Janeiro; ² University of Surrey, Reino Unido.

Palavras Chave: *Fipronil, single-walled carbon*

INTRODUÇÃO

Fipronil is a systemic insecticide, of the phenylpyrazole class, which has been widely used in the agricultural and veterinary sectors. The success of this asset, however, contrasts with episodes of contamination of surface waters and, as a result of excessive and disorderly use, fipronil and its metabolites have been detected and quantified in important water bodies, such as the Guandu River basin.¹ Therefore, chemical analysis and monitoring of fipronil in water bodies is imperative. Du et al. suggest that biosensors and electrochemical sensors can match or even surpass methods analysis methods due to its excellent performance.² Sensors composed of carbon nanotubes can be adopted, provided they demonstrate thermodynamic and kinetic properties favorable to adsorption processes and electron transfer.

MÉTODOS

In order to assess and quantify the adsorption of fipronil on carbon nanotubes, theoretical calculations have been performed adopting the spin-polarized density functional theory (DFT) with periodic boundary conditions, assuming the PBE functionals and ultrasoft pseudopotentials (USPP) for the description of the internal electrons. A 25 x 25 x 17 Å³ Tetragonal P cell has been adopted in order to guarantee the continuity of the carbon nanotube along the z direction and to avoid possible interactions among fipronil and its periodic images. Furthermore, calculations have been performed using a 90 Ry cutoff and 1 x 1 x 3 k-points. The SWCNT[10,0] has been chosen as a molecular model of the carbon nanotube.

RESULTADOS

Results suggest weak adsorption modes, with relative energies ranging from -2.81 to -7.92 kJ mol⁻¹. Stabilization of the best adsorption mode is controlled by π stacking interactions, in which the nearest distances between fipronil and the carbon nanotube range from 4.44 to 4.91 Å, as shown in Fig 1A.

The nature of the interaction between adsorbent and adsorbate was also identified with the aid of molecular orbitals, band structure and differential

nanotubes adsorption, density functional theory, charge density analysis. The latter is shown in Fig 1B, in which charge depletion is represented by red isosurfaces and positive charge accumulation is depicted in green isosurfaces.

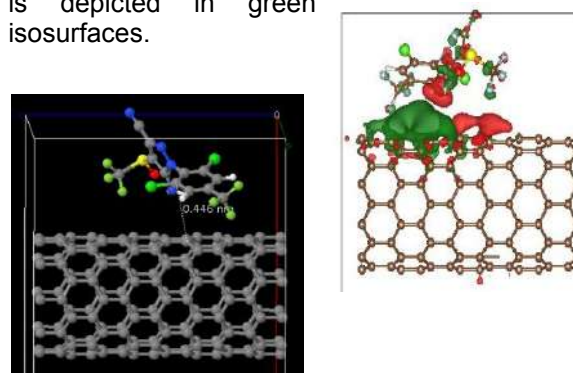


Figure 1. Left (A): Fipronil adsorption mode on SWCNT[10,0]. Right (B): Charge density difference plots.

CONCLUSÕES

Adsorption of fipronil on SWCNT[10,0] was studied with the aid of DFT calculations. Overall results suggest a weak physical interaction, probably due to the bulky structural characteristic of fipronil associated with the weak adsorption characteristic of the adsorbent, making difficult the docking of fipronil on unmodified carbon nanotubes walls difficult. New calculations are encouraged aiming at analyzing the effect of structural modifications, decoration and defects on CNT walls on the adsorption of fipronil.

REFERÊNCIAS

Fonte Arial 8 e espaçamento simples.

¹ L. Silva, M. Silva, PCCP, ano, vol. pg.

AGRADECIMENTOS



Elucidação dos Aspectos Dinâmicos de Liberação de Pesticidas Intercalados em Materiais Lamelares.

Sergio R. Tavares (PQ),^{1*} Pedro I. R. Moraes (PQ),^{2,3} Alexandre A. Leitão 3 (PQ).³

sergiotavares@iprn.ufrj.br¹

¹Instituto de Pesquisas de Produtos Naturais Walter Mors, Universidade Federal do Rio de Janeiro, Rio de Janeiro, RJ, 21941-599, Brasil ²Instituto de Química de São Carlos, Universidade de São Paulo, São Carlos, SP, 13560-970, Brasil

³Departamento de Química, Universidade Federal de Juiz de Fora, Juiz de Fora, MG, 36036-330, Brasil

Palavras Chave: DFT, Dinâmica Molecular, Interface .

INTRODUÇÃO

Pesticidas são substâncias puras ou uma mistura que repele organismos hostis a plantas ou animais. Seu uso indiscriminado é atualmente um tópico de grande preocupação em todo o mundo. A liberação controlada de pesticidas pode ser uma solução para esse impasse, visto que essas substâncias podem ser encapsuladas com materiais ecocompatíveis. Na busca pela compreensão dos efeitos microscópicos responsáveis pela liberação de pesticidas encapsuladas, este trabalho tem como objetivo elucidar as principais interações entre pesticida/cápsula, assim como entender os aspectos dinâmicos do processo. Para tal, foram realizadas simulações clássicas e quânticas (DFT) para os pesticidas 2,4-D e MCPA intercalados em hidróxidos duplos lamelares (HDL).

MÉTODOS

Simulações DFT foram inicialmente realizadas para a construção de uma estrutura de pesticidas intercalados. O funcional de troca e correlação utilizado foi o do tipo GGA-PW91. Os orbitais de Kohn-Sham foram expandidos por uma base de ondas planas com energia de corte de 60 Ry. Pseudopotenciais do tipo *Ultrasoft* foram utilizados para a descrição dos potenciais iônicos. O pacote Quantum Espresso¹ foi utilizado para a execução das simulações DFT com condições de contorno periódico. Quanto às simulações clássicas, as estruturas iniciais foram construídas a partir dos resultados obtidos pelas otimizações de geometria dos cálculos DFT. Uma superfície do nanocompósito foi gerada e colocada em contato com um reservatório de solvente (solução de carbonato de sódio). Trajetórias de produção foram obtidas em um ensemble NPT ($T = 300\text{ K}$ e $P = 1\text{ atm}$). As simulações de dinâmica molecular clássica foram feitas com o software LAMMPS²

RESULTADOS

Os parâmetros de rede simulados (tanto por DFT quanto por dinâmica molecular clássica) apresentaram um bom acordo com os valores experimentais, sendo os desvios relativos

menores que 3 %. A Figura 1 ilustra as diferentes conformações testadas pela etapa de simulações DFT.

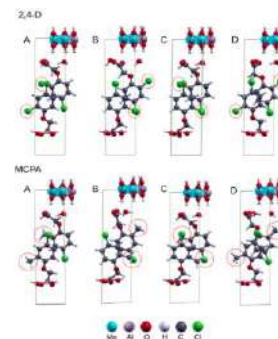


Figura 1: Estruturas das intercalações de pesticidas em HDL.

As interações foram estudadas por mapas de diferença de densidade, mostrando que os ânions de pesticida interagem fracamente entre si. As simulações clássicas indicaram que, no caso do pesticida 2,4-D, as moléculas de água do reservatório de solvente adentraram as galerias do material intercalado. O espaçamento basal do material apresentou um aumento acima de 5%. No caso do pesticida MCPA, tal aumento não foi observado.

CONCLUSÕES

Conclui-se que o processo de liberação controlada pode ser afetado pelo efeito de "inchamento" das galerias de HDL, já que, no caso do pesticida 2,4-D, houve uma grande absorção de água pelas lamelas. Tal efeito pode levar a uma facilitação da saída de ânions de pesticida com subsequente entrada de ânions carbonato para a região interlamelar.

REFERÊNCIAS

¹ P. Giannozzi et al. J. Phys.: Condens. Matter 2009, 21, 395502.

² S. Plimpton J. Comput. Phys. 1995, 117, 1–19.

AGRADECIMENTOS

Esse trabalho foi financiado em parte pela CAPES, CNPq e FAPEMIG. Parte das simulações foram realizadas no CENAPAD-SP.

Simulação de dinâmica molecular dos surfactantes dodecil-sulfato de sódio e dodecil-sulfato de colina em água

Kalil Bernardino (PQ),¹ Rafaela Eliasquevici* (IC)²

rafaela.eliasquevici@estudante.ufscar.br; kalib@ufscar.br

Rod. Washington Luís km 235 - SP-310 - São Carlos

Palavras Chave: Dinâmica Molecular, Auto-agregação, Surfactantes, Efeito Hidrofóbico, Dupla Camada Elétrica

INTRODUÇÃO

Surfactantes são moléculas anfifílicas com uma cabeça hidrofílica e uma cauda hidrofóbica. Acima da concentração micelar crítica, eles se agregam formando estruturas em que as cabeças ficam expostas ao solvente e as caudas ficam no interior do agregado, devido ao equilíbrio entre o efeito hidrofóbico e o caráter polar ou carregado da cabeça. Estruturas eletricamente carregadas em solução originam a chamada dupla camada elétrica, que consiste em uma distribuição de contra-íons ao redor do agregado, no caso, a micela que apresenta carga negativa. Ela é composta por íons aderidos à micela por interações específicas e outra composta por íons atraídos pela a superfície carregada da micela por forças eletrostáticas. Neste estudo, serão investigadas as micelas dodecil-sulfato de sódio (SDS) e dodecil-sulfato de colina (ChDS) em solução aquosa usando simulações computacionais de dinâmica molecular, a fim de caracterizar a dupla camada elétrica presente nas micelas e fazer uma análise qualitativa das diferentes estruturas de micelas formadas durante o processo de agregação.

MÉTODOS

- Simulação de dinâmica molecular: software GROMACS;
- T=323.15 K; P=1,0 bar; t = 240 ns;
- Empacotamento das moléculas: software Packmol;
- Simulação SDS em água: 60 íons dodecil-sulfato, 60 contra-íons sódio e 42000 moléculas de água;
- Simulação ChDS em água: 60 íons dodecil-sulfato, 60 contra-íons colina e 42000 moléculas de água.

RESULTADOS

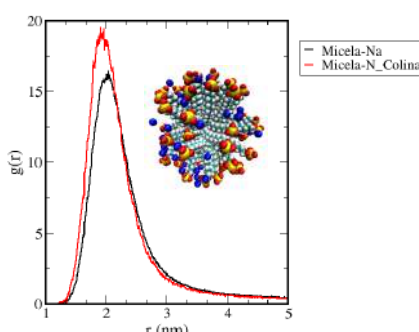


Figura 1 - Distribuição radial de pares dos contra-íons sódio e colina em relação ao centro de massa da micela e representação gráfica da micela de SDS.

A partir da análise da distribuição dos cátions ao redor das micelas (Figura 1), nota-se que a colina está mais concentrada na superfície da micela. Por outro lado, o sódio, sendo mais solvatado pela água, penetra menos na micela.

A distribuição radial de pares realizada entre os contra-íons (Na e N da colina) e os vários átomos do surfactante reforça que a colina penetra mais na micela que o sódio: há um pico grande entre o primeiro carbono depois da cabeça do surfactante e o nitrogênio da colina, já esse pico é muito menor e de maior raio para o sódio.

Tabela 1 - Resultados da análise de área de superfície acessível ao solvente para as micelas.

Micela	Área superficial surfactante (nm ²)	Área superficial surfactante - contra-íon (nm ²)	Blindagem do contra-íon (nm ²)
SDS	~109	~101	~8
ChDS	~109	~79	~30

A análise da superfície das micelas (Tabela 1) mostra que a quantidade de área disponível para a água é reduzida pelo contra-íon, sendo a colina mais eficiente em blindar a superfície do que o sódio. A área ocupada por uma única molécula de dodecil-sulfato é de aproximadamente 5 nm². Considerando a área total da superfície da micela e dividindo pelo número de moléculas de dodecil-sulfato presentes, chega-se a uma área de interação com o solvente de 1,82 nm² por molécula. Isso representa cerca de 36% da área que uma única molécula de dodecil-sulfato ocuparia se estivesse isolada.

CONCLUSÕES

Conclui-se que a colina está mais concentrada na primeira camada do surfactante, sendo mais eficiente em blindar a superfície, reduzindo a área disponível para a água em comparação com o sódio, que é mais solvatado pela água e penetra menos na micela. Tal compreensão será útil para entender quais são as forças motrizes de auto-agregação das micelas no solvente eutético profundo relina - formado pela mistura de cloreto de colina e uréia - que será o próximo passo do estudo.

REFERÊNCIAS

- ¹ H. J. C. Berendsen, D. van der Spoel, R. van Drunen, "GROMACS: A message-passing parallel molecular dynamics implementation," Comp. Phys. Comm. 91, 43–56 (1995).

AGRADECIMENTOS

FAPESP (2022/15862-7) e LNCC.

Molecular Dynamics Simulation of the Interaction of *n*-Octane with Clay Minerals

Stanislav R. Stoyanov (R)^{1*}, Jonathan Y. Mane (R)^{1*}

stanislav.stoyanov@nrcan-rncan.gc.ca; jonathan.mane@nrcan-rncan.gc.ca

¹ Natural Resources Canada, CanmetENERGY Devon, 1 Oil Patch Drive, Devon, Alberta T9G 1A8 Canada

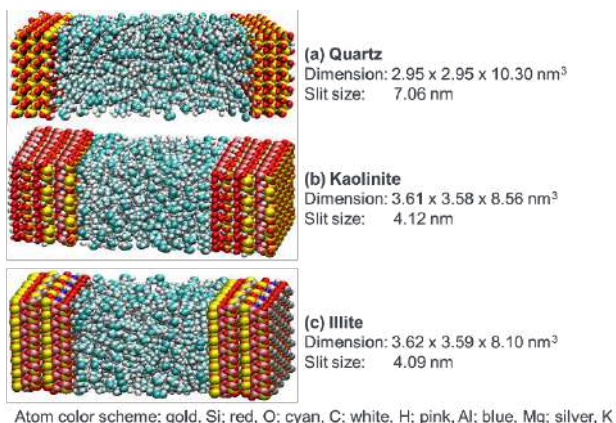
Keywords: molecular dynamics, layered aluminosilicates, clay interface, density profile, tight oil recovery

INTRODUCTION

The recovery of petroleum products from shale deposits highlights the need to study the interactions of model petroleum compounds with clay minerals under tight oil recovery conditions. We employ molecular dynamics (MD) simulations to study the behaviour of *n*-octane in rock nanopores. The MD simulations generate trajectories that contain large amounts of information, which provide valuable insights into the interactions, occurring in bulk hydrocarbons and with nanopore walls at conditions representative of tight oil recovery. The MD simulations enable the calculation of important thermodynamic and structural properties of model petroleum compounds near clay interfaces.

METHODS

Nanopore models¹ of (a) quartz, (b) kaolinite and (c) illite (representative of shale rock) are developed and then filled with *n*-octane (a representative hydrocarbon). The MD simulations are performed at the tight oil recovery conditions of 20–120°C and 1–300 bar for 100 ns using the Gromacs software under periodic boundary conditions. The force field CLAYFF is used for the bonding parameters and partial charges of the quartz, kaolinite, and illite atoms. The all-atom optimized parameters for liquid simulations OPLS-AA is used for the model *n*-octane.



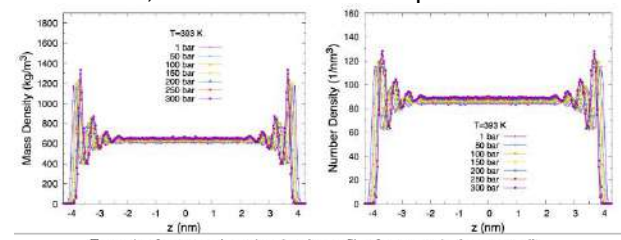
Atom color scheme: gold, Si; red, O; cyan, C; white, H; pink, Al; blue, Mg; silver, K

RESULTS

The trajectory analysis of *n*-octane molecules confined within the nanopore slit shows that the density distribution is not uniform. The intense oscillations of mass and number densities in the vicinity of nanopore surface indicate that strong intermolecular interactions exist, i.e. increased

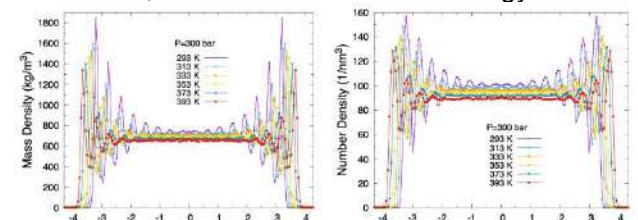
adsorption, between the nanopore and *n*-octane. The decreased adsorption of *n*-octane to the nanopore is indicated by the decreasing oscillation intensity towards the center of the slit. The density profiles within the nanopores also show the temperature (T) and pressure (P) effects on hydrocarbon organization:

- Increasing P at a given T resulted in increased *n*-octane density near the quartz surface and in the bulk, due to increased compression.



Example of mass and number density profile of *n*-octane in the quartz slit at T=393 K and P=1–300 bars.

- Increasing T at a given P resulted in decreased *n*-octane density near the quartz surface and in the bulk, due to increased kinetic energy.



Example of mass and number density profile of *n*-octane in the quartz slit at P=300 bars and T=293–393 K.

CONCLUSIONS

Changes and trends in the hydrocarbon densities near pore surfaces, including surface adsorption strength, as a function of temperature and pressure are observed. The calculated densities from the MD simulations are consistent with those published in the NIST Chemistry Webbook at the corresponding pressures and temperatures. The results of the MD simulations contribute to the development of mechanistic insights into the behavior of petroleum and its components that are key to improving hydrocarbon recovery from tight formations.

REFERENCES

- ¹ J.Y. Mane, S.R. Stoyanov, PCCP, 2023, **25**, 5638–5647.

ACKNOWLEDGMENTS

Program of Energy R&D (PERD), Government of Canada

© His Majesty the King in Right of Canada as Represented by the Minister of Natural Resources, 2023.

How domain segregation in ionic liquids controls nanoparticles aggregation - a molecular dynamics simulation study

Kalil Bernardino (R)¹

kalilb@ufscar.br

¹ Departamento de Química, Universidade Federal de São Carlos, São Carlos, SP, Brasil

Keywords: ionic liquids, domain segregation, nanoparticles, potential of mean force, molecular dynamics simulations

INTRODUCTION

Ionic liquids (ILs) have aroused interest as solvents due to several physical properties including negligible vapor pressure, chemical and thermal stability, and the ability to solvate both organic and inorganic species. Depending on the molecular structure of the ions, ILs can display polar and apolar domain segregation in a nanometric scale and the formation of those domains can stabilize nanoparticles dispersions without the need of additives like polymers or surfactants¹ and even be used as template to grow nanomaterials. In this work, the effect over the domain segregation over the stability of nanoparticles dispersions by means of molecular dynamics (MD) simulations.

METHODS

The potential of mean force for the association between two nanoparticles in ILs was computed to determine the aggregation free energy and the presence of solvent mediated barriers. To verify the effect of domain segregation, two different ILs were used: 1-octyl-3-methyl-imidazolium tetrafluoroborate, [OMIM][BF₄], and 1-butyl-3-methyl-imidazolium tetrafluoroborate [BMIM][BF₄], with only the former displaying significant domain segregation due to the longer alkyl chain of the cation. The Martini 3.0 force field² was employed to describe both the nanoparticles and the ILs. This force field was already used to study the structure and rheology of [BMIM][BF₄] both in the bulk liquid³ and confined between solid surfaces.⁴ The umbrella sampling method was used to compute the potential of mean force. Additional equilibrium MD simulations were performed to study the behavior of concentrated NPs dispersions. All the simulations were performed using Gromacs 2020.

RESULTS

The longer alkyl chain in [OMIM][BF₄] cation induces strong domain segregation in this IL. Depending on the hydrophilic or hydrophobic character of the NP surface, several polar and apolar shells are formed around it in an IL with strong domain segregation, while in the one without segregation, only a short-range order is observed (Figure 1 for a hydrophobic nanoparticle in both liquids). When two nanoparticles approach each other in an IL like [OMIM][BF₄], at some

distances there is a mixture between polar layers of the solvent around one particle with apolar layers around the other, which renders several local barriers for the aggregation observed in the potential of mean force, which stabilizes the dispersion and may result in complexes structures. This effect is absent in the liquid without domain segregation, which exhibits a simpler potential of mean force with only one barrier before the particles get in contact.

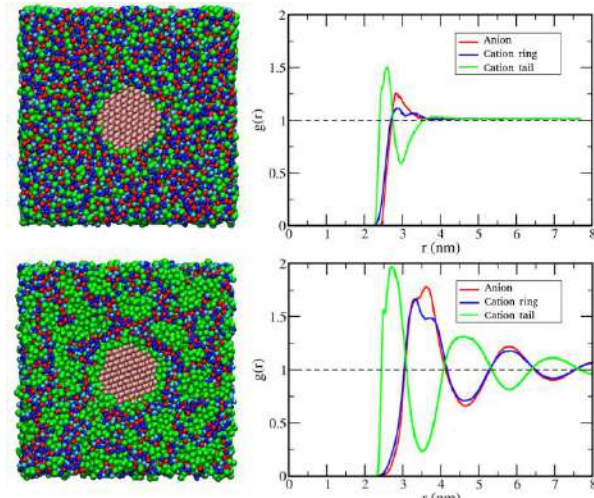


Figure 1 - Snapshots from the simulations (left) and radial distribution functions (right) showing the organization of the ILs [BMIM][BF₄] (top) and [OMIM][BF₄] (bottom) around a hydrophobic nanoparticle (showed in pink in the structures).

CONCLUSIONS

Domain segregation in ILs leads to polar and apolar shells around nanostructures which stabilizes their dispersions and may also be used to control complex hierarchical nanostructures formation.

REFERENCES

- 1 M. Iida, S. Kawakami, E. Syouno, H. Er, E. Taguchi, *J. Colloid Interface Sci.* 2011, 356, p. 630.
- 2 P. C. T Souza, R. Alessandri, J. Barnoud, S. Thallmair, I. Faustino, et al. *Nat. Methods* 2021, 18, p. 382.
- 3 K. Bernardino, M. C. C. Ribeiro, *PCCP*, 2022, 24, p. 6866.
- 4 K. Bernardino, M. C. C. Ribeiro, *JCP*, 2023, 158, p. 094712.

ACKNOWLEDGMENTS

The author is indebted with FAPESP (process 2019/04785-9) for financial support and with the LNCC-MCTI for the use of the SDumont supercomputer.



Estudo de Reações Químicas na Atmosfera de Titã

Isabela S. Vieira (PG),¹ Paulo T. C. Freire (PQ),² Rene F. K. Spada (PQ).^{1*}

isabeladvie@gmail.com; rfkspada@gmail.com

¹ Departamento de Física, Instituto Tecnológico de Aeronáutica, 12228-900, São José dos Campos, SP, Brasil;

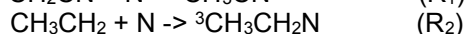
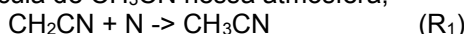
² Departamento de Física, Universidade Federal do Ceará, 60440-900, Fortaleza, CE, Brazil.

Palavras-Chave: *Termoquímica, Cinética Química, Titã.*

INTRODUÇÃO

Titã é a única lua do sistema solar a qual se tem informação acerca de uma atmosfera substancial. Sua composição química contém compostos orgânicos, e sua pressão atmosférica além da capacidade de abrigar líquidos em sua superfície indicam que Titã pode abrigar vida até mesmo diferente da que temos conhecimento. Portanto, contribuir para modelar a composição química de sua atmosfera é o foco deste trabalho em andamento. Krasnopolsky¹ publicou o modelo atual que temos de tal atmosfera, composto por cerca de 300 reações químicas. Entretanto, para estimar a viabilidade de cada uma delas é essencial o cálculo dos coeficientes de velocidade.

Algumas das reações propostas por Krasnopolsky chamam atenção devido à falta de informações na literatura e estudos aprofundados de cada uma individualmente. Portanto, decidimos estudar reações de formação da molécula de CH₃CN nessa atmosfera,



que apresentam seus coeficientes de velocidade estimados. A reação R₁ forma a acetonitrila em apenas uma etapa enquanto R₂ e R₃ constituem duas etapas na formação dessa molécula.

Nosso trabalho consiste na descrição da termoquímica, obtida por cálculos de estrutura eletrônica, e da cinética química, obtida por teoria do estado de transição e teoria de captura de R₁, R₂ e R₃.

MÉTODOS

Para obtermos dados acerca da termoquímica realizamos cálculos de estrutura eletrônica utilizando as metodologias de Møller-Plesset em segunda ordem (MP2), Coupled Cluster com excitações simples, duplas e triplas conectadas (CCSD(T)) e por fim a Teoria do Funcional de Densidade (DFT). Os resultados obtidos foram as energias das reações e as entalpias a 0K, além das barreiras clássicas e adiabáticas das reações caso haja ponto de sela na superfície de energia potencial. As propriedades de cinética química serão obtidas por teoria de captura para as reações sem barreira R₁ e R₂ e por teoria variacional do estado de transição (CVT) para R₃ a qual possui um ponto de sela.

Titã possui uma temperatura de cerca de 95K em sua superfície, dessa forma iremos calcular os efeitos de tunelamento a partir da abordagem de *Small-Curvature Tunneling* (SCT).

RESULTADOS

Até o devido momento realizamos cálculos de caminhos de mínima energia pelas abordagens de *Intrinsic Reaction Coordinate* (IRC) e *Nudged Elastic Band* (NEB) para garantir que os produtos estão corretamente conectados aos reagentes propostos. Cálculos de otimização de geometria e geometria fixa foram realizados para a descrição da termoquímica do problema. Nossos melhores resultados estão associados ao cálculo de geometria fixa CCSD(T)/CBS (extrapolando as bases aug-cc-pVTZ e aug-cc-pVQZ) considerando a geometria otimizada com a metodologia wb97x/def2-tzvp. A metodologia wb97x-d3/def2-tzvp retornou resultados satisfatórios em comparação com o nosso cálculo mais acurado, com divergências de: 2,5, 3,2 e 2,8 kcal/mol nas energias das reações R₁, R₂ e R₃, respectivamente. A distinção dos valores de barreira clássica de R₃ entre wb97x-d3/def2-tzvp e CCSD(T)/CBS é de 1,5 kcal/mol.

Os caminhos reacionais e as propriedades de cinética química estão em desenvolvimento tendo em vista que ainda estamos em busca do ponto de cruzamento que liga as reações R₂ e R₃ tornando possível a produção de CH₃CN no estado singuleto neste ambiente.

CONCLUSÕES

Nosso trabalho pretende contribuir para o conhecimento acerca da atmosfera de Titã e sua modelagem química. Dados de termoquímica já mostraram a viabilidade das reações R₁ e R₂ e seguimos investigando a viabilidade de R₃.

REFERÊNCIAS

¹ V. A. Krasnopolsky, A photochemical model of Titan's atmosphere and ionosphere, Icarus 201, 226 (2009).

AGRADECIMENTOS

O presente trabalho foi realizado com apoio do CNPq (projeto 143313/2020-7).



Emprego da técnica MIA-QSAR na proposição de novas tricetonas como potenciais inibidoras da enzima HPPD

Luiz R. Capucho (PG),^{1*} Elaine F. F. da Cunha (PQ),¹ Matheus P. de Freitas (PQ).¹

luiz.capucho2@estudante.ufla.br



¹ Departamento de Química do Instituto de Ciências Naturais da Universidade Federal de Lavras.

Palavras Chave: MIA-QSAR, Tricetonas, HPPD

INTRODUÇÃO

Descriptores químico-quânticos utilizados na análise quantitativa entre estrutura química e atividade biológica (QSAR), embora úteis e preditivos, não são facilmente obtidos, além de serem difíceis de se interpretar. Por outro lado, descritores digitais originados de imagens RGB (red-green-blue) correspondendo a estruturas químicas de uma classe congênere de compostos, podem ser obtidos rapidamente e fornecem uma relação direta sobre como determinados grupos químicos afetam a propriedade de interesse. Além disso, os átomos de uma molécula podem ser coloridos de tal forma que o seu valor RGB (que varia de 0 a 765) seja único para cada tipo de átomo; subsequentemente, esses valores podem ser substituídos por grandezas atômicas que representem, por exemplo, efeitos estéricos e eletrostáticos, tais como o raio de Van der Waals (r_{vdw}) e a eletronegatividade (ϵ). O método baseado nesses descritores digitais se chama *Multivariate Image Analysis applied to QSAR – MIA-QSAR*.

O método MIA-QSAR foi aplicado no design de novos candidatos a herbicidas. O conhecimento da relação entre o potencial herbicida e a estrutura de moléculas tricetonicas (inibidoras da enzima hidroxifenilpiruvato dioxigenase – HPPD) permitiu grandes avanços no controle de pragas, com destaque às culturas de milho e arroz. O problema de resistência gerado por mutações genéticas de espécies susceptíveis, porém, guiam pesquisas à busca de novos candidatos capazes de superar os fenômenos biológicos, garantindo assim maior segurança no manejo de herbicidas pela erradicação de práticas inadequadas, como o aumento de dosagem e misturas desconhecidas.

MÉTODOS

Dois conjuntos de amostras congêneres foram combinados e suas atividades herbicidas (IC_{50}) foram modeladas utilizando a técnica MIA-QSAR. As imagens obtidas pelo programa GaussView, capturadas e salvas em BMP, tiveram seus valores de pixel convertidos nas propriedades periódicas ϵ , r_{vdw} e r_{vdw}/ϵ , e pareados, na análise multivariada PLS (*Partial Least Squares regression*), com os respectivos valores de atividade em IC_{50} . O método *bootstrapping* de amostragem foi adotado

e reproduzido por 15 ciclos para cada propriedade. Por fim, os dados de validação estatística foram coletados, bem como os gráficos **b** (coeficientes de regressão PLS) e VIP (*Variable Importance in Projection*). Novas moléculas foram propostas e suas atividades foram preditas pelos modelos PLS confeccionados.

RESULTADOS

Os três tipos de descritores MIA foram igualmente preditivos, evidenciando a dependência da atividade herbicida dos compostos com efeitos estéricos e eletrostáticos.

Tabela 1. Média dos parâmetros de validação estatística da análise *bootstrapping* para as três propriedades periódicas (ϵ , r_{vdw} e r_{vdw}/ϵ).

Parâmetro	Média	Desv. Pad.
Componente PLS	3	0,00
RMSEC	0,40	0,02
r^2	0,72	0,02
RMSEy-rand	0,60	0,01
r^2_{y-rand}	0,36	0,02
$c_r^2_p$	0,51	0,01
RMSECV	0,54	0,00
q^2	0,51	0,00
RMSEP	0,43	0,01
r^2_{pred}	0,71	0,02
Avg. r^2_m	0,61	0,03
Δr^2_m	0,06	0,02
CCC	0,83	0,01

Através da análise dos gráficos **b** e VIP, 28 novas moléculas foram propostas, dentre as quais, 14 apresentaram valor de atividade predita superior ao composto padrão comercialmente utilizado, a mesotriona.

CONCLUSÕES

O método MIA-QSAR demonstrou satisfatória performance na proposição de novas moléculas com potencial herbicida, das quais 14 se mostraram promissoras. Os resultados foram corroborados por estudos de docking, que fazem uso da mecânica clássica para obter dados sobre a interação entre ligante e enzima HPPD.

REFERÊNCIAS

- ¹ L. Capucho, E. Cunha, M. Freitas, SQER, 2023, v. 34, pg. 231

AGRADECIMENTOS

Os autores agradecem às agências de fomento CNPq, CAPES e FAPEMIG.

Computer simulation of viscosity of fatty acid methyl ester derivatives

Lucas Q. dos Santos (PG)*,¹ Yaicel G. Proenza (PQ),¹ Ivani Malvestiti (PQ),¹ Ricardo L. Longo (PQ).¹

lucas.qsantos@ufpe.br;

¹Departamento de Química Fundamental, Universidade Federal de Pernambuco, 50740-560 Recife, PE, Brazil

Keywords: Biolubricants, Diffusion Coefficient, Stokes-Einstein Correlation, Molecular Dynamics, NMR-DOSY

INTRODUCTION

Viscosity is one of the three main transport properties, and it is the most important for characterizing biolubricants. Consequently, many attempts are being made to enhance and control this property. However, conventional measurement procedures require large sample quantities, which hinders the development of high-throughput approaches. In this context, the diffusion coefficient has been correlated with the medium viscosity through the Stokes-Einstein(SE) equation. The diffusion coefficient can be estimated by computer simulations from the temporal dependence of the mean squared displacement by the Einstein's relation¹, or determined by experimental methods such as the diffusion-ordered nuclear magnetic resonance spectroscopy (NMR-DOSY).

METHODS

Computational simulations were performed using Monte Carlo (MC) and molecular dynamics (MD) methods for methyl ricinoleate (MR) and its epoxidized derivative (EpMR) in NPT, NVE, and NVT ensembles with the multifunctional simulation package RASPA. The structures were optimized at the B3LYP/6-31+G(d,p) level, followed by the calculations of the atomic charges using the ChelPG-RESP² method with the G09 program.

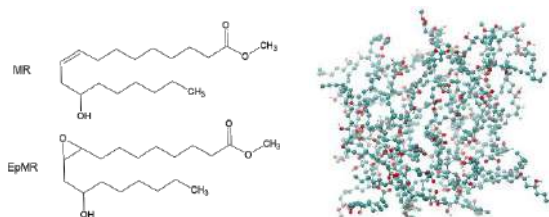


Figure 1.a) MR e EpMR molecular structures and b) simulation box with molecules of MR

Lorentz-Berthelot combination rules were employed to obtain Lennard-Jones parameters. The united-atom approach was employed for the -CH₃ and -CH₂- groups in semiflexible structures, where the molecules were divided into 4 groups, alternating flexible parts (aliphatic sections) with rigid fragments (unsaturation and oxygenated functions). Cubic boxes of 30.5 Å length were prepared, and the molecules were inserted using MC, with 10⁵ initialization cycles in the NVE ensemble and 2×10⁶ steps in the NPT ensemble, at 101.325 Pa and 298 K. A cutoff radius of 12 Å was applied. The final configurations from the MC-

NPT simulation were used for MD simulations with 2×10⁶ steps in the NVT ensemble with a time step of 0.5 fs. The diffusion coefficient was calculated in the linear region of the temporal dependence of the mean squared displacement, MSD(t).

RESULTS

The equilibration of each system was monitored by the temporal evolution of the potential energy and density. The calculated average density for MR was 0.925 ± 0.006 g/mL, in excellent agreement with the experimental value³ of 0.930 g/mL. For EpMR, the calculated average density was 0.967 ± 0.003 g/mL, slightly higher (+1.3%) than the experimental value³ of 0.956 g/mL. During the MD-NVT simulation, after 400 ps of propagation, both MR and EpMR exhibited linear MSD(t) behavior over time, yielding diffusion coefficients of 2.72×10⁻¹¹ m² s⁻¹ for MR and 9.5×10⁻¹² m² s⁻¹ for EpMR. The calculated diffusion coefficient for MR is in excellent agreement with the experimental measurement via NMR-DOSY of 2.70×10⁻¹¹ m² s⁻¹. The value obtained for EpMR suggests that this modified lubricant has a higher viscosity, which can be explained by the substitution of an unsaturation with a hydrogen bond acceptor (epoxide), compared to MR. This interpretation is further supported by the radial distribution function, which shows a significant frequency of oxirane groups in proximity to the hydroxyl hydrogen atoms, resulting in greater cohesion between the molecules compared to its precursor.

CONCLUSIONS

From the computational simulations, it was possible to estimate diffusion coefficients of fatty acid methyl ester derivatives. These measurements could be correlated with the dynamic viscosity of biolubricants using the SE equation, which was also validated for these fluids through experimental measurements by NMR-DOSY and rheological methods.

REFERENCES

- 1 M. P. Allen, D. J. Tildesley, *Computer Simulation of Liquids*, 2nd Ed., Oxford: OUP, 2017.
- 2 C. J. Cramer, *Essentials of Computational Chemistry: Theories and Models*, 2nd Ed., New York: Wiley, 2004.
- 3 V. B. Borugadda, V. V. Goud, *Energy Procedia*, v. 54, p. 75-84, 2014.

ACKNOWLEDGMENT

CNPq, CAPES, FACEPE, FINEP, CETENE, PRONEX.

Reinvestigating Parameters for Enhanced Identification of Antidepressant and Neuroleptic Drugs

Mylenna V. Ferro (IC),^{1*} Carlos M. R. Ribeiro (PQ),¹ Rodolfo G. Fiorot (PQ).¹

mvferro@id.uff.br; rodolfoviforot@id.uff.br

¹Departamento de Química Orgânica, Instituto de Química, Universidade Federal Fluminense

Keywords: psychotropic drugs, DFT, HOMO-LUMO gap

INTRODUCTION

Pharmacological interventions, particularly involving antidepressants and neuroleptics, offer therapeutic options for a subset of central nervous system (CNS) disorders. Neuroleptics are employed in managing psychotic disorders such as schizophrenia and bipolar disorder, while antidepressants are utilized for the treatment of anxiety, eating disorders and depression¹. By employing computational methods (in AM1) to analyze antidepressant and neuroleptic drugs, Cogordan and coworkers² proposed a correlation between their activities within the CNS and their values of HOMO, LUMO and ΔE (LUMO-HOMO) of the lowest energy conformers in the gas phase of certain drugs. Herein, we revisit these investigations by performing more modern computational methods, and broadening the sample space to encompass a more diverse array of drugs from the same class.

METHODS

The structures of the substances proposed by Cogordan (1-8) and of 20 commercial drugs divided between ADT neuroleptics and antidepressants (9-28) were subjected to conformational analysis using the Spartan'10 software, employing the Merck Molecular Force Field (MMFF) to explore a conformational space of up to 1000 conformers. All conformations with relative energies up to 10.0 kcal mol⁻¹ above the most stable conformer were subsequently fully optimized in Gaussian 09 software, using the following theory levels: Austin Model 1 (AM1) and Density Functional Theory (DFT) B3LYP-D3/Def2-TZVP, with further energy corrections being made by single-point calculations using the second order Møller–Plesset perturbation theory. Vibrational frequency calculations were performed to confirm their nature as a global minimum energy point on the potential energy surface.

RESULTS

When analyzing the AM1 method results, a discernible correlation seems to be present, corroborating the established trend hypothesized by Cogordan. Nevertheless, a closer examination of the computed ΔE (LUMO-HOMO) values in the same theory level for selected commercial

antidepressants and antipsychotics, utilizing identical methodologies, reveals a deviation from the aforementioned trend. To have more reliable results, the analysis was subsequently conducted employing bot MP2/Def2-TZVP//B3LYP-D3/Def2-TZVP method, resulting in findings that remain consistent with the preceding observations. The persisting nonconformity observed among several commercial drugs underscores their divergence from the trend originally proposed by Cogordan. Figure 1 shows the results of the aforementioned analysis.

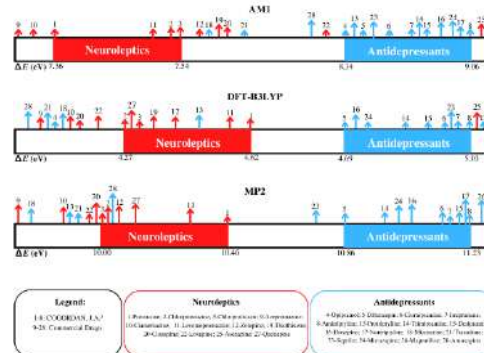


Figure 1. Representation of Cogordan's proposed activity interval.

CONCLUSIONS

Our outcomes suggest that there is no discernible direct relationship between the central nervous system (CNS) activity, particularly regarding antipsychotic and antidepressant effects, and the value of ΔE (difference in energy between LUMO and HOMO). The outcomes indicate that this particular method is unsuitable for predicting the activity of novel drugs within the CNS and should not be employed to expedite the drug development process. Further research will focus on the application of the Quantitative Structure Activity Relationship (QSAR) method.

REFERENCES

- SCHNEIDER, J. et al. Beyond depression: Other uses for tricyclic antidepressants. *Cleveland Clinic Journal of Medicine*, v. 86, n. 12, p. 807–814, 2019.
- COGORDAN, J. A. et al. Neuroleptic and antidepressant tricyclic compounds: Theoretical study for predicting their biological activity by semiempirical, density functional, and Hartree-Fock methods. *International Journal of Quantum Chemistry*, v. 71, n. 5, p. 415–432, 1999.

ACKNOWLEDGMENTS

To FAPERJ, CNPQ and Lattes.



Modelagem QSAR de uma série de *N*-(4-metanossulfônico) benzoil-*N'*-(pirimidin-2-il) tiureias com potencial herbicida

Natânia E. Rodrigues (PG),^{1*} Elaine F. F. da Cunha(PQ),¹ Matheus P. de Freitas (PQ).¹

natania.rodrigues2@estudante.ufla.br

¹ Departamento de Química do Instituto de Ciências Naturais da Universidade Federal de Lavras.



Palavras Chave: (MIA-QSAR, Tiureias, Herbicidas).

INTRODUÇÃO

Ureias e tiureias são grupos de herbicidas amplamente empregados no controle de ervas daninhas em práticas agrícolas. Exemplos de herbicidas *N*-fenil(tio)ureias comerciais incluem o diuron e o metiuron. É de suma importância o estudo do potencial herbicida desses compostos para o desenvolvimento de novos candidatos eficazes e resistentes para uso na agricultura. A ferramenta MIA-QSAR para estudos da relação quantitativa estrutura-atividade (QSAR) baseada em descritores de análise multivariada de imagens (MIA) torna-se aliada na modelagem molecular para encontrar uma correlação confiável das estruturas químicas de *N*-(4-metanossulfônico) benzoil-*N'*-(pirimidin-2-il) tiureias substituídas com suas respectivas atividades herbicidas. A técnica se fundamenta nas mudanças estruturais de uma série congênere de compostos que afetam as atividades biológicas, sendo que essas informações são codificadas através dos pixels (descritores) de imagens RGB (*red-green-blue*). O método MIA-QSAR tem demonstrado ser de fácil interpretação, por meio da análise dos coeficientes de regressão PLS (**b**) e dos scores *Variable Importance in Projection* (VIP), ao contrário, muitas vezes, de modelos baseados em descritores quânticos obtidos por meio de cálculos computacionais complexos.

MÉTODOS

A modelagem QSAR empregou as atividades herbicidas de 14 *N*-(4-metanossulfônico) benzoil-*N'*-(pirimidin-2-il) tiureias substituídas e imagens moleculares obtidas através do software GaussView. Os átomos foram representados por círculos proporcionais ao raio de VdW para codificar as propriedades estéricas e hidrofóbicas. Além disso, a cor de cada átomo foi numerada proporcionalmente à eletronegatividade de Pauling para formar a matriz descritora. A matriz de descritores foi calibrada com a matriz de porcentagem da inibição de raiz de *Brassica napus L.* por meio de regressão PLS (*Partial Least Squares*) e os dados estatísticos foram coletados para avaliar a qualidade do modelo. O modelo foi interpretado por meio dos gráficos MIA **b** (coeficientes de regressão PLS) e VIP (*Variable Importance in Projection*). Realizou-se também uma validação externa *bootstrap* em 10 ciclos,

para avaliar a robustez e estabilidade do método para o conjunto de dados selecionado. Por fim, novos compostos foram propostos e suas atividades foram preditas pelo modelo PLS gerado. Além disso, para entender o mecanismo de ação dos compostos sintetizados e propostos, realizou-se um estudo de *docking* molecular no sítio ativo da enzima fotossistema II (PSII).

RESULTADOS

A modelagem demonstrou-se adequada, robusta e preditiva, conforme parâmetros estatísticos de avaliação ($r^2 = 0,766$, RMSEC = 0,043, $\text{qr}^2_{\text{pred}} = 0,533$, $q^2=0.853$). Como o conjunto de dados é pequeno, a validação externa do tipo *bootstrap* é de suma importância para garantir que o modelo é robusto, estável e preditivo (Tabela 1).

Tabela 1. Desempenho estatístico da modelagem MIA-QSAR para validação externa usando o procedimento de *bootstrap* (10 ciclos).

Parâmetros ^a	média	Desv. Padrão
Componentes PLS	2,6	2.6±1.0
RMSEC	0.0372	0.037±0.016
r^2	0,8287	0.829±0.116
RMSEP	0,0744	0.074±0.034
r^2_{pred}	0,8333	0.833±0.222
r^2_m	0,5501	0.550±0.168

Por meio da análise dos gráficos **b** e VIP, as subestruturas que influenciam positivamente a atividade herbicidas foram detectadas e auxiliaram na proposição de 3 novos derivados de tiureias altamente promissores. Os resultados de *docking* demonstraram as interações ligante-PSII que justificam as atividades biológicas e corroboraram o potencial herbicida dos candidatos propostos.

CONCLUSÕES

A modelagem MIA-QSAR mostrou-se preditiva e confiável na proposição de novos candidatos a herbicidas para futuras sínteses e ensaios *in vitro* e *in vivo*.

REFERÊNCIAS

- ¹N. Rodrigues, E. F. F. da Cunha, M. P. Freitas. *Bull. Environ. Contam. Toxicol.*, 2022, v.108. pg. 1019-1025.

AGRADECIMENTOS

Os autores agradecem às agências de fomento CNPq, CAPES e FAPEMIG.



Construção de conjuntos de base relativísticos livres de prolapso variacional de tamanhos pequeno e médio para o sétimo período

Anne K. N. R. Dias (PG),¹ Eriosvaldo F. Gusmão (PQ),¹ Roberto L. A. Haiduke (PQ)¹

annekellenreis@usp.br; haiduke@iqsc.usp.br.

¹Instituto de Química de São Carlos (IQSC), Universidade de São Paulo, Avenida Trabalhador São Carlense, 400, São Carlos - SP.

Palavras Chave: conjunto de funções de base, prolapso variacional, elementos superpesados, cálculos relativísticos.

INTRODUÇÃO

A importância de se incluir os efeitos relativísticos se torna maior à medida em que os números atômicos dos elementos constituintes aumentam. Nesta situação, uma boa descrição de regiões da nuvem eletrônica mais próximas do núcleo exige o correto ajuste dos expoentes característicos das funções Gaussianas empregadas e a consequente eliminação do prolapso variacional.^{1,2,3} Dessa forma, conjuntos de base relativísticos livres de prolapso variacional vêm sendo produzidos em nosso grupo de pesquisa com resultados comprovando sua eficiência e competitividade.^{4,5} Considerando o desenvolvimento prévio de conjuntos de base de qualidade quadruplo-zeta (RPF-4Z), se torna agora necessária a construção de conjuntos de base de tamanho menor, principalmente para elementos pesados e superpesados. Dessa forma, o presente trabalho utiliza a versão polinomial do Método da Coordenada Geradora Dirac-Fock (p-GCDF) para a geração de tais conjuntos de base em conjunto com o modelo nuclear Gaussiano.

MÉTODOS

Os conjuntos de base livres de prolapso de tamanhos pequeno (SRPF) e médio (MRPF) foram desenvolvidos para os elementos do sétimo período utilizando o programa DFRATOM⁶ para os cálculos de estrutura eletrônica e o valor de 137,035999760 u.a. para a velocidade da luz.⁷ A otimização dos parâmetros do p-GCDF foi realizada por meio do algoritmo SIMPLEX,⁸ enquanto que a quantidade de funções foi definida por meio de balanço energético.

RESULTADOS

O estudo do balanço energético e o incremento do número de elétrons nas subcamadas permitiu estabelecer os tamanhos da base MRPF como 31s27p17d12f, 31s23p17d12f, 31s23p15d12f e 31s23p15d10f para os átomos 118-113, 112-103, 102-89 e 88-87, respectivamente. Por sua vez, para a base SRPF, encontramos tamanhos de 28s24p15d10f, 28s21p15d10f, 28s21p14d10f e 28s21p14d9f, respectivamente, para os mesmos elementos. Como esperado, foi detectado

prolapso variacional em todos os átomos e sua remoção deu-se pelo leve incremento de um dos parâmetros p-GCDF, onde o deslocamento das funções Gaussianas produzido neste processo proporciona uma melhor descrição das regiões mais internas sem causar prejuízos na descrição das energias obtidas. Assim, a eliminação do prolapso foi bem sucedida em todos os casos. Então, os maiores erros em relação aos resultados numéricos de referência^{7,9,10} observados para os conjuntos MRPF e SRPF foram de 43,1 e 100,9 mHartree, respectivamente, comprovando a excelente qualidade das bases aqui construídas.

CONCLUSÕES

Os conjuntos de base desenvolvidos neste trabalho para os elementos do sétimo período estão completamente livres de prolapso variacional, produzindo energias confiáveis e uma clara avaliação dos seus erros, os quais são de, no máximo, 43,1 e 100,9 mHartree, respectivamente, para conjuntos MRPF e SRPF. Em breve, a inclusão de funções de polarização deverá prover conjuntos de base prontamente adequados para uso com sistemas moleculares diversos.

REFERÊNCIAS

- 1 K. Faegri Jr, Theor. Chem. Acc., 2001, 105, 252.
- 2 H. Tatewaki, Y. Mochizuki, Theor. Chem. Acc., 2003, 109, 40.
- 3 H. Tatewaki, T. Koga, Y. Mochizuki, Chem. Phys. Lett., 2003, 375, 399.
- 4 T.Q. Teodoro, R.L.A. Haiduke, J. Comput. Chem., 2013, 34, 2372.
- 5 E.F. Gusmão, R.L.A. Haiduke, J. Comput. Chem., 2022, 43, 1901.
- 6 O. Matsuoka, Y. Watanabe, Comput. Phys. Commun., 2001, 139, 218.
- 7 L. Visscher, K.G. Dyall, At. Data Nuc. Data Tables, 1997, 67, 207.
- 8 J.A. Nelder, R.A. Mead, Comput. J., 1965, 7, 308.
- 9 K.G. Dyall, Theor. Chem. Acc., 2011, 129, 603.
- 10 K.G. Dyall, Theor. Chem. Acc., 2012, 131, 1172.

AGRADECIMENTOS

À CAPES (88887.653823/2023-00), CNPq (306763/2021-4) e FAPESP (2022/05138-0) pelo auxílio financeiro à pesquisa e ao IQSC pelo apoio e estrutura proporcionados.

Inclusion of the terpenes thymol and carvacrol into β -cyclodextrin through the GFN2-xTB multi-equilibrium quantum approach

Erick Ferreira Lacerda (UR)¹, Gleicy Teixeira (R)¹, Cleber Paulo Andrada Anconi (R)^{1*}

erick.lacerda1@estudante.ufla.br; cleberanconi@ufla.br

¹Laboratório de Química Fundamental (LQF), Department of Chemistry, Institute of Natural Sciences, University of Lavras, Lavras-MG, 37200-900, Brazil

Keywords: CD-based host-guest systems, GFN2-xTB semiempirical method, Binding constant, UD-APARM, Terpenes

INTRODUCTION

Terpenes, such as thymol and carvacrol, have been used in human history for their distinctive gastronomic aroma and therapeutic potential in traditional medicine from various cultures¹. These molecules exhibit hydrophobic characteristics². To advance in strategies to solve this limitation, researchers in supramolecular systems are investigating the complexation of terpenes (guest) with β -cyclodextrins (host). Cyclodextrins are easily absorbed in the organism and possess controlled absorption properties, making them promising candidates for overcoming the solubility barrier of terpenes in aqueous environments.

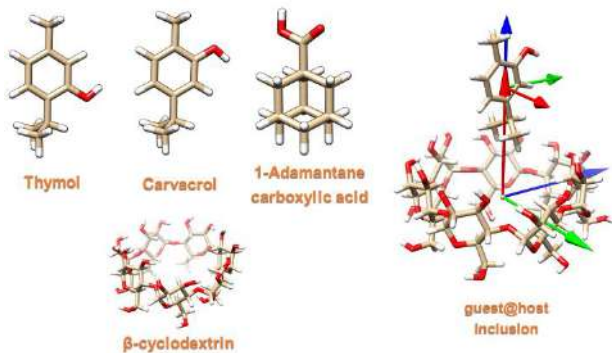


Fig. 1 Left: terpenes, β -cyclodextrin structure, and 1-Adamantane carboxylic acid. Right: UD-APARM axes of inertia for individual molecules in a supramolecular system formed with a CD as the host.

METHODS

- Each system was studied, considering more than 792 possible inclusion positions.
- The UD-APARM program was used to build these systems³.
- The GFN2-xTB method was employed to obtain theoretical data⁴.
- After optimizations and determination of free Gibbs energy, log K values were obtained in the condensed phase (Table 1) for the inclusion compounds Thy@ β -CD and Car@ β -CD. Additionally, for the sake of comparison, ADA-COOH@ β -CD was also investigated.

RESULTS

Table 1. Equilibrium constants obtained by the semiempirical method GFN2-xTB ($\log K_{xTB}$)

Terpenes	Systems	Log of binding constant	
		xTB	Expt. ^{5,6}
Thy@ β CD	10	2.28	3.16
Car@ β CD	6	4.19	3.31
ADA-COOH@ β CD	10	5.86	5.02

CONCLUSIONS

In previous investigations concerning cyclodextrin-based inclusion systems by our group, an excellent linear correlation between theoretical and experimental data was achieved. The data in Table 1 indicates that the potential energy surface (PES) exploration employed must be improved ($R^2=0.7752$). Finally, according to Table 1, the experimental trend was accomplished.

REFERENCES

- ¹Heusler, Friedrich. P. *Blakiston's son & Company*, 1902.
- ²Zhou, F.; Pichersky, E *Current Opinion in Plant Biology*. 2020, 55, 1-10.
- ³Anconi, C. P. A. *Acs Omega* 2020, 5 (10), 5013-5025.
- ⁴Bannwarth, C.; Ehlert, S.; Grimme, S. *Journal of Chemical Theory and Computation* 2019, 15 (3), 1652-1671.
- ⁵Palepu, R.; Reinsborough, V. C. *Australian Journal of Chemistry* 1990, 43 (12), 2119-2123.
- ⁶Cedillo-Flores, O. E.; Rodríguez-Laguna, N.; Hipólito-Nájera, A. R.; Nivón-Ramírez, D.; Gómez-Balderas, R.; Moya-Hernández, R. *Food Hydrocolloids* 2022, 124, 107307.

ACKNOWLEDGMENTS

The authors thank Professor Hélio Ferreira dos Santos for the access to the NEQC (Núcleo de Estudos em Química Computacional, UFJF, Brazil) computer facility and also thanks the Laboratório Central de Computação Científica (LCC) of UFLA for providing additional computing resources. Furthermore, professor Cleber Paulo Andrada Anconi also thanks the Fundação de Amparo à Pesquisa do Estado de Minas Gerais (FAPEMIG) for supporting the Laboratório de Química Fundamental (LQF), where the research was conducted.



Theoretical study XeF_n ($n = 2, 4, 6$): enthalpies of formation

Cleuton de Souza Silva (PG)^{*1,2}, Francisco das Chagas Alves Lima (PQ)³

cleutonsouza@yahoo.com.br

¹Instituto de Ciências Exatas e Tecnologia, Universidade Federal do Amazonas, Campus de Itacoatiara, 69100-021 Itacoatiara – Amazonas, Brazil; ²Departamento de Química, CCN, UFPI, 64049-550 Teresina, PI, Brazil; ³Centro de Ciências da Natureza–CCN, Universidade Estadual do Piauí, Teresina, Brazil

Keywords: G4(MP2)-XK, heat of formation, composite method, thermochemistry

INTRODUCTION

Dixon and collaborators [1] showed atomisation energies at 0 K and heats of formation at 0 and 298 K are predicted for XeF_6 , XeF_5^- , XeF_4 , XeF_2 , XeF^+ , and XeF^- using CCSD(T) calculations with correlation-consistent basis sets for Xe and Fluorine. The structure of XeF_6 is hard to acquire with the C3v and Oh structures having essentially the same energy. Dixon et. al [1] showed Oh structure is only 0.19 kcal/mol less than the C3v one at the CCSD(T)/CBS level using an approximate geometry for the C3v structure [1].

The composite methods that have gained prominence are the G4(MP2)-6X [2] G4(MP2)-XK methods. Many methods used a Pople basis set; the G4(MP2)-6X method used a Pople-type basis set, and G4(MP2)-XK used a Karlsruhe-type basis set with def2-ECP pseudopotential. The G4(MP2)-XK method is being applied in some studies, such as: enthalpies of formation for fullerenes, enthalpies of formation for a large set of C, H, N, and O species, and hydride affinities..

In this work, the thermochemical values of the considered XF_n ($n = 2, 4, 6$) compounds have been determined using the G4(MP2)-XK method, BMK and M06-2X with basis sets def2-QZVP and def2-ECP, where the G4(MP2)-XK presented the best results.

COMPUTATIONAL METHODS

The optimised geometries at the BMK with def2-QZVP in pseudo def2-ECP. Used zero-point vibrational energies (ZPVEs) and thermal corrections to enthalpy at 298 K (ΔH_{298}). All of our calculations were using the G09 program. The G4(MP2)-XK [2] was created to be a new version of the pan-periodic table of G4(MP2)-6X. It has a Karlsruhe basis set in order to cover most of the elements.

RESULTS

The value calculated by Dixon et al. [1] for the total bond dissociation energy of XeF_6 differs by 12.2 kcal/mol from the experimental value based on balance measurements while that calculated with G4MP2-XK differs by 2.1 kcal/mol. In the case of the atomisation energy of XeF_4 , Dixon et al. [5] determined the difference between the experimental and theoretical was 8 kcal/mol.

in the case of G4MP2-XK, this difference was 0.9 kcal/mol.

The results obtained by G4MP2-XK were closer to the experimental values based on balance measurements, so this method proves to be reliable for the study of XeF_x , since the results are very limited and can be compared to CCSD(T)/CBS.

The BMK calculations had a deviation between the experimental-theoretical results of 4.0 kcal/mol, 4.8 kcal/mol, and 4.6 kcal/mol for XeF_2 , XeF_4 , and XeF_6 , respectively, while the calculations of M06-2X had a deviation between the experimental-theoretical results of 2.0 kcal/mol, 3.2 kcal/mol, and -0.1 kcal/mol for XeF_2 , XeF_4 , and XeF_6 , respectively. Unlike CCSD(t)/CBS and G4MP2-XK calculations, BMK and M06-2X calculations are more negative than the experimental values.

Table I - Calculated and Experimental Heats of Formation (kcal/mol)

	CCSD	G4MP2-XK	BMK	M06-2X	expt (0K)
XeF_2	-23.3	-21.9	-29.3	-27.3	-25.3
XeF_4	-42.5	-46.6	-55	-53.4	-50.2
XeF_6	-55.9	-63.6	-72.7	-68	-68.1

CONCLUSIONS

The G4MP2-XK method presented the best results in this work with the molecules that were studied. The G4(MP2)-XK method gives a satisfactory performance on evaluating the enthalpies of formation for the majority of the examined compounds with results equivalent to the CCSD(T)/CBS for XeF_x compounds studied in this work.

REFERÊNCIAS

¹ D.A. Dixon, W.A. De Jong, K.A. Peterson, K.O. Christe, G.J.Schrobilgen, J. Am. Chem. Soc. (2005) 127 862.

² B. Chan, A. Karton, K. Raghavachari, J. Chem. Theory Comput. (2019) 15 447.

AGRADECIMENTOS

We acknowledge support from FAPEAM and CENAPAD-UFC.

Análise de estruturas exóticas metaestáveis ionizadas derivadas de anéis heterocíclicos aromáticos

Amir L. Perlin (PG),^{1*} Ricardo R. O. Junior (PQ),¹ Wania Wolff (PQ).²

amirperlin.94@gmail.com

¹Departamento de Química, Universidade Federal do Rio de Janeiro, Rio de Janeiro – RJ - Brasil; ²Departamento de Física, Universidade Federal do Rio de Janeiro, Rio de Janeiro – RJ - Brasil.

Palavras-Chave: Aromáticos, Heterocíclicos, DFT, AUTOMATON

INTRODUÇÃO

A detecção de espécies duplamente ionizadas,¹ assim como a determinação da geometria de mínimo global do benzeno² influenciou estudos do mecanismo de fragmentação e do mapeamento das possíveis estruturas de intermediários e produtos. Em particular das espécies, C₆H₆²⁺, C₆H₅²⁺, C₆H₄²⁺ e C₆H₃²⁺.³ Nesse estudo empregou-se o programa AUTOMATON⁴ utilizando em um algoritmo genético para a busca de estruturas mínimo global. Nesse novo estudo, busca-se verificar se há uma recorrência na produção da estrutura piramidal ao substituir um dos átomos de carbonos por outros átomos.

MÉTODOS

Primeiro realizou-se uma busca global em nível DFT com o programa AUTOMATON acoplado ao Gaussian utilizando o funcional PBE0 na base 6-31G(d,p). As espécies estudadas até o momento são os cátions da família 13, C₅H₆X⁺ (X = B, Al e Ga) e dicátions das famílias 14, C₅H₆Y²⁺ (Y = C, Si e Ge), e 15, C₅H₅Z²⁺ (Z = N, P e As).

As dez estruturas de menor energia foram reotimizadas com o mesmo funcional com a base cc-pVTZ, com cálculo de frequência e correção de energia de ponto zero (ZPE). Por fim, para recuperar, realizou-se um cálculo *single-point* CCSD(T) na mesma base. Para análise, organizou-se as cinco estruturas de menor energia em ordem crescente na escala kcal mol⁻¹.

RESULTADOS

A seguir, apresenta-se os resultados obtidos para a família 14, 15 e 13, respectivamente:

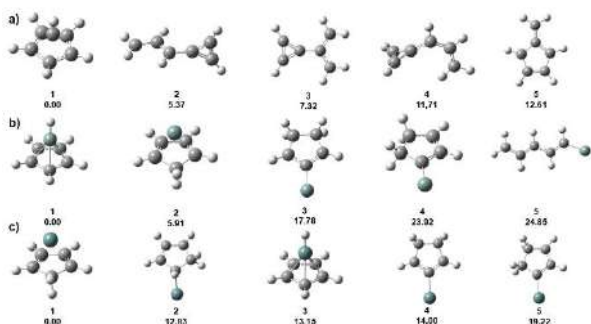


Figura 1: Isômeros de menor energia das moléculas a) C₆H₆²⁺, b) C₅H₆Si²⁺ e c) C₅H₆Ge²⁺

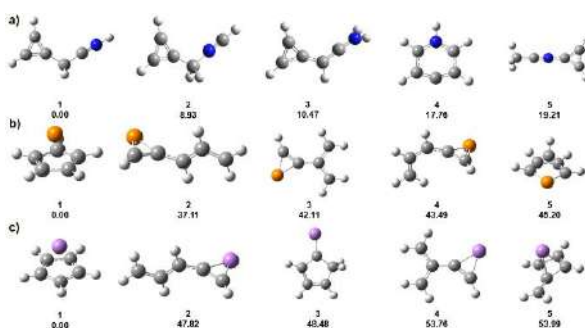


Figura 2: Isômeros de menor energia das moléculas a) C₅H₅N²⁺, b) C₅H₅P²⁺ e c) C₅H₅As²⁺

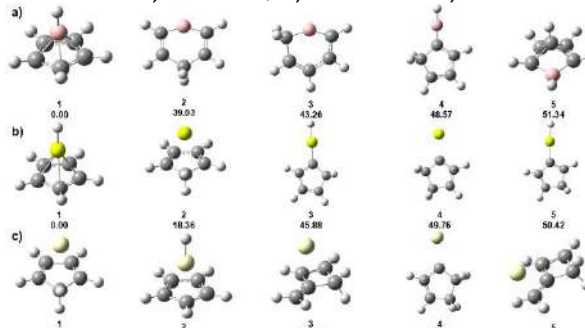


Figura 3: Isômeros de menor energia das moléculas a) C₅H₆B⁺, b) C₅H₆Al⁺ e c) C₅H₆Ga⁺

CONCLUSÕES

Os resultados indicam que é possível a produção de cátion na família 13 com a geometria piramidal. Obteve-se também outra forma piramidal para os dicátions contendo Ga e Ge, com todos os átomos de hidrogênio ligados aos carbonos. Por fim, o único sistema que não apresentou geometria piramidal de baixa energia foi o C₅H₅N²⁺.

REFERÊNCIAS

- KROGH-JESPERSEN, K. Journal of the American Chemical Society, v. 113, n. 2, p. 417–423, 1991.
- J. Jašík, D. Gerlich, J. Roithová, J. Am. Chem. Soc., 2014, 136, 2960–2962.
- O. Yañez, R. Báez-Grez, D. Inostroza, W. Rabanal-León, R. Pino-Rios, J. Garza, W. Tiznado, J. Chem. Theory Comput., 2019, 15, 1463–1475.
- W. Wania, et al. J. Phys. Chem. A 2020, 124, 44, 9261–9271

AGRADECIMENTOS

CNPq, a CAPES e a FAPERJ (JCNE, Nº DO PROCESSO E-26/200.249/2023). Agradecemos também ao LNCC por fornecer recursos computacionais via supercomputador SDumont.



Simulação do espectro eletrônico de um complexo de Fe^{II} contendo ligantes NHC para possível uso como fotossensor

Amanda D. Torres (PG),^{1*} Alexandre B. da Rocha (PQ),² Ricardo Rodrigues de O. Júnior (PQ).¹

dornelaamanda@gmail.com

¹Departamento de físico-química, Instituto de Química, Universidade Federal do Rio de Janeiro.

Palavras-Chave: Complexo, Espectro Eletrônico, TD-DFT, fotossensor.

INTRODUÇÃO

Uma classe de ligantes que vem sendo estudada nos últimos anos são os carbenos N-heterociclos (NHCs). Carbenos são uma classe de compostos neutros que possuem um átomo de carbono divalente e 6 elétrons de valência.¹ Já os NHCs são definidos como espécies heterocíclicas contendo um carbono carbênico e pelo menos um átomo de nitrogênio no anel.² Uma classe de aplicações que vem ganhando muito espaço na química dos NHCs são as que envolvem suas propriedades fotoquímicas.³ Com a crescente necessidade mundial por fontes de energia mais limpas, muito vem sendo feito para aprimorar o uso de energia solar e de energia provinda de hidrogênio. No entanto, além da mudança da fonte de energia, é preciso mudar o fornecimento e o consumo através de dispositivos mais eficientes e limpos. Por muitos anos foram usados complexos de metais nobres como fotossensores nessas aplicações. No entanto, eles são caros e envolvem reagentes tóxicos em sua exploração. Surge, então, a proposta de substitui-los por metais da primeira linha de transição, que são, além de mais baratos, menos tóxicos.⁴ O objetivo desse trabalho é, portanto, fazer um estudo do espectro eletrônico do [Fe(L₁)₂]²⁺ ($L_1 = 2,6\text{-bis}[3\text{-isopropilimidazol-2-ilideno]piridina}$), um representante de um conjunto de compostos que vêm sendo estudados como possíveis substitutos dos complexos de rutênio.⁵

MÉTODOS

A otimização de geometria foi feita usando o método DFT/B3LYP com a correção de dispersão D3BJ e as bases def2-TZVP no metal central e def2-SVP nos ligantes. Já para a estrutura eletrônica foi usado o método TDDFT/PBE0, com a base def2-TZVP. Deslocando-se cada região do espectro em uma quantidade diferente, pode ser obtida uma boa concordância entre os espectros simulado e experimental, mostrado na figura 2.

Esse tratamento diferente em diferentes regiões do espectro é válido já que os funcionais possuem aproximações distintas dependendo do alcance da interação. Sendo assim, um mesmo funcional pode descrever melhor uma região do que outra do espectro.

RESULTADOS

Figura 1. Espectro eletrônico simulado pelo método TD-DFT/PBE0 com a base def2-TZVP.

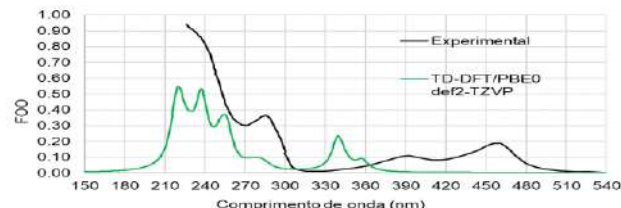
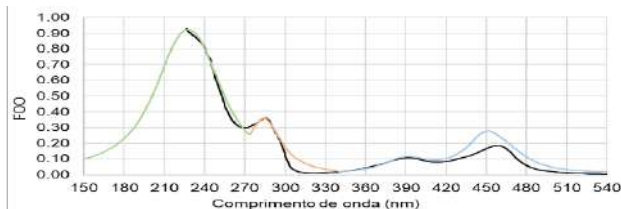


Figura 2. Espectro simulado usando o método TD-DFT/PBE0 com a base def2-TZVP. Cada região foi tratada separadamente, com deslocamentos de 113, 30 e 0 nm (0,91, 0,45 e 0 eV, respectivamente).



Foram testados, ainda, diversos outros funcionais, o método NEVPT2, efeitos de acoplamento vibrônico e acoplamento spin-órbita. Esses efeitos, no entanto, não melhoraram o espectro de forma geral.

CONCLUSÕES

Ainda que necessário certo deslocamento nas energias, a concordância com o espectro experimental é boa. O complexo apresenta uma boa absorção na região do visível, característica importante para a aplicação como fotossensor, mostrando-se promissor.

REFERÊNCIAS

- 1 HARDACRE, C., et al., Royal Society of Chemistry, 2017.
- 2 ARDUENGO, A. J., et al., J. Am. Chem. Soc 1992.
- 3 VISBAL, R., et al. Royal Society of Chemistry, 2014
- 4 FÖRSTER, et al, Royal Society of Chemistry, 2020
- 5 BOKAREVA, O. S., et al. Phys. Chem. Chem. Phys. 2020.; ZIMMER, P., et al., European J. of Inorg. Chem., 2017.

AGRADECIMENTOS

CNPq, CAPES, LNCC, DIRAC, PGQu, GETMM

Estudo computacional da dinâmica não-adiabática do CH₂FCI (HCFC-31)

Albert J. F. W. H. de S. Silva (PG),^{1*} Elizete Ventura (PQ),¹ Silmar A. do Monte (PQ).¹

albertwesleyhess@gmail.com

¹Departamento de Química, Universidade Federal da Paraíba, João Pessoa-PB.

Palavras Chave: Fotoquímica, CH₂FCI, Dinâmica de estados excitados.

INTRODUÇÃO

Muitos compostos interferem diretamente no equilíbrio químico $O_2 \rightleftharpoons O_3$ presente na Estratosfera. Um exemplo é o CH₂FCI (ou HCFC-31), que age por um mecanismo semelhante aos cloro-fluorocarbonetos (CFCs), e reduz a concentração de ozônio atmosférico a partir da liberação do radical Cl• após a absorção de radiação UV¹. Estudos acerca da fotodissociação dos CFCs e HCFCs são fundamentais para entender como essas moléculas são ativadas na Estratosfera. O objetivo deste trabalho é investigar a fotólise do CH₂FCI, utilizando CASSCF em conjunto com o método de dinâmica não-adiabática Surface Hopping (SH).

MÉTODOS

A geração das condições iniciais e espectros de fotoabsorção foram obtidos a níveis CASSCF e MR-CISD, ambos com a base d-aug-cc-pVQZ (C)/aug-cc-pVQZ (F, Cl, H), CAS (6,4) (σ_{CCl} , σ_{CCl}^* , n_1 [Cl] e n_2 [Cl]), e 2 orbitais de Rydberg no espaço auxiliar (3s [C] e 3p_σ [C]). Estes espectros foram gerados a partir de uma amostragem de 1000 pontos segundo a distribuição de Wigner. As simulações de dinâmica não-adiabática foram calculadas a nível CASSCF na janela de excitação 7,8 ± 0,25 eV, as quais 100 trajetórias estocasticamente escolhidas foram calculadas e as equações de movimento integradas a cada 0,5 fs. Todos os cálculos utilizaram 5 estados eletrônicos singletos e foram obtidos por meio do programa Newton-X em interface com Columbus.

RESULTADOS

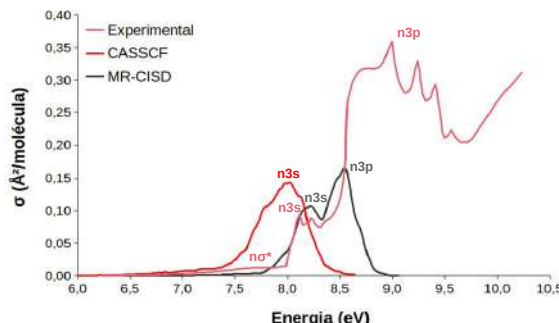


Figura 1 – Espectros de absorção UV para a molécula CH₂FCI. O espectro experimental encontra-se na referência². Na Figura 1, observa-se um grande deslocamento da banda n-3s do espectro CASSCF em relação a correspondente banda experimental. Contudo, o oposto ocorre para a mesma banda no nível MR-

CISD. Por outro lado, na janela de excitação estudada o rendimento de S₃, estado responsável pela formação do par iônico, HFC⁺H••Cl⁻, foi de 45% para as simulações de dinâmica. Esta alta porcentagem de trajetórias leva ao canal iônico, e a subsequente liberação de Cl⁻. Esse alto valor é resultante da maior eficiência computacional do CASSCF devido a sua boa capacidade de descrever certas regiões das curvas de energia potencial (CEPs) com significativo caráter multiconfiguracional e a disponibilidade de acoplamentos não-adiabáticos³. A Figura 2 apresenta uma trajetória representativa com fim em S₃ e algumas mudanças nucleares dessa mesma trajetória. Nota-se que até o final da simulação, para R_{ClI} = 2,12 Å os pares de estados S₁/S₂ e S₃/S₄ permanecem degenerados, em conformidade com as CEPs MR-CISD(+Q)⁴.

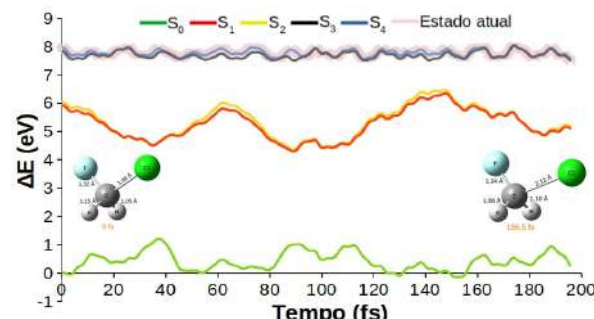


Figura 2 – Evolução temporal das energias para uma trajetória representativa do CH₂FCI, obtida a nível CASSCF/d-aug-cc-pVQZ (C)/aug-cc-pVQZ (F, Cl, H).

CONCLUSÕES

Este estudo apresenta a primeira descrição teórica à respeito da fotoquímica do CH₂FCI, com destaque para a dinâmica não-adiabática utilizando um método de estrutura eletrônica multiconfiguracional. Além disso, foi obtido um alto rendimento de S₃ nas simulações.

REFERÊNCIAS

- ¹ABAS, N. et al. *Renewable and Sustainable Energy Reviews*, v. 90, p. 557-569, 2018.
- ²DOUCET, J. et al. *The Journal of Chemical Physics*, v. 58, n. 9, 1973.
- ³CRESPO-OTERO, R.; BARBATTI, M. *Chemical Reviews*, v. 118, p. 7026-7068, 2018.
- ⁴SILVA, A. J. F. W. H. S. *Estudo teórico da Fotoquímica do 1-cloro-1-flúor-metano (HCFC-31)*. 2019. 77 f. Dissertação (Mestrado em Química) – Departamento de química, UFPB, João Pessoa, 2019.

AGRADECIMENTOS

CAPES, CNPq, FAPESQ, UFPB, PPGQ, LMMRQ.



Abstraction Reaction from Silane with Hydrogen and Methyl Radicals: Variational Transition State Theory Rate Constants

KANO, G. FILIPE (PG),^{1*} ROBERT-NETO O. (PQ),² FERRÃO, F. A. LUIZ (PQ),¹ CARVALHO, F. V. EDSON (PQ),³ MACHADO, B. C. FRANCISCO (PQ)¹

kanofilipe@gmail.com;

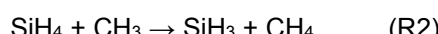
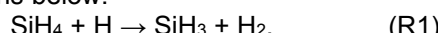
¹ Instituto Tecnológico da Aeronáutica, José dos Campos, São Paulo, Brazil; ²Instituto de Estudos Avançados, São José dos Campos, São Paulo, Brazil; ³Universidade Federal do Maranhão, São Luís, Maranhão, Brazil.

Key words: ω B97X-D, CCSD(T), Electronic structure, Chemical kinetics, Thermochemistry

INTRODUCTION

The gas phase reaction (R1) plays a significant role in chemical vapor deposition widely used in semiconductor industries¹. Its kinetic have been studied experimentally² and theoretically¹. Reliable kinetic data for the reaction (R2) are sparse and their study is essential to understanding the reactivity of Si-H bonds with alkyl radicals³.

The main purpose of this work is to compute accurate values of the rate constants from the reactions below:



Also, we have carried out calculations of the kinetic isotope effects (KIEs) for different deuterium combinations on (R1) and (R2).

METHODS

The geometries of reactants, products, and first-order saddle point of the reactions (R1) and (R2) were optimized using correlation consistent basis set with diffuse functions and various levels of theory, as Density Functional Theory (DFT) using ω B97XD and couple-cluster with single-double and perturbative triples CCSD(T). Single-point energy calculations were employed with CCSD(T)/aug-cc-pV(n+d)Z ($n= Q$ and 5) level with the energies extrapolated to the Complete Basis Set (CBS) limit using the CCSD(T)/aug-cc-pVTZ optimized geometries. The Dual-level strategy was used, and the low-level electronic energy was computed using ω B97X-D/aug-cc-pVTZ and the high-level corrections of electronic energies carried out with CBS_{Q-5}. The High-Level vibrational frequencies corrections were computed with the CCSD(T)/aug-cc-pVTZ level of theory.

The MEP of the reaction systems was calculated from $s = -1.5 \text{ \AA}$ to $s = +1.5 \text{ \AA}$.

Rate constants calculations were carried out with the Variational Transition State Theory (VTST) with small-curvature (SCT) and large-curvature (LCT) multidimensional tunneling corrections.

RESULTS

Table 1. list energetic data from reactions (R1) and (R2), including vibrationally adiabatic barrier ($\Delta V_a^{G,\#}$) and enthalpy of the reaction at 0 K (ΔH_0^0).

Table 1: Energetics (in kcal/mol) of the reactions (R1) and (R2).

Method	(R1)		(R2)	
	$\Delta V_a^{G,\#}$	ΔH_0^0	$\Delta V_a^{G,\#}$	ΔH_0^0
ω B97XD/ \emptyset	4.7	-11.8	6.6	-13.0
CCSD(T)/ \emptyset	4.2	-13.6	8.7	-13.2
CBS _{Q-5}	4.4	-13.0	9.2	-12.6
Exp	4.1 ± 0.7^2	-12.9 ± 0.6^2		-13.3^4

$\emptyset \equiv \text{aug-cc-pVTZ}$

The results calculated by CBS_{Q-5} approach for the reaction (R1) gave values for $\Delta V_a^{G,\#}$ and ΔH_0^0 in excellent agreement with the experimental² data. For the reaction (R2), experimental⁴ value for ΔH_0^0 also in good agreement with the present CBS_{Q-5}.

The CVT/SCT rate constants were calculated to the (R1) and (R2) paths at the temperature range of 200-1600 K providing the normal KIE (equal or larger than 1) for (R1), which converges to 1 at high temperatures. At 250 K for (R1) and (R2) paths, CVT/SCT is equal to 6.23×10^{-14} and 2.79×10^{-19} cm³molecule⁻¹s⁻¹ respectively.

CONCLUSIONS

Structures of the stationary states, energetics, and rate constants of the SiH₄ + {H, CH₃} hydrogen abstraction reactions were computed by DFT and CCSD(T) methods. For both (R1) and (R2) paths computed ΔH_0^0 agree well with experimental data. The rate constants calculated for (R1) are in excellent agreement with previous experimental and theoretical data. As far as we know, no previous CVT/SCT rate constants calculations for the (R2) path are provided here using the same methodology used for (R1).

REFERENCES

- J. Cao et al, J. Chem. Phys., 2011, 134, 24315.
- A. Goumire et al, Chemical Physics, 1993, 177, 233 - 241.
- O. P. Strausz et al, J. Chem. Phys., 1969, 51, 552 - 560.
- N. L. Arthur et al, Rev. Chem. Intermed., 1978, 2, 37.

ACKNOWLEDGMENTS

This study was financed in part by the Coordenação de Aperfeiçoamento de Pessoal de Nível Superior – Brasil (CAPES) Finance Code 001. We also acknowledgments to FAPESP and CNPq

Análise de Docking Consensual para a Avaliação e Predição de Novos Inibidores em PLpro de SARS-CoV-2

Flávio Vinícius da Silva Ribeiro (PG),^{1*} Jéssica de Oliveira Araújo (PG),¹ José Rogério de Araújo Silva (PQ).¹

flavio.silva.ribeiro@icen.ufpa.br

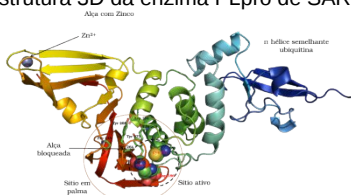
¹Computing Modeling of Molecular Biosystems (CompMBio), Universidade Federal do Pará, Belém, Pará 66075-110, Brazil.

Palavra-chaves: COVID-19, PLpro, Docking Molecular, Função de Pontuação.

INTRODUÇÃO

A enzima PLpro (Figura 1) vem sendo proposta como um potencial alvo para o desenvolvimento de medicamentos contra o SARS-CoV-2¹, o agente biológico responsável pela pandemia de COVID-19. Embora existam vacinas disponíveis, ainda há a urgência para o desenvolvimento clínico de medicamentos eficazes. Neste estudo, foi utilizado o docking consensual² como estratégia computacional para o desenho de inibidores de PLpro, a partir do uso de diferentes algoritmos de busca e funções de pontuação com predição da afinidade de ligação (AL) nos complexos.³

Figura 1: Estrutura 3D da enzima PLpro de SARS-CoV-2.



MÉTODOS

Um total de 4 (quatro) estruturas cristalográficas de PLpro foram extraídas do PDB, com os seguintes códigos e respectivos inibidores: 7CMD-GRL0617, 7SDR- Jun972-2, 7LBS- XR8-24 e 7D7L-YM155. Em seguida, cada sistema foi submetido ao procedimento de auto-ancoragem (no inglês, *redocking*) usando os seguintes programas: Autodock 4.5.6, Autodock Vina 1.2.3, GOLD 2022.3, Hybrid 4.2, DOCK 6.10 e Molegro Virtual Docker (MVD) 5.5. Para fins de validação, foram considerados os valores de menor desvio quadrático médio (sigla em inglês, RMSD, em Å) e os respectivos valores de AL (em kcal/mol) expressos em termos das funções de pontuação implementadas em cada programa. Ao final, 11 (onze) inibidores não cristalográficos foram submetidos aos procedimentos de ancoragem molecular no programa melhor avaliado¹.

RESULTADOS

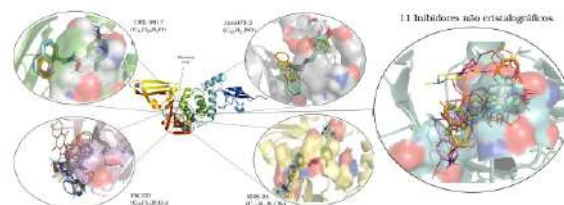
Na Tabela 1 são apresentadas as médias de RMSD (\bar{x}_{RMSD}) e de afinidade de ligação (\bar{x}_{AL}) calculadas pelos pacotes de ancogarem selecionados, considerando-se somente os sistemas com inibidores cristalográficos. Observa-se que o programa MVD apresentou os menores valores de \bar{x}_{RMSD} , bem como, para \bar{x}_{AL} .

Tabela 1: Valores médios de RMSD (em Å) e AL (em kcal/mol, exceto para o programa GOLD).

Programa	Função de Pontuação	\bar{x}_{RMSD}	\bar{x}_{AL}
Autodock4	ADT 4	1,88	-8,78
Autodock Vina	VINA	0,71	-8,52
MVD	MolDock	0,21	-127,00
GOLD	CHEMPLP	1,19	8,00
	Goldscore	1,76	65,09

Além disso, destaca-se (Figura 2) a conservação de interações de hidrogênios e contatos hidrofóbicos entre os resíduos Asp164, Pro248, Tyr264, Tyr268, Tyr273 e Gln269 em relação aos inibidores cristalográficos GRL0617, Jun972-2, XR8-24 e YM155. Analogamente, estas interações ocorreram para o conjunto de inibidores não cristalográficos submetidos a ancoragem molecular, onde os valores de afinidade de ligação variaram entre -155,25 e -81,65 kcal/mol, comparáveis ao valor de \bar{x}_{AL} apresentado pelo MVD.

Figura 2: Conformações obtidas após análises de docking consensual em PLpro de SARS-CoV-2.



CONCLUSÕES

Os procedimentos de ancoragem molecular adotados demonstraram-se satisfatórios como uma ferramenta para a avaliação de potenciais inibidores de PLpro de SARS-CoV-2, sugerindo que os resultados podem ser utilizados na triagem de potenciais medicamentos para o tratamento de COVID-19.

REFERÊNCIAS

1. Jiang et al., *Front. Chem.* 2022, 10, 1-14.
2. Ren et al., *J. Chem. Inf. Model.* 2018, 58, 1662-1668.
3. Costa et al., *Mol. Simul.* 2022, 48, 1678-1687.

AGRADECIMENTOS

À UFFPA e a CAPES



Influência de Substituintes na Redução de Barreiras Energéticas em Reações de Ativação do H₂ por Pares de Lewis Frustrados

Antonio Rafael de Oliveira (PG),¹ Roberto Luiz Andrade Haiduke (PQ),^{1*} José Walkimar de Mesquita Carneiro (PQ).^{2*}

rafaeldeoliveiraeu@gmail.com; haiduke@iqsc.usp.br; jose_walkimar@id.uff.br

¹ Instituto de Química de São Carlos, Universidade de São Paulo (IQSC/USP); ²Universidade Federal Fluminense (UFF)

Palavras Chave: Pares Frustrados de Lewis, centro ácido, centro básico, ativação, substituintes.

INTRODUÇÃO

O conceito de Pares de Lewis Frustrados (FLPs), introduzido por Stephan em 2006,¹ originou-se da observação da ativação reversível da molécula de H₂ em um sistema ausente de centros metálicos. Esse processo ocorre por meio de uma reação ácido-base de Lewis. Então, a reatividade dos FLPs tem sido amplamente empregada na ativação de moléculas pequenas e na hidrogenação de compostos insaturados, como iminas, cetonas, aldeídos e dióxido de carbono. A estrutura dos FLPs consiste em uma base de Lewis (BL) e um ácido de Lewis (AL), ambos apresentando impedimento estérico e/ou estrutural. A acidez e basicidade de Lewis, o impedimento estérico, bem como os grupos ligados a esses centros, determinam a reatividade dos FLPs. Adicionalmente, a aromaticidade e a antiaromaticidade podem modular o mecanismo da reação. Estudos recentes evidenciaram a estabilização do estereoisômero do ciclooctatetraeno (COT) e seu uso como esqueleto básico numa estrutura de FLPs.^{2,3} Nesse contexto, nossa pesquisa foi motivada a investigar em detalhes a estrutura do FLP usando o COT como modelo.³ Utilizamos a teoria do funcional da densidade (DFT) para calcular os mecanismos de reação dos FLPs, com o foco centrado nos efeitos dos substituintes investigados (-F, -CH₃, -OH, -NH₂, -SH, -OCH₃, -CF₃, -NO₂, -COH e -CN) considerando a ativação de hidrogênio. Assim, introduzimos substituições em pontos estratégicos, visando diminuir a barreira de ativação da molécula de H₂.

MÉTODOS

Os cálculos computacionais foram realizados utilizando o programa Gaussian 09.⁴ O funcional M06-2X foi empregado para descrever o mecanismo de ativação de H₂ mediado por FLPs, juntamente com o conjunto de base def2-TZVP. As otimizações de geometria foram conduzidas sem restrição de simetria, enquanto que a natureza dos pontos estacionários (mínimos e estados de transição) foi confirmada através de análises de frequências vibracionais. Todos os cálculos foram realizados na fase gasosa a 298 K, usando a pressão padrão de 1 atm.

RESULTADOS

Ao avaliar as substituições em diversas posições estratégicas na estrutura do sistema com FLPs, os resultados referentes aos valores termodinâmicos e cinéticos das barreiras energéticas demonstraram que a presença de um grupo -NO₂ ligado ao heterociclo contendo o átomo de boro (AL), do grupo -CHO ligado à estrutura do COT e do grupo -NH₂ ligado na posição "para" em relação ao nitrogênio inicialmente presente no anel de piridina (BL) consistentemente conduzem à uma redução nas barreiras energéticas da reação. Esses efeitos são notáveis nos casos em que estes e outros grupos substituintes (como -OH) estão estrategicamente posicionados dentro da estrutura com FLPs, resultando em reações acompanhadas por valores negativos de variação de energia de Gibbs da reação.

CONCLUSÕES

Através de cálculos DFT, realizamos uma análise estratégica de diversas substituições dentro da estrutura do sistema com FLPs abordado, no contexto da quebra heterolítica da ligação H-H. Avaliamos tanto os efeitos dos substituintes individuais quanto as combinações de 2 e 3 grupos distintos. Os resultados obtidos destacaram a relevância das estratégias de grupos substituintes para ampliar a reatividade do FLPs na ativação do H₂. Os resultados oferecem aos experimentalistas uma abordagem complementar para o desenvolvimento de sistemas mais eficientes com FLPs.

REFERÊNCIAS

- 1 G. C. Welch, R. R. S. Juan, J. D. Masuda and D. W. Stephan, *Science*, 2006, **314**, 1124–1126.
- 2 L. Li, M. Lei, Y. Xie, H. F. Schaefer, B. Chen and R. Hoffmann, *Proc. Natl. Acad. Sci. U.S.A.*, 2017, **114**, 9803–9808.
- 3 D. Zhuang, Y. Li and J. Zhu, *Organometallics*, 2020, **39**, 2636–2641.
- 4 M. J. Frisch, G. W. Trucks, et all., Gaussian 09 (Revisão E.01) 2001, 114, 9758–9763.

AGRADECIMENTOS

Os autores agradecem ao IQSC-USP, UFF, CAPES (88887-653938/2021-00), CNPq (306763/2021-4) e FAPESP (2022/05138-0).

Elucidação do mecanismo de reação para obtenção de fertilizantes nitrogenados com catálise heterogênea

Henrique Cury Boaro (IC),^{1*} Neubi Francisco Xavier Junior (PQ),² Glauco Favilla Bauerfeldt (PQ),¹ Antônio Marques da Silva Junior (PQ)¹.

hcboaro@gmail.com

¹Dep. de Química Fundamental, Universidade Federal Rural do Rio de Janeiro; ²University of Surrey, Reino Unido.

Palavras Chave: DFT, Catálise Heterogênea, Síntese de Ureia

INTRODUÇÃO

Diante da necessidade de atacar problemas de relevância social, econômica e ambiental, como o elevado consumo energético por processos industriais, bem como entender a físico-química do CO₂, este trabalho tem como objetivo contribuir para a proposição de modelo teórico para os mecanismos de reações envolvidas na obtenção de fertilizantes nitrogenados, como a ureia. Neste trabalho, buscamos elucidar o mecanismo pelo qual se processa a síntese de ureia na superfície Cu(100). A escolha deste metal como catalisador heterogêneo se deve a seu baixo custo e à eficiência catalítica relatada em trabalhos experimentais.¹ O plano 100 foi selecionado por ter sua atividade relatada na literatura.²

MÉTODOS

Para a descrição do processo de síntese de ureia,³ considerou-se as etapas:



Cálculos foram realizados com o programa Quantum Espresso,⁴ adotando a Teoria do Funcional da Densidade (DFT) com condições periódicas de contorno. Para o estudo de adsorção e de reações em superfície, considerou-se a expansão 3x3 da superfície de Cu(100). Ademais, visto que o material sugerido como catalisador possui configuração eletrônica com subcamadas abertas, são realizados cálculos spin-polarizados. Caminhos de reação foram obtidos através de cálculos CI-NEB.

RESULTADOS

O estudo da adsorção revelou que NH₃ é adsorvido preferencialmente sobre a superfície de Cu(100) em relação ao CO₂. A Figura 1 exibe um diagrama de energia do sistema. Nota-se que a adsorção de uma primeira molécula de NH₃ é acompanhada por diminuição da energia em 13,58 kcal.mol⁻¹, enquanto a interação de uma molécula de CO₂ aumenta a energia em 0,10 kcal.mol⁻¹. A adsorção de CO₂ sobre Cu(100) só é favorecida diante da interação com NH₃ na superfície, observando-se redução de energia de 8,27 kcal.mol⁻¹ (NH₃^{*} + CO₂(g) → NH₃^{*} + CO₂^{*}) e de 5,06 kcal.mol⁻¹ (2NH₃^{*} + CO₂(g) → 2NH₃^{*} + CO₂^{*}).

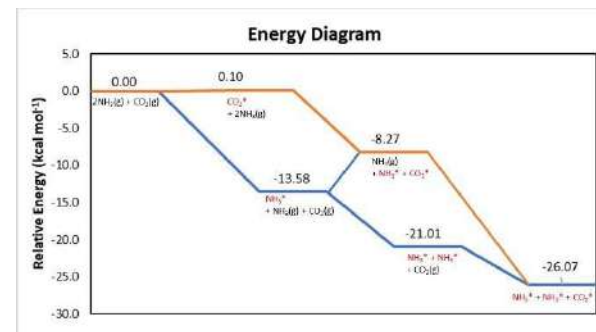


Figura 1 – Diagrama de energia compreendendo interações entre NH₃, CO₂ e Cu(100).

Ainda, mecanismos de reação baseados em caminhos molecular concertado e radicalar foram avaliados. A comparação das energias relativas dos intermediários do processo sugere que um mecanismo radicalar é favorecido. A adsorção das espécies NH₃ e COOH tem seu nível de energia estimado em valor 9,68 kcal.mol⁻¹ mais baixo do que a adsorção de NH₃ e CO₂. Cálculos CI-NEB também sugerem que a conversão de NH₃ e CO₂ em NH₂COOH tem como etapa lenta a dissociação de átomo de hidrogênio da amônia e consequente formação da espécie COOH, com barreira estimada em 13,37 kcal.mol⁻¹. Esta etapa elementar é seguida por uma rotação isoenergética da ligação H-O e por fim a formação da ligação N-C e adsorção de NH₂COOH, ligado à superfície pela carbonila, em que se espera a observação de uma transformação exoenergética.

CONCLUSÕES

Os resultados sugerem que a superfície de Cu(100) é ativa e eficiente para o processo de interesse, permitindo o recobrimento de NH₃ e subsequente reações com CO₂.

REFERÊNCIAS

- ¹Barzaghi, F.; Mani, F.; Peruzzini, M.. J. CO₂ Util.. **2016**, 13, 81.
- ²Eren,B.;Weatherup,R.S.;Liakakos,N.;Somorjai,G.A.;Salmeron ,M.B. J. Am. Chem. Soc. **2016**, 138(26), 8207.
- ³Souza, Mariana de Mattos Vieira Mello. Processos inorgânicos. Rio de Janeiro: Editora Synergia, **2012**.
- ⁴P. Giannozzi et al., J. Phys.:Condens. Matter. **2009**, 21, 395502

AGRADECIMENTOS

Os autores agradecem ao LNCC-SINAPAD – Santos Dumont (sdumont-chamadas/paper220119) pelo projeto em curso.



Estudo Termoquímico e Cinético da Reação $\text{CH}_3\text{NH}_2 + \text{N}$ Relevante para a Atmosfera de Titã

Ghuera I. Mayr (PG), Rene F. K. Spada (PQ).

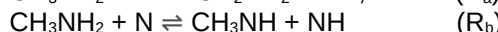
ghuerdamayr@ita.br; rfkspada@ita.br

Departamento de Física, Instituto Tecnológico de Aeronáutica, 12228-900, São José dos Campos, SP, Brasil;

Palavras Chave: Cinética Química, Termoquímica, Titã, Metilamina.

INTRODUÇÃO

A Atmosfera de Titã é composta por várias espécies moleculares e por átomos de Nitrogênio, Carbono e Hidrogênio que quando expostos a fontes energéticas como os raios solares podem produzir compostos orgânicos complexos como a metilamina. Krosnopolsky¹ simulou essa atmosfera e considerou a fotodissociação da molécula de metilamina (CH_3NH_2) em CH_3 e NH_2 , e o processo reverso na presença de um terceiro corpo inerte. A decomposição assistida por átomos de hidrogênio foi estudada por Kerkeni e Clary² e por Zhang et al.³ Nesse contexto, nosso objetivo foi estudar a termoquímica e a cinética das seguintes reações:



em que R_a e R_b ocorrem em uma superfície quarteto. O estudo dessas reações visa contribuir com a modelagem da atmosfera de Titã e foi realizado por métodos de estrutura eletrônica baseados em função de onda e em teoria do funcional de densidade, com o objetivo de adquirir propriedades termoquímicas e cinéticas relevantes.

MÉTODOS

As propriedades termoquímicas foram obtidas através de cálculos de estrutura eletrônica utilizando os métodos Møller–Plesset em segunda ordem (MP2), ω B97X, ω B97X-D3 e Coupled Cluster (CCSD(T)), com os conjuntos base cc-pVTZ e def2-tzvp. Os cálculos de cinética química foram obtidos através da teoria do estado de transição (sigla do inglês, TST) e da teoria variacional do estado de transição, em particular a teoria variacional canônica (sigla do inglês, CVT) na faixa de temperatura de 75 K a 2000 K. Também foram estimados os efeitos não-clássicos ao longo da coordenada reacional pela aproximação de pequena curvatura (sigla do inglês, SCT).

RESULTADOS

As geometrias de todos os pontos estacionários foram otimizadas com o conjunto de métodos MP2, ω B97X, ω B97X-D3 e devidamente reconhecidos por análise das frequências harmônicas que foram utilizadas para calcular a energia do ponto zero (EPZ). A conexão desses

pontos foi verificada pelo cálculo da coordenada de reação intrínseca (IRC). As propriedades termoquímicas obtidas foram a energia de reação eletrônica (ΔE), a entalpia da reação a 0 K (ΔH , $\Delta E + \Delta EPZ$), altura de barreira clássica (V^\ddagger) e barreira adiabática ($\Delta V_a^{\text{G}\ddagger}$, $V^\ddagger + \Delta EPZ^\ddagger$). Para obter valores confiáveis para as propriedades termoquímicas foram realizados cálculos de geometria fixa com o método CCSD(T)/CBS considerando primeiramente a geometria otimizada pelo método MP2/cc-pVTZ. A barreira clássica obtida por esse método para a formação de metilamina foi 5,5 kcal · mol⁻¹ para R_a e 3,4 kcal · mol⁻¹ para R_b . Também consideramos a geometria otimizada pelo funcional ω B97X para cálculos de geometria fixa utilizando o método CCSD(T)/CBS. Ambos os resultados obtidos pela abordagem CCSD(T)/CBS, não diferem por mais de 1,4 kcal · mol⁻¹. O método que obteve resultados mais próximos desses valores considerados como referência foi o ω B97X, e foi utilizado para os cálculos de cinética química. A partir desses cálculos foram obtidos os valores das constantes de velocidade na faixa de temperatura determinada. A 100 K a constante de velocidade para a formação de metilamina é igual a $2,5 \times 10^{-18}$ e $6,5 \times 10^{-17}$ cm³ · molécula⁻¹ · s⁻¹ para R_a e R_b , respectivamente.

CONCLUSÕES

Através das metodologias foi possível obter propriedades confiáveis de termoquímica. Das propriedades cinéticas foi possível calcular as constantes de velocidade das etapas elementares descritas (e sua viabilidade), que serão utilizadas em cálculos futuros visando contribuir para a modelagem da atmosfera de Titã.

REFERÊNCIAS

¹ Krasnopolksy, V. A. Icarus 2009, 201, 226–256.

² Kerkeni, B. et al. Chemical physics letters 2007, 438, 1–7.

³ Zhang, Q. et al. The Journal of Physical Chemistry A 2005, 109, 9112–9117.

AGRADECIMENTOS

O trabalho foi realizado com apoio da CAPES (projeto 711380/2022-00).



Estabilização e migração de átomos únicos de metais nobres suportados em magadiita

Monize F. Torres*(PG),¹ Márcio F. Santos (PG),¹ Bruna Nádia N. Silva (PQ),¹ Florence P. N. Antunes(PQ)¹, Alexandre A. Leitão(PQ).¹

monizetorres23@gmail.com

¹ Departamento de Química, Universidade Federal de Juiz de Fora-MG

Palavras Chave: (Catálise Heterogênea, Catálise por átomo único, Silicatos lamelares, Cálculos Ab initio, DFT).

INTRODUÇÃO

O conceito de catálise por um único átomo (single-atom catalysts - SACs) tem origem com a nanociência^[1], em que o refinamento das técnicas de síntese possibilitaram a redução das dimensões das fases catalíticas para um único átomo disperso na superfície do material suporte. Os SACs servem como uma ponte entre os catalisadores heterogêneos e homogêneos, onde o tamanho das partículas metálicas é um dos fatores que determinam o desempenho catalítico.

A magadiita, é um silicato lamelar hidratado, constituído de tetraedros de SiO_4 , cujas propriedades físico-químicas lhe permitem ser utilizada em vários processos, como adsorção, troca iônica e catálise heterogênea de moléculas orgânicas^[2].

Nesse trabalho, foram simulados modelos de metais nobres únicos suportados em superfície de magadiitas ácidas, M/H-Magadiita ($M = \text{Ag, Au, Pt, Pd}$), para avaliar sua capacidade de migração e estabilização em diferentes sítios e seus respectivos potenciais catalíticos através de cálculos computacionais ab initio baseados na teoria do funcional da densidade (DFT).

MÉTODOS

Todos os cálculos ab initio foram realizados com o pacote QUANTUM-ESPRESSO^[3], o qual é baseado na teoria do funcional da densidade e utiliza um conjunto de bases de ondas planas e condições de contorno periódicas. O funcional de troca e correlação foi do tipo GGA-PBE^[4], e os pseudopotenciais utilizados do tipo Vanderbilt Ultrasoft^[5]. A interação dos elétrons de valência com núcleos e elétrons do núcleo foram tratados pelo método do projetor de onda aumentada (PAW).

RESULTADOS

Foram testados 15 sítios (Figura 1a) agrupados em três regiões para a inserção dos metais nobres (Figura 1b), denominadas de "superfície"- oxigênios relativos às hidroxilas dos silanois ($\text{O}_3\text{-SiOH}$), sítios de "borda" - demais oxigênios dos silanois e oxigênios externos dos siloxanos vizinhos e "cavidade" - sítios de oxigênios internos da estrutura, relativos aos

demais siloxanos, para a inserção dos metais nobres.

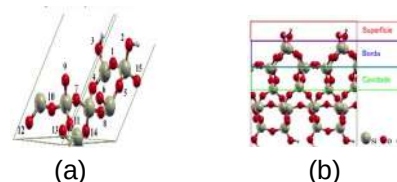


Figura 1 – (a) Identificação dos sítios testados e (b) Identificação das regiões de estabilização do metal.

A análise energética identificou dois sítios mais estáveis para os sistemas Au e Ag/H-Magadiita: na superfície e na cavidade, com diferença energética de 30 kcal/mol. Para a superfície de Pd e Pt/H-Magadiita foram observados três sítios (cavidade, superfície e borda) onde a variação de energia foi de 16 kcal/mol.

A barreira energética de migração dos modelos Ag, Au e Pd/H-Magadiita foram inferiores a 5 kcal/mol, dando indícios de sinterização destes metais. As estruturas de Pt/H-magadiita da cavidade apresentaram uma barreira de migração de 51 kcal/mol, se tornando o mais promissor dentre os modelos estudados.

CONCLUSÕES

Os testes para inserção e estabilização dos átomos únicos de metais nobres na H-magadiita mostraram que o metal tende a se estabilizar em três regiões específicas da estrutura, descritas como "superfície, borda e cavidade". Os sítios situados na região "superfície" são os mais estáveis para os sistemas Ag/H-magadiita, Au/H-magadiita e Pd/H-magadiita, diferindo do sistema Pt/H-magadiita em que o sítio mais estável se encontra na "cavidade".

REFERÊNCIAS

- [1] ACS Catal., v. 9, 8481–8502 (2019).
- [2] CrysEngComm, 13, 5428-5438 (2011).
- [3] Journal of CO₂ Utilization, 23, 29-41 (2018).
- [4] J. Molec. Catal A: Chem., 422, 43-50 (2016).
- [5] Journal of Physics: Condensed Matter., 21, 5502 (2009).
- [4] Physical Review B., 23, 5048-5079 (1981).
- [5] VANDERBILT, D.; Physical Review B, 41, 7892 (1990).

AGRADECIMENTOS

FAPEMIG,CAPES,CNPq,CENAPAD-SP,PETROBRAS CENPES.

The solubility of non-polar polymers in cyclohexane: molecular dynamics estimations of the Flory-Huggins interaction parameter

Gabriel P. Costa (PG),¹ Stanislav R. Stoyanov (PQ),² Qi Liu (PQ),¹ Phillip Choi (PQ).^{1,3*}

gpereir1@ualberta.ca; pchoi@ualberta.ca

¹Department of Chemical and Materials Engineering, University of Alberta, Edmonton, AB T6G 1H9, Canada;

²Natural Resources Canada, CanmetENERGY Devon, 1 Oil Patch Drive, Devon, Alberta T9G 1A8 Canada;

³Faculty of Engineering and Applied Science, University of Regina, Regina, SK S4S 2A0, Canada.

Keywords: Flory parameter, Non-polar polymers, Hildebrand solubility parameter, Enthalpy of mixing, Molecular dynamics.

INTRODUCTION

Polymer solubility is extremely relevant due to its applications, such as drug delivery, polymer design and polymer synthesis.¹ One of the established methods to identify polymer solubility is the Flory-Huggins interaction parameter χ , which is a dimensionless measure of the degree of interaction between solvent and polymer. One common approximation for this calculation is to use Hildebrand solubility parameters (δ) as in eq. (1).³

$$\chi = \frac{V_1^0(\delta_1^2 - \delta_2^2)}{RT} \quad (1)$$

Where V_1^0 represents a reference molar volume, usually taken as the solvent molar volume, and the subscripts 1 and 2 refer to solvent and polymer, respectively. This approach suffers from limitations inherent to the Regular Solution theory but can be very successful when strong polar interactions are not present. Flory defined χ based on the enthalpy of mixing (ΔH_{mix}), as presented in eq. (2).²

$$\chi = \frac{\frac{V_1^0}{RT\varphi_1\varphi_2} - \frac{\Delta H_{\text{mix}}}{V}}{V} \quad (2)$$

Where V represents the total volume and φ are the volume fractions of solvent (1) and polymer (2). The parameters in both equations can be derived from molecular dynamics (MD) simulations. Thus, this work aimed to compare the χ values obtained from both eq. 1 and eq. 2 via MD simulations.

METHODOLOGY

Seven nonpolar polymers, polyethylene (PE), isotactic and atactic polypropylene (iPP and PP), polyisobutylene (PIB), isotactic and atactic polystyrene (iPS and PS) and polyisoprene (PI), and one polar polymer, poly(ethylene oxide) (PEO), were simulated in the amorphous state, in vacuum and in a cyclohexane solution. Seven degrees of polymerization (DP), taken as 10, 20 30, 50, 100, 250, and 500 repeat units, were tested in every polymer sample. MD simulations were performed using GROMACS package.

The OPLS (optimized potential for liquid simulations) force field parameters were used for all polymers and cyclohexane. The simulations were performed in an isothermal-isobaric ensemble (NPT) with a Nosé-Hoover thermostat and a Parrinello-Rahman barostat for 5 ns.

RESULTS

Figure 1a presents the relation between experimental and calculated δ for all polymers with a DP=10. Most values are around the expected value. The solubility criterion was taken as $\chi_c < 0.5$.² The χ values calculated from eq. (1) indicated correctly the solubility trend (Figure 1b). Figure 1c presents χ_{PI} and χ_{PEO} vs. DP. It is worth mentioning that the values obtained did not reflect the exact experimental values due to the approximations associated. The χ values calculated from eq. (2) were expected to reflect more closely the experimental values as it can be seen in Figure 1d.

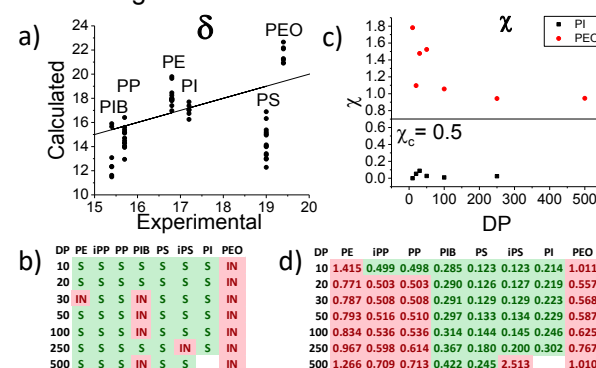


Figure 1. a) $\delta_{\text{experimental}}$ vs. $\delta_{\text{calculated}}$ b) Calculated χ from eq.1 c) Solubility evaluation based on $\Delta\delta^2$ approach d) Calculated χ values based on eq. 2.

CONCLUSIONS

Eq. 1 was successful in predicting polymer solubility. This is due to the nature of the solvent and the polymer evaluated. When eq. 2 was used instead, with less approximations inbuilt, the accuracy of the values increased significantly.

REFERENCES

- J. Nistane, L. Chen, Y. Lee, R. Lively, R. Ramprasad, MRS Commun., 2022, 12, 1-7.
- A. Rudin, P. Choi, The elements of polymer science and engineering. Academic press, 2012.
- S. Venkatram, C. Kim, A. Chandrasekaran, R. Ramprasad, J. Chem. information and modeling, 2019, 59(10), 4188-4194.

ACKNOWLEDGMENTS

The authors acknowledge Future Energy Systems for the funding and the Digital Research Alliance of Canada for the computational resources.

Experimental and molecular dynamics simulation ESI-CID spectrum of a Novichok nerve agent analog

¹Taynara Carvalho-Silva (PG), ¹Lucas Modesto-Costa, ^{1,2}Caio V.N. Borges, ¹Samir F.A. Cavalcante,
³Roberto B. Sousa, ²Antonio L.S. Lima ²Itamar Borges Jr. (PQ).

taynara.carvalho@eb.mil.br; itamar@ime.eb.br

¹ Instituto de Defesa Química, Biológica, Radiológica e Nuclear (IDQBRN), Exército Brasileiro, Avenida das Américas, 28705, Área 4, 23020-470, Rio de Janeiro-RJ, Brazil

² Departamento de Química, Instituto Militar de Engenharia (IME), Rio de Janeiro, RJ, 22290-270, Brazil.

³ Ministério da Ciência, Tecnologia e Inovação, Coordenação-Geral de Bens Sensíveis (CGBS), SPO, Área 5 - Quadra 3 - Bloco E, 20610-200, Brasília – DF, Brazil

Keywords: Novichok; A-242; Fragmentation pathways; Mass spectrometry; Molecular dynamics.

INTRODUCTION

Accurate mass spectral analysis is crucial for identifying compounds listed by the Chemical Weapons Convention (CWC) in environmental samples.¹ Due to the risks in handling nerve agents, a theoretical approach to study fragmentation pathways is highly desirable.²

In this work, we synthesized the O-2-methoxyethyl N-[bis(dimethylamino)methylidene]-P-methylphosphonamide (GND1), an analog of the Novichok nerve agent A-242, employing a one-pot microscale synthesis and measured its Electron ionization (EI) and electrospray ionization (ESI) mass spectra (MS) to determine data for CWC verification purposes.

ESI-MS/MS is a powerful method for analyzing degradation products of nerve agents, which we used for extensively investigating the ESI-(collision-induced dissociation) CID fragmentation pathways of the selected molecule. The spectra was compared with molecular dynamics simulations carried out with the Quantum Chemical Mass Spectrometry (QCxMS)³ method with the Triple Quadrupole experimental spectra in ESI positive ion mode.

METHODS

The CID calculations employed QCxMS version 5.0.3 with xTB version 5.8.1. Molecular nitrogen was used as the collision gas along with default parameters. The protonation of the targeted species was determined using the automated protonation protocol of CREST version 2.11 with the GFN2-xTB method. Free energy ranking of the ensemble was done using CENSO version 1.2.0 at the DFT level using the functional PBEh-3c with the def2-mSVP basis set. The DFT calculations employed the ORCA package version 4.2.1.

RESULTS

We investigated the four most populated protomers at 600 K indicated by CREST/CENSO at 600K (Figure 1)⁴. Their ESI-CID spectra were then calculated with QCxMS and compared with the experimentally measured spectrum.

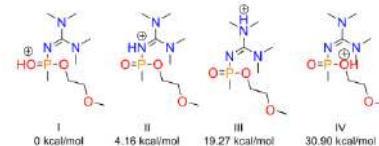


Figure 1. Protomers I-IV of the GND1 molecule with their assigned relative energies [kcal/mol] referred to the most stable structure protomer I (0.0 kcal/mol).

From the calculations, we identified 14 out of the 15 fragments generated by the mass spectrometer, resulting in a coverage of 93.3% of the signals (Figure 2(a))⁴.

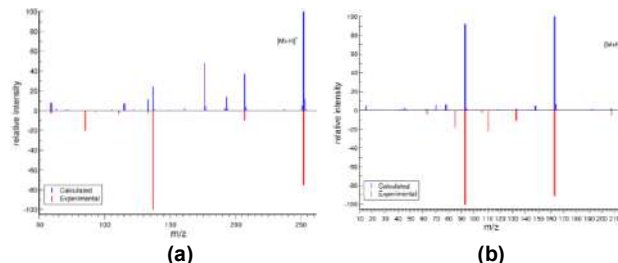


Figure 2. (a) QCxMS-calculated combined spectrum (blue) of GND1 protomers compared to experimental spectrum (red). (b) QCxMS-calculated spectra (blue) of O-methyl surrogate protomer IV compared to experimental spectrum (red).

Simulating other analogs, we found a good agreement with the experimental spectrum for one of the O-methyl surrogate protomers (Figure 2(b)).

CONCLUSIONS

Employing theoretical methods, a detailed view of dissociation mechanisms was obtained for experimentally measured spectra.

REFERENCES

- 1S.E. Hosseini, H. Saeidian, A. Amozadeh, M.T. Naseri, M. Babri, Rapid Commun. Mass Spectrom., 2016, 30, 2585–2593.
- 2F.C.S. Chernicharo, L. Modesto-Costa, I. Borges, J. Mass Spectrom., 2020, 55, 4513.
- 3J. Koopman, S. Grimme, J. Am. Soc. Mass Spectrom., 2021, 32, 1735–1751. DOI: 10.1021/jasms.1c00098.
- 4Carvalho-Silva, T., Modesto-Costa, L., Borges, C.V.N., Cavalcante, S.F.A., Sousa, R.B., Lima, A.L.S., Borges, I., 2023. Int J Mass Spectrom., 2023, 490, 117087.

ACKNOWLEDGEMENTS

We thank Prof. Stefan Grimme (Bonn University) for kindly making available the QCxMS program. I. B. thanks the Brazilian agencies CNPq and FAPERJ for support. We thank the Brazilian Army for supporting this research.

Cálculos *ab initio* de adsorção de moléculas de glicerol e água em MgO(001)

Isabelle C. R. Lourenço (PG),¹ Alexandre A. Leitão (PQ).^{1*}

isabelle.lourenco@ice.uff.br; alexandre.leitao@uff.br

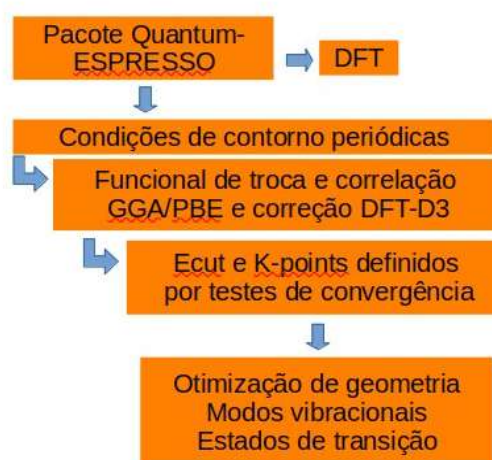
¹Departamento de Química, Universidade Federal de Juiz de Fora, Juiz de Fora, MG, 36036-330, Brasil

Palavras Chave: DFT, Adsorção, MgO, Glicerol, Material Refratário.

INTRODUÇÃO

Óxido de magnésio (MgO) é um sólido cúbico de face centrada, cuja superfície correspondente ao plano cristalográfico (001) é a mais estável e a que expõe a mesma fração de cátions e de ânions.¹ Um dos problemas relatados pela indústria de tijolos de MgO-C é o processo de hidratação do MgO e formação de hidróxido de magnésio, conhecido como brucita $[\text{Mg}(\text{OH})_2]$. A presença de $\text{Mg}(\text{OH})_2$ aumenta tanto a massa quanto o volume dos tijolos, ocasionando rachaduras no material e a diminuição do prazo de validade.² Na produção brasileira de biodiesel, há um excesso de glicerol proveniente da transesterificação de triacilgliceróis presentes em óleos e gorduras.³ Nesse contexto, o trabalho visou simular, por cálculos DFT, reações de adsorção de glicerol em MgO(001) e sua coadsorção com água para entender os processos termodinamicamente e cineticamente mais favorecidos.

MÉTODOS⁴



RESULTADOS

O sistema MgO(001)-gli-H⁺OH⁻ possuiu os menores valores de ΔG° (Figura 1a) e a menor barreira energética para a migração de prótons (Figura 1b). Até 600 K, os sistemas com glicerol são os mais estáveis e apresentam energias de ativação inferior a 5 kJ mol⁻¹. No caso do sistema contendo apenas moléculas de água, a barreira

de protonação da superfície a ser transposta é superior 20 kJ mol⁻¹.

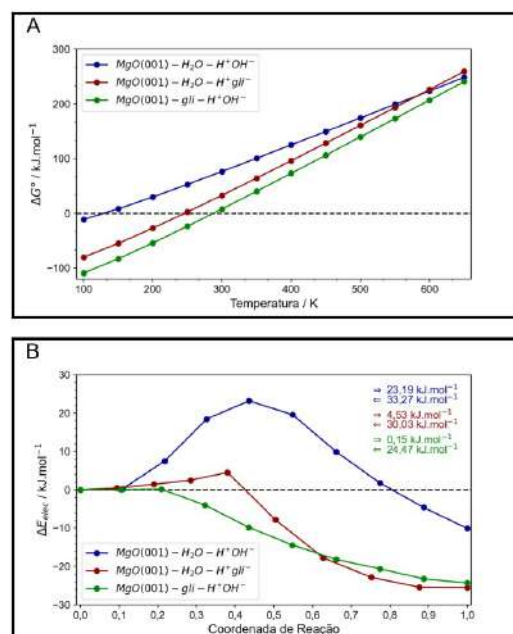


Figura 1 - (a) Relação da energia livre de Gibbs em função da temperatura e (b) caminho mínimo de energia para areação de protonação da superfície durante a coadsorção de moléculas.

CONCLUSÕES

Os sistemas com glicerol são termodinamicamente e cineticamente mais favorecidos. Espera-se que a protonação ocorra à temperatura ambiente com a adição de mais moléculas de água, sendo possível prever que a presença do glicerol na superfície dificulta a hidratação, levando a uma menor taxa de formação de brucita.

REFERÊNCIAS

- R. S. Alvim, *et al.* J. Phys. Chem. C, 2011, 116 v., 738-744 pg.
- J. A. Malarria, R. Tinivella, J. Am. Ceram. Soc. 2005, 80 v., 2262-2268 pg.
- I. R. F. S. Alves, *et al.* Energy, 2022, 241 v., 122818-122828, pg.
- P. Giannozzi, *et al.*, J. Phys. Condens. Matter, 2009, 21 v., 395502-395521 pg.

AGRADECIMENTOS

Agradecimentos a FAPEMIG, CAPES, CENAPAD-SP e UFFJ.

Unraveling Covalency in Actinides' Dithiocarbamate Complexes

William David Quintero Martinez (PhD)^{1,2*}, Dayán Páez-Hernández (R)^{1,2}

w.quinteromartinez@uandresbello.edu; dayan.paez@unab.cl

¹Doctorado en Fisicoquímica Molecular, Universidad Andres Bello, Santiago de Chile, Chile; ² Center of Applied Nanosciences (CANS), Universidad Andres Bello. Ave. República #275, Santiago de Chile, Chile

Keywords: Actinides, Covalency, Bonding, CASSCF, ligand-field theory

INTRODUCTION

The elucidation of f-element covalency is a current and challenging area of investigation for inorganic chemists. Therefore, several studies have been published in the last decade with the aim of understanding the covalency due to f orbitals¹⁻³, besides focusing on the design of selective extractants for the effective separation of actinides (An) and lanthanides (Ln), especially those found in nuclear fuel cycles⁴.

Traditionally, trivalent cations - especially lanthanides and heavy actinides - have been considered "hard acids" that show a preference for interacting with hard bases. However, experimental insights have led to purification strategies, have confirmed the selectivity of the S-donor ligand towards actinide ions Cm^{3+} and Am^{3+} compared to lanthanide ions Eu^{3+} and Tb^{3+} and even emphasize that more S atoms in the coordination sphere promote the selectivity⁵. In addition, a discussion of the covalency in some DTCs (S_2CNR_2) actinide complexes was provided by Kerridge *et al.*, who reported using DFT calculations that in $[\text{M}(\text{S}_2\text{CNPr}_2)_4]$ ($\text{M} = \text{Ti}, \text{Zr}, \text{Hf}, \text{Th}, \text{U}, \text{Np}$) complexes the degree of covalent bonding in the actinide is higher than in the group IV analogues⁶.

Nevertheless, there is currently no periodic trend for the actinide series. Therefore, in this work we systematically evaluate the role of f-orbitals and covalency across actinides with respect to interactions with the S-donor ligand in the DTC homoleptic complex.

METHODS

We used the Amsterdam Density Functional (ADF) package to optimize the molecular structures of $[\text{An}(\text{S}_2\text{CNH}_2)_4]$ using ZORA at the PBE0/TZ2P level. D_{2d} symmetry was used to ensure homogeneous structural effects. Since monodeterminantal methods are insufficient to describe the electronic structure of f-element complexes, we used CASSCF with a minimal active space ($n,7$) via ORCA 5.0.3; with DKH-optimized SARC and TZVP quality for actinides and def2-TZVPP basis set for all the others atoms. Covalent character bond was then analyzed using wave function and density based methods. Condon-Slater parameters were calculated by *ab-initio* ligand field theory, and natural bond orbital analysis was also performed. In addition, AIMALL was used to investigate quantum theory of atoms in molecules (QTAIM)

descriptors, including electron density (ρ), Laplacian ($\nabla^2\rho$), total energy density (H), virial ratio ($|V/G|$), and delocalization index ($\delta_{(A,B)}$), to gain insight into the nature of the bond.

RESULTS

AILFT analysis shows that the ratio $F^k/F_{\text{free-ion}}^k$ is <1 with variations from 2 to 9%, always higher than the lanthanide analogues. This observation suggests a nephelauxetic effect due to the interaction of the 5f orbitals with the DTC ligands. Figure 1 shows bonding orbitals between ion metal and sulfur and f-orbital contribution.

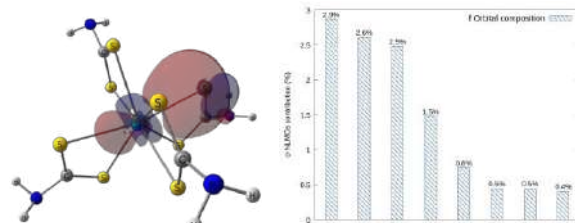


Figure 1. (a) Plot of a σ -Type NMLO for $[\text{U}(\text{S}_2\text{CNH}_2)_4]$ (b) f-orbital composition in NMLO for actinide ions QTAIM metrics indicate: $\rho < 0.2$, $\nabla^2\rho > 0$, $H < 0$, $|V/G|$ suggests partial covalency, and $\delta_{(A,B)}$ is greater in actinides than in lanthanides, and additionally in An(IV) compared to An(III).

CONCLUSIONS

Our study involved calculations to assess covalency in the bond between actinide ions and sulfur within the DTC ligand. Findings indicate decreasing covalency and f-orbital contribution across the series. Notably, heavy actinides exhibit higher covalency than corresponding lanthanides, with an increasing trend in covalency as oxidation numbers rise. Because of the QTAIM metrics, the covalency may be driven more by degeneracy energy than by overlap. This issue is not yet resolved, so other quantitative tools are needed, such as k-edge XAS spectra, which we're currently working on.

REFERENCES

- G. Chopin, J. Alloys Compd., 2002, 344, 55–59.
- A. Kerridge, Chem. Commun., 2017, 53, 6685–6695.
- M. Kelley, *et al.*, JACS, 2017, 139, 9901–9908.
- K. Pace, *et al.*, Chem. Eur. J., 2021, 27, 5835–5841.
- N. Bessen, *et al.*, Inorg. Chem., 2021, 60, 6125–6134.
- A. Behrle, *et al.*, Inorg. Chem. 2018, 57, 10518–10524.

ACKNOWLEDGMENTS

This work has been supported by Grants FONDECYT REGULAR 1220442 and acknowledges ANID/Doctorado Nacional/21222021 for his Ph.D. fellowship.



Estudo Teórico de Efeitos Solvatocrônicos e Modificação Estrutural de Cromóforos Sensibilizadores de Células Solares Derivados

Pierre Carlos de Souza Junior (PG),¹ Daniel Francisco Scalabrini Machado (PQ).^{1*}

pierrecarlosj@gmail.com; daniel_scalabrini@outlook.com

¹UnB (Universidade de Brasília) – IQ (Instituto de Química) - LMSC (Laboratório de Moléculas e Sistemas Complexos)

Palavras Chave: TDDFT, QM/MM, ASEC, UV-Vis, Monte Carlo

INTRODUÇÃO

Pesquisas em larga escala e esforços para o desenvolvimento de novas Células Solares Sensibilizadas por Cromóforos Orgânicos (em inglês Dye-Sensitized Solar Cells - DSSC's) tem atraído atenção desde sua demonstração seminal de viabilidade como tecnologia fotovoltaica com bom custo-benefício.¹ Em geral, os cromóforos orgânicos consistem em uma estrutura do tipo **D-π-A**, isto é, uma unidade doadora de elétrons **D**, **π** é uma unidade espaçadora π-conjugada e **A** é uma unidade acceptora de elétrons.³

MÉTODOS

O estudo usou-se da Teoria do Funcional da Densidade (DFT) para investigar as propriedades fotofísicas de cromóforos em solução. Como doadores de elétrons, foram utilizados a trimetilamina e a trifenilamina; como ponte π-conjugada; foram utilizados a benzotiadiazola e etilenodioxitifeno. Por fim, como unidades acceptoras de elétrons, temos o ácido acético-rodamina, diciano-rodamina e o ácido cianoacético. Os cromóforos (a combinação de um fragmento doador, seguido por uma ponte π-conjugada e uma unidade acceptora) foram otimizados usando o funcional de troca-correlação híbrido global B3LYP e as correções empíricas de dispersão foram incluídas no cálculo. O efeito do conjunto de funções de base foi avaliado investigando três conjuntos de base, 6-31G(d,p), 6-311G(d,p) e 6-311++G(d,p). As excitações e geometrias em solução foram avaliadas com três modelos de solvatação: implícito, ASEC e explícito.^{2,4} Todos os cálculos utilizaram metanol como solvente.

RESULTADOS

Começando pelo modelo implícito; foi verificado que após o término dos cálculos, todos os cromóforos testados que possuem o doador trimetilamina não estabeleceram transferência de carga para a região acceptora. Esses resultados foram de extrema importância para a continuidade do trabalho.

Para o modelo ASEC, foram obtidos resultados similares com o do modelo implícito. Quando comparado os dois modelos, os espectros

gerados pelo modelo ASEC apresentaram em sua maioria, efeito hipercrônico quando comparado com o método de solvatação implícito. No modelo explícito (em que o soluto é cercado pelas moléculas que formam a primeira camada de solvatação), foi verificado no espectro de absorção a ampla distribuição na posição de transição de menor energia (HOMO-LUMO), indicando que efeitos térmicos tem efeito de alargamento de banda.

CONCLUSÕES

Mesmo sendo um modelo simples quando comparado com os demais; o modelo implícito foi de extrema importância para o trabalho, já que com ele foi possível reduzir o número de cálculos. Já no método ASEC, as moléculas selecionadas apresentaram propriedades fotofísicas qualitativamente similares ao CPCM. Esta similaridade é atribuída a geometria molecular que é a mesma e foi mantida fixa nestes cálculos. O método de solvatação explícita é fundamental para determinar a maior potencialidade de um pigmento para aplicação em DSSC. Como alguns cromóforos apresentaram distribuições diedrais mais amplas do que outros, a escolha do melhor cromóforo baseado em solvente implícito não necessariamente será o mesmo resultado óptimo quando efeitos que simulam as condições experimentais de maneira mais sofisticada são considerados.

REFERÊNCIAS

- 1 O'Regan, B.; Grätzel, M. A Low-Cost, High-Efficiency Solar Cell Based on Dye-Sensitized Colloidal TiO₂ Films. *Nature* 1991, 353 (6346). <https://doi.org/10.1038/353737a0>.
- 2 Cezar, H. M.; Canuto, S.; Coutinho, K. DICE: A Monte Carlo Code for Molecular Simulation Including the Configurational Bias Monte Carlo Method. *J Chem Inf Model* 2020, 60 (7), 3472–3488. <https://doi.org/10.1021/acs.jcim.0c00077>.
- 3 Li, G.; Jiang, K. J.; Li, Y. F.; Li, S. L.; Yang, L. M. Efficient Structural Modification of Triphenylamine-Based Organic Dyes for Dye-Sensitized Solar Cells. *Journal of Physical Chemistry C* 2008, 112 (30). <https://doi.org/10.1021/jp802436v>.
- 4 Frisch, M. J.; Trucks, G. W.; Schlegel, H. B.; Scuseria, G. E.; Robb, M. A.; Cheeseman, J. R.; Scalmani, G.; Barone, V.; Petersson, G. A.; Nakatsuji, H. Gaussian 16, {Gaussian}. Inc., Wallingford CT 2016, 2016.

AGRADECIMENTOS

CNPq, CAPES, FAPDF, SBQT, IQ – UnB.



Effects of the concentration of seeds and finite time-dependent supersaturations on the crystallization kinetics of monosodium urate monohydrate

Lâna M. Sousa (PhD)¹, Leandro G. Rizzi (R)¹

lana.sousa@ufv.br ; lerizzi@ufv.br

¹Departamento de Física, Universidade Federal de Viçosa (UFV), CEP: 36570-000 Viçosa, MG, Brazil

Keywords: gout, crystallization, growth kinetics, master equation

INTRODUCTION

Gout^{1,2} is a rheumatic disease which generally occurs at the synovial fluid and is caused by the formation of needle-like crystals of monosodium urate monohydrate (MSUM), which is a by-product of the dissolution of uric acid at pH=7.4 and temperature T=37°C. Although the crystallization of MSUM plays a major role in the development of the gout disease, theoretical models which aim to describe its kinetics have been elusive, and only a few experiments under controlled conditions were performed until now^{3,4}.

Usually, the approach is to consider a high order rate equation which is given by^{5,6,7}

$$\frac{dC_1(t)}{dt} = -k_e C_s (C_1(t) - C_{1,e})^q , \quad (\text{Eq. 1})$$

where C_s is the concentration of crystalline seeds, k_e is the elongation rate constant, and $C_{1,e}$ is the solubility of MSUM molecules. Accordingly, Eq. 1 has solutions given by

$$C_1(t) = C_{1,e} + (C_{1,0} - C_{1,e}) e_q[x_q(t)] , \quad (\text{Eq. 2})$$

where $x_q(t) = -k_e C_s (C_{1,0} - C_{1,e})^{q-1} t$, with $e_q[x]$ being a q -exponential function⁷.

Burt & Dutt^{3,4} argued through experimental analyses that their results can be fitted using the solution of a 2nd order rate equation (*i.e.*, $q = 2$). However, a careful revision of their data indicates that Eq. 2 with $q = 2$ might not be used to describe the experimental results. Thus, here we present an alternative approach based on a master equation in order to consider more straightforward hypotheses. In particular, our modelling approach allows us to incorporate not only finite time-dependent supersaturation and concentration of seeds, but also how the crystallization kinetics can be affected by the viscosity of the solution.

METHODS

Here we consider a master equation⁸ which describes the attachment and the detachment of molecules to n -sized crystal, that is,

$$\frac{dC_1(t)}{dt} = - \sum_n A_{1,n} C_1 C_n + \sum_n F_{n+1} C_{n+1} , \quad (\text{Eq. 3})$$

where $A_{1,n}$ is the association kernel, which is related to the attachment of one particle to a n -

sized cluster, while F_{n+1} is the dissociation kernel, which describes the detachment of particles from a cluster with $n + 1$ molecules.

The viscosity of the solution η_s is incorporated into the model through a suitable approximation of the so-called Brownian kernels⁹.

RESULTS

Hence, in order to consider finite time-dependent supersaturations, we follow the approach of Ref.6, which led us to rewrite Eq. 3 as

$$\frac{dC_1(t)}{dt} = -k_e (C_1(t) - C_{1,e}) (C_{\text{tot}} - C_1(t)) \quad (\text{Eq. 4})$$

where $k_e \propto (k_B T / \eta_s)$ and C_{tot} is the total concentration of particles in the system, including not only the initial concentration of monomers $C_{1,0}$, but also the amount of monomers in the seeds. From Eq. 4 we obtain an analytical expression for $C_1(t)$ as a function of time t and explore it to investigate what happens for different k_s and C_{tot} .

CONCLUSIONS

By considering a master equation framework, our modelling approach resulted in a simple analytical expression which is capable of describing many features of the experiments on the growth kinetics of MSUM^{3,4} which the previous theoretical developments did not. Contrary to many modelling approaches^{3,4,5,6,7,10}, our kinetic model incorporates a few transparent hypotheses which can be readily tested through additional experiments.

REFERENCES

- Dalbeth *et al.*, Nature Rev. Disease Primers., 2019; **5**, 69.
- Martillo *et al.*, Curr. Rheumatol. Rep., 2014; **16**, 400.
- Burt & Dutt, Ann. Rheum. Dis., 1986; **45**, 858-864.
- Burt & Dutt, J. Cryst. Growth, 1989; **94**, 15-22.
- P. Atkins, J. de Paula, J. Keeler, *Physical Chemistry* (12nd ed), 2023; Oxford University Press.
- D. Kashchiev, Proteins, 2014; **82**, 2229-2239.
- Gell-Mann & Tsallis. *Nonextensive Entropy - Interdisciplinary Applications*, 2004; Oxford University Press.
- D. Kashchiev. *Nucleation: Basic Theory with Applications*, 2000; Butterworth-Heinemann.
- P. L. Krapivsky, S. Redner, E. Ben-Naim, *A Kinetic View of Statistical Physics*, 2010; Cambridge University Press.
- R. F. Pasternack *et al.*, J. Am. Chem. Soc., 1998; **120**, 5873-5878.

ACKNOWLEDGMENTS

The authors acknowledge the financial support from the Brazilian agencies CAPES (code 001), CNPq (Grant N°. 312999/2021-6), and FAPEMIG (Process APQ-02783-18).

Condensed matter models as a test bed for quantum information concepts

Tatiana Pauletti (PhD), Murilo A. Garcia (MSc), Guilherme A. Canella (PhD), Vivian V. França (R)*
vivian.franca@unesp.br:

Institute of Chemistry, São Paulo State University, UNESP, Araraquara, São Paulo, Brazil

Keywords: entanglement, Hubbard model, quantum phase transitions, superlattices, disordered systems

INTRODUCTION

Entanglement is conceived as a fundamental resource for quantum information process, including computation, communication and metrology, thus essential to quantum technologies. Condensed matter systems are considered good candidates for quantum technology devices due to their natural quantum fluctuations.

For bipartite pure states the von Neumann entropy is a proper measure of entanglement, while the linear entropy, associated to the mixedness of the reduced density matrices, is a simpler quantity to be obtained and is considered to be qualitatively equivalent to the von Neumann.

We investigate both linear and von Neumann entropies in homogeneous, superlattice and disordered Hubbard chains.

METHODS

The Hubbard Hamiltonian is given by:

$$H = -t \sum_{\langle ij \rangle \sigma} (\hat{c}_{i\sigma}^\dagger \hat{c}_{j\sigma} + h.c.) + U \sum_i \hat{n}_{i\uparrow} \hat{n}_{i\downarrow} + \sum_{i\sigma} V_i \hat{n}_{i\sigma}$$

where t is the hopping term, U the interaction, V the external potential and n the filling factor.

The ground-state single-site entanglement defined as the entanglement between a single site and the remaining $L - 1$ sites is quantified by the von Neumann entropy,

$$S = -\frac{1}{\ln(d)} \text{Tr} [\rho_i \ln \rho_i] = -\frac{1}{\ln(d)} \sum_k w_{ik} \ln w_{ik}$$

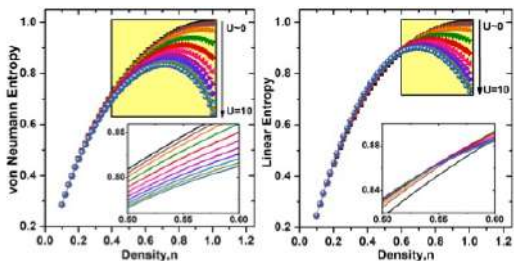
and by the linear entropy,

$$\mathcal{L} = \frac{d}{d-1} [1 - \text{Tr}(\rho_i^2)] = \frac{d}{d-1} \left(1 - \sum_k w_{ik}^2 \right)$$

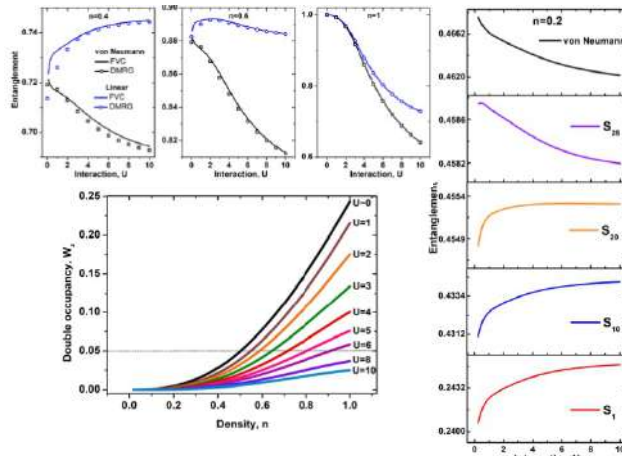
where d Hilbert space dimension, ρ_i reduced density matrix of site i , and w_{ik} occupation probabilities of site i , with $k = \uparrow, \downarrow, \uparrow\downarrow, 0$.

RESULTS

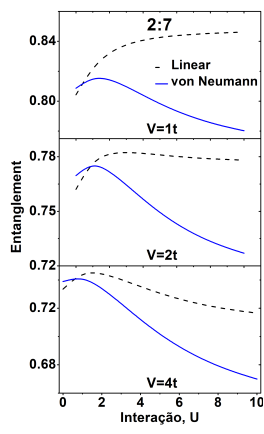
Homogeneous system x density



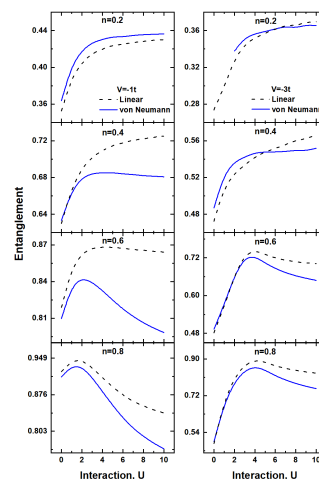
Homogeneous system x interaction



Superlattices



Disordered Chains



CONCLUSIONS

We find regimes of parameters for which the linear entropy fails in reproducing the qualitative behavior of the von Neumann entropy. This then may lead to incorrect predictions i) of maximum and minimum entanglement states and ii) of quantum phase transitions.

REFERENCES

¹ T. Pauletti, M. A. Garcia, G. A. Canella, V. V. França, arXiv: 2303.08075, 2023.

ACKNOWLEDGMENTS

Investigation of Metathesis Reactions Using Molybdenum Catalysts and Phenol Ligands: Kinetic Behaviors and Computational Insights

Attilio Chiavegatti Neto (PG),¹ Marco Antonio Barbosa Ferreira (PQ)¹

attilio@estudante.ufscar.br; marco@ufscar.br

¹Department of Chemistry, Federal University of São Carlos

Palavras Chave: Olefin Metathesis, Density Functional Theory, Semiempirical Quantum Mechanics, Reaction Kinetics

INTRODUÇÃO

Computational studies of transition metal complexes present significant challenges and modern semiempirical computational methods emerge as cost-effective alternatives.^{1,2} Catalyzed chemical synthesis enables the creation of previously nonexistent molecules. Olefin metathesis catalyzed by molybdenum complexes (Schrock catalysts) stands out for streamlining diverse multi-step syntheses.^{3,4} The use of bispyrrolide precursors enables a wide range of Schrock catalysts to be easily prepared. However, a study of ligand exchange mechanisms in these complexes is lacking. Here, we describe mechanistic aspects of this reaction. Particularly, we are interested in establishing a low-cost method for the estimation of the exchange rates, which is an important component of the framework for improving Schrock-type catalysts in terms of activity and selectivity currently under development in our group.

MÉTODOS

DFT calculations were performed with Gaussian 16. The best performing DFT functional were chosen by means of a benchmark against TPSSh/def2-tzvpp optimized geometries and DLPNO(T1)/def2-tzvpp energies. Optimizations and thermal corrections at 295.15 K (1 atm) were then computed at PBE0-D3BJ/def2-svp level. IRC calculations were performed to ensure that each transition state connects the expected minima. For all geometries, conformational searches were carried out using CREST 2.12 and xTB 6.5.1 using the GFN1-xTB under vacuum.

RESULTADOS

The investigation focused on the ligand exchange involving a bispyrrolide Mo complex and phenol. The preferred coordination of the entering phenol was identified as *trans* to the imido group. The favorable pathway is via a 4-membered transition state of proton transfer from phenol to pyrrole nitrogen. The C2-protonation route is higher in energy. The dissociation of a pyrrole ligand results in the formation of the MAP. A similar mechanism is proposed for bisaryloxyde formation (Figure 1). As our main interest is in the use of low-cost computational methods, we calculated the product distribution for a referenced reaction using single-

point calculations (SPE) of both the DFT-optimized and GFN1-xTB geometries (Table 1).

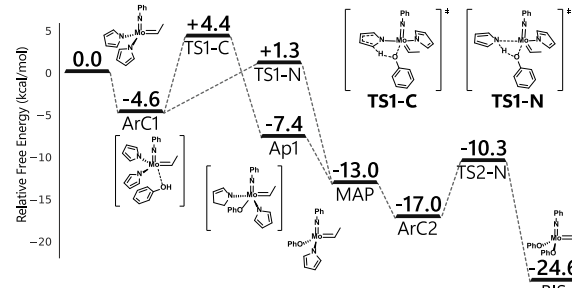
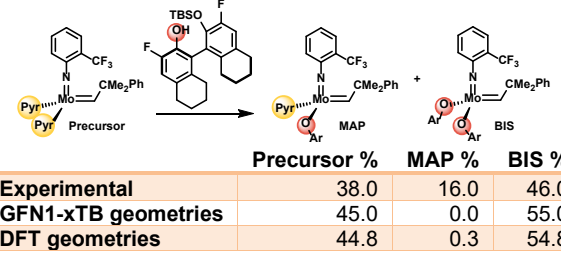


Figure 1. The calculated mechanism for ligand exchange (PBE0-D3BJ/def2-svp)

As demonstrated, accurate predictions of product distribution may be obtained using a combination of GFN1-xTB geometries and DFT for SPE effectively reducing computational costs.

Table 1. Calculated product distribution using kinetic equations.



CONCLUSÕES

The preferential mechanism for ligand exchange in Schrock-type Mo complexes involves the coordination of a phenol *trans* to the imido group followed by proton transfer to the pyrrolide nitrogen. Accurate approximations for the reaction rates of each proposed step may be achieved using semiempirical methods. This hybrid computational protocol thus enables a computational screening of a vast library of complexes. Such screening will then allow us to define which are the major catalysts, and their reactivity toward olefin metathesis reactions will be described using a second chemical model.

REFERÊNCIAS

- (1) Durand, D.; Fey, N. *Chem. Rev.* **2019**, 119 (11), 6561–6594.
- (2) Bursch, M.; Grimme, S.; et al. *Phys. Chem. Chem. Phys.* **2021**, 23 (1), 287–299.
- (3) Astruc, D. *New J. Chem.* **2005**, 29 (1), 42–56.
- (4) Benedikter, M. J.; Buchmeiser, M. R.; et al. *Coord. Chem. Rev.* **2020**, 415, 213315.

AGRADECIMENTOS

FAPESP (22/13563-7, 22/11314-5, 20/01255-6). CAPES (88887.597433/2021-00). NCC-UFSCar (CloudUFSCar) e NACAD. Departamento de Química da UFSCar.



Structural, vibrational, and electronic properties of the [Ni(Phen)(C₄H₂O₄)(H₂O)₃] coordination complex: Synthesis and DFT study

Jailton R. Viana (PG),¹ Antonio Douglas S. G. Lima (PG)¹, João G. Oliveira Neto (PG)¹, Rodrigo M. Gester (PQ),² José Walkimar M. Carneiro (PQ)³, Stanislav R. Stoyanov (PQ)⁴, Adenilson O. Santos (PQ)¹, Mateus R. Lage (PQ)⁵

jailton.viana@ufma.br

¹Universidade Federal do Maranhão, Imperatriz – MA; ²Universidade Federal do Sul e Sudeste do Pará, Marabá – PA;

³Universidade Federal Fluminense, Niterói – RJ; ⁴Natural Resources Canada, CanmetENERGY Devon, Devon, Alberta, Canada; ⁵Universidade Federal do Maranhão, Balsas – MA.

Keywords: Coordination complex, X-ray diffraction, hybrid density functional, non-linear optical materials.

INTRODUCTION

Coordination complexes have potential applications in several different areas, like in medicine, catalysis processes in redox and electrolytic reactions, dyes and pigments, optoelectronic devices, and non-linear optics (NLO), among others [1,2]. In coordination chemistry, ligands containing nitrogen (N) and oxygen (O) atoms have the ability to coordinate to metal ions, forming stable complexes, since N and O have enough electron densities to donate to metal ions [2]. The objective of this work is to synthesize the [Ni(Phen)(C₄H₂O₄)(H₂O)₃] coordination complex and study its structural, vibrational, and electronic properties. X-ray diffraction (XRD) crystallography and Fourier-Transform Infrared (FT-IR), and ultraviolet-visible (UV-Vis) spectroscopies were conducted to characterize the material. Density functional theory (DFT) and time dependent – density functional theory (TD-DFT) calculations were performed to study structural, spectroscopic, and NLO properties.

METHODS

The complex was synthesized by the slow solvent evaporation method, using the reagents nickel nitrate hexahydrate, 1,10-phenanthroline monohydrate, and maleic acid, in equimolar ratios (1/1) in a mixed solvent of methanol and water (1/1). After obtaining the crystals, they were experimentally characterized by XRD and FT-IR, and UV-Vis spectroscopies. The computational studies were carried out with the Gaussian16 software [3], using the hybrid exchange-correlation density functional PBE1PBE [4], with the 6-311++g(d,p) basis set for light atoms [5], and the SDD pseudopotential for the metal ion [6]. The PBE1PBE functional yields optimized structures of metal complexes in a very good agreement with XRD results [7]. Calculations were performed in a mixed solvent ($\epsilon = 42,686$), considering the integral equation formalism polarizable continuum model (IEFPCM) [8]. The TD-DFT and NLO calculations were performed at the same level of theory as the DFT calculations.

RESULTS

The XRD results showed that the complex has a monoclinic crystalline structure belonging to the P2₁ space group, with two metallic centers per unit cell.

The optimized geometry of the coordination complex obtained from DFT calculations was confirmed with the absence of negative vibrational frequencies. The complex has an octahedral geometry. The calculated structural data and spectroscopic parameters are in a good agreement with our experimental findings, contributing to the characterization of the material. The electronic UV-Vis transitions, calculated using TD-DFT, consisted of transitions at 790, 750, 660, 462 and 446 nm with low oscillator strengths. The NLO properties were also calculated. The dipole moment (μ), dipole polarizability in the isotropic (α) and anisotropic ($\Delta\alpha$) contributions, and first hyperpolarizability (β), in the static version, have values of 29.75 D, 48.10x10⁻²⁴ esu, 29.55x10⁻²⁴ esu and 3.60x10⁻³⁰ esu, respectively.

CONCLUSIONS

The successful synthesis of the complex was confirmed by XRD and the calculated structural parameters were in a good agreement with experimental data. The calculated spectroscopic IR and UV-Vis results revealed characteristic bands of d-d electronic transitions. The results of β in NLO of the complex was 10 times higher than that of urea, taken as a reference. These results suggest that the complex is suitable for potential applications in NLO.

REFERÊNCIAS

- [1] K. Sayin, D. Karakas, et. al., *Polyhedron*, 2015, 90, 139.
- [2] R. Chaurasia, M. K. Bharty, et. al., *Polyhedron*, 2019, 174, 114160.
- [3] Gaussian 16, Revision C.01, M. J. Frisch, G. W. Trucks, et. al., Gaussian, Inc., Wallingford CT, 2016.
- [4] C. Adamo, V. Barone, *J. Chem. Phys.*, 1999, 110, 6158.
- [5] K. B. Wiberg, *J. Comput. Chem.*, 2004, 25, 1342.
- [6] D. Andrae, U. Hässermann, et. al., *Theor. Chim. Acta*, 1990, 77, 123.
- [7] D.P. Rillema, S.R. Stoyanov et al. *Dalton Trans.*, 2015, 44, 17075.
- [8] R. Cammi; J. Tomasi, *J. Chem. Phys.*, 1994, v. 100, p. 7495.

ACKNOWLEDGMENT

CNPq, CAPES, FAPEMA, Digital Research Alliance of Canada, Program of Energy R&D (PERD), Government of Canada.

Avaliação das interações hidrogênio-oxigênio em aglomerados de água protonada

Társis C. Souza* (IC),¹ Gabriela R. Bastos (IC)¹ Italo C. Anjos (PQ).^{1*}

tarsisc.souza@hotmail.com; italo.anjos@ufmt.br

¹Departamento de Química, Universidade Federal do Mato Grosso, Cuiabá - MT - Brasil;
Palavras Chave: Aglomerados de água, ligação de hidrogênio, ligação química, ELF, QTAIM.

INTRODUÇÃO

O transporte de prótons entre moléculas de água é um fenômeno fundamental para muitos processos biológicos e químicos. Os prótons podem se mover de uma molécula de água para outra por meio de ligações de hidrogênio. Através dessas ligações, várias espécies protonadas são formadas em meio aquoso sendo que em cada uma delas o próton está ligado a uma ou mais moléculas de água de modo diferente. O objetivo central deste trabalho é caracterizar as ligações envolvidas nessas espécies aquosas protonadas e comparar com outras não protonadas.

MÉTODOS

Foram feitos cálculos de otimização de geometria e frequência no vácuo com o uso de M06-2X através dos softwares GaussView 5.0 e Gaussian 09. As estruturas investigadas foram: água (W), hidrônio (WH^+), dímero da água (W_2), cátion Zundel (W_2H^+), trímero da água (W_3) e cátion $H_7O_3^+$ (W_3H^+). Com as estruturas otimizadas, foram feitos cálculos usando a Teoria Quântica dos Átomos em Moléculas (QTAIM) e avaliados alguns parâmetros atômicos e de ligação. Posteriormente foram feitos cálculos usando a Função de Localização Eletrônica (ELF) para avaliar as bacias eletrônicas associadas a agrupamentos de elétrons.

RESULTADOS

Tabela 1 - Parâmetros das interações oxigênio-hidrogênio nos cátions WH^+ , W_2H^+ e W_3H^+

	WH^+	W_2H^+	W_3H^+ (c)	W_3H^+ (p)
d_{O-H} (Å)	0,952	1,188	1,025	1,438
ρ	0,331	0,165	0,259	0,0873
$\nabla^2\rho$	-2,516	-0,365	-1,648	+0,148
$\delta_{A,B}$	0,472	0,248	0,338	0,162
$q(O)$	-1,175	-1,216	-1,259	-1,203
$q(H)$	+0,725	+0,711	+0,710	+0,710

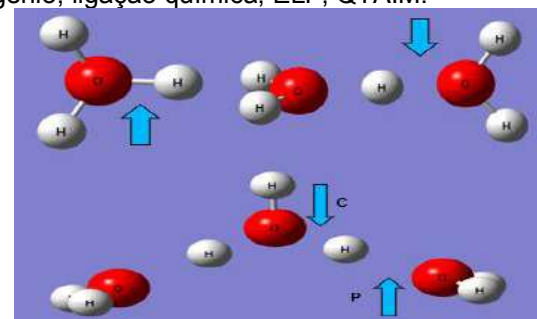


Figura 1 – Cátions estudados, com destaque para ligações investigadas: WH^+ (canto superior esquerdo), W_2H^+ (canto superior direito) e W_3H^+ (abaixo).

Comparando as quatro interações, o WH^+ é a mais forte por conta da sua curta distância, $\delta_{A,B}$ e ρ maiores. Posteriormente o W_3H^+ (c) tem uma força parcial e essa diferença ocorre por conta de ser um hidrônio ligado a duas águas. Esses dois casos possuem caráter covalente bem definido.

Para o W_2H^+ que possui uma ligação mais fraca, fatores como: ρ , $\nabla^2\rho$ e $\delta_{A,B}$ mostram um caráter intermediário entre uma ligação covalente e ligação covalente.

Por fim, a interação W_3H^+ (p) se caracteriza tipicamente como uma ligação de hidrogênio e isso é demonstrado pelo $\nabla^2\rho$ positivo, a ρ próximo a zero e a distância sendo a maior dentre as outras.

CONCLUSÕES

Moléculas de água e íons de hidrônio recebem o valor característico de ligações fortes. mas como mostrado acima, em alguns casos essas moléculas podem apresentar interações covalentes fracas e ligações de hidrogênio.

REFERÊNCIAS

1. Jieli M, Aida M (2009) Classification of OH Bonds and Infrared Spectra of the Topology-Distinct Protonated Water Clusters $H_3O + (H_2O)_n - 1$ ($n \leq 7$). J Phys Chem A 113:1586–1594. <https://doi.org/10.1021/jp810735>.

AGRADECIMENTOS

CNPq, FAPEMAT e UFMT.



Effects of Co doping in the CO₂ Reduction Reaction Catalyzed by Cu₅₅ Nanoclusters

Guilherme R. Nascimento (PG),^{1,2*} Marionir M. C. B. Neto (PG),¹ Breno R. L. Galvão (PQ),¹ Juarez L. F. Da Silva (PQ)³

guilhermevonrandon@gmail.com

¹Centro Federal de Educação Tecnológica de Minas Gerais, 30421-169, Belo Horizonte, MG, Brasil; ²Departamento de Química, Universidade Federal de Minas Gerais, Rua Mário Werneck, 2, Pampulha, Belo Horizonte, MG, Brasil;

³Instituto de Química de São Carlos, Universidade de São Paulo, PO Box 780, 13560-970, São Carlos, SP, Brasil.

Keywords: Electronic Structure, DFT, Nanoclusters, Catalysis, VASP.

INTRODUCTION

The burning of fossil fuels places a strain on the availability of energy and releases a large amount of CO₂ in the atmosphere, which leads to serious environmental problems that threaten sustainable economic development.¹ In this sense, the removal of CO₂ from the atmosphere has attracted great interest and strategies for CO₂ capture and CO₂ reutilization have been proposed.² In this sense, nanoparticles have been exploited as a new possibility for catalysis due to their properties on the activation and adsorption of this molecule.³ The focus of this work is to study the intermediates of CO₂ reduction reaction (CO₂ RR) using the Cu₅₅ nanocluster and its singly cobalt doped variant Cu₅₄Co as catalysts. Subsequently, with the most stable structures, we will perform a thermodynamics analysis using the computational hydrogen electrode (CHE)⁴ in order to obtain free energies and the onset potentials.

METHODS

All calculations were based on Density Functional Theory (DFT) and use the PBE⁵ functional with D3⁶ dispersion correction implemented in the Vienna *ab initio* simulation package (VASP). As a first step, calculations are made to determine the lowest energy structure for a cluster with 55 atoms. Afterwards, one atom of copper has been replaced by a cobalt atom in different possible positions. For investigating the interactions between the adsorbates and the clusters, preliminary screening calculations are performed to provide a first glimpse on the adsorption sites and possibilities. The most relevant configurations are later refined with calculations with larger plane wave cutoff energies and convergence criteria. After the refined calculations, we use the CHE model to compute free energy changes for the electrochemical steps.

RESULTS

In relation to unary clusters, the adsorbates have preference to hollow sites to adsorb, except for the HCO radical, which tends to be most stable in bridge sites. When the cluster is doped in subsurface and surface positions, the results are not changed, except for OH and CO. Through the

CHE model, we show that CO adsorption is favorable and the dopant in the surface makes the adsorption stronger and favors hydrogenation towards HCO. In the CO₂RR, there are parallel reactions, and one of them is the hydrogen evolution reaction, that will compete with the formation of more reduced products. We found that H₂ formation is extremely favorable and the dopant facilitates these paths too. Another possibility is the poisoning of the catalyst by OH, and the substrate must also favor its hydrogenation towards water, to avoid the poisoning. In this case the dopant hinders the formation of H₂O, but still the process is favorable to product formation.

CONCLUSIONS

Through DFT calculations, it was possible to study the interactions between the intermediates of CO₂RR with copper nanoclusters and to conclude that the doping mainly affected the CO and OH adsorptions due to the change of the orientation of the adsorbates in the clusters. The results obtained using the CHE model show that CO adsorption is favorable, however the COH and HCO formation requires more energy and the dopant influences more when it is in the surface of the nanoparticle.

REFERENCES

- P. Li, L. Liu, W. An, H. Wang, H. Guo, Y. Liang, W. Cui. Applied Catalysis B: Environmental 2020, 266 118618.
- J. Liu, Y. Cai, R. Song, S. Ding, Z. Lyu, Y. Chang, H. Tian, X. Zhang, D. Du, W. Zhu, Y. Zhou, Y. Lin. Materials Today, 2021, 48 95-114.
- L. Verga, G. Mendes, P. Ocampo-Restrepo, V. Ocampo-Restrepo, J. Da Silva. Catalysis Science & Technology, 2022, 12 869-879.
- J. Nørskov, J. Rossmeisl, A. Logadottir, L. Lindqvist, J. Kitchin, T. Bligaard, H. Jónsson. J. Phys. Chem. B 2004, 108 17886–17892.
- J. Perdew, P. Burke, K. Ernzerhof, M. Phys. Rev. Lett 1996, 77, 3865-3868.
- S. Grimme, J. Antony, Ehrlich, S. Ehrlich, H. Krieg. Chem. J. Chem. Phys 2010, 132 154104

ACKNOWLEDGMENTS

This research was supported by CEFET-MG, CINE, CNPq, CAPES, FAPEMIG (APQ-00597-22), FAPESP (2017/11631 – 2; 2018/21401 –7) and Shell.

COMPUTATION-GUIDED APPROACHES FOR RAPID DETECTION OF NEW PSYCHOACTIVE SUBSTANCES: CATHINONE FAMILY

José Renato D Fajardo (IC),^{1,2*} Eliani Spinelli (PQ),² Leonardo Moreira da Costa (PQ),¹ José Walkimar de Mesquita Carneiro (PQ)

joserdf@id.uff.br

¹ Fluminense Federal University. Institute of Chemistry. Niterói, RJ. Brazil;

² Fluminense Federal University. School of Pharmacy. Niterói, RJ. Brazil.

Palavras Chave: DFT, Spot test, Bathocuproine, Cathinones, Bath salts.

INTRODUCTION

The increasing prevalence of new psychoactive substances (NPS) poses challenges for public health and law enforcement agencies.^{1,2} Therefore, this study highlights the application of computational chemistry as a supporting tool for the development of spot test methodologies for synthetic drugs, commonly known as 'bath salts', which are analogs of cathinones, stimulating alkaloids derived from the plant *Catha edulis*.^{1,2}

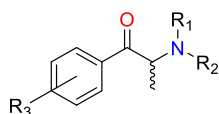


Fig. 1 – General structure of cathinone family.

METHODS

DFT calculations were employed to obtain a set of molecular parameters for the molecules of interest. The B3LYP functional and the Def2TZV basis set were employed in all calculations. After full geometry optimization, vibrational mode analysis were performed to confirm the optimized geometries as genuine minima energy points on the potential energy surface. A Python script was written to carry out a Principal Component Analysis (PCA) to identify the electronic properties that could correlate with the positive spot test.

RESULTS

The geometries of 33 molecules, including diverse members of the cathinone family and other substances, were fully optimized. Quantum calculations were conducted to derive essential parameters, such as reduction potential, oxidation potential, HOMO (Highest Occupied Molecular Orbital) and LUMO (Lowest Unoccupied Molecular Orbital) energies, and the HOMO-LUMO energy gap.

The substances with positive results in the rapid test were found to display a higher oxidation potential pattern than that of Bathocuproine (the copper complexing agent used in the rapid test method). Nevertheless, this correlation was not clear, as some substances with negative results exhibited similar oxidation potential values. To clarify this trend, we employed the PCA technique

to reduce data dimensionality. The PCA results are shown in Fig. 2.

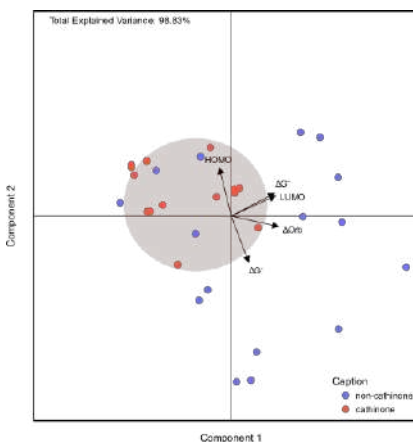


Fig. 2 – PCA1 x PCA2 graph.

The vertical orientation of the eigenvectors indicates parameters that strongly correlate with the positive test outcome, while the horizontal orientation represents parameters that have negligible impact on the test. The most correlated eigenvectors are oxidation potential and HOMO energy. The clustering of cathinones in a specific quadrant suggests that HOMO energy plays a crucial role in the positive test results. These results also demonstrate the test's specificity for cathinones, as they are all grouped together within the same quadrant.

CONCLUSIONS

The integration of molecular modeling and chemometrics analysis has allowed identification of molecular properties that may influence a positive spot test in cathinone identification. The HOMO energy, which also reflects in the oxidation potential, is the main parameter correlating with the positive prediction of drugs. This supports the improvement of detection tests and their application in diverse areas, including analytical chemistry and toxicology.

REFERENCES

- ¹ Novel Psychoactive Substances, 2 ed., 333-380, 2022.
² M. Philp, S. Fu, Drug Test. Anal., 2018, 20, 95-108.

ACKNOWLEDGEMENT

CNPq, CAPES, FAPERJ



Computational study of the formation of HCN in Titan's atmosphere

Daniel Moura (PG),^{1*} Adalberto Santana Lima Júnior (PG),¹ Maiara Oliveira Passos (PG),¹ Tiago Vinícius Alves (PQ).¹

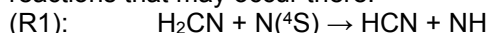
danieldemoura@ufba.br

¹Departamento de Físico-Química, Instituto de Química – Universidade Federal da Bahia, Rua Barão de Jeremoabo, 147, Salvador, 40170-115, Bahia, Brasil.

Palavras Chave: Hydrogen cyanide, Titan, Prebiotic chemistry, Reaction Kinetics.

INTRODUÇÃO

Since the detection of the HCN in Titan's atmosphere¹, the importance of this specie on prebiotic processes has been discussed². This molecule is connected to the formation of the nucleobases, as shown by LaWore e Regnier³. The formation of hydrogen cyanide was previously studied by Nesbitt *et al.*⁴, with the H₂CN and N(⁴S) as the starting reagents. In their experimental work, the rate constants were determined in a small range of temperatures. Later, Pearce *et al.*⁵ also determined the rate constants for the same reaction using the VTST approach, with the BHandHLYP/aug-cc-pVDZ level of theory. A difference of 47 orders from the experimental results was observed. Therefore, the main goal of this work is to study the reaction (R1), exploring its Potential Energy Surface (PES) and determining its thermal rate constant, in order to give a better understanding of Titan's atmosphere and the reactions that may occur there.



MÉTODOS

Geometry optimizations of the stationary points was performed with the M06-2X/aug-cc-pVQZ level of theory. This methodology was chosen based on recent works^{6,7} with similar reactions showing good agreement between DFT and highly correlated methods. The optimization was carried out using the Gaussian 09 program package. The thermal rate constants for the reaction were calculated using the canonical variational transition state theory (CVT) with multidimensional small curvature tunneling corrections (SCT). These rate constants were estimated with the Pilgrim code. The results were compared with the experimental results to evaluate the accuracy of the rate constants.

RESULTADOS

From the geometry optimization of the stationary points, we were able to estimate the relative energies of the stationary points. These results are shown in **Table 1**.

The calculated thermal constants are listed in **Table 2**, with the experimental result available in previous work. To evaluate the deviation of the results obtained, the ratio between these values is also listed.

Table 1 - Relative energies of the stationary points generated by the H₂CN + N(⁴S) reaction, at the M06-2X/aug-cc-pVQZ level of theory. All values are in kcal/mol.

Stationary Points	Relative Energies
H ₂ CN + N(⁴ S)	0.00
PRC	-1.15
TS1	1.33
HCN + NH	-62.30

Table 2 - Thermal rate constants ($\times 10^{-11}$) for the H₂CN + N(⁴S) → HCN + NH reaction together with the experimental values (in $\text{cm}^3 \text{molecule}^{-1} \text{s}^{-1}$).

T(K)	k _{Nesbitt}	k _{CVT/SCT}	k _{Nesbitt} / k _{CVT/SCT}
200	3.90	1.06	3.67
298	4.40	1.30	3.38
363	6.70	1.49	4.50

CONCLUSÕES

Four stationary points were identified for the reaction studied, with the most stable point located at -62.30 kcal/mol from the reactants. In terms of the kinetics, we were able to determine the rate constants in better agreement with the experimental results than the previous results available. The influence of the pre-reactive complex is being evaluated by applying the Canonical Unified Statistical (CUS) Theory.

REFERÊNCIAS

- R. Harnel *et al.*, Science, 1981, 10, 192.
- Z. Perrin *et al.*, Processes, 2021, 9, 965.
- D. LaWore, P. Regnier, Orig Life Evol Biosph, 2008, 38, 383.
- F. L. Nesbitt *et al.*, J. Phys. Chem. A, 1990, 94, 4946.
- B. K. D. Pearce *et al.*, J. Phys. Chem. A, 2019, 123, 1861.
- J. Bourgalais *et al.*, ApJ, 2015, 812, 106.
- J. C. Loison, K. M. Hickson, Chem. Phys. Lett., 2015, 635, 174.

AGRADECIMENTOS

CNPq, CAPES.



Avaliação topológica da ligação hidrogênio-flúor no ânion [FHF]⁻

Guilherme Arruda Belmonte Silva (IC),¹ Italo Curvelo dos Anjos (PQ).^{1*}

guilherme.silva14@sou.ufmt.br; italo.anjos@ufmt.br

¹Departamento de Química, Universidade Federal de Mato Grosso, Cuiabá –MT, Brasil.

Palavras Chave: Ligação Química, Ligação de Hidrogênio, QTAIM, ELF, Bifluoreto

INTRODUÇÃO

A ligação de hidrogênio é considerada uma interação intermolecular forte, que governa vários fenômenos importantes, como a solubilidade de substâncias, a preparação de nanomateriais, a formação do DNA, o enovelamento de proteínas e o projeto de novos fármacos.¹ Ainda assim, é mais fraca do que ligações químicas “convencionais” como a covalente e a iônica. Algumas interações, no entanto, apresentam características intermediárias entre as ligações químicas usuais e as interações intermoleculares, dificultando uma simples classificação em um desses grupos. É o caso da interação oxigênio-hidrogênio no cátion Zundel, $[H_5O_2]^+$.

Em 2021 uma publicação na revista Science, descrevia a interação no íon bifluoreto como um novo tipo de ligação química, similar a uma ligação de hidrogênio, porém bem mais forte que as ligações de hidrogênio conhecidas.²

Dante disso, o presente trabalho teve por objetivo caracterizar esta ligação, comparando o ânion bifluoreto $[FHF]^-$ com os cátions Zundel $[H_5O_2]^+$ e $[N_2H_7]^+$.

MÉTODOS

Foram realizados cálculos de otimização de geometria e de frequência buscando estruturas de mínimo e estados de transição com o funcional M06-2X e com o método MP2 e conjunto de funções de base aug-cc-pVTZ usando os pacotes Gaussian 09 e GaussView. Com as estruturas otimizadas, foram feitos cálculos de QTAIM e ELF usando os softwares AIMall e Multiwfn, respectivamente.

RESULTADOS

Para as estruturas de mínimo, tanto $[FHF]^-$ quanto $[H_5O_2]^+$ apresentaram duas ligações X—H equivalentes com certo caráter de compartilhamento de carga, embora menor do que uma ligação covalente usual, já $[N_2H_7]^+$ mostrou duas ligações X—H distintas: uma ligação covalente e uma ligação de hidrogênio.

Em relação às cargas dos hidrogênios centrais, $q(H)$, foi observada a seguinte tendência: $[FHF]^- > [H_5O_2]^+ > [N_2H_7]^+$, acompanhando a tendência de eletronegatividade dos átomos X. Já em relação às cargas nos átomos X, a tendência foi: $[H_5O_2]^+ < [N_2H_7]^+ < [FHF]^-$, evidenciando a influência dos hidrogênios periféricos. Os valores

da proriedades de ligação e de carga são mostrados na Tabela 1.

É importante ressaltar que não foram encontrados estados de transição para o íon bifluoreto, o que é compatível com dados de estudos recentes.³ Além disso, também não houve variações significativas entre os valores das propriedades calculados usando MP2 e M06-2X.

Tabela 1 – Propriedades das interações X-H das estruturas de mínimo de energia usando o funcional M06-2X e o método MP2 (entre parênteses)

	$[FHF]^-$	$[H_5O_2]^+$	$[N_2H_7]^+$	
d_{X-H} (Å)	1,14 (1,14)	1,20 (1,20)	1,51 (1,58)	1,15 (1,12)
θ (°)	180 (180)	175 (174)	180 (180)	
ρ	0,177 (0,176)	0,167 (0,168)	0,090 (0,077)	0,225 (0,251)
$\nabla^2\rho$	-0,556 (-0,570)	-0,458 (-0,504)	+0,005 (+0,026)	-0,937 (-1,332)
$\delta_{A,B}$	0,224 (0,208)	0,242 (0,222)	0,235 (0,188)	0,443 (0,415)
$q(H)$	+0,752 (+0,753)	+0,721 (+0,726)	+0,571 (+0,587)	
$q(X)$	-0,876 (-0,877)	-1,242 (-1,268)	-1,088 (-1,165)	-1,100 (-1,162)

CONCLUSÕES

Os dados topológicos e geométricos apontam para as interações H---F no íon $[FHF]^-$ não são compatíveis com as de ligação de hidrogênio usuais, na verdade essa ligação tem características que se aproximam mais de ligação covalente simples do que de uma interação intermolecular, semelhante à interação H---O no cátion Zundel, mas possivelmente com um grau de covalência ainda mais pronunciado.

REFERÊNCIAS

- Rocha, W. R. Interações Intermoleculares. *Química Nov. na Esc.* **2001**, No. 4, 31–36.
- Dereka, B.; Yu, Q.; Lewis, N. H. C.; Carpenter, W. B.; Bowman, J. M.; Tokmakoff, A. Crossover from Hydrogen to Chemical Bonding. *Science* (80-.). **2021**, 371 (6525), 160–164. <https://doi.org/10.1126/science.abe1951>.
- Feng, W.; Li, D.; Cheng, L. Theoretical Study on L—H+—L with Identical Donors: Short Strong Hydrogen Bond or Not? *J. Chem. Phys.* **2022**, 157 (9). <https://doi.org/10.1063/5.0103228>.

AGRADECIMENTOS

CNPq, Capes e UFMT.

Multiscale modelling to address the interaction of liquid acetonitrile with Mo-based bidimensional materials

Marcelo Albuquerque (PhD)¹, Flávia C. A. Silva (PhD)², Luciano T. Costa (R)², Pedro Venezuela (R)¹
marcelofilho@id.uff.br; pedrovenezuela@id.uff.br

¹Institute of Physics, Fluminense Federal University, Campus Praia Vermelha, Boa Viagem, Niterói-RJ, Brazil; ²MolModCS, Physical Chemistry Department, Institute of Chemistry, Fluminense Federal University, Campus Valongo, Niterói-RJ, Brazil

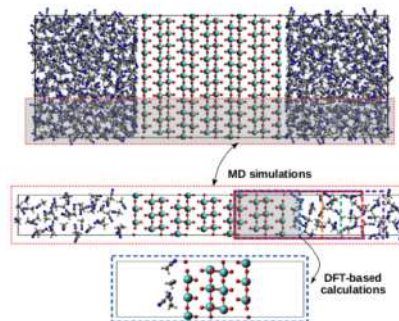
Keywords: Solid-liquid interface, multiscale, MD, DFT, charge transfer

INTRODUCTION

Since the successful mechanical cleavage of graphite into one single atomic-layered carbon plane, new atomic-size materials have been synthesized in the last almost two decades¹, including transition metal dichalcogenides (TMDs) and transition metal oxides (TMOs), which can be obtained through different experimental techniques. A few years ago, Schmidt and Zarbin² reported a simple, scalable and effective route to synthesize, disperse, exfoliate and process different molybdenum-based 2D material, such as molybdenum trioxide (MoO_3) and molybdenum disulfide (MoS_2), through the liquid-liquid interfacial route (LLIR). By handling the mixture of crystalline MoO_3 and MoS_2 with acetonitrile (ACN), layered MoS_2 becomes homogeneously dispersed, while MoO_3 becomes agglomerated as a bulk solid. Acetonitrile has a three-fold function in this process: separates the sulfide/oxide mixture, exfoliates the sulfide material and stabilizes the dispersion. In this process, the dispersed material seems to be negatively charged, and the deposited solid apparently does not show any signal of charge transferred to it. The origin of the charges in their samples are still unknown. In this work, we investigate the charge transfer at the solid-liquid interface.

METHODS

Stochastic dynamics (SD) simulations in the NVT ensemble were performed using GROMACS v. 2018.1 to sweep the phase space of the ACN molecules at the solid surfaces, which were kept ‘frozen’. From the trajectory of this system, the simulation box was cut out, whereon another SD simulation was performed. Then, different snapshots were sampled from the equilibrated MD trajectories and prepared to be inputs for the solid DFT calculations, according to the scheme below. Charge transfer was analyzed by integrating the electronic density in the solid volume.



RESULTS

Up to this point, we have seen through molecular density and RDF analysis that MoS_2 induce ACN ordering parallel to its surface, while ACN present a more random orientation at MoO_3 interface. Higher concentration of ACN at MoS_2 surface have been found compared to MoO_3 counterpart. Although DFT calculations did not show charge transfer to the solids, it indicated that MoS_2 plays a different role compared to MoO_3 . Calculations including O_2 and H_2O to account for environmental contaminants showed almost zero charge transfer for the former and an increase in almost twice in the latter case.

CONCLUSIONS

So far, we have seen that MoS_2 induces specific molecule ordering and charge transfer process as compared to the MoO_3 counterpart. However, it is necessary to investigate the effect of different force fields for ACN (polarizable one, for instance) on the ACN orientation at the solid interface, as well as different solid orientation on the charge transfer. Right now, we are working on the first proposition.

REFERENCES

- ¹ Gupta, A., Sakthivel, T. and Seal, S., Progress in Materials Science, 2015, 73, 44-126.
- ² Schmidt, A. and Zarbin, A.J., Journal of colloid and interface science, 2019, 554, 80-90.

ACKNOWLEDGMENTS

We greatly appreciate CAPES for funding and support, CENAPAD-SP for providing high-performance computing facilities and support, and the MolModCS group.

Chemical bond descriptors in a tripodal N_4O_3 ligand coordinated to $\text{Ln}(\text{III})$ ions: across the lanthanide series from La to Lu

Francielle C. M. Santos (PG),¹ Carlos V. Santos-Jr (PG),² Ricardo L. Longo (PQ),¹ Renaldo T. Moura Jr (PQ)^{3*}

franmachadosantos.20@gmail.com; renaldo.mourajr@cca.ufpb.br

¹Departamento de Química Fundamental, Universidade Federal de Pernambuco, Recife-PE; ²Departamento de Química, Universidade Federal da Paraíba, João Pessoa-PB; ³Departamento de Química e Física, Universidade Federal da Paraíba, Areia-PB.

Keywords: Localized polarizability, Local mode force constants, Lanthanide complex.

INTRODUCTION

The nature of the chemical bond between lanthanide ions and ligating atoms $\text{Ln}(\text{III})-\text{L}$ has been a subject of ongoing controversy. Central to this discussion are the extent to which the 4f orbitals and their electrons contribute to covalency, as well as the impacts of this covalency on 4f-4f transitions. The degree of covalency in $\text{Ln}(\text{III})-\text{L}$ bonds is primarily attributed to the more radially outer orbitals (5d, 6s, and 6p). Conversely, there is a consensus that the participation of 4f orbitals is minimal, though it could play a role in explaining variations in 4f-4f transitions. Analyzing these bonds through different chemical bond analyses poses challenges due to the complexity of the multiconfigurational nature, high multiplicity, and the large number of electrons involved. Considering these complexities, any information contributing to comprehending the nature of $\text{Ln}(\text{III})-\text{L}$ bonds is invaluable. This study presents an assessment of two properties associated with $\text{Ln}(\text{III})-\text{L}$ bonds: the local vibrational mode force constant and the ligand's effective polarizability.

METHODOLOGY

The compounds formed with the ligand trensal (Figure 1) binding to $\text{Ln}(\text{III})$ ions from La to Lu were investigated. Geometries, frequencies, and finite field calculations employed the B3LYP/MWBn(Ln)/6-311++G**, where n varies with the atomic number of $\text{Ln}(\text{III})$ ions with G09. Localized molecular orbitals (LMO) were obtained with Multiwfn, while ChemBOS¹ decomposed molecular polarizability into LMO contributions. Local force constants were determined using LModeA Software².

RESULTS

The ligand polarizabilities (α') and local force constants (k^a) for all $\text{Ln}(\text{III})-\text{L}$ bonds were obtained. The latter directly measures bond strength, while the former quantifies polarization of the chemical environment around the $\text{Ln}(\text{III})$ ion. The trensal ligand features three equivalent oxygen atoms (O), three equivalent nitrogen atoms (N), and one non-equivalent nitrogen (N'), all forming bonds with the $\text{Ln}(\text{III})$ ion.



Figure 1. Molecular structure of the complex (omitted H).

The $\text{Ln}-\text{N}'$ bonds have the lowest force constants (Figure 2) and the highest effective polarizabilities. $\text{Ln}-\text{N}$ and $\text{Ln}-\text{O}$ bonds exhibit systematically decreasing k^a values with increasing $\text{Ln}(\text{III})$ ionic radius, while their $\text{Ln}-\text{N}'$ counterparts display an opposite trend. Notably, $\text{Ln}-\text{N}'$ distances are larger than $\text{Ln}-\text{N}$ lengths, and the ionic radius expansion is followed by a subsequent bond length reduction.

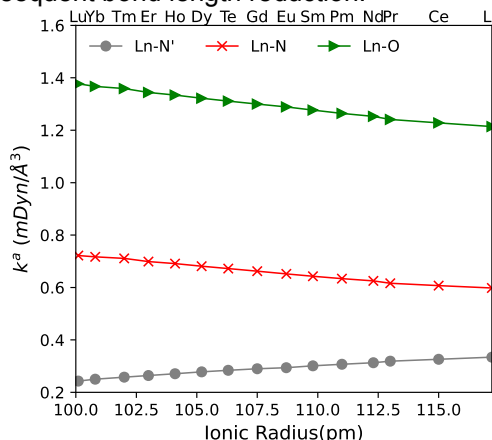


Figure 2. $\text{Ln}(\text{III})-\text{L}$ local force constants vs. $\text{Ln}(\text{III})$ ionic radius.

CONCLUSIONS

$\text{Ln}-\text{N}$ and $\text{Ln}-\text{O}$ bonds undergo the lanthanidic contraction, whereas $\text{Ln}-\text{N}'$ exhibit an opposing trend due to their frustrated coordination. Additional chemical bond descriptors are under evaluation.

REFERENCES

- R. T. Moura Jr *et al.* Optical Materials: X, 2022, 16, 139282.
- Zou, W.; Moura Jr., R.; Quintano, M.; Bodo, F.; Tao, Y.; Freindorf, M.; Makós, M.Z.; Verma, N.; Cremer, D.; Kraka, E. LModeA2023. CATCO, SMU: Dallas, TX, USA, 2023.

ACKNOWLEDGEMENTS

UFPE, UFPB, CNPq, CAPES, FACEPE, FINEP, CETENE.



Investigação QM/MM do Efeito de Solvatação sobre a Ancoragem de Cromóforos Sensibilizadores de Células Solares (DSSC)

Maria Luísa O. Lima (UR)¹, Daniel F. S. Machado (R)^{2*}

marialuisalimaa@gmail.com; daniel.scalabrin@unb.br

¹Universidade de Brasília, Instituto de Química, Laboratório de Modelagem de Sistemas Complexos

Palavras-chave: QM/MM, Monte Carlo, DFT, Cromóforos Orgânicos

INTRODUÇÃO

Foi realizado um estudo teórico para entender os efeitos de solvente nas propriedades eletrônicas e estruturais em um modelo de cromóforos orgânicos ancorados em um centro metálico de Titânio visando aplicações em células solares sensibilizadas por cromóforos orgânicos – DSSCs.

METODOLOGIA

As geometrias moleculares são obtidas a partir de cálculos de otimização empregando a DFT e sua variante do tempo TDDFT para simular as excitações. Nas otimizações foi adotado o funcional híbrido de troca-correlação B3LYP combinado com o conjunto de funções de base aug-cc-pVDZ para os elementos mais leves e a base com potencial efetivo aug-cc-pVDZ/PP para o átomo de Titânio. Na etapa de otimização, para levar em conta o efeito de solvente, utilizamos o modelo contínuo polarizável (PCM). Esses cálculos foram realizados através do pacote de química teórica Gaussian16 disponíveis nos clusters do Instituto de Química da UnB. A parte MM foi baseada no método Monte Carlo com algoritmo de Metropolis, utilizando o programa DICE.

RESULTADOS

Os espectros ocorreram na região UV/Vis, e o efeito do pseudo-potencial foi mais evidente na TPAR1 em gás, apresentando um deslocamento para a região vermelha. A TPAR1 também mostrou um efeito hipercrômico mais intenso que a TC1. O solvente também afetou os espectros, causando deslocamentos batocrómicos. A força do oscilador foi calculada para avaliar a eficiência de colheita de luz (LHE), e a TPAR1 foi identificada como um acceptor mais forte. O estudo dos orbitais mostra a transferência de carga para o átomo de Ti apenas na TC1, tornando-a mais eficiente como cromóforo. Analisando o solvente na abordagem Monte Carlo (MC), os parâmetros de densidade e entalpia conformacional da TC1 e TPAR1 apresentam flutuações em termos das interações intermoleculares, o que ressalta uma maior estabilidade intrínseca das interações soluto-solvente e solvente-solvente da molécula TC1. Pelo gráfico da função distribuição radial de pares, $g(r)$, dos cromóforos podemos verificar a

probabilidade de encontrar vizinhos em uma camada esférica conforme se afasta da molécula central, nesse caso a TC1 em distâncias menores é encontrado mais moléculas do solvente em volta do soluto do que na TPAR1.

CONCLUSÃO

O emprego do pseudo-potencial trouxe resultados semelhantes nos dois cromóforos quando os cálculos levam em conta o efeito do solvente. Em fase gás por outro lado, a omissão do tratamento explícito dos elétrons de caroço do Ti foi impactante apenas para a TPAR1. O tratamento implícito do solvente trouxe efeitos batocrómicos importantes nos dois cromóforos com uma grande variação do momento de dipolo em solução mostrando que a polarização do soluto é aumentada em fase líquida. Já o tratamento explícito demonstrou que em relação aos dois cromóforos temos flutuações distintas comparando a energia conformacional e sua densidade devido as interações entre soluto-solvente serem mais significativas na molécula TC1. E considerando a distribuição radial de pares temos mais soluto em volta do solvente em distâncias menores na TC1, o que elucida a presença de ligações de hidrogênio. Valores de LHE mostram que os dois cromóforos tem eficiência semelhante na coleta de luz na região do visível. Entretanto, observou-se que apenas a TC1 consegue injetar densidade de carga no centro metálico sob foto-exposição sendo um cromóforo potencialmente superior em relação a TPAR1.

REFERÊNCIAS

¹Brian O'Regan and Michael Graetzel. A low-cost, high-efficiency solar cell based on dyesensitized colloidal TiO_2 films. *Nature*, 353(1):737–740, 1991.

²Dyesensitized solar cells with conversion efficiency of 11.1%. *Japanese Journal of Applied Physics*, 45(No. 25):L638–L640, 2006.

AGRADECIMENTOS

Agradecimentos ao CNPq e FAP-DF pelo financiamento do projeto. À Universidade de Brasília por ceder o espaço de estudo. À SBQT por ceder o espaço de apresentação..

Exploring machine learning algorithms for the prediction of CO₂ and N₂ isotherm on nanoporous materials

João Matheus C. Sousa (UR)¹, Felipe L. Oliveira (PhD)¹, Pierre M. Esteves (R)^{1*}

joaosousa.chagas@gradu.iq.ufrj.br; pesteves@iq.ufrj.br

¹Instituto de Química, Universidade Federal do Rio de Janeiro

Keywords: machine learning, nanoporous materials, adsorption, CO₂ capture

INTRODUCTION

The increasing emissions of greenhouse gases, specially as CO₂, are directly linked to the growing environmental impacts caused by climate change.¹ One promising strategy to address this issue is the usage of nanoporous materials for the capture and storage of CO₂.

Reticular nanoporous materials such as MOFs and COFs have a great potential for CO₂ capture.² However, due to the large number of possible structures and its structural diversity their experimental exploration can be challenging. Computational techniques, including machine learning, offer a valuable tool for exploring these materials.

Here, we investigate the application of several machine learning methodologies for the prediction of adsorption isotherms of gases such as CO₂ and N₂ on nanoporous materials. Additionally, the impact of several dimensionality reduction techniques and feature selection methods on the predictive performance of the machine learning models was evaluated.

METHODS

For a set of porous materials taken from the CRAFTED³ database, we fitted a Dual-site Langmuir (DSL) isotherm model to the CO₂ and N₂ isotherms. Thus, each isotherm can be represented by 8 parameters by the equation

$$q_i^* = \sum_{j=1}^2 \left[q_{j,i}^s \frac{b_{j,i} P}{1 + b_{j,i} P} \right]$$

Four predictive models were evaluated: Decision Tree, Random Forest, xGBoost, and Neural Networks. For each model two distinct architectures were developed: *i.* a multi-objective architecture with a single model predicting all 8 parameters responsible for generating the adsorption isotherms, and *ii.* a single-objective architecture comprised of 8 separate models, each dedicated to predicting a single parameter of the isotherm.

The descriptors used to encode the structure features encompassed textural properties (specific surface area, pore volume, etc.) and chemical features calculated as the RAC descriptors.⁴

RESULTS

The fit of the DLS model on the adsorption data of the 1340 materials from CRAFTED presented a good fit ($R^2 > 0.9$) for 1223, as exemplified in Figure 1.

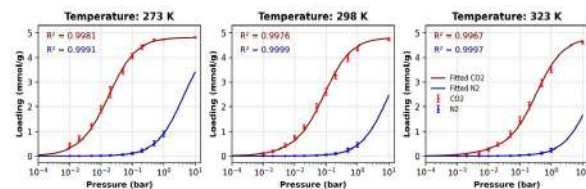


Figure 1: Isotherms fitted with the DSL model for CO₂ and N₂ at temperatures 273K, 298K, and 323K.

This fitted parameters were used to train the four different machine learning models. Among this models, at least three of them (Random Forest, xGBoost and Neural networks) presented good results ($R^2 > 0.8$), as exemplified in Figure 2. The Neural Network model presented the best result among the evaluated models.

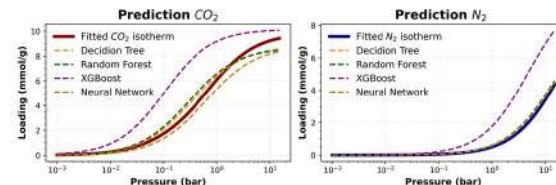


Figure 2: DSL models for CO₂ and N₂ isotherms at the temperature of 273K and the prediction with the evaluated ML models.

The combination of textural properties with RAC descriptors resulted in models with better predictive capabilities, followed by the versions with dimensionality reduction and textural and chemical descriptors individually.

CONCLUSIONS

We show that it is possible to develop Machine Learning algorithms capable of predicting adsorption isotherms for MOFs and COFs based on chemical (RACs) and geometric descriptors.

REFERENCES

- 1 STEFFEN et al. Philos. Trans. Royal Soc. A PHILOS T R SOC A, 2011, 369(1938), 842-867.
- 2 Yaghi, O. M. ACS Cent. Sci., 2019, 5(8), 1295-1300.
- 3 Oliveira et al. Sci Data, 2023, 10, 230.
- 4 Janet, J. P. et al. J. Phys. Chem., 2017, A121, 8939–8954.

ACKNOWLEDGMENTS

CNPq, CAPES, FAPERJ, FINEP-ANP.

Investigation of adsorption of sulfur compounds on CuCl₂ doped UiO-66

Amanda Cota Marques (UR),¹ Carla Vieira Soares (PhD),² Alexandre Amaral Leitão (R).^{1*}

amanda.cota@ice.ufjf.br; carlavieira@ice.ufjf.br; alexandre.leitao@ufjf.br

¹GFQSI, Departamento de Química, Universidade Federal de Juiz de Fora, Juiz de Fora-MG; ²LARHCO, Instituto de Química, Universidade Federal do Rio de Janeiro, Rio de Janeiro-RJ.

Keywords: DFT, MOFs, ADS, Sulfur Compounds.

INTRODUCTION

Waste gases containing sulfur compounds, which are generated and emitted from industrial processes, wastewater treatment and landfill waste may cause undesirable issues in adjacent areas and contribute to atmospheric pollution. In this context, adsorption desulfurization (ADS) is considered as a promising process, garnering attention due to its mild operation conditions, and no need of hydrogen or oxygen. Recently, Metal organic-frameworks (MOFs) have been reported to adsorb significant amounts of sulfur.¹ MOFs are highly porous crystalline compounds made of metallic clusters (or metal ions) and organic linkers connected by coordination bonds.²

The zirconium MOF UiO-66 has received considerable attention due to an easy lab-scale synthesis, great thermodynamic stability provided by the strong Zr-O bond, and a variety of applications.² Several studies have focused on the effect of introducing foreign metals to the MOF framework on gas adsorption. It has been concluded that metal doping increases gas uptake by providing additional sites for adsorption.³ Moreover, adsorbents containing metals such as Cu exhibit remarkable capabilities in selectively adsorbing sulfur compounds, as this process can occur via π -complexation, acid-base interactions, and direct sulfur-metal interactions.⁴ In this work Density Functional Theory (DFT) calculations have been used to investigate the effects of CuCl₂ on the adsorption of sulfur compounds on UiO-66.

METHODS

The calculations were carried out using the Quantum-ESPRESSO package⁵, which implements the DFT with periodic boundary conditions and a plane-wave basis set. The Perdew-Burke-Ernzerhof generalized gradient approximation (GGA-PBE) was employed to incorporate the exchange-correlation potential. To account for the long-range interactions, van der Waals correction DFT-D3 method of Grimme was applied. Interaction of valence electrons with nuclei and core electrons were treated by the projector augmented-wave (PAW) method.

RESULTS

A series of full geometry optimization calculations were made to reveal the preferential orientation of the CuCl₂ fragment within the pores of UiO-66.

The preferential arrangement of CuCl₂ was found to be in the tetrahedral cage, next to the oxygen bound to the Zr, as illustrated in Fig. 1.

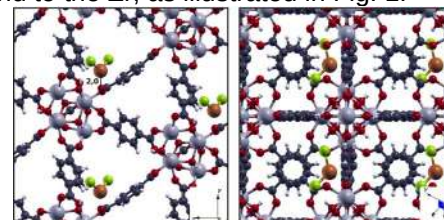


Fig. 1. Preferential location of CuCl₂ fragment on UiO-66.

Starting from the promising CuCl₂-UiO-66 structure, calculations were made to evaluate the adsorption capacity for water, CO₂, and the sulfur compounds H₂S, COS, and ethanethiol (EtSH). The adsorption energies for the Cu doped MOF compared to the ones in the pristine structure are depicted in Fig. 2.

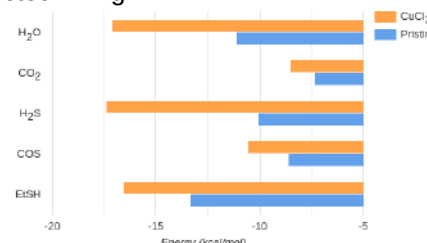


Fig. 2. Adsorption energies of pristine and doped UiO-66.

Charge density difference and Bader charge calculations indicate a significant charge transfer between MOF and the molecules, mostly observed in the vicinity of the CuCl₂ fragment.

CONCLUSIONS

The adsorption capacity of UiO-66 for the molecules was significantly increased upon introducing the CuCl₂ fragment. The most notable enhancement was observed for the adsorption of H₂S, showing a remarkable improvement of 72%. On the other hand, CO₂ adsorption experienced a comparatively lower increase of 15.7%. Charge density difference and Bader charge calculations confirmed evidence of chemisorption for the non-linear molecules H₂O, H₂S and EtSH.

REFERENCES

- ¹H. Zhang et al, IECR, 2012, 51, 12449-55.
- ²J. K. Cavka et al, JACS, 2008, 130, 42, 13850-51.
- ³A. M. Ebrahim, T. J. Bandosz, ACS, 2013, 92, 10565-73.
- ⁴B. Saha et al, 2021, FPT, 2014, 106685.
- ⁵P. Giannozzi et al. JPCM, 2009, 21, 395502.

ACKNOWLEDGMENTS

CAPES, CNPq, CENAPAD-SP, UFJF.



Estudo Cinético de Reações Uni e Bimoleculares de Trimetoximetano.

Daniel Rodrigues Mendes (IC),¹ Patrick José Mendes Ferreira (IC),¹ Glauco Favilla Bauerfeldt (PQ).^{1*}

danielrodrigues1509@gmail.com; bauerfeldt@ufrj.br

Universidade Federal Rural do Rio de Janeiro. Rodovia BR 465, km 7, Seropédica, RJ. Brasil.

Palavras Chave: Éteres de Oximetileno,

Combustão, Teoria de Estado de Transição

INTRODUÇÃO

Tecnologias voltadas a síntese e avaliação de combustíveis alternativos, visando diminuir a dependência global de combustíveis fósseis e inserir combustíveis de biomassa na matriz energética, têm sido continuamente investigadas. Para tal finalidade, os éteres de oximetileno têm se mostrado alternativas satisfatórias.¹ Éter dimetílico e dimetoximetano são encontrados neste grupo e os mecanismos de combustão cinética já foram extensivamente estudados. Neste trabalho é apresentado o estudo cinético das reações uni e bimoleculares que compõem um submecanismo de iniciação de combustão de trimetoximetano (TMM), um éter oximetileno mais complexo.

MÉTODOS

Métodos computacionais teóricos são adotados para a determinação precisa das constantes de velocidade, incluindo sua dependência de temperatura e pressão, para reações uni e bimoleculares de TMM. Os pontos estacionários foram localizados em nível M06-2X/aug-cc-pVTZ, bem como as frequências vibracionais e os caminhos de reação foram calculados. Coeficientes de velocidade foram previstos adotando os métodos de estado de transição variacional canônico e microcanônico.²

RESULTADOS

Atenção especial foi dedicada ao estudo de reações uni e bimoleculares de TMM, como indicado na Figura 1 e 2.

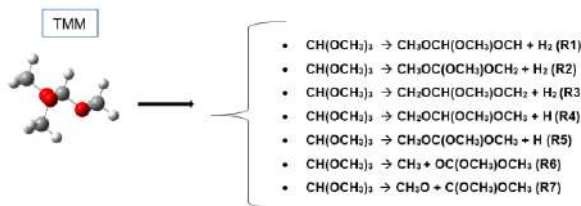


Figura 1. Reações Unimoleculares do TMM.

As alturas de barreira e as diferenças de energia de reação, obtidas no nível M06-2X/aug-cc-pVTZ, situam-se na faixa de 86,8 a 119,6 kcal mol⁻¹ e de 88,3 a 94,8 kcal mol⁻¹, respectivamente (reações unimoleculares, R1 – R7). A dissociação de CH_3 (R6) e as eliminações de H_2 (R1 e R2) têm alturas de barreira semelhantes, sendo as mais baixas do grupo de reações estudadas. Devido às

contribuições entrópicas, a dissociação é mais rápida e os coeficientes de taxa de alta pressão são expressos por $2,136 \times 10^{18} \times \exp(-46822/T)$.

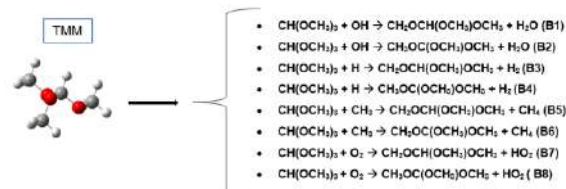


Figura 2. Reações Bimoleculares do TMM.

As barreiras obtidas para a abstração de hidrogênio, em nível M06-2X/aug-cc-pVTZ, encontram-se na faixa de 4,1 a -2,1 kcal mol⁻¹ (B1 e B2), 8,9 a 6,7 kcal mol⁻¹ (B3 e B4), 11,4 a 9,6 kcal mol⁻¹ (B5 e B6) e 40,8 a 38,2 kcal mol⁻¹ (B7 a B8). Percebe-se uma diminuição nos valores das barreiras quando o hidrogênio abstraído está ligado ao carbono central da molécula de TMM.

CONCLUSÕES

As reações OH são responsáveis pelo consumo rápido do combustível, embora as reações unimoleculares sejam responsáveis pelo consumo inicial do combustível, portanto, pela geração dos primeiros radicais que propagam a combustão. A competição entre reações unimoleculares e bimoleculares de O_2 pelo decaimento do TMM no mecanismo de consumo é fortemente dependente da temperatura inicial.

REFERÊNCIAS

- ¹ M. Hrtl, P. Seidenspinner, E. Jacob, G. Watch-meister, Oxygenate screening on a heavy-duty diesel engine and emission characteristics of highly oxygenated oxymethylene ether fuel, FUEL 153 (2015) 328 ±335.
- ² VIEIRA, G. S. S.; SANTOS, L. G. F.; ALMEIDA, C. S.; TEJERO, T. N.; XAVIER JUNIOR, N. F.; MACHADO, G. S.; BAUERFELDT, G. F. Assessment of Uni and Bimolecular Reaction Kinetics of Dimethoxymethane with the KINPRO Package. In: 10th European Combustion Meeting, 2021, Virtual Edition. Proceedings of the European Combustion Meeting 2021, 2021.

AGRADECIMENTOS

Os autores agradecem ao CNPq e a FAPERJ pelas bolsas de Iniciação Científica.

Structural Dynamics and Solvation a β -glucosidase in Aqueous Solutions containing Glucose

Felipe Cardoso Ramos, Munir Salomão Skaf and Leandro Martínez

felipecr@unicamp.br

Institute of Chemistry and Center for Computing in Engineering and Science - CCES, University of Campinas

Palavras Chave: Structural enzymology, Protein dynamics, Protein Solvation, Molecular dynamics, β -glucosidase.

INTRODUCTION

The enzyme β -glucosidase is a glycosyl hydrolase (GH) involved in the lignocellulose deconstruction and is of crucial importance for industrial processes, such as the manufacturing of second generation (2G) bioethanol. It is well known that the β -glucosidase (BG) enzyme, which breaks down the β -1,4 linkage of cellobiose (releasing two molecules of β -glucose), is inhibited by glucose (its own reaction product) at high concentrations (>375 mM) due to a competitive inhibition process. However, at lower glucose concentrations (~ 125 mM), the β -glucosidase from *Humicola insolens* (BGHI) undergoes an activation process that is not yet fully understood¹. Sugar molecules tend to favor the protein structure hydration in aqueous solutions, which generally promote its stabilization and, therefore, our guess is that this activation phenomenon may be due to indirect effects induced by the solvent arrangement around the protein^{2,3}.

METHODS

We have performed atomistic classical Molecular Dynamics (MD) simulations of BGHI at different glucose concentrations (0 mM, 125 mM, 250 mM and 1000 mM) in order to mimic the conditions found in the experiments. Our approach is based on a detailed examination of the solvent environment through the calculation of minimum distance distribution functions (MDDF) and Kirkwood-Buff integrals (KB)². Such quantities allow us to estimate thermodynamic properties of the systems such as the protein molecule preferential solvation parameter (Γ)³. The latter can help us to elucidate the structure of the solvent around the protein and provide information about the stability of the enzyme in solution.

RESULTS

The results indicate that the BGHI is preferentially hydrated and that Γ increases with the concentration of the glucose in medium. The glucose molecules made both specific (hydrogen bonds) and non-specific (hydrophobic) interactions with the protein surface, resulting in the formation of two and three solvation layers for glucose and water, respectively. The majority of the interactions between BGHI and glucose

consist of hydrogen bonding between the polar side chains of proteins and the hydroxyl groups of the co-solvent. Regarding the protein dynamics, the most flexible regions comprise loops at the entrance of the catalytic cavity. The loops dynamics control the size of the cavity leading to the catalytic residues (GLU 166 and GLU 377), which tends to adopt a more open conformation in the presence of glucose. The opening of the cavity, in turn, is related to the entry of glucose into the active site and, consequently, to product inactivation. Such opening of the protein structure was observed at all concentrations, although the frequency of glucose in the active site was lower at 125 mM.

CONCLUSION

Based on the analysis conducted here, it was possible to define the solvation structure of the enzyme in solutions containing glucose as a co-solvent, at different concentrations. The BGHI enzyme is preferentially hydrated at all concentrations, which, however, does not prevent direct (specific and non-specific) interaction between the enzyme and glucose molecules. These interactions with the co-solvent molecules change the structural dynamics of the enzyme (favoring its opening). Our guess is that at 125 mM, the enzyme presents better catalytic performance due to the lower entrance of glucose at the active site, which results in lower product inhibition. Mutagenesis approaches directed to the flexible loops of the enzyme could result in a better modulation of its activity and also better adaptation to industrial conditions.

REFERENCES

- ¹Meleiro, L. P., Salgado, J. C. S., Maldonado, R. F., Carli, S., Moraes, L. A. B., Ward, R. J., ... & Furriel, R. P. M. PLoS One, 2017, 12(11), e0188254.
- ²Martinez, L., & Shimizu, S. Journal of chemical theory and computation, 2017, 13(12), 6358-6372.
- ³Martinez, L. Journal of Molecular Liquids, 2022, 347, 117945.

ACKNOWLEDGMENTS

The authors acknowledge the support of FAPESP (2022/04810-6), the Center for Computing in Engineering and Sciences (CCES), CENAPAD-SP (National Center for High Performance Processing in São Paulo), and Martínez Molecular Modeling Group (M3G, <http://m3g.iqm.unicamp.br/>).



Avaliação da eficácia dos métodos CASSCF e MR-CISD na caracterização do espectro de fotoabsorção UV do Clorometano

Mariana G. Bezerra (PG),¹ Elizete Ventura do Monte(PQ),² Silmar Andrade do Monte (PQ).³

marianaguadez0298@gmail.com

¹Departamento de Química, Universidade Federal da Paraíba, João Pessoa-PB

Palavras Chave: Fotoquímica, dinâmica quântico-clássica.

INTRODUÇÃO

O Clorometano (CH_3Cl) é um composto de grande abundância atmosférica e está envolvido diretamente na emissão de radicais que atuam na degradação do ozônio atmosférico. Diante disso, é de grande interesse o entendimento acerca da fotoquímica do CH_3Cl , permitindo uma compreensão mais ampla acerca de seus processos de desativação na atmosfera. Logo, o estudo teórico da fotodinâmica dessa molécula pode contribuir diretamente na clarificação de tais processos. Portanto, este trabalho tem como objetivo caracterizar teoricamente o espectro de fotoabsorção UV da molécula de CH_3Cl por meio de dinâmica quântico-clássica não adiabática, baseando-se nos métodos multirreferenciais CASSCF (Complete Active Space Self-consistent Field) e MR-CISD (Multireference Configuration Interaction Single and Doubles), já usados na literatura na descrição da fotoquímica do clorometano¹, buscando, assim, avaliar a eficácia de tais métodos na descrição da fotodinâmica dessa molécula.

MÉTODOS

Para o cálculo de estados excitados tanto com o método MR-CISD quanto com o método CASSCF utilizou-se um espaço ativo que incluiu os orbitais de valência, configurando um CAS (6,4), e os orbitais de Rydberg 3s e 3p_o do carbono. As bases escolhidas para esses cálculos foram d-aug-cc-pVQZ (C) e aug-cc-pVQZ (Cl, H).

As condições iniciais da dinâmica e o espectro de fotoabsorção da molécula contendo a banda n3s para os dois métodos avaliados foram gerados no programa Newton-X em interface com o programa Columbus, no qual são realizados os cálculos eletrônicos.

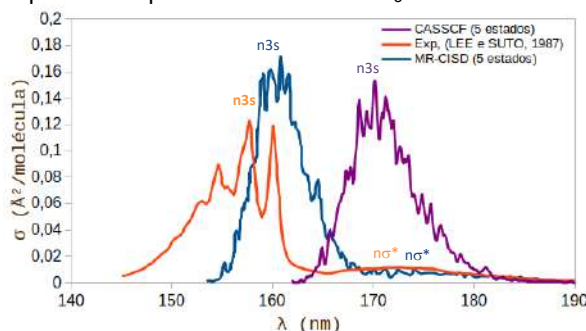
RESULTADOS

Foram construídos os espectros de fotoabsorção UV da molécula de CH_3Cl contendo a banda de interesse, n3s, nos níveis CASSCF e MR-CISD, exibidos na Figura 1. Em ambos os níveis de cálculo foram realizados cálculos com 5 estados, visto que este número é suficiente para descrever a formação do par iônico, conforme apontado

pelas curvas de energia potencial descritas no trabalho de Medeiros et al¹.

Em relação ao desempenho dos dois métodos, alcançou-se que com o método CASSCF a banda de interesse sofre um deslocamento significativo em comparação ao resultado experimental². Já o resultado MR-CISD se aproxima mais do experimental² e fornece uma descrição bastante melhorada em relação ao CASSCF. Isso sugere que o MR-CISD deve ser o método mais adequado para o estudo da fotodinâmica do clorometano, uma vez que descreve de forma aproximada o comportamento experimental da molécula.

Figura 1- Espectros de fotoabsorção UV teóricos e experimental para a molécula de CH_3Cl .



CONCLUSÕES

Através desse estudo concluiu-se que, apesar de apresentar um grande custo computacional, o método MR-CISD é o mais adequado na descrição da fotodinâmica do CH_3Cl , aproximando-se bastante da descrição experimental.

REFERÊNCIAS

- ¹ V. C. de Medeiros, et al. J. Am. Chem. Soc. 2016, 138, 1, 272–280.
² L. C. Lee, M. Suto. Chem. Phys. 1987, 114, 3, 423-429.

AGRADECIMENTOS

CAPES, CNPq, UFPB, PPGQ, LMMRQ.

DFT+U Study of Strain Engineered CO₂ Reduction on a CeO₂(110) Facet

Carla V. Soares (PhD)¹, Nilton Rosenbach Jr. (R)², Claudio J. A. Mota (R)^{1*}
carlavsoares@iq.ufrj.br

¹Universidade Federal do Rio de Janeiro, Instituto de Química, Av. Athos da Silveira Ramos 149, CT Bl A, Rio de Janeiro, RJ, Brazil; ²Universidade do Estado do Rio de Janeiro, Faculdade de Ciências Exatas e Engenharias, Av. Manuel Caldeira de Alvarenga, 1203, Rio de Janeiro, RJ, Brazil.

Keywords: CeO₂ surfaces, DFT, CO₂ conversion, hydrocarbons

INTRODUCTION

Excessive emission of CO₂ has emerged as an environmental challenge over the last few decades. This pressing issue calls for urgent exploration of efficient and cost-effective technologies aimed at mitigating atmospheric CO₂ and suppressing the greenhouse effect. One promising approach for producing clean energy involves the conversion of CO₂ into fuels like CH₄, higher hydrocarbons and CH₃OH. However, achieving a significant conversion through catalytic reactions remains a formidable obstacle due to the inherent thermal stability of CO₂ against its initial reduction. Among the potential catalysts, ceria (CeO₂) has garnered substantial attention for its viability in facilitating initial CO₂ reduction¹. Herein, a systematic investigation of the impact of oxygen vacancy on CeO₂ was investigated by periodic DFT calculations for the initial reduction of CO₂. Among the ceria polymorphs, CeO₂(110) has been chosen owing to its remarkable catalytic property and stability.

METHODS

DFT calculations were performed by using the Vienna ab initio Simulation Package (VASP)^{2,3}. The Perdew-Burke-Ernzerhof functional (PBE) is used for the exchange-correlation. Ionic cores are described by the projector augmented wave method (PAW) with a plane wave energy cutoff of 520 eV. The slab model of the ceria (110) surface was cleaved from the geometry-optimized bulk structure (lattice parameter of $a = 5.41 \text{ \AA}$), and the bottom two atomic layers of the five-layer slab are maintained fixed. A value of $U = 4.5 \text{ eV}$ was considered for the Ce 4f states. The Brillouin zones are sampled using a (3×2×1) Monkhorst-Pack grid.

RESULTS

The vacancy formation energy on the first layer of CeO₂(110) surface was calculated to be 44.0 kcal/mol. A similar value of oxygen vacancy formation energy was found by Cheng *et al.*⁴ Adsorbed CO₂, with adsorption energy of -41.1 kcal/mol, on the neighboring site of the oxygen vacancy is activated into a bent configuration with $\angle\text{OCO} = 123.9^\circ$ (Figure 1a). The two symmetrical C–O bonds in the bent structure are of length 1.28 Å and 1.30 Å, and the C–O bond in which the C atom interacts with the surface O atom of ceria is

1.33 Å. The energy required for the generation of oxygen vacancy in the second layer was 55.8 kcal/mol, in agreement with the value obtained by Pérez-Bailac *et al.*⁵. The CO₂ molecule is adsorbed, with binding energy of -59.8 kJ/mol, and bent configuration (with $\angle\text{OCO} = 126.7^\circ$ and C–O bond length of 1.28 Å), which is similar to the structure computed for the adsorption on the vacancy in the first layer (Figure 1b).

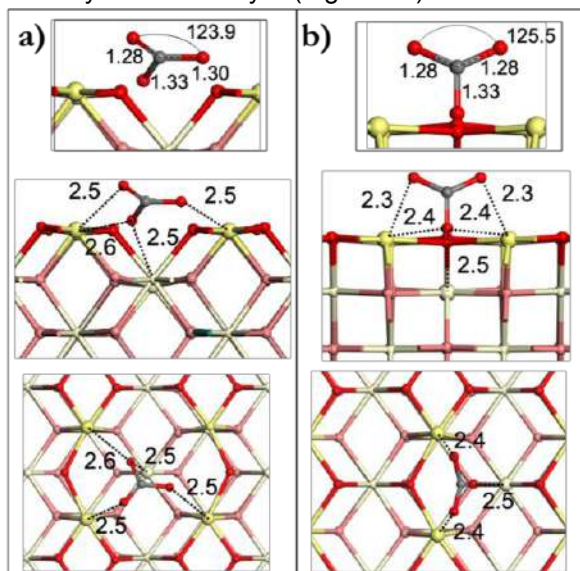


Figure 1: Adsorbed configuration of reactant of CO₂ conversion on surface ceria with vacancy (a) in the first layer and (b) in the second layer.

CONCLUSIONS

The most stable adsorbed configurations are the bent structure of CO₂. These configurations were used as reactants for CO₂ conversion to CO on ceria surfaces. The Nudged Elastic Band calculations are being performing to construct a reaction energy diagram for the mechanistic pathways for CO₂ reduction to CO and hydrocarbons on CeO₂(110) surface.

REFERENCES

- Ebrahimi, P., Kumar, A., Khraisheh, M. *Catalysts*, 2022, 12, 1101.
- G. Kresse and J. Hafner, *Phys. Rev. B*, 1996, 47, 558.
- G. Kresse and J. Furthmüller, *Comput. Mater. Sci.* 1996, 6, 15.
- Cheng, Z., Lo, C. S. *Phys.Chem.Chem.Phys.*, 2016, 18, 7987.
- Pérez-Bailac, P., Lustemberg, P. G., Ganduglia-Pirovano, M. *J. Phy. Cond. Matter*, 2021, 33, 504003.

ACKNOWLEDGMENTS

The authors acknowledge FAPERJ, CNPq and CENAPAD-SP.

Contribuições para o mecanismo reações do sítio ativo da proteína ATP7A com cis -[Pt(NH₃)₂(H₂O)₂]²⁺

Hercules Pereira da Silva (PG),¹ Juliana Fedoce Lopes (PQ).^{1*}

herculesps01@unifei.edu.br; jfedoce@unifei.edu.br

¹LaQC, Instituto de Física e Química, UNIFEI Avenida BPS, 1303, Pinheirinho, Itajubá-MG, 37500-903

Palavras Chave: cisplatina, ATP7A, estado de transição, IRC, DFT

INTRODUÇÃO

A cisplatina cis -Pt(NH₃)₂Cl₂ tem ação anticâncer, mas é sua forma cis -[Pt(NH₃)₂(OH₂)₂]²⁺ que possui atividade farmacológica. No entanto, as células são capazes de resistir à droga por meio de efluxo celular utilizando proteínas como a ATP7A, uma Cu-ATPase que contém 6 sítios ativos do tipo CXXC (C de cisteína e X, outros aminoácidos)¹, formando ligações Pt–S estáveis² como representado no modelo da Figura 1.

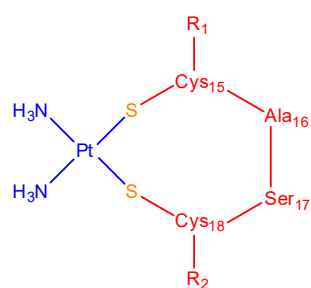


Figura 1: estrutura de cis -Pt(NH₃)₂(CXXC)

Seu mecanismo ainda é desconhecido, e a presença de Cu⁺ pode afetar a reação. É essencial seu estudo para compreensão de como esta rota de resistência celular pode ocorrer. Neste trabalho foram analisadas suas estruturas, cinética e termodinâmica desta reação contendo Cu⁺.

MÉTODOS

30 modelos estruturais do 6° CXXC complexados ou não com Cu⁺ foram obtidos pelo *Protein Data Bank* e otimizados. Com a estrutura mais estável, cálculos de TS de [Cu(CXXC)]⁻ e CXXC com cis -[Pt(NH₃)₂(OH₂)₂]²⁺ foram executados, iniciando-se por Cys₁₅. Cálculos de IRC foram executados e as estruturas finais, otimizadas. Foi empregado DFT, funcional M06-2X e conjunto de base 6-31g(d,p) com Lanl2dz para Pt.

RESULTADOS

No primeiro estado de transição encontrado, TS1 observou-se a geometria bipirâmide trigonal com Pt²⁺ como centro, e geometria tetraédrica com Cu⁺ como centro. Para o TS2 com [Cu(CXXC)]⁻, a estrutura indica possível ligação Pt²⁺-Cu⁺, onde Cu⁺ atua como uma “ponte” para Pt complexar-se com S_{Cys18}; sua geometria lembra uma pirâmide de base quadrada tendo Cu⁺ como centro metálico. A Figura 2 exibe as estruturas finais das reações.

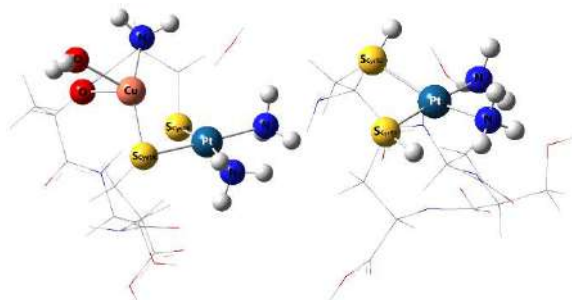


Figura 2: produtos de reações de [Cu(CXXC)]⁻ e de CXXC com cis -[Pt(NH₃)₂(OH₂)₂]²⁺

Todas as etapas da reação demonstraram serem exergônicas. A Figura 3 exibe o compilado dessas etapas

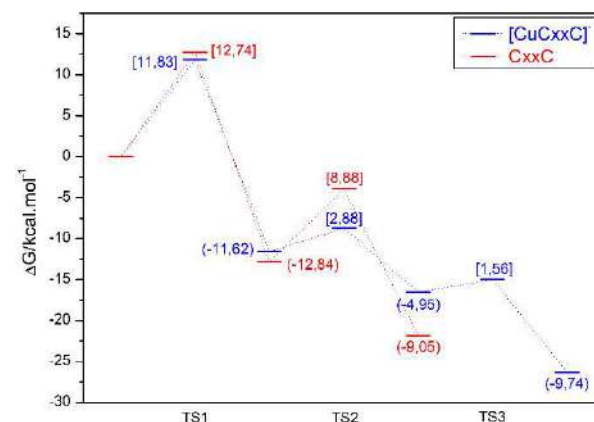


Figura 3: Coordenadas das reações de [CuCXXC]⁻ e CXXC com cis -[Pt(NH₃)₂(OH₂)₂]²⁺

CONCLUSÕES

A presença de Cu⁺ afeta a cinética da reação reduzindo as barreiras de energia de forma progressiva para formação de quelato bidentado mais estável. Isto pode ser um fator-chave para a resistência celular por efluxo da droga com ATP7A. A água também desempenha um papel essencial na estabilização de Cu⁺, o que aponta para necessidade de simulações em solvente explícito.

REFERÊNCIAS

¹ KATANO, K.; KONDO, A.; SAFAEI, R.; HOLZER, A. et al. CANCER RESEARCH, 2002, 62, p. 6559-6565.

² FANG, T.; TIAN, Y.; YUAN, S.; SHENG, Y. et al. Chemistry, 2018, 24, p. 8999-9003.

AGRADECIMENTOS

CNPq, CAPES, FAPEMIG, UNIFEI, PPGMQ-MG.



Chemical bonds in Lewis adducts: overlap descriptors and QTAIM in describing the covalent fraction from the ECW model.

Rachel Azevedo Maia (PG),¹ Carlos Vital dos Santos Junior (PG),² Francielle Caroline Machado Santos (PG),¹ Renaldo Tenório de Moura Junior (PQ)², Ricardo Luiz Longo (PQ)^{1*}.

rachel-maia@hotmail.com; ricardo.longo@ufpe.br

¹Departamento de Química Fundamental, Universidade Federal de Pernambuco, Recife-PE; ²Departamento de Química e Física, Universidade Federal da Paraíba, Areia-PB.

Keywords: Lewis Adducts, ChemBOS, Polarizability, Overlap Density.

INTRODUCTION

Lewis acid-base interactions have a wide relevance in chemistry and biology, for instance, in catalytic reactions present in industrial and biological processes. They arise from the interaction between a Lewis acid A (acceptor of an electron pair) and a Lewis base B (donor of an electron pair). The ECW¹ model is semi-quantitative, describing the enthalpy of the A–B bond in the adduct by the E, C, and W parameters of acid A and base B.

Several computational models investigate chemical bonds, including QTAIM (quantum theory of atoms-in-molecules) and LVM (local vibrational mode) theory. Additionally, the Overlay Model (OP)² has succeeded in describing chemical bonds in a wide range of molecules, including aspects of reaction mechanisms³.

One of the descriptors of the ECW model is the covalent fraction of the A–B interaction in Lewis adducts. In this context, this study aims at applying chemical bond descriptors from the OP, QTAIM, and LVM models to analyze A–B interactions in Lewis adducts, comparing them with the covalent fractions from the ECW model.

Fifteen Lewis A–B adducts were investigated, formed by combining acids A = I₂, IBr and ICl with bases B = (CH₃)₃P, (CH₃)₃N, C₅H₅N, (CH₃)₂SO, e (CH₃)₂CO. These adducts were selected to encompass a covalent fraction variation between 99% and 17%.

METHODS

All calculations were performed at the B3LYP/def2TZVP level of theory with the G09 program. QTAIM analysis and molecular orbital localization were done with the Multiwfn program. The overlap properties with localized molecular orbitals (LMOs), associated with the lone pairs of Lewis bases interacting with the acids, were obtained using the ChemBOS software (www.chembos.website).

RESULTS

Table 1 summarizes some results obtained for each A–B combination. It can be observed that for each acid A, the covalent fraction decreases in the order (CH₃)₃P > (CH₃)₃N > C₅H₅N > (CH₃)₂SO >

(CH₃)₂CO. On the other hand, for each base, the covalent fraction decreases as I₂ > IBr > ICl.

Table 1 - ECW, OP, and QTAIM descriptors of A–B interactions for Lewis adducts: covalent fraction f_{cov} (%), intra-overlap repulsion J_{OP}^{intra} (E_n), and Laplacian at the bond critical point $\nabla^2\rho_{BCP}$ (e a_0^{-5}) calculated with B3LYP/def2TZVP. Temperature maps were used for lower values (gray) and higher values (red, blue, and green, respectively, for f_{cov}, J_{OP}^{intra}, e $\nabla^2\rho_{BCP}$).

A / B	(CH ₃) ₃ P	(CH ₃) ₃ N	C ₅ H ₅ N	(CH ₃) ₂ SO	(CH ₃) ₂ CO
I ₂	f _{cov}	98.9	94.9	88.9	71.1
	J _{OP} ^{intra}	2.389	4.07	4.318	4.62
	$\nabla^2\rho_{BCP}$	0.045	0.072	0.081	0.083
IBr	f _{cov}	98.5	92.7	84.5	62.7
	J _{OP} ^{intra}	3.358	3.79	3.98	4.361
	$\nabla^2\rho_{BCP}$	0.041	0.078	0.091	0.094
ICl	f _{cov}	93.0	72.5	53.1	25.9
	J _{OP} ^{intra}	3.407	3.698	3.872	4.01
	$\nabla^2\rho_{BCP}$	0.041	0.08	0.094	0.099

It is noted that J_{OP}^{intra}, responsible for quantifying the repulsion energy of the bond overlap, shows a systematic increase with respect to acid A when the covalent fraction f_{cov} decreases. This trend can be attributed to the concentration of electron density at the acid, because of the reduced covalency. This increase in shared density, in turn, reflects in an elevation of overlap repulsion. Additionally, for each acid A, the descriptor $\nabla^2\rho_{BCP}$ follows the trend of increasing J_{OP}^{intra} as f_{cov} decreases, according to the following order (CH₃)₃P > (CH₃)₃N > C₅H₅N > (CH₃)₂SO, except for the interaction with the base (CH₃)₂CO. However, the descriptor J_{OP}^{intra} presents a stronger discrimination than the $\nabla^2\rho_{BCP}$ one.

CONCLUSIONS

Overall, the OP model corroborated the QTAIM trends by reproducing the covalent fraction estimated by the ECW model. More detailed analyses will be conducted on additional systems, employing OP descriptors augmented by the LVM theory, as well as other DFT functionals and basis sets.

REFERENCES

- ¹G.C. Vogel, R S. Drago, J. Chem. Educ., 1996, 73, 701.
- ²R.T. Moura Jr., et. al. J. Mol. Model., 2020, 301
- ³C.V. Santos-Jr., et.al. Chem. Phys. Lett., 2022, 787, 139282.

ACKNOWLEDGMENTS

CNPq, CAPES, FACEPE, FINEP, CETENE.

Reactive Molecular Dynamics Study of NOx Reduction with Urea and Ammonia

Maria E. A. Alves (IC)¹, Nilton Rosenbach Jr. (PQ)^{1*}, Adri C. T. van Duin (PQ)²

mariaeduarda@carvalhoz.org; nilton.rosembach.junior@uerj.br

¹Faculdade de Ciências Exatas e Engenharias, UERJ, Brasil.

²Department of Mechanical and Nuclear Engineering, Pennsylvania State University, United States

Keywords: NOx, Selective Catalytic Reduction (SCR), Reactive Molecular Dynamics, ReaxFF.

INTRODUCTION

NOx is a shorthand term used to designate nitric oxide (NO) and nitrogen dioxide (NO₂). These gases have serious impacts on the environment and human health, contributing to the formation of photochemical smog, acid rain, haze, and tropospheric ozone depletion¹. Selective Non-Catalytic Reduction (SNCR) or Selective Catalytic Reduction (SCR) utilizing ammonia (NH₃) or urea ((NH₂)₂CO) as reducing reagents are effective technologies for reducing NOx emissions².

The mechanism for SCR over catalysts is still widely debated in the literature. All theoretical studies have focused on a mechanism that involves two stages: oxidation and reduction, in which nitrosamine (NH₂NO) is a key intermediate³. In this study, we use the reactive molecular dynamics (ReaxFF) method to investigate the reduction of nitrogen oxides (NOx) utilizing ammonia and urea at the gas phase. The results of the study can provide insights into the molecular mechanism underlying the reaction and guide the development of more efficient and effective catalysts for NOx reduction.

METHODOLOGY

All simulations were carried out in a cubic periodic box with a side length of 60 Å, containing a mixture of NH₃ or (NH₂)₂CO with NO and O₂ at different concentrations. After a short 10 ps equilibration with switched-off bond parameters to prevent any reaction, MD simulations were carried out using the canonical (NVT) ensemble with a time step of 0.25 fs, and with trajectories spanning 1 ns. We use a reparameterized nitramine force field previously developed to study carbon cluster formation during the thermal decomposition of TATB and HMX high explosives⁴.

RESULTS

Figure 1(a) depicts the time-dependent behaviour of NO and H₂O concentration in the course of reactive molecular dynamics simulations on the mixture comprising NH₃, NO, and O₂ in a 4:4:1 ratio at the temperature of 1250 K. The reaction completely consumes NO within the first 100 ps, while the concentration of H₂O, a product of NOx reduction, gradually increases during that period.

All other mixtures studied in this work present a similar kinetic profile.

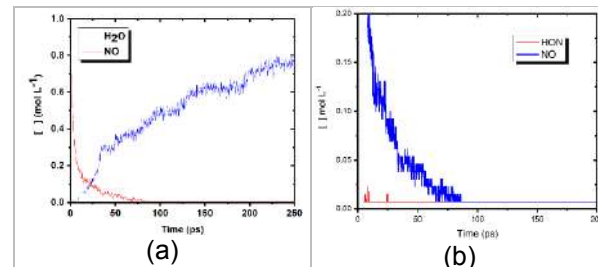


Figure 1: Temporal evolution of the (a) NO/H₂O (b) NO/HON concentration in simulations at 1250 K.

In addition to the nitrosamine pathway, our simulations revealed a distinct pathway for the formation N₂ from the reaction between HON and NO. The primary mechanism for this pathway is the hydrogen abstraction from NH₃ by NO. The time-dependent HON specie concentration is shown in Figure 1(b). The overall rate constant of $1.39 \times 10^{12} \text{ cm}^3 \text{ mol}^{-1} \text{s}^{-1}$, calculated from the fitted curve to the NO concentration at the kinetic regime, is consistent with previous studies and exhibits a negative temperature dependence within the optimal range of 1000 to 1500 K. The introduction of oxygen molecules (O₂) enhances the reaction rate.

CONCLUSIONS

The nitrosamine channel is the main pathway for NOx reduction at the gas phase according to reactive molecular dynamics simulations. However, an alternative route in which the HON intermediate play a major role in the formation of N₂ was identified. The results also indicate a negative temperature dependence kinetics and an increase in reaction rate when O₂ is introduced into the reaction medium.

REFERENCES

- 1 M. Z. Jacobson, *Atmospheric Pollution*, Cambridge University Press, 2002.
- 2 P. Granger, V. I. Parvulescu, *Chem Rev*, 2011, 111, 3155.
- 3 J. A. Miller, S. J. Klippenstein; *JPCA*, 2000, 104, 2061.
- 4 A. Strachan; et al. Goddard, *Phys Rev Lett*. 2003, 91 (9), 28.

ACKNOWLEDGEMENT

FAPERJ and CNPq.

Computational Study of CO₂ Capture Over MCM-41 Mesoporous Silica Impregnated with Chitosan

Nilton Rosenbach Jr. (PQ),¹ Carla V. Soares (PQ),² Claudio J. A. Mota (PQ).^{2*}

nilton.rosembach.junior@uerj.br; cmota@iq.ufrj.br

¹Faculdade de Ciências Exatas e Engenharias, UERJ, Brasil.

²Instituto de Química, UFRJ, Brasil.

Palavras Chave: CO₂ capture, MCM-41, Chitosan, GCMC simulations

INTRODUCTION

Atmospheric carbon dioxide (CO₂) levels are persistently rising due to fossil fuel combustion. In response, novel methodologies and materials are being developed to capture CO₂ before it has been emitted or directly from the air. Adsorption has become a promising approach, offering the advantage of generating high-purity streams with minimal energy demands. Many adsorbents have been developed, with mesoporous silicas MCM-41 and SBA-15 standing out due to their regular pore structure, extensive surface, and stability. However, non-functionalized silica can exhibit limited adsorption capacity, particularly for low CO₂ concentration gas streams, due to weak physisorption interactions. Incorporating basic compounds onto silica supports may overcome this limitation, enhancing CO₂ uptake. From an environmental perspective, the utilization of biomass to prepare adsorbents for CO₂ capture emerges as a promising option. Impregnating chitosan onto mesoporous silica supports, such as MCM-41 and SBA-15, has been reported as an effective adsorbent for CO₂ capture¹. In this work, we study the adsorption properties of MCM-41 impregnated with chitosan for CO₂ capture.

METHODOLOGY

CO₂ adsorption at 300 K was investigated by Grand Canonical Monte Carlo (GCMC) simulations, using an MCM-41 atomistic model, previously derived through *ab initio* calculations, impregnated with a small chitosan chain comprising nine deacetylated units². All charges and parameters to describe coulombic and dispersion interactions between CO₂ molecule and MCM-41/chitosan model were obtained from the COMPASS force field as implemented within the LAMMPS program.

RESULTS

Figure 1 displays experimental and simulated CO₂ adsorption isotherms at 300 K. The experimental isotherm for chitosan-impregnated MCM-41 reveals superior adsorption capacity compared to the non-functionalized material, particularly at low pressures. Nevertheless, as pressure rises, the adsorption capacity decreases and is surpassed by the non-functionalized material. Similar trends

are observed in the simulated isotherms, although the adoption capacity of the chitosan-impregnated MCM-41 persists at higher pressures. This behavior is attributed to the inherent basic nature of chitosan, which preferentially adsorbs CO₂ over MCM-41 surface, at low-pressure conditions. As the CO₂ loading increase, the presence of chitosan chains reduces the available pore space, leading to a lower adsorption capacity compared to the non-functionalized material. The CO₂ adsorption isotherm in the atomistic model of MCM-41 corresponds reasonably well with the experimental data. However, the simulations overestimate the adsorption capacity for chitosan-impregnated MCM-41. This discrepancy may be attributed to the limitations of the force field accuracy, as it might not adequately represent the specific interactions between CO₂ molecules and the chitosan-impregnated MCM-41 surface. Additionally, alterations in the conformation of the chitosan chain upon CO₂ adsorption could influence the accessibility of adsorption sites.

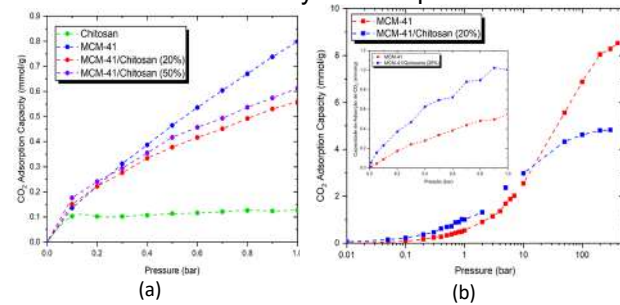


Figure 1. CO₂ adsorption isotherms: (a) experimental¹ and (b) GCMC simulations with zooming in the 0-1 bar pressure range.

CONCLUSIONS

Adsorption properties of chitosan-impregnated MCM-41 for CO₂ capture were explored using GCMC simulations. Experimental and simulated isotherms were compared, revealing that chitosan-impregnated MCM-41 had superior adsorption at low pressures but reduced capacity at higher pressures due to pore space limitations caused by the presence of chitosan chains.

REFERENCES

- D. E. F. Oliveira, et al., Ind. Eng. Chem. Res., 2022, 61, 10522.
- P. Ugliengo, et al., Adv. Mat., 2008, 20, 1.

ACKNOWLEDGEMENTS

FAPERJ, CNPq

Modelling of BODIPY's photophysical properties: Effect of solvent polarity and β substitution

Bruno S. Sampaio* (PG)¹, Joel L. Nascimento (PG),¹ Murillo H. Queiroz (PG),¹ Roberto Rivelino (PQ)²,
Tiago V. Alves (PQ)¹

*brunosamp08@gmail.com

¹Departamento de Físico-Química, Instituto de Química, Universidade Federal da Bahia

²Departamento de Física do Estado Sólido, Instituto de Física, Universidade Federal da Bahia

Palavras Chave: TD-DFT, BODIPY, Modelling

INTRODUÇÃO

Boron dipyrromethene (BODIPY) compounds are an important class of fluorophores that presents remarkable optical properties¹. However, owing to its low Stokes shift, BODIPYs are weakly or non-emissive at the solid state². This result limits the optoelectronic applications of these compounds³. In this context, to enhance the Stokes shift of this material, we adopted a donor acceptor strategy to investigate the effect of substitution of NH₂, COCl and phenyl groups at the β_1 position of BODIPY (Fig. 1). Seven different substitution schemes were adopted in three solvents with dielectric constants ranging from high to low (water, acetone and hexane), which allowed us to evaluate which solvent-substitution scheme presents the highest Stokes shift.

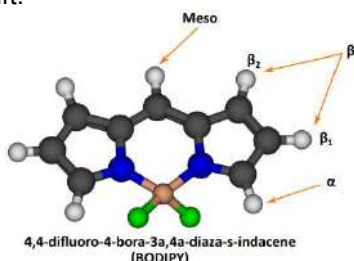


Figure 1 – BODIPY structure

MÉTODOS

For this proposal we performed electronic structure calculations using density functional theory (DFT) and time-dependent density functional theory (TD-DFT) to obtain the absorption and emission spectra of each compound. For all calculations, we have employed the M06-2X density functional with the Pople basis set 6-31+G(d,p), as implemented in the Gaussian 09 program package. The solvent effects were considered using the polarizable continuum model (PCM).

RESULTADOS

In a first step of our analysis was to compare the maximum wavelength of absorption (λ_{Max}) of all structures. We observed different trends depending on the donor-acceptor scheme adopted. For example, the λ_{Max} of the two-donor structure, NH₂-BODIPY-NH₂, is 568 nm in acetone, 573 nm in water and 520 nm in hexane. This

structure had a bathochromic shift, if compared with the BODIPY structure with no substituents, which presented λ_{Max} of 458, 463 and 421 nm, in acetone, water and hexane, respectively. The opposite was observed using two acceptors (COCl-BODIPY-COCl) as substituents, with λ_{Max} values of 449, 453 and 418 nm, in acetone, water and hexane, respectively. This result shows that the substituent type and the dielectric constant of the solvent presents considerable influence over the optical properties of BODIPY.

For the BODIPY structure with no substituents, we obtained λ_{Max} with a good approximation to the experimental values presented by Zhang and Zhu (2019)⁴, as shown in Table 1. We observed that in water and acetone, the method adopted in this work obtained a λ_{Max} value closer to the experimental value than the B3LYP/6-31++G method. However, in hexane, both methods performed similarly.

Table 1 - λ_{Max} for the BODIPY structure

Solvent	λ_{Max} (nm)	Experimental ⁴ (nm)	B3LYP/6-31++G (nm) ⁴
Water	462.6	498	417.6
Acetone	458.4	497	418.6
Hexane	421.2	502	419.1
Vacuum	400.0	-	433.2

CONCLUSÕES

The dielectric constant and the substituent type had a major influence in BODIPY's optical properties. Besides, the chosen method showed good results in polar solvents.

For the next step of this work, we will analyze the effects of the substituents and solvents in the fluorescence spectra of BODIPY, to evaluate the Stokes shift of all structures.

REFERÊNCIAS

1. M. Poddar, R. Misra, Coord. Chem. Rev., 2020, 421, 1-22.
2. B.M. Squeo, M. Pasini, Sup. Chem. 2020, 32, 56-70.
3. C.Liu et al. J. Mater. Chem C. 2014, 2, 5471-5478.
4. X.Zhang, J.Zhu. Jour. Lumi. 2019, 205, 148-157.

AGRADECIMENTOS



Complex networks, hydrogen bonds, and the structures of water

Jéssica I. R. de Souza (PG),¹ Amanda M. de Lima (PG),¹ Paulo M. C. de Oliveira (PQ),² Juliana A. B. da Silva (PQ),² Ricardo L. Longo (PQ).^{1*}

ricardo.longo@ufpe.br

¹Departamento de Química Fundamental, Universidade Federal de Pernambuco, 50740-540, Recife, PE, Brazil.

²Núcleo Interdisciplinar de Ciências Exatas e da Natureza, Campus do Agreste, Universidade Federal de Pernambuco, 55.014-900, Caruaru, PE, Brazil.

Keywords: Bulk water, Confined water, Topological descriptors, Simulations, Temperature dependence.

INTRODUCTION

Water, aqueous solutions, and other liquids are structured due to hydrogen bonds (HB). Many peculiar (or anomalous) properties of liquid water and solutions can be traced to the features of these HBs and, particularly, to the complex networks formed by the water molecules (nodes) and their connections (HBs). For nearly two decades, we have been employing methods of statistical mechanics applied to complex networks to describe structured liquid systems.

This presentation shall account for some of the pioneering applications¹ as well as recent developments and advances².

METHODS

The structures of liquids and solutions were obtained by computer simulations approaches such as Monte Carlo and molecular dynamics. Uncorrelated equilibrated simulation boxes (500 configurations) were used to obtain average properties, topological descriptors, and island (or cluster) statistics of the HB networks. A geometric criterium followed by an energetic one was employed to define a hydrogen bond between every pair of molecules in the simulation box.

The adjacency matrix \mathbf{A} , defined as $A_{ij} = 1$ if nodes (molecules) i and j are adjacent (i.e., connected by an edge = HB) or $A_{ij} = 0$ otherwise, is constructed and analyzed. This matrix \mathbf{A} is associated with a graph G representing a binary network (i.e., unweighted, and undirected).

The main topological descriptors are: *i*) clustering coefficient C , *ii*) average degree $z = \langle k \rangle$, and *iii*) degree distribution $P(k)$, which are local descriptors, *iv*) path length or geodesic distance L that is semiglobal, and *v*) graph of the spectral density $\rho(\lambda)$, which can be considered a global property. A program, called ANALYSIS, was developed and implemented (Fortran) to perform this topological and island analyses.

RESULTS

Liquid water at room conditions presented a percolated HB network with $L \gg L_{\text{rand}}$ and $C \gg C_{\text{rand}}$, where L_{rand} and C_{rand} are the corresponding path length and clustering coefficient of a random network. However, at critical conditions (673 K and 500 bar) the HB networks are described as

small-world characterized by $L \ll L_{\text{rand}}$ and $C \gg C_{\text{rand}}$, i.e., highly aggregated with short path lengths. Similar small-world behavior was observed for water-alcohol (methanol, n-butanol, t-butanol) and water-NH₃ mixtures at a wide range of mole fractions. The underlying topology of HB networks was shown to be tuned (or controlled) by the strength of the intermolecular interactions. Recently, the properties of HB networks of water confined within reverse micelles were investigated and shown to change regimes according to the degree of confinement. A trimodal distribution of the average path length L was obtained for liquid water employing simulation box with 2000 molecules. This distribution was attributed to three sets (A, B, and C) of structures and associated with the (micro) heterogeneity of liquid water. The areas of the peaks in the distribution varied with the temperature (Figure 1). Considering equilibria between these structures: $A \rightleftharpoons B \rightleftharpoons C$, the standard Gibbs energy, enthalpy, and entropy variations can be obtained for the first time².

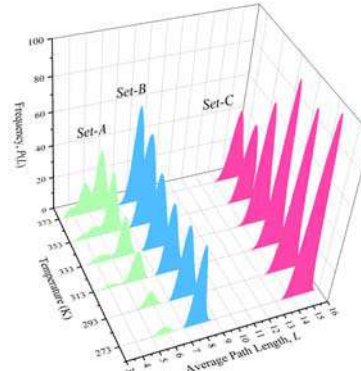


Figure 1. Distribution of the average path length, L , of HV networks of liquid water from 273 to 373 K.

CONCLUSIONS

New insights into the properties of liquids and solutions structured by hydrogen bonds were gained by topological descriptors of the networks.

REFERENCES

- V. M. L. dos Santos et al., Chem. Phys. Lett., 2004, 390, 157.
- P. M. C. de Oliveira et al., J. Phys. Chem. B, 2023, 127, 2250.

ACKNOWLEDGMENTS

CNPq, CAPES, FACEPE, FINEP, CETENE, dQF, UFPE.



Investigação de atividade óptica pela conversão de espectros ECD – ORD com a Transformada de Kramers-Kronig

Gabriel de A. Barros (PG),^{1*} Nelson H. Morgen (PQ).²

gabrieldealbuquerquebarros@gmail.com

¹Instituto de Química – Universidade Estadual de Campinas

Palavras Chave: Dicroísmo circular eletrônico, TD-DFT, Estado excitado, Dispersão rotatória óptica.

INTRODUÇÃO

A atividade óptica de sistemas quirais pode ser observada, em diferentes comprimentos de onda, pelo desvio da luz plano-polarizada (dispersão rotatória óptica – *ORD* em inglês) assim como pelo desvio de luz circularmente polarizada (dicroísmo circular eletrônico – *ECD* em inglês). A primeira pode ser modelada computacionalmente com cálculos no estado fundamental enquanto a segunda considera estados excitados.

Frente a problemáticas para cálculos de um dos espectros, a geração confiável (ou comparável com dados experimentais) de um dos dois pode fornecer o outro pela Transformada de Kramers-Kronig (KK). Neste trabalho, avaliamos conversão de espectros de ECD em ORD (este, com valores experimentais) em funções de Dunning (d)aug-cc-pVXZ (X=D,T).

MÉTODOS

Os sistemas quirais do 2-clorobutano e 3-cloro-1-buteno foram avaliados com análise conformacional, geração de espectros ECD e conversão em ORD¹ para comparação com valores experimentais.²

Os cálculos para o dicroísmo circular eletrônico foram calculados em TD-DFT considerando os 25 primeiros estados excitados, com o funcional CAM-B3LYP.

Distribuição populacional de Boltzmann após análise conformacional:

$$N_i/N = \exp(-G_i/kT) / \sum_j \exp(-G_j/kT)$$

Dispersão Rotatória Óptica – ORD:

$$N_i/N = \exp(-G_i/kT) / \sum_j \exp(-G_j/kT);$$



Dicroísmo Circular Eletrônico – ECD:

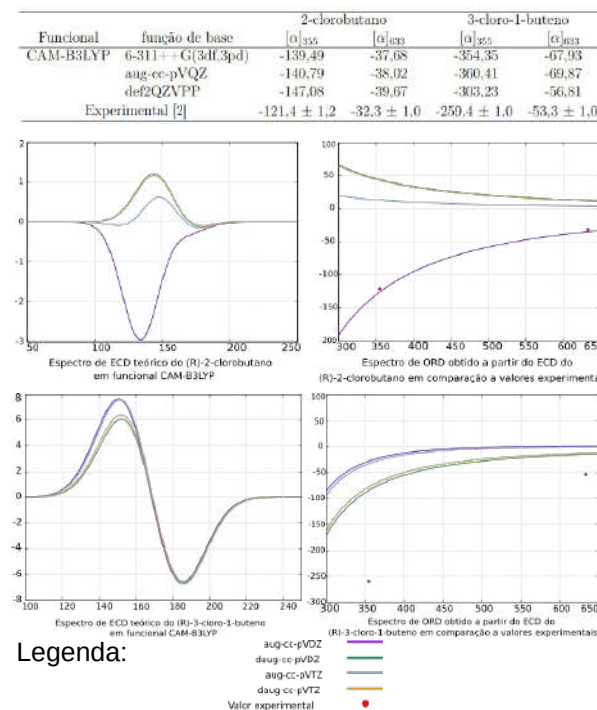
$$[\alpha(\lambda)] = 13,43 * 10^{-5} \frac{\beta}{\lambda^2 M}$$

Transformada KK (método Ohta-Ishida):



RESULTADOS

A tabela contém valores de rotação óptica calculados nos comprimentos de onda em que valores experimentais estão disponíveis. As imagens abaixo mostram espectros de ECD e o de ORD correspondente aplicando-se a transformadas.



CONCLUSÕES

A transformada de Kramers-Kronig é uma alternativa de obtenção de um espectro teórico de ECD confiável caso haja apenas valores experimentais de ORD disponíveis.

Nos sistemas em questão, o R-2-clorobutano apresentou sinal teórico indicativo do isômero S para os conjuntos de base usados, à exceção do aug-cc-pVDZ.

REFERÊNCIAS

¹P.L. Polavarapu, *J. Phys. Chem. A*, 2005, 109, 32, 7013-7023

²K.B. Wiberg, et al , *J. Phys. Chem. A*, 2005, 109, 3405-3410

AGRADECIMENTOS



Investigação da estabilidade de íons ferricianeto em materiais lamelares

Ana Carolina F. Hammes (PG),¹ Sérgio R. T. Filho (PQ),² Alexandre A. Leitão (PQ).^{1*}

anacarolina.ferreira@ice.ufjf.br; sergiotavares@iprn.ufrj.br; alexandre.leitao@ufjf.br

¹Departamento de Química, Universidade Federal de Juiz de Fora, Juiz de Fora, MG, 36036-330, Brazil; ²Instituto de Pesquisas de Produtos Naturais Walter Mors, Universidade Federal do Rio de Janeiro, Rio de Janeiro, RJ, 21941-599, Brazil

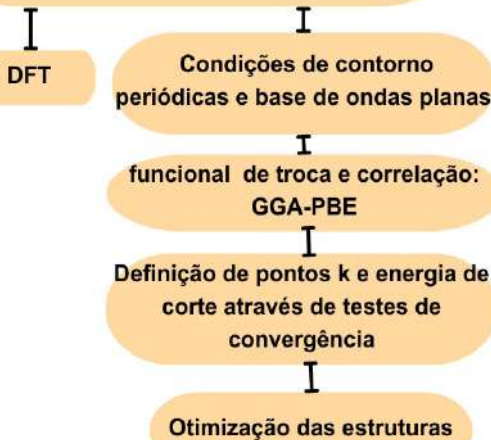
Palavras Chave: Ferricianeto, Compostos lamelares, DFT, Mineração aurífera, Toxicidade.

INTRODUÇÃO

O ferricianeto, $[Fe^{III}(CN)_6]^{3-}$, é classificado como o complexo cianometálico mais estável frente aos demais cianetos de ferro, sendo este o principal complexo gerado nos efluentes da mineração aurífera.¹ Ao descartar de forma inadequada seus efluentes, a mineração se torna uma das principais responsáveis pela degradação ou alteração da qualidade da água.² A toxicidade deste complexo é um dos principais pontos abordados atualmente, dado que quando exposto à luz solar este sofre fotodecomposição liberando CN^- livre, sendo extremamente prejudicial a saúde.³ Este fato evidenciou a necessidade de se retirar o ferricianeto dos efluentes gerados pela mineração aurífera, e com este objetivo este trabalho visa estudar a possibilidade de utilizar compostos lamelares para a captura deste complexo, em especial os hidróxidos duplos lamelares (HDL) e hidroxissais lamelares (HSL),⁴ por meio da avaliação da estabilidade estrutural de ferricianeto em materiais lamelares através de cálculos *ab initio* baseados na Teoria do Funcional de Densidade (DFT).

MÉTODOS⁵

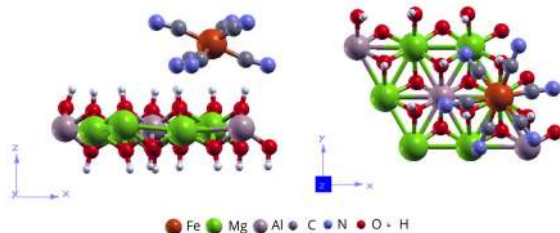
Pacote Quantum-ESPRESSO



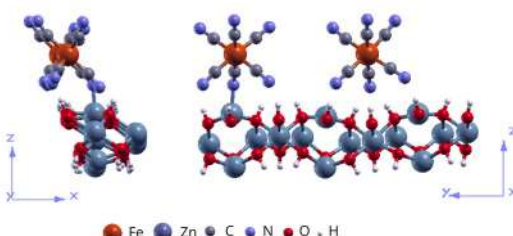
RESULTADOS

Foram testados 6 sítios para o ferricianeto na lamela do HDL- Mg_2Al . Ao analisar suas energias,

observou-se uma diferença abaixo de 0,1 kJ/mol de uma estrutura para outra, indicando que os diferentes pontos de partidas para as otimizações levaram à mesma estrutura final. A análise geométrica confirma que se trata da estrutura representada na Figura 1.



Para o HSL de zinco foi feito o mesmo procedimento, no entanto, para este caso foram testados apenas 3 sítios. A Figura 2 apresenta a estrutura otimizada.



PRÓXIMAS ETAPAS

Os sistemas HDL- $[Fe^{III}(CN)_6]$ e HSL- $[Fe^{III}(CN)_6]$ foram otimizados com sucesso encontrando desta forma a estrutura mais estável para cada um deles. A partir destas estruturas será realizada a análise termodinâmica.

REFERÊNCIAS

- ¹ T. Mansfeldt, *et al.*, Vadose Zone Journal, 2004, vol. 3, p. 471–479.
- ² L.R.G. Guilherme, *et al.*, Tópicos em Ciências do Solo, 2005, vol. 4, p. 345-390.
- ³ J. C. L. Meeussen, *et al.*, Environmental Science and Technology, 1992, vol. 26, p. 511–516.
- ⁴ G. G. C. Arizaga, *et al.*, Solid State Ionics, 2007, vol.178, p. 1143-1162.
- ⁵ P. Giannozzi, *et al.*, Journal Of Physics: Condensed Matter, 2009, vol. 21, p. 395502-395521.

AGRADECIMENTOS

Agradecimentos a CAPES, CENAPAD-SP e UFJF.

REVISITANDO A “ADAMANTANELAND”: the king is dead

Pedro, H. A. Silva (PG),¹ Pierre, M. Esteves (PQ).^{1*}

pedrohenrique.antunes15@gmail.com; pesteves@iq.ufrj.br

¹Instituto de Química – Universidade Federal do Rio de Janeiro

Palavras Chave: Rearranjo de carbocátions, Geoquímica, Monoterpenos, Adamantano.

INTRODUÇÃO

Amplamente conhecidos e estudados, os carbocátions são importantes intermediários reativos caracterizados por um átomo de carbono tricoordenado ou pentacoordenado¹. Essas espécies são importantes na biossíntese dos mais de 80 mil terpenóides catalogados, em que pode-se destacar a subclasse dos monoterpenos – os mais conhecidos e estudados². Os monoterpenos são formados a partir da ciclização do cátion linalila que, após eliminação de hidreto, abstração de prótons e rearranjos subsequentes formam os mais diversos monoterpenos conhecidos, como o limoneno, canfeno e terpineno. Um importante membro desta classe de monoterpenos encontrado no petróleo é o adamantano, um hidrocarboneto policíclico, saturado, do tipo gaiola de alta estabilidade térmica e termodinâmica do qual pouco se conhece a respeito do seu processo de formação. Na literatura é possível encontrar apenas um trabalho que descreve uma possível rota de rearranjo de carbocátions de hidrocarbonetos policíclicos para a formação do cátion 1-adamantila, um “poço” termodinâmico que, por abstração de hidreto, forma o isômero mais estável C₁₀H₁₆ conhecido, o adamantano³. Sendo assim, este trabalho tem por objetivo revisitar o trabalho de Engler e colaboradores (1973) utilizando bases e funcionais mais modernos e, além disso, introduzir uma novidade: a existência de carbocátions isômeros de maior estabilidade.

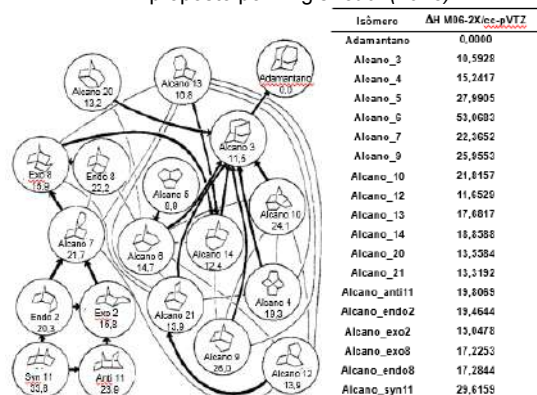
MÉTODOS

Os mecanismos de rearranjos de carbocátions foram estudados realizando-se cálculos baseados em primeiros princípios (DFT ou *ab initio*) das rotas carbocatiónicas conectando terpenos e diamantóides. A geometria dos intermediários foi otimizada em nível M06-2X/6-31G(d,p), M06-2X/cc-Pvtz. Além disso, utilizou-se o software AUTOMATOM para a busca de mínimos globais isoméricos do cátion 1-adamantila.

RESULTADOS

Os cálculos reproduzidos se mostraram majoritariamente em concordância com as energias originais propostas por Engler e colaboradores (1973) e apenas alguns valores de energia não se mostraram condizentes com o que foi proposto pelos autores. A Figura 01 abaixo permite observar as energias obtidas utilizando-se o funcional M06-2X e base cc-pVTZ.

Figura 01: Rearranjo dos triciclohexanos ao adamantano proposto por Engler et al (1973).



Fonte: Engler et al (1973), modificado pelo autor.

Com o auxílio do software Automaton foi possível constatar a existência de dois isômeros de menor energia do que o cátion 1-adantila. Essa informação é de extrema relevância pois coloca em dúvida a ideia de que este cátion seria o de menor entre os seus isômeros, o que faz necessário repensar a ideia de que sistemas tricíclicos evoluíram através do rearranjo de carbocátions para formar o cátion 1-adamantila, um “poço energético”.

CONCLUSÕES

Os cálculos realizados por Engler et al (1973) se apresentaram bem condizentes com os realizados através de métodos mais modernos. Além disso, foi possível observar a existência de espécies isoméricas mais estáveis do que o cátion 1-adamantila, o que colocou em dúvida as hipóteses iniciais do trabalho e as ideias iniciais de Engler e colaboradores (1973).

REFERÊNCIAS

- OLAH, George A.; LAALI, Kenneth K.; WANG, Qi; PRAKASH, G. K. Surya. **Onium ions**. [s.l.] : Wiley, 1998.
- KIM, Hoshin; SRIVIDYA, Narayanan; LANGE, Iris; HUCHALA, Eden W.; GINOVSKA, Bojana; LANGE, B. Markus; RAUGEI, Simone. Determinants of Selectivity for the Formation of Monocyclic and Bicyclic Products in Monoterpene Synthases. *ACS Catalysis*, v. 12, n. 12, p. 7453–7469, 2022
- ENGLER, E. M.; FARCAIU, M.; SEVIN, A.; CENSE, J. M.; SCHLEYER, P. V. R. On the Mechanism of Adamantane Rearrangements. *Journal of the American Chemical Society*, [S. I.], v. 95, n. 17, p. 5769–5771, 1973

AGRADECIMENTOS





pyCOFBuilder: A python package for automated creation of Covalent Organic Framework structures based on the reticular approach

Felipe Lopes Oliveira (PhD)¹, Pierre Mothé Esteves (R)^{1*}

felipe.lopes@nano.ufrj.br; pesteves@iq.ufrj.br

¹Instituto de Química, Universidade Federal do Rio de Janeiro, Rio de Janeiro 21941-909, Brazil

Keywords: covalent organic framework, reticular chemistry, python, CO₂ capture

INTRODUCTION

A class of materials that have attracted significant interest over the past years is the Covalent Organic Frameworks (COFs). COFs are materials with well-defined nanoporous architectures designed in a bottom-up approach by the covalent bonding of one or more organic molecules by strong covalent bonds, thus forming an extended nanoporous crystalline structure.

The general process for building a COF structure is commonly referred as the *reticular approach*. This starts with selecting a network topology and breaking it into building units. The underlying network's constraints determine the geometry and connectivity of these units. Building blocks are formed around an organic core, defining the size and chemical properties of the generated structure. Connection groups are chosen to create covalent connections between core units, forming the extended structure. Functional groups can be added to the core unit to control the pore surface characteristics.

Here we preset pyCOFBuilder, an open-source python package that automates the creation of computational models for COF structures based on the reticular approach. The current version offers a user-friendly platform with diverse features, including 2D/3D network implementation, stacking patterns, and a wide building block library with functionalization options. We also develop a new string-based representation to describe these reticular structures.

With these combined features, pyCOFBuilder can potentially generate millions of unique COF structures, enabling robust implementation of computational and machine learning techniques for novel COF material development.

METHODS

The *pyCOFBuilder* software was implemented using object-oriented Python, and utilizes several scientific programming libraries, such as Numpy, Scipy, and pymatgen to execute mathematical operations and symmetry analyses. The GitHub repository contains detailed instructions about the manual and automatic installation.

RESULTS

The code is designed with a focus on two primary objects namely *BuildingBlock*, intended to deal with the molecules that will form the COF, and *Framework* that represents the COF itself.

The COFs structure, referred in the code as *Framework*, can be created directly by their string-encoding as in the example shown on **Figure 1**. The COF referred in the literature as TpPa-1¹ or DAB-TFP² can be translated to the unique representation T3_BENZ_CHO_OH-L2_BENZ_NH2_H-HCB_A-AA.

```
1 import pycofbuilder as cof
2
3 name = 'T3_BENZ_CHO_OH-L2_BENZ_NH2_H-HCB_A-AA'
4
5 cof.Framework(name)
6 cof.save(fmt='cif', supercell=(1,1,2))
7
```

Figure 1. Example of code to generate a cif file of a COF structure.

We evaluated pyCOFBuilder's model quality using 33 diverse literature structures comparing their experimental cell parameters with those generated by pyCOFBuilder and after full DFT-PBE-D3, xTB-GNF1, and DFTB optimization. pyCOFBuilder produced cell parameters similar to experimental values, even without any geometry optimization process. This indicates its suitability for efficient high-throughput studies.

As an example of application we generate thousands of different COF structures and evaluate the influence of chemical properties on the discovery new materials for CO₂ capture.

CONCLUSIONS

Here we preset pyCOFBuilder as a tool for generating COF structures using a novel string-based approach. The implementation details, including design and libraries, are discussed. The generated structures presents good agreement with experimental and simulated data at various theory levels, emphasizing software accuracy.

REFERENCES

¹ Kandambeth, S. et al. J. Am. Chem. Soc. 2012, 134, 19524–19527.

² DeBlase, C. R. et al. J. Am. Chem. Soc. 2013, 135, 16821–16824.

ACKNOWLEDGMENTS

CAPES, CNPq, FAPERJ, NACAD

Predicting Biological Activity through Assessment of PLS-QSAR Models for 5-HT₆ Antagonists in the Context of Alzheimer's Disease

Daniel da Silva de Sousa (PhD)¹, Aldineia P. da Silva (PhD)², Laise P. A. Chiari (PhD)¹, Káthia M. Honório (R)², Albérico B. F. da Silva (R)^{1*}
daniel.silva.sousa@usp.br; alberico@iqsc.usp.br

¹ São Carlos Institute of Chemistry (IQSC), University of São Paulo (USP), 13560-970, São Carlos, SP, Brazil;

² School of Arts, Sciences and Humanities (EACH), University of São Paulo (USP), São Paulo, 03828-000, Brazil.

Keywords: Alzheimer's disease, 5-HT₆ receptor, Antagonists, PLS-QSAR.

INTRODUCTION

Alzheimer's disease (AD) is the primary cause of global dementia, with approximately 55 million cases and a projected increase to 74.7 million by 2030.¹ This rising prevalence emphasizes the urgent need for effective treatments. Numerous studies are investigating treatment strategies based on various theories about its origin, which remains incompletely understood. One promising approach is targeting the 5-HT₆ receptor, associated with memory loss, as a symptomatic treatment for AD.² This receptor, part of the GPCR family, could be modulated using antagonists to potentially enhance cognition and memory. Our research addresses this challenge through PLS-QSAR models,³ using computational chemistry to systematically predict the biological activity of potential drug candidates.

METHODS

The methodology involved optimizing a molecular set of 5-HT₆ antagonists using DFT with B3LYP exchange and correlation functional and 6-31++G basis functions (d,p) in Gaussian9. Energetics and electronic descriptors were derived from DFT calculations, while topological, geometric, and constitutional descriptors were obtained through e-Dragon software. Selected descriptors determined through a Genetic Algorithm and Pearson's coefficient (> 0.3) were used for QSAR model construction with Pirouette® and MatLab. PLS models were developed and evaluated using SEV, PRESS validation, SEC, PRESS calibration, R², and Q². The best PLS model's predictive ability was assessed using an independent test set.

RESULTS

The optimal PLS-QSAR model (Fig. 1) with minimal prediction errors exhibited Q² = 0.87 and R² = 0.94. This model encapsulates 57.16% of the original dataset's information. External analyses yielded the following results: SEP = 0.29, Press = 0.76.

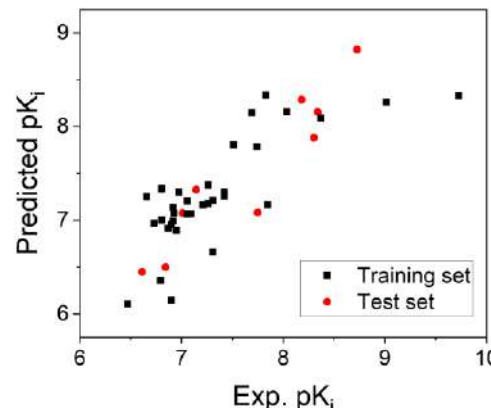


Fig. 1: Prediction of pKi values in the PLS model.

CONCLUSIONS

In conclusion, our analysis and validation of the PLS-QSAR models have led us to the identification of a collection of promising compounds that exhibit strong potential for therapeutic intervention against AD. These findings not only emphasize the robustness of our approach but also pave the way for further exploration and development of novel treatments for this challenging neurodegenerative condition. Our results underscore the importance of computational methodologies in accelerating drug discovery and highlight the potential of these compounds to make a meaningful impact on the future of AD therapy.

REFERENCES

- ¹ Alzheimer's & Dementia 2023, 19, 1598–1695.
- ² Andrews, M.; Tousi, B.; Sabbagh, M. N. Neurology and therapy 2018, 7, 51–58.
- ³ da Silva, A.P., de Angelo, R.M., de Paula, H. et al. Struct Chem, 2020, 1585–1597.

ACKNOWLEDGMENTS

National Council for Scientific and Technological Development (CNPq). Process number: 140894/2021-7 and 152105/2022-0

Assessment of a computational protocol for predicting the Xe-129 NMR chemical shift of xenon fluorides using the new NMR-ZORA basis sets

Simone F. T. Marques (IC)^{1*}, Diego F. S. Paschoal (PQ)¹

simoneflorencey@gmail.com; diegopaschoal01@gmail.com

¹Núcleo de Química Teórica e Computacional de Macaé, Polo Ajuda, Instituto Multidisciplinar de Química, Centro Multidisciplinar UFRJ-Macaé, Universidade Federal do Rio de Janeiro, Macaé, RJ, Brasil.

Keywords: Xenon, NMR, DFT, Computational Protocol, Basis sets, Relativistic Effects

INTRODUCTION

Since the discovery of Noble Gases reactivities and their specific chemistry, a variety of applications for Xenon (Xe) has been developed¹. Thus, there is a demand for a description of new Xe compounds, where NMR spectroscopy can be a powerful tool given the suitability of Xe-129 nucleus due to its favorable magnetic properties². Therefore, computational chemistry resources are advantageous for the prediction of NMR properties. The present study aims to develop a computational protocol for predicting the Xe-129 NMR chemical shift ($\delta^{129}\text{Xe}$) using the new NMR-ZORA basis sets.

METHODS

The molecules XeF_2 , XeF_4 , and XeF_6 , that present experimental data for $\delta^{129}\text{Xe}$ available in the literature, were selected. The structures of the molecules were optimized at DFT-Functional/def2-SVP, considering 32 functionals and the Xe-129 NMR shielding constants ($\sigma^{129}\text{Xe}$) were obtained at SSD-D-SC-ZORA/NMR-ZORA protocol. Furthermore, the role of the DFT-functionals for predicting the $\delta^{129}\text{Xe}$ was also evaluated. Finally, other ZORA basis sets and 4-components calculations (performed with ReSpect 5.1.0 program) were carried out. The calculations were performed with the NWChem 7.0.2 program.

RESULTS

The optimized geometries for the xenon fluorides presented mean relative deviation (MDR) in relation to the experimental bond lengths between 0,51% (M11) and 2,40% (BHandH). It was observed in a previous paper that there is a tendency to only DFT-functionals with at least 28% of HF Exchange being able to describe the experimentally observed C_{3v} symmetry for the XeF_6 molecule³. The same relation was observed in the present study, except for the meta-GGA M11-L functional.

Concerning the influence of the structure on the NMR, the structures obtained with the PW6B95, B1B95, and CAM-B3LYP functionals presented MDR of 3,79%, 3,93%, and 3,99%, respectively, for the $\delta^{129}\text{Xe}$ in XeF_2 , XeF_4 , and XeF_6 (Figure 1). Furthermore, the role of the DFT functional in predicting the $\delta^{129}\text{Xe}$ was also assessed. The

calculated results showed that the SSB-D presents the most accurate results, followed by the PBE0 and PBE functionals (Figure 2).

The role of the NMR-ZORA basis sets was evaluated when protocols with the jorge-TZP-ZORA basis sets were considered, with the best result obtained, SSB-D-SC-ZORA/jorge-TZP-ZORA/B1B95/def2-SVP, presenting a MRD of 22,6%.

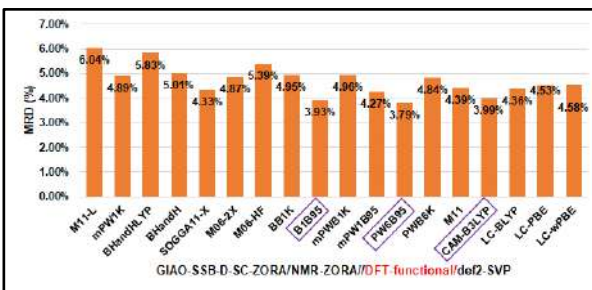


Figure 1. Mean relative deviation for the calculated $\delta^{129}\text{Xe}$ in XeF_2 , XeF_4 e XeF_6 with distinct structures.

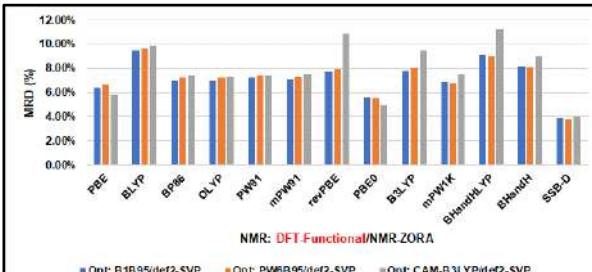


Figure 2. Mean relative deviation for the calculated $\delta^{129}\text{Xe}$ in XeF_2 , XeF_4 e XeF_6 with distinct DFT functionals.

CONCLUSIONS

This study investigated the influence of structure and DFT functional in predicting the $\delta^{129}\text{Xe}$ of the xenon fluorides using the new NMR-ZORA basis sets. The best protocol, SSB-D-SC-ZORA/NMR-ZORA//PW6B95/def2-SVP, with a MRD of 3,79%, will be applied in studying the $\delta^{129}\text{Xe}$ of other xenon compounds.

REFERENCES

- A. Chhandak et al., Int. J. Curr. Microbiol. App. Sci., 2017, 6, 2063.
- D. Raftery, Annu. Rep. NMR Spectrosc., 2006, 57, 205.
- D. F. S. Paschoal, H. F. Dos Santos, PCCP, 2021, 23, 7240.

ACKNOWLEDGMENTS

The authors would like to thank the Brazilian agency FAPERJ (E-26/201.336/2022 – BOLSA and E-26/210.070/2022) and PIBIC-UFRJ for the financial support.

CONFINEMENT OF QUANTUM PARTICLES IN CURVED SPACES

Eduardo V. S. Anjos¹ (PG), Antonio C. Pavão¹ (PQ) e Cristiano C. Bastos² (PQ);

eduardo.anjos@ufpe.br;

¹Departamento de Química Fundamental, Universidade Federal de Pernambuco, Recife – PE - Brasil.

²Departamento de Química, Universidade Federal Rural de Pernambuco, Recife – PE - Brasil;

Key-words: Quantum Confinement, Differential Geometry, Geometric Potential

INTRODUCTION

In this work we solve the Schrödinger equation using a Hamiltonian with Da Costa's geometric potential¹ to describe the confinement of a particle in a spiral curve.

METHOD

The Schrödinger equation with the attractive potential of Da Costa ($V_{geo} = k_s^2/4$) is:

$$-\frac{\hbar^2}{2m} \frac{\partial^2 \Psi}{\partial s^2} - \frac{\hbar^2 k(s)^2 \Psi}{8m} = E\Psi \quad (1)$$

We analyze cases where, given the curvature, it is possible to find the corresponding curve, the wave function and the spectrum. The Dirichlet boundary condition ($\psi(0)=\psi(L)=0$) was used for confinement in open curves.

RESULTS

The solution of Eq. 1 for $k(s) = \frac{1}{\sigma s}$ spiral curve is a Bessel function J of first kind:

$$\Psi(s) = c_1 \sqrt{s} J_{\frac{1}{2} \sqrt{1 - \frac{4a}{\sigma}}}(\sqrt{bs}) \quad (2)$$

where $b = \frac{2mE}{\hbar^2}$, $a = \frac{1}{4}$ and $\sigma \geq 1$ is a parameter. The behavior of the potential for $\sigma = 1$ and $\sigma = 10$ is shown in Fig. 1. The spectrum depends of the Bessel zero function ($j_{\frac{1}{2} \sqrt{1 - \frac{1}{\sigma}}, n}$):

$$E = \left(\frac{\hbar^2}{8\pi^2 m L^2} \right) \left(j_{\frac{1}{2} \sqrt{1 - \frac{1}{\sigma}}, n} \right)^2 \quad (3)$$

As shown in Fig. 2, there is a shift in the spectrum when comparing the canonical case ($V_{geo}=0$) with the spiral. The 2→3 transition, which corresponds to cyan in the observable spectra, in the curved system $\sigma = 1$ turns blue-green. However, as we increase the parameter σ , we see that the spiral spectrum tends towards the canonical case. An application of this spiral model would be in polyenes and nanostructures, where the geometry of these compounds can be controlled in the synthesis.

Unlike the classical case ($V_{geo}=0$), equation 3 does not admit $n = 0$. However, we also analyze the zero mode ($E = 0$) of the spiral, which represents

a transition state between confined and ionized. The wave function of this state is:

$$\Psi(s) = \sqrt{\frac{2d+1}{L^{d+1}}} s^d \quad (4)$$

where $d = \frac{1}{2} - \frac{\sqrt{\sigma-1}}{2\sqrt{\sigma}}$, and can be controlled by the σ parameter.

Figure 1. Comparison between V_{geo} when $\sigma = 1$ e $\sigma = 10$.

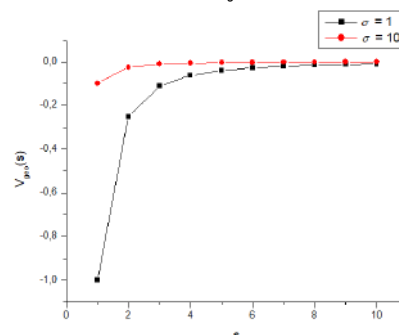
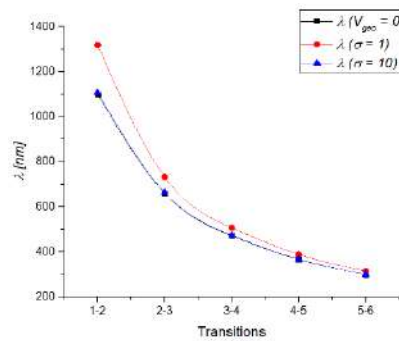


Figure 2. Comparison between λ (nm) of the spiral transitions (T), when, $\sigma = 1$ e $\sigma = 10$, and the canonical case ($V_{geo} = 0$).



CONCLUSION

We obtained the wave function, spectrum and zero mode for a particle confined in a spiral curve. The potential $k(s) = 1/\sigma s$ allows the modulation of energy levels with the parameter σ , which leads to a better description of the experimentally observed spectrum.

REFERENCE

¹Da Costa, R. C. T. Quantum mechanics of a constrained particle. Phys. Rev. A **23**, 1982 (1981).

ACKNOWLEDGMENT

CAPES, UFPE, <QQ>, LnP e UFRPE.

Design de novo dirigido por descritores quimioinformáticos em receptores de serotonina 5-HT2A 5-HT6 e 5-HT7: é possível gerar candidatos seletivos?

Anelisa G. de Sousa (IC)¹, Guilherme D. R. Matos (R)^{1,2*}.

anelisa.gs@gmail.com; guilhermedrmatos@gmail.com

¹Universidade de Brasília, Instituto de Química, Laboratório de Modelagem de Sistemas Complexos, Brasília, DF, 70910-900, Brasil;

²Department of Applied Mathematics and Statistics, Stony Brook University, EUA

Keywords: Design de novo, receptores de serotonina, seletividade.

INTRODUÇÃO

Receptores de serotonina¹ são componentes importantes da transmissão de sinais biológicos no sistema nervoso e em tecidos não-neuronais. Dada a associação desses receptores à depressão, cognição e até mesmo ao uso de drogas recreativas, o design de novos ligantes deve tentar buscar seletividade com o receptor de serotonina de interesse. Este trabalho propõe o uso de design de novo para a geração de ligantes seletivos (potencialmente específicos) para três receptores de serotonina, 5-HT2A (PDB: 7WC6), 5-HT6 (PDB: 7XTB) e 5-HT7 (PDB: 7XTC).

MÉTODOS

A geração de novas moléculas foi realizada por meio do software DOCK6 com o uso do algoritmo de design de novo² dirigida por descritores. Essa metodologia explora preferencialmente o espaço químico e cria moléculas a partir de uma biblioteca de fragmentos, levando em consideração propriedades de interesse (descritores quimioinformáticos calculados em interface com o pacote RDKit) ao longo do processo de construção da molécula. O design foi feito dentro do sítio de ligação dos três receptores e os ensembles das moléculas geradas apresentavam valores de “druglikeness,” acessibilidade sintética, LogP e número de centros estereogênicos que nos permitem inferir se a molécula é um bom candidato a fármaco. As moléculas geradas em cada receptor foram, então, submetidas a cross-docking, onde os ligantes de um sítio foram ancorados nos sítios dos outros receptores com o propósito de separar ligantes promíscuos de ligantes mais seletivos.

RESULTADOS

Com o uso do D3N foram gerados 1202 ligantes para a proteína 5-HT2A, 488 para a proteína 5-HT6 e 1212 ligantes para a proteína 5-HT7. Por meio da análise da energia de interação (energia eletrostática e energia contínua) entre os resíduos da proteína e os ligantes gerados foi feita a comparação entre ligantes capazes de se ligar a uma proteína de forma específica.

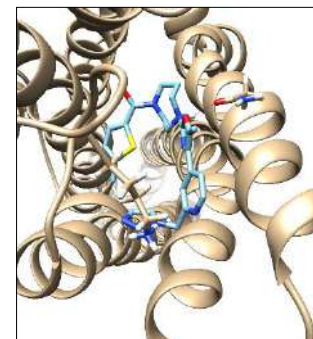


Figura 1. Sítio de ligação do receptor 5-HT2A com o ligante 5_1 gerado pelo Design de novo.

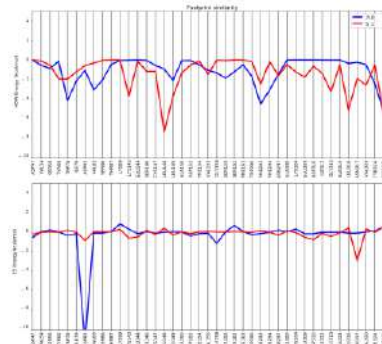


Figura 2. Gráfico com quarenta resíduos de maior interação com o receptor 5-HT2A e seu ligante natural dietilamida do ácido lisérgico e o ligante 5_1.

CONCLUSÕES

O experimento conjunto de design de novo e cross-docking não revelou candidatos marcadamente seletivos para as proteínas 5-HT6 e 5-HT7, mas encontrou bons candidatos para o receptor 5-HT2A, como a molécula das figuras 1 e 2. Ligantes escolhidos tem indicadores de seletividade quando as diferenças de energia de interação são grandes o suficiente para indicar uma interação preferencial. Estudos dos sítios de ligação estão sendo feitos para guiar experimentos futuros.

REFERÊNCIAS

¹ Hannon, J.; Hoyer, D. Molecular Biology of 5-HT Receptors. Behavioural Brain Research 2008, 195.

² Allen, W. J.; Balius, T. E.; Mukherjee, S.; Brozell, S. R.; Moustakas, D. T.; Lang, P. T.; Case, D. A.; Kuntz, I. D.; Rizzo, R. C. DOCK 6: Impact of New Features and Current Docking Performance. J. Comput. Chem. 2015, 36 (15).

AGRADECIMENTOS

Agradecimentos à Universidade de Brasília e ao Prof. Daniel F. Scalabrin Machado.

Copolymerization of Carbon Dioxide and Cyclohexene Oxide by Bimetallic Homogeneous Catalysts: A DFT Study

Lucas W. de Lima (PhD)¹, Michael Roemelt (R)², Atualpa A.C. Braga (R)^{1*}

lucas.welington.lima@usp.br; atualpa@iq.usp.br

¹Institute of Chemistry, University of São Paulo, São Paulo, Brazil; ²Institute für Chemie, Humboldt-Universität zu Berlin, Berlin, Germany

Keywords: CO₂, ROCOP, bimetallic catalyst, DFT, reaction mechanism

INTRODUCTION

The effects caused by the increase of carbon dioxide (CO₂) released in the atmosphere due to human activities are considered to be detrimental to the environment.¹ As an alternative to diminishing the release of CO₂, its conversion into valuable products is one of the most promising processes.² In this work we investigate the reaction mechanism of the copolymerization of CO₂ and cyclohexene oxide (CHO) catalysed by bimetallic homogeneous catalysts composed by Mg²⁺, Mn²⁺, Co²⁺, Cu²⁺, and Zn²⁺ at position 1 (vide Figure) and Mg²⁺ in position 2.

METHODS

Geometry optimization and frequency calculations were performed at the BP86-D3(BJ)/def2-SVP/CPCM($\epsilon=2.82$) level of theory. Single point calculations on top of the optimized geometries were performed at the TPSS0-D3(BJ)/def2-TZVP/CPCM($\epsilon=2.82$) level of theory. Thermal corrections were calculated at 298.15 K. All calculations were performed with the ORCA 5.0.3 software package.

RESULTS

The presented figure shows the main reaction (a) and the studied catalyst, along with the Gibbs free energy profile of the initiation (c) and propagation

(d) of the polymerization reactions. In both steps, the TOF-determining transition state is the CHO epoxide ring opening, where the transition state 1 (TS1) is the TOF-determining transition state for the reaction. Those results shows that the best catalysts to perform this reaction are in the following order: CuMg, CoMg, MnMg, ZnMg, and MgMg.

CONCLUSIONS

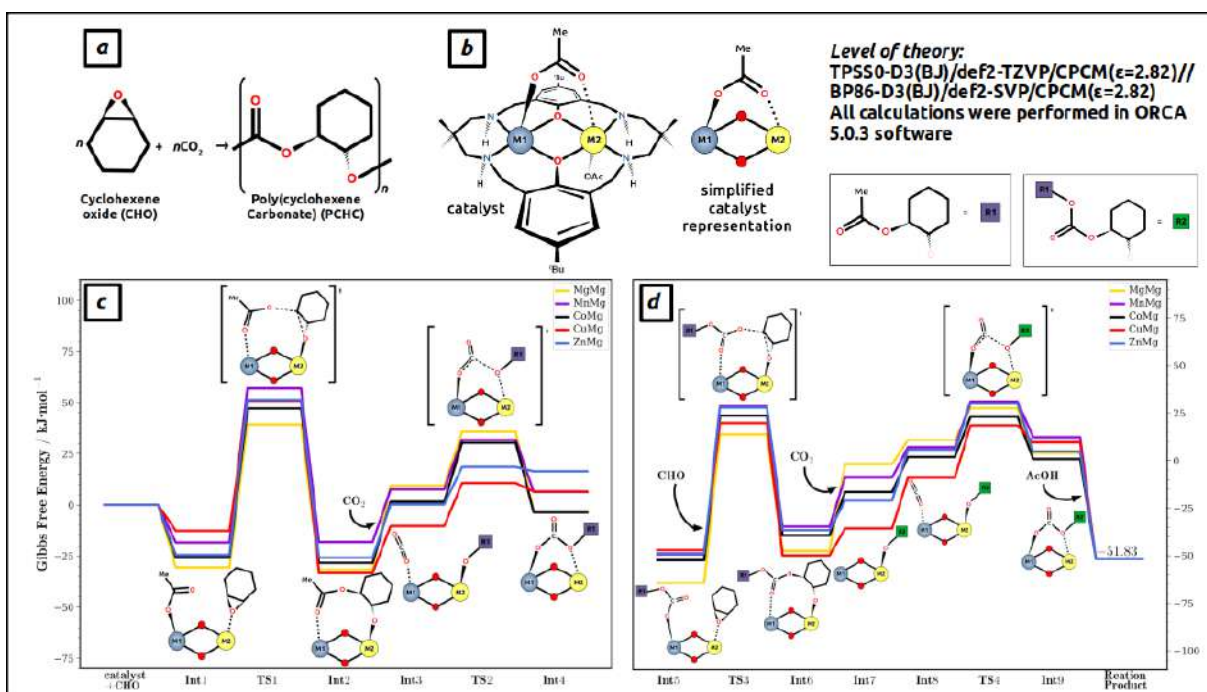
In conclusion, with the presented results we improved the understanding of the reaction mechanism catalysed by the systems studied, which may allow experimentalists to improve their systems.

REFERENCES

- S. Klaus, M. W. Lehenmeier, et al. *Coord. Chem. Rev.*, 2011, 255(13). 1460-1479.
- A. Buchard, F. Jutz, et al. *Macromolecules*, 2012, 45(17). 6781-6795.

ACKNOWLEDGMENTS

We would like to thank Coordenação de Aperfeiçoamento de Pessoal de Nível Superior (CAPES) agency for grants 88887.694552/2022-00 and 88887.341693/2019-00.





Estudo da Estabilidade e da Aromaticidade de Anéis Aromáticos Lineares Substituídos com Átomos de oxigênio

Kássio Henrique Souza Silveira (IC),^{1;2*} Júlio Cesar Verli Chagas (PG),¹ Luan G. F. dos Santos (PG),¹ Francisco Bolívar Correto Machado (PQ).¹

kassio.silveira@aluno.ifsp.edu.br

¹Instituto Tecnológico de Aeronáutica - ITA, Brasil;

²Instituto Federal de Educação, Ciência e Tecnologia de São Paulo – IFSP, Brasil.

Palavras Chave: Benzeno, Antraceno, Aromaticidade, Gap Singlet-Tripleto.

INTRODUÇÃO

Compostos aromáticos podem ser definidos como sendo aqueles que possuem um sistema de elétrons π deslocalizados. A partir de medidas de calor de formação e dos estados de energia, é possível classificar compostos em aromáticos, anti-aromáticos e não-aromáticos, onde tal classificação pode ser obtida através de critérios geométricos, energéticos, entre outros. Para uma melhor compreensão dessas estruturas aromáticas e derivadas, métodos de química computacional são utilizados, obtendo-se assim dados das estruturas eletrônicas, caráter radicalar, energias totais e gaps de energia entre os estados fundamental e excitados.

Neste sentido, este estudo consistiu em estudar os efeitos da inserção de dois átomos de oxigênio em substituição a dois átomos de hidrogênio em várias posições nas moléculas de benzeno, naftaleno e antraceno. Um total de vinte e uma estruturas foram caracterizadas e analisadas. A análise foi voltada para compreender a relação entre a posição da substituição e a aromaticidade do sistema, sua estabilidade energética e o caráter radicalar.

MÉTODOS

As geometrias do estado fundamental de simetria singlet foram otimizadas utilizando o método da teoria do funcional de densidade, UwB97XD com a base def2-TZVP. A seguir, cálculos pontuais para o estado tripleno foram calculados com a mesma metodologia para determinar os gaps de energia singlet-triplet (S-T). Usando as geometrias, a aromaticidade foi estimada pelo método HOMA (*Harmonic Oscillator Model of Aromaticity*)¹. A estabilidade do estado fundamental também foi caracterizada pelo número de elétrons desemparelhados através do método *Fractional Occupation Number Weighted Electron Density* (FOD)². Cálculos de estrutura eletrônica foram realizados utilizando os códigos Gaussian 09 e Orca.

RESULTADOS

As substituições foram realizadas em todas as possíveis posições para as três moléculas citadas anteriormente. Contudo, para termos uma ideia do conjunto de informações, apresentamos na

Figura 1 as possíveis posições de substituição dos átomos de hidrogênio por átomos de oxigênio no antraceno.

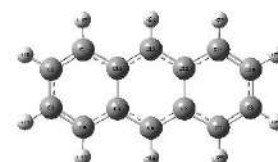


Figura 1. Estrutura do antraceno, com as posições de substituições enumeradas.

Na Figura 2, apresenta-se os resultados dos gaps verticais S-T. Observa-se que dependendo da posição de substituição, a estabilidade, maior gap, aumenta ou diminui. A maior estabilidade, comparada ao antraceno, é obtida quando da substituição central.

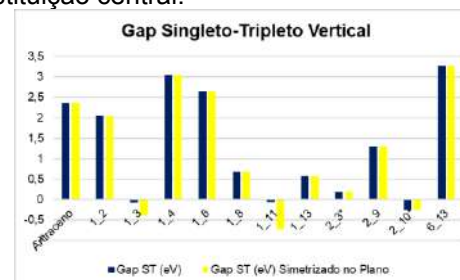


Figura 2. UwB97XD/def2-TZVP gaps S-T.

CONCLUSÕES

Os resultados obtidos sobre o aumento ou diminuição da estabilidade via gap S-T das estruturas substituídas, tanto no antraceno, como no naftaleno e benzeno, também estão de acordo com os obtidos pelo número de elétrons desemparelhados, N_{FOD}, assim como pelo método geométrico de aromaticidade HOMA.

REFERÊNCIAS

¹ T. M. KRYGOWSKI, et al., Chem. Rev., 2001, 101. 1385-1420.

² C. GRIMME, et al., Chem. Eur. J., 2017, 23. 6150-6164.

AGRADECIMENTOS

CAPES, CNPq, FAPESP.

Mechanistic Study of Palladium(II)-Catalyzed C-H Bond Activation and Benzyne Insertion of N-Methoxy Amides

Erick H. de S. Alves (IC),^{1*} Daniel A. S. Oliveira (PG),¹ Ataulpa A. C. Braga (PQ).¹

erick_004@iq.usp.br;

¹Department of Fundamental Chemistry, Institute of Chemistry, University of São Paulo, São Paulo - SP, Brazil

Keywords: C-H activation, annulation, DFT, catalysis

INTRODUCTION

In recent years, C-H functionalization reactions have received much attention from specialized authors. Countless products can be conceived under propitious conditions and catalysts, typically exhibiting a higher atom economy compared to other techniques.

Based on the experimental work of Xiu-Feng Cheng and Ting Yu *et al.*,¹ our objective is to establish a reliable computational model for the palladium(II) complex-catalyzed N-Methoxy amide directed C-H activation reaction. .

METHODS

The calculations were performed using M06L density functional,² with the basis set Def2-SVP³ for geometry optimizations and frequency calculations and Def2-TZVP³ for energy corrections. Transition States confirmed by an imaginary frequency and confirmed by IRC. The solvent effects were simulated with the method of implicit solvent SMD,⁴ with acetonitrile, as done in the experimental work.¹ All calculations were performed using Gaussian 16.

RESULTS

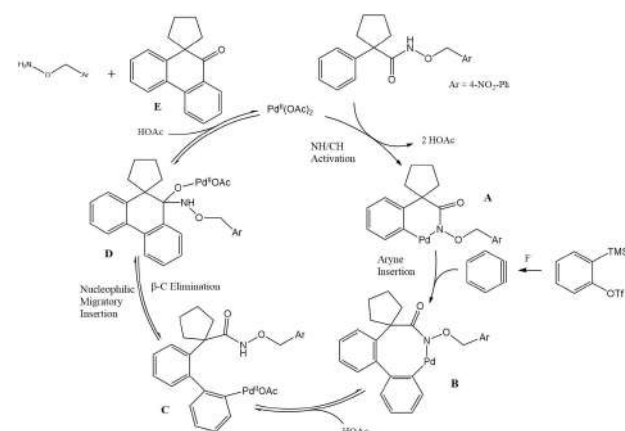


Figure 1. Proposed mechanism for the reaction

A probable mechanism has been proposed for the reaction (**Figure 1**).¹ To date, all the intermediates and the N-H/C-H activation transition states have been determined in the condensed phase, shown in **Figure 2**. The C-H activation represents the highest free-energy activation barrier up to now and it takes place through a concerted metalation-deprotonation (CMD) mechanism. The latter was facilitated by the N-methoxy amide group, which serves as a directing group for *ortho* C-H activation.

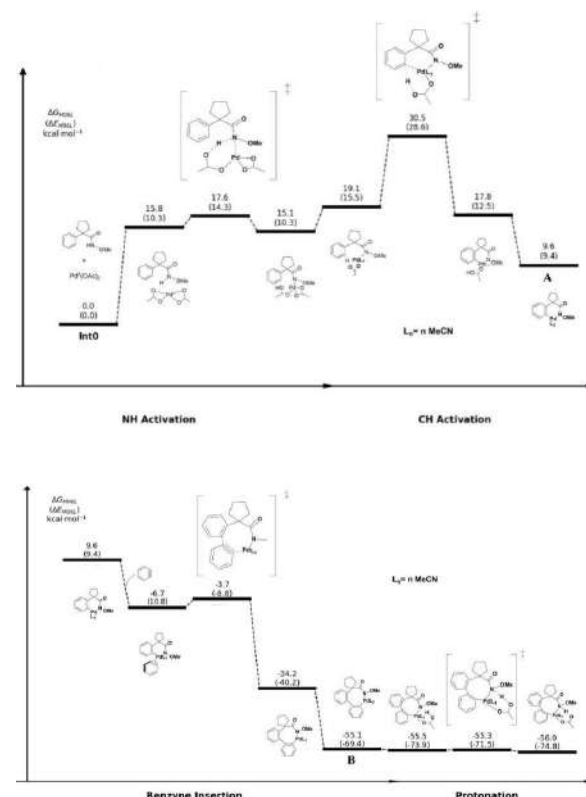


Figure 2. Energetic profile of reaction

CONCLUSÕES

Up to this point, the obtained results have consistently conformed to the proposed mechanism. Under the specific conditions, the C-H functionalization presents the highest energy barrier, *ortho* directed due to the presence of the amide group. In all cases, acetonitrile has proven to be a more stable ligand than acetic acid. Furthermore, the reaction has displayed significant exothermic behavior. Further research is currently being conducted in our laboratory.

REFERENCES

- X. Cheng, T. Yu, Y. Liu, N. Wang, Z. Chen, G. Zhang, L. Tong, B. Tang, *Organic Letters* 2022, 24, 11, 2087-2092.
- Y. Zhao, D. G. Truhlar, *J. Chem. Phys.* 2006, 125, 194101.
- F. Weigend, R. Ahlrichs, *Phys. Chem. Chem. Phys.*, 2005, 7, 3297. *Phys. Chem. Chem. Phys.*, 2006, 8, 1057.
- A. V. Marenich, C. J. Cramer, D. G. Truhlar, *J. Phys. Chem. B*, 2009, 113, 6378.

ACKNOWLEDGMENTS

We acknowledge the Institute of Chemistry of University of São Paulo and the financial support from FAPESP.

Kinetics of the initiation pathways of *trans*-crotonaldehyde oxidation by the OH radical.

Adalberto Santana Lima Junior (PG),^{1*} Tiago Vinicius Alves (PQ).¹

adalbertoslj@hotmail.com

¹ Instituto de Química (UFBA), R. Barão de Jeremoabo, 147 - Ondina, Salvador - BA, Brasil

Palavras Chave: Combustion, kinetic, *trans*-crotonaldehyde, CUS.

INTRODUÇÃO

Trans-crotonaldehyde (CROT) is one of the main α,β -unsaturated carbonyl compounds of atmospheric interest.¹ Emitted through different sources such as combustion and chemical industries and produced from atmospheric oxidation of volatile organic compounds (VOCs), CROT is a primary and secondary pollutant.^{1,2} It is well-established that oxidation by OH radical is the dominant pathway in typical atmospheric conditions for the CROT.^{1,2} In this way, Atkinson *et al.*³ performed the first experimental investigation of the reaction between OH radical and CROT. More recently, experimental studies performed by Orlando and Tyndall⁴ indicated that abstraction and addition processes occur parallelly and at equal extents. In the only theoretical investigation until now, El-Taher¹ performed an exploration of the potential energy surface (PES) at the CCSD(T)/cc-pVDZ//MP2(Full)/6-31G(d,p) level theory. In this work, he considered two processes: the abstraction of the aldehydic hydrogen and the radical OH addition. Hence, our work aims to elucidate the mechanism reaction between the OH radical and CROT. More specifically, we estimate the thermal rate constants for abstractions and additions of OH-initiated reactions employing the canonical unified statistical (CUS) theory.

MÉTODOS

All stationary points generated by CROT + OH reaction were optimized at the M06-2X/aug-cc-pVTZ level. The accuracy of this level of theory was checked for oxidation reactions in our previous work.⁵ All electronic structure calculations were performed using the Gaussian 09 program package. Thermal rate constants for the elementary steps involving a saddle point were calculated by applying canonical variational transition state theory with small-curvature tunneling corrections (CVT/SCT) using the Pilgrim code. For the association reaction, we employed long-range transition state theory (LR-TST). We apply the canonical statistical model (CUS) to determine the rate coefficient of the pathways with pre-reactive complexes (PRCs). A comparison with previous experimental results was also made.

RESULTADOS

Fig. 1 shows the Arrhenius plot from our work to the addition rate constants obtained with CUS and competitive-CUS (CCUS) models compared to previous studies. Our results are shown in good concordance with experimental results. The rate coefficients for the abstraction processes are two magnitude orders higher than the experimental data.

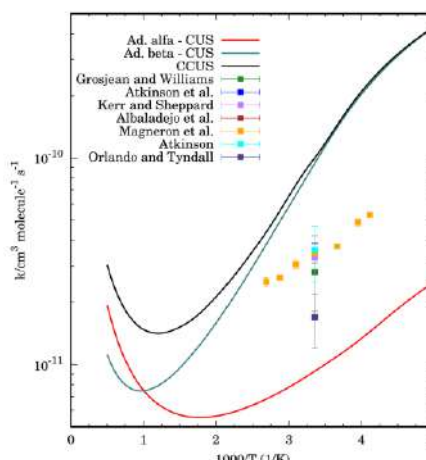


Fig. 1: Arrhenius plot of the thermal rate constants for addition reactions between 200 and 2000 K. Previous experimental estimations are also shown.

CONCLUSÕES

The kinetics mechanism of the CROT + OH reaction was investigated. Our best estimation of the rate constants presents good agreement with the tendency of the experimental data. We expect to improve these results by applying the multi-structural treatment in CVT/SCT constants.

REFERÊNCIAS

- S. El-Taher, Can. J. Chem., 2009, 87. 1716-1726.
- I. Magneron, R. Thévenet, A. Mellouki, G. Le Bras, J. Phys. Chem. A, 2002, 106. 2526-2537.
- R. Atkinson, S. M. Aschmann, J. N. Pitts Jr., Int. J. Chem. Kin., 1983, 15. 75-81.
- J. J. Orlando, G. S. Tyndall, J. Phys. Chem. A, 2002, 106. 12252-12259.
- A. S. Lima Junior, J. L. Nascimento, D. Moura, T. V. Alves, Comput. Theor. Chem., 2023, 1222. 114073.

AGRADECIMENTOS

FAPESB, CNPq, CAPES.

Chemical bond overlap descriptors from MCSCF wavefunctions

Carlos V Santos Jr (PG),¹ Renaldo T Moura Jr (PQ)^{2*}

cvdsj3@academico.ufpb.br; renaldo.mourajr@cca.ufpb.br

¹Departamento de Química, Universidade Federal da Paraíba, João Pessoa-PB; ²Departamento de Química e Física, Universidade Federal da Paraíba, Areia-PB.

Keywords: overlap model, canonical molecular orbital, configuration interaction, CASSCF, topology.

INTRODUCTION

Chemical bond overlap (OP) descriptors were initially introduced¹ by employing analytical calculations based on an overlap electron density constructed from localized molecular orbitals (LMOs). Subsequently, it was demonstrated that these OP descriptors, along with their topological (TOP) extension², agreed with the quantum theory of atoms in molecules (QTAIM) and their corresponding local modes analysis (LMA) counterparts³. Building upon this foundation, the current work further advances the decomposition of the total electron density, obtained from a multiconfigurational self-consistent field (MCSCF) wavefunction, into atomic and overlap contributions, thereby improving the description of OP/TOP descriptors.

METHODOLOGY

By assuming an orthogonal N -electron basis function set of configuration state functions (CSFs), the overlap electron density in the position (\vec{r}) can be written in the form:

$$\rho_{OP}(\vec{r}) = 2 \sum_k^{\text{CSFs}} \mathbb{C}_k^2 \sum_l^{M_k} n_l \sum_{i \in A}^N \sum_{j \in B}^N c_i^l c_j^l \varphi_i(\vec{r}) \varphi_j(\vec{r}) \quad (1)$$

where \mathbb{C}_k^2 represents the MCSCF expansion coefficient for the k -th CSF. l runs over M_k molecular orbitals (MOs) constituting the k -th CSF, with n_l denoting the occupation of the l -th MO. $\varphi_i(\vec{r})$ and $\varphi_j(\vec{r})$ are spin-orbitals inspected in position \vec{r} , and c_i^l and c_j^l their coefficients. OP/TOP descriptors are derived from $\rho_{OP}(\vec{r})$ in the ChemBOS (www.chembos.webpage) package. Archetype systems H_nX-OH ($X = Li, B, C, N, O$, and F) were studied to demonstrate the feasibility of obtaining OP/TOP descriptors at CASSCF(8,8) /def2QZVP level of theory from Gaussian 16.

RESULTS

The remarkable equivalence between OP density maps obtained from LMOs and CMOs is demonstrated in Figure 1 for density functional theory (DFT). This equivalence leads to highly similar OP/TOP descriptors, highlighting that the locality of the overlap density remains independent of the MO basis used.

Table 1 presents the OP/TOP descriptors obtained at the CASSCF(8,8) level of theory. It demonstrates a consistent decrease in ρ_{OP} and

J_{intra} from C to O, followed by an increase in the overlap critical point Laplacian.

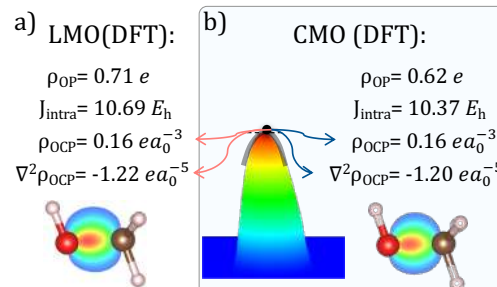


Figure 1. OP/TOP descriptors: LMOs and CMOs (H_3C-OH).

In Figure 2, it is evident that $\rho_{OP}(\vec{r})$ decreases from the more covalent bond C–O to the O–O counterpart, being the last composed by³ resonant covalent and ionic contributions.

Table 1. CASSCF(8,8) OP/TOP descriptors for X–O bonds.

X	ρ_{OP} (e)	ρ_{OCP} (ea_0^{-3})	J_{OP}^{intra} (E _h)	$\nabla^2\rho_{OCP}$ (ea_0^{-5})
O-C	0.617	0.157	10.37	-1.204
O-N	0.454	0.129	8.26	-0.999
O-O	0.339	0.103	3.33	-0.703

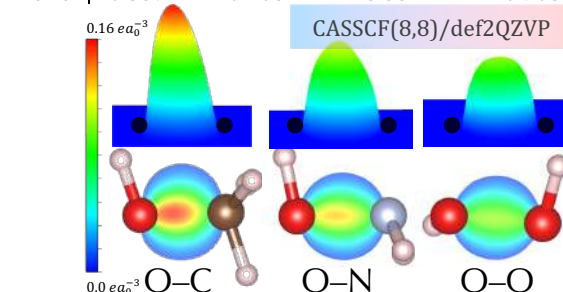


Figure 2. MCSCF ρ_{OP} for O–C, O–N, and O–O bonds.

CONCLUSIONS

The study demonstrates that LMOs and CMOs provide a consistent localized representation of the overlap electron density. Utilizing the orthogonal set of CMOs improves the description of chemical bonds and enables incorporating a multiconfigurational character to enhance its reliability. The forthcoming comprehensive assessment of OP/TOP descriptors will reinforce these findings and pave the way for future advancements in this field.

REFERENCES

- R. T. Moura Jr. J. et al. Mol. Model. 2020, 26. 301.
- C. V. dos Santos-Jr, et al. In peer review.
- C. V. dos Santos-Jr, et al. CPL, 2022, 787. 139282.
- M. Fugel. et al. Chem. Eur. J. 2018, 24. 6248.

ACKNOWLEDGEMENTS

CAPES, CNPq, UFPB, PPGQ.

Tunning the electronic bands of Covalent Organic Frameworks with functional groups

Jéssica Mendonça Bayer(UR)¹, Felipe L. Oliveira(PhD) ¹, Pierre M. Esteves(R)^{1*}

bayer@nano.ufrj.br; pesteves@iq.ufrj.br

¹Institute of Chemistry, Universidade Federal do Rio de Janeiro, Rio de Janeiro – RJ, Brazil.

Keywords: Covalent Organic Frameworks, DFT calculations, functional groups, electronic bands

INTRODUCTION

Covalent Organic Frameworks (COFs) are an emerging class of nanoporous organic and reticulated materials, build by the covalent bond of two organic building blocks.¹ These materials present a crystalline extended structure with a defined topology, which is dictated by the geometry of its building blocks.² Usually, two-dimensional COFs are built with building blocks presenting aromatic rings and several points for possible functionalizations, which confer these materials a high degree of modularity. Consequently, COFs have attracted a great deal of attention over the past years, particularly for their potential for applications in catalysis, spintronics, or optoelectronics.³

Computational studies have predicted that even slight modifications of the COF building blocks can heavily change the electronic structure characteristics around the Fermi level of these structures. Certain modifications can give rise to exotic electronic states such as Dirac cones, high delocalized electronic states as presented by graphene, or Van Hove singularity, high localized electronic states that generate flat bands.⁴

Here we explore the influence of functional groups on the electronic structure characteristics of an azine-based two-dimensional covalent organic framework built from the covalent bond of a functionalized-1,3,5-triformylbenzenes and 1,4-benzenediamine forming an augmented honeycomb (HCB-A) net.

METHODS

We combine calculations based on the density functional theory (DFT) using the PBE exchange-correlation functional with band structure and density of states analysis to explore the influence of several functionalizations (Br, CH₃, CHO, Cl, CN, COOH, F, H, NH₂, NO₂, OH e OMe) on the electronic states near to Fermi level of the isolated 2D COF structures.

RESULTS

Our results show that functional groups such as Br, Cl, F, CN, H, NH₂, and OH do not generate a relevant geometric change on the COF backbone but can change the band gap and the dispersion of the valence bands presenting Dirac cones by tuning the electronic states dispersed over the COF backbone and acting as dopant agents, as shown in Figure 1. Other groups such as CH₃, CHO, COOH, NO₂, and OMe induce strong conformational change over the COF structure, reducing the π-electron conjugation and modifying electronic structure characteristics of the valence bands.

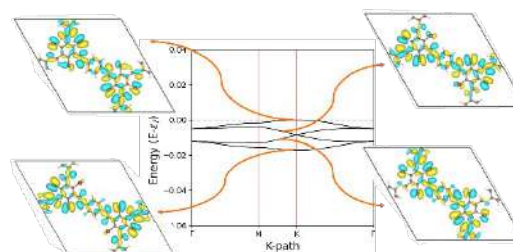


Figure 1. Bands of Br functional group.

CONCLUSIONS

The influence of these functional groups on the valence bands induced changes in the band gap ranging from 1.5 to 2.4 eV through different mechanisms. This indicates that it is possible to fine-tune the electronic properties of COFs in a specific way by the auspicious selection of the functional groups.

REFERENCES

- ¹ C.S. Diercks and O.M. Yaghi, Science, 2017, v. 355, n. 6328
- ² R.S.B. Gonçalves, et al, ChemCatChem. (2016) 8 743–750.
- ³ THOMAS, Simil et al. Chem Mater, v. 31, n. 9, p. 3051-3065, 2019.
- ⁴ SPRINGER, Maximilian A. et al. Chem Soc Rev, v. 49, n. 7, p. 2007-2019, 2020.

ACKNOWLEDGMENTS

UFRJ, NACAD, CAPES, CNPq, FAPERJ.

Development of a computational protocol for predicting the first hyperpolarizability of coumarin dyes

Gabriel de S. Martins (IC)^{1*}, Diego F. S. Paschoal (PQ)¹

gabrielmartins1102@gmail.com; diegopaschoal01@gmail.com.

¹NQTCM: Núcleo de Química Teórica e Computacional de Macaé, Polo Ajuda, Instituto Multidisciplinar de Química, Centro Multidisciplinar UFRJ-Macaé, Universidade Federal do Rio de Janeiro, Macaé, RJ, Brazil.

Keywords: Nonlinear optics, First hyperpolarizability, Organic dyes, DFT, Basis sets.

INTRODUCTION

Nowadays, nonlinear optics (NLO) help in several areas such as solar energy and telecommunications which have been growing increasingly around the world¹. The first molecular hyperpolarizability (β) is the key property for the development of new NLO materials. However, the theoretical determination of β is a difficult task, quantum mechanics methods with extended basis sets and electronic correlation being of fundamental importance². In this context, it was evaluated and developed computational protocols for predicting β in coumarin dyes, a family of organic molecules that present π conjugation and push-pull and conjugation groups.

METHODS

Initially, a new specific NLO basis sets for 1st and 2nd row atoms, named as nqtcm-VDZP, was developed from modifications of the methodology of Paschoal et al.^{2,3}. Subsequently, a set of 14 coumarins⁴ (Figure 1) were selected and had their geometry optimized at B3LYP/6-31G(d,p)/IEF-PCM(UFF) protocol. Then, β was calculated at CAM-B3LYP/Basis set/IEF-PCM(UFF), where a set of 24 distinct basis sets were considered. Finally, for the best basis set, the role of the DFT functional was also assessed with a set of 31 distinct functionals. For calculating β , the eq. (1) was used².

$$\beta_t = \sqrt{\beta_x^2 + \beta_y^2 + \beta_z^2} \quad (1)$$

with $\beta_i = \beta_{iii} + \frac{1}{3} \sum_{i \neq j}^3 \beta_{iij} + \beta_{jij} + \beta_{iji}$ ($i = x, y, z$).

The β tensor elements obtained from the Coupled-Perturbed Kohn-Sham (CPKS) method, considering the field dependency (1064 nm). All calculations were carried out in the GAUSSIAN 16 Rev. C.01. program.

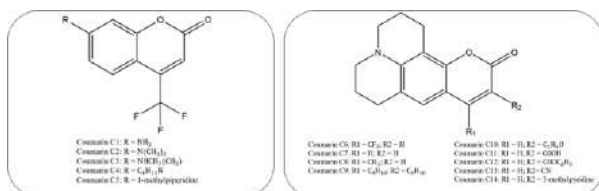


Figure 1. Coumarin dyes studied

RESULTS

First, the role of the basis sets for predicting β was assessed. For a set of distinct 24 basis sets, the mean relative deviation (MRD) varied between 24.5% (jorge-TZP) and 120.8% [6-311G(2d,2p)], with the triple-zeta basis sets presenting, in general, the smallest MRD. The new nqtcm-VDZP basis set presented MRD of 34.0%. However, for the C10 to C14 coumarines, that presented the largest β values ($> 100 \times 10^{-30}$ esu), the nqtcm-VDZP basis set showed the best description, with a MRD of 28.6%, in addition to presenting a low computational cost.

Then, the role of the DFT functional was assessed with the protocol DFT-Functional/nqtcm-VDZP/IEF-PCM(UFF), considering 31 distinct functionals. The calculated results showed that β is very sensitive to the functional used, with MRD varying between 282.5% (mPWLYP) and 8.0% (MN15). Furthermore, the inclusion of %HF Exchange was of fundamental importance in the description of β , with the pure GGA functionals showing the highest MRD.

CONCLUSIONS

In the present work, the role of the basis sets and DFT functionals in predicting the first hyperpolarizability of coumarin dyes was assessed, considering a set of 24 distinct basis sets, including a new nqtcm-VDZP basis set, and 31 distinct DFT functionals. The calculated results showed that the MN15/nqtcm-VDZP/IEF-PCM(UFF) presented itself as an excellent alternative for predicting β values, mainly for $\beta > 100 \times 10^{-30}$ esu.

REFERENCES

- 1 GARMIRE, E. Opt. Express 2013, 21, 30532.
- 2 MOYLAN, C. J. Phys. Chem. 1994, 98, 13513
- 3 Paschoal, D.; DOS SANTOS, H. F. Org. Electron. 2016, 28, 111
- 4 KANIS, D.R.; RATNER, M.A.; MARKS, T.J. Chem. Rev., 1994, 94, 195

ACKNOWLEDGMENTS

The authors would like to thank the Brazilian agency FAPERJ (E-26/210.070/2022 and E-26/201.336/2022 – BOLSA) and Prefeitura Municipal de Macaé by the research grants.

Theoretical study and QTAIM analysis of the interaction between pure and N-substituted coronene monomers

Kelly F.P. Laeber (PG),^{1*} Letícia M. Prates (PQ),² Leonardo Baptista (PQ),³ Maurício T.M. Cruz (PQ).¹

kellylaeberdo20201@ppqq.uerj.br*

¹Departamento de Química Geral e Inorgânica, Universidade do Estado do Rio de Janeiro, Rio de Janeiro-Brasil;

²Centro de Tecnologia Mineral, Rio de Janeiro-Brasil³Departamento de Química e Ambiental, Universidade do Estado do Rio de Janeiro, Faculdade de Tecnologia, Rio de Janeiro-Brasil.

Keywords: Asphaltene Aggregation, $\pi - \pi$ stacking, Coronene, DFT, QTAIM.

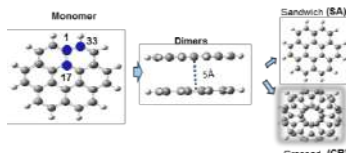
INTRODUCTION

The $\pi - \pi$ stacking forces are widely explored in diverse applications within chemistry, biology, and materials science. These interactions can be modulated by the geometric configuration and the presence of heteroatoms (N, O, and S).¹ Hence, understanding the influence of these factors on the magnitude of $\pi - \pi$ interactions bears significant importance within supramolecular systems, particularly in the context of asphaltene aggregation.² Therefore, the present work aims to evaluate the interaction between two pure and N-substituted coronene ($C_{24}H_{12}$) monomers, serving as a model for the aromatic portion of these structures.

METHODS

The construction of the structures (Figure 1) has been described previously.³

Figure 1: Structure construction scheme.



The dimers were optimized at the DFT level with the CAM-B3LYP/6-311G (d,p) methodology, adding D3 empirical dispersion in the Gaussian16 program. The aggregation energy ($E_{agg} = E_{dim} - (E_{mon(A)} + E_{mon(B)})$) was corrected for basis set superposition error (BSSE). Based on these results, a QTAIM analysis for each structure was performed using the AIMAll software.

RESULTS

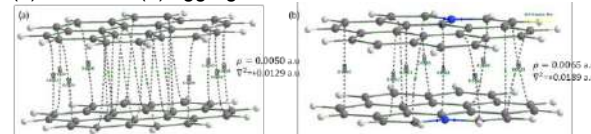
The Table 1 displays the E_{agg} of pure and N-substituted coronene dimers, considering both the sandwich (SA) and crossed (CR) conformations, three positions for N-substitution (N1, N17 and N33), and the variation of the dihedral angle (Θ) between the N atoms.

Table 1: E_{agg} (kcal mol⁻¹) for optimized structures of pure and N-substituted COR dimers. *Calculations did not converge.

Conf.	Θ	COR	N1	N17	N33
SA	0°	-16.19	*	-16.66	-16.54
	60°		-18.04	*	-17.51
	120°		-16.88	-16.61	-17.52
	180°		-17.90	-17.06	-17.81
CR	30°	-15.43	-15.82	-17.20	-16.20
	90°		-17.95	*	-16.54
	150°		-18.28	-16.29	-16.58

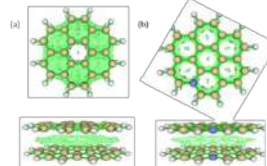
The addition of N increases the module of E_{agg} compared to the pure dimers (COR). The strongest interaction is observed for the N1-CR/150° dimer (-18.28 kcal mol⁻¹), and the weakest for COR-CR/30° (-15.43 kcal mol⁻¹). The QTAIM analysis (Figure 2) performed on the less (a) and more (b) aggregated dimer indicates only the contribution of van der Waals interactions between the monomers. However, as indicated by ρ and $\nabla^2\rho$ values, the magnitude of this contribution increases in the substituted dimer, even with the N atom not participating directly in the interaction. Such result suggests that the aggregation of these dimers may not depend solely on the C-C interaction.⁴

Figure 2: Bond critical points (BCPs) of the structure of the less (a) and more (b) aggregated dimer.



Based on the reduced density gradient (RDG) analysis (Figure 3), it is possible to observe that the addition of the N atom leads to a change in the electronic density in the interaction between the monomers.

Figure 3: RDG isosurface of (a) COR/30° (b) COR-N1/150°.



CONCLUSIONS

The presence of N increases the aggregation, regardless of the arrangement of the dimers. QTAIM indicates the contribution of van der Waals forces to aggregation, wherein even though N may not participate directly, its presence influences the magnitude of interaction between the monomers. Analysis of QTAIM and RDG in the other dimers is currently ongoing.

REFERENCES

- K.C. Fenk; J.H. Herbert. P.C.C.P., 2020, 22, 24870.
- Y. Ruiz-Morales et al. Energy Fuels, 2019, 33, 9, 7950–7970.
- K.F.P. Laeber et al, In: ANAIS DO XXI SBQT, 2021.
- U. Koch; P.L.A. Popelier. T.J.P.C., 1995, 99, 24, 9747-9754.

ACKNOWLEDGMENT

This study was financed in part by the Coordenação de Aperfeiçoamento de Pessoal de Nível Superior - Brasil (CAPES) - Finance Code 001, and FAPERJ.

Automatic generation of local vibrational mode parameters: from small to large Molecules, QM/MM systems, and lanthanide complex

Renaldo T. Moura Jr.^{1,2*}, Mateus Quintano², and Elfi Kraka².

renaldo.mourajr@cca.ufpb.br

¹Department of Chemistry and Physics, Federal University of Paraíba, Areia, Paraíba, Brazil; ²Department of Chemistry, Southern Methodist University, Dallas, Texas 75275, USA,

Keywords: Vibrational spectroscopy, Local vibrational mode theory, LModeA, Chemical graphs, Intrinsic bond properties.

INTRODUCTION

Vibrational spectroscopy provides in-depth insights into electronic structure and bonding, with recent interest in its applications and enhancements. Yet, the nature of a normal vibrational mode (NVM) in polyatomic systems is marked by delocalization, complicating the extraction of intrinsic bond properties or assignment of contributions. The local vibrational mode (LVM) theory tackles this by deriving local vibrations from NVMs, forming the basis for characterization procedures like the composition of normal modes (CNM) and adiabatic connection scheme (ACS)¹. ACS and CNM offer comprehensive insights but need a nonredundant set of local vibrational modes, which is challenging for complex systems.

LModeAGen, a new protocol for the automatic determination of a non-redundant, complete set of local vibrational modes is reported¹, which is based on chemical graph concepts. Whereas local mode properties can be calculated for a selection of parameters targeting specific local modes of interest, a complete set of non-redundant local mode parameters is requested for the ACS, relating each local vibrational mode with a normal mode counterpart, and for the CNM in terms of local mode contributions, a unique way to analyze vibrational spectra. LModeAGen was successfully applied for a test set of eleven systems, ranging from small molecules to the large QM (>100 atoms) subsystem of carbomonooxy-neuroglobin protein, described with a hybrid QM/MM method. LModeAGen is totally embedded in our new LModeA 2023² software version.

METHODOLOGY

The ω B97X-D/aug-cc-pVDZ, M06L/def2-TZVP, and QM/MM ω B97X-D/6-31G(d,p)/AMBER model chemistries were adopted for the description of the molecules in the test set. The new algorithm was also applied to lanthanide base compounds with organic ligands, allowing the utilization, for the first time, of local vibrational mode theory for obtaining local Ln-ligand force constants, an underlying property in intramolecular energy transfer mechanisms theory².

RESULTS

In the LModeAGen protocol, each LVM parameter is considered as a path with up to four vertices (connected by three edges) determined from the molecular graph. While each bond leads to one parameter, the presence of linear or cyclic subfragments (see Figure 1) defines the balance between angles and dihedral parameters. The ACS and CNM plots of test examples give a flavor of the rich information obtained in normal vibrational modes, for example, by shedding new light on the clustering of local vibrational modes in molecular motions of fragments (see Figure 1) or the change of vibrational modes upon substitution which lowers the symmetry.

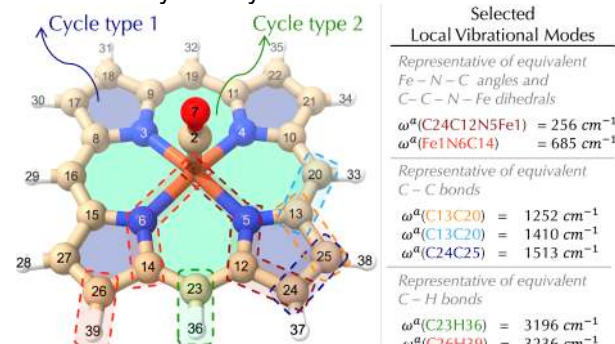


Figure 1. Selected local mode frequencies of Fe(II)-porphyrin coordinated with CO indicating corresponding parameters in the structure. Cycles are indicated as well.

Our new protocol has facilitated the investigation of a diverse array of systems.

CONCLUSIONS

Our new protocol LModeAGen is a significant advance for routine local mode analysis in intricate and extensive systems. Our approach facilitates obtaining reliable LVM parameters for generic systems with over ca. 60 atoms, an achievement made possible only by our new protocol.

REFERENCES

- ¹ Moura Jr., R. T.; Quintano, M.; Antonio, J. J.; Freindorf, M.; Kraka, E.; J. Phys. Chem. A, 2022, 126, 9313–9331.
- ² Zou, W.; Moura Jr., R.; Quintano, M.; Bodo, F.; Tao, Y.; Freindorf, M.; Makós, M.Z.; Verma, N.; Cremer, D.; Kraka, E. LModeA2023. CATCO, SMU: Dallas, TX, USA, 2023.
- ³ Moura Jr., R. T.; Quintano, M.; Santos-Jr, C. V.; Albuquerque, V. A. C. A.; Aguiar, E. C.; Kraka E.; Carneiro Neto, A. N; Opt. Mat. X, 2022, 16, 100216.

ACKNOWLEDGEMENTS

NSF Grant CHE 2102461; SMU's Center for Scientific Computing for providing generous computational resources.

Density Functional Theory Investigation of the Contributions of π - π Stacking and Hydrogen Bonding to the Supramolecular Aggregation Interactions of Asphaltene Heterocycles

Milena D. Lessa (PQ),^{1*} João Victor S. B. de Mello (PG)¹ Stanislav R. Stoyanov (PQ),^{2*} José Walkimar M. Carneiro (PQ),¹ Leonardo M. da Costa (PQ).³

lmcosta@id.uff.br, stoyanov@ualberta.ca

¹Programa de Pós graduação em Química, Universidade Federal Fluminense, CEP 24020-141, Niterói-RJ.

²Natural Resources Canada, Canmet ENERGY Devon, 1 Oil Path Drive, T9G 1A8 Devon, Alberta, Canada.

³Departamento de Química Orgânica, Universidade Federal Fluminense, CEP 24020-150, Niterói-RJ.

Palavras-Chave: Heterocycles Dimers; DFT; Interaction Analysis; Chemical Scaling.

INTRODUCTION

The aggregation of asphaltenes, the heaviest fraction of petroleum, is associated with the formation of organic chemical scaling that severely reduces the oil recovery. The precipitation occurs practically along all the production line, transport and upgrading, thus being a challenge to industry [1]. The affinity of these molecules is driven by a complex supramolecular sum of electrostatic, dispersion, orbital and acid-base interactions [2]. In the present study, we compared the interaction strength of hydrogen bonding and π - π stacking in stacked homodimers of asphaltene heterocycles (containing N, O and S atoms) linked by water bridges to evaluate the strongest driven interaction.

METHODS

DFT calculations were performed in Gaussian09 with the wB97X-D functional and the Def2-SVP basis set. The B3LYP/Def2-SVP method was employed for the EDA using the GAMESS software. The non-covalent interactions were also analyzed using NCIplot software. The heterocycles pyridine, thiophene, isoquinoline and furan are selected due to their presence as moieties in asphaltene structures [2]. Additionally, the heterocycles pyrazine, 1,3-oxazole and 1,3-thiazole were included to study aromatic compounds with two heteroatoms. The dimerization of each heterocycle was calculated with 0, 1, 2 and 3 water molecules forming a bridge between the organic moieties (Figure 1).

RESULTS

The geometries of the 28 homodimers with and without water molecules were fully optimized. Additionally, frequency calculation was performed to confirm that the optimized geometry was a genuine minimum on the potential energy surface.

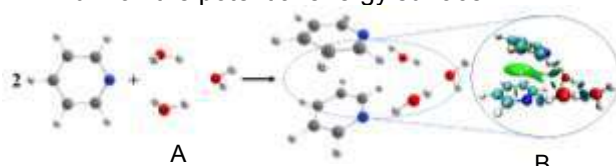


Figure 1. (A) Dimerization reaction of pyridine with a 3 water molecules bridge. (B) Stabilizing non-covalent interactions map obtained with NCIplot.

The enthalpy (ΔH) and Gibbs free energy (ΔG) for the supramolecular aggregation were calculated. The π - π stacking interaction ΔE_{INT} between the rings in each dimer structure was accounted using the ASM method [3]. The distance (D) between the planes of the aromatic rings was also obtained. The NCI plots of the optimized structures of the supramolecular aggregates were used to examine the non-covalent interactions between the monomers in the dimer structure and between the monomers and water bridges. The analysis shows that the green area (weak interactions) corresponds to the π -stacking interaction between the heteroaromatic rings. We also have light blue areas representing strong attractive interactions due to hydrogen bonding.

CONCLUSION

The distance between the planes of the aromatic rings is correlated with the π - π stacking interaction strength. All the dimerization reactions are exothermic and not spontaneous. This is mostly modulated by the strength of the hydrogen bond of the water bridge and the π - π stacking interaction. Dimers bridged by two water molecules are the most stable. The magnitude of the hydrogen bond and the π - π stacking interaction is similar. EDA results show that the electrostatic and polarization components are the main stabilizing terms for the hydrogen bond interaction in the bridge, with almost 80% for all dimers. The non-covalent interaction analysis confirms the molecular sites that have the strongest (hydrogen bond) and weak (π - π stacking) attractive interactions. They are concentrated in the water bridge (localized interactions) and in the plane between the aromatic rings (delocalized interactions), respectively.

REFERENCES

- Ali, S. I. et al. *Pet. Explr. Prod. Technol.* **2021**, 11, 3599.
- Ok, S.; Mal, T. K.; *Energy Fuels.* **2019**, 33, 10391.
- Fernández, I.; Bickelhaupt, F. M.; *Chem. Soc. Rev.* **2014**, 43, 4953.

ACKNOWLEDGMENT

Reaction mechanism of furan oxidation by OH radical: A protocol for kinetic studies

Joel Leitão Nascimento (PG),^{1*} Murillo H. Queiroz (PG),¹ and Tiago Vinícius Alves (PQ)¹.

joeInascimento@ufba.br

¹Departamento de Físico-Química, Instituto de Química - Universidade Federal da Bahia, Rua Barão de Jeremoabo, 147, Salvador, 40170-115, Bahia, Brasil.

Palavras Chave: Atmospheric, Furan, SOA, Protocol, Kinetics.

INTRODUCTION

Furans are volatile organic compounds (VOCs), considered atmospheric pollutants, generally emitted by burning biomass. The presence of these compounds in the atmosphere, followed by their degradation, resulted in the formation of secondary organic aerosols (SOA), responsible for decreasing air quality. In this context, theoretical and experimental studies aimed to understand the tropospheric degradation mechanisms of furanic compounds by the OH, O₃, and NO₃ radicals. Lee and Tang¹ determined experimentally kinetic parameters for the reaction of furan with OH. Previous theoretical results² employing TST and RRKM approaches provide the rate constant with one order of magnitude from the experimental study. Based on this discrepancy, this work aims to provide a mechanistic overview of the furan + OH reaction through a kinetic protocol that includes multiple structures and torsional anharmonicity effects.

METHODS

In this work, we employ M06-2X/aug-cc-pVTZ for geometry optimizations, conformational searches, and rate coefficient calculations. The MPW1K/aug-cc-pVTZ were used to calculate anharmonic scale factors (λ^{ZPE}). Conformational searches were performed using the TorsiFlex code. Rate coefficients for each elementary reaction were obtained using multistructural canonical variational transition state theory with small curvature tunneling corrections (MS-CVT/SCT). The influence of the pre-reactive complexes was evaluated with the Canonical Unified Statistical Model (CUS), combining the long-range transition state theory (LR-TST) and MS-CVT/SCT approaches. Furthermore, the overall rate coefficients were calculated by Kinetic Monte Carlo (KMC). All geometry optimizations were performed using the Gaussian 09. The MS-CVT/SCT rate constants and KMC simulations were carried out with the Pilgrim code.

RESULTS

Based on the geometry optimizations and frequency calculations of the stationary points, we constructed the energy profile, Figure 1, for the

oxidation reaction of furan with OH. We verified that the anharmonic scale factors for OH ($\lambda^{\text{ZPE}} = 0.978$) reproduce the experimental ZPE with only a discrepancy of 0.02 kcal/mol. Therefore, the λ^{ZPE} is considered to be applicable to all stationary points.

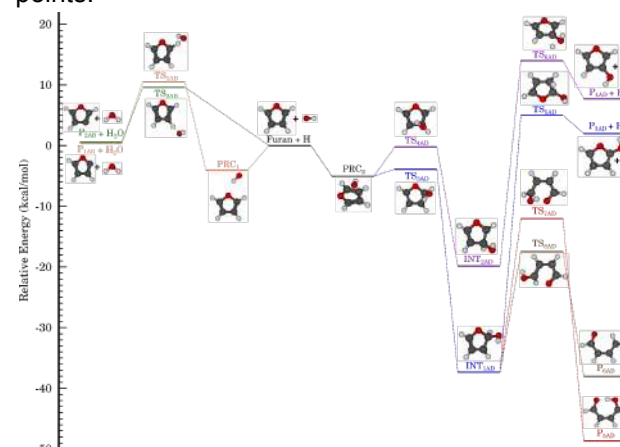


Figure 1 - Relative energies of the stationary points (in kcal/mol) on the potential energy surface for the Furan + OH reaction.

Through KMC simulations, we identify that P_{6AD} (4-hydroxybut-2-enal radical), at 298.15 K, is majority formed (approximately 90%). The overall rate coefficient for this mechanism at the same temperature is $6.40 \times 10^{-11} \text{ cm}^3 \text{ molecule}^{-1} \text{ s}^{-1}$. This value agreed with the experimental result reported by Bierbach et al.³ ($4.19 \times 10^{-11} \text{ cm}^3 \text{ molecule}^{-1} \text{ s}^{-1}$). According to our results, the tropospheric residence time of furan in the atmosphere is 9h, corroborating the experimental results.

CONCLUSIONS

Based on the KMC simulations, we identified that the most favorable product channel, at 298.15 K, is the 4-hydroxybut-2-enal radical. Our overall thermal rate constants are also shown in good concordance with the experimental results.

REFERENCE

- [1] J. Lee and I. Tang, *J. Chem. Phys.*, 1982, 77, 4459.
- [2] Mousavipour et al., *J. Phys. Chem. A*, 2009, 113, 2838.
- [3] Bierbach et al., *Atmos. Environ., Part A*, 1992, 26, 813.

ACKNOWLEDGMENT

CNPq, CAPES and CNPq/AWS (Grant No.421795/2022-0).



Exploring the influence of explicit solvation and ion interactions on energy barriers for the photodegradation reaction of sulfapyridine

José Luiz Felix Santos (PG)¹, Gabriel Luiz Cruz de Souza (PQ),² Roberto Luiz Andrade Haiduke (PQ)¹

jlfelix@felix.br ; haiduke@iqsc.usp.br ; gabrielucs@pq.cnpq.br

¹Department of Chemistry and Molecular Physics, São Carlos Institute of Chemistry, USP, São Carlos – SP;

²Natural Science Center – Campus Lagoa do Sino, UFSCar, Buri – SP.

Keywords: Sulfapyridine, photodegradation, Gibbs activation energies, solvation effects, DFT.

INTRODUCTION

Sulfonamides constitute one of the most widely used classes of antibiotics, being among the first of these compounds to be synthesized.¹ They are prescribed in both human and veterinary medicine and, due to their extensive use, the contamination of water bodies by sulfonamides also generates negative consequences for the environment and human health.^{2,3} Thus, in order to contribute to the investigation of degradation methodologies, we carried out a computational study about the effects of explicit solvation and interactions with ions (Mg^{2+} , Zn^{2+} , Br^- , Cl^- , and NO_3^-) on the energy barrier of the rate-determining elementary step of the sulfapyridine (SPY) photodegradation mechanism via triplet-sensitized SO_2 extrusion.

METHODS

Geometry optimizations and calculations of harmonic vibrational frequencies in the ground state (S_0) and in the lowest triplet excited state (T_1) were done by using a Density Functional Theory (DFT) approach with dispersion corrections and a triple- ζ basis set, PBE-D3/cc-pVTZ. The solvent effect of water was considered by the polarizable continuum method (PCM) and also by the inclusion of a few explicit water molecules. Thermodynamic quantities were determined at 298 K. All electronic structure calculations for the stationary points along the reaction coordinate (reactants, intermediates, transition states and products) were performed within the Gaussian 09 package⁴ and the Gibbs energy values obtained were corrected to the standard concentrations using the GoodVibes software⁵.

RESULTS

First, the lowest energy structure that favors the photodegradation mechanism was found from a preliminary conformational analysis. However, unlike what was previously observed in the literature⁶, T_1 excitation leads to spontaneous SPY fragmentation. The rate-determining step of the SPY photodegradation reaction was carefully investigated and the Gibbs energies of activation (ΔG_{act}) seen in Table 1 are given by

$$\Delta G_{act} = \Delta G_{TS} - \Delta G_R . \quad (1)$$

where Gibbs energies of transition states (ΔG_{TS}) and reactants (ΔG_R) were computed in the standard state.

Table 1 – Gibbs energies of activation (ΔG_{act}) of the SPY photodegradation rate-determining reaction as given by the DFT/PBE-D3/cc-pVTZ level in water with PCM and PCM plus one (+1W) and two (+2W) explicit solvent molecules (in kcal mol⁻¹).

	PCM	+1W	+2W
SPY	16.15	13.53	10.54
SPY-Mg ²⁺	-4.43	-12.18	-20.98
SPY-Zn ²⁺	-10.10	-26.77	-26.26
SPY-Cl ⁻	13.80	8.68	8.02
SPY-Br ⁻	14.52	11.76	8.32
SPY-NO ₃ ⁻	13.96	-	6.10

CONCLUSIONS

First, the interaction with cations lowered the height of the reaction barrier for SPY photodegradation. However, the inclusion of explicit water molecules shows that this effect can be underestimated with PCM. The effect on anions is less relevant.

REFERENCES

- ¹ F. Carta; A. Scozzafava, C.T. Supuran, Expert opinion on therapeutic patents (2012), 22, 747.
- ² P. Sukul, M. Spiteller, Reviews of environmental contamination and toxicology (2006), 67.
- ³ X. Yang *et al.*, Chemical Engineering Journal (2021), 405, 126806.
- ⁴ M.J. Frisch *et al.*, Gaussian 09, Revision D.01, Gaussian, Inc., Wallingford CT, 2013.
- ⁵ G. Luchini *et al.*, F1000Research (2020), 9, 291.
- ⁶ H. Zhang *et al.*, Chemosphere (2018), 191, 1021.

ACKNOWLEDGMENTS

The authors thank the institutions that provided infrastructure and funding for this project: IQSC-USP, CNPq (141684/2022-4) and FAPESP (2022/14780-7 and 2022/05138-0).



Estudo teórico sobre adsorção de fosfato em minerais ricos em alumínio.

Jared S. Martins (PG),¹ Viviane S. Vaiss (PQ),¹ Jonathan B. Brum (PG),¹ Luciano T. Costa (PQ),¹ Deyse G. Costa (PQ).^{2*}

jaredemartins@id.uff.br; deysegcosta@ufv.br

¹Instituto de Química – Universidade Federal Fluminense; ²Departamento de Química – Universidade Federal de Viçosa.

Palavras Chave: (*Gibbsita, Fosfato, DFT, solo*).

INTRODUÇÃO

Um dos grandes desafios do agronegócio brasileiro é a dependência da importação de fósforo (P) e outros fertilizantes. Além das flutuações do mercado internacional, o agronegócio sofre com o intemperismo do solo brasileiro, que torna baixa a disponibilidade de P em decorrência da sua interação com os componentes do solo tais como argilas, óxidos e hidróxidos de ferro e alumínio (hematita e gibbsita), tornando-o indisponível às plantas.^{2,3} A imobilização desse macronutriente no solo ou liberação para as plantas depende marcadamente do pH, das propriedades físico-químicas e mineralógicas do solo.¹ É de notar que são várias as questões que enlaçam e interpenetram com a questão do uso eficiente do fósforo como fertilizante, e dada a sua complexidade muitas propostas de estudo e soluções podem ser levantadas. Desta forma, o objetivo deste trabalho é desenvolver estudos teóricos a fim de ampliar a compreensão acerca do mecanismo de reação da adsorção de íons fosfato (HPO_4^{2-} e $H_2PO_4^-$) em gibbsita ($\alpha\text{-Al(OH)}_3$), um mineral rico em alumínio.

MÉTODOS

Realizou-se a caracterização estrutural e energética de todas as espécies envolvidas no processo de adsorção dos íons fosfato nas superfícies (001) e (100) da gibbsita. As simulações foram desenvolvidas com base na Teoria do Funcional da Densidade (DFT) e executadas com o Quantum-Espresso, software de livre distribuição pela General Public License.⁴ A superfície do mineral adsorvente foi modelada com condições de contorno periódicas, funcionais de troca e correlação GGA do tipo PBE, método PAW para descrever os núcleos e os elétrons internos, e conjunto de bases de autofunções dado por ondas planas.

RESULTADOS

Os testes de convergência indicaram que os valores de energia de corte de 40 Ry e amostragem de pontos k de $4 \times 4 \times 4$ são suficientes para descrever o sistema. Para a simulação das adsorções foi necessário a construção de uma superfície. Para tanto, foram investigadas supercélulas construídas através de dois modelos: o primeiro monolamelar com dimensões $2 \times 3 \times 1$ e o segundo bilamelar com

dimensões $1 \times 2 \times 1$. Em ambas foi inserida uma camada de vácuo de 12 Å. As análises de estabilidade mostraram que apenas a superfície bilamelar é adequada para os estudos de adsorção. Para a avaliação da adsorção dos íons fosfato na superfície (001) foram analisados a formação de complexos monodentados e bidentados. A análise dos resultados sugere que a imobilização dos grupos fosfatos se dá pela alta estabilidade que é alcançada, quando o fosfato é adsorvido na superfície formando um complexo monodentado. Tendo em vista a importância da água para o transporte de nutrientes no solo, sua influência foi avaliada em três condições: I-complexos bidentados e monodentados na presença de água, II-formação de complexos de esfera interna, na qual ocorre fisssorção do H_3PO_4 na presença de água e III-formação de complexo de esfera externa, na qual existem moléculas de água entre o H_3PO_4 e a superfície. A presença de água na superfície contribui favoravelmente para a formação de complexos de esfera externa.

CONCLUSÕES

Com a execução deste trabalho, conclui-se que uma superfície bilamelar é um modelo mais adequado para a simulação da superfície da gibbsita. Na investigação da adsorção do fosfato na superfície (001), apenas os complexos formados através do modo de coordenação monodentado se mostraram energeticamente favoráveis. Na presença de água, o complexo de esfera externa se mostrou mais energeticamente favorável. Análises futuras irão permitir avaliar o comportamento para a superfície (100).

REFERÊNCIAS

- A.F.C. Bahia Filho, et al. Revista Brasileira de Ciência do Solo, 1983, v 7, p. 221-226,
- P. S. Pavinato. C. A. Rosolem. Revista Brasileira de Ciências do Solo, 2008 v.32, p. 911-920.
- I. C. Mendes, F. B. Reis júnior. Embrapa Cerrados. 2003.
- P. Giannozzi , et al. Journal of Physics: Condensed Matter, 2009 v.21, p. 395502-395521.

AGRADECIMENTOS

Agradeço à CAPES pelo apoio de fomento, Ao Grupo MolMod-CS da UFF e ao cluster da UFV pela disponibilização de sua infraestrutura computacional.

Theoretical GFN2-xTB study of the inclusion of Linuron, Diuron, and Neburon into β -CD

Carolina Lúcia Cardoso Ribeiro (UR)¹, Júlia Alves Ferreira (UR)¹, Cleber Paulo Andrade Anconi (R)¹ (UR)

carolinalcribeiro@gmail.com; julia.ferreira9@estudante.ufla.br; cleberanconi@ufla.br

¹Laboratório de Química Fundamental (LQF), Department of Chemistry, Institute of Natural Sciences, University of Lavras, Lavras-MG, 37200-900, Brazil

Keywords: pesticides, cyclodextrin, host-guest system, GFN2-xTB, UD-APARM

INTRODUCTION

Cyclodextrins (CDs) are cyclic oligosaccharides formed through the degradation of starch. Their structure comprises a hydrophilic exterior and a hydrophobic cavity that can accommodate distinct organic molecules. These compounds have demonstrated efficacy as pesticide complexation agents [1]. Experimentally, the determination of formation constants for inclusion complexes between cyclodextrins and pesticides has been reported.

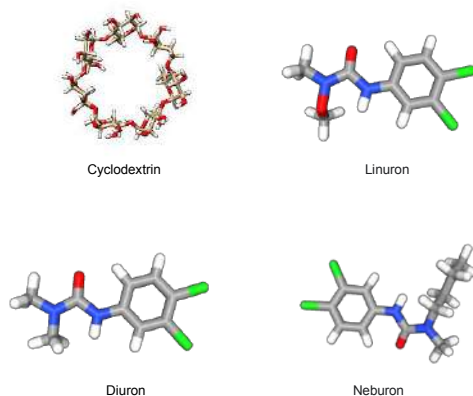


Figure 1. Host (cyclodextrin) and guests (linuron, diuron, neburon) studied herein

METHODS

- Each system was studied, considering 300 and 792 supramolecular starting systems.
- The UD-APARM program [2] was employed in constructing these systems.
- The GFN2-xTB method was utilized to obtain the theoretical data [3].
- Following optimizations and determination of Gibbs free energy in the condensed phase, log K values were obtained for the inclusion compounds DIUR@ β -CD, NEBU@ β -CD, and LINU@ β -CD in a multi-equilibrium scope [4].

RESULTS

The logarithmic values of the formation constant increased with a broader scan range (Table 1). However, the experimental trend was not achieved. The Potential Energy Surface (PES) will be further

explored since the approach gives reasonable results [4].

Table 1. Equilibrium constants obtained by the semiempirical method GFN2-xTB ($\log K_{xTB}$)

Pesticides	Log of binding constant		
	Expt ^{5,6}	300 points	792 points
DIU@ β CD	2.10	5.03	6.30
NEB@ β CD	2.26	4.72	5.14
LIN@ β CD	2.81	3.50	3.85

CONCLUSIONS

The logarithmic values of the formation constant increased with a broader scan range. The experimental trend was not achieved, and additional exploration of the GFN2-xTB PES has to be conducted.

REFERENCES

- ¹FLAHERTY, Ryan J.; NSHIME, Bertil; DELAMARRE, Michael; DEJONG, Sam; SCOTT, Pamela; LANTZ, Andrew W., Chemosphere 91 (2013) 912–920
- ²Anconi, C. P. A. Acs Omega 2020, 5 (10), 5013-5025.
- ³C. Bannwarth, S. Ehliert, S. Grimme. J. Chem. Theory Comput. 15 (2019) 1652–1671.
- ⁴C. P. A. Anconi and L. C. A. Souza, Comput. Theor. Chem., 2022, **1217**, 113916.

ACKNOWLEDGMENTS

The authors thank Professor Hélio Ferreira dos Santos for the access to the NEQC (Núcleo de Estudos em Química Computacional, UFJF, Brazil) computer facility and also thanks the Laboratório Central de Computação Científica (LCC) of UFLA for providing additional computing resources. Furthermore, professor Cleber Paulo Andrade Anconi also thanks the Fundação de Amparo à Pesquisa do Estado de Minas Gerais (FAPEMIG) for supporting the Laboratório de Química Fundamental (LQF), where the research was conducted.

Estudo de Caminhos de Energia Mínima na Transição de Fases Entre Alótropos de Carbono

Geisa Pires N. Lima (PG),¹ Ricardo Rodrigues de O. Junior (PQ),² Pierre Mothé Esteves (PQ).^{1*}

geisapiresnogueira@gmail.com; pesteves@iq.ufrj.br

¹Avenida Athos da Silveira Ramos, nº 149, Bloco A, 6º andar, sala 607; 3º andar, sala 304.

Palavras-Chave: Alótropos de Carbono, Transição de Fases, DFT, NEB.

INTRODUÇÃO

Alótropos de carbono são compostos baseados apenas em carbono que podem assumir diversas estruturas cristalinas. A miríade de compostos de carbono que podem ser idealizados e sintetizados é extensa, assim, a busca teórica e experimental por novos alótropos e sua caracterização experimenta vertiginoso crescimento desde o isolamento e caracterização do grafeno em 2004¹. Apesar dos mecanismos que levam uma fase alotrópica a outra não serem bem estabelecidos, alguns estudos exploram essas transições de fase de forma teórica e experimental^[2,3]. Neste trabalho, serão estudadas as transições entre carbina e grafeno, carbina e bifeníleno, e grafite e diamante, através de cálculos de Caminho de Energia Mínima (*Minimum Energy Path* – MEP), analisando qualitativamente as estruturas intermediárias em termos de modos normais⁴ vibracionais dos alótropos de partida.

MÉTODOS

Os cálculos periódicos de otimização e modos normais vibracionais das células de carbina (32 átomos e 24 átomos), bifeníleno, grafite e diamante foram realizados em nível DFT (PBE, base de ondas planas, $E_{corte} = 540$ eV). Os cálculos dos MEPs foram realizados com o método *Nudged Elastic Band* (NEB) com e sem a aproximação de *Climbing Image* (CI) em nível DFT (PBE, base de ondas planas, $E_{corte} = 410$ eV).

RESULTADOS

As otimizações das células unitárias dos alótropos mostrou uma diminuição nos parâmetros das células em todos os casos. Os modos normais vibracionais calculados foram comparáveis aos valores da literatura para todos os alótropos calculados. Os cálculos dos MEPs para as 3 transições (Figuras 1, 2 e 3) indicaram que as estruturas intermediárias passam por distorções qualitativamente semelhantes aos modos vibracionais indicados.

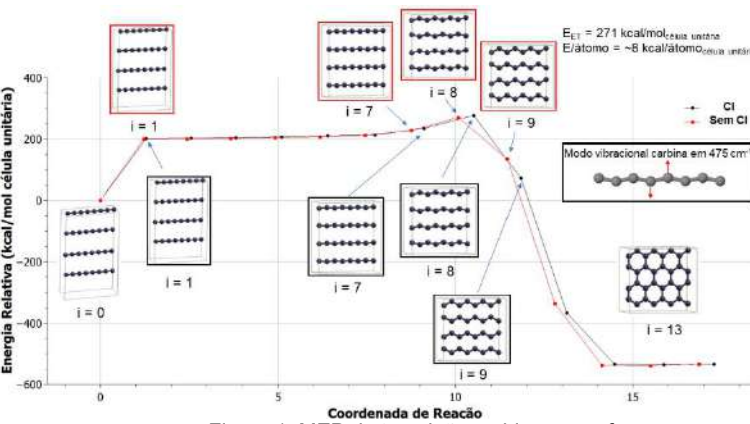


Figura 1: MEP da transição carbina → grafeno

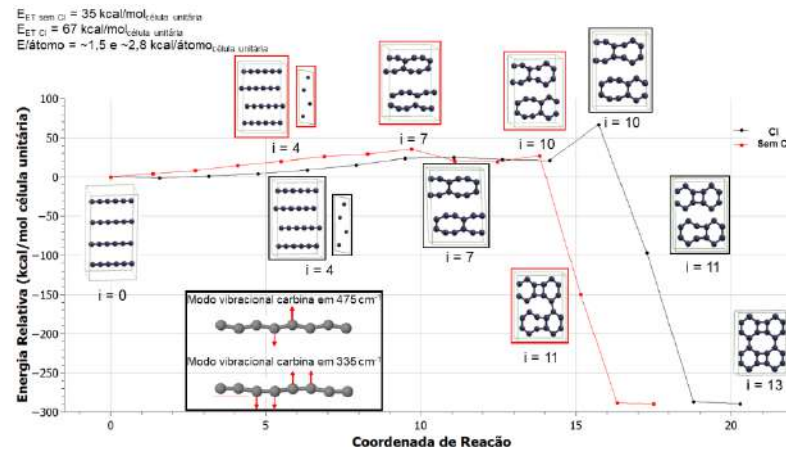


Figura 2: MEP da transição carbina → bifeníleno

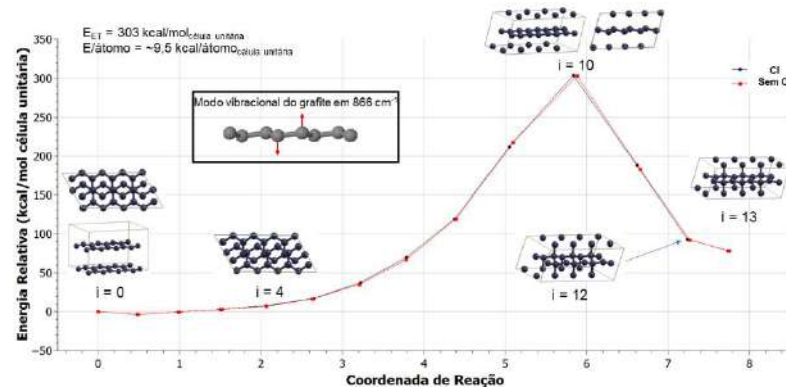


Figura 3: MEP da transição grafite → diamante

CONCLUSÕES

Ao diminuir os parâmetros de célula, as cadeias de carbinas e folhas de grafite se alinham para gerar novas fases alotrópicas, passando por estruturas intermediárias que seguem qualitativamente 1 ou mais modos vibracionais para grafeno, bifeníleno e diamante ($E_{ET} = 268$, 35 e 67, e 303 kcal/mol de célula unitária, respectivamente).

REFERÊNCIAS

- NOVOSELOV, K. S., et al. Science. 2004, 306, 666-669.
- DONG, X., et al. Journal of Physics: Condensed Matter, 2013 v. 25. p. 145402.
- O'BANNON, et al. Diamond and Related Materials, 2020. 107876.
- Oliveira, F. L. Estudo de novos alótropos de carbono usando Teoria do Funcional da Densidade. 2020. – Dissertação de mestrado.

AGRADECIMENTOS

CNPq, CAPES, FAPERJ, LNCC, NACAD, DIRAC

Investigação Teórica de Espécies com Ligação Mg–C, MgC_nH , de Interesse Astrofísico

Anna Karolyna M. S. Gomes (PG),¹ Felipe Fantuzzi Soares (PQ),² Thiago M. Cardozo (PQ).^{1*}

gomes.ak@pos.iq.ufrj.br; thiago@iq.ufrj.br

¹Av. Athos da Silveira Ramos 149, Rio de Janeiro 21941-909, Brasil.

²Park Wood Rd, Canterbury CT2 7NH, UK.

Palavras-Chave: Magnésio, Astroquímica, DFT, Coupled-Cluster.

INTRODUÇÃO

Desde 1993, compostos de magnésio têm sido encontrados em ambientes interestelares e, mais recentemente, espécies como MgC_4H [1], MgC_2H [2] e MgC_6H [3] foram detectadas, embora espécies do tipo $MgC_{(2n+1)}H$ continuam sem serem detectadas. Devido à dificuldade de obtenção de dados experimentais sobre essas moléculas, estudos teóricos podem ser muito importantes para auxiliar na detecção dessas espécies. Este estudo tem como objetivo investigar as estruturas de isômeros de baixa energia das fórmulas químicas MgC_nH , com n variando de 4 a 6. Além disso, busca-se obter propriedades espectroscópicas e termoquímicas relevantes para esses compostos, a fim de orientar pesquisas futuras relacionadas a essas moléculas e auxiliar na seleção de possíveis alvos para tentativas de detecção astronômica.

MÉTODOS

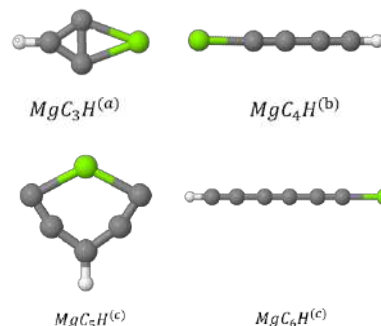
Cálculos teóricos foram realizados para MgC_nH , $n=4,5,6$. As geometrias iniciais foram geradas usando o software CLUSTER 1.0 em nível UB3LYP-def2-SVP e as geometrias foram reotimizadas usando UB3LYP/aug-cc-PTVZ. Os cálculos de energia e as densidades de spin foram realizados usando CCSD(T)/aug-cc-PTVZ na geometria mínima obtida usando DFT. Para validar o uso de métodos de referência única, cálculos SA-CAS(5,5)/def2-SV(P) também foram realizados para algumas das moléculas obtidas. Os cálculos de estrutura eletrônica foram realizados usando o software ORCA 5.0.3.

RESULTADOS

Foram obtidos 2, 11 e 6 isômeros abaixo do limite de 50kcal/mol para $n=4,5$ e 6, respectivamente. Os dados obtidos para o isômero de menor energia do MgC_4H são concordantes com os reportados na literatura [4]. Além disso, verificou-se que para n par, a geometria mínima global é linear enquanto para n ímpar, obteve-se geometria cíclica, conforme ilustrado na figura 1.

Figura 1 Isômeros menor de baixa energia para a fórmula química MgC_nH . $n=3,4,5,6$. (a) UwB97XD75/6-311++G(2d,2p) [4] (b)

CCSD(T)/aug-cc-pVTZ [5]. (c) UB3LYP/aug-cc-PVTZ.



As geometrias lineares, MgC_4H e MgC_6H , apresentaram alternância de comprimentos de ligação C–C, indicando uma estrutura poliínica. Além disso, a densidade de spin apresentou componente majoritária sobre o átomo de magnésio. No caso da estrutura de mínimo do MgC_5H a densidade de spin apresentou componente sobre 3 átomos de carbono e os comprimentos de ligação C–C são intermediários entre ligações triplas e duplas ou simples e duplas, indicando possíveis estruturas de ressonância.

CONCLUSÕES

Isômeros de baixa energia foram obtidos para MgC_nH , $n=4,5,6$. Além disso, parece haver um padrão para as geometrias de menor energia para diferentes valores de n , de modo que, estruturas de n par são lineares e para n ímpar observou-se estruturas cíclicas.

REFERÊNCIAS

- 1 Cernicharo, José, et al. *Astronomy & Astrophysics*. 2019, 630, L2.
- 2 Agúndez, Marcelino, José Cernicharo, and Michel Guélin. *Astronomy & Astrophysics*. 2014, 570, A45.
- 3 Pardo, Juan Ramón, et al. *Astronomy & Astrophysics* 652 (2021): L13.
- 4 Baldea, Ioan.. *Monthly Notices of the Royal Astronomical Society*. 2020, 498, 4316.
- 5 Panda S., et al. *The Journal of Physical Chemistry A*. 2022, 126 (27), 4465.

AGRADECIMENTOS

O presente trabalho foi realizado com apoio do Conselho Nacional de Desenvolvimento Científico e Tecnológico (CNPq).

Predicting first hyperpolarizability of new stilbene-quinones hybrids with potential technological application

Júlio P. C. Oliveira (PG)^{1*}, Diego F. S. Paschoal (PQ)¹

oliveira.julio@ufrj.br; diegopaschoal01@gmail.com

¹Núcleo de Química Teórica e Computacional de Macaé, Polo Ajuda, Instituto Multidisciplinar de Química, Centro Multidisciplinar UFRJ-Macaé, Universidade Federal do Rio de Janeiro, Macaé, RJ, Brazil.

Keywords: First hyperpolarizability, Stilbene-quinones hybrids, DFT, Basis Sets, NLO.

INTRODUCTION

Molecular materials that have nonlinear optical (NLO) properties are studied due their technological applications¹. To intensify the NLO properties, the inclusion of electron acceptor (A) and donor (D) groups linked to π -conjugated electron system (D- π -A)² is required. Stilbenes are known in the literature to have NLO potential³. However, studies involving stilbene-quinones hybrids are scarce. Considering that the experimental obtaining of the NLO properties is a difficult task, theoretical calculations based in quantum mechanics can help to overcome this disadvantage³. From this, the present work aims to evaluate the first hyperpolarizability (β) for a group of stilbene-quinones hybrids present in literature, in addition to proposing a new set of stilbene-quinones hybrids aiming to intensify their NLO properties to potential technological application.

METHODS

The geometry of the studied compounds was optimized and characterized as stationary points on potential energy surface through harmonic frequency calculations at the B3LYP/6-31G(d,p)/IEF-PCM(UFF) level. For the calculations of β , the CAM-B3LYP/NLO-V/IEF-PCM(UFF) methodology³ was validated, using stilbene 4-amine-4'-nitrostilbene as reference. Subsequently, the methodology was applied to a set of stilbene-quinones hybrids⁴ for β evaluation, a 1907 nm laser was considered. From the stilbene-quinone hybrid named SQ04, new stilbene-quinone hybrids have been proposed. All calculations were performed using the GAUSSIAN 16 Rev. C.01 computational package, considering chloroform as the solvent.

RESULTS

The methodology for calculating β was validated, with a calculated value of 35×10^{-30} esu for the reference compound, showing excellent agreement with the experimental data of 40×10^{-30} esu. After validation, the methodology was applied to a set of stilbene-quinone hybrids. The calculated results showed that the addition of electron donor groups in the *para* position of the stilbene moiety, present the highest values of β for the stilbene-quinone hybrids found in the

literature. The compound named SQ04 had the highest value for β (65×10^{-30}). From compound SQ04, new molecules were proposed replacing electron acceptor groups in the quinone moiety. All substituents caused an increase in property. The compound named SQ04N14 had the highest β (144×10^{-30}) value. Then, new substituents evaluated in the stilbene moiety. The new evaluated substituents presented higher values for β when there was only substitution, with the substituents in the *para* position. The highest β value was obtained for compound named SQ04N25 (Figure 1), $\beta = 217 \times 10^{-30}$ esu. This β value is approximately 20 times higher than the unsubstituted stilbene-quinone hybrid (SQ01), and approximately 24 times greater than the experimental value of *para*-nitroaniline (9.2×10^{-30} esu), used as a reference to evaluate the potential application in NLO of a compound.

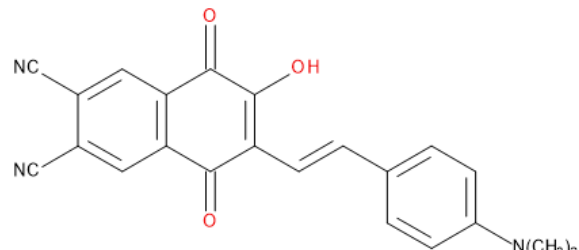


Figure 1. Proposed SQ04N25 stilbene-quinone hybrid that presented the highest β value.

CONCLUSIONS

In this study, it was found that the addition of electron donor groups on the stilbene moiety, and electron acceptor groups on the quinone moiety, significantly increases the β values of stilbene-quinone hybrids. The proposed stilbene-quinone hybrid, SQ04N25, which presented a β of 217×10^{-30} esu, showing a well-designed methodology for proposing new stilbene-quinone hybrids with potential technological application.

REFERENCES

- ¹E. Garmire, Opt. Express, 2013, 21, 30532.
- ²D. F. S. Paschoal et al., Bol. Ciência Macaé, 2022, 2, 8-26.
- ³D. Paschoal et al., J. Mol. Model., 2013, 19, 2079.
- ⁴F. C. Demidoff et al., Synthesis, 2017, 49, 5217.

ACKNOWLEDGMENTS

The authors would like to thank the Brazilian agencies FAPERJ (E-26/201.336/2022 – BOLSA and E-26/210.070/2022), CAPES (Finance Code 001), and Prefeitura Municipal de Macaé for the financial support.

Theoretical studies of decavanadate containing copper(II) complexes

Heloísa de Souza Camilo (PhD)¹, Lucas Gian Fachini (PhD)¹, Gabriel Barros Baptista (PhD)¹, Juliana Morais Missina (R)¹, Patrizia Rossi (R)², Paola Paoli (R)², Giovana Gioppo Nunes (R)¹, Eduardo Lemos de Sá (R)^{1*}.

edulsa@ufpr.br

¹Departamento de Química, UFPR, Brazil; ²Dipartimento di Ingegneria, Università degli Studi di Firenze, Firenze, Italy.

Keywords: (Decavanadate, copper(II), NCI, IGM, IBSI)

INTRODUCTION

Decavanadate (V_{10}) is a polyoxometalate used as a building block for creating supramolecular structures containing a second metal transition (M).¹ Herein, the atomically precise $\{[Cu_2(cyclen)_2](H_2V_{10}O_{28})\} \cdot 6H_2O$ (CuV_{10}), where cyclen = 1,4,7,10-tetraazacyclododecane, was studied. This compound presents unusual Cu-V₁₀ bonds that were explored through computational methods, such as Density Functional Theory (DFT), Non-Covalent Interaction (NCI), and Independent Gradient Model (IGM).

METHODS

The DFT modeling was performed on Gaussian16 using the molecular geometry obtained through crystallographic data in a single-point calculation, employing B3LYP/LANL2DZ theory level. Electrostatic potential surfaces (ESP) were generated from the DFT converged wave function, using the Multiwfn code; NCI and the IGM results were calculated through the IGMPPlot software.^{2,3} Finally, the IGM and its δg descriptor were used to evaluate the Intrinsic Bond Strength Index (IBSI).

RESULTS

The coordination mode of V_{10} to a second metal generally involves the terminal (V–O–M) or the bridged (V– μ_2 O–M) oxide groups. In the CuV_{10} , the unexpected V– μ_3 O–Cu coordination mode is described for the first time. Aiming to elucidate the interaction between V_{10} and the metal complex, ESP were generated for $[Cu(OH_2)(cyclen)]^{2+}$ and $[H_2V_{10}O_{28}]^{4-}$ isolated ions and for the complex CuV_{10} (Fig. 1).

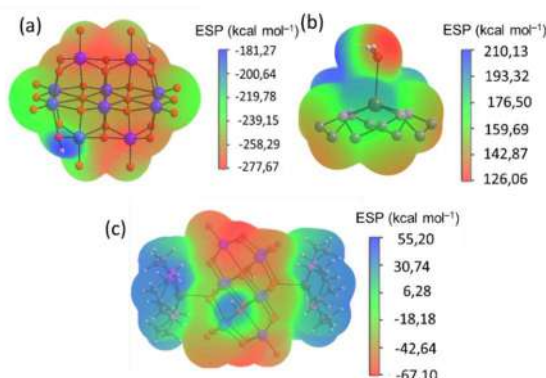


Figure 1. ESP for (a) $[H_2V_{10}O_{28}]^{4-}$, (b) $[Cu(OH_2)(cyclen)]^{2+}$ and (c) CuV_{10} .

Regions close to the triple-bridging oxide group of V_{10} , colored red, present the most negative electrostatic potential. On the other hand, the region near the copper(II) center in the precursor has positive potential, indicating attractive electrostatic forces between these fragments. The low IBSI values (Table 1) for both axial bonds in $[Cu(OH_2)(cyclen)]^{2+}$ and CuV_{10} indicate similar weak Cu–O covalent interactions, which is ca 2/3 of a usual coordination bond.

Table 1. IBSI values for Cu_{aqua} and CuV_{10}

Compound	Bonding	IBSI
$[Cu(OH_2)(cyclen)]^{2+}$	Cu–O	0.100
CuV_{10}	Cu– μ_3 O	0.105

The NCI analysis revealed that CuV_{10} exhibits strong intermolecular interactions between the V_{10} and copper(II) complex (Fig. 2), reflecting the N–H···O hydrogen bonds. Blue and green colored regions represent strong and weak attractive interactions, respectively.

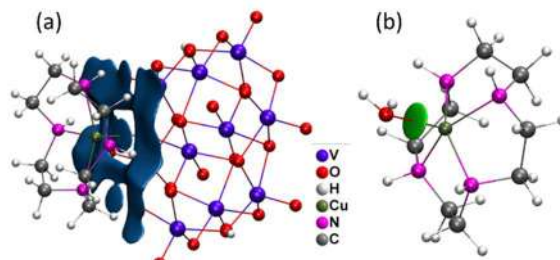


Figure 2. NCI for (a) CuV_{10} and (b) $[Cu(OH_2)(cyclen)]^{2+}$ isolated cation.

CONCLUSIONS

The analysis of ESP, IBSI and NCI results indicate that the formation of the CuV_{10} complex is not only related to the Cu–O covalent interaction but also due to the additional stabilization got by the particular conformation presented in Figure 1. The computational approach used here was a helpful tool for understanding the factors contributing to the prevalence of MV₁₀ complexes over ionic pairs.

REFERENCES

- D. Eder, et al. J. Inorg. Biochem. 2023, 239, 112067.
- R. Johnson, et al. J. Am. Chem. Soc., 2010, 132, 6498-6506.
- J. Klein, et al. J. Phys. Chem., 2020, 124, 1850-1860.

ACKNOWLEDGMENTS

LCPAD (UFPR) / CAPES/ CNPq / FUNDAÇÃO ARAUCÁRIA



Rumo a uma Ligação Nobre: Estudo Computacional de Complexos Metaestáveis Contendo Hélio.

Lucas A. L. Dias (PG),¹ Felipe Fantuzzi (PQ),² Thiago M. Cardozo (PQ).^{1*}

lucaraujo.quim@gmail.com; thiago@iq.ufrj.br

¹Av. Athos da Silveira Ramos 149, Rio de Janeiro 21941-909, Brasil.

²Park Wood Rd, Canterbury CT2 7NH, UK.

Palavras-Chave: Química de gases nobres, dicátons, compostos metaestáveis, astroquímica, química quântica.

INTRODUÇÃO

Os gases nobres não costumam participar nem perturbar os sistemas químicos, mesmo assim, existem importantes exceções.¹ Desde a descoberta de Bartlett, diversos compostos contendo xenônio foram sintetizados. Porém, compostos com gases nobres mais leves ainda são um grande desafio, apesar de serem possíveis. Por exemplo, núcleos de hélio são capazes de erodir superfícies de grafite, via formação rápida de moléculas (HeC)², relevante para tecnologia nuclear. Além disso, íons moleculares como HeH⁺, clusters do tipo He_xH⁺ e He₂H₂⁺ são de enorme interesse astrofísico.³ No presente trabalho, buscamos desenhar e prever a existência de dicátons de inserção (X-He-Y) contendo He ligado a elementos do grupo principal, pois não há evidência experimental para essas estruturas,¹ além de poderem atuar como um novo tipo de propelente.⁴ Procuramos ainda descrever o esquema de ligação nessas moléculas e suas principais vias de dissociação.

MÉTODOS

Cálculos exploratórios foram feitos (otimização e frequências) para algumas estruturas contendo hélio em nível wB97X-D3/def2-SVP. Os compostos de inserção testados foram [H-He-L]²⁺, [F-He-L]²⁺ e [L-He-L]²⁺, com L=CO, OC, CN, NC, HCN, HNC, BO, BOH, BN, BNH, CC, CCC, CCH, CCHe, NH₃, PH₃, carbenos NHC, aNHC e CAAC, além dos superhalogênios BO₂, BF₄⁻ e AlF₄⁻. Superfícies de energia potencial foram feitas variando a distância da ligação He-E a partir da geometria otimizada em nível DFT, onde E é um elemento do grupo principal. Em função do caráter multireferencial, as dissociações, foram investigadas utilizando métodos *State-Average* e *State-Specific* CASSCF, com uso dos métodos NEVPT2 e MRCI+Q, para inclusão dos efeitos de correlação eletrônica.

RESULTADOS

As estruturas de dicátons mais promissoras foram do tipo [L-He-L]²⁺ com ligantes com L= CO, HCN, HNC, CC, CCC e HeCC. Dentre as estruturas dos dicátons obtidas,

[HCN-He-NCH]²⁺ mostrou a menor diferença entre a distância de ligação calculada e a estimada utilizando raios covalentes. A Figura 1 mostra a curva de dissociação da ligação He-N mantendo fixas as outras ligações. A energia de dissociação estimada é de aproximadamente 16 kcal/mol.

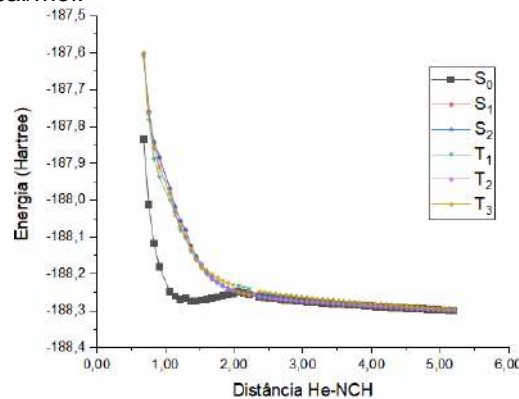


Figura 1: Superfícies de energia potencial para ligação He-NCH no dicáton [HCN-He-NCH]²⁺. Curvas obtidas utilizando SA-CASSCF(10,10)-MRCI+Q/def2-TZVPP. Todas as outras ligações são mantidas fixas.

CONCLUSÕES

Novos complexos de inserção contendo átomos de hélio ligado se mostraram promissores através de cálculos de DFT. Ligações curtas foram obtidas para as algumas moléculas como [HCN-He-NCH]²⁺ e [HeCC-He-CCHe]²⁺. Os resultados preliminares desse trabalho apontam para algumas estruturas de inserção inéditas contendo hélio. Verificou-se ainda que carbenos e superhalogênios não são particularmente interessantes para estabilizar as estruturas.

REFERÊNCIAS

- 1 R. Saha, et al. *Molecules*, 2019, v. 24, p. 2933.
- 2 E. Creutz, S. Cunningham, General Atomic Div. General Dynamics Corp., 1959, San Diego, Calif.
- 3 S. Jaksch et al. *Chem. Eur. J.*, 2009, v. 15, p. 4190-4194.
- 4 S. Falcinelli, M. Rosi, *Molecules* 2020, v. 25, p. 4157.

AGRADECIMENTOS

O presente trabalho foi realizado com apoio da Coordenação de Aperfeiçoamento de Pessoal de Nível Superior - Brasil (CAPES) e da Fundação Carlos Chagas Filho de Amparo à Pesquisa do Estado do Rio de Janeiro (FAPERJ).



Investigating Lipid Composition and Curvature in Osteoblast Membrane Mimetics: A Multi-Approach Study

Diane C. A. Lima (PhD)^{1*}, Pietro Ciancaglini (R)¹, Ana Paula Ramos (R)¹, Thereza A. Soares (R)¹
danelima@usp.br

¹Department of Chemistry, University of São Paulo, Ribeirão Preto, SP.

Keywords: Bilayer, Lipid Composition, Molecular Dynamic Simulation, Langmuir films.

INTRODUCTION

This project aims to explore the molecular mechanisms driving vesicle formation in osteoblast membranes, investigating how lipid composition and spatial variation impact membrane curvature. Employing an integrated approach, we combine computational membrane simulations with structural and thermodynamic methods, including Langmuir monolayers. The hypothesis being examined is that changes in lipid composition within the membrane alter the lamellar system's curvature, ultimately leading to vesicle formation¹. In the context of osteoblast membrane mimetics, different proportions of two characteristic lipids of this membrane class, sphingomyelin (SM) and ceramide (Cer), are examined to identify lipid ratios that induce alterations in membrane curvature²⁻³. Additionally, we conduct experiments to study the conversion of SM to Cer catalyzed by the enzyme sphingomyelinase (SMase).

METHODS

The present work presents both experimental and computational approaches, as shown below:

Atomistic Simulations

CHARMM-GUI online platform used for biomimetic membrane setup based on literature data. Bilayers are constructed with varying proportions of sphingomyelin (SM) and ceramide (Cer) lipids using CHARMM36 force field parameters⁴. Each bilayer: 256 lipids/monolayer, solvated with TIP3 water model, CaCl₂ concentration ~0.15 molar. Seven molecular systems simulated for 1 μs each, with duplication for validation. Analyses were performed by the SuaVE Software⁵.

Coarse-Grained Simulations:

Similar setup as Atomistic simulations using CHARMM-GUI platform and appropriate force field parameters. System tested: 25% Ceramide and 75% Sphingomyelin, enriched with DPPC and DPPE lipids. Five systems simulated for 12 μs each, duplicated. Analyses were performed by the SuaVE Software.

Experimental Procedure:

Lipid molecules palmitoyl sphingomyelin (SM) and palmitoyl ceramide (Cer) sourced from Avanti Polar Lipids®, purity 99%. Langmuir films are prepared by dissolving lipids in a 7:3 mixture of

chloroform (CHCl₃) and methanol (CH₃OH). Enzyme assays involving sphingomyelinase (SMase) conducted using enzymes from Merck® in Tris-based buffer solution. Langmuir films prepared using KSV Instruments mini Langmuir trough.

RESULTS

Preliminary findings suggest that osteoblast membrane mimetics with a 25% Ceramide proportion exhibit higher fluidity, while a composition of 75% Ceramide results in a nearly flat curvature profile. Both experimental findings and computational simulations consistently highlight the potential of the 75% SM - 25% Cer composition as the most promising proportion. The enzymatic conversion of SM to Ceramide, catalyzed by SMase, exhibits a qualitatively similar pattern to the control isotherm with the 75% SM - 25% Cer composition. This convergence in behavior between experimental and simulated data reinforces the robustness of our approach. Additionally, increased membrane compaction disturbs the conversion via SMase, underscoring the significance of membrane compaction/fluidity in this process.

CONCLUSIONS

The consistent alignment between experimental results and computational simulations, particularly in the context of the 75% SM - 25% Cer lipid composition, underscores the potential of our approach. This ongoing research not only contributes to our understanding of cellular dynamics but also lays the groundwork for future investigations in the realm of vesicle biogenesis and related cellular phenomena.

REFERENCES

- ¹ Helfrich, W. 28, 693–703 (1973).
- ² Jon V. Busto, Bruno Maggio, 2009, Biophysical J., 97, 2717-2726.
- ³ Bottini, M. et al. Biochimica et Biophysica Acta - General Subjects, V. 1862, 532-546, 2018.
- ⁴ J. Chem. Theory Comput. 2016, 12, 1, 405–413
- ⁵ Santos, D. E. S., Pontes, F. J. S., Lins, R. D., Coutinho, K. & Soares, T. A. J Chem Inf Model 60, 473–484 (2020).

ACKNOWLEDGMENTS

The completion of this academic summary would not have been possible without the funding and support from CAPES, CNPq, FAPESP and the HPC2N Supercomputing Center.

Electronic analysis of *n*-propyl xanthate complexes with group 12 metals: a theoretical-experimental study

Daniella B. Miranda (PG),¹ Susana Quintal (PQ)¹; Glaucio B. Ferreira (PQ).^{1*}

daniellabrito@id.uff.br; *glauciobf@id.uff.br

¹Programa de Pós-graduação em Química, Universidade Federal Fluminense, Niterói – RJ - Brasil

Keywords: Xanthates, UV-Vis spectroscopy, Zn²⁺, Cd²⁺, Hg²⁺

INTRODUCTION

Xanthates or dithiocarbonates ($R-OCS_2^-$) are organic compounds known for their application as a flotation agent, and exhibit electron density donor sulfur and oxygen atoms, allowing these compounds to coordinate in different ways with metal centers.¹ In coordination chemistry, spectroscopy in the UV-Vis region is one of the widely used to understand the M-L bond through the information provided by the electronic transitions.² In addition, this technique can be employed in different areas, since several substances have chromophores groups, such as carbonyl, carboxyl, among others.

METHODS

The theoretical calculations, realized for bidentate complexes of Zn(II), Cd(II), and Hg(II) with the *n*-propyl xanthate ligand, were performed with DFT level: M06L/6-311++G**+LANL2TZ-ECP with Gaussian 09 software. The electronic structure, its normal modes, and UV-Vis spectroscopy calculations with TD-DFT were used to investigate the components and parameters associated with experimental data of solids and solutions obtained in the 200-800 nm of these previously prepared compounds.³ Also, extended structure calculations were performed with M06L/LANL2TZ-ECP to understand solid-state properties. The population analyses were performed with GaussSum software.

RESULTS

Metal xanthate compounds can present different coordination modes. Thus, we consider in this study two different structures of *n*-propyl xanthate complexes with group 12 metals: Two S,S-bidentate coordinated xanthate ligands and a structure simulating a polymeric complex, in which it presents two monodentate ligands and two bridging xanthate ligands with another unit of the metal center. The experimental results showed bands around 220 and 300 nm in solid state spectra. In the solution, bands at 220, 240 and 300 nm were observed, as shown in figure 1 for the Zn²⁺ complex. Theoretical UV-Vis spectrum for the bidentate Zn²⁺ complex (blue), exhibit bands at 238, 266 and 309 nm, which was similar to the spectrum of the complex in solution (*n*-hexane). The same trend was observed for the Cd²⁺ and Hg²⁺ complexes. The force of the oscillator obtained in TD-DFT made it possible to associate the observed bands to the electronic transitions. Thus, in the Zn²⁺ complex the bands at 309, 266 and 238 nm were associated with the transitions H-1 → L+1, H-3 → L+1 and H-1 → L+2, respectively. In the bidentate Cd²⁺ complex, the HOMO → L+1 and H-2 → L+1 transitions were associated with

bands at 321 and 256 nm, respectively. Finally, Hg²⁺ complex showed H-3 → L+2 and H-4 → LUMO transitions, corresponding to the bands at 258 and 236 nm, respectively.

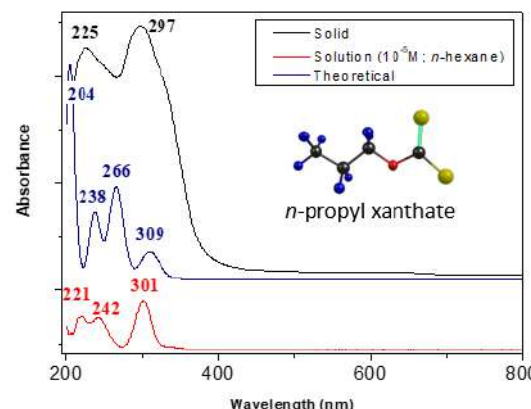


Figure 1. UV-Vis spectra for Zn²⁺ bidentate complex

Through population analysis, the orbitals involved in electronic transitions could be described, as showed in figure 2.

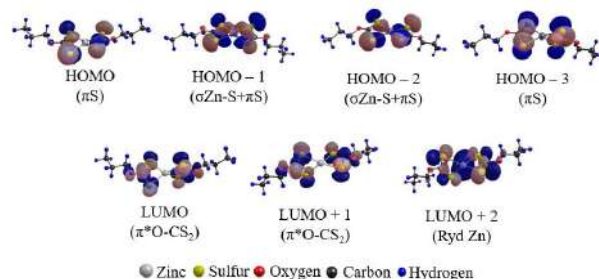


Figure 2. Molecular orbitals of the bidentate Zn²⁺ complex

CONCLUSIONS

Theoretical results indicated that the bidentate *n*-propyl xanthate complexes with the group 12 metals show similar profile to experimental UV-Vis analysis in solution (*n*-hexane). In addition, population analysis indicated the orbitals involved. Similar calculations of the polymeric complexes are being finalized.

REFERENCES

- E. J. Mensforth, R. Matthew, Inorg. Chem, 2013, 9, 403.
- Chen. Z., Dinh. H. N., Miller E., Springer Briefs in Energy, 2013.
- Miranda, D. B.: Complexos de íons metálicos do grupo 12 com ligantes xantatos: síntese, caracterização e cálculos computacionais; MSc Dissertation, UFF, RJ, Brazil, 2022.

ACKNOWLEDGEMENTS

CNPq, CAPES, FAPERJ, PROPPi UFF, and LMQC-UFF.

Effects of conformational flexibility and torsional anharmonicity on the products distribution of 2-pentanone + H reaction

Maiara Oliveira Passos (PG),¹ Tiago Vinicius Alves (PQ)^{1*}.

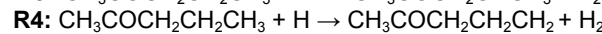
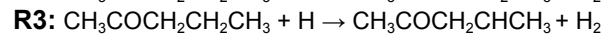
maiapassos05@gmail.com; tvinalves@gmail.com

¹Departamento de Físico-Química, Instituto de Química - Universidade Federal da Bahia, Rua Barão de Jeremoabo, 147, Salvador, 40170-115, Bahia, Brasil.

Palavras Chave: Conformational Flexibility, Torsional Anharmonicity, Kinetics.

INTRODUÇÃO

The ketones are volatile organic compounds (VOCs), considered the most common atmospheric pollutants. The hydrogen abstraction reactions by OH radicals, H, and HO₂, are considered important to remove this species from the environment^{1,2}. In the present study, we focus on the influence of the multiple structures and the torsional anharmonicity on the product branching ratio from the hydrogen abstraction reactions from the 2-pentanone + H. This reaction the four following possibilities were assumed:



MÉTODOS

The distributions over the different products of these reactions were obtained through kinetic Monte Carlo simulations using the rate constants obtained by approximations based on the transition state theory. More specifically, we apply the variations that consider single-structure (SS), multiple-structures (MS), and multiple-paths (MP) of reactants and transition states. Additionally, the quantum tunneling effect was incorporated with the multidimensional small-curvature tunneling (SCT) model. The torsional anharmonicity was introduced through the rotational-vibrational partition functions, using the model Multi-Structural Method with Torsional Anharmonicity Based on a Coupled Torsional Potential - MS-T(C). The electronic structure calculations were performed at the M06-2X/6-31+G(d,p) level of theory using the GAUSSIAN 09. The thermal rate constants and the product distribution were estimated using the PILGRIM conde. The rovibrational partition functions were calculated with the MsTor program.

RESULTADOS

The product distributions are shown in **Figure 1**. As we can see, the hydrogen abstraction corresponding to reaction (**R2**) is predominant in temperatures higher than 2000 K. Above this temperature, the reaction channel (**R3**) becomes

more relevant. The comparison between the different kinetic approximations is also shown in **Figure 1**. Our results indicate that the occurrence of the products of (**R1**) is favored when multiple paths and torsional anharmonicity are considered [MP-CVT/SCT(Anh.)]. Regarding the reaction (**R3**), the product distribution estimated with SS-TST, SS-CVT/SCT, and MP-CVT/SCT(Anh.) approximations suggested that the inclusion of torsional anharmonicity decreases the formation of the products of (**R3**). For (**R4**), our estimations that do not consider the dynamic and non-dynamic effects, multiple reaction paths, and torsional anharmonicity (i.e., SS-TST), underestimates significantly the formation of 2-pentan-5-yl + H₂.

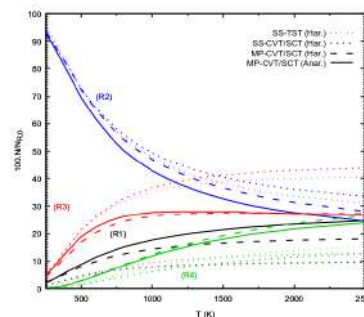


Figure 1. Product branching ratios obtained by different kinetic models.

CONCLUSÕES

In this study, we found that dynamic (variational) and non-dynamical effects affect the estimative of the product branching ratios of the 2-pentanone with atomic hydrogen reactions.

REFERÊNCIAS

- 1 L. Gasnot *et al.*, Combust. Sci. Technol., 2000, 161, 1.
- 2 K. Lam *et al.*, J. of Phys. Chem. A, 2012, 116, 5549.

AGRADECIMENTOS

The authors are grateful for the financial support of CNPq and CAPES.

Mechanical Properties and Fracture Dynamics of Collagen Fibers Using Reactive Force Fields

Matheus B. da Silva (IC),¹ Nilton Rosenbach Jr (PQ).^{1*}

matheusbs12@hotmail.com; nilton.rosembach.junior@uerj.br

¹Faculdade de Ciências Exatas e Engenharias, UERJ, Brasil.

Palavras Chave: Biomaterials, Collagen, Reactive Force Fields.

INTRODUCTION

The meniscus is a fibrocartilage structure present in the knee joint, that plays a crucial role in shock absorption, force distribution and overall stability. Its intricate architecture comprises three distinct layers formed by fibroblast-like cells, chondrocytes, and fibro-chondrocytes. The extracellular matrix of fibroblastic cells, located in the peripheral region of the meniscus, is predominantly composed of type II collagen. The increasing incidence of irreparable meniscus injuries has led to synthetic meniscus implantation. The development of novel materials capable of replacing the meniscus in the treatment of injuries must combine resistance, tenacity, softness, and human tissue-like flexibility¹. Although the mechanical properties of collagen fibers have been extensively studied using classic force field simulations, only a limited number of studies have reported simulations based on reactive force fields². In this work, we use the reactive molecular dynamics (ReaxFF) method to investigate collagen behavior within simulations mimicking natural meniscal fiber conditions.

METHODS

All simulations were conducted using the ReaxFF version in LAMMPS. Collagen structures 1QSU and 1BKV were directly obtained from the Protein Data Bank (PDB). Upon introducing hydrogen atoms, the collagen structure was placed in a box, and energy minimization was carried out to prevent unrealistic interactions arising from potential hydrogen atom overlaps. Subsequently, the temperature was gradually elevated to 310 K in the NVT ensemble until structure equilibration was achieved. Following equilibration, MD simulations were performed in the NVE ensemble. We applied tension in both axial and perpendicular directions, inducing segments of the collagen molecules to shift at a rate of 0.001 Å/step rate, while other regions remained stationary. For this study, a reparameterized nitramine ReaxFF force field, previously developed to study carbon cluster formation during the thermal decomposition of high explosives TATB and HMX, was utilized³.

RESULTS

Figure 1 illustrates a stress-strain curve obtained from MD simulations on the 1BKV collagen

structure under axial displacement. The high tensile stress displayed in this figure correlates with the mechanical failure of the fiber. The fracture is preceded by an increase in the radius of curvature, resulting in a transition from fiber's linear configuration to a curved one. These regions characterized by augmented curvature, typically situated near the fiber's end in mostly of the MD trajectories, correspond to occurrences of mechanical failure. This behavior is in fair agreement with simulations using classical force fields¹. Young's modulus is estimated as the tangent's slope in the elastic deformation regime of the stress-strain curve. For 1BKV collagen structure, the Young's module obtained is 10.3 GPa. The 1QSU collagen structure shows comparable behavior, yet some trajectories lack well-defined elastic regimes. Comparable results also arise from perpendicular loading on both collagen structures.

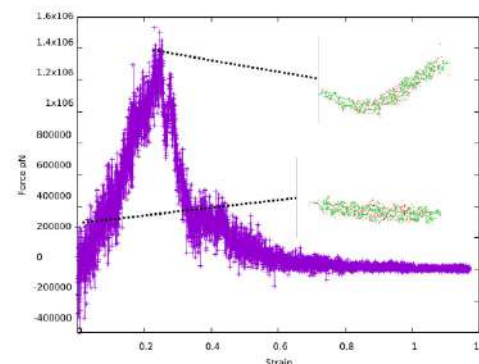


Figure 1. Stress-strain curve of 1BKV collagen structure under axial loading obtained in ReaxFF MD simulations.

CONCLUSIONS

ReaxFF force field method is used to simulate collagen behavior under natural conditions. Results showed stress-strain behavior and failure correlated with increased curvature, while Young's modulus was estimated at 10.3 GPa for the 1BKV collagen structure.

REFERENCES

- A. Kara et al., J. of Biomat. Appl., 2021, 35, 1192.
- M. J. Buehler, J. Mater. Res., 2006, 21, 1947.
- A. Strachan; et al. Goddard, Phys Rev Lett. 2003, 91 (9), 28.

ACKNOWLEDGEMENTS

FAPERJ, CNPq

Adaptive Steered Molecular Dynamics Study of Mutagenesis Effects on Arabinoxylan Substrate Affinity in GH62

Clauber Henrique Souza da Costa¹; Munir S. Skaf¹.

¹ Institute of Chemistry and Center for Computer in Engineering and Sciences, UNICAMP, SP, Brazil

The demand for economically viable and environmentally friendly processes in plant biomass bioconversion has spurred increasing interest in hemicellulose polysaccharides. Hemicellulose is a polysaccharide with significant economic and environmental relevance, as it can be converted into biofuels, pharmaceuticals, and other valuable materials using glycoside hydrolases (GHs). Adaptive Steered Molecular Dynamics (ASMD) has been successfully employed to obtain energy profiles from various challenging systems, including characterizing complex dynamics mechanisms, mutagenesis, binding affinity, protein-ligand interactions, and protonation effects. ASMD has proven effective in determining energy landscapes for challenging systems, spanning complex dynamics, mutagenesis, binding affinity, protein-ligand interactions, and protonation effects. In this study, we utilized ASMD to analyze the binding affinity of the Arabinoxylan substrate and the resulting effects of mutations in the glycoside hydrolase family 62 (GH62) enzyme from a Filamentous Bacterium. The distance between the catalytic Asp348 Oδ1 atom and the oxygen of the arabino ring of the substrate was determined as a displacement coordinate, ranging from 3.0 to 30.0 Å. This coordinate is divided into stages to conduct Steered Molecular Dynamics (SMD), with Jarzynski averages (JA) calculated throughout each stage. The trajectory with the work value closest to the JA average is selected for use in the next step. A potential mean force (PMF) was generated for each ASMD simulation (1000 ps = 1 ns with CHARMM36m). The results reveal that mutations induce conformational effects in the loop, highlighting crucial residues for substrate binding. Loop 9 proves critical for substrate recognition and binding; the Y461A mutation in this loop resulted in increased catalytic activity. Simulations suggest modifications in loop interactions to modulate the binding process. With the N462Q mutation and heightened catalytic activity, intensified interactions were observed with catalytic residues (Asp28, Asp348, and Glu361), underscoring the importance of positions 461 and 462 in loop 9 for substrate recognition and binding. Our findings imply that GH62 (Y461W) inactivation can be attributed to low substrate affinity with catalytic residues, coupled with increased interactions in other substrate areas, limiting access to the catalytic cavity. Thus, our simulations identify key amino acids for substrate binding, highlighting loop9's importance in substrate recognition and accessibility. Furthermore, mutation analyses emphasize enhancement of the active site affinity profile and, notably, specific interactions with catalytic residues, providing insights for GH62 design and engineering improvements.

Keywords: Hemicellulose polysaccharides; Adaptive Steered Molecular Dynamics (ASMD);

Substrate binding; Mutagenesis effects.

Sponsorship: FAPESP.

Molecular Dynamics Simulations and Free Energy Calculations of Selective Magnetic Coating of Mineral Surfaces

Lucas A. Silva(PG),^{1*} Alexandre M. Pereira(PG),¹ Tatiane A. R. Gonçalves(PG),² Julio C. G. Correia(PQ)¹

lucasandrade.chem@gmail.com

¹Laboratório de Modelagem Molecular, Centro de Tecnologia Mineral, Rio de Janeiro (RJ), Brasil; ²Vale S. A., Nova Lima (MG), Brasil.

Keywords: Magnetic Nanoparticles; Selective Magnetic Coating; Molecular Dynamics; Free Energy Calculations.

INTRODUCTION

Magnetic nanoparticles have diverse scientific and technological applications. An example is the selective magnetic coating technique aimed at the selective adsorption of these colloidal particles on the surface of minerals to improve the recovery of slimes by magnetic separation,¹ as in iron ore processing, where the separation of iron-bearing minerals from the silicates is targeted. As such, physicochemical aspects of such process must be investigated to optimize the industrial application, operational conditions and reagent usage, such as the common hydrophobization by oleic acid.

METHODS

Equilibrium and Steered Molecular Dynamics Simulations were performed to estimate the adsorption free energy, ΔG_{ads} , from the potential of mean force (PMF) of a cubic magnetite nanoparticle-mineral surface adhesion process for different surfaces of hematite, goethite, quartz and kaolinite, under different conditions of surface coverage by oleic acid as hydrophobizing agent in water medium. LAMMPS was used for running the simulations along with the CLAYFF, OPLS-AA and SPC/E forcefields. Along the thermodynamic, structural insights were also sought.

RESULTS

The adhesion of the bare hydrated nanoparticle on the also hydrated surfaces is highly impacted by the structured water layers, and low selectivity can be achieved. The average ΔG_{ads} values (kcal/mol) from all systems are -10.33 ± 4.8 for the silicates and -8.81 ± 6.8 for the iron minerals. When the nanoparticle is coated by oleic acid but the mineral surfaces are hydrated, the interaction is worse. The average values (kcal/mol) from all systems are -2.86 ± 0.5 for the silicates and -2.11 ± 1.2 for the iron minerals. When both the nanoparticle and the iron minerals are coated by oleic acid, the ΔG_{ads} values are much more negative, reaching almost 5 times the highest values in the previously reported conditions (Figure 1). The hydrophobic interaction is the key mechanism. Interdigitation was observed between the adsorption layers (Figure 2), helping in explaining why full coverage was not necessarily the best condition. Also, magnetic separation

experiments using real samples were performed and met the expected results from the simulations.

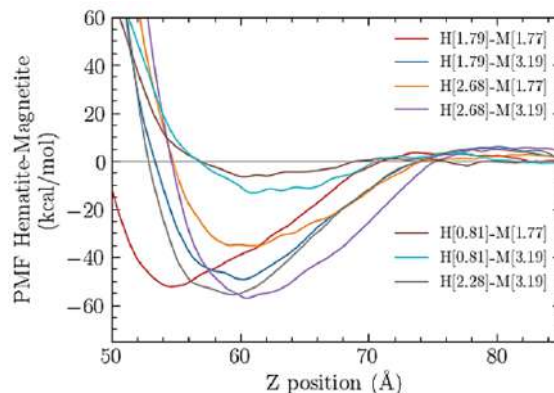


Figure 1. PMF for the interaction of magnetite nanoparticle with hematite (001) surface at different oleic acid coverages.

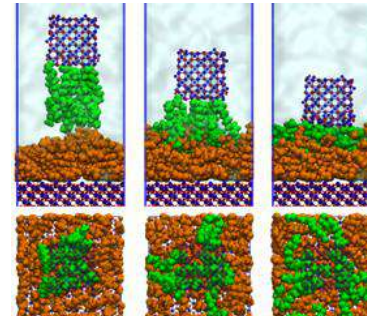


Figure 2. Interaction between colloidal magnetite and hematite coated with 9 and 28 molecules of oleic acid, respectively.

CONCLUSIONS

The molecular level interactions behind selective magnetic coating and the influence of the hydrophobization of the iron minerals' surfaces were elucidated. Our *in-silico* observations guided the tuning of the experimental ore separation process, meeting a successful theory-experiment nexus. The best adhesion was obtained when both the nanoparticle and the iron minerals' surfaces were hydrophobized. Also, surface coverage of less than the hypothetical monolayer leads to better cost-benefit of ΔG_{ads} /oleic acid.

REFERENCES

- ¹ P. Parsonage, Int. J. Miner. Process., 1988, 24, 269–293.

ACKNOWLEDGMENTS

The authors thank CETEM, MCTI, CNPq and VALE. S. A.

Cannabinoid receptors in motion: a Molecular Dynamics exploration of CB1 and CB2 interactions with cannabinoid compounds

Laise P. A. Chiari (PhD)¹, Michael K. Gilson (R)², Albérico B. F. da Silva (R)^{2*}

laisechiari@usp.br; alberico@iqsc.usp.br

¹Universidade de São Paulo, Instituto de Química de São Carlos

²University of California San Diego, Skaggs School of Pharmacy and Pharmaceutical Sciences

Keywords: cannabinoids, drug discovery, molecular dynamics

INTRODUCTION

Cannabinoid receptors (CB1 and CB2) and compounds greatly influence physiological processes like pain perception, appetite control, and inflammation modulation¹.

This study initiates the investigation of interactions between psychoinactive cannabinoids and CB1/CB2 receptors within cell membranes. It emphasizes building an accurate simulation system as a foundation for subsequent detailed calculations that uncover binding free energy differences. A comparative exploration is undertaken, contrasting their behavior with prominent psychoactive cannabinoid compounds, Δ^9 -THC and Δ^8 -THC. The selected cannabinoid compounds show similar structures, enhancing the comparison's importance. Molecular Dynamics, a potent tool, was used to gain atomic-level insights into dynamic molecule behavior and interactions², allowing to explore intricate molecular details behind these interactions, potentially opening therapeutic avenues.

METHODS

Molecular dynamics simulations were conducted to explore the interactions between selected cannabinoid compounds and CB1 and CB2 receptors. The NAMD2³ software was employed for the simulations.

Initial crystalline structures of CB1 and CB2 proteins were acquired from the Protein Data Bank. These structures were then embedded in lipid membranes using the CHARMM-GUI platform. The CHARMM36⁴ force field was utilized, and simulations were performed under periodic boundary conditions utilizing NPT ensemble (T=310K and P=1 bar).

The systems underwent energy minimization phases (20 ns) followed by the equilibration (100 ns). Subsequent visualization and analysis were carried out using VMD⁵.

RESULTS

Visual analysis of the molecular trajectories using VMD allowed to observe the dynamic behavior of the CB1 and CB2 membrane systems throughout the simulations, showing to be stable. The Root Mean Square Deviation (RMSD) profiles extracted from CB1 MD simulations illuminate a noteworthy observation:

psychoinactive cannabinoid compounds Ic2 and Ic19 exhibit greater stability compared to the prominent psychoactive counterparts, Δ^9 -THC and Δ^8 -THC, as showed in Figure 1.

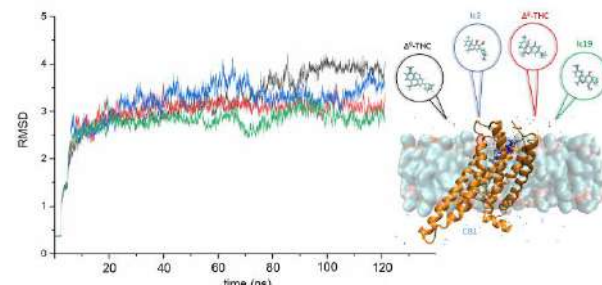


Figure 1. RMSD analysis from MD simulations for CB1.

In the CB2 context, the RMSD profiles prominently highlight the stability of compound Ic18, which is notably more stable than both Δ^9 -THC and Δ^8 -THC, as depicted in Figure 2.

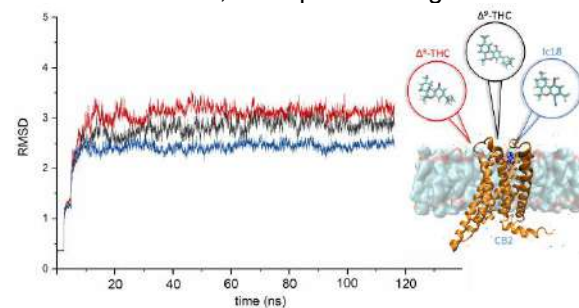


Figure 2. RMSD analysis from MD simulations for CB2.

CONCLUSIONS

Certain psychoinactive compounds have demonstrated highlighted stability in their interaction with CB1 and CB2 receptors. This stability not only enables a comprehensive exploration of their potential therapeutic effects but also offers insights into their underlying chemical structures, as well as making it possible to suggest new psychoinactive cannabinoid compounds with prospective therapeutic applications.

REFERENCES

- ¹M. B. Amar, J. Ethnopharmacol., 2006, v. 105, p. 1-25.
- ²J. D. Durrant, J. A. McCammon, BMC Biology, 2011, v. 9.
- ³J. C. Phillips Et al, J. Chem. Phys., 2020, v. 153.
- ⁴J. Lee Et al., J. Chem. Theory Comput., 2016, v. 12, p. 405-13.
- ⁵W. Humphrey Et al., J. Molec. Graphics, 1996, v. 14, p. 33-38.

ACKNOWLEDGMENTS

CAPES, CNPq, FAPESP and Gilson Lab.

Estudo mecanístico da Reação Multicomponente de Hantzsch a partir de métodos teóricos e experimentais.

Nicola L. Rocha (PG),¹ Rodrigo A. Cormanich (PQ)^{2*}

n209740@dac.unicamp.br; cormanich@unicamp.br

¹Universidade Estadual de Campinas

Palavras Chave: DFT; Estados de Transição; Mecanismo de Reação, MCRs

INTRODUÇÃO

A reação multicomponente (MCR) de Hantzsch corresponde a uma das reações com maior complexidade mecanística entre o grupo das MCRs clássicas,¹ sendo três caminhos reacionais mais discutidos atualmente para a formação do produto.² Assim, neste trabalho, cálculos teóricos foram realizados para a determinação dos diagramas de energia dos três caminhos reacionais propostos para o mecanismo da reação.

MÉTODOS

A Figura 1 apresenta os três mecanismos avaliados.

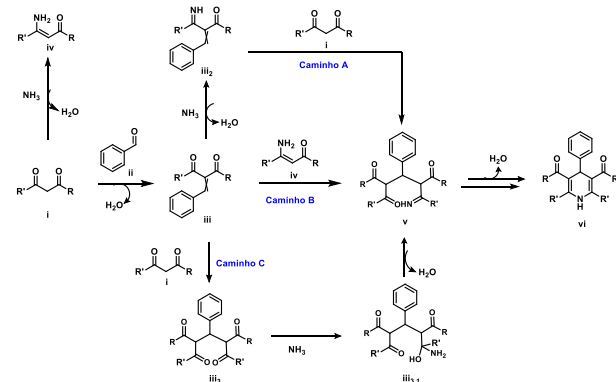


Figura 1. Caminhos reacionais avaliados para a formação do produto de Hantzsch vi (etapas simplificadas).

Para determinação dos diagramas de energia os seguintes procedimentos teóricos foram utilizados: (1) Avaliação de funcionais de densidade (B3LYP, M06L, M062X, HSEH1PBE e ω B97X-D): barreiras energéticas responsáveis pela formação do intermediário **iii** foram calculadas a partir de cada um dos funcionais, com o conjunto de bases 6-311++G(2d,p) nos cálculos de energia *single-point* e 6-31G(d) nas etapas de otimização de geometria. As barreiras obtidas foram comparadas com as do método DLPNO-CCSD(T)/def2-pvTZ//M06L/6-311++G(2d,p). O funcional com energias mais próximas do método de referência foi utilizado nas etapas subsequentes. (2) Solvatação: método de solvatação implícita IEF-PCM, utilizando etanol como solvente. (3) Para buscas conformacionais utilizou-se metadinâmica estática-iterativa (GFN2-xTB | CREST). Cálculos de energia *single-point* e otimizações de geometria foram realizadas utilizando-se os softwares G16 e ORCA5.0.

RESULTADOS

A comparação de todos os funcionais testados com o modelo de referência indicou que o funcional ω B97X-D apresenta a melhor representação energética, com um erro médio absoluto de apenas 1,0 kcal mol⁻¹.

As maiores barreiras energéticas presentes no diagrama de energia calculado estão associadas a reação entre: (A) **iii**₂ e β -cetoéster **i** (B) **iii** e **iv** e (C) **iii** e o β -cetoéster **i** (Figura 2).

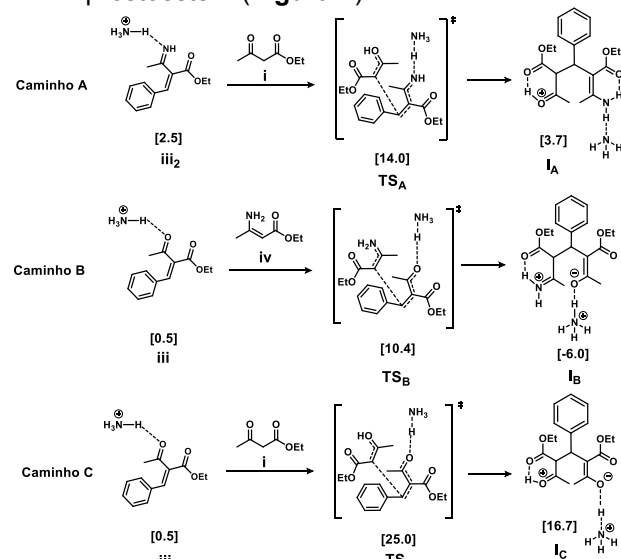


Figura 2. Modelo simplificado indicando estados de transição de maior energia para a formação do produto de Hantzsch (ΔG kcal mol⁻¹). *Energias calculadas no nível ω B97xd/6-311++G(2d,p).

Todos estes estados de transição levam à formação do produto. Como indicado na Figura 2, o estado de transição de menor energia está associado ao caminho reacional **B**, envolvendo os intermediários **iii** e **iv**, com energia equivalente à 10,4 kcal mol⁻¹ quando comparado aos reagentes iniciais.

CONCLUSÕES

Os cálculos realizados indicam que o **Caminho B**, envolvendo as espécies **iii** e **iv**, apresentou a menor energia entre os caminhos reacionais avaliados.

REFERÊNCIAS

- H, Alvim, RSC Adv, 2014, 97, 54282-54299
- V, Santos, Chem. Eur. J, 2014, 20, 12808-12816

AGRADECIMENTOS

CNPq, CAPES, FAPESP, FAEPEX, CENAPAD-SP e CESUP.

Atomistic modeling of plant cell wall and mechanical properties using molecular dynamic simulations

Carlos Guilherme Tissi Batista (PhD)¹, Lucas Nascimento Trentin (PhD)^{1*}, Amadeus Cavalcanti Salvador de Alcântara (PhD)², Munir Salomão Skaf (R)¹
c203748@dac.unicamp.br; lucas.trentin.unicamp@gmail.com

¹Institute of Chemistry, University of Campinas, Barão Geraldo, 13083-970, Campinas – SP; ²School of Mechanical Engineering, University of Campinas, Barão Geraldo, 13083-860, Campinas - SP

Keywords: Molecular dynamics, plant cell wall, biofuels, mechanical properties, atomistic model.

INTRODUCTION

Cellulose, hemicellulose, and lignin are the major components of lignocellulosic material. This biomass is under the spotlight due to the saccharification process of your polysaccharides to produce microbial enzymes and biofuels. However, these polymers are interconnected by covalent and non-covalent interactions, hardening the sugar hydrolysis.^{1,2} Likewise, the interactions among this components and their implications on the mechanical properties of this material are still not fully understood.³ Experimental methods are limited to explore the compositional interactions since they can lack a limit of detection to evaluate some molecular interactions or are disturbed by methodological limitations (such as low water solubility of lignin).⁴ Hence, the molecular dynamics approach helps to study the relationship between molecular interaction and the properties of this biomaterial. In this way, our group has been modeling a secondary plant cell wall to describe a softwood applying molecular dynamics to study the interactions and implications on mechanical properties of this material.

METHODS

The softwood atomistic model is compound of cellulose, hemicellulose, lignin and water.

Cellulose	30.6% - β-D-Glc-(1→4)-D-Glc with PBC bond (DP 100) - 7 hexagonal microfibrils with 18 chains on each microfibril (2-3-4-4-3-2 scheme)
Hemicellulose	DP 96 (45 mannan and 30 xylan chains) 12.8% – Mannan w/ 4:1:0.3 (0.4 Ac) and 3:1:1.2 (0.1 Ac) Man:Glc:Gal patterns and acetylation degree 7.60% – Xylan chains w/ evenly spaced D-GlcA and D-Ara decorations (17:10)
Lignin	28.9% (DP from 6 to 249) - 19:1 Linked G and H units (0.3 branching degree) - 300 chains with some of them assembling LCC (close to 90% of total lignin mass)
Water and Ions	20.00% – water TIP3P water molecules (68909 atoms) 0.10% – Ca ²⁺ ions (255 atoms)

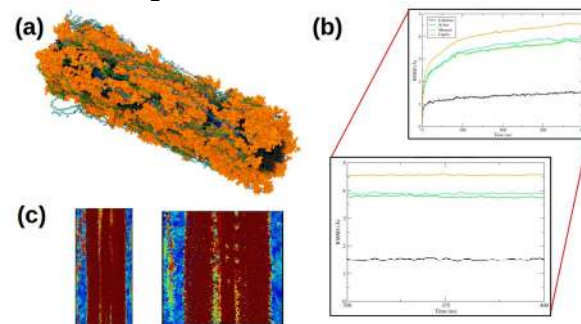
We assemble the system on Cellulose-Builder, VMD, and PACKMOL and we are running the simulations with NAMD using CHARMM force field. The LigninBuilder package crafted the spruce lignin structures and generated additional simulation parameters. We are checking the mechanical properties with uniaxial tensile stress essays using LAMMPS:

$$\sigma_v^k = \sqrt{\frac{1}{2} \sum_{i < j} (\sigma_{ij}^k - \bar{\sigma}_{ii}^k)^2 - 6(\bar{\sigma}_{ij}^k)^2}$$

RESULTS

The softwood model can be visualized on Fig. 1a, where the cellulose chains (black) are filled with xyloans (blue), mannans (green), and wrapped by lignin (orange). The Fig. 1b shows that the system can be treated as equilibrated.

Figure 1. Large-scaled atomistic softwood secondary cell wall (a) model (~900K atoms), (b) RMSD of 400 ns simulation, and (c) by atom von Mises loadings.



The von Mises stress scalars show that hemicellulose neighboring cellulose can hold a lot of mechanical strength of the material in a fast uniaxial tensile stress, such as the microfibrils. This indicate that this cross glycans help to disperse the overburden tension along cellulose, sustaining the molecular ensemble and crystalline the I-β cluster.

CONCLUSIONS

The softwood system is practically equilibrated and could be used in mechanical stress essays. The xylan and mannan can help to dissipate the load of tensile strain over cellulose microfibrils. We are studying the water role on this phenomena now.

REFERENCES

1. M. Busse-Wicher et al., Plant J., 2014, 79, 492–506.
2. R. Cresswell et al., Biomacromolecules, 2021, 22, 4669–4680.
3. C. Zhang et al., Sci. Adv., 2021, 7, eabi8919.
4. W. Zhao et al., J. Magn. Reson., 2022, 341, 107263.

ACKNOWLEDGMENTS

This work was supported by CNPq (140772/2023-5) and by the FAPESP (2013/08293-7 and 2019/17373-0).

Reactivity of carbonyl compounds explored by DFT: nucleophilic addition to aldehydes and ketones

Ricardo C.S. Neves (IC)¹, Rodolfo G. Fiorot (PQ) ^{1*}.

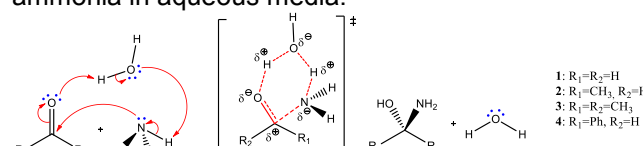
ricardo.caldeira@id.uff.br; rodolfofiorot@id.uff.br

¹Department of Organic Chemistry, Chemistry Institute, Universidade Federal Fluminense (UFF), Outeiro de São João Batista, 24020-141, Niterói, RJ, Brazil.

Keywords: Ammonia, Chemical Reactivity, Reaction Mechanism.

INTRODUCTION

Carbonyl compounds are interesting substances due to their synthetic versatility and reactivity associated to the C=O unit, making them appealing building blocks to synthesize valuable materials. By reacting with a nucleophile, these compounds can undergo nucleophilic addition reactions producing a tetrahedral product.¹ It is assumed that the reactivity of carbonyl compounds are controlled by its distortion (going from a trigonal planar to a tetrahedral geometry), and to its electron deficiency. Both factors depends on the R₁ and R₂ groups connected to the carbonyl moiety. However, literature lacks a proper quantification and rationalization of how these features influences their reactivity. Reacting with ammonia in aqueous media, the carbonyl compounds yields an aminoalcohol product² (Scheme 1). This reaction is important for several areas of chemistry, such as the synthesis of amines for the production of pharmaceuticals.³ Herein, we investigated the origin of the reactivity of different carbonyl compounds (aldehydes and ketone) towards ammonia in aqueous media.



Scheme 1: Nucleophilic addition of ammonia to carbonyl compounds in aqueous media.

METHODS

We investigated the origin of the reactivity of carbonyl compounds by simulating the nucleophilic addition of ammonia in aqueous media varying the substrate structure: formaldehyde (1), acetaldehyde (2), propanone (3), and benzaldehyde (4) – Scheme 1. The geometry optimizations were performed at **wB97XD/def2-TZVPP** level. Further, the physical factors behind their reactivity were assessed using the activation-strain model (ASM)⁴, considering the substrate as fragment 1, and (H₂O+NH₃) as fragment 2 at the transition state structure.

RESULTS

Figure 1 shows that aldehydes are more reactive towards nucleophiles than ketones. The reactivity

order follows: formaldehyde > acetaldehyde > benzaldehyde > propanone.

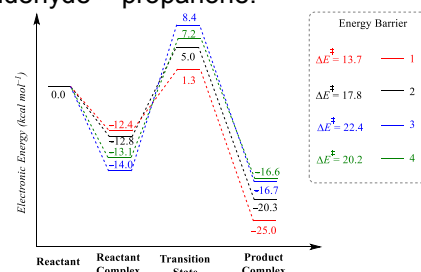


Figure 1: Diagram of electronic energies relative to reactants along reaction coordinates.

Figure 2 shows the ASM analysis in the TS structure. As the R size increase, the barrier increases mostly because the distortion energy.

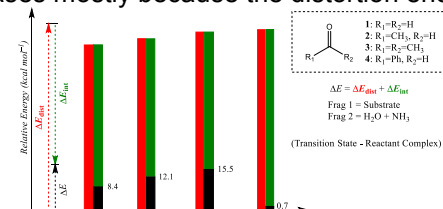


Figure 2: Activation strain model applied to the TS structure for the four reactions, using only the energies relative to the fragments of the transition states and reactive complexes.

CONCLUSION

The smaller the substituents of a carbonyl, the higher its reactivity. Except in cases where the substituent group has a large contribution to the interaction energy of the reaction, due to some chemical characteristic of its own. Next, we will employ the ASM along the entire reaction coordinate for a more complete assessment of the interaction/distortion energies, and subsequently decompose the interaction energy via the EDA method.

REFERENCES

- A. Ingersoll *et al*, *J. Am. Chem. Soc.* 1936, 58, 9, 1808–1811
- E. Goller, *Chem. Educ.* 1974, 51, 3, 182.
- O. Afanasyev *et al*, *Chem. Rev.* 2019, 119, 23, 11857–11911.
- FM Bickelhaupt, KN Houk, *Angew. Chem. Int. Ed.* 2017 , 56, 10070.

ACKNOWLEDGMENTS

CNPq, CAPES, FAPERJ, PROAES, UFF, LAMMECT, LMQC.

UV-Vis da merocianina em metanol utilizando TD-DFT, partindo de solvatação explícita.

Débora Assumpção Cunha (PG),^{1*} Juliana Fedoce Lopes (PQ)

deboracunha@unifei.edu.br

¹Laboratório de Química Computacional (LaQC), Instituto de Física e Química, Universidade Federal de Itajubá, Itajubá, 37500-903, Minas Gerais, Brazil.

Palavras Chave: Merocianina, UV-Vis, TD-DFT, Solvatação explícita.

INTRODUÇÃO

A merocianina apresenta o fenômeno do solvatocromismo¹ assim, diferentes interações soluto-solvente resultam em diferenças nas energias de absorção, e na cor observada. Estudos anteriores do grupo de pesquisa indicaram que apenas a solvatação implícita² não é suficiente para descrever esse tipo de cromismo. Neste trabalho, investigamos essas interações por meio de solvatação explícita.

MÉTODOS

Para as etapas de cálculos de otimização, frequência e cargas utilizou-se M06-2X/6-31G(d,p) com IEFPCM, por meio do G09. Seguiu-se para simulação de Monte Carlo no DICE. Com 50 configurações descorrelacionadas foram realizados TD-DFT, incluindo a primeira camada de solvatação.

RESULTADOS

A Figura 1 apresenta a sobreposição das 50 configurações com distribuição do solvente assim como seus espectros UV-Vis.

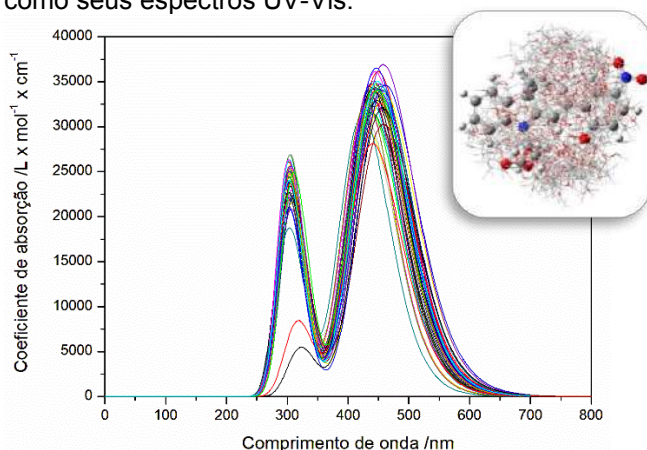
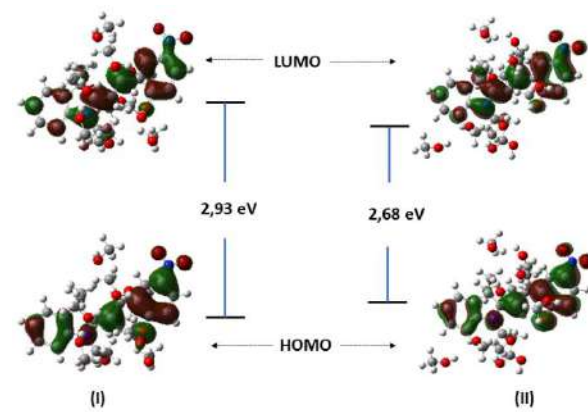


Figura 1. UV-Vis de 50 configurações da merocianina com metanol. Destaque da distribuição estrutural do solvente ao redor do soluto

Percebe-se que a primeira camada de solvatação não envolve toda a estrutura do soluto, o que pode negligenciar interações com grupos em suas extremidades. A faixa de pico máximo de absorção varia entre 420 e 460nm, demonstrando a diferença que há entre as configurações

geradas. Para as configurações de maior separação de λ_{\max} , foram detalhados os orbitais envolvidos na transição eletrônica (Figura 2).

Figura 2. Orbitais HOMO e LUMO de duas



configurações e seus λ_{\max} .

Os orbitais das duas configurações são bem semelhantes, mantendo a densidade sobre a estrutura da merocianina e seus grupos cromóforos. Mesmo com essa similaridade as energias diferem entre si, e uma vez que não há mudança na configuração do soluto, são resultados das interações com o solvente, que interfere em propriedades como polarizabilidade e de dipolos, tendo como consequência a diferença nos comprimentos de onda.

CONCLUSÕES

Os resultados atestam que para uma melhor representação do fenômeno de solvatocromismo é necessário incluir solvatação explícita. Assim é possível avaliar a influência dos solventes nas propriedades eletrônicas da merocianina em metanol, podendo estender esses estudos para outros solventes.

REFERÊNCIAS

¹P. Bamfield, M. Hutchings. *Chromic Phenomena Technological Applications of Colour Chemistry*. 2010, 3rd ed., p. 3-10, 160-167.

²T.G. Menzonatto, J. F. Lopes. Chemical Physics, 2022.

AGRADECIMENTOS

UNIFEI, CNPq, CAPES, FAPEMIG e PPGMQ-MG.



Estudo da Interação de Pares de Bases Nitrogenadas com Complexos de Platina

Marlon de Assis Modesto(PG)*, Arthur A. de Oliveira Rocha(IC), Valdemir Ludwig(PQ), Zelia M. da Costa Ludwig(PQ)

marlonmodesto.assis@estudante.ufjf.br

¹Departamento de Física, Universidade Federal de Juiz de Fora

Palavras Chave: xTB, DFT, ligações de hidrogênio.

INTRODUÇÃO

A cisplatina é um agente antineoplásico utilizado no tratamento de diversos tipos de câncer. Este tipo de medicamento visa induzir a morte programada de células cancerosas. A falta de especificidade afeta as células sadias resultando em uma série de efeitos colaterais. Do ponto de vista molecular há um grande esforço em entender o mecanismo da atividade anticancerígena. Estudos usando as propriedades quânticas em geral requerem um grande esforço computacional. Propomos neste trabalho o uso de métodos semi-empíricos combinados com métodos de teoria do funcional da densidade. Utilizamos uma estrutura dupla hélice DNA constituída por um par afim de analisar seu comportamento em meio aquoso e gasoso em fase gasosa.

MÉTODOS

O uso de softwares para visualizar moléculas Avogadro e Gabedit é nosso inicial para obter as estruturas dos pares de base a pentose e o grupo fosfato. A Teoria do Funcional de Densidade (DFT) é uma ferramenta já estabelecida na área da Química computacional. Recentemente uma extensão de um modelo semi-empírico foi implementado pelo grupo do professor S. Grimme [1], denominado xTB. Realizamos os cálculos no método DFT e xTB utilizando o software ORCA para a otimização das estruturas em vácuo e solução aquosa de forma implícita. O cálculo das energias de interação entre as ligações de hidrogênio é outro parâmetro importante em nossa análise.

RESULTADOS

A análise das estruturas de mínima energia foi feita para as diferentes estruturas estudadas. As estruturas dos pares de bases Watson-Crick são ponto de partida em nossa análise. A comparação entre as distâncias de ligação dos pares Guanina-Citosina (Tabela 1) no modelo DFT e xTB mostram diferenças da ordem de 0,07 Å. As estruturas no modelo apresentaram uma boa concordância o que nos motivou a estudar outras propriedades como a energia de interação. Os valores (tabela 2) da ligação tripla

na Guanina-Citosina (GC) tem uma energia de ligação que é estimada [2,3] como sendo 21 kcal/mol. Nossos valores em solução aquosa estão próximos aos já reportados indicando que a metodologia tem potencial para ser aplicada a sistemas mais realistas, com mais bases.

Tabela 1: Distâncias de ligação das ligações de hidrogênio entre as moléculas Guanina (G) e Citosina (C) isoladas.

Dist. de lig. de hidrogênio (Å)	cam-b3lyp/aug-ccpvdz	xTB
G(H)...C(O)	1.854	1.778
G(H)...C(N)	1.857	1.781
G(O)...C(H)	1.700	1.638

Tabela 2: Energias de interação das ligações de hidrogênio (kcal/mol).

modelo	CG_fase gás	CG_solvante
DFT/aug-ccpvdz	-34.07	-21.56
xTB	-33.75	-20.46

CONCLUSÕES

Os valores encontrados para as distâncias de ligação e energias de interação das bases Guanina-Citosina apresentaram boa concordância com valores já reportados na literatura, a metodologia se mostrou robusta na descrição das propriedades estudadas. É nosso interesse aplicar a metodologia a sistemas de vários pares com os grupos fosfato e pentoses além da interação com a cisplatina.

REFERÊNCIAS

- C. Bannwarth, E. Caldeweyher, S. Ehlert, A. Hansen, P. Pracht, J. Seibert, S. Spicher, S. Grimme *WIREs Comput. Mol. Sci.*, **2020**, 11, e01493.
- I. K. Yanson, A. B. Teplitsky, and L. F. Sukhodub, *Biopolymers* **18**, 1149 (1979).
- J. Sponer, J. Leszczynski, and P. Hobza, *J. Phys. Chem.* **100**, 1965 (1996).

AGRADECIMENTOS

CNPq, CAPES, FAPEMiG.





Grafite como Sensor de Gases Orgânicos

Isabelle Leão Gomes (IC),^{1,2*} Amanda Fernandes Gouveia (PG),³ Elson Longo (PQ).¹

paraabell@usp.br*

¹Centro de Desenvolvimento de Materiais Funcionais (CDMF), Universidade Federal de São Carlos, São Carlos, SP, Brasil; ²Instituto de Química de São Carlos, Universidade de São Paulo, São Carlos, SP, Brasil; ³Department of Analytical and Physical Chemistry, University Jaume I (UJI), Castelló 12071, Spain

Palavras Chave: GRAfite, DFT, CRYstal,

INTRODUÇÃO

Materiais nanoestruturados à base de carbono do tipo sp^2 , como nanotubos de carbono, grafeno, grafite, são candidatos promissores na área de desenvolvimento de sensores altamente sensíveis [1]. O grafite, material alvo deste projeto de pesquisa, é aplicado como sensor de gases orgânicos [2]. Assim, o foco do presente estudo foi construir e determinar os parâmetros que melhor descrevessem a estrutura do grafite em um modelo computacional, bem como a investigação de sua interação com moléculas orgânicas.

MÉTODOS

Para as simulações teóricas foi utilizada a Teoria do Funcional de Densidade (DFT) implementada no programa CRYSTAL17 [3], associada ao funcional híbrido B3LYP. O átomo de carbono foi descrito *all-electron* pela base C_6-21G*_catti_1993, encontrada no banco de dados do CRYSTAL.

Cálculos mecânicos envolvendo a otimização do bulk do grafite, da sua superfície de plano (001), e das moléculas orgânicas (metanol, etanol e acetona) foram realizados para auxiliar na análise das alterações causadas pela reação de adsorção. Os sistemas adsorvidos foram produzidos por meio de algoritmos de agrupamento e clusterização, e os cálculos foram realizados a partir da SUPERCELL (3x3x3) do grafite (Figura 1). A otimização do modelo de superfície com as moléculas orgânicas foi realizada utilizando uma otimização parcial, na qual apenas as posições atômicas da primeira camada e da molécula foram otimizadas. Para isso, utilizou-se o método de otimização ATOMONLY juntamente com FRAGMENT.

RESULTADOS

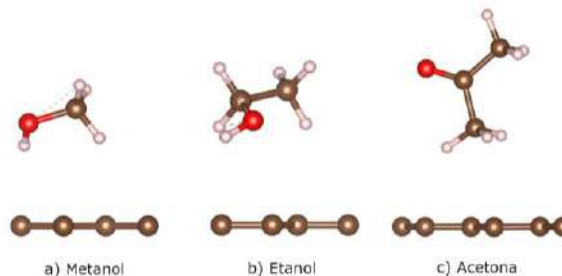
As adsorções apresentaram em sua maioria uma rotação das moléculas orgânicas com a hidroxila em direção à superfície do grafite, indicando uma forte interação $C_{(\text{superfície})}-O$. Para as moléculas de metanol e etanol, as distâncias de ligação OH e CO apresentaram resultados iguais a 0,97 Å e 1,44 Å para ambas as moléculas e um ângulo de ligação COH de 109,48° e 110,60°, respectivamente. Quando esses valores são comparados aos encontrados na literatura (valores

ideais), é possível afirmar que houve a ativação dessas moléculas, visto que, apesar do comprimento de ligação da hidroxila tenha se mantido, as ligações CO apresentaram estiramento, assim como também houve um aumento no ângulo COH. Para a acetona, a adsorção ocorreu com a carbonila estando perpendicular à superfície do grafite, com o ângulo CCC apresentando 117,51° e o comprimento da ligação dupla CO sendo de 1,22 Å.

CONCLUSÕES

Os resultados obtidos permitem afirmar que a reação de adsorção entre moléculas/superfície do grafite provocou uma ativação dessas moléculas, com base na alteração dos seus parâmetros estruturais. Este mecanismo é relacionado à interação entre os elétrons dos orbitais p desemparelhados presentes na superfície do grafite, que permite diferenças na transferência de carga entre molécula-superfície. A próxima etapa do projeto consiste em propor um mecanismo de detecção dessas moléculas orgânicas, ajudando, assim, no desenvolvimento de novos sensores.

Figura 1. Gases orgânicos alvos de estudo neste trabalho adsorvidos na superfície do grafite.



REFERÊNCIAS

- [1] Costa, J.; et al. IEEE Sensors Journal 2022.
- [2] Vieira Segundo, J.; et al. Revista Eletrônica de Materiais e Processos, 2017
- [3] Dovesi, R., et al., CRYSTAL17 User's Manual. University of Torino. 2017, Torino.

AGRADECIMENTOS

Fapesp (nº 2013/07296-2, 2022/16219-0) e Generalitat Valenciana (CIAPOS/2021/106).



DockThor-VS: a Free Brazilian Platform for Protein-Ligand Virtual Screening Using the Supercomputer Santos Dumont

Isabella A. Guedes (PQ),^{1*} Matheus M. P. da Silva (PG),¹ Eduardo K. da Silva (PQ),² Camila S. de Magalhães (PQ),³ Laurent E. Dardenne (PQ)¹

isabella@lncc.br

¹Laboratório Nacional de Computação Científica, LNCC, Petrópolis-RJ; ²Fundação Oswaldo Cruz, Fiocruz, Rio de Janeiro-RJ; ³Universidade Federal do Rio de Janeiro, UFRJ, Xerém-RJ

Keywords: drug design, molecular docking, virtual screening, supercomputer.

INTRODUCTION

Docking-based virtual screening is a structure-based drug design approach widely used by the scientific community in Medicinal Chemistry^{1,2}, assisting the process of drug discovery to search for new lead compounds against relevant therapeutic targets. The DockThor program³, developed by our group GMMSB/LNCC, has obtained promising results in comparative studies compared to other well-established docking programs for predicting experimental binding modes⁴ and binding affinities⁵ considering several molecular targets and chemical classes of ligands, including highly flexible peptides. We recently developed several scoring functions with protein-ligand interaction-driven features trained with machine learning techniques for predicting binding affinities of protein-ligand complexes. The DockThor-VS portal (available at www.dockthor.lncc.br) was developed to facilitate and enable the use of the docking program by the academic community using the computational facilities provided by the SINAPAD Brazilian high-performance platform SDumont.

METHODS

The DockThor program employs a steady-state genetic algorithm for multiple solutions and the MMFF94S force field as the scoring function for pose prediction. The affinity prediction is performed by an empirical scoring function developed by our research group that considers different terms relevant to the binding event, such as intermolecular interactions, conformational entropy of the ligand and desolvation. The DockThor-VS web server provides the main steps of ligand and protein preparation, being possible to change the protonation states of residues and to define the degree of flexibility of the ligand. During the COVID-19 pandemic, we provided curated structures of key SARS-CoV-2 therapeutic targets, including the wild-type and clinically relevant non-synonym variations and a prepared dataset with the drugs approved by the FDA up to 2021 to be virtually screened⁶. Guest users can submit experiments with up to 200 compounds, while registered users with approved projects can submit up to 5,000 compounds per job.

RESULTS

Compared to the state-of-the-art docking programs in the literature, the DockThor program obtained encouraging results in redocking experiments using benchmarking datasets in pose and affinity predictions. As a result of our efforts during the COVID-19 pandemic, the DockThor-VS currently provides the structure of six relevant SARS-CoV-2 therapeutic targets, including clinically relevant non-synonym variations and distinct conformations representative of the flexibility of each receptor. Twenty-seven structures are currently available and ready-to-dock, providing a free large-scale virtual screening service to the scientific community to help fight against COVID-19 and further emergence situations.

CONCLUSIONS

The validated accuracy of the DockThor program for binding mode and affinity predictions encouraged us to improve the portal DockThor-VS to accelerate the fight against de COVID-19 pandemic as a free and reliable tool for virtual screening. The portal utilises the computational facilities provided by the SINAPAD Brazilian high-performance platform and the supercomputer Santos Dumont.

REFERENCES

- ¹Guedes, I. A., Magalhães, C. S. de & Dardenne, L. E. Receptor-ligand molecular docking. *Biophys Rev* **6**, 75–87 (2014).² Guedes, I. A., Pereira, F. S. S. & Dardenne, L. E. Empirical Scoring Functions for Structure-Based Virtual Screening: Applications, Critical Aspects, and Challenges. *Front. Pharmacol.* **9**, 1–18 (2018).³ de Magalhães, C. S., Almeida, D. M., Barbosa, H. J. C. & Dardenne, L. E. A dynamic niching genetic algorithm strategy for docking highly flexible ligands. *Information Sciences* **289**, 206–224 (2014).⁴dos Santos, K. B., Guedes, I. A., Karl, A. L. M. & Dardenne, L. Highly Flexible Ligand Docking: Benchmarking of the DockThor Program on the LEADS-PEP Protein-peptide Dataset. *J. Chem. Inf. Model.* (2020).⁵ Guedes, I. A. et al. New machine learning and physics-based scoring functions for drug discovery. *Sci Rep* **11**, 3198 (2021).⁶Guedes, I. A. et al. Drug design and repurposing with DockThor-VS web server focusing on SARS-CoV-2 therapeutic targets and their non-synonym variants. *Sci Rep* **11**, 5543 (2021).

ACKNOWLEDGEMENT

Santos Dumont Brazilian High-Performance Platform (SINAPAD). Financial Support: FAPERJ, CNPq and CAPES.

DFT Functional Dependence and Solvent Effects on the NMR $^1J_{\text{PtPt}}$ Coupling Constants by *Ab Initio* Molecular Dynamics

Pedro P. R. Oliveira (MSc)¹, Patrick R. Batista (PhD)¹, Lucas C. Ducati (R)¹

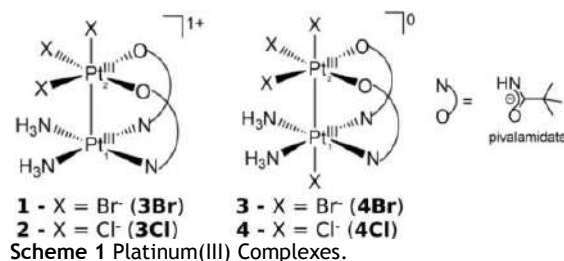
oliveirapedro@usp.br;

¹Department of Fundamental Chemistry, Institute of Chemistry, University of São Paulo, São Paulo, Brazil.

Keywords: (Molecular Dynamics, NMR, DFT)

INTRODUCTION

Dinuclear Pt(III) complexes, characterized by d⁷-d⁷ electronic configuration and octahedral coordination, possess potential in catalytic reactions and technological applications.¹ NMR spectroscopy parameters, such as 1J -coupling constants, are widely employed to unambiguously infer about molecular structure. However, static calculations involving implicit solvation have shown limited accuracy.² To address this limitation, we have employed Car-Parrinello *ab initio* Molecular Dynamics and relativistic KS-DFT calculations to investigate the solvent effect on NMR parameters of the complexes (Scheme 1) in aqueous media.^{2,3}



Scheme 1 Platinum(III) Complexes.

METHODS

B3LYP/TZP and PBE0/TZP geometry optimization, as well as calculations of $^1J_{\text{PtPt}}$ with ZORA-SR(SO)/jcpl for **1-4** complexes, were performed using the Amsterdam Density Functional (ADF) package, both with and without the implicit solvation (COSMO). The optimized structures, organized within a cubic cell of 64 solvent molecules ($\rho = 1.0 \text{ g cm}^{-3}$), underwent CPAIMD simulations using Quantum ESPRESSO software with BLYP (and PBE) ultrasoft pseudopotentials (NVT = 3 ps at 350 K and NVE = 30 ps). The ensemble average was estimated by sampling over 64 even spaced configurations from the NVE trajectory. 1J -coupling constants of these configurations were calculated at the ZORA-SR/B3LYP(PBE0)/jcpl level of theory. The reliability of AIMD was verified by examining radial pair distribution functions (RDFs).

RESULTS

The magnetic and structural properties trends in the **1-4** complexes evaluated are the same using both functionals (PBE0, B3LYP). Implicit solvation induces a systematic reduction in $^1J_{\text{PtPt}}$, leading to results that better match existing experimental values for both functionals (**1-2** complexes).⁴ In

general, $^1J_{\text{PtPt}}$ are more accurate when calculated with PBE0. Incorporating explicit solvent molecules also tends to promote more accurate results and convergence is reached after considering 10 explicit solvent molecules (Figure 1). Additionally, analysis of Pt-O radial pair distribution functions from the CPAIMD trajectory confirms the presence of around 10 solvent molecules within the first solvation shell. Furthermore, NVE trajectory analysis reveals the formation of a stable H₂O-Pt₁ coordination in **1-2** complexes. O-O RDFs shows that PBE's AIMD simulation tends to result in a more structured liquid. Static calculations revealed that PBE0 geometries presents a lower Pt-Pt distance and a lower $^1J_{\text{PtPt}}$, which is the opposite of the expected. Further investigation will be done to relate the $^1J_{\text{PtPt}}$ with structure in the AIMD configurations.

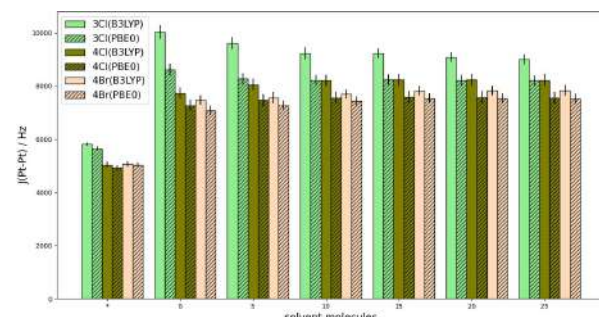


Figure 1 $^1J_{\text{PtPt}}$ dependence on explicit nearest neighbor solvent count for 2-4 platinum complexes. Data corresponds to NVE trajectory averages (64 configurations). Asterisk corresponds to bare structures. Counts (0-25) correspond to structures including the given number of explicit nearest solvent molecules and implicit COSMO solvation.

CONCLUSIONS

The magnetic and structural trends of **1-4** Pt(III) complexes were consistent under both PBE0 and B3LYP functionals. The analysis of RDFs indicates the presence of approximately 10 water molecules in the first solvation shell. PBE0 tends to yield improved alignment with experimental data for $^1J_{\text{PtPt}}$, in accordance with previous works.²

REFERENCES

- X. Wu, et al. *J Am Chem Soc*, 2020, 142, 16, 7469–7479.
- P. R. Batista, L. C. Ducati, J. Autschbach, *Phys. Chem. Chem. Phys.*, 2021, 23, 12864–12880.
- L. C. Ducati, et al. *J. Inorg. Chem.* 2016, 55, 12011–12023.
- K. Matsumoto, et al. *Inorg. Chem.* 2005, 44, 23, 8552–8560.

ACKNOWLEDGMENTS

University of São Paulo, FAPESP (2022/12004-0) and to the Laboratório Nacional de Computação Científica (LNCC).



Programa para cálculo da Força do Oscilador Generalizado

Amanda Alencar (PG),¹ A. P. de Oliveira (PQ),¹ A. B. Rocha (PQ),² Ginette Jalbert (PQ).^{1*}

a.alencar@pos.if.ufrj.br; ginette@if.ufrj.br

¹Instituto de Física da Universidade Federal do Rio de Janeiro, 21941-972 Rio de Janeiro, RJ, Brasil; ²Instituto de Química da Universidade Federal do Rio de Janeiro, 21941-972 Rio de Janeiro, RJ, Brasil.

Palavras Chave: Força do Oscilador Generalizado, Impacto de elétrons, Primeira aproximação de Born.

INTRODUÇÃO

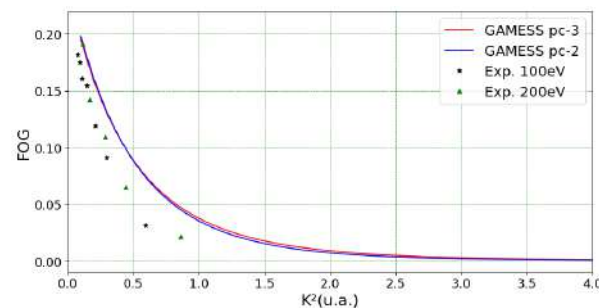
A força do oscilador generalizado (FOG) é uma propriedade essencial para o estudo de transições moleculares causadas pelo impacto de elétrons. No entanto, a maioria dos pacotes de química computacional existentes carecem da capacidade de calcular esta propriedade diretamente. No final de 2019, André Pacheco de Oliveira defendeu a sua tese de doutorado tratando do desenvolvimento de um programa para cálculo da FOG com base em informações provenientes do cálculo eletrônico da molécula sob estudo realizado pelo software PSI4, com destaque para a diferença de energia e a matriz de densidade de transição referentes à transição de interesse^{1,2}.

MÉTODOS

Como o programa existente foi desenvolvido para trabalhar especificamente com a saída do PSI4, o que limita sua aplicação, estamos desenvolvendo mecanismos para aumentar a flexibilidade do programa, permitindo que ele funcione com qualquer software a partir do qual as informações necessárias possam ser obtidas. Para tal, padronizamos o formato de entrada de dados para o programa de cálculo da FOG e automatizamos a criação desta entrada padrão a partir da saída do PSI4, como primeiro teste, e da saída do GAMESS.

RESULTADOS

Após a adaptação do programa para seu funcionamento com os dados oriundos do GAMESS, realizamos testes para validar os resultados obtidos comparando-os com resultados obtidos a partir do PSI4 e com resultados experimentais. A imagem a seguir mostra resultados obtidos para a transição $X^1\Sigma_g \rightarrow B^1\Sigma_u$ da molécula de hidrogênio comparada com resultados experimentais para impacto com elétrons de 100 eV e 200 eV ³.



CONCLUSÕES

As melhorias que estão sendo desenvolvidas permitem a integração do programa para cálculo da FOG com diversos pacotes de química computacional, aumentando assim as possibilidades de uso do programa. As modificações que estão sendo implementadas permitirão, inclusive, calcular a FOG para transições de elétrons provenientes de camadas internas (elétrons do caroço), ampliando muito a região de energia que poderá ser estudada.

REFERÊNCIAS

¹ Oliveira, A. P. ; Jalbert, Ginette ; Rocha, A. B.. Generalized oscillator strengths of carbon disulfide calculated by multireference configuration interaction. Journal of Chemical Physics, v. 150, p. 174116 (2019).

² Oliveira, A. P. ; Alencar, Amanda ; Jalbert, Ginette ; Rocha, A. B.. Electron-molecule collisions with explicit rovibrational resolution at MRCl level and using even tempered basis sets. Journal of Chemical Physics, v. 155, p. 194110 (2021).

³ H Kato, H Kawahara, M Hoshino, Hiroshi Tanaka, Laurence Campbell, and MJ Brunger. Electron-impact excitation of the b σ 1 u+ and c π 1 u electronic states of h 2. Physical Review A, 77(6):062708, 2008

AGRADECIMENTOS

Agradecemos à CAPES, ao CNPq e à FAPERJ pelo auxílio financeiro que possibilitou o desenvolvimento deste trabalho.

Insights into the value of statistical models, solvent and relativistic effects for investigating Re complexes: a potential spectroscopic probe

Gustavo A. Andolpho (PG),^{1*} Elaine F. F. da Cunha (PQ),¹ Teodorico C. Ramalho (PQ).¹

gustavo.andolpho@outlook.com

¹Chemistry Department, Natural Sciences Institute, Federal University of Lavras (UFLA) P.O. Box 3037 – 37200-900 – Lavras, MG – Brasil

Palavras Chave: *ReCO₃, DFT, RMN, HCA.*

INTRODUCTION

Breast cancer is responsible for a large part of the cancer cases in the world, therefore, early diagnosis is essential. For this, MRI is used with the help of contrast agents (Cas), which, although essential, can be harmful. Thus, new CAs have been studied, such as the Re(CO)₃(NNO) conjugated with 2-(4'-aminophenyl)benzothiazole (ReABT), proposed by Tzanopoulou (2006)¹, which we studied for its interaction with the PI3K enzyme and the changes in its chemical shift.

METHODOLOGY

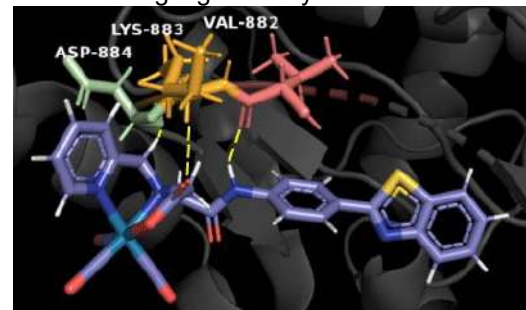
The optimized geometries for the studied complex have been got using the ω B97X-D3 functional, the SARC-ZORA-TZVP basis set for rhenium, and the TZVP basis set for all other atoms. We also used the zeroth-order regular approximation (ZORA) in Hamiltonian. After the optimization, a factorial 2^K model calculation was performed using the Chemoface software, to evaluate the influence of basis set, DFT functional, and relativistic effects on spectroscopic parameters. The NMR properties were computed at the GIAO-DFT method. In order to evaluate the best calculation protocol, a hierarchical cluster analysis, HCA, was performed using the Chemoface software. Once the calculation protocol was defined, the solvent effect has been evaluated on chemical shifts values, using water with the CPCM method. Then, NMR calculations were carried out using the ReABT complex docked in the active site of the target enzyme, considering the amino acids residues that form hydrogen bonds with ReABT. All DFT calculations were performed using the ORCA 5.0.0 software and the docking study was performed with Molegro Virtual Docking software, using the PI3K enzyme (Protein Data Bank (PDB) code 3QJZ).

RESULTS

The ReABT geometry was obtained with no imaginary frequencies, i.e., local minima. In the sequence the HCA results, indicates that protocol using PBE0|ZORA-TZVP|ZORA is the best for the shielding tensors (σ) calculations. To do that, all the δ values for 26 carbon atoms and 19 hydrogen atoms were considered, and compared with reference values¹. Then, the docking studies

pointing that ReABT interacts via H-Bond with some amino acids residues (Figure 1).

Figure 1. ReABT with amino acids residues. The H-Bonds are highlighted in yellow.



After that the $\sigma(187\text{Re})$ were obtained in the gas phase, 1630.49 ppm, solution, 1666.51 ppm, and enzymatic environment, 1514.65 ppm.

This behavior can be explained by the hydrophobic characteristic of the enzyme active cavity. The ReABT complex docked in the PI3K enzyme can put in evidence the importance of H-bond interactions on the changes that occur in the shielding tensors when ReABT moves from water to the enzyme cavity environment. In this sense, the difference of σ values in solvent and enzyme environment is a very interesting result, once this finding indicates that $\sigma(187\text{Re})$ values are quite sensitivity the change of chemical environments.

CONCLUSIONS

The HCA analysis points out that the best functional is the PBE0, considering the relativistic effects, both in the (i) system Hamiltonian, with ZORA, and in the (ii) basis set, with SARC-ZORA-TZVP for rhenium and ZORA-TZVP for all other atoms. NMR calculations for ReABT point out that the $\sigma(187\text{Re})$ changes significantly when the complex is in the enzyme environment. Thus, from our theoretical findings, this complex is a promising spectroscopic probe and could be an alternative to the traditional contrast agents, such as Gd-based, once it presents activity in NMR spectroscopy and the metal center is less toxic.

REFERENCES

- ¹Tzanopoulou, S. et. al., J Med Chem, 2006, 49(18), 5408-5410.
²Andolpho, G.A. et al., J Mol. Model, 2022, 28, 154.

ACKNOWLEDGMENTS

We thank the CNPq, CAPES, FAPEMIG.



DFT and Reactive Force Field Study of Ethanol Dehydration Catalyzed by Metalorganic Framework UiO-66(Zr)

Guilherme da S. G. Maria (IC),¹ Fabio J. da S. Henrique (PQ),² Nilton Rosenbach Jr. (PQ),^{1*} Claudio J. A. Mota (PQ),² Adri C. T. van Duin (PQ).³

gs300.gh@gmail.com; nilton.rosembach.junior@uerj.br

¹Faculdade de Ciências Exatas e Engenharias, UERJ, Brasil.

²Instituto de Química, UFRJ, Brasil.

³Department of Mechanical and Nuclear Engineering, Pennsylvania State University, United States

Palavras Chave: Metal-Organic Frameworks, ReaxFF Force Field, Ethanol Dehydration

INTRODUCTION

Metal-Organic Frameworks (MOFs) are a class of porous hybrid solids, formed by inorganic subunits connected by organic ligands. Due to their structural and chemical flexibility, MOFs have been considered the catalysts of the future with shape selectivity, higher catalytic site density than zeolites and adjustable acid properties. The zirconium-based MOF UiO-66 has a surface area of 1200 m²gm⁻¹ and two types of cavities: an octahedral one with a diameter of 11 Å and a tetrahedral one with a diameter of 8 Å¹. Due to its high thermal and chemical stability and good resistance to water and alcohol, its catalytic activity/selectivity has been investigated in a wide variety of reactions^{2,3}. In this work, we investigated the ethanol dehydration reaction catalyzed by UiO-66(Zr), using DFT and ReaxFF force fields methods.

METHODOLOGY

The parameters used in the description of the bond and non-bonded interactions between Zr/C/O/H were reparametrized from the combination of two force fields, originally developed to describe zirconia-based fuel cells and tautomerization reactions of glycine and conformational dynamics of biomolecules in H₂O. This ReaxFF force field has been successfully used to study the atomistic mechanism of thermal transformation in zirconium-based MOF MIL-140C⁴. In this work, we evaluate the performance of this force field to describe the thermal stability and catalytic properties of UiO-66(Zr) in ethanol dehydration. We investigated three reaction mechanisms using DFT methods and representative clusters of the UiO-66(Zr), and the results were compared with that obtained using ReaxFF force fields.

RESULTS

ReaxFF MD simulations performed using a representative UiO-66(Zr) unit cell demonstrates the capability of the force to reproduce the crystalline structure of the MOF. The volume discrepancy between theoretical and experimental data is below 1%. Notably, unit cell volumes

undergo significant changes between 600 and 800 K, corroborating experimental evidence that indicates the UiO-66(Zr)'s thermal decomposition within this temperature range¹. The ethanol dehydration catalyzed by UiO-66(Zr) may involve three different mechanisms. In the first, oxygen atoms within the MOF structure participate in the dehydration step. The second is a concerted mechanism wherein the Zr-O-H site accepts a proton. The third mechanism involves two steps: (i) formation of a zirconium-coordinated alkoxide intermediate (Zr-ethoxide), (ii) followed by the dehydration step. The results are reported in Table 1, which includes only the highest energy barrier (dehydration step) of the third mechanism. The alkoxide formation involves a small activation energy of 5.3 kcal.mol⁻¹. ReaxFF force field results are consistent with DFT data, demonstrating its satisfactory performance in describing the catalytic properties of MOF UiO-66(Zr).

Table 1. Adsorption (E_a), activation (E_c), and reaction (E_r) energy (values in kcal.mol⁻¹) for ethanol dehydration catalyzed by UiO-66(Zr).

Mechanism	Method	E_a	E_c	E_r
I	DFT	-10.9	59.4	17.4
	ReaxFF	-10.1	56.3	17.4
II	DFT	-13.1	41.6	17.4
	ReaxFF	-8.1	35.7	16.8
III	DFT	-10.9	46.2	17.4
	ReaxFF	-5.1	45.1	18.2

CONCLUSIONS

Both DFT and ReaxFF force field methods were used to investigate UiO-66(Zr)-catalyzed ethanol dehydration. The ReaxFF force field describes accurately UiO-66(Zr)'s crystalline structure and thermal stability. Three reaction mechanisms were explored using ReaxFF, yielding comparable kinetic and thermodynamic parameters to DFT calculations.

REFERENCES

- 1 J.H. Cavka, et al., J. Am. Chem. Soc., 2008, 13850.
- 2 J. Hou, et al., J. Mol. Catal. A., 2015, 407, 53.
- 3 F. Vermoortele et al., Chem. Comm., 2011, 47, 152.
- 4 S. Dwivedi, et. al., JPCL, 2021 12, 177.

ACKNOWLEDGEMENTS

FAPERJ, CNPq

Improving Optical Property Predictions in Solvated Systems: Combining tuning of RSH functional and sequential QM/MM approach

Pedro Henrique Ferreira Matias (PG),^{1*} Mateus Rodrigues Barbosa (PG), Daniel Francisco Scalabrini Machado (PQ),² Heibbe Cristhian Benedito de Oliveira (PQ).¹

phfmatias@discente.ufg.br

¹*Instituto de Química - Universidade Federal de Goiás*

²*Instituto de Química - Universidade de Brasília*

Palavras Chave: DFT, JGAP, Solvated Systems.

INTRODUCTION

Discrepancies between theoretical and experimental results can arise from the choice of molecular modeling. Add solvation effects can enhance theoretical accuracy. Another way is performing functional optimization. However, trying to mix this practice with solvation methodologies, some barriers arise. Optimizing RSH functionals in implicit solvation methodologies leads to artificially low values of range separation parameter ω (bohr $^{-1}$)¹. Looking for explicit solvation methodologies, HOMO and LUMO orbitals become spread over onto solvent molecules instead of solute². The present work aims to overcome the problems of functional optimization in solvated systems combining the JGAP tuning scheme with explicit solvation methodology carried out by s-QM/MM.

METHODOLOGY

The para-Nitroaniline (pNA) molecule was the object of study due to its frequent use as a reference system for property responses as it is a π conjugated system with high π delocalization and push-pull mechanism. Photophysical properties were calculated using TD-DFT in Gaussian 16 software³. The solvent employed was Water. OPLS parameters were obtained through the LigParGen server⁴. The s-QM/MM solvation method was performed using DICE⁵ software in conjunction with ASEC-FEG approximations with 1 solute and 500 solvent molecules. Functional optimization was performed by Golden Omega software in Python 3.x/C++ programming language. The golden ratio search algorithm was implemented to reduce computational cost. The procedure was performed in order to minimize the equation (1):

$$Jgap(\omega)C = C\sqrt{(Jip)^2 + (Jea)^2} \quad (1)$$

RESULTS

The functional optimization process resulted in 0.27 ω (bohr $^{-1}$) for all systems.

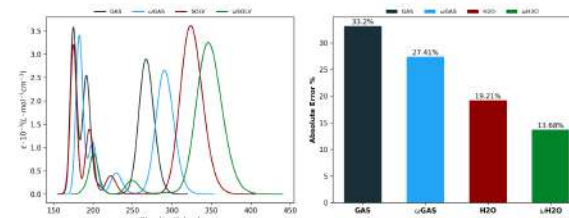


Fig 1. Theoretical UV-Vis spectrum (left), Relative error between theoretical and experimental (right). Dark blue is the isolated system, light blue is the optimized isolated system, red is the solvated system, and green is the optimized solvated system.

In Fig 1 (left), a red shift is observed in optimized systems and the inclusion of the charge points also presents a redshift. This behavior is due to the optimization process minimizing the GAP, leading to low-energy excitation. Also, due to the polarity of water, the charge points stabilize the solute LUMO, decreasing the GAP and consequently leading to redshift. The relative errors present a trend, when the approximation becomes more robust the relative error decreases, the lowest being the solvated optimized with 9.92% of error.

CONCLUSION

Combining functional optimization with an explicit solvation method was successful being the best approximation for photophysical properties of pNA in water solvent compared to experimental.

BIBLIOGRAPHY

¹ Bhandari et. al., JCTC, 2018, 14. 6287–6294.

² de Queiroz, T. JCP, 2015, 143.

³ Frisch, M. J. et al. Gaussian 16 Revision C.01. 2016; Gaussian Inc. Wallingford CT.

⁴ Dodd, L. S et. al., Nucleic Acids Research, 2017, 45. W331–W336.

⁵Coutinho, K et. al., Journal of Chemical Information and Modeling, 2020, 60. 3472–3488

ACKNOWLEDGEMENTS

CNPq, CAPES, FAPEG, LAMCAD, PPGQ-UFG, IQ-UFG, LEEDMOL-IQ-UFG.



Physicochemical properties and phase transitions of $(\text{NH}_4)_2\text{Zn}(\text{SO}_4)_2(\text{H}_2\text{O})_6$ crystals: a theoretical and experimental study

João G. de Oliveira Neto (PQ),¹ Jailton R. Viana (PG),^{1*} Luiz F. L. da Silva (PQ),² Mateus R. Lage (PQ),¹ Stanislav R. Stoyanov (PQ),³ Rossano Lang (PQ),⁴ Francisco F. de Sousa², Adenilson O. dos Santos (PQ),¹

joao.gomes.quimico@gmail.com; jrvfisica@gmail.com

¹Universidade Federal do Maranhão – campus Imperatriz; ²Universidade Federal do Pará – campus Belém; ³Natural Resources Canada, CanmetENERGY Devon – Canadá; ⁴Universidade Federal de São Paulo – campus São José dos Campos.

Keywords: Tutton salts, Structural-thermal properties, Density functional theory, Hirshfeld surfaces, Dehydration Enthalpy.

INTRODUÇÃO

In recent years, hydrated inorganic materials have been studied due to the structural and thermal properties that make them promising candidates for developing systems for storing thermal energy.¹ The class of isomorphic crystals, called Tutton salts, attracted attention due to the thermodynamic parameters associated with their chemical composition.² From this perspective, we present a comprehensive characterization study associated with density functional theory (DFT) calculations and Hirshfeld surfaces analysis.

MÉTODOS

Crystals with composition $(\text{NH}_4)_2\text{Zn}(\text{SO}_4)_2(\text{H}_2\text{O})_6$, NHZnSO, were grown by the slow evaporation method, using equimolar proportions of $(\text{NH}_4)_2\text{SO}_4$ and $\text{ZnSO}_4(\text{H}_2\text{O})_7$ in 40 ml of deionized water. Structural, thermal, and vibrational properties were obtained by X-ray diffraction (XRD), thermos-analytical techniques, and infrared (IR) and Raman spectroscopies. Complementarily, vibrational properties were calculated at DFT level using the Cambridge Serial Total Energy Package (CASTEP) software. Electron exchange and correlation were treated using norm-conserving pseudopotential and Local Density Approximation (LDA) with Ceperley and Alder data, parameterized by the Perdew and Zunger (CA-PZ) functional,³ with a $2 \times 2 \times 2$ medium k-set point, an energy cut-off of 600 eV and energy tolerance selected per atom. Geometry optimization was performed using the Broyden-Fletcher-Goldfarb-Shanno (BFGS) algorithm. Furthermore, a detailed study of the intermolecular interactions was conducted through Hirshfeld surfaces by the CrystalExplorer program.

RESULTADOS

The NHZnSO double salt was obtained after 10 days in acidic pH (≈ 4.5) and crystallized in a monoclinic system with space group $P2_1/a$ ($Z=2$). Hirshfeld surfaces combined with the fingerprint results were used to verify that the molecular fragments NH_4^+ , SO_4^{2-} , and $[\text{Zn}(\text{H}_2\text{O})_6]^{2+}$ are co-crystallized in the structural lattice. The contacts $\text{H}\cdots\text{O}/\text{O}\cdots\text{H}$, $\text{H}\cdots\text{H}/\text{H}\cdots\text{H}$, and $\text{O}\cdots\text{O}$, contributed to

interactions in the crystal with the percentages of 73.8%, 25.2%, and 1.0%, respectively. In addition, through surface mapping, it was observed that the H_2O atoms are associated with the most intense and predominant interactions. The experimental IR and Raman spectra showed a good correlation with the theoretical spectra obtained through DFT calculations. This correlation allowed a spectral band assignment, corresponding to vibrational modes in the crystal. According to the simulations, active modes corresponding to irreducible representations A_g and B_g were observed in the Raman, and A_u and B_u were in the IR spectra. Through thermogravimetry, it was observed that NHZnSO crystals exhibit thermal stability up to 61°C, followed by a phase transformation intermediated by the evaporation of the six coordinated water molecules. An endothermic peak observed in the differential thermal analysis curve at 98°C confirmed this dehydration process. For this event, an enthalpy of 736.70 kJ/mol was estimated using differential scanning calorimetry, which is equivalent to 122.78 kJ per mol of H_2O and an energy density of 3.54 GJ/m³. These results make the Tutton salt NHZnSO a promising material for energy storage in thermochemical systems.

CONCLUSÕES

The NHZnSO Tutton salt was synthesized, and its structural, vibrational, and thermal properties were characterized. Using Hirshfeld surfaces and DFT calculations, it was possible to develop a better understanding of the intermolecular interactions in this system, as well as to properly assign the Raman and IR modes. The thermal analyses showed the changes occurring in the crystal, when subjected to heat variation and suggest it would be attractive for storing thermal energy.

REFERÊNCIAS

- 1 J. G. de Oliveira Neto, et al., JMM, 2022, 28, 341.
- 2 A. C. Morales, et al., JTAC, 2018, 132, 1523.
- 3 J. P. Perdew, A. Zunger, PRB, 1981, 23, 5048.

AGRADECIMENTOS

CAPES, CNPQ, FAPEMA, Digital Research Alliance of Canada, and Program of Energy R&D (PERD), Government of Canada.

Theoretical Investigation of Regiodivergent Addition of Anilines and Phenolates to *p*-Benzoquinone Ring

Haroldo C. Da Silva¹, Talita O. C. Leite², Searitha C. Rodrigues³, Beatriz L. C. De Carvalho³, Maria Tereza Martins³, Rodolfo G. Fiorot³, Flaviana R. F. Dias³, Vinícius R. Campos³, Vitor F. Ferreira⁴, Anna C. Cunha³ e Wagner B. De Almeida¹

haroldocandal@id.uff.br; annacunha@id.uff.br; wbdealmeida@gmail.com.

¹Laboratório de Química Computacional e Modelagem Molecular, Departamento de Química Inorgânica, Universidade Federal Fluminense, Niterói 24020-150 RJ, Brazil;

²Faculdades Integradas Maria Thereza, Niterói 24020004 RJ, Brazil.

³Departamento de Química Orgânica, Universidade Federal Fluminense, Niterói 24020-141 RJ, Brazil.

⁴Faculdade de Farmácia, Departamento de Tecnologia Farmacêutica, Programa de Pós-Graduação em Química, Universidade Federal Fluminense, Niterói 24241-000 RJ, Brazil.

Palavras Chave: (Regiodivergência, DFT, Estados de Transição, Adição, Mecanismos).

INTRODUCTION

Benzoquinones are extensively studied with the aim of synthesizing new derivatives with relevant biological activities^{1,2}, particularly those exhibiting antitumor properties³⁻⁶. In this study, we will address the molecular, kinetic, and thermodynamic factors of the syntheses of amino- and aryl-oxi benzoquinones through regiodivergent nucleophilic conjugate addition to the 2-bromo-1,4-benzoquinone ring. Experimentally, the reaction with phenolates eliminates the halogen from the molecule, but surprisingly, the reaction with aniline does not yield the same product (Figure 1).

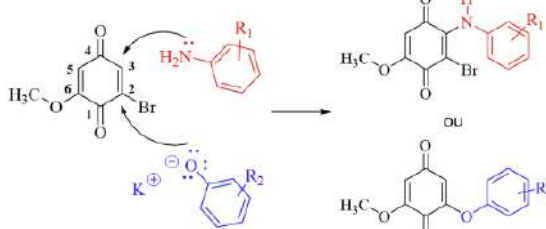


Figure 1.
Regiodiver-
gence.

METHODS

The mechanisms of halogen substitution (nucleophilic attack at carbon 2) and addition/oxidation (nucleophilic attack at carbon 3) were thermodynamically and kinetically analyzed. The $\Delta_r G$ values, energies of transition states (TS), molecular orbitals, atomic charges, and Fukui indices were calculated using the ω B97X-D/6-31G(d,p)-PCM theory (in water or acetonitrile solvent). NBO analysis of the reactants and the TS of the first step in each mechanism was also performed at the same theory level.

RESULTS

The charges, molecular orbitals, and Fukui indices are highly similar for the substrate molecule and the nucleophiles in both solvents. The $\Delta_r G$ indicates that the reaction with phenolates via substitution is thermodynamically more favorable. However, for the reaction with aniline, the addition/oxidation product is thermodynamically favored. (Figure 2).

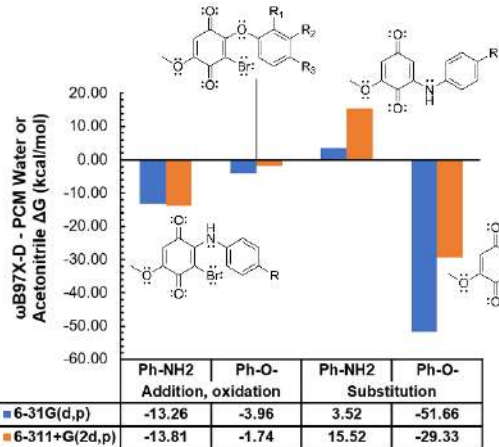


Figure 2.
 $\Delta_r G$ for the
reactions
in Figura
1.

The energies of the TS for the first steps of the mechanisms reveal that the TS formed by the attack of aniline at carbon 3 is associated with a lower energy barrier, which confers kinetic preference to the addition/oxidation product.

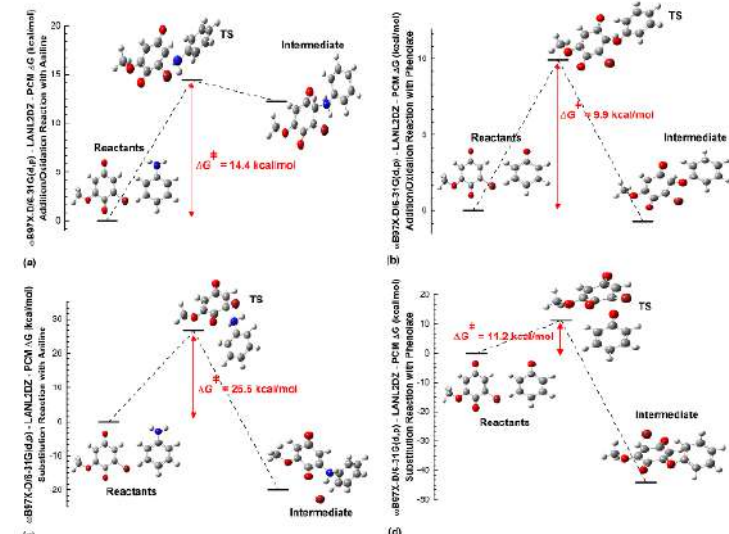


Figure 3. $\Delta_r G^+$ for the TSs in each mechanism.

One of the hypotheses considered for the preference of aniline for carbon 3 involves a possible clustering of nucleophile molecules in this region through the establishment of an O...H2NAr hydrogen bond, which was confirmed by NBO analysis, as shown in the Table 1.

Table 1. NBO Analysis of the reactant pairs.

Par	ΔE_{rel} (kcal/mol)	HB	NBO1	NBO2	$E(2)$ (kcal/mol)
NH...O1	0,00	1	LP(O1)	σ_{NH}^*	4,66
		2		σ_{CH}^*	0,74
NH...O4	-2,8	1	LP(O4)	σ_{NH}^*	7,19
		2		σ_{CH}^*	0,19
		3		σ_{C3H}^*	3,03

CONCLUSIONS

The calculated data indicates that the product obtained from substitution with phenolates exhibits thermodynamic preference, while those obtained from addition/oxidation with aniline shows kinetic preference, which is entirely consistent with the experimentally obtained products.

REFERENCES

- Da Silva, R. E., et al. A. Microb Pathog, 2020, 149, 104513.
- Abraham, I., et al. J. Braz. Chem. Soc., 2011, 3, 385.
- Dias, F. R., et al. J. Braz Chem Soc., 2021, 32, 476.
- Leite, T. O. C., et al. Curr Top Med Chem, 2019, 20, 192.
- Da Silva, W. A., et al. Future Med Chem, 2018, 10, 527.
- Campos, V. R., et al. RSC Adv, 2015, 5, 96222.

ACKNOWLEDGMENTS

We thank CNPq and FAPERJ for funding the research.

DFT Study of the interaction between chlorobenzene and Palladium clusters supported on different types of β -cyclodextrins

Verônica Ferreira Lima (PG),¹ Jaqueline Dias Senra (PQ),² Maurício Tavares de Macedo Cruz (PQ).^{1*}

vroniklima@gmail.com; cruzmtmr@gmail.com

¹Universidade do Estado do Rio de Janeiro, Rio de Janeiro – RJ – Brasil

Keywords: DFT, Cross-coupling reactions C-C, β -cyclodextrin, Palladium, Methyl- β -cyclodextrin.

INTRODUCTION

There is a wide applicability in C-C cross-coupling reactions in the synthesis of new compounds, such as drugs.¹ For many years, palladium catalysts with phosphine ligands were preferred in these reactions, with the disadvantages of environmental contamination and incompatibility with some organic functions.² A promising alternative is the use of Palladium combined with different types of β -cyclodextrins (β CD), natural and modified, which increase the stability and selectivity of the catalyst, and reactions in aqueous media.^{3,4} Thus, the present work has been investigated computationally the interaction between a Pd₄ cluster and β CD monomers and Methyl- β CD (M β CD) against the interaction with chlorobenzene substrate molecule, to collaborate in understand the influence of β CDs in the oxidative addition step.

METHODOLOGY

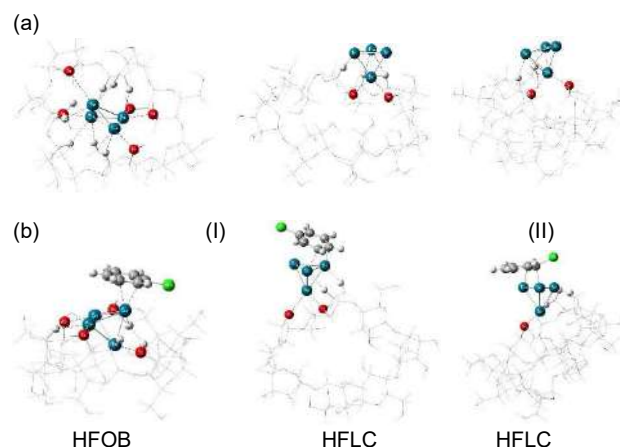
Based on the literature a structural model to represent a monomer of different types of β CDs was built from crystallographic data and were optimized. A bulk of Pd₄ with tetrahedral geometry was approximated to β CDs by two distinct regions: hydrophobic (HFOB) and hydrophilic (HFLC). In a next step, a single chlorobenzene (ArCl) molecule was approached directly on the Palladium cluster deposited on the β CDs monomers. This methodology was carried out for natural β CD and functionalized with methyl groups. All calculations were performed at B3LYP/LANL2DZ/6-31G(d,p) method with Grimme and Becke-Jonhson dispersion correction. However, the Cl atom was described with the 6-311G(d) basis set. The interaction energies were corrected with counterpoise method to eliminate the BSSE. The orbitals were evaluated through NBO method. All complexes present the singlet state as the lowest energy state.

RESULTS

The structural optimization of the complex between Pd₄ and M β CD monomer shows a migration of the metallic agglomerate from the HFOB region to the HFLC and a closure of the monomer cavity (Fig. 1 – IIa). The calculation of HOMO/LUMO gap energies indicates a slightly higher value for M β CD monomer in relation to β CD when obtained for isolated cyclodextrins

(0,75 eV against 0,72 eV). In complexes with β CD, the gap is greater when Pd₄ complexation occurs in the HFOB region (0,20 eV) compared to HFLC (0,14 eV). This last value is maintained in the monomer is M β CD. The electronic effect promoted by β CD on ArCl anchoring is more prominent when Pd₄ is in the HFLC region than in the HFOB (-33,5 kcal.mol⁻¹ against -31,7 kcal.mol⁻¹). In M β CD, Pd₄ behaves similarly to HFLC in β CD, leading to an approximately 12,0 kcal.mol⁻¹ higher anchoring energy (-45,3 kcal.mol⁻¹).

Figure 1. Optimized complexes of (a) Pd₄ and (b) Pd₄/ArCl with (I) β CD and (II) M β CD.



CONCLUSIONS

The increase in the energy of the border orbitals and the HOMO/LUMO gap in β CD/Pd₄ complex suggests greater stability of the Pd₄ supported in the HFOB region. The functionalization of cyclodextrin results in the narrowing of the hydrophobic cavity, which makes it impossible to include Pd₄ in this region.

REFERENCES

- ¹K. Hong et al, App nano materials, 2020, 3.2070-2103.
- ²F. Han, Chem.Soc.Rev., 2013, 42. 5270-5298.
- ³B. Poulsou et al, Polys., 2020, 3. 1-31.
- ⁴S.Kanchana et al, Carb.Res., 2020, 489. 1-12.

ACKNOWLEDGMENT

The authors thank CNPQ and FAPERJ for the financial support.

MD and DFT Study of the Driving Forces for Extraction of Fe³⁺, Co²⁺ and Ni²⁺ in PEO/SCN Salt Aqueous Two-Phase Systems

Letícia M. Prates (PQ),^{1*} Lucas A. Silva (PG),¹ Alexandre M. Pereira (PG),¹ Heyder P. Neves (PG),² Julio C. G. Correia (PQ),¹ Aparecida B. Mageste (PQ),² Gabriel M. D. Ferreira (PQ)²

leticiamaiapr@gmail.com

¹Laboratório de Modelagem Molecular, Centro de Tecnologia Mineral, Rio de Janeiro (RJ), Brasil; ²Laboratório de Físico-Química e Química Ambiental, Universidade Federal de Ouro Preto, Ouro Preto (MG), Brasil

Keywords: Aqueous Two-Phase Systems, Extractive Metallurgy, Molecular Dynamics, Density Functional Theory.

INTRODUCTION

Aqueous two-phase systems (ATPS) have been increasingly applied as environmentally friendlier alternatives for extractive processes.¹ However, the fundamental aspects behind metal partition are yet in discussion. The main mechanisms proposed to explain this partition are (1) coordination bonding between metal and poly(ethylene oxide) (PEO), (2) interaction between metalate anions and pseudo-polycations (PPC) formed by the solvation of the polymer with cations of the ATPS-forming salt, (3) hydrophobic solvation. In this work, we investigate the mechanisms for ATPS formed by PEO and SCN⁻ salts (Na⁺, K⁺) in the extraction of Fe³⁺, Co²⁺ and Ni²⁺, relevant for green energy applications.

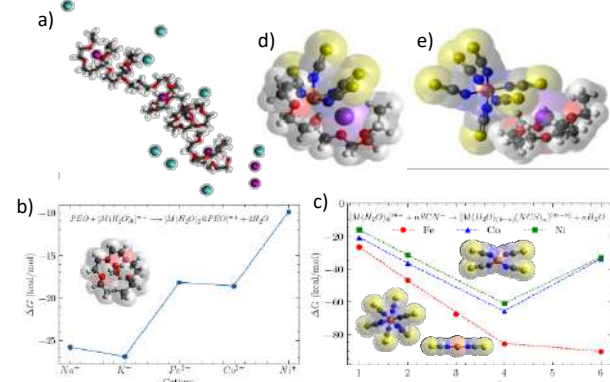
METHODS

To probe the formation of the PPC, Molecular dynamics (MD) simulations were performed for different PEO-NaCl-water systems compositions using GROMACS software and SPC/E and OPLS-AA force fields. Simulations were run for at least 80 ns generating a reliable sample. Also, the most stable structures of the complexes (M@PEO, M(SCN)_n) and the reaction free energies (ΔG_r) were investigated with Density Functional Theory (DFT) in the presence of implicit SMD solvent. Orca package and B97-3c method were employed.

RESULTS

Formation of the PPC was observed in the MD simulations (Fig. 1a). The PEO coils around the Na⁺ cations and the Cl⁻ anions distribute close to PPC. This result supports mechanism 1 and 2 by the hypothesis that Fe³⁺, Co²⁺ and Ni²⁺ could replace Na⁺ or K⁺ in the PPC and/or form metalate anions that could replace Cl⁻ and interact with PPC. To investigate via 1, the ΔG_r of the metal complexation by a PEO fragment was calculated. The values indicate the favoring of the reaction in the order K⁺ > Na⁺ > Co²⁺, Fe³⁺ > Ni²⁺ (Fig. 1b), which indicates that this step alone is not enough for the extraction. To explore via 2, the ΔG_r for the complexation of M by SCN⁻ was computed. Fig. 1c shows an order for reaction favorability of Fe³⁺ > Co²⁺ > Ni²⁺, which agrees with the extraction experiments,² indicating the relevance of this step.

Figure 1. (a) Formation of PPC in PEO-NaCl-water system; ΔG_r for the formation of (b) [M@PEO] and (e) [M(SCN)_n]-[M@PEO] interaction for (b) n=4 and (c) n=6.



The feasibility of the interaction between the PPC and [M(SCN)_n]^{m-n} (Fig. 1d,e) was investigated. The binding energy (E_b) indicates a stronger interaction with the low charged M(SCN)₄ complexes, favoring Fe over Co and Ni, again in accordance with the experimental findings (Tab. 1). For M(SCN)₆, the module of E_b values are lower and no metal selectivity is observed. The bulky size of the metalates produces a steric hindrance, impeding the close interaction with the PPC. Also, via 3 was probed by calculations under different solvents which pointed to further increase in extraction for ether-like solvents, close to the ATPS top-phase.

Table 1. E_b (kcal/mol) in [M(SCN)_n]-[M@PEO] aggregates.

Complex	M	q_{complex}	E_b	
			[Na@PEO] ⁺	[K@PEO] ⁺
[M(SCN) ₄] ^{m-4}	Fe ³⁺	-1	-32.72	-36.83
	Co ²⁺	-2	-9.52	-17.29
	Ni ²⁺	-2	-5.85	-9.66
[M(SCN) ₆] ^{m-6}	Fe ³⁺	-3	-7.74	-17.64
	Co ²⁺	-4	-7.25	-16.34
	Ni ²⁺	-4	-7.46	-15.91

CONCLUSIONS

The three mechanisms proposed were proved to influence metal partition behavior. The thiocyanate ability to act as phase forming salt and complexing agent simultaneously is paramount in these ATPS.

REFERENCES

- H. P. Neves et al., Sep. Purif. Technol., 2022, 282. 120064.
- G. M. D. Ferreira et al., J. Mol. Liq., 2021, 327. 114803.

ACKNOWLEDGMENTS

The authors thank CNPq, MCTI, CETEM and CAPES.

Avaliação topológica das interações intermoleculares em anéis mesoiônicos 1,3-diazólio-4-tiona; 1,3-tiazólio-5-tiona e 1,3-oxazólio-5-ona

Antoni Souza Strozzi (IC),¹ Italo Curvelo dos Anjos (PQ).^{1*}

antonisouza1999@gmail.com; italo.anjos@ufmt.br

¹Departamento de Química, Universidade Federal do Mato Grosso, Cuiabá - MT - Brasil;

Palavras Chave: Ligação Química, Ligação de Hidrogênio, QTAIM, Mesoiônicos.

INTRODUÇÃO

Os compostos mesoiônicos são moléculas sintéticas compostas por heterocílicos de 5 membros com elevada separação de cargas e estrutura eletrônica pouco usual. Vários desses compostos possuem atividade biológica, , além de terem aplicação em dispositivos de ótica não linear e serem usados em síntese orgânica. Os mesoiônicos são normalmente mais estáveis quando apresentam grupos aromáticos ligados ao anel mesoiônico, formando sólidos isoláveis em condições ambiente, enquanto os mesoiônicos sem esses grupos aromáticos costumam se decompor nas mesmas situações. Neste trabalho, investigou-se a formação de interações intra e intermoleculares em monômeros e dímeros de três compostos mesoiônicos distintos.

MÉTODOS

Foram realizados cálculos de varredura para avaliar a posição relativa dos grupos fenila em relação ao anel mesoiônico. A seguir, foram realizados cálculos de otimização e frequência tanto para as moléculas isoladas quanto para os dímeros nos arranjos paralelo e antiparalelo. Em ambos os casos foram usados o funcional M06-2X e a função de base 6-311+g(d,p).

A partir das estruturas otimizadas, foram feitos cálculos de QTAIM e do índice NCI.

Foram utilizados o programa Gaussian 16 para os cálculos de scan, otimização e frequência; AIMall para QTAIM e Multiwfn para NCI.

RESULTADOS

Na Tabela 1 estão as propriedades das interações do átomo exocíclico Z (enxofre para os anéis NNS e NSS, e oxigênio para NOO) com o hidrogênio do grupo fenila.

Tabela 1 Propriedades da interação intramolecular Z --- H: distância interatômica, densidade eletrônica e laplaciano da densidade eletrônica no BCP e índice de delocalização

	NOO	NNS	NSS
$d_{X-H} (\text{\AA})$	2,39	2,68	2,75
$\rho (\times 10^{-2})$	1,21	1,25	1,16
$\nabla^2 \rho (\times 10^{-2})$	+4,20	+3,65	+3,54
$\delta_{A,B} (\times 10^{-2})$	4,51	6,63	5,42

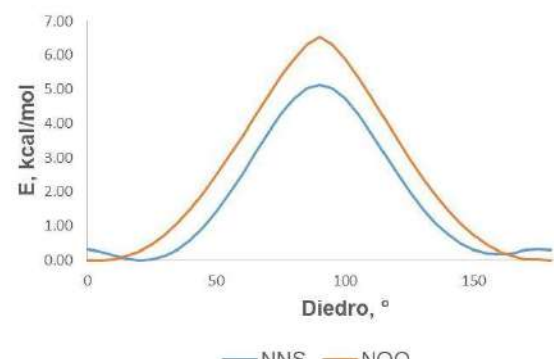


Figura 1 Energias relativas à rotação do grupo fenila

Na Figura 1, encontram-se os resultados dos cálculos de scan com os pontos máximo e mínimo de energia da rotação dos grupos fenila em função do diedro, em kcal/mol.

CONCLUSÕES

Para os monômeros, o diedro entre o anel mesoiônico de menor energia é de 0 e 35° enquanto a maior energia é 90°, com uma diferença entre 4 e 7 kcal/mol entre os pontos mínimo e máximo. Além disso, uma ligação de hidrogênio intramolecular parece contribuir para a estabilização de cada um dos compostos.

A dimerização é mais favorável nos arranjos antiparalelos, o que pode ser facilitado pela alta separação de cargas em cada anel mesoiônico. Já a formação dos dímeros paralelos, ocorre com certo desalinhamento entre os polos de mesma carga dos monômeros, de modo a minimizar interações repulsivas

REFERÊNCIAS

Anjos, I. C.; Rocha, G. B. A Topological Assessment of the Electronic Structure of Mesoionic Compounds. *J. Comput. Chem.* 2015, 36 (25), 1907–1918. <https://doi.org/10.1002/jcc.24027>.

Zhao, Y.; Truhlar, D. G. Density Functionals with Broad Applicability in Chemistry. *Acc. Chem. Res.* 2008, 41 (2), 157–167. <https://doi.org/10.1021/ar700111a>.

AGRADECIMENTOS

CNPq e UFMT.

Predicting Pt-195 NMR chemical shift in Pt(II)-Sn(II) complexes using the NMR-DKH basis sets

Milena A. Pereira (PG)^{1*}, Larissa P. N. M. Pinto (PG)¹, Hélio F. Dos Santos (PQ)², Diego F. S. Paschoal (PQ)¹

milenaaguiarj18@gmail.com; diegopaschoal01@gmail.com

¹Núcleo de Química Teórica e Computacional de Macaé, Polo Ajuda, Instituto Multidisciplinar de Química, Centro Multidisciplinar UFRJ-Macaé, Universidade Federal do Rio de Janeiro, Macaé, RJ, Brazil. ²NEQC: Núcleo de Estudos em Química Computacional, Departamento de Química – ICE, Universidade Federal de Juiz de Fora, Juiz de Fora, MG, Brazil.

Keywords: (catalysts, Pt(II)-Sn(II) Complexes, NMR, computational protocol)

INTRODUCTION

Pt(II)-Sn(II) complexes are known as excellent homogeneous catalysts. Thus, there is great interest in studying the structure and mechanism of catalysis of these complexes.¹ A fundamental technique for this study is Nuclear Magnetic Resonance (NMR) spectroscopy, where the use of Pt-195 NMR is an important tool for studying the Pt(II)-Sn(II) complexes. Considering that studies involving Pt-195 NMR chemical shift in Pt(II)-Sn(II) complexes are scarce,² the present study aims to predict the Pt-195 NMR chemical shift ($\delta^{195}\text{Pt}$) in Pt(II)-Sn(II) complexes employing nonrelativistic and quasi-relativistic approximations.

METHODS

A set of 100 Pt(II)-Sn(II) complexes, which present experimental data for the $\delta^{195}\text{Pt}$, were selected. The structure of the complexes were obtained at B3LYP/LANL2DZ/def2-SVP/IEF-PCM(UFF) using the GAUSSIAN 16 Rev. C.01 program, which is the same protocol used in the paper of Paschoal et al.². Subsequently, an evaluation of the computational protocol for predicting the $\delta^{195}\text{Pt}$ was carried out using the Cpx39 and Cpx61 complexes as models. For this, nonrelativistic (P1: $\delta^{195}\text{Pt} = -0,925 \times \sigma^{195}\text{Pt} - 2065,7558$)² and quasi-relativistic (P2 – P9: $\delta^{195}\text{Pt} = \sigma_{\text{ref}} - \sigma_{\text{calc}}$) protocols were tested using the GAUSSIAN 16 Rev. C.01 and ORCA 5.0.4 programs, respectively. Finally, the $\delta^{195}\text{Pt}$ for the 100 selected Pt(II)-Sn(II) complexes was calculated using the selected protocol.

RESULTS

Initially, considering the complex models (Cpx39 and Cpx 61), the results obtained with the nonrelativistic P1 protocol [GIAO-PBE/NMR-DKH/IEF-PCM(UFF)] presented the best agreement with the experimental values, with a relative deviation (RD) of only 0.4% and 1.6% for the Cpx39 and Cpx61 complexes, respectively. The best quasi-relativistic protocol, P3 (GIAO-OPBE-SC-ZORA/SARC-ZORA-TZVPP/ZORA-def2-TZVPP/CPCM, presented a RD of 1.1% (Cpx39) and 13.3% (Cpx61).

Thus, the P1 protocol was applied in the study of the 100 selected Pt(II)-Sn(II) complexes. The calculated results showed a good correlation between the calculated and experimental values. The determination coefficient (R^2) of 0.8462, the angular coefficient of 1.0032 and the linear coefficient of 86.2890 show that the model presents a good prediction quality (Figure 1).

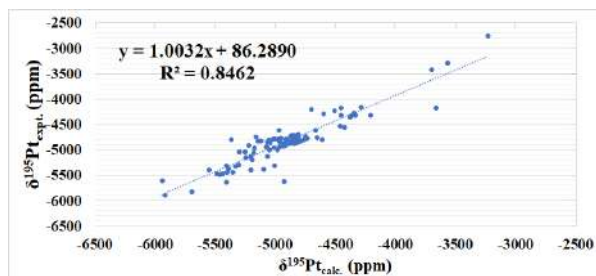


Figure 1 Correlation between calculated and experimental values of $\delta^{195}\text{Pt}$ for the 100 Pt(II)-Sn(II) complexes studied with the P1 protocol.

Considering the 100 complexes studied, a mean absolute deviation (MAD) of 140 ppm was found, which corresponds to a mean relative deviation (MRD) of only 3.0%. Finally, for some complexes that present similar structures, for example, *trans*-[Pt(C₆H₄-m-Br)(SnCl₃)(PEt₃)₂] – $\delta^{195}\text{Pt}_{\text{expt/calc}} = -4851$ ppm / -4827 ppm, and [Pt(C₆H₄-m-CH₃)(SnCl₃)(PEt₃)₂] – $\delta^{195}\text{Pt}_{\text{expt/calc}} = -4868$ ppm/-4843 ppm, the P1 protocol is able to distinguish variations in $\delta^{195}\text{Pt}$ caused by small structural changes.

CONCLUSIONS

The P1 protocol is an excellent alternative for studying the $\delta^{195}\text{Pt}$ in the search for new Pt(II)-Sn(II) complexes with potential catalytic application, presenting a MRD of only 3.0% for a set of 100 complexes.

REFERENCES

- ¹C. H. Fricke et al., ACS Catal., 2023, 13, 10627-10640.
²D. Paschoal et al., J. Comput. Chem., 2016, 37, 2360-2373.

ACKNOWLEDGMENTS

The authors would like to thank the Brazilian agency FAPERJ (E-26/201.336/2022 – BOLSA and E-26/210.070/2022) and CAPES (Finance Code 001) for the financial support.

Ligação S–H no aminotiofenol: descritores de recobrimento e QTAIM

Willis G. Barbosa (PG),¹ Carlos V. Santos-Jr. (PG),² Juracy R. Lucena Jr (PQ)¹, Renaldo T. Moura Jr. (PQ).^{3*}

willis.galvacio.barbosa@gmail.com; renaldo.mourajr@cca.ufpb.br

¹Universidade Estadual da Paraíba, Campina Grande-PB, Brasil; ²Universidade Federal da Paraíba, João Pessoa-PB, Brasil; ³Universidade Federal da Paraíba, Departamento de Química e Física, Areia, PB, Brasil.

Palavras Chave: Aminotiofenol, DFT, Propriedades de recobrimento, QTAIM.

INTRODUÇÃO

Atualmente esforços direcionam-se à investigação da captura de radicais livres e à redução da oxidação induzida por eles. O mecanismo HAT na formação do radical tiofenóxido ($\text{ArS}\cdot$) a partir do tiolfenol e seus derivados (ArSH) é objeto de intensa pesquisa, abordando a entalpia de dissociação da ligação S–H (BDE)¹. A BDE considera diversos fatores ligados à dissociação de ligações, como reorganização eletrônica e relaxamento geométrico, não sendo o descritor ideal da ligação química. Assim, para compreender efeitos ligados à situação da ligação S–H em derivados do tiofenol, é crucial aplicar metodologias de análise de ligações químicas, como a teoria quântica de átomos em moléculas (QTAIM)², o modelo de recobrimento (OP/TOP)³ ou a teoria de modos locais. Neste estudo, várias substituições nas posições *ortho*, *meta* e *para* do tiofenol foram investigadas, com foco nas substituições do aminotiofenol sendo apresentadas aqui.

MÉTODOS

As otimizações de geometria e frequência para as moléculas de aminotiofenol nas posições *ortho*, *meta* e *para* foram executadas no programa Gaussian 09, empregando o nível de teoria $\omega\text{B97X-D}/\text{def2TZVP}$. Os descritores QTAIM foram determinados por meio do software Multiwfn, enquanto os descritores OP foram computados usando o software ChemBOS.

RESULTADOS

A Figura 1 apresenta as densidades de recobrimento dos sistemas investigados, evidenciando a semelhança nas ligações S–H, que se manifesta em contraste com os valores dos descritores de ligação química exibidos na Tabela 1. Através dos descritores QTAIM, é notável uma redução nos valores de ρ_{BCP} , H_{BCP} e $\nabla^2\rho_{BCP}$ nas espécies *ortho* e *para* aminotiofenol, em comparação com o tiofenol não substituído, com pouca variação observada para o *meta* aminotiofenol. Os descritores OP/TOP acompanham a tendência observada nos descritores QTAIM, onde a substituição na posição *meta* torna o composto mais semelhante ao

tiofenol em comparação com as substituições nas posições *ortho* e *para*. Embora os mapas da Figura 1 pareçam similar, a análise topológica da densidade OP revela, por exemplo, a posição *ortho* com $\nabla^2\rho_{OCP}$, o Laplaciano no ponto crítico de recobrimento (OCP) mais negativo, revelando uma depleção de carga pouco captada pela QTAIM.

Figura 1. Densidades OP das ligações S–H para tiofenol (a) e seus derivados *ortho*- (b), *meta*- (c) e *para*- aminotiofenol.

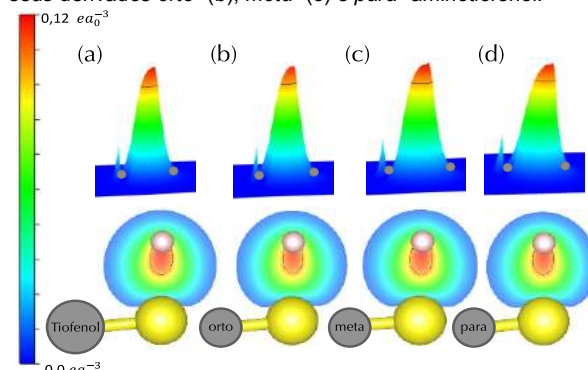


Tabela 1. Propriedades de recobrimento e QTAIM da ligação S–Hs: distância de ligação R (Å), polarizabilidade OP α_{OP} (\AA^3); densidade OP ρ_{OP} ($e\text{a}_0^{-3}$), repulsão intra-recobrimento J_{OP}^{intra} (E_h); densidade no OCP ρ_{OCP} ($e\text{a}_0^{-3}$), Laplaciano no OCP $\nabla^2\rho_{OCP}$ ($e\text{a}_0^{-5}$); densidade no BCP ρ_{BCP} ($e\text{a}_0^{-3}$); densidade de energia no BCP H_{BCP} ($e\text{h}\text{a}_0^{-3}$); Laplaciano de ρ_{BCP} no BCP $\nabla^2\rho_{BCP}$ ($e\text{a}_0^{-5}$).

S–H	Tiofenol	<i>o</i> -atf	<i>m</i> -atf	<i>p</i> -atf
R	1,338	1,343	1,338	1,342
α_{OP}	0,548	0,631	0,607	0,914
ρ_{OP}	0,818	0,808	0,824	0,809
J_{OP}^{intra}	11,87	11,47	12,08	11,56
ρ_{OCP}	0,119	0,118	0,120	0,118
$\nabla^2\rho_{OCP}$	-1,048	-2,108	-1,134	-1,290
ρ_{BCP}	0,220	0,218	0,220	0,217
H_{BCP}	-0,212	-0,206	-0,212	-0,208
$\nabla^2\rho_{BCP}$	-0,657	-0,638	-0,656	-0,641

CONCLUSÕES

Os descritores OP/TOP acompanham a tendência observada nos descritores QTAIM, mas foram mais sensíveis. Análises de modos locais e com outros substituintes estão em curso.

REFERÊNCIAS

1. J. Rimarčík, V. Lukeš, E. Klein, L. Rottmannová. Comput. Theor. Chem. 967 (2011) 273.
2. R. F. W. Bader. Chem. Rev. 91 (1991) 893.
3. R. T. Moura, et al. J. Mol. Mod. 26 (2020), 301.

AGRADECIMENTOS

UEPB, UFPB, CAPES.

Viriális: A Web-based Program that Calculates the Second Virial Coefficient

Alberto Seleto de Souza(IC)*¹, Patrícia Regina Pereira Barreto(PQ) ².

albertoseleto@usp.br; prpbarreto@gmail.com

¹Departamento de Engenharia de Materiais, Escola de Engenharia de Lorena da USP - Área II - Lorena – SP,

²Laboratório Associado de Plasma, Instituto Nacional de Pesquisas Espaciais, CP515, São José dos Campos – SP – Brasil.

Keywords: Monte Carlo Integration, Potential Energy Surface, Second Virial Coefficient, Interactive web based program, non linear regression.

INTRODUCTION

A web-based program called *Viriális* has been developed in order to calculate the classical second virial coefficient $B(T)$ ¹, alongside with its quantum corrections, for a molecular system of A_2-B_2 type as a rigid rotor. The intermolecular interaction energy $V(R, \theta_a, \theta_b, \varphi)$ is defined as:

$$V(R, \theta_a, \theta_b, \varphi) = 4\pi \sum_{L_a, L_b, L} V^{L_a, L_b, L}(R) Y_{L_a L_b}^{L_0}(\theta_a, \theta_b, \varphi)$$

Where R is the distance between the centers of mass, θ_a and θ_b are the angles between the molecule axis and the center of mass coordinates, and φ is the dihedral angle between A_2 and B_2 . $Y_{L_a L_b}^{L_0}$ represents the bipolar spherical harmonics, and $V^{L_a, L_b, L}$ are the moments, that can be write in terms of the leading configuration (LCs) and can be described as Pirani potential² or the fifth degree Rydberg potential³.

The goal of this work is to obtain the value of the second virial coefficient through a computational numeric method hosted in the web, so other research can avail from it.

METHODS

Using ab initio points from electronic structure calculation made in *Molpro*, *Gaussian*, and *SAPT*, it was possible to create a code in *Python* that fits these points to the fitting function of choice, and calculates B for various temperatures(T) using Monte Carlo integration through the *VEGAS* library⁴. The final outputs are a downloadable information table, and plots of $B \times T$, $V \times R$, and $V^{L_a, L_b, L} \times R$. Several different systems were used to test the code, but only the results for H_2F_2 will be shown here.

RESULTS

The software can be accessed through <https://viriialis.streamlit.app/>. Figure 1 represents the Home Page of *Viriális*. From there, the user can read the instructions on how to use it, and proceed to page “Regression”, where he can input his ab initio points’ files and choose the desired fitting function. Once the fitting is done, the energy information is displayed in a plot (figure 2), and the

generated information can be used as input for the page “Polyatomic Molecules A_2B_2 ”. There, a few options ought to be specified, such as the number of temperatures, and the atoms that are being used. *Viriális* uses the equation of state⁵ as a reference data.

Welcome to Virialis!



Figure 1: Virialis Home Page.

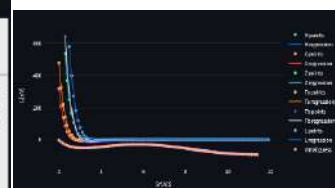


Figure 2: Graph of $V \times R$ of H_2F_2 , for the six LCs.

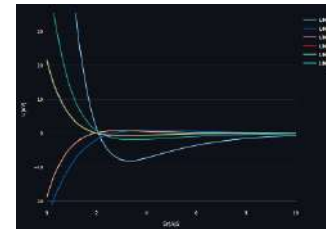
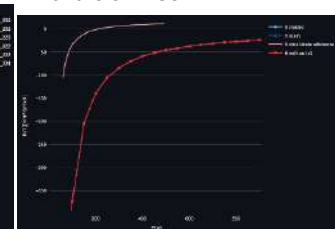


Figure 3: Graph $V^{L_a, L_b, L} \times R$ of H_2F_2 .



CONCLUSIONS

As shown in the previous figures, *Viriális* is a working and functioning code that returns valuable information about $B(T)$ of A_2-B_2 type systems. However, its precision is imperfect, and corrections are still underway. Apart from A_2-B_2 , it also works for $A-B$ molecules, and we wish to expand it to a wider range of molecules, including the most general case $AB-CD$.

REFERENCES

- BARRETO, P.; CRUZ, A.; EUCLIDES, H.; ALBERNAZ, A.; CORREA, E. J. Mol. Mod., v. 26, p. 277, 09 2020. 3, 5
- CORREA, E.; ALBERNAZ, A.; BARRETO, P.; AQUILANTI, V. Chem. Phys. Lett., v. 779, p. 138845, 06 2021. 5, 6
- CORREA, E.; ALBERNAZ, A.; BARRETO, P.; AQUILANTI, V.. Chem. Phys. Lett., v. 779, p. 138845, 06 2021. 5, 6
- LEPAGE, G. P. J. of Comp. Phys., v. 27, n. 2, p. 192–203, 1978.
- MENG, L.; DUAN, Y.-Y.; WANG, X.-D.. Fluid Phase Equilibria, v. 260, n. 2, p. 354–358, 2007.

ACKNOWLEDGEMENTS

I thank CNPq for funding my undergraduate research for the past three years.

Minimal model of the catalytic site of human thioredoxin reductase: A molecular prototype to study biocatalytic reactions

Daniel B. Quintanilha (IC)^{1*}, Hélio F. Dos Santos (PQ)¹

daniel.quintanilha@estudante.ufjf.br; helio.santos@ufjf.br

¹ Núcleo de Estudos em Química Computacional, Departamento de Química, UFJF

Keywords: ONIOM, TrxR, Biocatalysis.

INTRODUCTION

Thioredoxin reductase (TrxR) is a homeostasis regulator in mammalian cells. This enzyme is associated with higher expression in tumor cells, which makes it a potential target for chemotherapy. The catalytic site of TrxR has been characterized as a deep cavity within the protein dimer, comprising an internal N-terminal domain and a lengthy and mobile C-terminal domain (Figure 1a). The natural substrate for TrxR is the thioredoxin,¹ one of the proteins associated with the induction of apoptosis cascade in human cells.

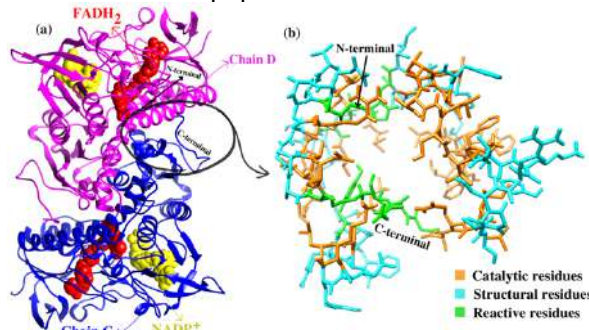


Figure 1. Structure of TrxR (PDB:2J3N) (a), and the molecular model of the TrxR catalytic site (b).

The catalytic action of TrxR is based on an electron transfer mediated by a redox reaction between pairs of Cys at the N- and C-terminal domains. Regarding the enzyme inhibitors, two interaction modes are described: (1) by forming a non-covalent network of contacts that stabilizes the drug-receptor complex, thereby blocking the interaction between N- and C-terminal; (2) by forming a covalent bond with the Cys at C-terminal, leading to the deactivation of the TrxR.

This study describes a molecular model for the catalytic site of TrxR. This was built based on our previous paper where organic inhibitors were evaluated and the main residues identified.² Our current focus is on the TrxR-inhibitor covalent interaction, aiming to provide kinetic and thermodynamic data for biocatalytic reactions under confinement regime.

METHODS

The model was constructed based on our previous study. It represents the catalytic site by 80 residues (38 from the chain C and 42 from chain D), which comprises 8% of the enzyme structure (Figure 1b). The residues were selected based on their contacts with the ligands.² The structural residues are responsible to maintain the

active form for the site; the catalytic residues stabilize the ligand-receptor complex; the reactive residues are essential for catalysis. The reactions were modeled at QM/MM (ONIOM) level, employing B3LYP/6-31G(d) level for the high-layer (QM), and the UFF force field for the low-layer (MM). The high-layer included the ligand and H463, G487, C488, C489, Gly490, K513, C543, C548, Y600, I831 residues. The other residues were defined as low-layer. Besides, the C_α of the structural residues was frozen (35 atoms).

RESULTS

The optimized geometry of the catalytic site preserved its native structure, with the overall RMSD found 1.4 Å.

The TrxR inhibition has been studying in our group for organic (pleurotin) and inorganic (auranofin) molecules. The DTNB, a standard for TrxR activity assay, was used as reference. For pleurotin, it was observed that the ligand fits at the catalytic site with the carbonyl groups of quinone and lactone rings near to the S of C489 (S...CO = 3.60 Å) and C488 (S...CO = 3.64 Å), respectively. Moreover, the lactone carbonyl forms a H-bond with Y600 (OH...O = 2.01 Å), which actives the carbonyl for nucleophilic attack. These preliminary results, suggests a feasible pathway to alkylate C489.

CONCLUSIONS

A molecular model for the catalytic site of TrxR was built and the geometry optimized at hybrid QM/MM method. The final structure was satisfactorily predicted, differing from X ray by 1.4 Å. When the pleurotin was included, a pre-reactive arrangement emerged, in which the Cys in the C-terminal were close to the carbonyl groups of pleurotin. This favors a nucleophilic attack, mainly at the lactone carbonyl that is activated by short H-bond with Tyr. Work is currently in process in order to represent the full reaction pathway for alkylation of Cys at C-terminal.

REFERENCES

- ¹K. Fritz-Wolf, et al., *Nat. Commun.* 2, 383 (2011).
²D. B. Quintanilha, H. F. Dos Santos, *J. Biomol. Struct. Dyn.* 41, (2023) 5646–5659.

ACKNOWLEDGMENT

CNPq (307018/2021-0), FAPEMIG and CAPES.



Improving the path to obtain spectroscopic parameters for the PI3K-(Pt Complex) system: Theoretical evidences for using ^{195}Pt NMR as a probe

Taináh M. R. Santos (PQ),^{1*} Gustavo A. Andolpho (PG),¹ Camila A. Tavares (PQ),¹ Mateus A. Gonçalves (PQ),¹ Teodorico C. Ramalho (PQ).¹

teo@ufla.br; tainah-martins@hotmail.com

¹Chemistry Department, Natural Sciences Institute, Federal University of Lavras (UFLA) P.O. Box 3037 – 37200-900 – Lavras, MG – Brasil

Palavras Chave: Platinum Complex, Spectroscopic Probes, PI3K, NMR, Molecular Dynamics.

INTRODUCTION

The absence of adequate force field (FF) parameters to describe certain metallic complexes makes new and deeper analyses impossible. In this context, after a group of researchers developed and validated an AMBER FF for a platinum complex (PC) conjugated with AHBT, new possibilities emerged¹. Thus, in this work, we propose an improved path to obtain NMR spectroscopic parameters, starting from a specific FF for PC, allowing to obtain more reliable information and a longer simulation time.

METHODOLOGY

A docking study was carried out, using Molegro Virtual Docker, between a PC and PI3K enzyme. From this result, to carry out a simulation of classical molecular dynamics (MD), using Amber 20, with an explicit solvent and 50 ns. To explore a new PC environment, a second MD simulation was performed only between the complex and water molecules, under the same conditions as the first MD. In addition, we also selected the best frames from the two MDs through the OWSA algorithm. Thus, we performed NMR calculations, using Gaussian 09 package, in two chemical environments, enzymatic and aqueous, with theory level GIAO–PBE/PBE/NMR-DKH.

RESULTS

After analyzing the 100 poses obtained from the docking calculation, the best orientation was selected, three hydrogen bonds (H-Bonds) were identified involving PC and the valine (Val882) and glutamic acid (Glu880) amino acids. After that, a MD calculation was performed. Changes in the spatial coordinates of PC and PI3K along the entire trajectory are indicated using the RMSD, where is possible to notice the excellent evolution of the PC over time, presenting an average of only 1.42 Å and standard deviation of 0.14 Å. For PI3K, the oscillation resulted in an average of 3.68 Å, and the standard deviation of its oscillation was only 0.65 Å, which shows that there were no large variations. The analysis of the H-bonds formed between the PC and PI3K indicates two, both involving the Val882. For the selection of the best frames, a

sophisticated computational resource was used, the OWSA algorithm. The original signal obtained by MD simulations generated 2000 conformations. Thus, the treatment of the signal of the first system resulted in the selection of 93 structures, whereas the treatment of the signal of the second system resulted in the selection of 98 structures. We proposed to reduce the PC:PI3K system to be able to perform GIAO-DFT calculations without a very high computational cost, the reduced system is composed by the PC and the residue Val882. Chemical shifts calculations were performed using the 93 and 98 frames selected. The average chemical shifts values are presented in table 1.

Table 1. Theoretical ^{195}Pt chemical shifts in different chemical environments performed at theory level PBE/PBE/NMR-DKH.

Chemical Environment	$\delta(^{195}\text{Pt})$ (ppm)
Enzymatic	-1309.58 ± 25.33
Aqueous	-2911.25 ± 9.66

These calculations point out that, as expected, there is a difference when the chemical environment was changed from water to enzymatic of around 1600 ppm. These results indicate that the PC shows a different behavior in both environments, showing the sensitivity of the Pt chemical shift to these media, which is an interesting result for the application of this complex as a spectroscopic probe.

CONCLUSIONS

This work proposes a strategic path to obtain the chemical shifts in enzymatic and aqueous environments. When starting a study containing a specific FF for the PC, this leads to a more reliable investigation with, therefore, more refined results. In addition, in the selection of the best frames and residues, we achieved a decrease in the quantum calculations and computational cost.

REFERENCES

- ¹Pereira, A.F. et. al., Int. J Quantum Chem, 2021, 121, e26525.
²Santos, T. M. R. et al., Magnetochemistry, 2023, 9(4), 89.

ACKNOWLEDGMENTS

We thank the CNPq, CAPES, FAPEMIG.



TEORIA DO FUNCIONAL DE DENSIDADE E MODELOS DE CONFINAMENTO QUÂNTICO PARA SISTEMAS CURVOS

Bruna M. G. Oliveira^{1*} (IC), Eduardo V. S. Anjos² (PG) e Cristiano C. Bastos¹ (PQ);

bruna.mgoliveira@ufrpe.br;

¹Departamento de Química, Universidade Federal Rural de Pernambuco, Recife – PE - Brasil;

²Departamento de Química Fundamental, Universidade Federal de Pernambuco, Recife – PE - Brasil.

Palavras Chave: polienos, Confinamento Quântico, Modelos Moleculares, Cálculos de Química Quântica

INTRODUÇÃO

A equação de Schrödinger¹ para sistemas quânticos inspirou novas formulações para o problema do confinamento de partículas, a forma com que o espaço é considerado leva a diferentes hamiltonianos. Da Costa², por exemplo, obteve um potencial geométrico dependente da curvatura da curva.

A Teoria do Funcional de Densidade evidencia que elétrons de valência de certos sistemas podem se comportar como partículas confinadas. Isto ocorre para elétrons π como no benzeno, piridina, pirazina, diazina e triazina³.

Aqui buscamos observar novas relações entre elétrons de valência e modelos de confinamento para moléculas contendo ligações simples e duplas alternadas, em particular polienos, incluindo algumas já obtidas experimentalmente⁴.

MÉTODOS

Elaboramos modelos para polienos já sintetizados: decatetraeno, dodecapentaeno, tetradecahexaeno e hexadecaheptaeno. Expandimos o estudo para quatro moléculas de polienos, variando o número de carbono: dez, vinte, trinta e quarenta. Todos as moléculas foram construídas seguindo distâncias e ângulos típicos de sistemas deste tipo. Usamos o comando *clean* do programa *GaussView* que gera uma otimização prévia da geometria. Criamos a partir disto, três tipos de cálculo: sem otimização, otimizando e impondo a linearidade para a molécula. As otimizações foram feitas em nível PM3 com o programa MOPAC. Em todos os casos realizamos para as estruturas finais cálculos B3LYP/6-31G. Para cada sistema geramos suas respectivas moléculas encurvadas em uma das extremidades.

Consideramos o modelo de confinamento canônico e o confinamento descrito por Da Costa:

$$-\frac{\hbar^2}{2m} \frac{\partial^2 \psi}{\partial s^2} - \frac{\hbar^2 k(s)^2 \psi}{8m} = E\psi \quad (1)$$

Onde temos, o operador Laplaciano e um operador geométrico atrativo, dependente da curvatura $k(s)$ da curva.

RESULTADOS

Os sistemas lineares parecem se aproximar mais dos sistemas experimentais. Em geral, a distribuição do *HOMO* (último orbital molecular ocupado) correspondeu ao número de nós na função de onda definida pelo modelo canônico da partícula confinada. Nos sistemas curvos, houve uma diminuição no número de elétrons de valência e número de nós do *HOMO*. Os elétrons se concentram mais na parte curva da molécula, remetendo ao potencial geométrico.

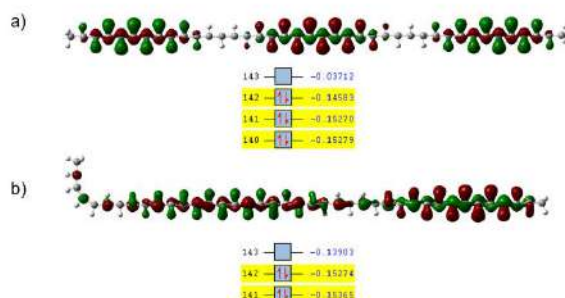


Figura 1. Densidade de orbitais HOMO dos sistemas. a) polieno linear e b) polieno com curvatura induzida.

Para os $C_{40}H_{44}$, identificamos seis elétrons (Fig.1a) e quatro elétrons (Fig.1b) de valência se comportando como confinados. O *HOMO* apresenta três e duas regiões de distribuição, que associamos aos nós das respectivas funções de onda no modelo de partículas confinadas.

CONCLUSÕES

Por meio de cálculos de química quântica para polienos foi possível observar elétrons de valência se comportando como confinados. A distribuição dos elétrons pode ser associada ao potencial geométrico descrito por Da Costa.

REFERÊNCIAS

- ¹SCHRÖDINGER, E. *Annalen Der Physik*, 384(4), 361, 1926.
- ²DA COSTA, R. C. T. *Phys. Rev. A*, 23, 1986, 1981.
- ³BASTOS, C. C. et al. *J. Math. Chem.*, 54(9), 1822, 2016.
- ⁴Christensen, R. L. et al *The J. Phys. Chem. A*, 112(49), 12629, 2005.

AGRADECIMENTOS

CNPq, CAPES, UFPE, LnP e UFRPE.

COMPUTATIONAL STUDY OF CO₂ REDUCTION REACTION WITH A MOLECULAR MANGANESE COMPLEX GENERATING ACETIC ACID

Gabriela Garcia (PG),^{1*} Ataulpa A. C. Braga (PQ)¹.

ggarcia@iq.usp.br

¹Departamento de Química Fundamental, Instituto de Química da USP (IQ-USP).

Palavras Chave: Computational Chemistry, Electrochemistry, Homogeneous Catalysis, Electrocatalysis, CO₂.

INTRODUCTION

Inspired by the work of Ratnadip De, *et al*¹, a manganese complex with corrole ligand was used as the catalyst (Figure 1) for the theoretical calculations of CO₂ electroreduction's reaction path to form acetic acid. Based on this, a reaction mechanism was proposed, through computational methods, as a proof of concept to this type of reaction (Figure 2).

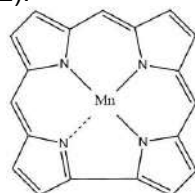


Figure 1: Mn-Corrol Catalyst

METHODES

Geometry optimizations were carried out in the Gaussian 16 software, with unrestricted B3LYP functional, Def2-SVP basis set, and single-point calculations, with Def2-TZVP. Since this is an open shell system, all structures were optimized with different multiplicities, and the ones with lowest energy were elected as the most stable multiplicity. No spin contamination was found in any structure.

RESULTS

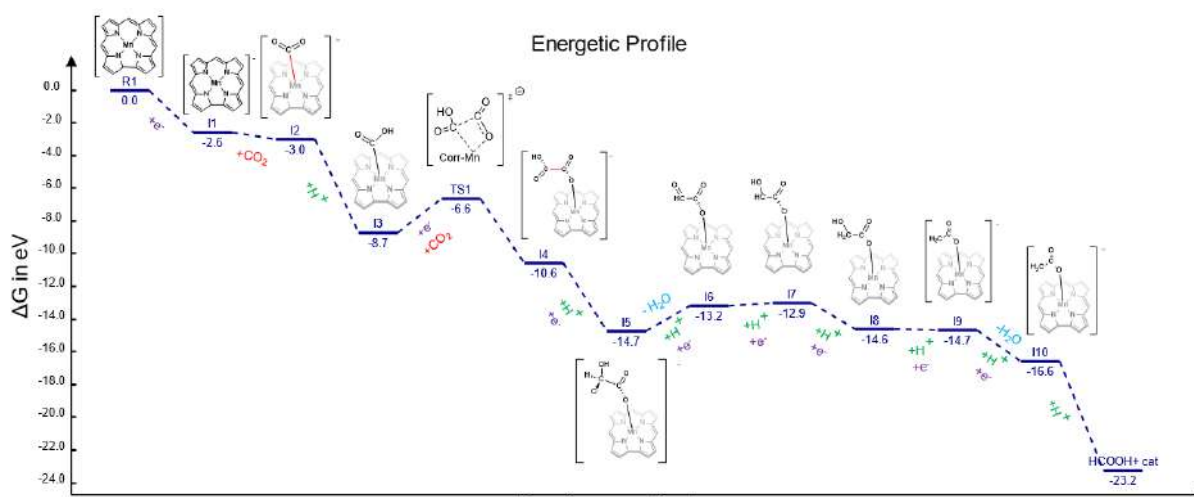


Figure 2: Energetic profile

The electroreduction of the initial Mn (III) (R1) to Mn (II) (I1) forms a species that can activate a carbon dioxide molecule from saturated atmosphere. As it follows, the intermediate I2 receives a proton from water (20% in acetonitrile solution), leaving the carbon more electrophilic. When receiving another electron, I3 becomes able to bind a second CO₂ molecule, forming the carbon-carbon bond, which is the most interesting step for this work, since our goal is to form C₂₊ products. On the following ones, the reaction undergoes successive proton coupled electron transfers, that in the end will release acetic acid and restore the initial catalyst. The missing transition states are being sought and still need energy calculation at a higher level of theory, as for the other species.

CONCLUSIONS

It is possible to obtain C₂₊ products from CO₂ molecules using a homogeneous manganese electrocatalyst. Although several possible pathways can be thought of, only the one presented had its intermediates reached stable geometries.

REFERENCES

¹ De, R.; *et al.* *Angew. Chem. Int. Ed.*, 2020, 59, 9228–9232.

AKNOWLEDGEMENTS

CNPq, CAPES, FAPESP

Unveiling the Flexibility of the Active Site of SARS-CoV-2 Protease: Exploring New Avenues for Virtual Screening of Multiconformer Inhibitors

Luiz E. G. da Cruz¹ (PG), Rafael E. O. R. (PQ)², Elton J. F. C. (PQ)¹, Pedro H. C. F. (PG)², Leon S. C. C. (PG)³, Igor B. G. (PQ)¹, Fabiana C. G. (PQ)⁴, Carlos. H. da S. (PQ)⁴, Marcus T. S., Alex D. C. (PG)⁵, Karina S. M. (PG)¹, Adriano V. W. (PG)², Rafaela S. F. (PG), Leonardo H. F. de Lima (PQ)² and Gerd B. Rocha (PQ)¹.

luiz_eduardo_gc@hotmail.com;

¹ Universidade Federal da Paraíba, João Pessoa, Brasil; ² Universidade Federal de São João Del Rei, Sete Lagoas, Brasil;

³Laboratório Nacional de Computação Científica, Petrópolis, Brasil; ⁴Universidade Federal de Itajubá, Itabira, Brasil; ⁵s, Universidade Federal do Rio Grande, Rio Grande, Brazil.

Palavras Chave: COVID-19; SARS-CoV-2; metadynamics simulation; multiconformational drug targeting; quantum chemical calculations.

INTRODUCTION

The main protease (Mpro) catalyses a crucial step in the SARS-CoV-2 life cycle. The recent SARS-CoV-2 presents the main protease (MCoV2pro) with 12 mutations compared to SARS-CoV-1 (MCoV1pro). Recent studies pointed out that these differences lead to mobility variances at the active site loops with functional implications. We used metadynamics simulations and a sort of computational analysis to probe the dynamic, pharmacophoric, and catalytic environment differences between the monomers of both enzymes.

METHODS

To comprehensively explore the free energy landscape of the Mpro protomers from SARS-CoV-1 and SARS-CoV-2, a preliminary equilibrium MD stage was executed. Subsequently, both well-tempered and non-tempered MetaDy simulations were conducted. For assessing solvation enthalpies, the PM7 method was employed. To comprehend solvent interactions at position SER46 for both enzymes, we utilized NCIPLOT and Primordia to study the variation of electronic quantum chemical descriptors related to catalysis. In pursuing an optimal Mpro active site ligand, a hierarchical virtual screening cascade was employed: (i) structure-based pharmacophore screening and (ii) ensemble docking. We used the following ligand databases: (i) Drugbank, (ii) ZINC15 database, and (iii) SistemX. To validate the efficacy of the docking protocol, we leveraged both GOLD and Molegro Virtual Docker (MVD) software platforms.

RESULTS

We observe a significantly greater availability of open binding conformations in the MCoV2pro monomer compared to MCoV1pro. The A46S substitution in the MCoV2pro S2 loop appears to contribute significantly to this increased hydration tendency (Figure 1.a). QM calculations suggest that the broader conformations of MCoV2pro exhibit reduced catalytic activity in the monomer. Nevertheless, the statistical data for interactions involving the N-finger imply that this activity is better in the dimer. Docking analyses indicated that the ability to modulate the width of the active site could play a crucial role in facilitating ligand

access in various manners. Thus, we conducted a multi-conformational virtual screening using different ligand libraries (Figure 1.c). Our findings emphasize the significance of accounting for protein conformational diversity when seeking potential anti-MCoV2pro compounds.

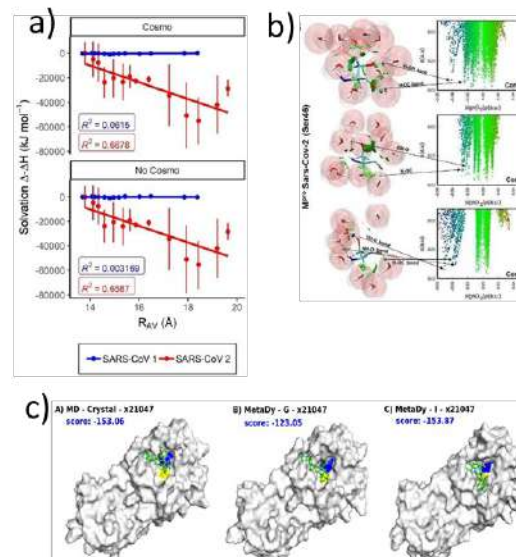


Figure 1. (a) Variation in the hydration enthalpy; (b) Hydration effects on the residue SER46; (c) Multi-conformerflexible docking's hits explore the MCoV2Pro active site space in different ways.

CONCLUSIONS

By employing a combination of computational tools, we shed light on the distinctions in motion, druggability, and activity between Mpro monomers in both SARS-CoV-1 and SARS-CoV-2. We found a new set of notably open conformations that arise in MCoV2pro and are potentially facilitated by solvation effects.

REFERENCES

¹Rocha REO, et al, JBSD, 2022;40(19):9214-9234. <https://doi.org/10.1080/07391102.2021.1924271>.

AGRADECIMENTOS

The authors thank UFPB, LNCC, CENAPAD-SP, NPAD/UFRN, Capes, and CNPQ.

Molecular Dynamics study of imidazolium based ionic liquids in aqueous system applied to osmosis technologies

Matheus Signorelli* (PhD)¹, Marie-Madeleine Walz (R)², Carl Caleman (R)², Luciano T. Costa (R)¹, Olle Björneholm (R)²
matheussignorelli@id.uff.br; lcosta@id.uff.br

¹Universidade Federal Fluminense, Department of Physics and Astronomy

Department of Physical-Chemistry;

²Uppsala

Keywords: Ionic Liquids, Molecular Dynamics, Osmosis

INTRODUCTION

The present work evaluates by molecular dynamics the mobility of different ionic liquids derived from cations containing imidazolium ring in aqueous system. The aim was to elucidate their characteristics and look for patterns in their molecular compositions capable of predicting the behavior of new ionic liquids with potential application for desalination by direct osmosis. The study draws a parallel with the literature¹ and submits dynamic calculations for different systems, seeking to find the influence of many factors as well as the interface phenomena resulting from the hydrophobicity of some chains.

METHODS

This study was based on imidazolium ionic liquids varying the alkyl chain length and the anions regards to the hydrophobicity features. The force fields used for all ILs are based on CL&P development, which has already been used for ionic liquids with good experimental data agreement². The force field for the water molecule was based on TIP4P-2005. The protocol used is shown in Figure 1. A mixture of 25 ion pairs and 2000 water molecules was built for each simulated systems with the use of the Packmol software. MD simulations were performed for all systems by using the Gromacs 2022 suite package at the NpT ensemble. After the equilibration of the density, a slab was built with vacuum interfaces. Once these slabs were made, all systems were again simulated in NVT ensemble. In this way, the mobility of the species, their distribution in the simulation box and their hydrophobicity were evaluated.

RESULTS

Phase separations were observed in systems with higher hydrophobicity as expected. Such systems contain cations with a longer carbon chain or anions such as $[\text{TFSI}]^-$, bis-trifluoromethanesulfonylimide. Such systems formed surface layers in contact with the vacuum as also evidenced by XPS and allowed the verification of lateral mobility confined to the surface. The orientation of the ions was also obtained with the carbonic chains oriented to the vacuum and solvation of the imidazolium rings in

water allowing the formation of small charge distributions between the layers.

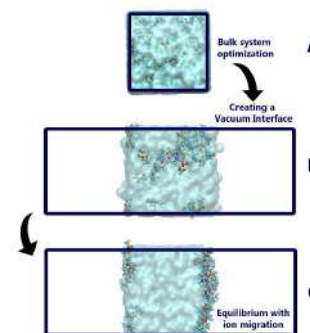


Figure 1. Representation of the protocol used for the simulations with a bulk NpT equilibration (A), a slab building with the vacuum interfaces (B) and the NVT ensemble simulations until the system reach the equilibrium.

CONCLUSIONS

The present work showed a comparison between different ionic liquids in aqueous solution by the optic of the molecular dynamics simulation. Based on that, this study helped to elucidate the influence of the alkyl chain in the displacement and the interface enrichment of ionic liquids in hydrophobic systems generating a quantitative analysis for that. These results are useful when trying to create mechanisms of desalination that requires multiple steps such as the forwards osmosis with recover of the draw solution.

REFERENCES

1. DUTTA, S.; NATH, K. Prospect of ionic liquids and deep eutectic solvents as new generation draw solution in forward osmosis process. *Journal of Water Process Engineering*, v. 21, p. 163–176, fev. 2018.
2. Fuentes-Azcatl, R.; Araujo, G. J. C.; Lourenço, T. C.; Costa, C. T. O. G.; Walkimar de M. Carneiro, J.; Costa, L. T. Dielectric behavior of water in $[\text{bmim}][\text{Tf}_2\text{N}]$ room temperature ionic liquid: molecular dynamics study. *Theor. Chem. Acc.* 2021, 140, 125–134.

ACKNOWLEDGMENTS

The authors would like to thank CAPES, CNPq and the postgraduate program in chemistry at the UFF Institute of Chemistry and Uppsala University.

Estudo teórico do impacto da dimerização do complexo $[Bi(dmit)_2]^-$ sobre o espectro Ultravioleta-Visível em solução de acetonitrila

Heloisa N. S. Menezes (IC)^{1*}, Henrique C. S. Júnior (PQ)², Glaucio B. Ferreira (PQ)¹.

heloisanaomy@id.uff.br

¹Pós-Graduação em Química, Universidade Federal Fluminense – Niterói (RJ); ²Pós-Graduação em Química Universidade Federal do Rio Grande do Sul – Porto Alegre (RS).

Palavras-Chave: Química Computacional, Métodos Ab Initio, Complexos dmit, Espectro UV-Vis.

INTRODUÇÃO

Os complexos do ligante 1,3-ditiola-2-tiona-4,5-ditiolato (dmit) são estudados há décadas e possuem propriedades químicas com aplicações em supercondutores, compostos magnéticos e óptica não-linear^[1-3].

O complexo $[Bi(dmit)_2]^-$, diferente do reportado para complexos de Zn(II), Sb(III) e Sn(IV), contém uma banda de média intensidade em 365 nm no espectro Ultravioleta-Visível (UV-Vis)^[4,5]. Porém, estudos computacionais com métodos *Ab Initio* e *Density Functional Theory* (DFT) para cálculo do espectro UV-Vis não foram capazes de representar de modo conclusivo o espectro nessa região utilizando a estrutura monomérica do complexo^[4]. Esse resultado abre a possibilidade de novas geometrias em solução como responsáveis pela transição encontrada no dado experimental.

MÉTODOS

O cálculo de Dinâmica Molecular *Ab Initio* (AIMD) foi feito com o software GFN2-XTB para uma célula unitária experimental de $[Bi(dmit)_2][NBu_4]$ retirada do Cambridge Crystallographic Data Centre (CCDC)^[6] em solvente explícito acetonitrila. As geometrias usadas foram otimizadas pelo método PBEh-3c e os cálculos de espectro UV-Vis dos complexos dmit de Bi(III) foram feitos com o método *Similarity Transformed Equations of Motion Coupled Cluster with Singles and Doubles* com aproximação *Domain-Based Local Pair Natural Orbital* (STEOM-DLPNO-CCSD) com o software ORCA versão 5.0.3^[7] com funções de base Def2-TZVP. Os resultados obtidos foram comparados ao espectro UV-Vis experimental do complexo de Bi(III)^[4].

RESULTADOS

O cálculo AIMD apresentou a dimerização entre complexos bisdmit de Bi(III) com estrutura estável após o cálculo de otimização geométrica.

O cálculo STEOM-DLPNO-CCSD para $[Bi(dmit)_2]^-$ possui transições de alta intensidade em 432 e 408 nm do tipo intraligante $\pi-\pi^*$; uma transição de baixa intensidade em 364 nm de transferência de carga ligante-metal (TCLM); e uma transição de alta intensidade 277 nm do tipo TCLM. Já o resultado STEOM-DLPNO-CCSD do dímero do complexo bisdmit de Bi(III) mostra transições em 423 nm de alta intensidade intraligante $\pi-\pi^*$; uma transição TCLM 375 nm de média-alta intensidade; uma transição de média-alta intensidade em 308 nm $\sigma-$

σ^* entre metais e TCLM; e uma transição em 275 nm de média intensidade intraligante $\pi-\pi^*$.

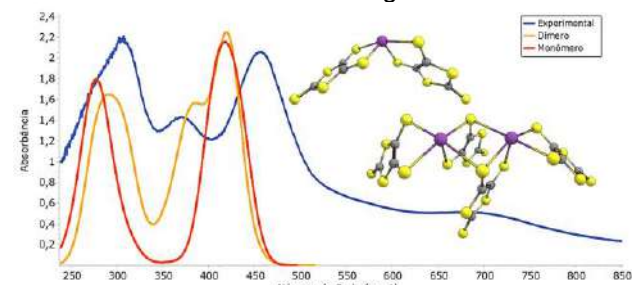


Figura 1: espectros UV-Vis dos complexos calculados comparados ao dado experimental.

Assim, se observa que a banda experimental para o espectro UV-Vis do complexo bisdmit de Bi(III) em 365 nm é encontrada computacionalmente para o cálculo de espectro utilizando o dímero do composto. O que não se verifica para o complexo dissociado, mesmo com um nível de teoria sofisticado. Em outros compostos bisdmit, como Sb(III) e Zn(II), essa banda não é encontrada^[4,5].

CONCLUSÕES

Os dados computacionais de espectro UV-Vis obtidos para o dímero do complexo bisdmit de Bi(III), mostram que a banda em 365 nm reportada experimentalmente é reproduzida pelo dímero do complexo em alta intensidade. Esse dado demanda a investigação experimental do comportamento em solução deste composto.

REFERÊNCIAS

- [1] A. Albino, S. Benci, L. Tesi, M. Atzori, R. Torre, S. Sanvito, R. Sessoli, A. Lunghi, *Inorg. Chem.* **2019**, 58, DOI 10.1021/acs.inorgchem.9b01407.
- [2] D. Espa, L. Pilia, L. Marchiò, F. Artizzu, G. Di Carlo, D. Marinotto, A. Serpe, F. Tessore, P. Deplano, *Dalt. Trans.* **2016**, 45, DOI 10.1039/c6dt02911f.
- [3] L. Valade, D. de Caro, C. Faulmann, K. Jacob, *Coord. Chem. Rev.* **2016**, 308, 433.
- [4] G. B. Ferreira, E. Hollauer, N. M. Comerlato, J. L. Wardell, *Spectrochim. Acta - Part A Mol. Biomol. Spectrosc.* **2008**, 71, DOI 10.1016/j.saa.2007.12.010.
- [5] G. B. Ferreira, E. Hollauer, N. M. Comerlato, J. L. Wardell, *Inorganica Chim. Acta* **2006**, 359, DOI 10.1016/j.ica.2005.11.041.
- [6] Cambridge Crystallographic Data Centre, “CCDC Home | CCDC,” **1965**.
- [7] F. Neese, *WIREs Comput. Mol. Sci.* **2022**, 1.

AGRADECIMENTOS

Agradecemos ao NACAD-UFRJ e LNCC pelo uso dos supercomputadores Lobo Carneiro e Santos Dumont. Agradecemos às instituições de fomento CNPq e FAPERJ pelo suporte financeiro prestado.

Efeito de grupos sulfonato em ftalocianinas para aplicação em terapia fotodinâmica

Maíra Guimarães Nobrega (PG), Jhonathan R. de Souza (PG), Antônio Moraes Neto (PG), Mateus Zanotto (PG), Paula Homem-de-Mello (PQ)

nobreaga.maira@ufabc.edu.br, paula.mello@ufabc.edu.br

ABCSim, Centro de Ciências Naturais e Humanas (CCNH), Universidade Federal do ABC (UFABC)

Palavras Chave: Câncer de mama, Fotossensibilizadores, Teoria Funcional da Densidade, Terapia Fotodinâmica.

INTRODUÇÃO

Estudos mostraram que compostos fotossensibilizadores derivados de macrociclos podem ser eficazes contra o câncer de mama.¹ Um fotossensibilizador eficiente deve apresentar alta absorção na região do vermelho, rendimento quântico e tempo de vida de tripleto elevados. Com a finalidade de atender a estes critérios para uma sensibilização eficaz, é possível inserir um íon metálico ou metaloide, como zinco, alumínio, estanho, germânio ou silício no macrociclo da ftalocianina.^{1,2} Soluções contendo uma mistura de ftalocianinas de Al(III) e Ge(IV) (AlPcSmix e GePcSmix) com diferentes graus de sulfonação têm se mostrado promissoras no tratamento do câncer de mama.¹⁻³ Neste trabalho, o efeito dos diferentes graus de sulfonação na ftalocianina livre (Fig. 1) e na ftalocianina de Al(III) foi avaliado por meio da (TD)DFT. Um baixo grau de sulfonação impede a agregação e aumenta a hidrofilicidade sem, no entanto, comprometer a interação com a membrana celular.⁴ Assim, aqui foram avaliadas substituições simétricas e assimétricas, com a introdução de um grupo sulfonato (estrutura assimétrica) ou dois (estrutura simétrica).

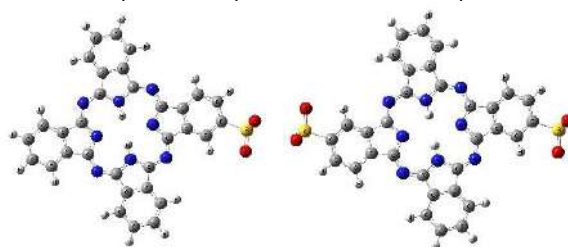


Fig. 1: Estrutura da ftalocianina livre com 1 e 2 grupos SO_3^- .

MÉTODOS

A fim de comparar com o banco de dados QM9, as geometrias e frequências vibracionais das moléculas em estudo foram obtidas em nível de teoria B3LYP/6-311G(d,p) enquanto que os espectros de absorção foram obtidos em mesmo nível usando a TDDFT. Cargas atômicas foram calculadas pelo método de Mulliken e somadas sobre o macrociclo (Σ cargas) para avaliar os efeitos dos substituintes e do Al(III).

RESULTADOS

Tabela 1. Resultados obtidos para ftalocianina livre (H2Pc) e complexada a Al(III) (AlPc) sem e com 1 (S1) ou 2 (S2) grupos sulfonato

	E_{HOMO} (eV)	E_{LUMO} (eV)	GAP (eV)	Dipolo (D)	Σ cargas
H2Pc	-5,22	-3,08	2,14	0,00	0,30
H2PcS1	-2,65	-1,30	1,36	27,73	-1,64
H2PcS2	-1,41	0,35	1,76	0,00	-1,66
AlPc	-5,35	-3,24	2,10	3,89	-0,63
AlPcS1	-2,85	-1,48	1,37	27,37	-0,67
AlPcS2	-1,57	0,19	1,76	0,14	-0,70

A energia de HOMO aumenta significativamente com o aumento do número de grupos sulfonato, dado que são grupos bastante eletronegativos (Tabela 1). O mesmo ocorre para o LUMO, e na presença de dois grupos sulfonato, o LUMO se torna positivo. No entanto, o impacto de dois grupos sulfonato é pequeno no gap HOMO-LUMO, se comparado ao efeito de 1 grupo sulfonato, que o diminui mais expressivamente. Como esperado, as moléculas simétricas (sem e com dois sulfonatos) são apolares, com exceção da AlPc, cujo metal e ligante cloreto se posicionam acima do plano do macrociclo, enquanto as assimétricas são bastante polares e não há efeito significativo do metal. Há um efeito doador de carga dos grupos sulfonato para o macrociclo (Σ cargas), que é mais expressivo para a ftalocianina livre.

PERSPECTIVAS

Estão em andamento estudos para as ftalocianinas assimétricas duplamente sulfonadas para então podermos correlacionar com os achados da literatura para atividade antitumoral desses compostos.

REFERÊNCIAS

- 1 H. Abrahamse, et al. Proc. SPIE 6139, 2006, XV, 613904.
- 2 T. K. Horne et al. Photodiag Photodyn Therapy, 2012, 9, 215.
- 3 N. A. Kuznetsova, et al. J. Porph and Phthal, 2003, 07, 147.
- 4 H. van Leengoed et al. Photochem Photobio, 1993, 58, 233.

AGRADECIMENTOS

UFABC, CNPq, FAPESP, CAPES.

Strategies to Incorporate a Variable Reduced Mass Into Analytical Quantum Tunneling Calculations

Caio M. Porto (PhD)¹, Nelson H. Morgan (R)^{1*}
c145568@dac.unicamp.br; nhmorgan@unicamp.br

¹Universidade Estadual de Campinas - Unicamp

Keywords: Quantum Tunneling, APS, CHE, DFT, DWP

INTRODUCTION

The Quantum Tunneling (QT) process involves a particle or a system of particles moving through regions with higher potential energy than the particle itself possesses. This phenomenon is prohibited by classical mechanics. To assess the impact of QT on reaction rates, various methods have been developed over the years. The most commonly used methods employ the approximation of the tunneling particle's mass as a fixed value. Nevertheless, the motion of the atoms in a system may involve motion of atoms of different masses in different parts of the potential energy surface (PES), which can introduce significant errors. The objective of the present work is to investigate the use of new strategies in order to incorporate a variable mass in QT calculations of double well potential (DWP) systems.

METHODS

The model system chosen was the ammonia molecule. It has the advantages that its energy levels and tunneling frequency are well known. The QT calculations were performed using the angular prolate spheroidal (APS) method, developed by the group for tunneling in DWP systems.¹ The electronic structure calculations were carried out using the BP86 functional in density functional theory (DFT), together with the 6-311G(3df,3pd) basis set. The functional and basis set were chosen based on previous work from the group. All electronic structure calculations were carried out in Gaussian09 software.

RESULTS

The ammonia molecule mass is known to not vary much during the umbrella motion. Figure 1 shows the values for the reduced mass at each point of the IRC calculation.

Three methods have been implemented and tested in the present work. The first one uses the displacements of the atoms as the reaction coordinates, and the mean calculated reduced mass (MM). It does not use a variable reduced mass but it may be an approximation for a number of reactions. The second uses the mass weighted Cartesian coordinates (MWC), which employed the reduced mass calculated at each point of the intrinsic reaction coordinates (IRC). The third was created as explained by Fernandez-Ramos *et al* (FR).²

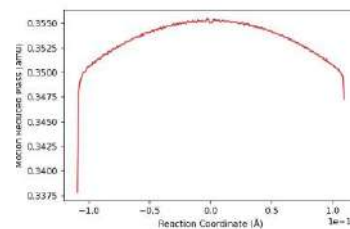


Fig 1. Reduced mass, in amu, versus the reaction coordinate, in Å.

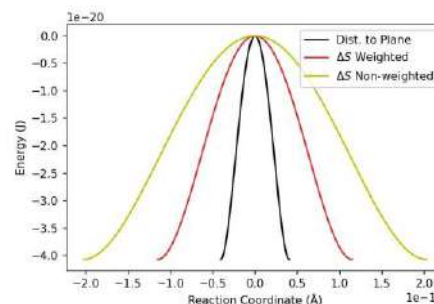


Fig 2. Calculated barriers to the inversion motion of ammonia using the distance from the plane of H atoms to the N atom, and weighted and non-weighted displacements.

Table 1. Results for the tunneling frequency, in s^{-1} , using the methods and masses, in amu, investigated.

Method	Mass (amu)	Tun. Freq. (s^{-1})
Reference ¹	2.47	2.69×10^{10}
MM	0.34	3.07×10^{10}
MWC	1	0.15×10^{10}
FR ²	1	1.61×10^7
Experimental	-	2.40×10^{10}

CONCLUSIONS

Both the MM and MWC methods have generated good results. The somewhat small tunneling frequency for the latter may be caused by the functional used, as it makes the barrier width slightly larger. The work is still in progress and the next step is to test both methods with molecules that have a larger variation in mass.

REFERENCES

¹ Porto, C. M., Morgan, N. H., Comput. Theor. Chem., 1187, 112917, 2020

² Fernandez-Ramos, A, *et al*. Reviews in computational chemistry, 23, 125, 2007.

ACKNOWLEDGMENTS

The authors would like to thank CNPq, Fapesp (2021/11039-1) and the Institute of Chemistry for the computational infrastructure.

Potential Energy Surface for H₂O ... CO₂

Patrícia Regina Pereira Barreto(PQ)¹, Alessandra Ferreira. Albernaz (PQ)², Eberth Correa³

prpbbarreto@gmail.com, albernalessandra@gmail.com, eberthcorrea@gmail.com

¹Laboratorio Associado de Plasma, Instituto Nacional de Pesquisas Espaciais, CP515, São José dos Campos, SP CEP 12247-970, Brazil, ²Instituto de Física, Universidade Brasília, CP04455, Brasília, DF CEP 70919-970, Brazil, ³Ciências Naturais Aplicadas, Universidade de Brasília, Campus do Gama, Gama, DF CEP 72444-240, Brazil

Keywords: Potential Energy Surface, H₂O-CO₂, second virial calculation

INTRODUCTION

We have been working in the development of potential energy surface (PES) for several years.

Basically, for system as AB-CD¹, were A, B, C and D are atoms, that can equals or not, and H₂O-X₂, where X can be any atom². Now, we propose a new surface, based in the H₂O-X₂ PES for H₂O ... CO₂, according to:

$$V(R_{CM}, \alpha, \theta_1, \theta_2, \phi) = \sum_m F_m(\Omega) v_m(R_{CM})$$

Where R_{CM} is the distance between the centers of mass, $F_m(\Omega)$ is an angular function and $v_m(R)$ are the moments.

METHODS

The system are treated as rigid motor, were the geometries of H₂O and CO₂ are kept frozen in theirs equilibrium. Fig. 1 shows the coordinate system used.

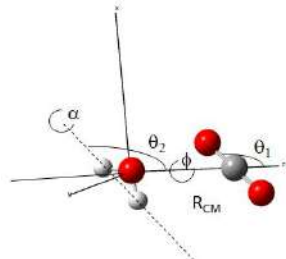


Fig 1: Coordinate system, where R_{CM} is the distance between the centers of mass (CM) of H₂O and CO₂, θ_1 is the angle of CO bond with the Z axis, θ_2 is the angle formed by the imaginary axis that pass through the CM of H₂O and parallel to the line connecting the H atoms of H₂O and the Z axis, ϕ is the dihedral angle and α is the angle that describes the rotation of H₂O around the the line connecting the H atoms.

The angular function is written as:

$$F(\Omega) = \sum_i \omega_i(\alpha) \sum_{L_1, L_2, L} Y_{L_a L_b}^{L, 0}(\theta_1, \theta_2, \phi)$$

Where $\omega_i(\alpha)$ is a cosine expansion in α angle, $Y_{L_a L_b}^{L, 0}(\theta_1, \theta_2, \phi)$ represents the bipolar spherical harmonics. The angles ($\alpha, \theta_1, \theta_2, \phi$) are given in Fig. 1.

To determine the moments $v_m(R_{CM})$, we choose 18 leading configurations whose choice is due to physical and geometric considerations. These configuration are divided in three groups, each group for three different α angle, as 0, $\pi/2$ and π . In each group we have six configuration, as H($\pi/2, \pi/2, 0$), L(0,0,0), T_a($\pi/2, 0, 0$), T_b(0, $\pi/2, 0$), Z($\pi/4, \pi/4, 0$) and X($\pi/2, \pi/2, \pi/2$).

RESULTS

The H₂O and CO₂ are optimized using the Gaussian code³ for different basis set and the geometric and electrical properties were determined, the results as shown in Tab.1.

Table 1: Geometric and electrical properties of H₂O and CO₂ calculated at aug-cc-pVDZ (aDZ), aug-cc-pVTZ (aTZ), aug-cc-pVQZ (aQZ),in comparison with experimental data.

	aDZ	aTZ	aQZ	Ref.
H ₂ O				
r _{OH}	0.967	0.962	0.959	0.958
A _{HOH}	103.9	104.2	104.4	104.5
E _{ZEP}	13.34	13.40	13.47	12.88
μ	1.995	1.970	1.963	1.857
α	9.239	9.493	9.538	10.128
Θ	12.553	12.509	12.488	13.184
IP	12.33	12.49	12.55	12.62
EA	0.69	0.56	0.51	1.20
PA	162.24	163.46	163.63	165.00
CO ₂				
r _{CO}	1.177	1.167	1.163	1.162
A _{CCO}	180	180	180	180
E _{ZEP}	7.11	7.21	7.26	7.17
μ	0	0	0	0
α	17.466	17.514	17.473	16.916
Θ	41.288	39.722	39.129	27.452
IP	9.72	12.52	13.77	13.78
EA	3.70	3.81	4.23	-0.60
PA	122.79	151.35	0.00	129.20

As one can see the aQZ basis set are in good agreement with experimental data, and this base will set for future calculation.

Molpro and SAPT determined the Leading Configuration energies at aug-cc-pVQZ. Fig. 2(a) shows the results for few LC, while Fig. 2(b) compares the SAPT and Molpro energies for Ta LC with $\alpha=\pi$, and Fig. 2(c) shows the SAPT contribution.

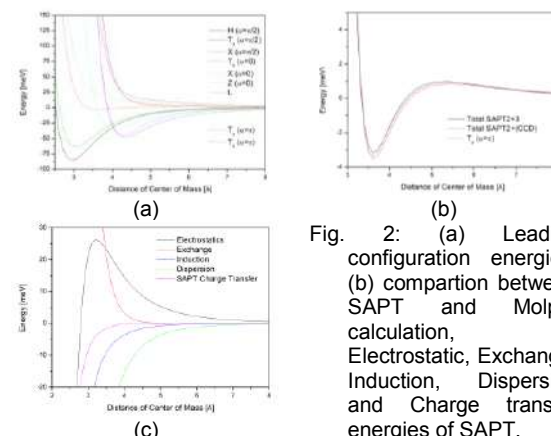


Fig. 2: (a) Leading configuration energies, (b) compartion between SAPT and Molpro calculation, (c) Electrostatic, Exchange, Induction, Dispersion and Charge transfer energies of SAPT.

ACKNOWLEDGEMENTS

I thank FAPESP and FADF.

Estudo das Propriedades Eletrônicas E Espectroscópicas de 2-Arilbenzimidazóis A Partir da Teoria de Funcional da Densidade

Maurício Rocha de Brito (PG)^{1*}, Leandro da Silva Pereira (PG),¹ Henrique Cury Boaro (IC),¹ Cláudio Eduardo Rodrigues dos Santos (PQ),¹ Glauco Favilla Bauerfeldt (PQ)¹.

mauriciorochasic@gmail.com

¹Instituto de Química (IQ), Universidade Federal Rural do Rio de Janeiro - Seropédica/RJ - Brasil.

Palavras Chave: Benzimidazóis, espectroscopia de absorção molecular, estrutura eletrônica, DFT.

INTRODUÇÃO

Benzimidazóis compreendem uma classe de compostos nitrogenados heteroaromáticos de interesse exploratório devido suas aplicações farmacêuticas, bem como no desenvolvimento de materiais eletrônicos de alto desempenho.

Quanto aos métodos sintéticos, se destacam a condensação de carbonilados com o-fenilenodiaminas na presença de nucleófilos. No entanto, os mecanismos reacionais ainda representam importantes lacunas para a compreensão das observações experimentais. Tendo isso em vista, o presente trabalho tem como objetivo o estudo das estruturas eletrônicas de dois derivados benzimidazólicos sintetizados em estudos anteriores do mesmo grupo de pesquisa (estruturas **1** e **2**), de maneira a contribuir com ferramentas para investigação teórico-experimental dessa classe de substâncias.

MÉTODOS

Primeiramente, foram realizadas otimizações geométricas das duas moléculas a nível de teoria de funcional de densidade utilizando o funcional B3LYP, empregando a base de cálculo cc-pVTZ para o composto **1** e aug-cc-pVDZ para o composto **2**. A partir das estruturas otimizadas, os cálculos foram então realizados a nível DFT/CAM-B3LYP empregando a base DEF2-TZVP. Efeitos de solvatação do etanol foram ainda inclusos através do modelo CPCM.

RESULTADOS

Tanto nas otimizações iniciais, quanto nos cálculos a nível DFT/CAM-B3LYP, as estruturas atingidas possuem ângulo diedro próximo a 180°, como esperado para um sistema conjugado de anéis aromáticos. A partir da ausência de frequências vibracionais imaginárias, foi constatado que as estruturas convergidas se tratam de pontos de mínimo e a partir de então, os espectros de absorção eletrônica foram obtidos a nível DFT/CAM-B3LYP DEF2-TZVP. Os espectros de absorção no UV teóricos obtidos coincidem satisfatoriamente com os correspondentes experimentais: no composto **1**,

os sinais experimentais centrados em 321 e 223 nm podem ser atribuídos aos estados excitados teóricos mais prováveis, atingidos através de absorções em 299,6 nm ($f_{osc} = 0,7043$, $\pi \rightarrow \pi^*$) e 220,2 nm ($f_{osc} = 0,7672$, $\pi \rightarrow \pi^*$). Na substância **2**, os estados excitados mais prováveis são 289,8 nm ($f_{osc} = 0,7774$, $\pi \rightarrow \pi^*$); 245,2 nm ($f_{osc} = 0,6601$, $\pi \rightarrow \pi^*$); 208,1 nm ($f_{osc} = 0,5137$, $\pi \rightarrow \pi^*$) atribuídos aos sinais no espectro experimental centrados em 309, 248 e 213 nm.

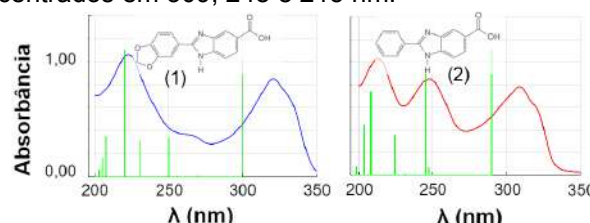


Figura 1: Espectros de absorção no UV.

Por fim, seguem as representações dos orbitais HOMO e LUMO dos dois arilbenzimidazóis, obtidas com valores de isosuperfícies de 0,02 au:

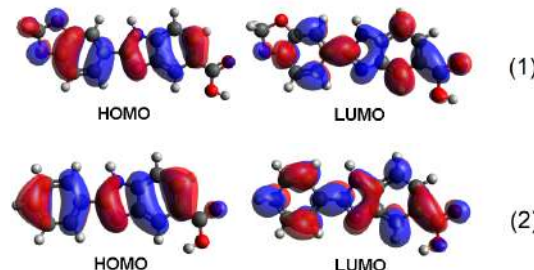


Figura 2: Representação dos orbitais de fronteira.

CONCLUSÕES

A partir do presente trabalho, foi possível a obtenção dos espectros de absorção eletrônica dos benzimidazóis estudados, bem como a descrição das energias e morfologias dos orbitais moleculares. Contribuindo assim com ferramentas teóricas a serem empregadas em futuras investigações dessa classe.

REFERÊNCIAS

¹ Salahuddin *et al.*, Arab. J. C., 2017, v. 10. p. S157-S173.

² Rodrigues-Santos *et al.*, 42RASBQ, 2019, p. 816.

AGRADECIMENTOS

CNPq, CAPES, FAPERJ.

Development, Optimization and Application of Density Functionals in Nanomaterials

Tatiana Rossafa Pauletti (PhD),^{1*} Isaac Martins Carvalho (PhD),¹ Tamiris Trevisan Negri Borges (PQ)², Vivian Vanessa França (PQ).¹

tatiana.pauletti@unesp.br

¹ Institute of Chemistry, São Paulo State University, UNESP, Araraquara, São Paulo, Brazil,

²Federal Institute of São Paulo, Araraquara, São Paulo, Brazil.

Keywords: Density Functional Theory, quantum phase transitions, magnetic susceptibility, Hubbard model.

INTRODUCTION

In nanomaterials, solids and cold atoms, one of the quantum properties that stand out, both from a fundamental point of view and in technological applications, is quantum entanglement. At the experimental level, quantification of entanglement is still elusive and remains an open problem in many contexts. A possible way to do this is through the measure of magnetic susceptibility, extracted from the second derivative of energy with respect to magnetization. Although via density functional theory (DFT) it is possible to extract the energy of quantum systems, the quality of the results depends on the functionals used in tracking the solutions.

In this work, we propose the development and optimization of a new density functional capable of providing accurate results for the ground state energy of the Hubbard model - a paradigmatic model in theoretical chemistry, condensed matter physics and materials science.

METHODS

The first analytical functional designed for the one-dimensional Hubbard model was developed by building a Local Density Approximation (LDA) based on Lieb and Wu's Beth-ansatz (BA) exact solution, called the LSOC¹ functional. Even though it is an efficient functional for non-magnetized systems has it, problems with the Mott gap and is not Applied to magnetized systems.

Starting from the same mathematical structure, the FVC² functional was created with the objective of correcting the problems of the LSOC functional:

$$e^{FVC}(n, m, U) = -\frac{2\beta(n, m, U)}{\pi} \sin\left(\frac{\pi n}{\beta(n, m, U)}\right) \cos\left(\frac{\pi m}{\gamma(n, m, U)}\right),$$

where,

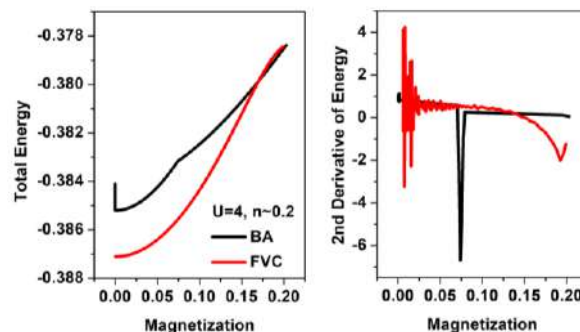
$$\begin{aligned}\beta(n, m, U) &= \beta(U)^{\alpha(n, m, U)}, \\ \gamma(n, m, U) &= 2\exp\left[\frac{\sqrt{U}}{1-\left(\frac{m}{n}\right)^{3/2}}\right], \\ \alpha(n, m, U) &= \left[\frac{n^2 - m^2}{n^{15}/m^8}\right]^{3\sqrt{U}}\end{aligned}$$

Even though the new functional is more accurate than the LSOC, correcting the Mott gap problem and describing magnetized systems, we observe that the derivatives of energy are not precise enough. Due to its importance in the investigation of observables

derived from the derivative of energy, it is necessary to develop a new functional that maintains the mathematical structure and reduces the problems faced by the FVC functional.

RESULTS

Our preliminary results shows a low performance of the FVC in the representation of the second derivative of the energy with respect to the magnetization, as seen in Figure 1.



The deviations observed in the Figure 1 are caused by the propagation of errors arising from numerical approximations made in the development of the functional.

Furthermore, we observe a small peak in the exact curves (via BA) could be related to a new quantum phase transition.

CONCLUSION

The analyzes carried out so far provided a greater understanding of the performance of the FVC and LSOC functionals when compared to exact results (via BA). From these data we will start the development of the new density functional as well as the understanding of a possible phase transition in systems with low magnetization.

REFERENCES

¹N. A. Lima, M. F. Silva, L. N. Oliveira, and K. Capelle, Phys. Rev. Lett., 2003, 90, 146402.

²V. V. França, D. Vieira, and K. Capelle, New J. Phys., 2012, 14, 073021.

ACKNOWLEDGMENT

This research is supported by: CNPq (140854/2021-5), FAPESP (2021/06744-8) and FAPESP (2023/00510-0).

Estudo Computacional da Influência de Interações Não Covalentes em Reações de Funcionalização C–H Catalisadas por Paládio.

Daniel Arley Santos Oliveira (PG),^{1*} Ataulpa Albert Carmo Braga (PQ).¹

danielarley452@usp.br;

¹Instituto de Química, Departamento de Química Fundamental, Universidade de São Paulo, São Paulo-SP, Brasil.

Palavras Chave: Funcionalização C–H, Interações não covalentes, Paládio, DFT, Catálise.

INTRODUÇÃO

O uso de interações não covalentes para direcionar a seletividade em reações de funcionalização C–H tem ganhado cada vez mais destaque na literatura especializada.^{1,2} Contudo, para nosso conhecimento, ainda não existem estudos computacionais que investiguem as reais influências dessas interações nos mecanismos e na seletividade dessas reações. Dessa forma, neste trabalho realizamos um estudo computacional da reação de funcionalização C–H *meta*-seletiva, catalisada por paládio, e dirigida por interações não covalentes desenvolvida experimentalmente por Li *et al.*² (Figura 1).

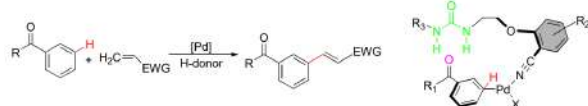


Figura 1: Reação de olefinação *meta*-C–H catalisada por paládio e dirigida por ligações de hidrogênio.¹

MÉTODOS

Os cálculos de otimização de geometria e frequência foram realizados com o software Gaussian16 ao nível de teoria M06/Def2-TZVP//M06/Def2-SVP em conjunto com o modelo de solvatação implícita SMD (Solvente= 2-metil-1-propanol). Todos os estados de transição foram confirmados pelo método da Coordenada Intrínseca de Reação (IRC). Cálculos QTAIM (*Quantum Theory of Atoms in Molecules*) foram realizados através do software Multiwfn.

RESULTADOS

A reação estudada se processa através de quatro etapas principais: ativação N–H, ativação C–H, inserção de alceno e β -eliminação de hidreto. O perfil energético da reação é apresentado na Figura 2. Nessa reação a acetil glicina (Ac-Gly-OH) é utilizada como ligante auxiliar e desempenha papel fundamental na abstração de hidrogênio na etapa de ativação C–H, processo conhecido como metalação-desprotonação concertada (CMD). De acordo com o perfil energético, essa é a etapa que determina a velocidade da reação, além de ser nela que a seletividade é definida. A Figura 3 apresenta os gráficos QTAIM das estruturas relacionadas a essa etapa. Na estrutura anterior ao TS, dois

pontos críticos de ligação são formados entre a carbonila e os hidrogênios do anel aromático, com valores de ρ de 0.0135 e 0.0170 e.a₀⁻³ para as interações com os hidrogênios *ortho* e *meta*, respectivamente. Evidenciando um maior acúmulo de densidade eletrônica no hidrogênio abstruído.

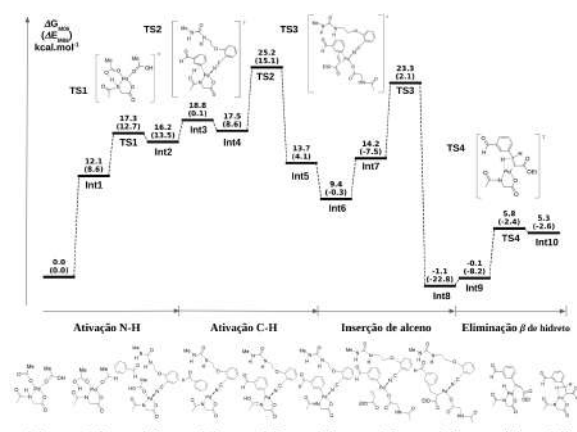


Figura 2: Perfil energético.

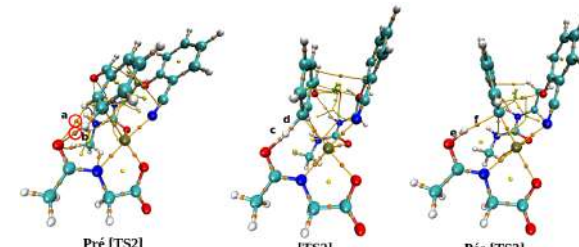


Figura 3: Gráficos QTAIM para etapa de ativação C–H.

CONCLUSÕES

Todo o ciclo catalítico da reação de olefinação C–H foi caracterizado. A etapa de ativação C–H se mostrou como a etapa determinante da velocidade e da seletividade da reação. Os resultados QTAIM suportam a seletividade encontrada experimentalmente.¹

REFERÊNCIAS

¹G. Li, Y. Yan, P. Zhang, X. Xu, Z. Jin. ACS Catal. 2021, 11, 10460.

²Y. Kuninobu, H. Ida, M. Nishi, M. Kanai. Nat. Chem. 2015, 7, 712.

AGRADECIMENTOS

Os autores agradecem à Fundação de Amparo à Pesquisa do Estado de São Paulo (FAPESP) (2022/01685-6) e ao CNPq (162366/2021-3) pelo apoio financeiro.

Theoretical Absorption Spectrum of Nitroguanidine in water: competition between conformation and dimer

Lucas Modesto da Costa (PQ),^{1*}

lucmod@ufrj.br;

¹Departamento de Física, Universidade Federal Rural do Rio de Janeiro, Seropédica, RJ, Brasil;

Palavras Chave: Nitroguanidine, absorption spectrum, sequential QM/MM.

INTRODUÇÃO

The nitroguanidine is an energetic molecule with high detonation velocity widely used as a propellant and explosive. The experimental absorption spectrum of nitroguanidine in water is characterized by two bands in 263 nm and 214 nm.^{1,2} A single shoulder is observed in the first band, around 300 nm.² Using the continuum model to represent the solvent, there is no evidence of the presence of excitations that form the shoulder. The two conformers of nitroguanidine are studied, figure 1. The origin of this shoulder is investigated in this work, comparing the presence of less stable conformer (B) or the dimer effect of most stable conformer (A), with the drawing of molecules plotted in figure 1.

Most stable (A)

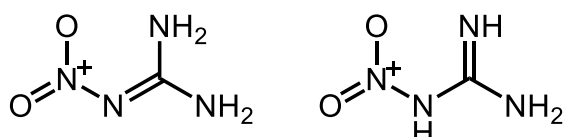


Figure 1: Two conformers of nitroguanidine.

MÉTODOS

Geometry and IRC was obtained by MP2/aug-cc-pvdz. The solvent effect was described with sequential QM/MM method.^{3,4} The classical simulation was performed with Dice program,⁵ at 25 °C and 1 atm. The OPLS-AA force field was used to describe nitroguanidine, and SPC/E for water. The thermalization was performed with 1×10^5 MC steps, equilibrium with 5×10^5 MC steps and production with 1×10^6 MC steps. The peak of the first maximum of the radial distribution function includes 10 water molecules, and this was the number of solvent molecules explicitly used in the electron absorption calculations. The absorption spectrum was performed with B3LYP/aug-cc-pvdz level, with Gaussian 09 package.

RESULTADOS

We evaluated the difference energy between two conformers, and obtained 11.1 kcal/mol favorable to conformation A. The height of the barrier was also calculated with a value of 43.4 kcal/mol. The

two results then in good agreement with other studies: 6.73 kcal/mol and 38.5 kcal/mol.⁶

The convoluting absorption spectrum for each species shows that there are no excitations for the A conformer for wavelengths greater than the first peak. Overall, the shape of the two-band spectrum is similar to the experimental result. In conformer B, there is a shoulder in the first peak for longer wavelengths, consistent with the experimental result. Different DFT functionals and post-Hartree-Fock methods are being employed to better describe the spectrum.

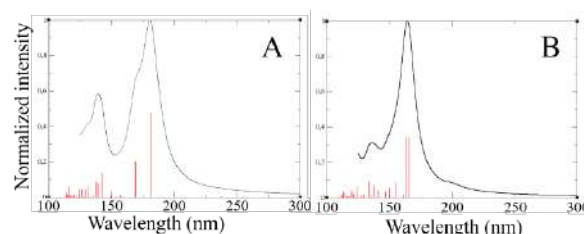


Figure 2: Calculated absorption spectrum

CONCLUSÕES

Due to the barrier height, barrier overlap is not anticipated under normal temperature and pressure conditions. But still the difference in energy allows the two conformations to be present in solution. The calculations for the absorption spectrum of the dimer are being conducted, since results with a continuous solvent model have shown the existence of excitations with longer wavelengths.

REFERÊNCIAS

Fonte Arial 8 e espaçamento simples.

¹ A. F. McKay, Chem. Rev. 1952, 51, 301

² A. F. McKay, J. P. Picard, P. E. Brunet, Can. J. Chem. 1951, 29, 746.

³ K. Coutinho, S. Canuto, Adv. Quantum Chem. 1997, 28, 89.

⁴ K. Coutinho, S. Canuto, J. Chem. Phys. 2000, 113, 9132.

⁵ H. M. Cezar, S., Canuto, K. Coutinho, Int. J. Quantum Chem. 2019, 119, e25688.

⁶ W. W. R. Fude, B. W. Wenliang, W. Chinese J. Chem. Phys. 2005, 18, 765.

AGRADECIMENTOS

CAPES, UFRJ e IME





Estudo QTAIM da regiosseletividade e do efeito químico do grupo metil como substituinte do tiofenol

¹ Adriano Oliveira da Silva (IC),² Juracy Régis de Lucena Júnior (PQ).^{1*}

adriano.oliveira@aluno.uepb.edu.br; juracylucena@servidor.uepb.edu.br

¹Universidade Estadual da Paraíba – Campus I

²Universidade Estadual da Paraíba – Campus I

Palavras Chave: QTAIM, Metil tiofenol, Efeito químico, hiperconjugação.

INTRODUÇÃO

O substituinte metil no tiofenol se comporta como doador de elétrons ao anel aromático. A doação ocorre através da hiperconjugação entre o orbital molecular σ do carbono do metil e o orbital molecular π da ligação dupla do anel aromático, isso quando eles estão alinhados. Com esse efeito químico, ocorre mudança de densidade eletrônica em parte do monômero, desestabilizando a ligação S-H do tiofenol. A metodologia DFT tem sido bastante utilizada para o estudo da reatividade de tiofenóis e seus derivados^{1,2,3}. Afim de investigar o efeito da hiperconjugação do metil no tiofenol e a consequência na reatividade desse sistema, realizou-se a otimização dos monômeros do metil tiofenol, com o substituinte nas posições *ortho*, *meta* e *para* no nível de cálculo ω b97x-d/6-311++G(3d,3p) e com as estruturas de mínimos, re realizou-se o estudo QTAIM com objetivo de caracterizar o efeito da hiperconjugação do grupo CH_3 no tiofenol e a sua regiosseletividade.

MÉTODOS

O estudo da análise conformacional dos isômeros do metil tiofenol e a otimização das estruturas de mínimo obtidas foram realizados com a metodologia DFT no nível de cálculo ω b97x-d/6-311++G(3d,3p) usando o programa Gaussian 09. A partir das estruturas de mínimos, confirmados com o cálculo de frequências, com ausências de frequências imaginárias, realizou-se o cálculo *single point* dos isômeros *ortho*, *meta* e *para* metil tiofenol e obteve-se o *input* para ser usado no programa Multiwfn⁴. Os parâmetros do QTAIM foram calculados com o Multiwfn.

RESULTADOS

As geometrias moleculares dos isômeros do metil tiofenol foram encontradas todas como planares. Os parâmetros analisados do QTAIM foram a densidade eletrônica, a densidade de energia, o laplaciano, as energias cinética e potencial. Com o efeito doador de elétrons ao anel aromático do grupo metil por hiperconjugação espera-se que ocorra variação nos descritores QTAIM densidade eletrônica do ponto crítico da ligação (ρ_{BCP}) do S-H dos isômeros do metil tiofenol, quando

comparados com o monômero do tiofenol, como também variação de ρ_{BCP} do anel aromático (Tabela 1),

Tabela 1. QTAIM da ligação S-H do tiofenol (T), *ortho* metil tiofenol (o-m-T), *meta* metil tiofenol (m-m-T) e *para* metil tiofenol (p-m-T): densidade no BCP ρ_{BCP} ; densidade de energia no BCP H_{BCP} ; laplaciano de ρ_{BCP} no BCP $\nabla^2\rho_{BCP}$, energias potencial e cinética,

S-H	T	o-m-T	m-m-T	p-m-T
ρ_{BCP}	0,2141	0,2165	0,2176	0,2161
H_{BCP}	-0,1947	-0,1912	-0,2100	-0,2063
$\nabla^2\rho_{BCP}$	-0,5672	-0,6114	-0,6114	-0,6115
Potencial	-0,3417	-0,2600	-0,2650	-0,2598
Cinética	0,1912	0,2064	0,2100	0,2063

Anel _{BCP}	T	o-m-T	m-m-T	p-m-T
ρ_{BCP}	$0,232 \cdot 10^{-1}$	$0,223 \cdot 10^{-1}$	$0,228 \cdot 10^{-1}$	$0,216 \cdot 10^{-1}$
H_{BCP}	$0,598 \cdot 10^{-2}$	$0,698 \cdot 10^{-2}$	$0,711 \cdot 10^{-2}$	$0,706 \cdot 10^{-2}$
$\nabla^2\rho_{BCP}$	0,158	0,158	0,164	0,161
Potencial	$-0,276 \cdot 10^{-1}$	$-0,255 \cdot 10^{-1}$	$-0,268 \cdot 10^{-1}$	$-0,262 \cdot 10^{-1}$
Cinética	$-0,598 \cdot 10^{-2}$	$-0,698 \cdot 10^{-2}$	$-0,711 \cdot 10^{-2}$	$-0,706 \cdot 10^{-2}$

As variações dos descritores QTAIM não foram observadas no resultados para os isômeros estudados, usando como referência a molécula do tiofenol, indicando que o efeito de hiperconjugação do substituinte metil não deve ter ocorrido (Tabela 1).

CONCLUSÕES

Os descritores QTAIM dos isômeros do metil tiofenol calculados indicaram que não houve desestabilização do monômero pelo efeito do substituinte metil. Esse resultado pode estar associado ao efeito de hiperconjugação que é relativamente fraco, como também relacionado a condição do alinhamento dos orbitais σ do carbono do metil e dos orbitais das ligações π do anel.

REFERÊNCIAS

- Igor Reva, Maciej J. Nowak, Leszek Lapinski e Rui Fausto, PCCP, 2015, Vol.17, 4888-4898.
- Jean Sun Lim, Hyun Sik You, Songhee Han e Sang Kyu Kim, J. Phys. Chem. A, 2019, Vol. 123, 2634–2639.
- Ján Rimarc įk, Vladimír Lukeš, Erik Klein e Lenka Rottmannová, Computational and Theoretical Chemistry, 2011, Vol. 967, 273–283.
- Tian Lu, Feiwei Chen, Multiwfn: A Multifunctional Wavefunction Analyzer, J. Comput. Chem. 2012, Vol. 33, 580-592.

AGRADECIMENTOS

CNPq e INCT-CiMol.

Estudo teórico comparativo dos modos de adsorção das formas iônicas do herbicida glifosato na superfície de materiais lamelares

Jackson H. Cardoso de Lima (PG),^{1*} Neubi F. Xavier Jr. (PQ),² Marcelo H. Herbst (PQ),¹ Glauco F. Bauerfeldt (PQ).¹

jackh.c.lima@icloud.com

¹ Instituto de Química – Universidade Federal Rural do Rio de Janeiro, Brasil. ² University of Surrey, England.

Palavras Chave: Hidróxidos Duplos Lamelares, Quantum Espresso, Química Teórica, Adsorção, Glifosato.

INTRODUÇÃO

Os Hidróxidos Duplos Lamelares (HDLs) são materiais formados por estruturas bidimensionais (2D) ligadas ao longo das duas dimensões (eixos 'a' e 'b'), onde interagem com uma terceira dimensão (eixo 'c') formando um material com dimensões tridimensionais (3D).¹ Resultante dessas interações, os cristais são construídos a partir do empilhamento de várias unidades, denominadas "lamelas". Devido a carga residual positiva das lamelas, são necessárias inserções de ânions na região que fica entre as lamelas e também a hidratação do meio,² além da possibilidade de serem usados como materiais adsorventes para diversos tipos de espécies aniónicas.

Neste trabalho, o objetivo foi avaliar as interações dos diferentes modos de adsorção de glifosato (N-(fosfonometil) glicina) na superfície da estrutura do HDL, nas suas formas aniónicas: Gli⁻, Gli²⁻ e Gli³⁻. O herbicida glifosato é o princípio ativo de diversos herbicidas, um deles é o Roundup, um importante herbicida sistêmico, pós-emergente, não seletivo e de alto espectro de ação, o qual é produzido pela empresa Monsanto e tem se mostrado um preocupante poluente de solos e corpos hídricos.

MÉTODOS

Os cálculos foram realizados através do pacote Quantum ESPRESSO,³ usando a Teoria do Funcional da Densidade (DFT).⁴ O funcional de correlação PBE⁵ foi adotado e pseudopotenciais ultrasoft de Vanderbilt foram considerados para descrever os elétrons das camadas internas. Os cálculos da equação de Schrödinger⁶ foram realizados em espaço recíproco e os estados de um elétron de Kohn-Sham foram expandidos em uma base de ondas planas definidas com uma energia cinética de corte de 140 Ry e amostragem de pontos k de 1x1x1 por ponto gama.

RESULTADOS

A estrutura cristalográfica do HDL de MgAl/CO₃²⁻, desenvolvida em trabalho anterior em nosso grupo de pesquisa, foi adotada para estudar a interação do material lamelar com a molécula de glifosato, apresentada na Figura 1.

A energia de adsorção (E_{ads}) foi usada como parâmetro para verificar os modos de adsorção energeticamente mais favoráveis. Os cálculos iniciais foram utilizados com a molécula de glifosato em seus diferentes modos iônicos e nas sequências foram obtidos os valores da E_{ads} em kJ/mol, conforme são apresentados na Tabela 1.

Figura 1. Estrutura otimizada utilizada nos cálculos de adsorção.

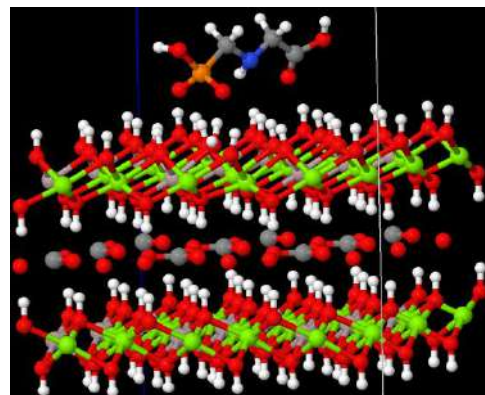


Tabela 1. Relação das E_{ads} obtidas para os diferentes modos de adsorção.

Modo de Adsorção	E_{ads} (kJ/mol)
HDL-Gli ¹⁻	-157,84
	-179,74
	-216,80
HDL-Gli ²⁻	-211,26
	-233,26
HDL-Gli ³⁻	-164,82

CONCLUSÕES

Conclui-se que a estrutura mais favorável para adsorver na superfície do HDL seria a do Gli²⁻, devido ao seu estado de mais baixa energia.

REFERÊNCIAS

- Ray, S. S. & Okamoto, M. *Prog. Polym. Sci.*, 2003, 28, 1539.
- Ravenna, R. R. A. *Universidade Federal Do Paraná*, 2018.
- Giannozzi, P. et al. *J. Phys.: Condens. Matter* 2009, 21, 395502.
- Hohenberg, P.; Kohn, W. *Inhomogeneous Electron Gas*. *Phys. Rev.* 1964, 136, B864.
- Perdew, J. P.; Ernzerhof, M.; Burke, K. *J. Chem. Phys.* 1996, 105, 9982.
- Monkhorst, H. J.; Pack, J. *D. Phys. Rev. B*, 1976, 13, 5188.

AGRADECIMENTOS

À CNPq, CAPES e SDumont.

Adsorção de clorotalonil em CNT (10,0) e BNNT (10,0): um estudo DFT

Francisco Gleidson de S. Ferreira (PG)^{1*}, Caio V. Caetano (PG)², José Milton Elias de Matos (PQ)³, Alexandre Araujo de Souza (PQ)³.

caioviniuscaetano@hotmail.com; gleidsonqmc@hotmail.com

¹Programa de Pós-Graduação em Química, Universidade Federal do Piauí, Teresina – PI - Brasil; ²Programa de Pós-Graduação em Química, Universidade Federal de São Carlos, São Carlos – SP – Brasil; ³Departamento de Química, Universidade Federal do Piauí, Teresina – PI - Brasil

Palavras Chave: *DFT, Nanotubos de carbono, Nanotubos de nitreto de boro, Adsorção de contaminantes, Clorotalonil.*

INTRODUÇÃO

Dentre as várias técnicas de remoção de contaminantes no ambiente, a adsorção é uma das mais utilizadas e promissoras na remoção de poluentes, pois permite alcançar altas taxas de remoção mesmo em concentrações muito baixas desses contaminantes¹. Os nanotubos em geral, são usados como sensores e removedores de contaminantes devido a sua alta área superficial. Nesse sentido, este trabalho apresenta um estudo teórico da adsorção do fungicida clorotalonil (CLT) na superfície dos nanotubos de carbono (CNT) e de nitreto de boro (BNNT) com quiralidade (10,0).

MÉTODOS

Utilizando cálculos de primeiros princípios baseados na teoria do funcional da densidade (DFT) implementados no software SIESTA², usando base DZP, funcional vdW-DF2³ e o pseudopotencial de Troullier-Martins⁴. O critério de convergência para a otimização de geometria foi de 0,05 eV/Å. As propriedades eletrônicas foram analisadas através da densidade de estados projetada (PDOS). A energia de adsorção (E_{ads}) foi calculada subtraindo a energia do sistema nanotubo+CLT (E_{NT+CLT}) da energia total do nanotubo (E_{NT}) e da molécula (E_{CLT}) isolados, e adicionando a correção BSSE (E_{BSSE}) posteriormente, assim,

$$E_{ads} = E_{NT+CLT} - E_{NT} - E_{CLT} + E_{BSSE}$$

RESULTADOS

O CLT foi colocado em várias configurações na superfície dos nanotubos, sendo que a configuração mais estável foi a com o CLT horizontalmente paralelo aos nanotubos. Para o sistema CLT+CNT a energia de adsorção (E_{ads}) foi de -0,76 eV, indicando que houve uma fissão moderada com transferência de carga quase nula (+0,0006 e⁻), o sinal positivo indica que a molécula tem tendência de doar elétrons ao CNT. Também houve uma pequena diferença no band-gap passando de 0,60 eV (CNT puro) para 0,58 eV (CLT+CNT), como mostra a PDOS da Figura 1a e 1b. Já o sistema CLT+BNNT apresentou E_{ads} de -0,66 eV, com uma transferência de carga de +0,12 e⁻, e uma redução do band-gap de 1,85 eV em relação ao BNNT puro (Figura 1c), a qual se deve ao aparecimento de novos níveis de energia na região do band-gap (Figura 1d).

A comparação entre a E_{ads} dos dois sistemas indica que os ciclos de adsorção e desorção são mais favoráveis no BNNT, devido a E_{ads} ser menor.

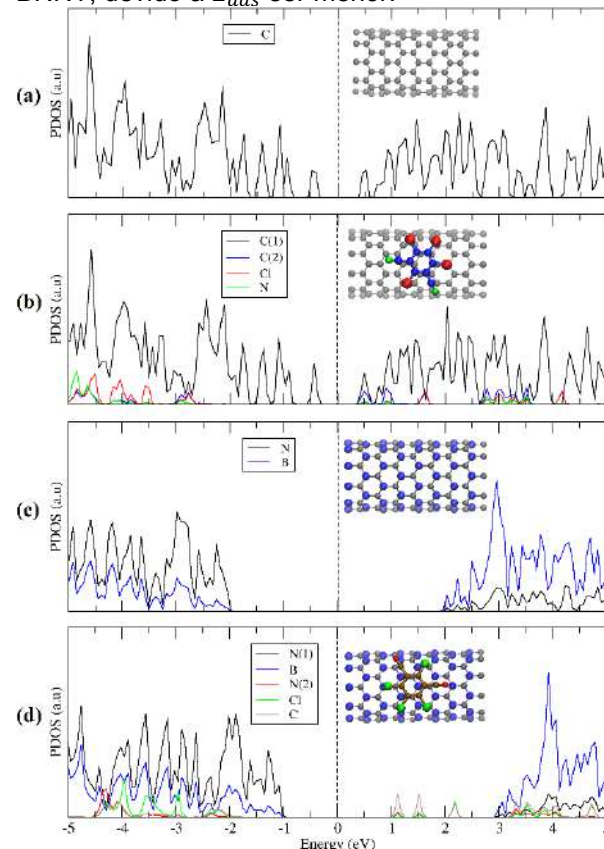


Figura 1: Densidade de estados projetada para o sistema (a) CNT puro, (b) CNT+CLT, (c) BNNT puro e (d) BNNT+CLT.

CONCLUSÕES

Os resultados mostram que o BNNT é um candidato promissor para detecção e remoção do CLT em ambientes contaminados, pois ele produz uma E_{ads} moderada em relação ao CNT, o que facilita os ciclos de adsorção e desorção.

REFERÊNCIAS

- 1 DERYLO-MARCZEWSKA, A. *Chemosphere*, 214, 349-360, 2019.
- 2 ORDEJÓN, P. et al. *Phys. Rev. B*, 53, R10441–R10444, 1996.
- 3 LEE, K. et al. *Phys. Rev. B*, 82, 081101, 2010.
- 4 TROULLIER, N., MARTINS, J. L. *Phys. Rev. B*, 1991, 43, 1993–2006.

AGRADECIMENTOS



Cálculo das propriedades fotoquímicas da base nitrogenada artificial 2-amino-6-(2-tiazolil) purina

Tuan C. Pacheco (IC)*,¹ Thiago M. Cardozo (PQ).²

tuanpcpacheco@gmail.com; thiago@iq.ufrj.br

¹Instituto de Química, Universidade Federal do Rio de Janeiro. ²Instituto de Química, Universidade Federal do Rio de Janeiro

Palavras Chave: Fotoquímica, Fotofísica, Estados Excitados, Bases Nitrogenadas, Bases Nitrogenadas Artificiais

INTRODUÇÃO

A base artificial 2-amino-6-(2-tiazolil) purina (UNBv) apresenta perda de fluorescência no pareamento com a imidazolin-2-ona (UNBz)¹, porém se isolada ou inserida numa cadeia de DNA, a fluorescência é observada. Em contrapartida, as bases naturais são foto-estáveis quando isoladas ou no DNA, devido à rápida desativação de seus estados excitados².

Nesse trabalho, cálculos *ab initio* foram conduzidos para obter as geometrias de equilíbrio e as energias de excitação vertical. O caráter das excitações foi investigado por métodos de análise da matriz de transição.

MÉTODOS

Usamos DFT e TDDFT, respectivamente, para otimizar as geometrias e calcular as excitações, sob o funcional híbrido ω B97X-D3, o mais adequado para o sistema quando comparado com o método coupled-cluster usado como referência³ e a base utilizada foi cc-pVTZ. Usamos o pacote ORCA 5.0.3 para fazer os cálculos e a matriz de transição eletrônica foi analisada com o pacote TheoDORE 3.0.

RESULTADOS

A geometria otimizada do estado fundamental do par, é estabilizada em quase 20kcal.mol⁻¹ pelas ligações de hidrogênio com os anéis aromáticos e o grupo tiazolil no mesmo plano. As figuras 1 e 2 exibem, simultaneamente, os NTOs (natural transition orbitals) e essas estruturas.

Estado	dE (eV)	f	CT
LE- $\pi\pi^*$ (S_1)	4,025	0,286	0,007
CT- $\pi\pi^*$ (S_3)	4,846	0,01	0,979

Tabela 1: Excitações verticais, força de oscilador (f) e charge-transfer (CT). (TDDFT/ ω B97X-D3)

Pela depleção de carga no orbital buraco do primeiro singuleto (S_1) no anel purina e ocupação do anel tiazolil no orbital partícula do mesmo estado (Fig. 1), caracterizamos esse estado como 1 LE (local excitation). O S_3 é uma transferência de carga entre as bases (Fig. 2) e

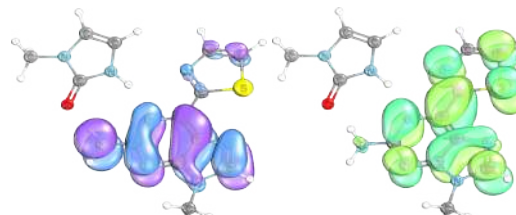


Figura 1: NTOs do primeiro singuleto (TDDFT/ ω B97X-D3)

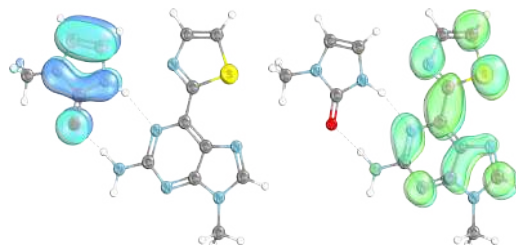


Figura 2: NTOs do terceiro singuleto. (TDDFT/ ω B97X-D3)

por isso é nomeado 1 CT (charge-transfer). Embora sua força do oscilador seja pequena (Tabela 1), esse estado pode ser crucial para a fotofísica do par porque é similar ao S_3 -CT encontrado no par guanina-citosina que induz uma SPT (single proton-transfer) da citosina para a guanina, contribuindo para a desativação não-radiativa no par⁴.

CONCLUSÕES

Há fortes indícios de que uma SPT estabilize o estado 1 CT- $\pi\pi^*$ promovendo o cruzamento entre esse estado e o estado fundamental, esse mecanismo pode contribuir para a fotostabilidade do par UNBv-UNBz assim como ocorre para o par de bases naturais (ver Ref. 4). A otimização desses estados e a busca por interseções cônicas em andamento poderão em breve concretizar essa expectativa.

REFERÊNCIAS

- ¹Mitsui, T. et al. Characterization of fluorescent, unnatural base pairs. *Tetrahedron*, v. 63, n. 17, p. 3528–3537, 2007.
- ²Barbatti, M. et al. Relaxation mechanisms of UV-photoexcited DNA and RNA nucleobases. *Proceedings of the National Academy of Sciences*, v. 107, n. 50, p. 21453–21458, 2010
- ³Souza Mattos, R. Estudo teórico da fotofísica da 2-amino 6-(2-tiazolil) purina, 2021.
- ⁴Sobolewski, A. Domcke, W. Ab initio studies on the photophysics of the guanine-cytosine base-pair, *Phys. Chem. Chem. Phys.*, 2004, 6, 2763–2771

AGRADECIMENTOS

À FAPERJ pelo apoio financeiro.

Molecular modeling of multi-target analogs of Huperzine A and applications in Alzheimer's disease

Leonardo F. de Sousa (PG)^{1*}, Diego F. S. Paschoal (PQ)¹, Willian T. G. Novato (PQ)¹

leonardowfs.97@gmail.com; willian.tg.novato@gmail.com

¹Núcleo de Química Teórica e Computacional de Macaé, Polo Ajuda, Instituto Multidisciplinar de Química, Centro Multidisciplinar UFRJ-Macaé, Universidade Federal do Rio de Janeiro, Macaé, RJ, Brazil.

Keywords: Molecular modeling, Molecular docking, Alzheimer's disease, Density Functional Theory.

INTRODUCTION

Since Alzheimer's disease has a complex pathophysiological mechanism, it is unlikely that a single targeted drug will be successful as a therapeutic strategy. Then exploring the various hypotheses in drug design is a critical path. The capture of Fe(II) and Zn(II) cations is an important mechanism based on the reduction of reactive oxygen species. On the other hand, the inhibition of acetylcholinesterase represents an important strategy to increase acetylcholine levels in the synaptic cleft. Thus, the objective of this research is to investigate select analogs of Huperzine A through the lens of these two hypotheses¹.

METHODS

The chemical speciation of the structures with Fe(II) and Zn(II) was analyzed using computational chemistry calculations at B3LYP/6-31G(d)/IEF-PCM(UFF) level, with the GAUSSIAN 16 Rev. C.01 program. The coordination complexes were analyzed using the variation of the Gibbs free energy and Hard and Soft Acids and Bases (HSAB) theory. Molecular docking calculations were performed using the GOLD program, based on the crystal structure of the acetylcholinesterase protein (pdb code=4EY5). The pharmacokinetic properties were predicted with SwissADME².

RESULTS

From the prediction of the pharmacokinetic properties, only two analogs are permeable to the blood-brain barrier: HupA-A1 and HupA-A2. The enantiomers with the best interaction parameters were: S'R'HupA-A1($\Delta G_{\text{BIND}} = -40.0 \text{ kcal mol}^{-1}$, fitness score=35.5) and R'R'HupA-A1 ($\Delta G_{\text{BIND}} = -35.5 \text{ kcal mol}^{-1}$, fitness score=22,61), compared to HupA (-41.75 kcal mol⁻¹, fitness score=39.95).

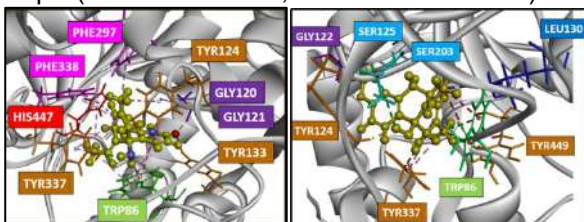


Figure 1. Comparison between HupA (left) and S'R' HupA-A1 (right).

These enantiomers showed favorable values for the speciation reaction with both with Fe(II) and

Zn(II) ions. The S'R'HupA-A1 was more specific for Fe(II), according to thermodynamic and hardness analysis, from the perspective of HOMO-LUMO gap.

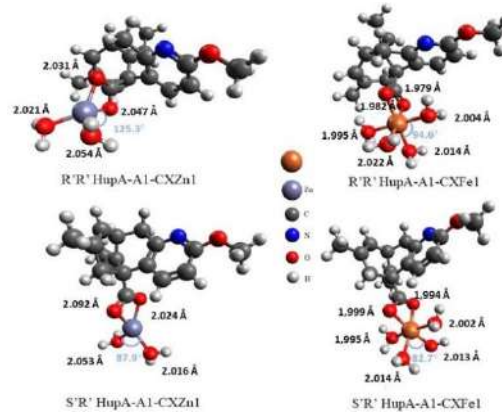


Figure 2. Structure of the best scored complexes.

Table 1. Parameters of the studied chemical speciation

Analogs	ΔG_{Fe}^{0+} (mol/L)	ΔG_{Zn}^{0+} (mol/L)	η^+ (mol/L)
R'R' HupA-A1	-29.038	-27.442	51.78
R'S' HupA-A1	-25.644	-23.804	54.68
S'R' HupA-A1	-28.263	-23.860	55.58
S'S' HupA-A1	-28.557	-28.576	47.94
S'R' HupA-A2	-3.652	+5.391	61.18
S'S' HupA-A2	+26.894	+0.467	60.24
R'R' HupA-A3	-23.368	-24.656	50.77
R'S' HupA-A3	-25.455	-24.104	53.36
S'R' HupA-A3-CX1	-31.577	-27.826	54.20
S'R' HupA-A3-CX2	-29.829	-25.568	54.20
S'S' HupA-A3-CX1	-30.017	-25.710	53.73
S'S' HupA-A3-CX2	-29.137	-29.342	53.73

CONCLUSIONS

The candidates for useful drugs in this research were S'R'HupA-A1 and R'R'HupA-A1, due to the thermodynamically favorable chelating ability and the possible anticholinesterase mechanism.

REFERENCES

- P. LEI, J. Biol. Chemistry. 2021, vol. 296 pg.100-105
- J. Cheung et al., J. Med. Chem., 2012, 55, 10282-10286.

ACKNOWLEDGMENTS

The authors would like to thank the Brazilian agency FAPERJ (E-26/201.336/2022 – BOLSA and E-26/210.070/2022) and CAPES (Finance Code 001) for the financial support.

In silico investigation of the role of halogen bonds in the design of 5-HT₆ receptor antagonists against Alzheimer's Disease

Aldineia P. Da Silva (PhD)¹, Daniel S. De Sousa (PhD)², Laise P. A. Chiari (PhD)^{2*}, Káthia M. Honório (R)¹, Albérico B. F. Da Silva (R)^{2*}

aldineiapereira@hotmail.com; alberico@iqsc.usp.br

¹School of Arts, Sciences and Humanities (EACH), University of São Paulo (USP), São Paulo, 03828-000, Brazil;

²São Carlos Institute of Chemistry (IQSC), University of São Paulo (USP), 13560-970, São Carlos, SP, Brazil.

Keywords: Alzheimer's Disease, 5-HT₆ Receptor Antagonists, In Silico Study.

INTRODUCTION

Alzheimer's disease is a neurodegenerative disorder that may affect about 152 million individuals by 2050¹, which is a challenging problem, as the understanding of the molecular basis of this disease is still not completely understood. Addressing this problem, the 5-HT₆ receptor as a potential anti-Alzheimer drug target has been the subject of study for the design of anti-amnesic drugs and in addiction efforts to several studies focused on this molecular target, our aim was to investigate the role of halogen bonds in increasing the inhibitory activity of potential 5-HT₆ receptor antagonist candidates through *in silico* studies.

METHODS

Our compounds were designed using information from QSARs models built in our research group (using PLS and ANN methods)^{2,3}. We chose the compounds with the highest and lowest values of biological activity to carry out the structural modifications through the addition of halogens. Subsequently, we submitted these new compounds to previously constructed QSAR models to obtain biological activity values. Molecular Docking simulations were performed in Glide (software included in the Maestro bundle) with the 5-HT₆ receptor and the previously designed ligands. The Protein Preparation Wizard (PPW) module was used to add hydrogens, maintain the pH at 7 and add fillers to the waste. The 5-HT₆ receptor site pocket was defined using the Receptor Grid Generation module and a box of size 10 x 10 x 10 was constructed. For this simulation, the extra precision XP score function was chosen and at the end, an evaluation of the main types of interactions between the 5-HT₆ molecular target and the new compounds was carried out.

RESULTS

The information extracted from the analyzes of the QSAR models pointed to the importance of halogen atoms in the structures of the compounds, so new compounds were proposed with the presence of halogens in their structures. The result obtained were compounds with pronounced

antagonistic activity values. The results showed that the compound **C4704** interacts by halogen binding (Figure 1), a type of interaction that has been widely explored in the field of drug design.

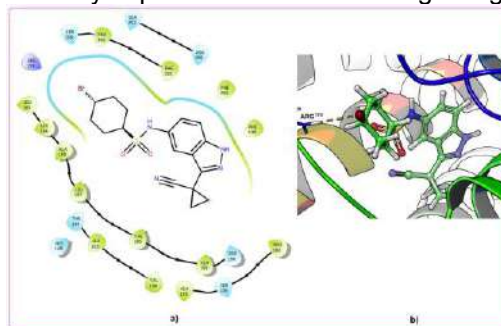


Figure 1- Simulation of Molecular Docking between the 5-HT₆ receptor and compound **C4704**. **a**) bidimensional diagram of amino acid residues that interact with C4704; **b**) main type of interaction between compound **C4704** and residue ARG¹⁷⁴.

Halogenated compounds have been widely used by the pharmaceutical industry to increase membrane permeability while decreasing metabolic degradation, in addition to contributing to increasing the effectiveness of several drugs. Several of the new compounds planned have halogen atoms in their structures (**C4701**, **C4702**, **C4703**, **C4704**, **C2502**, **C2506**), whose biological activity values predicted by the generated QSARs models^{2,3} proved to be promising.

CONCLUSIONS

The presence of halogen atoms (mainly Br) linked to aromatic rings in the *para*-position contributes to significantly increasing the antagonistic effect of the compounds. This study qualifies the new compounds to go on further with experimental procedures and thenceforth their drug-likeness features can be confirmed.

REFERENCES

- ¹ Alzheimer's Disease International, World Alzheimer report 2019 Attitudes to dementia disponível em: <https://www.alz.co.uk/research/WorldAlzheimerReport2019.pdf>.
- ²da Silva, A.P.; Chiari, L.P. A et al. J.Mol.Graph, 2021,104, 107844.
- ³da Silva, A.P.; de Angelo, R.M.; de Paula, H. et al, Struct Chem, 2020, 1585-1597.

ACKNOWLEDGMENTS

National Council for Scientific and Technological Development (CNPq). Process number: 140894/2021 and 152105/2022-0.

An investigation into the conformational flexibility of the Papain-like protease using molecular simulation methods

José Gutembergue de Mendonça (PG),¹ Leonardo Henrique Franca de Lima (PQ),² Gerd Bruno da Rocha (PQ).^{1*}

Gutembergue.13@gmail.com

¹Universidade Federal da Paraíba-UFPB; ²Universidade Federal de São João del-Rei-UFSJ

Keywords: Papain-Like Protease, SARS-CoV's, Molecular Dynamics, Zinc Finger domain, Conformations.

INTRODUCTION

The emergence of SARS-CoV-2 in Wuhan, China, triggered the global COVID-19 pandemic, mobilizing scientists to understand its extent in order to stop its rapid spread¹. The study of viral proteases, such as papain-like viral protease (PLpro), which are critical for replication and the host immune response, is a valuable key¹. Computer simulations play a key role in discovering the structure of proteases and understanding their conformation, which is essential for drug development². Although the PLpro of SARS-CoV-1 and SARS-CoV-2 are quite similar in structure³, they have different substrate preferences, which can influence the behavior of the virus. Molecular dynamics simulations explore the interactions of PLpro with compounds to guide drug development for COVID-19². These simulations allow the analysis of the conformational behavior of this protease in detail and reveal potential drug targets.

METHODS

PLpro crystal structures (2FE8 for SARS-CoV-1, 6WRH for SARS-CoV-2 with C111S mutation) were retrieved from the PDB database and mutation-free models were generated through SWISS-MODEL. Protonation was determined using the H++ tool considering physiological conditions. The proteins were parameterized by using AmberTools 21. For this, we built systems solvated in a cubic box with a minimum edge distance of 12 Å, considering ff14SB, GLYCAM-06, and ZAFF force fields for proteins. Salinities were achieved by adding Na⁺ and Cl⁻ ions. The equilibration protocol NPT included minimization, restricted/unrestricted equilibration, and pre-productive MD simulations. For zinc-finger PLpro, an extra equilibration step was added. Three productive MD simulations (100 ns each) per system were carried out. PCA (principal component analysis) was performed for internal motions analysis (PC1, PC2, PC3). Structural distinctions were visualized through average projections.

RESULTS

Our aim was to investigate how the presence of the zinc finger domain affects the conformational

balance of other regions, such as the ubiquitin-like domain (Ubl) and the BL2 loop. We selected representative conformations of each system studied by PCA. Our results indicated that the tetracoordinate Zn(II) cations, coordinated by cysteines in the PLpro structure, contribute to the stabilization of the zinc finger domain. This stabilization in turn reduces the mobility of specific β sheets (β4, β5, β6, and β7). However, we observed an increase in the mobility of the Ubl domain, particularly in the PLpro of SARS-CoV-2, figure 1.

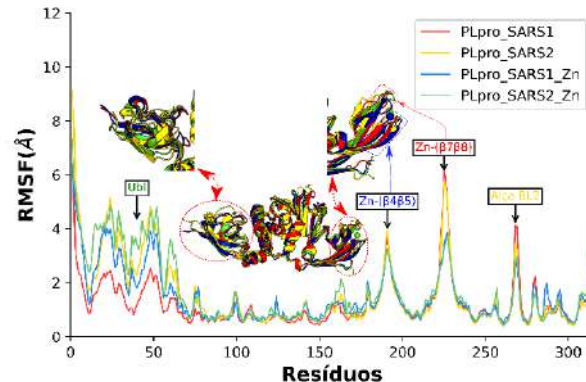


Figure 1 RMSF plots of PLpro. The main conformations of PLpro with and without zinc are highlighted, observed by Principal Component Analysis (PCA) for the ubiquitin and zinc-finger domains.

CONCLUSIONS

Molecular dynamics simulations were used to investigate the effect of Zn(II) on PLpro of SARS-CoV-1 and SARS-CoV-2. Our results showed that zinc induces structural changes in the zinc finger and Ubl domains, which may influence substrate capture and immune response. Principal component analysis revealed that the Zn(II) decreased the mobility in the zinc finger region, while the absence of zinc increased mobility in the Ubl domain, zinc finger, and BL2 loop.

REFERENCES

- ¹Klemm, T. et al.. The EMBO Journal 2020, 39.
- ²Arnettali, M. et al. Procedia Computer Science, 2019, 156, 69–78.
- ³Gao, X. et al. Acta Pharmaceutica Sinica B 2021, 11, 497–506.

ACKNOWLEDGMENTS

CAPES, CNPq, FAPESQ, FINEP, FACEPE, SDumont, Cenapad-SP, and UFPB.



Positronium atoms in liquids

Mateus Bergami(PhD)^{1*}, Jorge Charry(R)², Andres Reyes(R)³, Kaline Coutinho(R)¹, Márcio Varella(R)¹
mbergami@if.usp.br

¹*Instituto de Física, Universidade de São Paulo, Rua do Matão 1371 CP 66318, CEP 05508-090 São Paulo, SP, Brazil*

²*Department of Physics and Materials Science, University of Luxembourg, L-1511 Luxembourg City, Luxembourg*

³*Department of Chemistry, Universidad Nacional de Colombia, Av. Cra. 30 #45-03, 111321 Bogotá, Colombia*

Keywords: sequential-QM/MM, Monte Carlo simulation, molecular dynamic, positronium

INTRODUCTION

Positrons and positronium (Ps) atoms have long been known as nanoscale probes in materials sciences. Positron Annihilation Lifetime Spectroscopy (PALS) measurements have been applied to investigate conformational, structural, and microenvironmental properties of biomimetic systems [1], as well as phase transitions of lipid bilayers [2] and pharmaceutically relevant compounds [3]. The Ps contribution to the annihilation signals is expected to allow improvement of accuracy and diagnosis in Positron Emission Tomography (PET) as indicated in recent studies [4,5]. Motivated by biomedical applications, we have combined computational techniques to model Ps atoms in the liquid phase.

METHODS

We considered the sequential Quantum Mechanics/Molecular Mechanics (s-QM/MM) approach [6], composed of classical simulations (MM step) followed by quantum calculations (QM step). The MM step considers a force field composed of the Lennard-Jones potential to describe Ps-solvent interaction during classical simulations, and this step provides liquid structures and thermodynamical properties. The QM step considers the Ps-solvent configurations for quantum calculations with the Any Particle Molecular Orbital (APMO) method [7], which generalizes the electronic structure techniques for systems with more than a single fermionic species. The Hartree-Fock wave functions obtained were considered to account for the pick-off annihilation rates and vertical detachment energies of hydrated Ps.

RESULTS

Our classical simulations indicate a hydrophobic character of Ps, and the vertical detachment energies obtained in the quantum calculations are smaller than the ionization potential of isolated Ps. On the other hand, the main experimental property of Ps in the liquid phase is the pick-off lifetime measured in experiments with the PALS technique. The pick-off lifetime of Ps atoms solvated in water at a temperature of 20°C is

1.84ns [8], while our QM/MM protocol proposed in this work provides 1.90ns.

CONCLUSIONS

We have proposed a QM/MM model for solvated Ps atoms [9], exploring classical simulations and APMO quantum calculations. The classical force field for Ps atoms can be readily obtained, and our protocol is general because it can be applied to other liquids and materials, as we will discuss in this talk.

REFERENCES

- ¹C. Fong et al. Phys. Chem. Chem. Phys. 2015, 17, 17527.
- ²L. A. B. Garcia-Arribas et al. Langmuir 2016, 32, 5434.
- ³N. Chieng et al. Eur. J. Pharm. Biopharm. 2013, 85, 197.
- ⁴P. Moskal et al. Phys. in Medicine & Biology 2019, 64, 055017.
- ⁵K. Shibuya et al. Communications Physics 2020, 3, 1.
- ⁶K. Coutinho et al. Adv. Quantum Chem. 1997, 28, 89.
- ⁷A. Reyes et al. Int. J. Quantum Chem. 2019, 119, e25705.
- ⁸K. Kotera et al. Phys. Lett. A 2005, 345, 184.
- ⁹M. Bergami et al. J. Phys. Chem. B 2022, 126, 2699.

ACKNOWLEDGMENTS

This work has been supported by CAPES, CNPq, FAPESP and IFUSP.

A DFT study of a novel Zn(II) coordination complex with 1,10-phenanthroline and purpurin ligands

Diego C. Abreu (PG),^{1,2*} Regina M. M. Oliveira (PQ)³, Antonio Douglas S. G. Lima (PG),¹ Stanislav R. Stoyanov,⁴ Mateus R. Lage (PQ)^{1,3}

diego.abreu@ifma.edu.br, regina.oliveira@ufma.br, antonio.guedes@discente.ufma.br, stoyanov@ualberta.ca, mateus.lage@ufma.br.

¹ Graduate Program in Materials Science, Center of Science of Imperatriz, Federal University of Maranhão, CEP 65900-410, Imperatriz, MA, Brazil.

² Federal Institute of Education, Science and Technology of Maranhão, Campus Imperatriz, CEP 65906-335, Imperatriz, MA, Brazil.

³ Coordination of Science and Technology, Federal University of Maranhão, Campus Balsas, CEP 65800-000 Balsas, MA, Brazil.

⁴ Natural Resources Canada, CanmetENERGY Devon, Devon, AB, Canada.

Keywords: Aromatic diimine ligands, Purpurin complexes, Octahedral complexes of Zn(II), DFT, continuum solvation methods

INTRODUCTION

Coordination complexes of Zn(II) have been widely studied by means of DFT calculations, associated with experimental techniques, as well as other complexes containing 1,10-phenanthroline (PHEN) and purpurin (PURP) ligands. Previous studies explore a wide spectrum of potential applications for coordination complexes with the PHEN ligand, including magnetic¹ and photovoltaic² properties, and antimicrobial activity.³ Antibacterial activity has also been observed for complexes with Zn(II). It is also important to mention that some studies reported the optical and electrical properties of complexes containing PURP.⁴ We report a theoretical study of a new Zn(II) coordination complex containing two PURP and one PHEN ligands, recently synthesized by our group.

METHODS

All the DFT calculations were developed using the software *Gaussian16*,⁵ employing the DFT functional PBE1PBE,⁶ with the basis set 6-311g (d,p), for C, H, O, and N atoms, and the Stuttgart-Dresden pseudopotential (SDD) for the Zn atom. Calculations were developed for each of the ligands PHEN and PURP and for the complex in vacuum and in methanol, with the IEFPCM solvation method.⁷ A neutral charge and a spin multiplicity of 1 were considered for the Zn(II) complex. All the data obtained were analyzed using the software *Chemcraft1.8*.⁸

RESULTS

The results obtained from the DFT study indicated that the Gibbs free energy (ΔG^{298}) of complexation is -599,85 kcal/mol in vacuum, indicating that the complex formation is a spontaneous process. This is an important parameter since some properties reported in the literature of Zn(II) complexes, such as oxidative catalysis in organic reactions may be associated with the value of ΔG^{298} .⁹

The dipole moment of the Zn complex is 12.23 D, while the HOMO-LUMO gap is 2.87 eV, which indicates possible applications in photovoltaic devices.¹⁰ Figure 1 presents the spatial distributions of HOMO and LUMO orbitals,

calculated for the complex. The HOMO-LUMO transition is a ligand-to-ligand charge transfer.

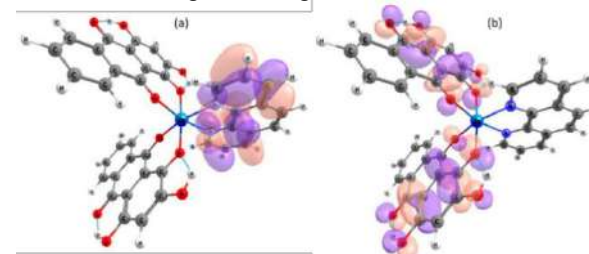


Figura 1. Frontier molecular orbitals (a) LUMO and (b) HOMO

The calculated vibrational results corroborate experimental FT-IR spectra, confirming the attribution of the vibrational mode of $\nu\text{C=O}$ from 1620 and 1667 cm⁻¹ in PURP to 1583 and 1623 cm⁻¹ in the complex. The $\nu\text{C=N}$ also changes from 1566 in PHEN to 1556 cm⁻¹ in the complex. These results highlight a shift towards lower wavenumbers in Zn(II) complex than free ligands.

CONCLUSIONS

Relevant alterations in experimental spectroscopic data were observed, which agreed with the calculations and confirmed complexation. It should also be noted that the coordination of the complex is spontaneous at 298 K, which implies a low production cost. The low value of HOMO-LUMO gap indicates it would be attractive for photovoltaic energy production.

REFERÊNCIAS

- Teixeira, F. J. et al. *J. Molec. St.* 2022, 1261, 132820.
- Stoyanov, S. R. et al. *ACS Omega* 2020, 5, 12944–12954.
- Gulab, H. et al. *J. Molec. St.*, 2018, 1154, 140–144.
- Ali, Z. et al. *J. King Saud Univ. Sci.*, 2022, 34, 102117.
- Frisch, M. J. et al. *Gaussian16*. Wallingford CT, 2016
- Adamo, C.; Barone, V. *J. Chem. Phys.*, 1999, 110, 13, 6158–6170.
- Marenich, A. V. et al. *J. Phys. Chem. B*, 2009, 113, 6378–6396.
- Chemcraft – graphical. Software. for visualization. of quantum. Chemistry. computations. build 648.
- Adam, M. S. S. *J. Molec. Liq.*, 2023, 381, 121841.
- De Lile, J. R. et al. *ACS Omega*, 2020, 5, 15052–15062.

ACKNOWLEDGMENT

UFMA-PPGCM, IFMA, CAPES, CNPQ, FAPEMA, Digital Research Alliance of Canada, and Program of Energy R&D (PERD), Government of Canada.

Assessment of a computational protocol to study the aquation reaction of Pt(II) complexes containing N-Ligands

Letícia S. Amorim (PG),^{1*} Willian T. G. Novato (PQ),¹ Diego F. S. Paschoal (PQ)¹

leticia.amorim05@gmail.com; diegopaschoal01@gmail.com

¹Núcleo de Química Teórica e Computacional de Macaé, Polo Ajuda, Instituto Multidisciplinar de Química, Centro Multidisciplinar UFRJ-Macaé, Universidade Federal do Rio de Janeiro, Macaé, RJ, Brazil.

Keywords: Cancer, Pt(II) complexes, Kinetics, Aquation, Computational Protocol.

INTRODUCTION

Considering that the aquation reaction of Pt(II) complexes is an important descriptor to be considered in the search for new Pt(II) complexes with antineoplastic potential,¹ Paschoal et al.² assessed the role of the platinum basis set (PTBS) and relativistic effects (REL) in predicting the reactivity of cisplatin. However, a gap still remained regarding the role of the DFT functional and the ligands basis set (LBS).² Thus, the present study aims to extend these analyzes evaluating the role of the DFT functional and the LBS, and applying in the study of the aquation reaction of the other Pt(II) complexes with N-ligands.

METHODS

First, the cisplatin, *cis*-[Pt(NH₃)₂Cl₂], aquation reaction was studied through the supermolecule approximation, considering an associative mechanism, where the transition state (TS) was proposed as a distorted trigonal bipyramidal and the intermediate 1 (I1) was found through intrinsic reaction coordinate (IRC) calculation. The Gibbs free energy of activation (ΔG_a) was calculated using the equation: $\Delta G_a = G(TS) - G(I1)$. Computational protocols considering 5 PTBS, 6 LBS and 17 DFT functionals were constructed. Solvent effects were considered using the CPCM implicit solvation model and scalar relativistic effects were considered in some protocols using the 2nd-Order Douglas-Kroll-Hess (DKH2) approach. Then, 32 protocols that presented ΔG_a data within the available experimental range were selected to evaluate the *trans*-[Pt(NH₃)₂Cl₂], [Pt(en)Cl₂], and *cis*-[Pt(py)₂Cl₂] complexes. Finally, 05 protocols with absolute deviations (AD) ≤ 1.0 kcal mol⁻¹ were selected to evaluate the [Pt(NH₃)₃Cl]⁺ and [Pt(dien)Cl]⁺ complexes. The calculations were performed in ORCA 4.2.1 program.

RESULTS

In the first step, a total of 32 computational protocols presented ΔG_a values for cisplatin aquation reaction within the experimental range available in the literature with a maximum relative deviation (RD) of only 1.66%. So, after applying

these protocols to *trans*-[Pt(NH₃)₂Cl₂], [Pt(en)Cl₂], and *cis*-[Pt(py)₂Cl₂] complexes, 05 protocols presented AD ≤ 1.0 kcal mol⁻¹ (Fig.1), being considered suitable for application in the study of the aquation reaction of [Pt(NH₃)₃Cl]⁺ and [Pt(dien)Cl]⁺ complexes (Table 1).

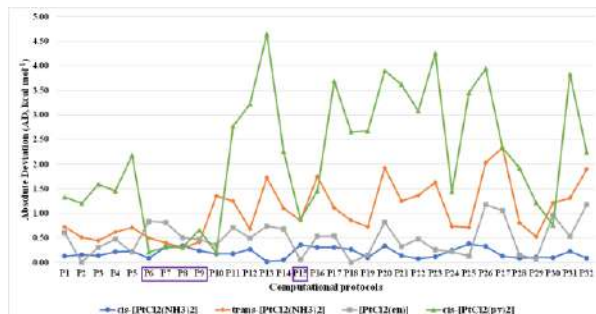


Fig. 1: Absolute deviations of the ΔG_a obtained for the first aquation reaction of the complexes *cis*-[Pt(NH₃)₂Cl₂], *trans*-[Pt(NH₃)₂Cl₂], [Pt(en)Cl₂] and *cis*-[Pt(py)₂Cl₂].

Table 1: Absolute deviations (kcal mol⁻¹) of the ΔG_a calculated for the first aquation reaction of the complexes [Pt(dien)Cl]⁺ and [Pt(NH₃)₃Cl]⁺.

	[Pt(dien)Cl] ⁺	[Pt(NH ₃) ₃ Cl] ⁺	
P6	B3LYP/def2-SVP/def2-SVP/CPCM	0.75	0.26
P7	mPW1LYP/def2-SVP/def2-SVP/CPCM	0.96	0.10
P8	B3LYP/LANL2TZ(f)/def2-SVP/CPCM	0.35	0.08
P9	mPW1LYP/LANL2TZ(f)/def2-SVP/CPCM	0.29	0.74
P15	PBE0-DKH2/Sapporo-DKH3-DZP-2012/jorge-DZP-DKH/CPCM	0.57	0.01

CONCLUSIONS

Considering all the studied complexes, 05 computational protocols presents absolute deviations < 1.0 kcal mol⁻¹ in predicting the Gibbs free energy of activation for the first aquation reaction of these complexes, with an emphasis on P8 - B3LYP/LANL2TZ(f)/def2-SVP/CPCM that presents a mean absolute deviation (MAD) of only 0.32 kcal mol⁻¹.

REFERENCES

- ¹Ahmad, S.; Polyhedron, 2017, 138, 109-124.
²Paschoal, D.F.S.; Gomes, M.S.; Machado, L.P.N.; Santos, H.F.; Basis Sets for Heavy Atoms. In: E. Perlt (eds). Lecture Notes in Chemistry: Basis Sets in Computational Chemistry. Springer, 2021, 107, 183-214.

ACKNOWLEDGMENTS

The authors would like to thank the Brazilian agency FAPERJ (E-26/201.336/2022 – BOLSA and E-26/210.070/2022) and CAPES (Finance Code 001) for the financial support.



Magnetic properties of organolanthanide complexes through $4f^n5d^1$ electron configuration as potential applications as SMMs

Kevin Parco – Valencia¹, Dayán Páez – Hernández^{2*}

k.parcovalencia@uandresbello.edu; dayan.paez@unab.cl

¹Doctorado en Fisicoquímica Molecular, Facultad de Ciencias Exactas, Universidad Andrés Bello, República 498, Santiago, Chile.

²Center of Applied Nanoscience (CANS), Universidad Andrés Bello, República 330, Santiago, Chile.

Keywords: SMMs, divalent lanthanides, electronic structure, magnetic properties

INTRODUCTION

SMMs (single – molecule magnets) have caught the attention of many researchers as their properties make them suitable candidates to be the building blocks of future data storage units, quantum bit carriers (qubits) or components of spintronic devices. These magnets consist of one or more magnetic cores surrounded by ligands guaranteed to have high spin ground states. When the lanthanide ions are incorporated into SMMs, many novel magnetic phenomena were discovered mainly because of the strong magnetic anisotropy of 4f electrons arising from the strong spin–orbital coupling interactions.¹ However, the electronic structure of divalent lanthanides $4f^n5d^1$ could allow the synthesis of complexes of predictable, high - symmetry geometries arising from covalent interactions between ligands and the valence 5d electron, that also maintain the high anisotropy provided by the $4f^n$ electrons. Linearly aligned sandwich complexes introduce some desirable properties like a bistable ground state and reduction of the state mixing due to the pseudo-axial character of the structures. Moreover, divalent lanthanide ions also give the opportunity to consider how it is possible to improve magnetic properties beyond modifying the crystal field, by intrinsically enhancing the magnetic moment of the ion.²

METHODS

$\text{Ln}(\text{CNT})_2$ structures where $\text{Ln} = \text{Pr, Nd, Gd, Tb, Dy, Ho, Er, Yb}$ and $\text{CNT}^- = \text{cyclononatetraenyl}$ were selected to test the active space performance. CAS(n,8), which includes the seven orbitals of the 4f shell and the $5d_{z^2}$ orbital, was considered as the minimum active space followed by a CAS(n,12) where both 4f and 5d shells were completely included. The SO was introduced by a state interaction within the basis of spin–orbit free states using the restricted active space state interaction (RASSI) approach. After obtained the electronic structure, the magnetic properties (effective magnetic moment, g matrix and magnetic susceptibility) were calculated using the SINGLE_ANISO module of ORCA code.³

RESULTS

$\text{Ho}(\text{CNT})_2$ revealed a room temperature χT value of $16.50 \text{ emu.K.mol}^{-1}$, being the highest value reported in this work. In the case of Gd(II), it

should remain isotropic with the addition of an electron into an orbital of primarily $5d_{z^2}$ character. Indeed, the χT for $\text{Gd}(\text{CNT})_2$ reveals a nearly temperature independent χT product, with a room temperature magnitude of $9.98 \text{ emu.K.mol}^{-1}$. These factors support a $4f^n5d^1$ assignment. Ho(II) (${}^6\text{I}_{17/2}$) ion (Kramer ion) obtained a value of $g_{||} = 21.90$, which reflects a large component of g-tensor thus characterizing a strong axiality. On the other hand, the transversal components (g_x and g_y or g_{\perp}) provide the quantitative description of the low symmetry of the ligand field , which is of great importance in explaining the relaxation dynamics in the low-temperature region. The value obtained for this parameter was $g_{\perp} = 0$, meaning that the relaxation dynamics in the low-temperature region are negligible.

Ln	g	μ_{eff} (free ion)	$\chi T - \text{Ln}(\text{CNT})_2$		$\chi T - \text{Ln}(\text{CNT})_2$	
			CAS(n,8)SCF	CAS(n,12)SCF	CAS(n,8)SCF	CAS(n,12)SCF
Pr	0.67	2.64	3.50	3.58	0.78	0.88
Nd	0.60	2.68	3.34	3.36	0.91	1.08
Gd	2.00	6.94	8.94	8.93	9.98	9.98
Tb	1.54	10.74	10.64	8.61	14.82	13.78
Dy	1.37	11.67	11.42	11.44	16.24	16.28
Ho	1.29	11.63	11.53	11.46	16.50	16.52
Er	1.25	10.64	10.63	10.64	13.97	13.97
Yb	1.25	5.59	5.79	5.66	3.394	3.39

CONCLUSIONS

Dy(II) and Ho(II) exhibit room temperature magnetic moments and magnetic susceptibilities (χT) that are the highest reported in this work. The accessibility of such enormous moments could have intriguing implications in single-molecule magnetism and in the design of new bulk magnet materials. Larger magnetic moments and a high - symmetry geometries can diminish tunneling of the magnetization (QTM) in molecular materials as well as the Orbach relaxation processes, currently both major drawbacks in the design of SMMs. Thus, it is interesting to consider that within this ligand field symmetry, such accessible moments may enhance single-molecule magnet properties.

REFERENCES

- 1 Tang, J., & Zhang, P, Berlin: Springer, 2015, 2. 41-90.
- 2 Solís-Cespedes, E., & Páez-Hernández, D, Dalton Transactions, 2021, 50(28), 9787-9795.
- 3 Neese, F.; Wennmohs, F.; Becker, U.; Ripplinger, C, J. Chem. Phys., 2020, 152. 224108.

ACKNOWLEDGMENTS

This work has been supported by FONDECYT Regular 1220442.

Desenvolvimento de uma Metodologia de Otimização de Funcionais RSH Fisicamente Inspirada no Princípio da Mínima Polarizabilidade

Ana Carolina Felisberto Araujo (PG),^{1*} Pedro Henrique Ferreira Matias (PG),² Mateus R. Barbosa (PG),³ Heibbe Cristhian Benedito de Oliveira (PQ),⁴ Daniel Francisco Scalabrini Machado (PQ).⁵

carol.felisbertoa@gmail.com

¹Universidade Federal de Goiás (UFG), Instituto de Química (IQ), Laboratório de Estrutura Eletrônica e Dinâmica Molecular (LEEDMOL), Goiânia, Brasil; ²Universidade de Brasília (UnB), Instituto de Química, Brasília, Brasil.

Palavras Chave: RSH, Polarizabilidade, Polímeros Orgânicos.

INTRODUÇÃO

Existe uma grande demanda em protocolos para correção de descrições de propriedades de caráter local obtidas pela Teoria do Funcional de Densidade (DFT), destacando-se a otimização do parâmetro ômega (ω). Uma alternativa para minimizar o valor de ω em funcionais RSH pode ser fisicamente inspirada no princípio da mínima polarizabilidade, a medida que, esta requer apenas informações sobre polarizabilidade linear do estado fundamental e, por conseguinte, é capaz de reduzir o número de cálculos necessários em três vezes quando comparada aos demais métodos^{1,2}.

Os materiais ópticos podem ter suas propriedades optoeletrônicas aprimoradas seguindo o princípio da mínima polarizabilidade, logo, espera-se que a otimização do parâmetro ω visando a minimização da polarizabilidade linear acarrete em uma melhora sensível de suas propriedades ópticas.^{1,2,3}

MÉTODOS

Este trabalho propõe uma otimização do parâmetro ω fisicamente inspirada no princípio da mínima polarizabilidade para o funcional LC-BLYP⁴ em polímeros orgânicos. Após a otimização, será possível predizer propriedades optoeletrônicas que são diretamente dependentes da polarizabilidade linear (α): Índice de Refração (n) e Número de ABBE (v).

RESULTADOS

A otimização do parâmetro ω resultou nos seguintes valores de polarizabilidade (α):

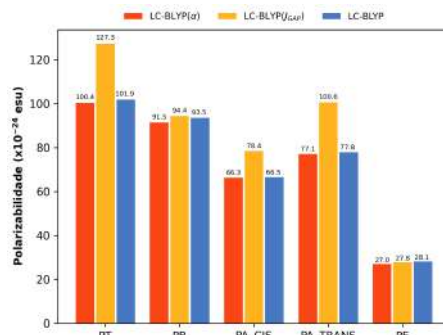


Figura I. Polarizabilidade (ESU) obtida para o Politiofeno (PT), Poli(1,4-fenileno) (PB), cis-poliacetileno (PA_CIS), trans-poliacetileno (PA_TRANS) e Polietileno (PE) através de LC-BLYP (α) (vermelho), LC-BLYP (J_{GAP}) (amarelo) e default LC-BLYP (azul), respectivamente.

A partir das polarizabilidades obtidas foi possível calcular o Índice de Refração (n) e Número de ABBE (v) para os polímeros. Podemos destacar que o PE, por exemplo, indicou valores de “ n ” igual a 1,4815 e “ v ” 63,2910 após a otimização do funcional LC-BLYP baseando-se na mínima polarizabilidade. Entretanto, o funcional otimizado via J_{GAP} resulta em propriedades ópticas de valores iguais a 1,4990 para “ n ” e 58,1379 para “ v ”.

CONCLUSÕES

A proposta metodológica forneceu resultados satisfatórios, com valores mínimos para ômega e polarizabilidade. Foram obtidos valores de “ α ” menores em nossa metodologia, quando comparados à varredura do parâmetro ômega via esquema JGAP, pois este resultou em valores mais elevados até mesmo em referência à “ α ” obtida por meio do funcional *default*. As propriedades ópticas calculadas se aproximam do valor experimental encontrado na literatura.

REFERÊNCIAS

- Maekawa, S.; Moorthi, K. Polymer Optical Constants from Long-Range Corrected DFT Calculations. *The Journal of Physical Chemistry B* 2016, 120, 2507–2516, PMID: 26918918.
- Neto, A. P.; Machado, D. F. S.; Lopes, T. O.; Camargo, A. J.; de Oliveira, H. C. Explicit Aqueous Solvation Treatment of Epinephrine from Car-Parrinello Molecular Dynamics: Effect of Hydrogen Bonding on the Electronic Absorption Spectrum. *The Journal of Physical Chemistry B* 2018, 122, 8439–8450.
- Machado, D.F.S. Desenvolvimento de Métodos Fisicamente Inspirados Para Cálculos de Ótica Não-Linear e Efeitos de Solventes nas Propriedades ópticas Não-LInearas em Derivados de Azo-Enaminonas. 2017. Tese (Doutorado) - Universidade de Brasília, Brasília, 2017.
- Chai, J.-D., & Head-Gordon, M. (2008). Systematic optimization of long-range corrected hybrid density functionals. *The Journal of Chemical Physics*, 128(8), 084106.

AGRADECIMENTOS

CNPq, CAPES, FAPEG, LaMCAD, LEEDMOL, UFG.

QTAIM topological analyses of zinc(II), cadmium(II), and mercury(II) xanthate complexes

Daniella B. Miranda (PG),¹ Henrique C. Silva Junior (PQ),² Glaucio B. Ferreira (PQ)^{1*}

daniellabrito@id.uff.br; *glauciofb@id.uff.br

¹Programa de Pós-graduação em Química, Universidade Federal Fluminense, Niterói – RJ – Brasil; ²Instituto de Química, Universidade Federal do Rio Grande do Sul, Porto Alegre – RJ - Brasil.

Palavras Chave: Xanthates, DFT, QTAIM, Zn²⁺, Cd²⁺, Hg²⁺

INTRODUCTION

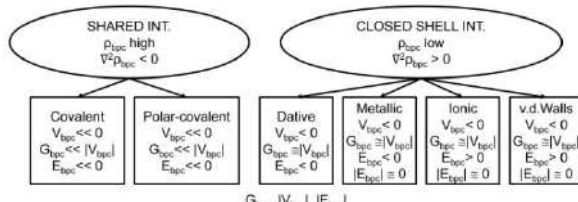
The xanthate ligand is a low-cost, easy-to-prepare flotation agent still widely used today.¹ In addition to the known environmental action in removing heavy metals, xanthates stand out for the versatility of coordination modes with metallic centers. Recently, Miranda and coworkers carried out thermodynamic studies and electronic analysis with Density Functional Theory (DFT) to investigate xanthate complexes with group 12 metals.^{2,3} The results indicated M-S interactions with ionic and covalent characters and the influence of intermolecular interactions.

MÉTODOS

The theoretical studies for twenty-seven structures optimized of Zn(II), Cd(II), and Hg(II) xanthate complexes with an alkyl group (n-propyl) were performed with DFT level: M06L/6-311++G**+LANL2TZ-ECP, as described in the literature with Gaussian 09 software.^{2,3} The quantum theory of atoms in molecules (QTAIM) topological analyses were used to refine the characterization of the chemical bonds. This analysis was performed with DFT level: M06L/def2TZVP to obtain wfx files utilized in MultiWFN software. The studies focused on M-S and M–O bonds and the presence of hydrogen bond (HB) and S–H interactions.

The topological analysis of the electron density $\rho(r)$ allows for defining bond paths and bond critical points (BCPs). The nature of the chemical bond is characterized by properties of $\rho(r)_{\text{BPC}}$, especially the sign of the Laplacian $(\nabla^2\rho)_{\text{BPC}}$ and the values of the kinetic energy density $(G)_{\text{BPC}}$, of the potential energy density $(V)_{\text{BPC}}$ and the energy density: $E_{\text{BPC}} = G_{\text{BPC}} + V_{\text{BPC}}$. Negative and positive values for $(\nabla^2\rho)_{\text{BPC}}$ are assigned to “electron-shared” and “closed-shell” interactions, respectively.⁴ Macchi’s scheme below describes the bonding regimes, where the first is associated with covalent bonds, and the second includes ionic bonds or van der Waals interactions. Intermediate systems are dative and ionic bonds of weak covalent character.⁵

Scheme 1. Classification of the atomic interactions.⁵



RESULTS

The analysis of the topological descriptors allowed the identification of intramolecular BPCs in mono- and bi-coordinated cationic and neutral complexes, with a refined classification of atomic interactions. For example, in Figure 1, data are presented for some complex cations where HB and van der Wall interactions were evident. In addition, the descriptors confirmed the increase in electron sharing in the comparison between M-S and M–O, with greater emphasis on the mercury complex.

Figure 1. QTAIM descriptors (in a.u.) of the BPC related to M-S e M-O bonds in cationic complexes.

Bond	Zn-S ₆	Zn-O ₃
R	2.362	2.207
ρ	0.067	0.046
$\nabla^2\rho$	0.157	0.221
V	-0.069	-0.059
G	0.054	0.057
E	-0.014	-0.002
Bond	Cd-S ₃₀	Cd-O ₁₃
R	2.506	2.401
ρ	0.064	0.040
$\nabla^2\rho$	0.140	0.179
V	-0.064	-0.048
G	0.049	0.046
E	-0.014	-0.002
Bond	Hg-S ₃₀	Hg-O ₁₄
R	2.493	2.438
ρ	0.076	0.045
$\nabla^2\rho$	0.107	0.175
V	-0.066	-0.050
G	0.047	0.047
E	-0.020	-0.003

The figure displays three molecular models of cationic complexes. The top model shows a central Zinc atom (Zn) coordinated to six sulfur atoms (S) from six n-propyl xanthate ligands, with one water molecule (H₂O) also present. The middle model shows a central Cadmium atom (Cd) coordinated to three sulfur atoms (S) from three ligands, with one water molecule (H₂O) present. The bottom model shows a central Mercury atom (Hg) coordinated to four sulfur atoms (S) from four ligands, with one water molecule (H₂O) present. All models include green lines representing bond paths and small grey spheres representing bond critical points (BCPs).

CONCLUSION

The QTAIM descriptors complemented the evaluations previously obtained in the literature's electronic energy decomposition analysis (EDA) and natural bond orbitals (NBO) studies. Furthermore, the presence of HB and S---H interactions and the influence of bond distance on the coordination sphere were confirmed.

REFERÊNCIAS

1. M. Zhao M, et al., Appl. Microbiol. Biotechnol. 2016, 100, 6509;
2. D.B. Miranda, S. Quintal, G.B. Ferreira, JBCS, 2023, in press;
3. D.B. Miranda, S. Quintal, G.B. Ferreira, J.Mol.Mod., 2023, 26, 146;
4. C. Lepetit, M. L. Kahn, Res. Chem. Intermed., 2021, 47, 377;
5. R. Bianchi, et al., Inorg. Chem., 2000, 39, 2360

AGRADECIMENTOS

CNPq, CAPES, FAPERJ, PROPPi UFF, and LMQC-UFF.

Aplicação de Aprendizado de Máquina na Interpretação de Rearranjo de Claisen

Rafael Ferreira Veríssimo (IC),¹ Ana Gabriela Coelho Oliveira (PQ),¹ Mateus Rodrigues Barbosa (PQ),¹ Pedro Henrique Ferreira Matias (PQ),¹ Ângelo Henrique Lira Machado (PG),² Daniel Francisco Scalabrini Machado (PG)², Hebbe Cristhian Benedito de Oliveira (PG).¹

rafaelfv27@gmail.com;

¹Instituto de Química - Universidade Federal de Goiás; ²Instituto de Química - Universidade de Brasília

Palavras Chave: *machine learning, estereoseletividade, rearranjo de Claisen.*

INTRODUÇÃO

A reação de Morita-Baylis-Hillman (MBH) ocorre entre olefinas e compostos carbonílicos, contando com uma transição seguida de um rearranjo de Claisen^{1,2}. Silva e colaboradores (2019) publicaram o primeiro estudo teórico experimental do rearranjo de Hurd-Claisen para adutos de MBH obtendo-se uma seletividade *E* sem precedentes, levantando questionamentos de como a estereoseletividade pode ser controlada, nesta etapa por meio de modificações estruturais². Este trabalho propõe, a utilização de *machine learning* como ferramenta de análise em um banco de dados reduzido³, visando determinar quais possíveis modificações estruturais influenciam a estereoseletividade dos rearranjos de Claisen.

MÉTODOS

A partir de cálculos quantum-mecânicos de 72 estados de transição dos adutos de MBH (etapa sigmatrópica [3,3]) foi gerado um banco de dados. Os 67 descritores químicos (parâmetros geométricos e eletrônicos) foram retirados da porção central do anel da TS.

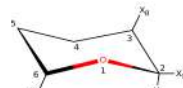


Figura 1: Estrutura genérica do estado de transição do rearranjo de Claisen.

Foi necessário reduzir a multicolinearidade do banco de dados, removendo-se 33 descritores altamente correlacionados juntamente com a seleção dos descritores por meio da penalização L1 e L2 do Elastic-Net, resultando em 23 descritores. Dez modelos de *machine learning* foram utilizados na validação. Vabalas (2019) menciona que banco de dados reduzidos devem ser validados pelo método de validação cruzada aninhada (*Nested-CV*)³. O modelo final foi escolhido com base nos valores de R^2 do erro médio absoluto da validação aninhada. Por fim, os resultados foram analisados via *SHAP values*,

quantificando a contribuição de cada descritor da estereoseletividade.

O modelo final implementado foi a rede neural *MLP*, obtendo um R^2 de 0,89 e MAE de 0,74 kcal/mol.

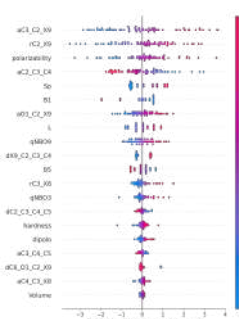


Figura 2: Gráfico de dispersão do impacto do modelo final.

O gráfico da Figura 2 indica que valores altos entre os ângulos dos átomos (C3-C2-X9) tem um grande impacto na estereoseletividade do rearranjo, como também de grandes distâncias de ligações entre C2-X9. Em contrapartida, valores elevados do ângulo (C2-C3-C4) tem um impacto negativo na predição da estereoseletividade.

CONCLUSÕES

O modelo de *machine learning* apresentou boas métricas de validação mesmo com banco de dados reduzido. Ademais, sendo capaz de predizer o impacto de diferentes descritores geométricos e eletrônicos sobre a variação da energia livre de Gibbs das TS, indicando quais mudanças estruturais devem ser engenhadas para controle estereoseletivo.

REFERÊNCIAS

1. Lima-Junior, C. G., & Vasconcellos, M. L. (2012). Bioorganic & medicinal chemistry, 20(13), 3954-3971.
2. Silva, V. S. et al. (2019). Organic & biomolecular chemistry, 17(18), 4498-4511.
3. Vabalas, A. et al. (2019). PloS one, 14(11), e0224365.

AGRADECIMENTOS

CNPq, CAPES, FAPEG, LAMCAD, UFG, UNB, LEEDMOL, LITMO, LMSC.

PROSPECÇÃO IN SILICO DE INIBIDORES DA SAP5 DE CANDIDA ALBICANS EM ONICOMICOSSES

Lorrany K. C. Queiroz (PG),¹ Gunar V. da S. Mota (PQ),² Fabio L.P. Costa (PQ).¹

fipcosta@ufj.edu.br

¹Universidade Federal de Jataí-ICET; ²Universidade Federal do Pará-ICEN

Palavras Chave: SAPs, Dinâmica molecular, Docking, C. Albicans

INTRODUÇÃO

A onicomicose é uma doença fúngica prevalente, com disseminação influenciada por fatores imunossupressores.¹ O tratamento é limitado por efeitos colaterais, custos e resistência a antifúngicos.¹ Considerando o aumento de casos, é necessário investigar novas terapias, como inibidores de proteases de *C. albicans*, como a SAP5 (Protease Aspártica Secretada 5). Neste estudo realizou-se simulações de docking molecular (DOC) e dinâmica molecular (DM) entre a SAP5 e 130 ligantes, entre fármacos antifúngicos e metabólitos vegetais. Foram analisados parâmetros de interação, e as propriedade ADMET (absorção (A), distribuição (D), metabolismo (M), excreção (E) e toxicidade (T)).

MÉTODOS

Nos estudos de DOC utilizou-se o programa AutoDock Vina.² A definição da grid box foi realizada com base no ligante cristalizado a pepstatina A. As propriedades ADMET foram obtidas na plataforma ADMETlab 2.0.³ As simulações de DM foram realizadas no módulo DESMOND do pacote Maestro21.⁴

RESULTADOS

Assim, foram selecionados 7 complexos para os estudos de DM. Os melhores resultados foram obtido para a molécula de cubenol (figura 1) e para a molécula de 2-metóxi-4-propil-fenol (figura 2) nas figuras abaixo os resultados são apresentados em relação ao desvio quadrático-médio das distâncias dos átomos (do inglês root-mean-square deviation, RMSD).

Figura 1: Variação RMSD temporal para a simulação SAP5-cubenol.

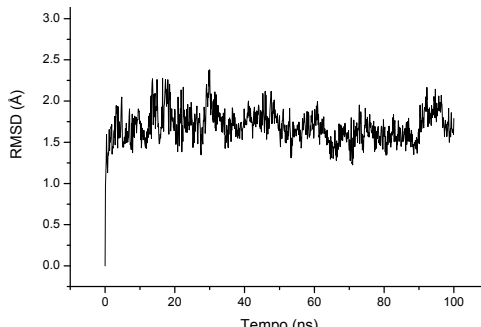
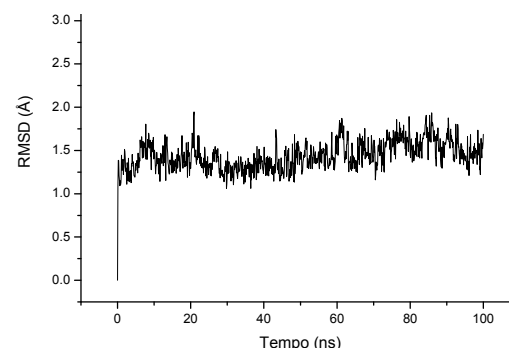


Figura 2: Variação RMSD temporal para a simulação SAP5-2-metóxi-4-propil-fenol



O comportamento foi comum às 7 simulações, com desvios muito pequenos que não ultrapassaram 0,20 nm (2,0 Å), para a proteína e para o ligante. Isso sugere que há uma interação estável entre os ligantes e a SAP5, ou seja, os eles se acomodaram bem no sítio ativo da enzima durante os 100 ns simulados, confirmando os resultados obtidos por meio do cálculo de energia total da DM e DOC.

CONCLUSÕES

Os resultados de DOC e de DM obtidos neste estudo indicam o potencial de alguns metabólitos secundários como possíveis inibidores da enzima SAP5 de *C. albicans*. Os 7 complexos enzima-ligante selecionados apresentaram interações e estabilidade consideradas favoráveis segundo parâmetros da literatura.⁵ Esses compostos são alvos promissores para investigação experimental a fim de confirmar a predita atividade antifúngica contra essa protease.

REFERÊNCIAS

- ¹ A. M. et al., Infect Drug Resist, 2021, 14, 5543.
- ² O. Trott, A. J. Olson, J Comput Chem, 2010, 31, 455.
- ³ G. Xiong et al., Nucleic Acids Res, 2021, 49(W1): W5.
- ⁴ K. J. Bowers et al., Proceedings of the 2006 ACM/IEEE Conference on Supercomputing, 2006, 43.
- ⁵ D. Ramírez, J. Caballero, Molecules, 2018, 23, 1038.

AGRADECIMENTOS

À CAPES

Studies of energy transfer processes in structures derived of NH₂-UiO-66 MOF

Vinicius Gonçalves Souto Fontenelle (PG)*, Willian Ricardo Rocha (PQ), Guilherme Ferreira de Lima (PQ).

vifontenelle@gmail.com.

Departamento de Química, Universidade Federal da Minas Gerais, Belo Horizonte - MG

Palavras-Chave: DFT, MOFs, NH₂-UiO-66, TD-DFT.

INTRODUCTION

Reducing CO₂ through photochemical processes is a key strategy for combatting climate change. Solar energy, with the assistance of appropriate catalysts, can convert CO₂ into C₁ and C₂ fractions, which holds significant potential as renewable energy sources and raw materials for industries. However, optimizing the efficiency of this process necessitates catalysts capable of effectively absorbing solar energy. Regrettably, in MOFs there exist energy and symmetry discrepancies between the metal and the ligand orbitals, resulting in insufficient ligand-to-metal-charge-transfer (LMCT) and low electron-hole separation efficiency. To address this issue, one approach involves modifying well-established, stable MOFs with electron-rich systems to augment LMCT. Our project centers on investigating the electronic behavior of NH₂-UiO-66 functionalized with compounds designed to enhance LMCT of the material, such as ferrocene. To achieve this goals, molecular models and periodic calculations will be done.

METHODS

The investigations will be carried out using computational simulations grounded in Density Functional Theory (DFT). For periodic models, *Quantum Espresso* software will be utilized, incorporating the PBE exchange correlation functional, ultrasoft pseudopotentials, and plane waves as the foundational basis. Regarding molecular models, ORCA 5.0.3 will be employed, utilizing the PBE functional and the split valence basis set. Studies involving excited states will be undertaking using TD-DFT, incorporating different functionals.

RESULTS

Based on the CIF file of the UiO-66 MOF structure, a calculation protocol was established for the periodic system computations. Molecular approximations of the MOF were constructed, which will be employed for excited-states studies to analyze the material's electronic behavior. Figure 1 displays one of the approximations of NH₂-UiO-66 and the structure functionalized with ferrocene.

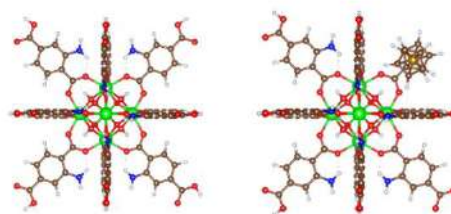
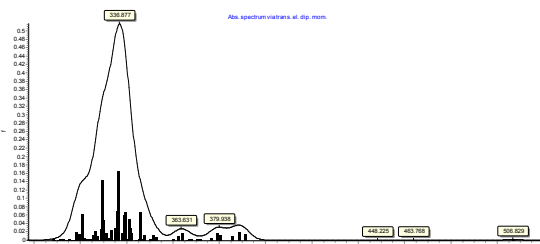


Figure 1: Molecular model of NH₂-UiO-66 and NH₂-UiO66-Fc, where carbon, hydrogen, nitrogen, oxygen, zirconium and iron are depicted in brown, white, blue, red, green and golden respectively.

TD-DFT calculations were conducted to analyze the excited states of the systems within the Franck-Condon region. Figure 2 displays the absorption spectrum via transition dipole moments for the MOF with ferrocene, employing PBE0 functional.



Based on the natural transition analysis (NTA) obtained, following the functionalization with Fc, the state with the greatest contribution of the electron – hole pair was identified as 41(1), involving the transition 608(HOMO-4) to 633(LUMO+6). According to the results, a portion of the electrons from the BDC and the Fc is transferred to the oxygen atoms of the Zr-O cluster, indicating a LMCT type interaction.

CONCLUSIONS

The initial results indicate that the functionalization of the BDC ligand with NH₂ increases the absorption wavelength of the system. However, the addition of a unique Fc to the model does not appear to significantly influence the absorption spectrum. The next step is to determine the optimal proportion of ferrocene to enhance the LMCT.

REFERENCES

- Xia, L. et al. *Chemical Engineering Journal*. 2023, 451.
- Cavka, J. H. et al. *JACS*. 2008, 130(42) 13850-13851.
- Li, R. et al. *Advanced Materials*. 2018, 30(35).

ACKOWLEDGEMENT

CNPq, CAPES, FAPEMIG.

Unraveling a homogeneous route to glycerol valorization: a DFT study

Rodrigo S. Bitzer (R)¹, Marco A. C. Nascimento (R)^{1*}

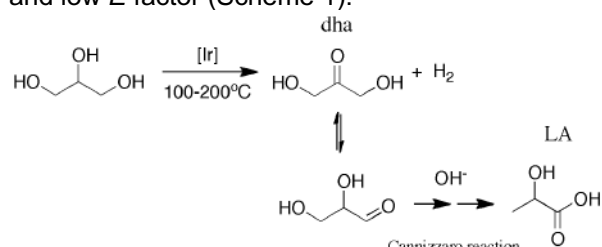
bitzer@iq.ufrj.br; chaer01@gmail.com

¹Instituto de Química, Universidade Federal do Rio de Janeiro, Brazil

Keywords: biodiesel, glycerol, acceptorless dehydrogenation, iridium, DFT.

INTRODUCTION

Glycerol valorization embraces catalytic processes aiming to transform glycerol, a coproduct of biodiesel production, into value-added chemicals, such as propanediols, acrolein, dihydroxyacetone (dha), glyceraldehyde (gca), and lactic acid (LA).¹ Both heterogeneous and homogeneous strategies have been employed in the catalytic valorization of glycerol.^{1–3} Among them, homogeneous glycerol dehydrogenation and hydrogenolysis have been widely investigated because these processes can directly transform crude glycerol, freshly obtained from biodiesel manufacture, into commodity chemicals.^{2,3} In particular, acceptorless glycerol dehydrogenation (AGD) catalyzed by 14-electron iridium(I) complexes has emerged as one of the most efficient homogeneous routes to glycerol valorization.^{2,3} In effect, AGD reactions produce dha/gca, LA, and H₂, exhibiting high atom economy and low E factor (Scheme 1).



Scheme 1. AGD catalyzed by iridium complexes.

Unraveling the catalytic mechanisms of iridium complexes in AGD reactions contributes to the design of improved catalysts with tailored properties.^{2,3} In this work, we carried out DFT calculations on a homogeneous Ir(NHC)-based catalytic system for the acceptorless dehydrogenation of glycerol in basic medium.³

METHODS

All DFT calculations were performed using Jaguar. Geometry optimizations and vibrational frequency calculations were carried out at the PBE0/LACVP** level. Energy values were refined, including PBF solvation (neat glycerol), by single-point calculations at the M06-D3/LACV3P**++ level.

RESULTS

The catalytic system studied in this work operates through 14-electron iridium(I) species obtained by thermal activation (145°C) of Williams' precatalyst: [(NHC)Ir(cod)]⁺ [NHC = (2-pyridylmethylene)NHC; cod = cyclooctadiene] (Fig. 1).³

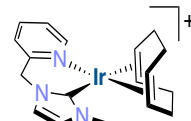


Fig. 1. Williams' precatalyst.³

Our mechanistic approach encompasses the following steps: (1) precatalyst deprotonation; (2) precatalyst reprotonation by neat glycerol; (3) cod displacement; (4) β-hydride elimination; and (5) H₂ formation and release. Steps (1)–(3) concern precatalyst speciation and activation, whereas steps (4) and (5) account for the catalytic cycle. According to our results, (NHC)Ir^l(glycerolate) complexes are the catalytically active species. In addition, the turnover-limiting step involves H₂ release and catalyst regeneration, rather than β-hydride elimination (Fig. 2).

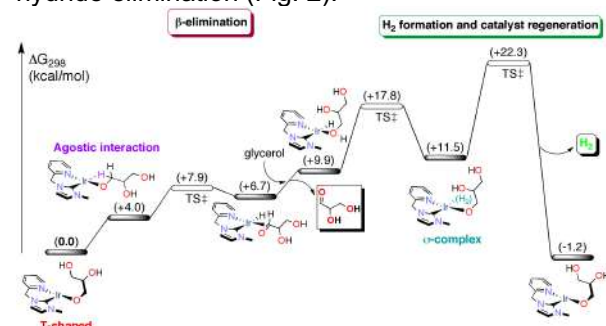


Fig. 2. Calculated reaction diagram for gca and H₂ formation. Three pathways for H₂ formation and release have been investigated in this work: (i) glycerol-assisted Ir–H bond protonation (non-oxidative pathway); (ii) glycerol-assisted Ir protonation (oxidative pathway); and (iii) intramolecular proton migration (oxidative pathway). The non-oxidative pathway leads to the lowest energy barriers (Fig. 2).

CONCLUSIONS

In contrast to literature proposal,^{2,3} our DFT calculations have shown that catalyst turnover is governed by H₂ release, rather than β-hydride elimination. Also, H₂ formation and dissociation proceed through σ(H₂) intermediates.

REFERENCES

- C.-H.C. Zhou, J.N. Beltramini, Y.-X. Fan, G.Q.M. Lu, Chem. Soc. Rev., 2008, 37, 527.
- R.H. Crabtree, Chem. Rev., 2017, 117, 9228.
- Z. Lu, I. Demianets, R. Hamze, N.J. Terrile, T.J. Williams, ACS Catal., 2016, 6, 2014.

ACKNOWLEDGMENTS

FAPERJ, CAPES, and CNPq.

Quiralidade Axial Induzida Através de LHS Não-Clássicas ($\text{CH}\cdots\text{F}$)

Bruno A. Piscelli (PG),¹ Lucas A. Zeoly,¹ Luciana P. S. Viana (PG),² Cleiton M. da Silva (PQ),² Rodrigo A. Cormanich (PQ).^{1*}

b195034@dac.unicamp.br; cormanich@unicamp.br

¹Instituto de Química, Universidade de Campinas, UNICAMP, 13083-970; ²Departamento de Química, Universidade Federal de Minas Gerais, UFMG, 31270-901.

Palavras Chave: Isomeria Rotacional, Ligação de hidrogênio, Organofluorados, DFT, NBO.

INTRODUÇÃO

A isomeria rotacional refere-se aos estereoisômeros que podem interconverter entre si através da rotação da uma ligação simples, sendo assim chamados de rotâmeros.¹ O butano é um alifático simples que apresenta dois rotâmeros acessíveis, o *anti* e o *gauche*, e que podem se interconverter através da rotação do diedro C-C-C-C com uma barreira energética de $\sim 3,5 \text{ kcal mol}^{-1}$.² Em casos em que a barreira energética de rotação é suficientemente alta ($>22 \text{ kcal mol}^{-1}$ à 300K), como no BINAP ($\sim 49,2 \text{ kcal mol}^{-1}$), os isômeros rotacionais apresentam tempo de meia-vida longo o bastante para que eles possam ser separados quimicamente, recebendo o nome de atropoisomeria.^{3,4}

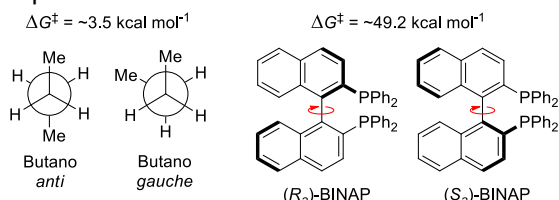


Figura 1. Barreira energética para (a) a interconversão dos rotâmeros *anti* e *gauche* do butano e (b) interconversão dos atropoisômeros *R*_a e *S*_a do BINAP.

Diferentemente dos casos reportados na literatura, neste estudo reportamos um composto orgânico que exibe uma ligação σ com alta barreira de rotação devido à formação de interações não-covalentes, especificamente ligações de hidrogênio (LHS) entre uma ligação CH e um átomo de flúor, que por sua vez é reconhecido como um mal aceptor de LH.⁵

MÉTODOS

- Busca Conformatinal: Metadinâmica estática-iterativa GFN2-xTB | CREST.
- Otimização de geometria, frequência e NBO: M05-2X/6-311++G(d,p) | Gaussian16.
- Scans: M05-2X/6-31G(d,p) | Gaussian16.

RESULTADOS

Apesar de não apresentar centros estereogênicos, o composto **1F** apresenta hidrogênios diastereotópicos que foram identificados por experimentos de RMN (Figura 2). Cálculos de NBO feitos para os confôrmeros do composto **1F** mostram que há a formação de LHS não-

convencionais de caráter eletrostático entre os hidrogênios H₂₀ e H₂₁ e o flúor na posição *ortho*, estimadas em $\sim 10 \text{ kcal mol}^{-1}$.

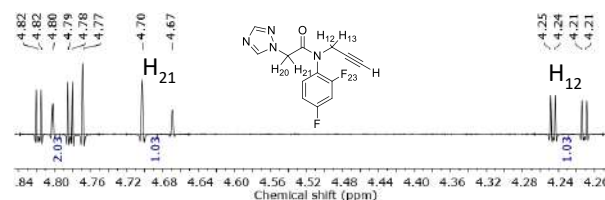


Figura 2. Espectro de RMN de ^1H (500MHz) do composto **1F** obtido em CDCl_3 .

O scan realizado para a rotação da ligação C-N do composto **1F** indica uma barreira teórica de 16,8 kcal mol⁻¹ em DMSO, em ótima concordância com o valor obtido experimentalmente (16,4 kcal mol⁻¹). A barreira de rotação calculada para o composto **1**, análogo ao **1F** sem o flúor em *ortho*, é expressivamente menor (9,1 kcal mol⁻¹), o que indica o papel central das LHS para o surgimento da quiralidade axial observada.

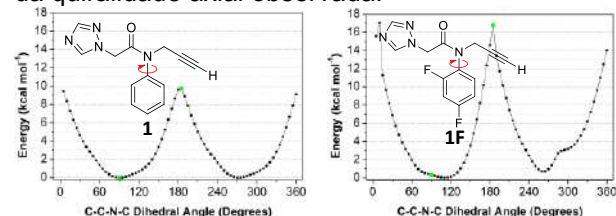


Figura 3. Scans da rotação da ligação C-N no composto **1** (esquerda) e **1F** (direita).

CONCLUSÕES

O composto **1F** apresenta quiralidade axial devido à alta barreira energética de rotação da ligação Ar(C)-N, decorrência da formação de LHS não-convencionais CH \cdots F. A indução de quiralidade axial através de LHS não clássicas é novo na literatura, visto que a vasta maioria dos casos reportados são decorrência dos efeitos estéricos promovidos por grupos volumosos.

REFERÊNCIAS

- ¹ G. P. Moss, Pure Appl. Chem., 1996, 68, 2193.
- ² R. A. Cormanich, M. P. Freitas, J. Org. Chem., 2009, 74, 8384.
- ³ M. Oki, Topics in Stereochemistry, 1983.
- ⁴ J. S. García, C. Lepetit, Y. Canac, R. Chauvin, M. Boggio-Pasqua, Chem. Asian J., 2013, 9, 462.
- ⁵ J. A. K. Howard, V. J. Hoy, D. O'Hagan, G. T. Smith, Tetrahedron, 1996, 52, 12613.

AGRADECIMENTOS

Modeling Electronic Transport in Fullerene-Based Materials using a Wide-Band Limit Complex Absorbing Potential Self-Energy Approach.

Gabriela M. B. da Silva (UR)¹, Roberta P. Dias (R)², Augusto C. L. Moreira (R)², Júlio C. S. Da Silva (R)^{1*}
gabriela.balbino@iqb.ufal.br; julio.silva@iqb.ufal.br

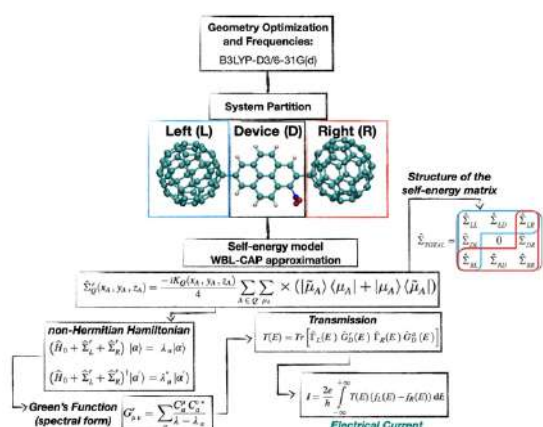
¹Instituto de Química e Biotecnologia, UFAL; ²Núcleo Interdisciplinar de Ciências Exatas e da Natureza, CAA-UFPE.

Keywords: (transmission function, conductance, complex absorbing potential, DFT)

INTRODUCTION

The prevailing method for calculating current and conductance through a molecule involves utilizing non-equilibrium Green's function (NEGF) in conjunction with Density Functional Theory (DFT). Within this context, two distinct approaches emerge: (1) the self-consistent (SC) approach and (2) the non-self-consistent (non-SC) approach. For the acquisition of precise (current x voltage) curves, the full SC methodology within the NEGF+DFT framework necessitates a substantial computational capacity. Upon considering the Complex Absorption Potential (CAP) as a means to replicate an infinite environment at the termini of a finite system, it becomes feasible to employ this as a self-energy model with low computational demands. This allows the matrices essential for transport calculations to be derived from a DFT assessment of extended molecules, all in a single step using an adaptable model.^{1,2} Thus, in the present study, we have employed the self-energy model grounded in the CAP methodology and scattering theory. Our aim is to investigate electron transport in the systems involving (C₆₀)-pyrene-(C₆₀) as well as (C₆₀)-pyrene units functionalized with NO₂ and NH₂ groups at various positions.

METHODS



Scheme 1: Steps of the WBL-CAP approximation used to calculate the transmission and electrical current.

RESULTS

Figure 1 shows the Kohn-Sham frontier molecular orbitals (KSFMO) calculated for the (C₆₀)-pyrene-(C₆₀) and (C₆₀)-pyrene-(C₆₀) functionalized with NO₂ in the position defined as 1 and 2. The analysis of the KSFMO orbitals indicates a possible

formation of an electron transport channel although the extended molecular systems. Also, it is possible to note that the position of the NO₂ in the pyrene molecule affects the shape of the KSFMO.

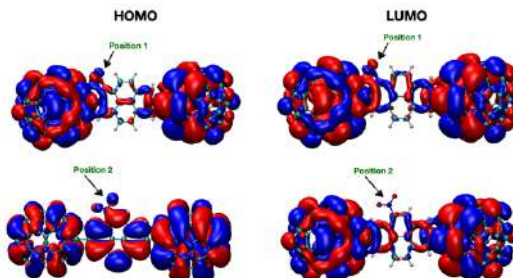


Figure 1: Kohn-Sham frontier molecular orbitals for systems with NO₂ in positions 1 and 2.

Fig. 2 shows the transmission function calculated with WBL-CAP model for (C₆₀)-pyrene(NO₂ in different positions)-(C₆₀) systems.

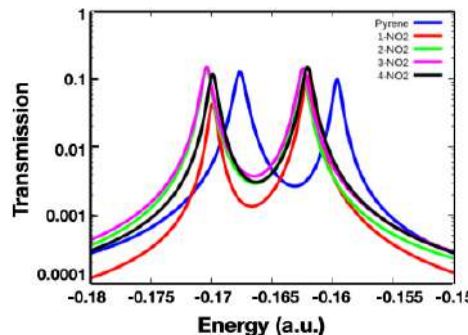


Figure 2: Calculated transmission function.

Fig. 2 illustrates that introducing NO₂ into the pyrene molecule alters the regions of peak transmission compared to the system without NO₂. This observation highlights the sensitivity of the Wide-Band Limit Complex Absorbing Potential (WBL-CAP) approximation concerning the chemical composition of the extended system.

CONCLUSIONS

Our findings affirm that the WBL-CAPs model effectively captures essential characteristics of the transmission function in fullerene-based systems.

REFERENCES

- A. C. L. Moreira, C. P. Melo, L. S. Marques, J. Phys. D.: Appl. Phys., 2022, 55, 055306.
- A. C. L. Moreira, R. P. Dias, J. C. S. Da Silva, Comp. Theo. Chem., 2023, 1221, 114033.

ACKNOWLEDGMENTS

CNPq, FAPEAL, FACEPE and CAPES.



valiação de propriedades óticas não-lineares em nanoclusters de ouro e influência dos efeitos de simetria

Mário Gutfilen Grünbaum (IC),² Thiago Messias Cardozo (PQ).^{1*}

mggrunbaum@eq.ufrj.br; thiago@iq.ufrj.br

¹Laboratório de Físico-Química teórica IQ/UFRJ

Palavras Chave: Ótica não-linear, Simetria, Hiperpolarizabilidade, Ouro, Prata

INTRODUÇÃO

As propriedades óticas não-lineares consistem da capacidade de alguns materiais de modificarem propriedades de luz incidente, como a sua frequência ou sua fase. Materiais com essas propriedades apresentam um número grande de propriedades de interesse com potenciais aplicações, como a geração de segundo harmônico, retificação ótica e absorção multi-fotônica. Essas propriedades são dependentes das hiperpolarizabilidades dos constituintes dos materiais.

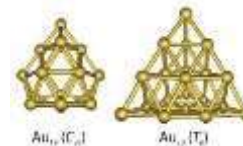
Nanoclusters de ouro e prata têm sido explorados como potenciais materiais para este fim [2][3][4][7] devido aos seus altos valores do tensor hiperpolarizabilidade, e uma série de aglomerados de ouro de alta simetria foi divulgada por Pykkö *et al.* Ainda, Zyss *et al.* [5] já avaliou o comportamento da primeira hiperpolarizabilidade (tensor β) com os grupos de ponto mais usuais, porém os maiores aglomerados de ouro da série são raros casos de simetria icosaédrica.

O presente trabalho tem como objetivo avaliar o tensor β de aglomerados de ouro da série apresentada por Pykkö *et al.* e determinar como a eliminação gradual de elementos de simetria por meio da substituição de átomos de prata afeta essa propriedade.

MÉTODOS

Os cálculos foram conduzidos com o método DFT usando o funcional PBE e a base com pseudopotenciais iMCP. Os cálculos executados até o momento foram conduzidos no estado singlet. As geometrias do Au₁₈ (C_{2v}) e Au₂₀ (T_d) foram otimizadas a partir das estruturas divulgadas por Pykkö *et al* [1]. Um *script* foi desenvolvido para a determinação do conjunto de átomos simetricamente únicos de cada um dos subgrupos próprios dos grupos de ponto dos aglomerados. Foram feitas substituições sistemáticas de átomos simetricamente únicos por átomos de prata, de modo a verificar o comportamento do tensor β , calculado com o método CPDFT. Os tensores calculados para os aglomerados modificados foram reorientados de modo que todos estivessem expressos no mesmo conjunto de coordenadas do aglomerado original. Estimou-se então o EFISH

(Electric Field Induced Second Harmonic Generation), uma propriedade ótica não-linear observável que pode ser aproximadamente dada por $I_{2w} \approx \sum_i \sum_j \mu_i \beta_{ijj}$, a fim de estimar a atividade ótica não-linear.



RESULTADOS

A molécula com total substituição de átomos de ouro por átomos de prata apresenta valores maiores nos componentes octopolares da primeira hiperpolarizabilidade, bem como do EFISH. O Au₁₈ tem EFISH 0.2 Debye*esu*10⁻³⁰ e o Ag₁₈ apresenta EFISH 0.7 nas mesmas unidades.

Observaram-se valores significativamente maiores de EFISH em aglomerados parcialmente substituídos por átomos de prata, com valores comparáveis a moléculas de referência [6]. Alguns exemplos dos valores obtidos para estruturas mistas apresentaram EFISH 22.7 (C₂), 65.2 (C_s), 77.5 (C_{2v}) e 82.0 (C_{2v}).

CONCLUSÕES

Foram identificadas posições de interesse para substituições, e observou-se que é possível obter modificações significativas nas propriedades dos aglomerados com substituições que modificam a simetria do sistema.

REFERÊNCIAS

1. A. J. Karttunen, M. Linnolahti, T. A. Pakkanen, P. Pyykkö, Chem. Commun., 2008, 465-467
2. L. François, M. Mostafavi, J. Belloni, J. A. Delaire, PCCP, 2001, 3, 4965-4971
3. R. L. M. Giesecking, Chem. Mater., 2019, 31, 17, 6850-6859
4. R. Antoine, Frontier Research Today, 2018, vol 1, article No 01001
5. J. Zyss, I. Ledoux, Chem. Rev., 1994, 94, 77-105
6. T. M. Cardozo, M. A. C. Nascimento, THEOCHEM, 2007, 811, issues 1-3, 337-343
7. S. Lakhera, M. Rana, K. Devlal, Optical and Quantum Electronics, 2023, 55, article 178

AGRADECIMENTOS

FAPERJ pelo financiamento da Bolsa de IC e Projeto Redes de Pesquisa em Nanotecnologia. O ex-administrador Rodrigo de Oliveira prestou auxílio técnico durante toda a execução do trabalho.

Predicting Os-187 NMR chemical shift using the NMR-DKH basis sets

Carolina M. Santos (IC)^{1*}, Diego F. S. Paschoal (PQ)¹

carolinamanhaessantos@gmail.com; diegopaschoal01@gmail.com

¹Núcleo de Química Teórica e Computacional de Macaé, Polo Ajuda, Instituto Multidisciplinar de Química, Centro Multidisciplinar UFRJ-Macaé, Universidade Federal do Rio de Janeiro, Macaé, RJ, Brazil.

Keywords: Osmium, NMR, Os-187, NMR-DKH basis sets, Computational Protocol.

INTRODUCTION

Osmium (Os) complexes have attracted interest in areas such as metal-based anticancer drug development, homogenous catalysis, bioelectrocatalysis and photophysics^{1,2}. On the other hand, NMR spectroscopy is a very powerful tool for structural characterization and has also been used in the designing of new drugs and studying reaction mechanisms³. The present study aims to develop a new NMR-DKH basis set for Os atom and a computational protocol for predicting the Os-187 NMR chemical shift ($\delta^{187}\text{Os}$) in Os(II) complexes.

METHODS

Initially, the NMR-DKH basis set for Os atom was developed using the same methodology of Paschoal et al.³. Subsequently, a set of 37 Os(II) complexes with experimental data for $\delta^{187}\text{Os}$ found in the literature were selected.

The role of the structure in predicting the $\delta^{187}\text{Os}$ was evaluated with calculations performed at GIAO-PBE / NMR-DKH /IEF-PCM(UFF) // B3LYP / OSBS / def2-SVP / IEF-PCM(UFF), where OSBS = LANL2DZ or LANL2TZ(f). After defining the osmium basis set (OSBS) to be used in obtaining the structures, the role of the DFT functional in the description of $\delta^{187}\text{Os}$ was evaluated, considering the following functionals: PBE, OPBE, BP86, BLYP, TPSS, PBE0, B3LYP, TPSSh, LC-BLYP, LC- ω PBE, and CAM-B3LYP.

The eq. (01) was used for calculating the $\delta^{187}\text{Os}$, which was obtained from a linear regression model between calculated $\sigma^{187}\text{Os}$ and experimental $\delta^{187}\text{Os}$ for the set of 37 Os(II) complexes studied, with each computational protocol. The calculations were performed in GAUSSIAN 16 Rev. C.01 program. Eq. (01): $\delta^{187}\text{Os} = a \times \sigma^{187}\text{Os} + b$, with "a" and "b" being the angular and linear coefficient, respectively, obtained from linear regression.

RESULTS

From the calculated results with geometries obtained with ECP LANL2DZ and LANL2TZ(f) for Os, a mean relative deviation (MRD) of 4.52% and 4.37% was found, respectively, showing that the B3LYP/LANL2TZ(f)/def2-SVP/IEF-PCM(UFF) is the best choice for obtaining the structures of Os(II) complexes.

When the distinct DFT-functionals were considered in predicting the $\delta^{187}\text{Os}$, the results obtained with GIAO-OPBE/NMR-DKH/IEF-PCM(UFF) protocol presented the best description, with a MRD of 4.30% and a mean absolute deviation (MAD) of 114 ppm. In addition, the model proved to be statistically relevant, with a coefficient of determination (R^2) of 0.9686 (Figure 1). Figure 2 shows that the protocol was able to adequately describe the trends in experimental values.

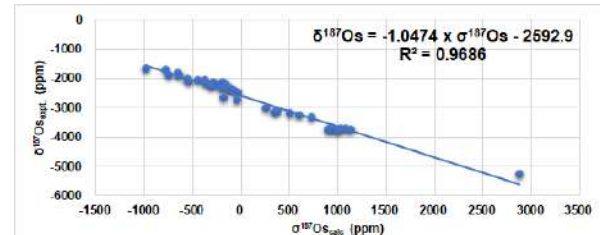


Figure 1. Linear regression model between $\sigma^{187}\text{Os}_{\text{calc}}$ x $\delta^{187}\text{Os}_{\text{expt}}$ with GIAO-OPBE/NMR-DKH/IEF-PCM(UFF) protocol.

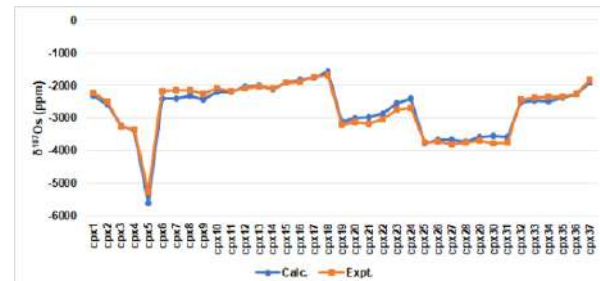


Figure 2. Calculated $\delta^{187}\text{Os}$ with GIAO-OPBE/NMR-DKH/IEF-PCM(UFF) protocol.

CONCLUSIONS

The calculated results showed that the NMR-DKH basis sets, with GIAO-OPBE/NMR-DKH/IEF-PCM(UFF) // B3LYP/LANL2TZ(f)/def2-SVP/IEF-PCM(UFF) protocol, is an excellent alternative for predicting the $\delta^{187}\text{Os}$ in Os(II) complexes. Besides, the protocol was able to describe the trends in experimental values.

REFERENCES

1. R. Cerón-Camacho et al., Molecules, 2021, 26, 1563
2. M. Hanif, M. V. Babak, C. G. Hartinger. Drug Discovery Today, 2014, 19, 1640–1648.
3. D. Paschoal et al., J. Comput. Chem., 2016, 37, 2360–2373.

ACKNOWLEDGMENTS

The authors would like to thank the Brazilian agency FAPERJ (E-26/201.336/2022 – BOLSA and E-26/210.070/2022) and PIBIC-CNPq for the financial support.

A Theoretical Investigation into the Mechanisms of Electrocatalytic CO₂ Reduction Using an Exceptionally Efficient Mn-based Homogeneous System

Murugesan Panneerselvam (PQ)¹, Marcelo Albuquerque (PQ)², Luciano T Costa (PQ)^{1*}

panneerchem130491@gmail.com; ltcosta@id.uff.br

¹Institute of Chemistry - Department of Physical Chemistry, Universidade Federal Fluminense (UFF), Niterói – RJ, Brazil;

²Institute of Physics Universidade Federal Fluminense (UFF), Niterói – RJ, Brazil.

Keywords: CO₂ reduction, Electrocatalysts, Value-added products, Mn-based Polypyridyl and DFT Study

INTRODUCTION

The conversion of CO₂ into sustainable solar fuels and chemicals offers a promising solution to the energy and environmental challenges we face today. This project focuses on developing new molecular electrocatalysts for CO₂ reduction and hydrogen production using computational tools. Given the current energy crisis, there is a growing interest in the development of efficient and cost-effective molecular electrocatalysts. This proposed theoretical study aims to provide new and innovative designs of molecular electrocatalysts that offer improved efficiency and performance, requiring only a small budget and a short timeframe. Through quantum chemical modeling, we can develop innovative design strategies and provide theoretical explanations for experimental studies in this field.

METHODS

We are aiming to study the structure and bonding aspects of diimine complexes. In this purpose, we performed the detailed DFT calculations on diamine ligand based Mn complexes [Mn(pyrox)(CO)₃Br] using ORCA and Gaussian software packages. The structural optimization and investigation of various metal-ligand catalysts will be carried out by using the scalar relativistic DFT method. This method can calculate essential quantities such as redox potential and pK_a values of catalysts and catalytic intermediates. From the thermodynamic aspects, DFT calculations provide an efficient way to calculate the electronic energetics of molecular systems by the polarizable continuum model (SCRF-PCM). M06/LANL2DZ/6-31G(d) level of theory will also be used to reveal the electronic structure of reactive species involved in the reaction profiles.

RESULTS

To calculate the thermodynamic and kinetic aspects of photo- and electrocatalytic processes involving imine based Mn-complexes. By understanding the system, we have determined its exclusive selectivity for CO generation and achieve high turnover numbers, which are among the highest reported for fully earth-abundant photocatalytic systems. Redox properties and reactivity can be regarded as two sides of a coin, as a slight perturbation in the redox & pKa values

can influence the reactivity as well as in the geometrical parameters as we observed in the diimine based Manganese complexes.

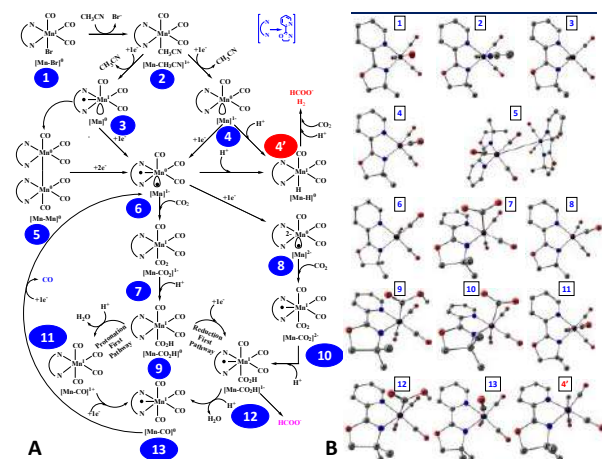


Figure 1. Scheme of the reaction mechanism for CO₂ reduction involving protonation & reduction steps (A) and all the optimized geometries at M06/LANL2DZ/6-31G(d) (B).

CONCLUSIONS

Our research involves the development of a distinctive computational protocol that allows us to calculate the energy landscape and spectroscopic parameters for the electrochemical aspect of our investigations. By analyzing the computed reaction profile (PES), we can assess how different factors, such as steric and electrostatic interactions, impact the kinetics of the reaction. In summary, our primary objective is to contribute to the reduction of the greenhouse effect by enhancing the electrochemical conversion of CO₂ into fuel and improving the production of C1 building blocks.

REFERENCES

- ¹Takeda, H.; Cometto, C.; Ishitani, O.; Robert, M. ACS Catal. 2017, 7, 70–88.
²C. Steinelechner, A. F. Roesel, E. Oberem, A. Päpcke, N. Rockstroh, F. Gloaguen, S. Lochbrunner, R. Ludwig, A. Spannenberg, H. Junge, R. Francke, M. Beller, ACS Catal. 2019, 9, 2091–2100.

ACKNOWLEDGMENTS

Authors acknowledge the financial support from FAPERJ (204.539/2021 – SEI-260003/014963/2021), APQ-1, CAPES/PRINT 1038152P and 88881.465529/2019-01 and also thanks for the Computing Resources from Feynman, DIRAC and CENAPAD Server.



Estudo estrutural e eletrônico do politiofeno e derivados via DFT

Rafael H. Rosário (PG),¹ Ricardo R. Oliveira (PQ),¹ Alexandre B. Rocha (PQ).¹

rafsario@pos.iq.ufrj.br

¹Instituto de Química, Departamento de Físico-Química, Universidade Federal do Rio de Janeiro.

Palavras Chave: Politiofeno, Célula Solar Orgânica, energia renovável.

INTRODUÇÃO

A crescente demanda global por energia gera diversos desafios para o setor. Nesse cenário, as células solares desempenham papel crucial para a mudança na matriz energética atual.¹ Em particular, as células solares orgânicas (CSO), que empregam polímeros como o politiofeno, apresentam algumas vantagens em relação às inorgânicas, por exemplo, leveza, baixo custo e flexibilidade.²

MÉTODOS

Um estudo inicial sobre o tamanho da cadeia, a geometria e primeira energia de transição eletrônica do politiofeno foi conduzido a fim de utilizar esse polímero como ponto de partida para o estudo de CSO. O tamanho dos oligômeros foram de 2, 4, 8, 10 e 12 unidades de tiofeno. Os cálculos de otimização de geometria utilizaram a teoria do funcional da densidade (DFT) com os funcionais B3LYP e wB97X-D. A base utilizada foi a 6-31G(d,p) com correção de dispersão de Grimme D2. Para as transições eletrônicas, 20 estados foram determinados a partir da teoria do funcional da densidade dependente do tempo (TD-DFT) com o funcional CAM-B3LYP e a mesma base. Todos os cálculos foram feitos com o software GAUSSIAN 2009.

RESULTADOS

As geometrias otimizadas dos oligômeros com 2, 4 e 8 unidades foram semelhantes. Para 10 e 12 unidades, o funcional wB97X-D produziu estruturas com torções que fugiram da linearidade esperada para a cadeia (Figura 1).

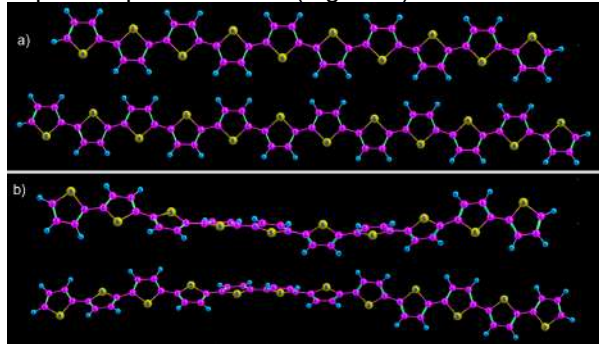


Figura 1. Geometria otimizada para o oligômero de politiofeno com 10 e 12 unidades nos funcionais a) B3LYP e b) wB97X-D, ambos na base 6-31G(d,p).

A TD-DFT forneceu os dados expostos na Tabela 1. A energia para a primeira transição diminui

com o aumento da cadeia, enquanto a força do oscilador aumentou.

Tabela 1. Resultados para oligômeros de tiofeno a nível TD-DFT/CAM-B3LYP/6-31G(d,p).

Politiofeno	Energia para a primeira transição (eV)	Força do Oscilador	Orbital (maior contribuição)
T2	4,3224	0,4148	43 → 44
T4	3,2203	1,2196	85 → 86
T8	2,6085	2,9276	169 → 170
T10	2,503	3,7859	211 → 212
T12	2,4558	4,637	253 → 254
Energia de Transição ²		Experimental	2,3 eV
		Teórico para T8 B3LYP 6-31G(d)	2,48 eV

Percebe-se que os valores encontrados para a primeira energia de transição são condizentes com o valor experimental. O mesmo ocorre para o valor teórico em condições semelhantes.

A partir da geometria otimizada por B3LYP, os funcionais em estudo foram também comparados na TD-DFT. Avaliando-se apenas os extremos, a Tabela 2 não revela diferenças significativas.

Tabela 2. Comparação entre os funcionais CAM-B3LYP e wB97X-D na TD-DFT para os oligômeros T2 e T12.

Politiofeno	Energia para a primeira transição (eV)		Força do Oscilador	
	CAM-B3LYP	wB97X-D	CAM-B3LYP	wB97X-D
T2	4,3224	4,3396	0,4148	0,4184
T12	2,4558	2,5382	4,637	4,6965

CONCLUSÕES

O funcional wB97X-D produziu geometrias que fugiram da linearidade esperada para o politiofeno, e, na TD-DFT, não foram observadas diferenças significativas ao compará-lo com CAM-B3LYP. Pela primeira energia de transição, o oligômero T12 se aproximou mais do valor experimental. Diante do exposto, os estudos prosseguirão com oligômeros de 12 unidades de tiofeno no funcional B3LYP-D2/6-31G(d,p).

REFERÊNCIAS

¹ L. Rinaldi, M. V. Rocco, E. Colombo, Resources, Conservation and Recycling, 2023, v. 191, p. 106900.

² S. Garg, N. Goel, The Journal of Physical Chemistry C, 2022, v. 126, p. 9313-9323.

AGRADECIMENTOS

CNPq, a CAPES e a FAPERJ. Agradecemos também ao LNCC por fornecer recursos computacionais via supercomputador SDumont.

Conjugate vs direct nucleophilic addition on α,β -unsaturated carbonyl compounds

Lilah F. Freire (IC), Rodolfo G. Fiorot (PQ).

lilahfreire@id.uff.br

Universidade Federal Fluminense, Instituto de Química, Niterói, Rio de Janeiro, Brasil

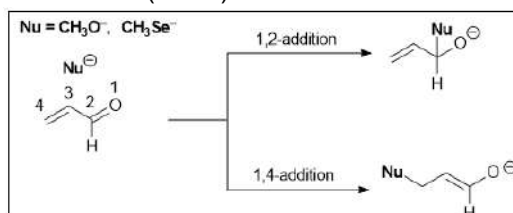
Keywords: Chemical Reactivity, Chemoselectivity, DFT, Reaction Mechanism.

INTRODUCTION

α,β -unsaturated carbonyl compounds react with nucleophiles via conjugate (1,4) or direct (1,2) addition. Under specific conditions, the preference for which attack site is favored depends on some factors. Classical textbooks state that conjugate addition to α,β -unsaturated carbonyls compounds is privileged by “soft” nucleophiles (lower electron density, more spontaneous, and controlled by orbital overlap), which produces the thermodynamic product (more stable). Conversely, “hard” nucleophiles (small, electronegative, low polarizable) favor direct addition, yielding kinetic products, facilitated by electrostatic attraction for faster formation.^{1,2} However, literature does not provide a suitable quantification of how these factors actually determine which site will undergo attack. Studying these reactions not only helps predict outcomes but also aids synthetic transformation, including polymers³. Therefore, this work examines reaction coordinates for conjugate and direct nucleophilic additions, employing computational tools.

METHODS

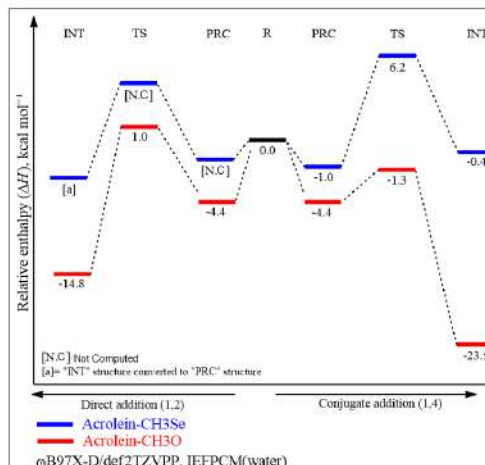
The conjugate (1,4) and direct (1,2) nucleophilic addition reaction between acrolein (the most simple α,β -unsaturated carbonyl compound) and organochalcogen CH_3X^- ($\text{X} = \text{O}, \text{Se}$) were assessed to investigate how the different nucleophiles with distinct polarizability (thus, hardness or softness) affects the energy profile and the thermodynamic/kinetic control (Scheme 1). The energy parameters change was computed by performing geometry optimization and frequency calculations at DFT level ($\omega\text{B97X-D}/\text{def2-TZVPP}$) with the Gaussian 09. All calculations were performed considering the implicit solvent (water) with IEFPCM.



Scheme 1: Reaction with acrolein and nucleophiles to quantify kinetic and thermodynamic effects on the mechanism.

RESULTS AND DISCUSSION

Scheme 2 shows that CH_3O^- is more reactive and produces more stable products by reacting with acrolein than CH_3Se^- regardless of the reaction pathway. Comparing the reactive sites of acrolein, conjugate addition with CH_3O^- forms the most stable product, as expected. In contrast with classical textbooks, this reaction should also be faster (kinetic control). For CH_3Se^- as a nucleophile, only the intermediate formed by the conjugate addition (1,4) could be optimized. The optimization of the intermediate from the direct (1,2) addition converged to its reactants. It suggests that soft and bigger nucleophiles, such as CH_3Se^- are not able to form a stable bond with the carbonyl, converting it into the tetrahedral intermediate.



Scheme 2: Relative enthalpy (ΔH) changes along the reaction coordinate during the interaction between acrolein and CH_3X^- ($\text{X} = \text{O}, \text{Se}$).

CONCLUSIONS

The nucleophilic addition reaction can occur in two sites: conjugate or direct. Although oxygen is a “hard” nucleophile, the conjugate addition has a lower activation barrier. This study will incorporate in the future sulfur molecules and consider gas-phase interactions to enhance understanding, as well as utilize energy decomposition analysis to quantify the effects that control reactivity.

REFERENCES

- [1] J. Am. Chem. Soc. (1963). 85, 22, 3533–3539
- [2] Clayden, J., Greeves, N., & Warren, S. (2012). Organic Chemistry (2nd ed.). Oxford University Press
- [3] Chem. Rev. (2021). 121, 12, 6744–6776

ACKNOWLEDGMENTS

CAPES, CNPq, FAPERJ.



Predicting Glycosyl Hydrolase Interactions and Components using Advanced Machine Learning Techniques

Alberto M. dos Santos (PQ),^{1*} Munir Skaf (PQ)¹

*albertos@unicamp.br

¹CCES, Department of Chemistry, State University of Campinas, Campinas, SP, Brazil

Palavras Chave: Machine Learning, Enzymatic Mechanism, QM/MM, Semantic Segmentation

INTRODUCTION

The precise assessment of electrostatic energy contributions and the ability to forecast enzymatic components accurately are of the utmost importance in comprehending molecular interactions, elucidating reaction mechanisms, and pressing the field of enzyme engineering forward. The use of Quantum Mechanics/Molecular Mechanics (QM/MM) provides significant and crucial insights into the understanding of these interactions. However, the computing expenses associated with QM/MM provide obstacles when conducting extensive investigations. Here, we integrated QM/MM with machine learning and, in conjunction with computer vision methodologies like semantic segmentation, explored a novel approach to address these difficulties.

METHODS

In this study, a dataset consisting of 40 structures was employed to estimate electrostatic energy. These structures mainly correspond to the first reaction step of Glycosyl Hydrolase 6. The electrostatic energy contribution associated with each structure was determined using quantum mechanics/molecular mechanics (QM/MM) hybrid approaches. The data underwent training, validation, and testing procedures within a neural network model that was constructed using the TensorFlow framework. Additionally, the prediction of components was facilitated through the utilisation of semantic segmentation techniques, with a specific emphasis on the RandLANet and PointNet designs. The methodology employed point cloud data, wherein the initial framework focused on semantic segmentation, while the subsequent framework directly processed the data. The training process was conducted on a local GPU using Python3 with the utilisation of Open3D, TensorFlow, and ML3D libraries.

RESULTS

The accuracy rate of the neural network model in predicting electrostatic contributions was found to be 85%. Concurrently, the use of the semantic segmentation methodology, based on a comparable dataset obtained from QM/MM

simulations, yielded a remarkable accuracy rate of 95.1% in predicting enzyme components. Nevertheless, our approach encountered difficulties in accurately forecasting negative residues (7.7%), aromatic residues (92.9%), and extremities (0%).

CONCLUSION

The field of machine learning exhibits considerable potential in its ability to accurately estimate electrostatic contributions using quantum mechanics/molecular mechanics (QM/MM) computations, as well as forecast the components of enzyme systems. Although the current findings show promise, there are still areas that require further enhancement, particularly in regard to the challenges associated with predicting specific residues. We aim to enhance accuracy by integrating the training methodologies employed in both investigations into a unified convolutional neural network. These developments not only facilitate the advancement of academic knowledge but also create opportunities for practical implementation, particularly in the fields of enzyme engineering and industrial biotechnology. Subsequent research efforts will focus on developing algorithms with the ability to forecast crucial enzymatic attributes, hence facilitating the enhancement and optimization of enzymatic systems.

REFERENCES

1. Hu, Q. et al (2020). RandLA-Net: Efficient Semantic Segmentation of Large-Scale Point Clouds.
2. Qi, C. et al (2017). PointNet: Deep Learning on Point Sets for 3D Classification and Segmentation. The Computer Vision Foundation.
3. Roshan, V. et al (2022). Optimal ratio for data splitting. Statistical Analysis and Data Mining: The ASA Data Science Journal, 15(4), 531–538.

ACKNOWLEDGMENT

This work was supported by the São Paulo Research Foundation (FAPESP, Brazil) (grant numbers 2022/04695-2, 2013/08293-7).

Molecular dynamics simulations of organic-aqueous interfaces under influence of organophosphorus extractants

Alexandre M. Pereira (PG),^{1,2*} Letícia M. Prates (PQ),¹ Lucas A. Silva (PG),^{1,3} Julio C. G. Correia (PQ),¹ Alexandre N. M. Carauta (PQ),⁴ Marcelo B. Mansur (PQ),³ Luciano T. Costa (PQ)²

monipereira.alexandre@gmail.com

¹Laboratório de Modelagem Molecular, Centro de Tecnologia Mineral; ²MolMod-CS – Instituto de Química, Universidade Federal Fluminense; ³PEMM/COPPE, Universidade Federal do Rio de Janeiro; ⁴FTESM – Fundação Técnico-Educacional Souza Marques;

Keywords: Solvent Extraction; Molecular Dynamics (MD); Liquid-Liquid Interface; Critical Micelle Concentration (CMC).

INTRODUCTION

Organophosphorus extractants play an important role in the extraction, recovery, and purification of strategic metals. Interfacial properties govern the mechanism and kinetics of the processes. Molecular modeling allows to characterize interfaces using different metrics. Thus, we applied MD (molecular dynamics) to study interfacial properties of the water/dodecane interface when D2EHPA (di-2-ethylhexyl phosphoric acid) and two isomers DOP and DTTP (Fig. 1) fill the interface.

METHODS

Gromacs 2023.1 was used to simulate the systems as shown in Fig. 1. The molecular topologies were obtained from ATB under GROMOS forcefield for the organics and SPC/E for water. 60 ns of NVT simulation was performed to generate enough sampling data to evaluate density, interfacial tension (IFT), and other interfacial properties.

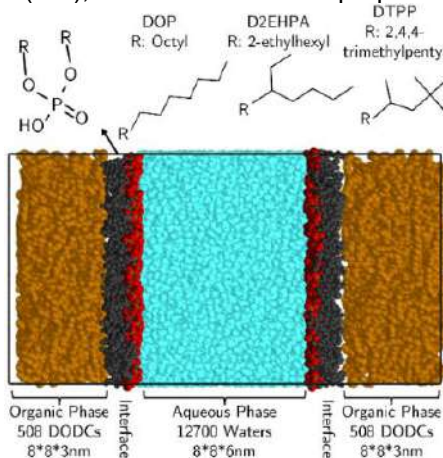


Figure 1. Simulation system and structure of the extractants.

RESULTS

Through Gromacs analysis, we have obtained density profiles along the Z direction for each studied concentration. Thus, we could compute the extractant concentration in the interface using the P density peaks. DOP and DTTP reach higher equilibrium concentrations when compared with D2EHPA (Fig. 2). The packing of D2EHPA is less effective, even with the most branched carbon chain of DTTP. The CMC obtained by MD for DOP,

DTTP, and D2EHPA were 86.14, 91.57, and 95.4 Å², respectively; for D2EHPA, the reported CMC is 94.7 Å² in n-hexane and 113.6 Å² in kerosene¹. Fig. 3 shows the obtained IFT values, and they match the literature data, D2EHPA stands out with the most different values, reiterating the relation between the packing at the surface with the IFT.²

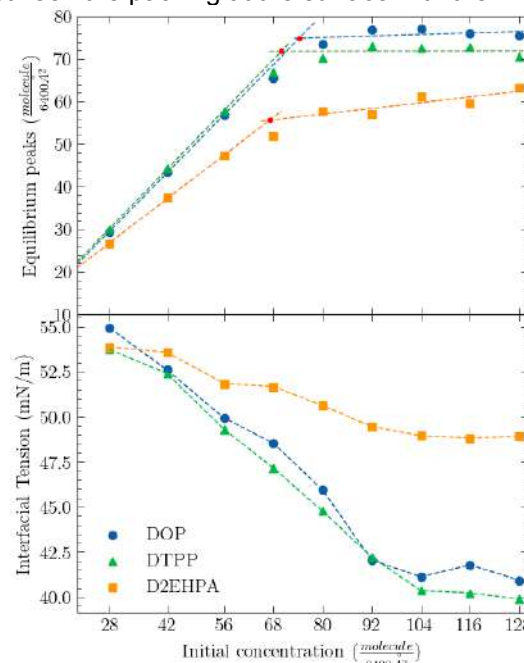


Figure 2. Peak P density and IFT x extractant concentration.

For solvent extraction (SX), an intermediate IFT promotes both the partitioning of metals between the phases and the phase separation. This is why D2EHPA is widely applied.

CONCLUSIONS

The relationship between CMC and IFT could be reinforced through the properties computed. For SX, an intermediate IFT is ideal, and to reach these values a branched but not rigid carbon chain is desirable.

REFERENCES

- ¹R. K. Biswas et al, Hydrometallurgy, 2003, 69. 157.
²Z. Y. Liu et al, J. Mol. Model., 2017, 23. 112.

ACKNOWLEDGMENTS

The authors thank CNPq, MCTI, CETEM and CAPES.

Molecular modeling investigation of Impact of Tyrosine Y73 mutation in Thermobifida fusca Endoglucanase Cel6A on substrate ring distortion.

Shabir, Ahmad (PhD)¹; Munir, Skaf (R)^{1*}

Categories: PhD Student

shabirjan427@gmail.com; skaf@unicamp.com

¹Authors' affiliation(s) (Institute of Chemistry; University of Campinas, 13083-970, Campinas, São Paulo, Brasil)

Keywords: (GH6, endoglucanases, *Thermobifida fusca*, Molecular Dynamics)

INTRODUCTION

Glycoside hydrolase Family 6 (GH6) cellulases are enzymes of paramount importance in the context of biomass degradation. Their role within natural enzyme mixtures is pivotal, as they are the primary agents responsible for breaking down cellulose, a complex and resilient component of plant cell walls. GH6 cellulases function through a mechanism known as "inverting," a process that involves cleaving cellulose molecules from their non-reducing ends, ultimately facilitating their conversion into simpler sugars.

METHODS

In this comprehensive study, we undertake an exploration of the cellulose-degrading capabilities of endoglucanase Cel6A derived from *Thermobifida fusca*. Our investigation predominantly focuses on the catalytic domain of this enzyme, employing molecular dynamics simulations. We chose the crystallographic structure of the Wild and mutant type PDB from the protein databank. The system was prepared using CHARMM36m forcefield and GPU version of AMBER20 software

RESULTS

By employing molecular dynamics simulation, each of 600ns using a Wild and Mutant type system in the presence of a Cellooctaoose substrate, we uncovered distinctive molecular interactions. We observed distorted ring conformation in the presence of the Tyr73 in the -1 subsite region of the protein while in the mutant type system the ring adopt chair conformation, further enhancing our grasp of cellulose degradation mechanisms. Notably, the amino acid Tyr73 was recognized as a trigger for subsite -1 distortion, mitigated by a Tyr73-to-serine mutation.

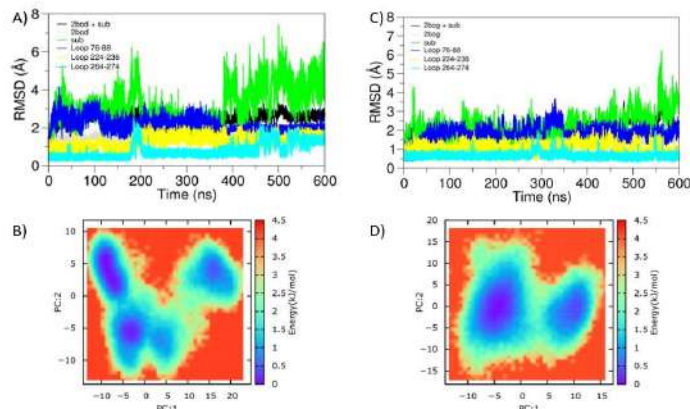


Figure 1: Root Mean Square Deviation (RMSD) and Principal Component Analysis (PCA) of the Wild type (A,B) and mutant type (C,D) glycosidic hydrolase family 6 (GH6) of the *Thermobifida fusca*.

CONCLUSIONS

Crucially, these findings bear pertinent consequences for fine-tuning enzymes via bioengineering, propelling the evolution of strategies for more efficacious biomass utilization.

REFERENCES

- ¹ Larsson, A.M., et al., 2005. Crystal structure of *Thermobifida fusca* endoglucanase Cel6A in complex with substrate and inhibitor: the role of tyrosine Y73 in substrate ring distortion. *Biochemistry*, 44(39), pp.12915-12922.
- ² Case, D.A., Aktulga, H.M., Belfon, K., Ben-Shalom, I., Brozell, S.R., Cerutti, D.S., Cheatham III, T.E., Cruzeiro, V.W.D., Darden, T.A., Duke, R.E. and Giambasu, G., 2021. Amber 2021. University of California, San Francisco.
- ³ Jo, S., Kim, T., Iyer, V.G. and Im, W., 2008. CHARMM-GUI: a web-based graphical user interface for CHARMM. *Journal of computational chemistry*, 29(11), pp.1859-1865.

ACKNOWLEDGMENTS

The authors sincerely acknowledge FAPESP for financial support.

Molecular Dynamics Simulations of Amine-Starch Clathrate formation

Lucas A. Silva (PG),¹ Alexandre M. Pereira (PG),¹ Leonardo C. Bastos (PQ),^{1,3} Julio C. G. Correia (PQ),¹ Elayne R. Peçanha (PG),² Marisa B. M. Monte (PQ)^{3*}
lbastos@cetem.gov.br; mmonte@cetem.gov.br

¹Laboratório de Modelagem Molecular, Centro de Tecnologia Mineral, RJ, Brazil; ²Departamento de Físico-Química, UNICAMP, SP, Brazil; ³Laboratório de Química de Superfície, Centro de Tecnologia Mineral, RJ, Brazil.

Keywords: Clathrates; Non-Covalent Complexes; Amines; Polysaccharides; Molecular Dynamics.

INTRODUCTION

Surfactant-polymer clathrates are intriguing molecular assemblies resulting from the intricate balance between hydrophobic and hydrophilic forces. These complexes garnered significant attention due to their potential applications in diverse fields, from drug delivery and materials science to environmental remediation. However, in the context of mineral froth flotation, these clathrates can be detrimental. Their formation and deposition on mineral surfaces can adversely affect flotation¹ efficiency by altering hydrophobic interactions, bubble attachment, and froth stability. In this work we study the formation of etheramine-starch clathrate formation.

METHODS

Molecular Dynamics Simulations were performed using GROMACS. CHARMM36 and CgenFF force fields were used alongside TIP3P water. The etheramine 3-decoxypropan-1-amine ($C_{13}H_{29}NO$) and an amylose chain of 18 glucose units were simulated in bulk solution systems and gas-liquid interfacial systems. Simulations were run for $\sim 0.5 \mu s$ to allow extensive sampling of the configurational space. Structural analyses such as solvent accessible surface area (SASA) were used to characterize the clathrate formation.

RESULTS

The bulk solution simulations showed the spontaneous formation of the clathrates from the initially separated amine and amylose molecules within few nanoseconds. They persisted complexed throughout the long simulations in a dynamic equilibrium, in which they were rapidly recomplexed after any decomplexation events that occurred. Figure 1 shows this by the analysis of the SASA of the solutes. When unbound, the total SASA value is higher, because of the inclusion of the etheramine inside the amylose helix. The etheramine surfactant was coiled by the polymer, forming a helical structure, with the amine located in the center of the helix, in the internal hydrophobic region of the amylose chain as seen in Fig. 1. The interfacial simulations showed that the amine prefers to adsorb at the gas-liquid interface while the amylose chain stays in the solution region (Fig. 2). That is in line with

the interfacial activity of both molecules in solution as probed by surface tension measurements.

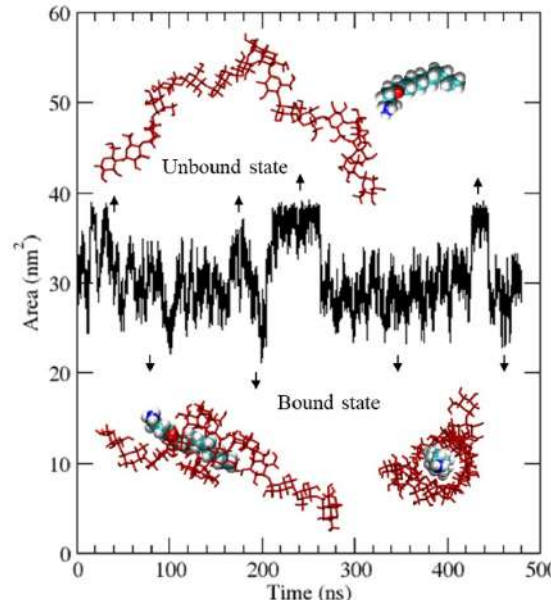


Figure 1. Total solute SASA x time and the molecular structures of amylose, etheramine, and their clathrates.

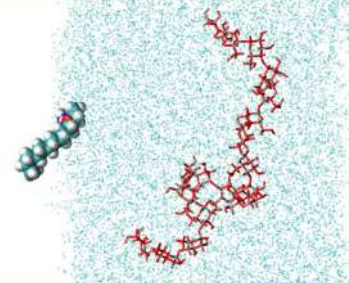


Figure 2. Equilibrium configuration snapshot of the gas-liquid interfacial system.

CONCLUSIONS

Long molecular dynamics simulations revealed the behavior of clathrate formation in bulk solution while not present in gas-liquid interfacial systems. This indicates that one must guarantee that there is not enough starch and/or amine together in solution so that they can reach the interfaces where they are supposed to adsorb in flotation processes.

REFERENCES

- ¹ M. Albuquerque et al., Miner. Eng.. 2021, 170, 106988.

ACKNOWLEDGMENTS

The authors thank CETEM, MCTI, CNPq, CAPES.



Predicting the ^1H , ^{13}C , and ^{15}N NMR chemical shift in Pd(II) complexes and application in studying drug delivery system with cyclodextrin

Catherine R. S. de Souza (UR)^{1*}, Willian T. G. Novato (R)¹, Diego F. S. Paschoal (R)¹

catherinesiqueira1@hotmail.com; diegopaschoal01@gmail.com

¹Núcleo de Química Teórica e Computacional de Macaé, Polo Ajuda, Instituto Multidisciplinar de Química, Centro Multidisciplinar UFRJ-Macaé, Universidade Federal do Rio de Janeiro, Macaé, RJ, Brazil.

Keywords: Cancer, Pd(II) complexes, NMR, chemical shift, cyclodextrin.

INTRODUCTION

Pd(II) complexes are a promising alternative for the development of new antitumor drugs.¹ Aiming to improve antitumor treatments, cyclodextrins have shown great application. Therefore, computational chemistry is an advantageous tool to obtain information about the formation of the inclusion system through nuclear magnetic resonance (NMR).² In the present study, computational protocols for predicting the ^1H , ^{13}C , and ^{15}N NMR chemical shift (δ) were developed and applied in the characterization study of the inclusion complexes between palladium complexes and β -cyclodextrin.

METHODS

Initially, a new NMR-DKH basis set for Pd atom was developed. The Pd(II) complex *trans*-[Pd(py)₂Cl₂], *trans*-[Pd(isoquin)₂Cl₂], and [Pd(bquin)Cl₂], that present experimental data for $\delta^1\text{H}$, $\delta^{13}\text{C}$, and $\delta^{15}\text{N}$ available in the literature were selected. The role of the structure, DFT functional, palladium basis set (PDBS), and ligands basis sets (LBS) in predicting the chemical shifts were assessed. First, the structures were optimized at DFT-functional/def2-SVP/def2-SVP/C-PCM level, considering 17 different functionals, and the chemical shifts were calculated at GIAO-PBE0/Paschoal-DZP/pcSseg-2/C-PCM level. After defining the computational protocol for the description of the structures, computational protocols at GIAO-Functional-DFT/PDBS/LBS/C-PCM were considered. Finally, in order to validate the obtained computational protocol (NMR//geometry), new Pd(II) complexes were studied. Then, the best protocol is being applied in the study of inclusion complexes with β -cyclodextrin. The calculations were performed using the ORCA 5 program.

RESULTS

For the description of the structural parameters, considering that all protocols presented an excellent description of the geometries, the $\delta^{15}\text{N}$, which is very sensitive to the considered structure, was used as reference for defining the best protocol. So, the structure BLYP/def2-SVP/C-

PCM, that presented a relative deviation (RD) of only 0.48% for the $\delta^{15}\text{N}$, was selected.

Furthermore, the role of the DFT functional, PDBS, and LBS in predicting the $\delta^1\text{H}$, $\delta^{13}\text{C}$, and $\delta^{15}\text{N}$ was assessed. The results showed that the $\delta^1\text{H}$ and $\delta^{13}\text{C}$ were less sensitive to the PDBS employed than $\delta^{15}\text{N}$, which N nucleus is coordinated to the Pd atom. Regarding the LBS, the $\delta^{13}\text{C}$ proved to be more sensitive when compared to the other nuclei. When the distinct DFT functionals are considered, the hybrid PBE0 functional presented the best results for $\delta^{15}\text{N}$ and the GGA OPBE functional for the $\delta^{13}\text{C}$. In addition, the same analyzes were performed considering the NMR-DKH basis sets for Pd and ligands atoms.

Table 1. Mean relative deviation (MRD) calculated at GIAO-NMR-protocol//BLYP/def2-SVP/C-PCM, considering the three Pd(II) complexes selected.

Computational protocols	MRD
PBE0/def2-TZVP/jorge-TZP	2.40%
$\delta^{15}\text{N}$ PBE0/def2-TZVP/def2-SVP	2.44%
PBE0/NMR-DKH/NMR-DKH	3.06%
OPBE/def2-TZVP/jorge-TZP	0.92%
$\delta^{13}\text{C}$ OPBE/Sapporo-TZP-2012/jorge-TZP	0.92%
OPBE/NMR-DKH/NMR-DKH	1.17%

Finally, the protocols will be validated in studying new Pd(II) complexes and applied in the characterization of the inclusion compounds between Pd(II) complexes and β -cyclodextrin.

CONCLUSION

The study presented the construction of computational protocols for predicting the NMR chemical shift of ^1H , ^{13}C , and ^{15}N nuclei in Pd(II) complexes. In addition, a new NMR-DKH basis set for Pd atom was also proposed. The results showed MRD below 3%, indicating that the protocols are a good choice for studying NMR properties in Pd(II) complexes.

REFERENCES

- E. Z. Jahromi et al., J. Iran. Chem. Soc., 2016, 13, 967-989.
- L. A. Souza et al., Chem. Phys. Lett., 2021, 774, 1-22.
- D. Paschoal et al., J. Comput. Chem., 2016, 37, 2360-2373.

ACKNOWLEDGMENTS

The authors would like to thank the Brazilian agency FAPERJ (E-26/201.336/2022 – BOLSA and E-26/210.070/2022), PIBIC-UFRJ, and CAPES (Finance Code 001) for the financial support.

Computational Study of the Adsorption of Lithium, Aluminum, and Lead Ions on COF RIO-12

¹Correa, Letícia (PG), ¹Oliveira, Felipe* (PG), ²Freitas, Sunny (PQ), ²Branco, Luis (PQ) ¹Esteves, Pierre (PQ); leticiarccorrea@gmail.com; felipe.lopes@nano.ufri.br.

1Instituto de Química, Universidade Federal do Rio de Janeiro, Avenida Athos da Silveira Ramos, nº 149, Bloco A—7º andar Centro de Tecnologia—Cidade Universitária, Ilha do Fundão, Rio de Janeiro 21941-909, Brazil 2LAQV-REQUIMTE, Department of Chemistry, NOVA School of Science and Technology, NOVA University of Lisbon, Campus de Caparica, 2829-516 Caparica, Portugal.

Keywords: COFs, Adsorption, Heavy metals, CP2K.

INTRODUCTION

The quality of water plays a crucial role in ensuring human consumption safety, catalyzing investigations and technological advancements. The high occurrence of toxic metals in various environments, stemming from their use in pharmaceutical, medical, cosmetic, and electronic products, has led to the generation of contaminated waste. Emerging inorganic pollutants, such as lithium, lead, arsenic, mercury, and cadmium, are identified in wastewater, carrying adverse implications that encompass hormonal, neurological, and cancerous dysfunctions. Due to their affinity for organic groups and resistance to degradation, these elements accumulate in organisms, categorizing them as hazardous substances. Adsorbent materials, such as Covalent Organic Frameworks (COFs), Covalent Organic Networks (CONs), and Porous Organic Polymers (POPs), exhibit remarkable potential in removing unwanted agents^[1,2]. These porous and crystalline structures emerge as promising candidates for purifying toxic metals from water, with nitrogen-rich materials like RIO-12 standing out^[3]. They reveal intrinsic potential for selective adsorption due to their configuration and functionalized sites. This study presents the computational analysis of the adsorption of Li⁺, Al³⁺, and Pb²⁺ ions on COF RIO-12, aiming to provide insights into the understanding of these intricate interactions.

METHODS

DFT calculations were performed using the Perdew–Burke–Ernzerhof (PBE) exchange-correlation functional with DFT-D3(BJ) dispersion corrections. The Quickstep code of the CP2K v2023.1 package was used, employing GTH pseudopotentials, TZV2P-MOLOPT-SR contracted Gaussian basis sets, and an auxiliary plane wave basis set. The plane waves cutoff is set to 600 Ry cutoff mapped on a 5-level multigrid with the orbital transformation (OT) method^[4]. The calculations have been conducted for the species listed below: Li⁺, LiCl, LiOH, LiClO₄, Al³⁺, AlCl₃, Al(NO₃)₃, Pb²⁺ and Pb(NO₃)₃ adsorbing on the COF RIO-12.

RESULTS

The obtained results suggest an adsorption trend in the order of atomic charge, with Al³⁺ exhibiting

the strongest interaction, followed by Pb²⁺, and Li⁺ showing the weakest interaction. The electronic interaction energies are -1279.0, -411.7, and -170.69 kcal/mol, respectively. The binding energies between the isolated ion and the COF are higher in all cases compared to other molecules. In all three cases, the ion interacts directly with the =O present in the tripodal building block and the N of the hydrazine, with bond lengths smaller than 2 Å. The short bond length indicates a strong charge transfer bond between the COF structure and the ions. In Figure 1, it is clearly evident the charge transfer both from the O atoms and the N atoms to form the bond with the Li⁺ ion.

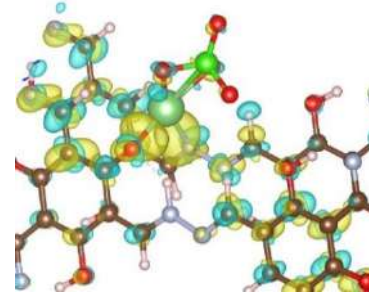


Figure 1: Charge transfer during the adsorption process between Li⁺ and RIO-12.

CONCLUSIONS

Upon a comparison of the acquired results with the experimental data, a distinct reversal in the order of aluminum and lead ion affinities towards the COF emerged, remarkably positioning lithium with the least affinity. Further comprehensive studies are currently underway to meticulously validate and elucidate this inversion.

REFERENCES

- [1] Christie, L. Captivating COFs. *Nature Chem* 8, 406 (2016).
- [2] Gendy, M. A., et al. Removal of heavy metals by covalent organic frameworks (COFs): A review on its mechanism and adsorption properties. *Journal of Environmental Chemical Engineering*, 9(4), 105687. (2021).
- [3] MAIA, R. A. et al. CO₂ Capture by Hydroxylated Azine-Based Covalent Organic Frameworks. *Chemistry – A European Journal*, v. 27, n. 30, p. 8048–8055, 27 April 2021. Christie, L. Captivating COFs. *Nature Chem* 8, 406 (2016).
- [4] HUTTER, Jürg et al. cp2k: atomistic simulations of condensed matter systems. *Wiley Interdisciplinary Reviews: Computational Molecular Science*, v. 4, n. 1, p. 15–25, 2014.

ACKNOWLEDGMENTS

The authors thank the financial support from CAPES. The program FCT/CAPES project (34/2018) and Associate Laboratory for Green Chemistry LAQV.

Cinética das Etapas de Consumo de Radicais Dimetoximetil Oxidanol.

Caio Fabio Gomes Oliveira (IC),¹ Franklyn da Costa Campos (IC),¹ Glauco Favilla Bauerfeldt (PQ),^{1,2}

caiofab@ufrj.br; bauerfeldt@ufrj.br

¹Dep. de Química Fundamental, Universidade Federal Rural do Rio de Janeiro.

Palavras Chave: Mecanismos de Reação. Éteres de Oximetileno. Teoria de Estado de Transição.

INTRODUÇÃO

Trimetoximetano (TMM; ortoformato de trimetil; **Figura 1**), um composto da classe de éteres de oximetileno de cadeia ramificada, tem sido apontado como combustível alternativo.¹⁻³ Seu perfil de combustão, emissão de resíduos e mecanismo de combustão têm sido investigados intensamente. Entre as etapas de ignição do mecanismo, destacam-se as bimoleculares de abstração de hidrogênio por O₂ e as unimoleculares, entre as quais a demetilação, com formação de radicais dimetoximetil oxidani (I, **Figura 1**), se mostra a principal reação em regime de alta temperatura e pressão.

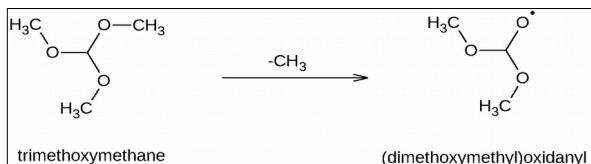


Figura 1 – Etapa do Mecanismo de Combustão de TMM.

As etapas que permitem o consumo destes radicais e propagam o mecanismo de combustão, entretanto, ainda não foram elucidadas.³ Neste trabalho, buscamos contribuir para a arquitetura do mecanismo de combustão dos éteres de oximetileno através do estudo cinético das etapas de consumo do intermediário *I*. Especificamente, o objetivo deste trabalho é propor e obter dados termodinâmicos e cinéticos para possíveis etapas de consumo de *I*.

MÉTODOS

Cálculos teóricos foram realizados em nível M06-2X/aug-cc-pVTZ. Geometrias de todas as espécies envolvidas, incluindo pontos de sela, foram otimizadas e os mínimos globais foram confirmados por cálculos de varredura em função de ângulos diedros e análise conformacional. As características dos pontos estacionários localizados foram confirmadas por cálculos de frequências vibracionais, no mesmo nível de teoria. Etapas de reação foram confirmadas por cálculos de coordenada de reação. Coeficientes de velocidade foram determinados pelo método do estado de transição variacional canônico.⁴

RESULTADOS

As etapas estudadas foram: $I \rightarrow CH_3OC(O)OCH_3 + H$ (R1a), $I \rightarrow CH_3OC(OH)OCH_3$ (R1b), $I \rightarrow OCOCH_3 + CH_3OH$ (R1c) e $I \rightarrow CH(O)OCH_3 + CH_3O$ (R1d), sendo a primeira a de menor

barreira, como apresentado na **Figura 2**. O estudo das etapas consecutivas, de consumo de cada produto, mostra que as barreiras encontradas na decomposição de $\text{CH}_3\text{OC(O)OCH}_3$ são muito altas, permitindo a abertura do canal de reação reversível $\text{CH}_3\text{OC(O)OCH}_3 + \text{H} \rightarrow I$. Situação semelhante é encontrada em R1d. Assim, espera-se que *I* seja preferencialmente consumido pelos canais R1b e R1c, em regime de controle termodinâmico, formando, após algumas etapas, CH_3 , CH_3OH e CO_2 , como produtos de R1b e OCH_3 , CH_3 e CO_2 , como produtos de R1c.

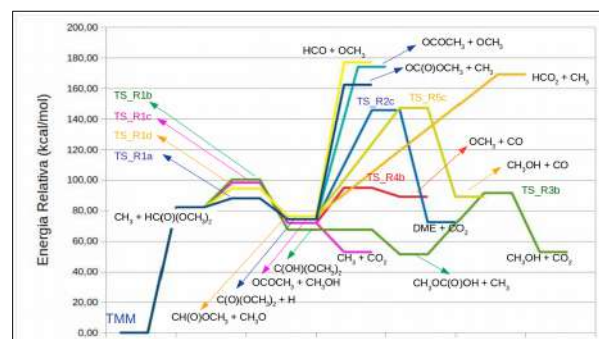


Figura 2 – Diagrama de energia mostrando as etapas de consumo de I_1 .

CONCLUSÕES

Os resultados mostram que as vias de isomerização (R1b) e decomposição (R1c) são os caminhos preferenciais de consumo de radicais dimetoximetil oxidanil, tanto do ponto de vista cinético quanto termodinâmico e levam as espécies que já constam dos mecanismos de combustão de dimetil éter, o que permite a inclusão das etapas e a extensão do mecanismo para o estudo cinético da combustão de TMM. O estudo de reações de outras espécies primárias está sendo conduzido, o que deverá permitir a formação de um mecanismo de combustão do TMM mais amplo e capaz de fornecer previsões de seu perfil de combustão.

REFERÊNCIAS

- ¹Härtl, M. et al. *Fuel* **2015**. 153, 328–335.
²Döntgen, M. et al. *Combust Flame* **2022**. 242, 112186.
³Döntgen, M. et al. *Proc. Combust. Inst.* **2023**. 39, 305–314.
⁴Vieira, G. S. S. et al. Assessment of Uni and Bimolecular Reaction Kinetics of Dimethoxymethane with the KINPRO Package. In: 10th European Combustion Meeting, 2021, Virtual Edition. *Proc European Combust Meeting*, 2021.

AGRADECIMENTOS

Os autores agradecem ao CNPq pelas bolsas de Iniciação Científica.

Glucose Impact on the Solvation of Polyacrylamide

Eduard David Simões Mourão (PhD)^{1*}, Leandro Martínez (R)¹

e219542@dac.unicamp.br

¹Institute of Chemistry and Center for Computing in Engineering and Science - CCES, University of Campinas

Keywords: Molecular dynamics, Solvation, Polyacrylamide, MDDF, Kirkwood-Buff integrals.

INTRODUCTION

Water-soluble polymers, exemplified by polyacrylamide (PAm), exhibit distinctive properties with applicability across diverse sectors¹. Non-ionic solutes, such as sugars, exert significant influence on polymer stability and structures in aqueous environments. Interactions between glucose and PAm can impact colloid, rheological, and interfacial properties. Experimental findings underscore a pronounced correlation between swelling of PAm gel matrices in glucose solutions. Tools such as Minimum Distance Distribution Functions (MDDFs) and Kirkwood-Buff integrals offer insights into solute-solvent interactions and bridging microscale solvation perspectives^{2,3}.

METHODS

PAAm polymer structures were generated using the charmm-gui web-based platform with Polymer-Builder⁴. Three polymer models, with lengths of 20, 50, and 100 monomers, were created. Simulations ran in triplicates of 300 ns, starting from widely different structures. GROMACS performed energy minimization and Molecular Dynamics (MD). Analysis utilized GROMACS tools, ComplexMixtures.jl⁵ for MDDF and KB.

RESULTS

The KB integrals results indicate that polyacrylamide is preferentially hydrated at all simulated glucose concentrations and across all studied systems. Both glucose and water form solvation layers on the polymer's surface. Glucose establishes specific and non-specific interactions with polyacrylamide, with hydrophobic interactions predominating. Analysis of the MDDF data reveals that hydrogen and oxygen atoms of the co-solvent are the primary contributors to the polymer interaction.

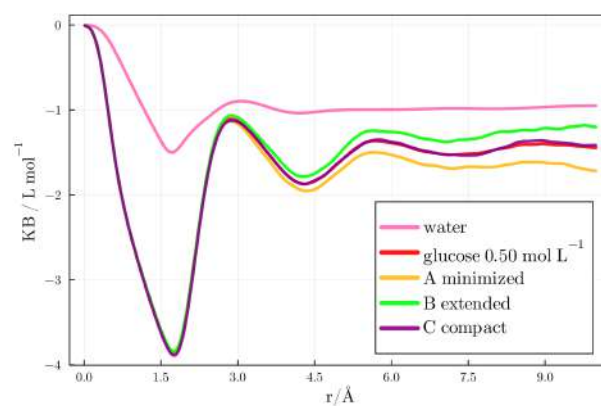


Figure 1. Polymer-solvent Kirkwood-Buff integrals for all replicas, where A represents the minimized structure, B represents the extended structure, C represents the compact structure and the line red represents the average integral.

CONCLUSION

In conclusion, based on the simulation outcomes, we have successfully replicated the mechanisms governing the influence of glucose on PAAM hydration. These simulations are consistent and enable us to faithfully reproduce experimental observations within a system involving polyacrylamide in a glucose solution. Furthermore, the theoretical results of this study demonstrate remarkable agreement with the experimental findings.

REFERENCES

- ¹Livney, Y. D., Portnaya, I., Faupin, B., Fahoum, L., Ramon, O., Cohen, Y., Mizrahi, S., & Cogan, U. *Journal of Polymer Science*, 2003, 41, 3053–3063.
- ²Martinez, L., & Shimizu, S. *Journal of chemical theory and computation*, 2017, 13(12), 6358-6372.
- ³Martínez, L. *Journal of Molecular Liquids*, 2022, 347, 117945.
- ⁴Choi, Y. K., Park, S.-J., Park, S., Kim, S., Kern, N. R., Lee, J., & Im, W. *Journal of Chemical Theory and Computation*, 2021, 17, 2431–2443.
- ⁵Martinez, L. *Journal of Molecular Liquids*, 2022, 347, 117945.

ACKNOWLEDGMENTS

The authors acknowledge the support of Coordination for the Improvement of Higher Education Personnel (CAPES), Center for Computing in Engineering and Sciences (CCES), CENAPAD-SP (National Center for High Performance Processing in São Paulo), and Martínez Molecular Modeling Group (M3G, <http://m3g.igm.unicamp.br/>).

A Relação Estrutura-Atividade de Derivados da Cumarina Contra as Bactérias *Staphylococcus aureus* e *Escherichia coli*

Ana Paula Oliveira (PG)^{1,2}, Alexandre Santiago Silva Cardoso (PG)¹, Hudieyllen Alves Moreira (PG)¹, Rodrigo Aparecido Lemos Silva (PQ)¹, Luciano Ribeiro (PQ)², Luciana Machado Ramos (PQ)¹

LRIIBEIRO@ueg.br

¹ Laboratório de Química Medicinal e Síntese Orgânica, Câmpus Central, Universidade Estadual de Goiás (UEG), Anápolis – GO – Brasil

² Grupo de Química Teórica e Estrutural de Anápolis, Câmpus Central, Universidade Estadual de Goiás (UEG), Anápolis – GO – Brasil

Palavras-Chave: SAR, PCA, DFT, Cumarina.

INTRODUÇÃO

A cumarina é alvo de frequentes investigações de interesse farmacológico. Entre as características que fazem a cumarina ser uma substância tão relevante está na sua origem natural e abundante. Seu baixo custo, ser um composto estável e além de assumir conformações diversas. Neste trabalho apresentamos a avaliação de 12 derivados de cumarina ao potencial antibacteriano para duas bactérias: o *Staphylococcus aureus* e a *Escherichia coli*.

MÉTODOS

Os cálculos foram feitos no funcional de troca e correlação híbrido M062X e o conjunto de base 6-311++G(d,p), usando o pacote Gaussian G16. O tratamento estatístico utilizado foi a análise de componentes principais na linguagem R empregando a função *prcomp* do pacote *stats* no R. Foi seguido os protocolos da literatura [1, 2].

RESULTADOS

O composto ilustrado na Fig. 1 pode assumir várias conformações geométricas distintas por apresentar diversos graus de rotação nas ligações da sua composição estrutural.

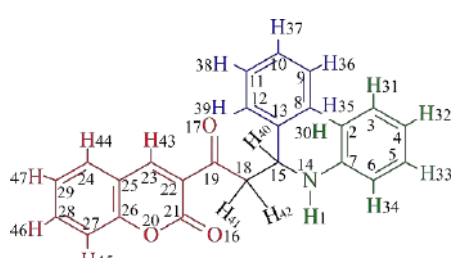


Figura 1. Representação da estrutura molecular da 3-[3-fenil-3-(fenil amino) propanoil]-2H-cromen-2-ona.

Staphylococcus aureus

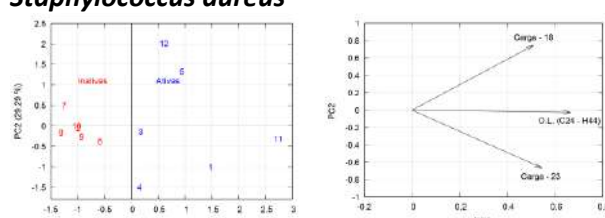


Figura 2. Gráfico de escores para as ativas e inativas e o dos pesos para os descritores que influenciam a atividade.

A Eq. 1 que relaciona as variáveis e coeficientes do componente principal PC1, é possível prever como a atividade biológica para o *S. aureus*.

$$PC1 = 0,510C_{18} + 0,6650L_{43} + 0,545C_{23} \quad (1)$$

Escherichia coli

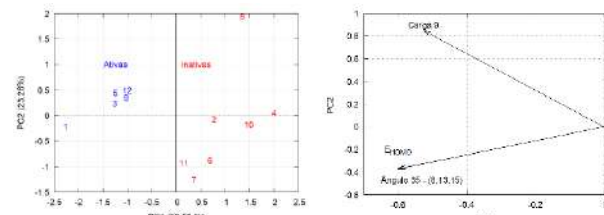


Figura 3. Gráfico de escores para as ativas e inativas e o dos pesos para os descritores que influenciam a atividade.

A Eq. 2 que relaciona as variáveis e coeficientes do componente principal PC1, é possível prever como a atividade biológica para o *E. coli*.

$$PC1 = -0,526C_9 - 0,6010E_{HOMO} - 0,6012A_{35} \quad (2)$$

CONCLUSÕES

O estudo teórico estrutura-atividade utilizando cálculos de mecânica quântica molecular realizados usando a teoria do funcional da densidade, por meio do funcional de troca e correlação híbrido M062X e utilizando o conjunto de base 6-311++G(d,p) se mostrou eficaz na descrição qualitativa quanto aos descritores geométricos e eletrônicos das moléculas análogas da cumarina.

REFERÊNCIAS

1. De Paiva RKC, Da Silva JF, Moreira HA, et al (2019) Synthesis, Antimicrobial Activity and Structure-Activity Relationship of Some 5-Arylidene-thiazolidine-2,4-dione Derivatives. J Braz Chem Soc 30:. <https://doi.org/10.21577/0103-5053.20180167>

2. Vieira I, Camargo LTFM, Ribeiro L, et al (2019) Structure-activity relationship of tacrine and its analogues in relation to inhibitory activity against Alzheimer's disease. J Mol Model 25:116. <https://doi.org/10.1007/s00894-019-3993-8>

AGRADECIMENTOS

Os autores agradecem o suporte dado pela UEG e FAPEG.

Estudo computacional de O-glicosídeos 2,3-insaturados com terpenos

Yuri Antonio Fortunato da Silva* (PG)¹, **João Rufino de Freitas Filho** (PQ)¹, **Cristiano Costa Bastos** (PQ)¹

yuri_antonio97@hotmail.com

¹Departamento de Química, Universidade Federal Rural de Pernambuco, Recife -- Pernambuco – PE - Brasil;

Palavras-Chave: Química, Orgânica, Computacional, O-glicosídeos, Terpenos.

INTRODUÇÃO

Os glicosídeos são uma classe de compostos que possuem em sua estrutura uma unidade de glicona (geralmente um monossacarídeo) e uma unidade de aglicona. Na síntese de glicosídeos é possível formar os anômeros α e β , sendo necessário analisar os fatores que podem interferir na formação majoritária de determinado isômero (em geral mais α).¹ Os terpenos ou terpenóides são considerados como alcenos de origem natural e apresentam em sua estrutura básica mínima uma unidade de isopreno (C_5H_8). Há na literatura muitos trabalhos envolvendo a aplicação de terpenos, um exemplo disso é o Geraniol, que apresenta atividade antifúngica, anti-inflamatória e antioxidante.^{2,3} Os terpenóides também ocorrem como isômeros (R, S, E e Z) permitindo uma diversidade química estrutural e reacional. A Química Computacional e Teórica permite obter dados que podem contribuir para o melhor entendimento de como estas reações acontecem, quais estruturas químicas são mais estáveis e possíveis novos compostos.

MÉTODOS

Foram construídos modelos para as inéditas moléculas de tri-O-acetil-D-glucal e dos glicosídeos formados pela reação da glicona com os seguintes terpenos: E-Geraniol; Z-Geraniol; 3R-Citronelol; 3S-Citronelol; 3R-Linolol; 3S-Linolol; α -Terpineol; E-Nerolidol e Z-Nerolidol. As estruturas foram otimizadas em nível semi-empírico AM1. Após a otimização, foram obtidas as energias eletrônicas, frequências, propriedades termodinâmicas e cargas atômicas em nível B3LYP/6-31g+.

RESULTADOS

A energia livre de Gibbs de formação dos O-glicosídeos e constantes da força de ligação indicaram equilíbrio de proporção para síntese dos compostos (Figura 1). Os cálculos indicam que, com exceção dos isômeros (3R)-Linolol e (3S)-Linolol, a maior constante de força da ligação glicosídeo-terpeno se dá para a menor variação da energia livre de Gibbs, indicando a maior estabilidade. Os isômeros do Linolol, por terem cadeias maiores, mostram sua diferenciação de estabilidade pela ligação dupla dos carbonos terminais. Assim, por exemplo, o E-Geraniol seria mais estável para o anômero α , enquanto o Z-Geraniol para o anômero β . Temos então que para estas novas moléculas, o anomero α não deve ser totalmente preferencial em relação ao anomero β .

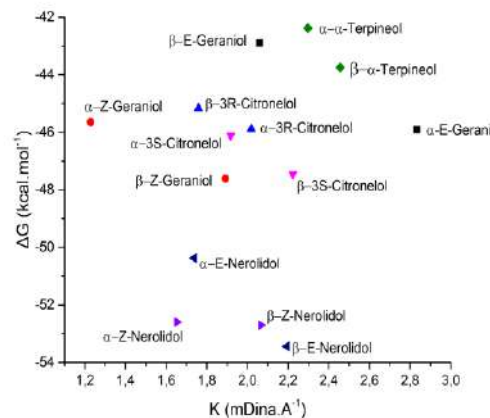


Figura 1: Energia livre de Gibbs vs Constante de força

Além disso, analisando a distribuição de cargas os cálculos indicam que os terpenos apresentam uma maior carga negativa no oxigênio e após a formação do glicosídeo, ele demonstra ter carga positiva para os glicosídeos com o 3R-Linolol, α -Terpineol e os isômeros do Nerolidol, enquanto que para os glicosídeos restantes há uma diminuição da carga menos pronunciada. Isso parece ter relação com a estrutura dos terpenos que causam um efeito indutivo deslocando a carga do oxigênio para os carbonos mais afastados.

CONCLUSÕES

Um maior valor da constante de força da ligação glicosídeo-terpeno geralmente é um indicativo de maior estabilidade da molécula. Os anômeros α com E-Geraniol, 3R-Citronelol, 3S-Citronelol, 3R-Linolol, 3S-Linolol são mais estáveis que seus respectivos isômeros. Os anômeros β com Z-Geraniol, α -terpineol, E-Nerolidol e Z-Nerolidol são os mais estáveis dentre os isômeros de acordo com os cálculos. A adição de terpenos diminui a carga negativa do oxigênio após a formação do glicosídeo.

REFERÊNCIAS

- ¹MOURA, Aldiceia Luiz de et al. O-glicosídeos 2,3-insaturados: aplicações, rearranjo de Ferrier e reações. *Química Nova*, v. 41, p. 550-566, 2018.
- ²GUIMARÃES, Adriana G.; QUINTANS, Julliana SS; QUINTANS-JÚNIOR, Lucindo J. Monoterpenes with analgesic activity—a systematic review. *Phytotherapy research*, v. 27, n. 1, p. 1-15, 2013.
- ³DE SÁ, Rodrigo Elísio et al. Geraniol, um componente dos óleos essenciais de plantas—um mapeamento científico de suas propriedades farmacológicas. *Research, Society and Development*, v. 10, n. 12, p. e508101220805-e508101220805, 2021.

AGRADECIMENTOS

CNPq, CAPES, LnP e UFRPE.

TD-DFT analysis of tryptophan from the vitamin D receptor binding site

Vanessa Regina Miranda (PG),^{1*} Nelson Henrique Morgan (PQ).¹
miranda.vanessar@gmail.com*

¹Institute of Chemistry, University of Campinas, 13083-970, Campinas, SP, Brazil

Keywords: (Tryptophan, Vitamin D Receptor, TD-DFT, Circular Dichroism Spectra).

INTRODUCTION

The vitamin D receptor (VDR) belongs to the nuclear receptor superfamily¹ and mediates the action of 1 α ,25-dihydroxyvitamin D3 (calcitriol) in transcriptional regulation.² The interaction of calcitriol with the amino acid residues of the ligand-binding domain (LBD) causes conformational changes in these residues. To gain insights into protein secondary and tertiary structures, circular dichroism (CD) spectroscopy is employed. The positive and negative bands in the CD spectrum directly correspond to different conformations. In the near-UV CD spectrum (250 to 300 nm), it is possible to observe bands originating from residues such as tryptophan, tyrosine and phenylamine, which, due to their aromaticity, are sensitive to the electronic environment around them.³ However, it is experimentally unfeasible to carry out individual CD studies for each residue in the specific conformation in complexation with the ligand. Within this context, *in silico* approach makes it possible to understand the contribution of each residue in the CD spectrum. Thus, this work has sought to understand, through electronic studies, using TD-DFT, the near-UV CD signal of TRP-286 from the LBD of the VDR, considering the presence and absence of calcitriol, verifying its influence on the neighborhood of the TRP-286. This study may contribute to the development of new analogues of the calcitriol aiming at therapeutic profiles.

METHODS

The studies involving L-tryptophan⁴ (CAS: 73-22-3) were conducted in ethanol solvent ($\epsilon=24.852$), with an explicit description, as well as using the SMD approach (solvent model density). Optimization and frequency calculations were carried out at B3LYP/6-31++G(2d,p) and excited state by TD-PBE1PB1/6-311++G(3df,2p) levels of theory, respectively. The same functional was used in the electronic study of the tryptophan residue (TRP-286) from the LBD of the vitamin D receptor (PDB ID: 1DB1).⁵ The active site was defined in 6Å (using molden software), and the hydrogens were added at physiological pH, and their coordinates were optimized at PM7 method. After that, TRP-286, calcitriol and the TRP286-calcitriol complex were isolated and subjected to the corrected complexation energy calculation using the Counterpoise⁶ (CP) method. The TD-DFT study was performed at the same level as defined for L-tryptophan. Calculations were performed using Gaussian 16.⁷

RESULTS

The CD result obtained for L-tryptophan was corroborated with experimental data available in the literature.⁵ The corrected complexation energy of TRP286-calcitriol resulted in 2.32 kcal/mol. TD-DFT calculations show that tryptophan is located very close to the calcitriol HOMO/LUMO regions, with practically an alignment of the indole ring of TRP-286 with one calcitriol rings (Fig.1, TRP-286 + calcitriol).

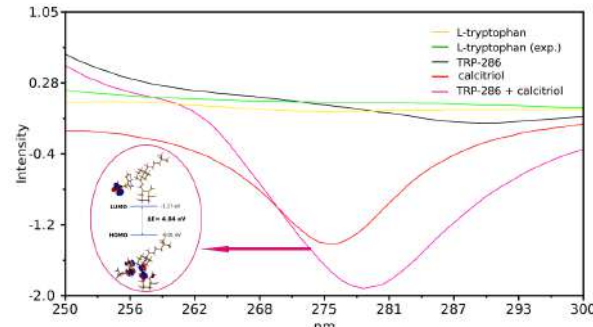


Figure 1: Near-UV CD (250 – 300 nm) of L-tryptophan in ethanol and TRP-286 from the LBD of the vitamin D receptor with and without the calcitriol presence.

The near-UV CD spectra, Fig.1, show that isolated TRP-286 has a smooth signal, that is negative after 277 nm. However, in the presence of the ligand (TRP-286 + calcitriol), an intensification of a negative peak around 279 nm is observed, indicating that the aromatic ring of TRP-286 was sensitive to the induction of this band by interaction with calcitriol, which already had a slightly less intense negative peak (276 nm). Similar near-UV CD results were also observed experimentally, after saturation of the rat VDR LBD with calcitriol, showing the induction of a large and strong peak around 277 nm.⁸

CONCLUSIONS

The results showed that the appearance of the band at 279 nm in the near-UV CD is due to a change in the electronic environment around TRP-286 when calcitriol complexes with VDR. We plan to perform fluorescence studies on TRP-286 in future work.

REFERENCES

1. Mangelsdorf, D.J. et al. Cell, 1995, 83, 835-839.
2. Rochel, N. et al. Molecular Cell, 2000, 5, 1, 173-179.
3. Strickland, E. H.; Beychok, S. CRC Crit. Rev. in Bioch., 1974, 2, 113-175.
4. PubChem. National Center for Biotechnology Information, 2023, CID 6305, Tryptophan.
5. Sousa, I. L. et al. J. Braz. Chem. Soc., 2020, 31, 3, 613-618.
6. Boys, S. F.; Bernardi, F. Mol. Phys., 1970, 19, 553.
7. Gaussian16,RevA.03. Frisch,M.J. et al. Gaussian,Inc, 2016.
8. Strugnell, S. A. Arch. Biochem. Biophys.,1999, 364,1,42-52.

ACKNOWLEDGEMENTS

CAPES; FAPESP – Procs. 2013/08293-7 e 2015/22338-9; CNPq – Proc. 303581/2018-2).

Predicting ^{49}Ti , ^{51}V , and ^{57}Fe NMR chemical shifts using the new NMR-DKH basis sets

Matheus G. R. Gomes (PG)^{1,2*}, Diego F. S. Paschoal (PQ)², Wagner B. De Almeida (PQ)¹

matheusgunar@id.uff.br; diegopaschoal01@gmail.com; wbdealmeida@gmail.com

¹Laboratório de Química Computacional e Modelagem Molecular (LQC-MM), Departamento de Química Inorgânica, Instituto de Química, Universidade Federal Fluminense, Outeiro de São João Batista s/n, Campus do Valongo, Centro, Niterói, RJ, Brazil; ²Núcleo de Química Teórica e Computacional de Macaé, Polo Ajuda, Instituto Multidisciplinar de Química, Centro Multidisciplinar UFRJ-Macaé, Universidade Federal do Rio de Janeiro, Macaé, RJ, Brazil.

Keywords: NMR, Basis Sets, DFT, Transition Metals, Computational Protocol.

INTRODUCTION

One of the applications of Nuclear Magnetic Resonance (NMR) spectroscopy is in studies involving the characterization and reactivity of coordination compounds with transition metals. However, many active metal nuclei are quadrupole ($I > 1/2$), causing additional difficulties in obtaining spectra^{1,2}. In this way, Computational Chemistry can strongly contribute to the interpretation of experimental data³. Therefore, the present study aims to obtain a computational protocol for predicting the ^{49}Ti , ^{51}V , and ^{57}Fe NMR chemical shifts (δ) in coordination complexes involving these transition metals.

METHODS

Initially, the new NMR-DKH basis sets for the Ti, V, and Fe atoms were constructed using the same methodology as Paschoal et al.⁴ For the construction of the computational protocol for predicting the NMR chemical shifts, the role of the structure and the DFT functional in obtaining of the shielding constants was assessed. A set of three V and Fe complexes, and six Ti complexes, with experimental data available in the literature for the $\delta^{49}\text{Ti}$, $\delta^{51}\text{V}$, and $\delta^{57}\text{Fe}$ were selected (Fig. 1). The structures of the complexes were obtained at DFT-Functional/def2-SVP/IEF-PCM(UFF) level, with a set of 12 functionals being tested. After, the chemical shifts were calculated at GIAO-PBE/NMR-DKH/IEF-PCM(UFF) level. The structures that resulted in the best NMR description were selected and then the role of the DFT functional in predicting the chemical shifts was also evaluated at GIAO-DFT-Functional/NMR-DKH/IEF-PCM(UFF) level, with a set of 21 functional being tested. The computational protocols obtained are being validated for a larger set of complexes. All calculations were carried out in GAUSSIAN 16 Rev. C.01 program.

RESULTS

For the $\delta^{57}\text{Fe}$, considering a set of two Fe complexes, the combination of structures obtained with GGA functionals with NMR obtained with hybrid functionals resulted in the lowest mean relative deviations (MRD). The protocols

(NMR/Geometry) B3PW91/PW91 and B3LYP/PBE resulted in MRD of 2.14% and 2.24%, respectively. For the $\delta^{51}\text{V}$, the better results were obtained with GGA functionals for both NMR and geometries, with PBE/BLYP protocol obtaining a MRD of 15.6%, corresponding a mean absolute deviation (MAD) of 56 ppm. The largest MRD obtained can be explained by the smaller range of variation of $\delta^{51}\text{V}$. Finally, for the $\delta^{49}\text{Ti}$, the hybrid B3PW91/B3LYP hybrids functionals presented the best results, with a MAD of 144 ppm.

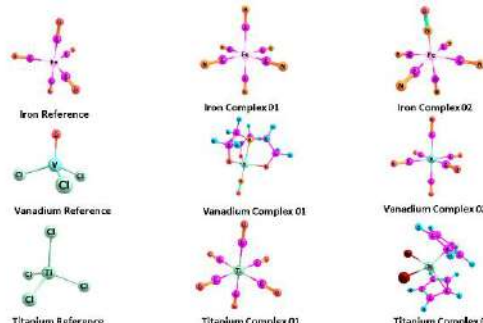


Fig. 1. Some of the Fe, V, and Ti complexes used in the benchmarking.

CONCLUSIONS

The computational protocols proposed in this work for predicting the $\delta^{49}\text{Ti}$, $\delta^{51}\text{V}$, and $\delta^{57}\text{Fe}$ are a good alternative for studying the NMR properties of Fe, V, and Ti complexes.

- $\delta^{57}\text{Fe}$: GIAO-B3PW91/NMR-DKH/IEF-PCM(UFF)//PW91/def2-SVP/IEF-PCM(UFF)
 - $\delta^{51}\text{V}$: GIAO-PBE/NMR-DKH/IEF-PCM(UFF)//BLYP/def2-SVP/IEF-PCM(UFF)
 - $\delta^{49}\text{Ti}$: GIAO-B3PW91/NMR-DKH/IEF-PCM(UFF)//B3LYP/def2-SVP/IEF-PCM(UFF)
- The protocols are being applied in a larger number of complexes aiming at validation.

REFERENCES

- ¹ Ronconi, L.; Sadler, P. J. *Coord. Chem. Rev.* **2008**, 252, 2239.
- ² Bühl, M. *Annu. Rep. NMR Spectrosc.* **2008**, 64, 77.
- ³ Gomes, M. G. R. et al. *Magnetochemistry* **2023**, 9, 172.
- ⁴ Paschoal, D. et al. *J. Comput. Chem.* **2016**, 37, 2360.

ACKNOWLEDGMENTS

The authors would like to thank the Brazilian agency FAPERJ (E-26/201.336/2022 – BOLSA and E-26/210.070/2022) and CAPES (Finance Code 001) for the financial support.

Obtention, characterization, and DFT study of the [Cu(Phen)(L-Asparagine)H₂OCl] coordination complex

Jéssica A. O. Rodrigues (PQ)¹, Antonio D. S. G. Lima (PG)¹, João G. de Oliveira Neto (PQ)¹, Mateus R. Lage (PQ),¹ Adenilson O. dos Santos (PQ),¹ Francisco F. de Sousa (PQ),² Alan S. de Menezes (PQ),¹.

antonio.guedes@discente.ufma.br; jessicaufma@gmail.com; mateus.lage@ufma.br.

¹Universidade Federal do Maranhão; ²Universidade Federal do Pará.

Keywords: [Cu(Phen)(L-Asparagine)H₂OCl]H₂O, DFT, Solvation Effect.

INTRODUCTION

Coordination complexes with organic ligands have attracted the attention of researchers due to their interesting properties and possible applications in different fields. Complexes containing amino acids as ligands have been the subject of research with studies of their solubility in different kinds of solvents, redox properties, and structural variability, as well as to study their potential antibacterial activity ^{1,2}. In the present study, a crystal of the complex [Cu(Phen)(L-Asparagine)H₂OCl] was obtained, and structural, spectroscopic, electronic, and thermodynamic properties of the complex were investigated through DFT calculations. The stability, electronic properties, and spectroscopic data of the complex were studied, considering solvation effects.

METHODS

The crystal of the [Cu(Phen)(L-Asparagine)H₂OCl] complex was obtained by the slow solvent evaporation method, using the molar ratio 1:1:1 of L-asparagine, 1,10-phenanthroline and CuCl₂.2H₂O, considering a mixture of water and ethanol as solvent. The crystal was characterized by X-ray diffraction (XRD), infrared (FT-IR), Raman and UV-vis spectroscopy. The theoretical calculations were performed employing the PBE1PBE DFT functional, as implemented in the Gaussian16 software³. The 6-311G(d,p) basis set was applied to carbon, nitrogen, oxygen, chlorine, and hydrogen atoms. The Stuttgart-Dresden pseudopotential (SDD) was used to treat inner electrons of the metal. The DFT calculations were developed considering neutral charge and doublet state, including solvation effects using the Integral Equation Formalism variant of the Polarizable Continuum Model (IEFPCM)⁴.

RESULTS

The crystal belongs to the triclinic system with a spatial group of $P\bar{1}$ e Z = 2. The XRD results show a good agreement with the theoretical structural parameters obtained for complex from the DFT calculations. The optimized geometry of the [Cu(Phen)(L-Asparagine)H₂OCl] complex was optimized and it was confirmed as a minimum in the potential energy surface since the vibrational frequencies calculated are positive.

The HOMO and LUMO spatial distributions and energy values were calculated in water solvent, as presented in Figure 1. The HOMO-LUMO gap was also calculated and is equal to 4.55 eV. These parameters obtained enable the calculation of reactivity indices for the complex.

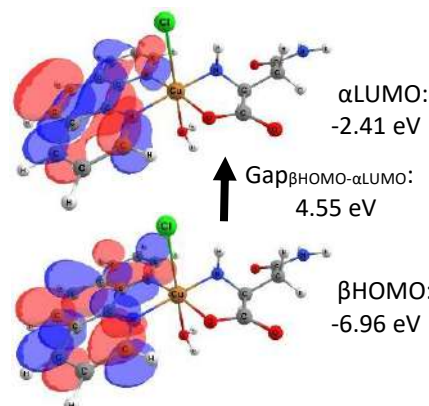


Figure 1. Isosurface and energy values of HOMO and LUMO orbitals of the [Cu(Phen)(L-Asparagine)H₂OCl] complex in water solvent.

The electrostatic potential surface indicated the charge distribution in the complex, suggesting the type of intermolecular force that can occur in each site. Characteristic bands of *d-d* transitions for Cu(II) pentacoordinate were identified from the experiments, with changes in accord with the solvent used. The theoretical IR and Raman spectra obtained are in good agreement with the experimental data. These results contributed to the characterization and better understanding of the material properties.

CONCLUSION

The study describes the structural, electronic, and vibrational properties of the complex. Additional steps of the study are needed for a better understanding of the properties of the complex, which is important for the analysis of technological applications of the material.

REFERENCES

- X. Li, et al., J Inorg Biochem. 105 (2011), 23–30.
- X. Liu, et al., Biol Trace Elem Res. 154 (2013), 150–155.
- M. J. FRISCH et al. Gaussian16 Rev.B.01, 2016
- J. Tomasi, et al. Chem. Rev. 105 (2005), 2999–3094

ACKNOWLEDGMENT

CAPES, CNPQ, FAPEMA, AllianceCanada.



Investigations on potential drug candidates targeting cholinesterase enzymes for AD treatment

Alexandre A. de Castro (PG),^{1*} Henrique F. Silva (IC),² Teodorico C. Ramalho (PQ),² Paula Homem-de-Mello.¹ alexandre.a.castro@hotmail.com

¹Center for Natural and Human Sciences, Federal University of ABC, Brazil; ²Department of Chemistry, Federal University of Lavras, 37200-000, Lavras, Brazil.

Keywords: Alzheimer, Cholinesterase enzymes, Computational chemistry, Inhibitors, Pharmacology.

INTRODUCTION

Alzheimer's disease (AD) may be denoted as a progressive neurodegenerative illness. This disorder has reached worrying epidemic proportions related to the aging of the global population. Currently, there is a prediction that the number of patients with AD will reach an impressive 115 million by 2050 [1]. Dementia affects millions of people around the world, and the majority of them present with AD, characterized by a devastating state that leads to progressive cognitive deterioration and functional injury, in addition to the loss of personal independence [2]. In this line, this work aims to computationally propose new therapeutic solutions for AD treatment, based on the cholinergic hypothesis, which postulates that reduced levels of neurotransmitters are observed in patients with AD [3].

METHODS

The crystallographic structure for the human acetylcholinesterase (AChE) enzyme, as well as for butyrylcholinesterase (BChE), were obtained from the Protein Data Bank (PDB). After choosing the bioactive compounds, the technique of virtual screening was carried out through two screening platforms and different databases. The molecular docking was conducted with the tool AutoDock Vina, which was validated for both enzymatic systems by plotting the ROC curve. The compounds obtained from virtual screening were protonated at physiological pH and then filtered by employing computed pharmacological parameters from SWissADME and ADMET. These parameters were high gastrointestinal absorption, blood-brain barrier permeability, toxicity, and Lipinski's rule of five, among others. The set of approved compounds was forwarded to molecular docking simulations.

RESULTS

The virtual screening brought an amount of 986 compounds. After applying the pharmacological filters, the final set was constituted of 50 compounds, which were forwarded to molecular docking calculations. To validate the molecular docking software for the molecular targets, the

ROC curve was plotted for both enzymes, showing satisfactory values of 0.75 for AChE and 0.70 for BChE. After docking, the compounds were ranked according to the best interaction energies. The results for the top 5 are shown in Table 1.

Table 1. Interaction energies of ranked top 5 compounds.

COMPOUNDS	AChE kcal mol ⁻¹	BChE kcal mol ⁻¹
Top 1	-13.1	-10.9
Top 2	-12.1	-11.8
Top 3	-13.0	-10.3
Top 4	-12.3	-10.3
Top 5	-11.5	-10.8

According to these results, compound top 1 presented the best interaction energy (-13.1 kcal mol⁻¹) with AChE, and compound top 2 had the most stabilizing interaction energy (-11.8 kcal mol⁻¹) with BChE. In general, these dual inhibitors presented stabilizing energies in both molecular targets. They performed several intermolecular interactions, mostly of long-distance type. In addition, the compounds performed strong hydrogen bonds with a range of residues in the active site, such as Gly121, Tyr124, Tyr72, His447 (AChE) and Glu197, Gln71, Ser198, His438 (BChE), among others. They also interacted with catalytic triad residues.

CONCLUSIONS

The screened compounds were approved and ranked according to different pharmacological parameters. Furthermore, they show close stabilizing interaction energies for both targets. Further studies must certify their efficacy as drug candidates for AD treatment.

REFERENCES

- Appleby, BS. et al. *Dement. Geriatr. Cogn. Disord.* 35, 1–22 (2013)
- Corbett, A. et al. *Nat. Rev. Drug Discov.* 11, 833–846 (2012)
- Contestabile, A. *Behav. Brain Res.* 221, 334–340 (2011)

ACKNOWLEDGMENTS

CNPq, UFABC, UFLA



In Silico studies of nitro derivatives of quinoline and quinoline N-oxide as low-cost alternative for the SARS-CoV-2 treatment

Henrique F. Silva (IC)^{1*}, Letícia C. Assis (PQ)¹, Alexandre A. de Castro (PG)¹, João P.A de Jesus (PG)², Eugenie Nepovimova (PQ)³, Kamil Kuca (PQ)³, Teodorico C. Ramalho (PQ)^{1,3}, Felipe A. La Porta (PQ)²
henriquefs63@gmail.com

¹Department of Chemistry, Federal University of Lavras, Minas Gerais CEP 37200-000, Brazil. ²Laboratório de Nanotecnologia e Química Computacional, Universidade Tecnológica Federal do Paraná, Londrina, PR 86036-370, Brazil.

³Department of Chemistry, Faculty of Science, University of Hradec Králové, Rokitanskeho 62, 500 03 Hradec Králové, Czech Republic.

Keywords: SARS-CoV-2; In Silico studies; M^{pro}; Quinoline; Quinoline N-oxide

INTRODUCTION

In 2019, the world faced a pandemic caused by a new coronavirus disease designated as COVID-19. It started in China and spread rapidly around the world. Researchers worldwide struggled to find an effective vaccine as well as forms of treatment targeting SARS-CoV-2 [1]. *In silico* methods aid in the path of finding new potential drugs to treat the disease. In this regard, the combination of quantum mechanics and molecular mechanics calculations are robust tools for investigating a vast range of drug candidates, as well as identifying potential molecular targets for the sites of actions of these therapeutic agents [2]. In this work, nitro derivatives of quinoline (Q) and quinoline N-oxide (QO) were computationally investigated targeting SARS-CoV-2 M^{pro} and chosen due to nitration reaction, which is attractive once the synthesis requires low-cost materials and simple reaction paths.

METHODS

The crystal structure for the SARS-CoV-2 virus M^{pro} enzyme was obtained from de Protein Data Bank (PDB; accession ID: 5R82, resolution 1.31 Å). The molecular docking was conducted with the tool AutoDock Vina (version 1.1.2), as implemented in the MolAr (Molecular Architecture) software. The ions and water molecules were removed from the original PDB, except for water molecules that were in the M^{pro} active site. The addition of polar hydrogen atoms was performed according to the protonation state of the receptor at pH 7.4, by using Chimera software. In further theoretical insight, the key docking complexes were evaluated by molecular dynamics (MD) simulations using the GROMOS54A7 all-atom force field and performed using GROMACS 5.1 software.

RESULTS

A comparison of the difference between the total electronic energy (ΔE) for the computed Q and QO isomers suggests that both N-4-Q and N-4-QO compounds are energetically more stable.

From docking studies, compounds N-4-QO, N-9-QO, N-8-QO, together with QO, had slightly more stabilizing interaction energy values than those of their corresponding nitro-quinolines. The N-4-QO performed hydrogen bonds with the residues Cys145 and His41 and a water molecule, which constitute the catalytic triad.

Table 1. Interaction energy (in kcal mol⁻¹) of nitro derivatives.

Nitro group position	Interaction Energy (kcal mol ⁻¹)	Nitro group position	Interaction Energy (kcal mol ⁻¹)
N-4-QO	-5.0	N-4-Q	-4.6
N-9-QO	-5.0	N-9-Q	-4.6
N-7-QO	-4.9	N-7-Q	-5.0
N-2-QO	-4.8	N-2-Q	-4.8
N-5-QO	-4.8	N-5-Q	-4.8
N-8-QO	-4.8	N-8-Q	-4.6
N-3-QO	-4.5	N-3-Q	-4.5
QO	-4.5	N-1-Q	-4.3
CQO	-3.0	CQ	-2.8
HCQO	-3.1	HCQ	-2.3

MD simulations estimated the interaction energies for nitro derivatives of quinoline (Q) and quinoline N-oxide (QO). For instance, N-4-Q and its oxo form presented values of -96.54 kJ mol⁻¹ and -107.35 kJ mol⁻¹, respectively. Most N-oxide compounds showed stronger affinity for the M^{pro} active site than their Q counterparts in the study.

CONCLUSIONS

From this structure-based study, the nitro derivatives of QO showed to be better inhibitors than their Q counterparts. These compounds can be easily produced on a large scale (at a low-cost), making them a promising treatment option against SARS-CoV-2 infection.

REFERENCES

- ¹ Zhou, P. et al. Nature 579, 270–273 (2020).
² La Porta, F. A. & Taft, C. A. (Springer, Cham, 2020).

ACKNOWLEDGMENTS

CNPq, CAPES, FAPEMIG, UFLA

Computational study of the Tc-99 NMR chemical shift

Taís F. C. B. Andrade (PG)^{1*}, Hélio F. dos Santos (PQ)², Célia F. Guerra (PQ)³, Diego F. S. Paschoal (PQ)¹

tais.andrade.ufrj@gmail.com; diegopaschoal01@gmail.com

¹Núcleo de Química Teórica e Computacional de Macaé, Polo Ajuda, Instituto Multidisciplinar de Química, Centro Multidisciplinar UFRJ-Macaé, Universidade Federal do Rio de Janeiro, Macaé, RJ, Brazil; ²NEQC: Núcleo de Estudos em Química Computacional, Departamento de Química – ICE, Universidade Federal de Juiz de Fora, Juiz de Fora, MG, Brazil;

³Department of Theoretical Chemistry, Amsterdam Institute of Molecular and Life Sciences (AIMMS), Amsterdam Center for Multiscale Modeling (ACMM), Vrije Universiteit Amsterdam, 1081 HV Amsterdam, The Netherlands.

Keywords: Radiopharmaceutical, Technetium, NMR, Computational protocol.

INTRODUCTION

The ^{99m}Technetium (^{99m}Tc) is the most used element in radiopharmaceuticals designed for imaging diagnosis, where it is applied as a radioactive tracer. It can exist in 9 oxidation states, which allows this element to form many coordination complexes with a variety of chelating agents, assuming different geometries¹. The Nuclear Magnetic Resonance (NMR) spectroscopy is widely used to monitor the chemical surroundings of ⁹⁹Tc complexes¹. This study aims to evaluate relevant aspects for predicting the Tc-99 NMR chemical shift ($\delta^{99}\text{Tc}$), such as level of theory, basis set, relativistic and solvent effects.

METHODS

There are few studies in the literature regarding the theoretical prediction of $\delta^{99}\text{Tc}$ ^{2,3}. Thus, this work suggests the development of a computational protocol for predicting $\delta^{99}\text{Tc}$ in Tc(0), Tc(I), and Tc(V) complexes⁴. The role of the structure, DFT functional, basis set, solvent effects (gas phase, implicit and explicit solvent), and relativistic effects (nonrelativistic, quasi relativistic and 4-component approaches) were considered. The best models were named as Model 1, quasi relativistic model with calculations performed with ADF 2019.3 program and Model 2, nonrelativistic model with calculations performed with GAUSSIAN 09 Rev. D.01 program. It was also proposed an empirical nonrelativistic protocol (Model 3) from the linear regression model between $\delta^{99}\text{Tc}_{\text{calc}} \times \delta^{99}\text{Tc}_{\text{expt}}$. In addition, a new relativistic gaussian basis set (NMR-DKH) was developed for Tc atom. The 4-component calculations were performed with ReSpect 5.1.0 program. The $\delta^{99}\text{Tc}$ were calculated according to eq. (1), Models 1 and 2, and eq. (2), Model 3.

$$\delta^{99}\text{Tc} = \sigma_{\text{ref}} - \sigma_{\text{calc}} \quad (1)$$

$$\delta^{99}\text{Tc} = -2218.4 - 0.9256 \times \sigma^{99}\text{Tc}_{\text{calc}} \quad (2)$$

RESULTS

The proposed models were applied to a set of 41 Tc complexes, with oxidation states 0, I e V. From the calculated results (Figure 1), a mean absolute deviation (MAD) and a mean relative deviation (MRD) were of 67 ppm/4.8% (Model 1: SO-ZORA-

SSB-D / TZ2P-ZORA / COSMO // SC-ZORA-B3LYP / TZP-ZORA / COSMO, 92 ppm/6.2% (Model 2: B3LYP / NMR-DKH /IEF-PCM(UFF) // TPSS /def2-SVP /IEF-PCM(UFF)), and 65 ppm/4.9% (Model 3: B3LYP / NMR-DKH /IEF-PCM(UFF) // TPSS /def2-SVP /IEF-PCM(UFF)).

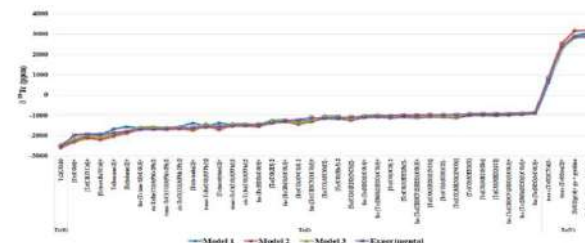


Figure 1. Relation between the experimental and calculated $\delta^{99}\text{Tc}$ with Models 1, 2, and 3.

The explicit solvent model was also evaluated for a Tc(V) complex, $[\text{Tc}(\text{en})_2\text{O}_2]^+$. The results showed an absolute deviation/relative deviation of only 7 ppm/0.3%, when implicit solvent model and 14 water molecules were included (first solvation shell) at SO-ZORA-SSB-D/TZ2P-ZORA/COSMO // TPSS/def2-SVP/IEF-PCM(UFF).

Finally, the proposed Models 1, 2, and 3, presented results of the same quality as those obtained when a 4-component approximation was considered.

CONCLUSIONS

Relevant aspects were accounted for a computational prediction of the $\delta^{99}\text{Tc}$ in Tc(0), Tc(I), and Tc(V) complexes. This work suggests the following protocols for predicting $\delta^{99}\text{Tc}$:
Model 1 – SO-ZORA-SSB-D/TZ2P-ZORA/COSMO // SC-ZORA-B3LYP/TZP-ZORA/COSMO
Model 3 – B3LYP/NMR-DKH/IEF-PCM(UFF) // TPSS/def2-SVP/IEF-PCM(UFF).

REFERENCES

- D. Papagiannopoulou, J. Label. Compd. Radiopharm., 2017, 60, 502-520.
- G. Hall et al., Inorg. Chem., 2016, 55, 8341-8347.
- M. Bühl, V. Golubnychiy, Magn. Reson. Chem., 2008, 46, S36-S44.
- T. F. C. B. Andrade et al., J. Phys. Chem. A, 2022, 126, 5434-5448.

ACKNOWLEDGEMENTS

The authors would like to thank the agencies FAPERJ (E-26/010.002261/2019 – EMERGENTES), CAPES (Finance Code 001), CNPq, and NWO - Netherlands for the financial support.

Ajuste espectral e determinação dos fatores de Franck-Condon usando a lei do gap de energia, uma comparação com cálculos DFT

Luiz S. R. Lamego (PQ),¹ Ana Carolina C. do Nascimento (PQ),¹ Nathan B. Soares (IC),¹ Fabio da S. Miranda (PQ).^{1*}

fsmiranda@id.uff.br

¹Instituto de Química, Universidade Federal Fluminense, Niterói, RJ, 24.220-071

Palavras Chave: Fatores de Franck-Condon, Lei do gap de energia, Ajuste espectral, Estados Excitados.

INTRODUÇÃO

A análise espectral é uma ferramenta importante para entender o estado excitado de qualquer molécula. A lei do gap de energia¹ permite determinar os fatores de Franck-Condon através do ajuste espectral de espectros de emissão. Nesse trabalho foram usadas duas equações para o ajuste espectral. A equação de 1 modo, para espectros sem estrutura vibrônica:

$$I(\bar{v}) = \sum_{v_M=0}^5 \left\{ \left(\frac{E_0 - v_M \hbar \omega_M}{E_0} \right)^3 \binom{S_M^{v_M}}{v_M!} \exp \left[-4 \ln(2) \left(\frac{\bar{v} - E_0 + v_M \hbar \omega_M}{\Delta \bar{v}_{1/2}} \right)^2 \right] \right\}$$

Onde: E_0 é o gap de energia entre o estado fundamental e o estado excitado, S_M é o fator de Huang-Rhys (constante de acoplamento vibrônico), $\hbar \omega_M$ é o espaçamento vibracional médio e Δv é a largura de cada componente vibrônica. Já para os espectros com estrutura vibrônica foi usada a equação de dois modos:

$$I(\bar{v}) = \sum_{v_M=0}^5 \sum_{v_L=0}^{15} \left\{ \left(\frac{E_{00} - v_M \hbar \omega_M - v_L \hbar \omega_L}{E_{00}} \right)^3 \binom{S_M^{v_M}}{v_M!} \binom{S_L^{v_L}}{v_L!} \times Q \right\}$$

$$Q = \exp \left[-4 \ln(2) \left(\frac{\bar{v} - E_{00} + v_M \hbar \omega_M + v_L \hbar \omega_L}{\Delta \bar{v}_{1/2}} \right)^2 \right]$$

Esta equação conta com dois modos vibracionais e duas constantes de acoplamento vibrônico, diferenciados pelas letras M (médio) e L (baixa frequência).

MÉTODOS

Para o ajuste espectral foi desenvolvido um Software dedicado que foi chamado de FCspec, escrito em Free Pascal (FPC 3.0.0) usando o Lazarus (1.6+dfsg-1). Os ajustes empregaram o método de Levenberg-Marquardt. Para testar o modelo de 1 modo foi usado o espectro de emissão do composto $[\text{Ru}(\text{bpy})_3(\text{PF}_6)_2$ a 298K dissolvido em acetonitrila, já para testar o modelo de 2 modos foi utilizado o espectro do $[\text{Ru}(\text{bpy})_3(\text{PF}_6)_2$ a 77K (EtOH/MeOH 4:1 vítreo) e do ligante dpqQX² a 298K dissolvido em CH_2Cl_2 . Para o ligante ainda foram realizadas análises vibrônicas usando os funcionais B3LYP, PBE0, cam-B3LYP, M06-2X e WB97XD (Gaussian09).

RESULTADOS

A Figura 1 mostra os ajustes espetrais dos espectros de emissão experimentais.

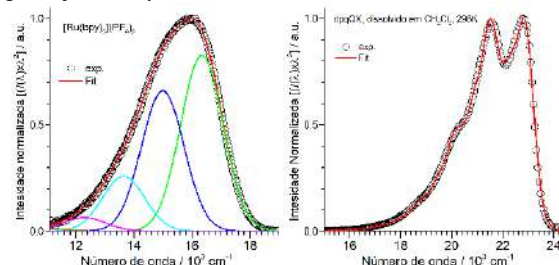
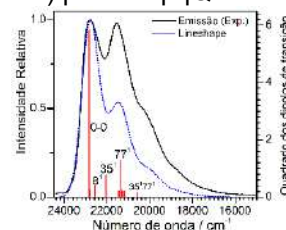


Figura 1. (Esquerda) ajuste de 1 modo juntamente com as contribuições vibrônicas para o $[\text{Ru}(\text{bpy})_3(\text{PF}_6)_2$. (Direita) Ajuste usando a equação de 2 modos para o ligante dpqQX.

A Figura 2 apresenta o espectro de emissão teórico (TD-DFT) para o dpqQX.





Theoretical Studies of the Hydrodehalogenation Reactions of CBrX₃ (X= H, F, Cl)

Alessandra F. Albernaz (PG),^{1*} Patrícia R. P. Barreto (PQ)².

albernaz@unb.br; prpbarreto@gmail.com

¹Instituto de Física, Universidade de Brasília - UnB, Brasília, DF, Brazil; ² Instituto Nacional de Pesquisas Espaciais, São José dos Campos, SP, Brazil

Palavras-Chave: (ozone-depleting substances, Halons, CH₃Br, CF₃Br, CCl₃Br).

INTRODUCTION

Halons, a group of chemicals with diverse industrial and consumer applications such as refrigeration, fire suppression, and foam manufacturing, possess desirable properties. Unfortunately, they are also potent ozone-depleting substances (ODSs) and greenhouse gases (GHGs), contributing to environmental harm. Their widespread use has led to significant ozone layer depletion and exacerbated global warming. To address this, the Montreal Protocol mandated the gradual phase-out of ODS production globally, sparking research into ODS treatment¹. Developing models for the thermal degradation of halogenated compounds in flames requires a deep understanding of reaction mechanisms, kinetic data, and thermodynamics. This knowledge is crucial for comprehending the incineration of hazardous industrial waste and developing more environmentally friendly incineration methods. It's particularly relevant when studying halogen abstraction from CBrF₃ (halon-1301) by hydrogen atoms during combustion, a process central to incineration but capable of producing toxic by products. Their potency to destroy ozone is measured by their Ozone Depleting Potential (ODP). Ozone depleting substances controlled by Montreal Protocol include:

- CFCs
- Halon (CF_xCl_yBr_z)
- Chlorocarbons
- Hydrochlorofluorocarbons (HCFCs)
- Hydrobromofluorocarbons (HBFCs)
- Bromocarbons
- Bromochloromethane

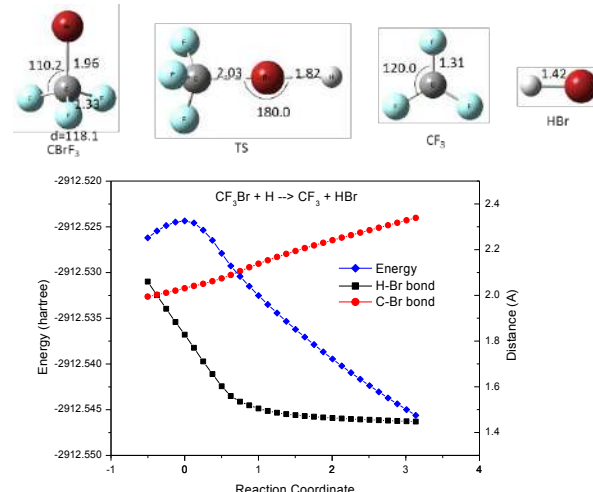


METHODS

The several Method was employed in our work to determine the potential energy surface (PES), geometries, vibrational frequencies and energies

of the reactants, transition states and products of the CBrX₃ + H₂ (X = H, F, Cl) reactive process. Vibrational frequencies were used to characterize the stationary points as minimum or transition states; the number of imaginary frequencies (0 or 1) indicates whether a minimum or a transition state has been located. To confirm that the transition state really connects reactants and products, the intrinsic reaction coordinate (IRC) calculations were determined. All calculations were performed with Gaussian16 program. Researchers employ advanced tools like RRKM/Master Equation, Transition State Theory (TST), and programs like MESMER² and Apuama³ to investigate the kinetics of hydrodehalogenation reactions of CBrX₃ (where X = H, F, Cl) across a wide temperature range (298–1500 K). These studies involve detailed potential energy surface mapping and utilize density functional theory (DFT) with various basis sets for all reaction species.

RESULTS



REFERENCES

- ¹ UNEP (2000) <http://www.unep.org/ozone/pdf/Montreal-Protocol2000.pdf>
- ² D. R. Glowacki, C.-H. Liang, C. Morley, M. J. Pilling and S. H. Robertson, MESMER: an open-source master equation solver for multi-energy well reactions, *J. Phys. Chem. A* 116 (2012) 9545–9560.
- ³ H. O. Euclides, P. R. P. Barreto, *J. Mol. Model.* (2017) 23: 176.

ACKNOWLEDGEMENTS

FAPDF - Institutional Process Number 00193.00001811/2022-95

Dynamics of vibronic intersystem crossing in lanthanide(III) complexes

Leonardo F Saraiva (PG)¹, Albano N. C. Neto (PQ)², Airton G. Bispo Jr (PQ)³, E. Kraka (PQ)⁴, Sergio A. M. Lima (PQ)¹, Ana M. Pires (PQ)^{*1}, Renaldo T. Moura Jr (PQ)⁵

Leonardo.f.saraiva@unesp.br; lsaraiva35@gmail.com

¹ São Paulo State University (UNESP), School of Technology and Sciences, Presidente Prudente, SP, Brazil; ² Physics Department and CICECO – Aveiro Institute of Materials, University of Aveiro, Portugal; ³ Institute of Chemistry (Unicamp), Campinas, SP, Brazil; ⁴ Department of Chemistry, Southern Methodist University, Dallas, TX, USA; ⁵ Department of Chemistry and Physics Center of Agrarian Sciences, Federal University of Paraíba.

Palavras Chave: *Eu(III) complexes, vibronic coupling, excited state dynamics.*

INTRODUCTION

Photonic materials based on trivalent lanthanide ions, Ln^{3+} , coordinated with organic ligands have garnered much attention due to their unique photophysical properties stemming from transitions across the $4f$ manifolds¹. Owing to the parity forbidden nature of such transitions, it is essential to populate the ligand excited state for an efficient energy transfer process from the S_1 and/or T_1 state to the Ln^{3+} ¹. While the direct excitation of S_1 occurs with high oscillator strength, the excitation of T_1 involves a spin-forbidden process, where alternative routes such as intersystem crossing (ISC) induced by the presence of Ln^{3+} are the main pathways to its population. However, ISC ($S_1 \rightarrow T_1$) strongly depends on the overlapping vibrational levels of the two excited states. In this sense, this work aims to introduce a theoretical procedure to derive the effect of vibronic coupling while rationalising the rates of intersystem crossing (ISC) in $[\text{Eu}(\text{TTA})_3(\text{H}_2\text{O})_2]$ complex.

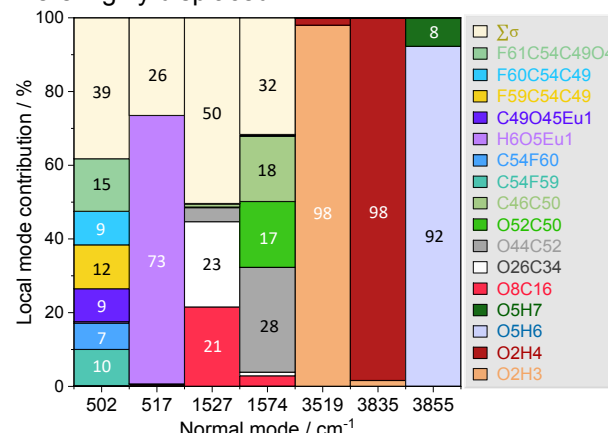
METHODS

All electronic structure calculations were performed in Orca 5.0.4 package², employing the Def2-TZVP basis set to describe all atoms besides Eu^{3+} , where an effective-core potential (MWB52) was used. The adopted methodology involves optimising both ground (S_0) and triplet excited state (T_1) geometries at the DFT level with the B3LYP functional, whereas singlet excited state (S_1) was optimised using TDDFT. Using their respective geometries, a numerical hessian calculation was performed for each state to access the excited-state dynamics, and the obtained parameters were used to calculate the ISC rates from Marcus-Levich theory.

RESULTS

The aforementioned methodology applied to $[\text{Eu}(\text{TTA})_3(\text{H}_2\text{O})_2]$ complex (*tris*-TTA) yielded an adiabatic energy difference of 6012 cm^{-1} . Despite this being a relatively high energy gap, the estimated ISC assumed reasonably large values of $8.3 \times 10^7 \text{ s}^{-1}$, indicating that large $S_1 - T_1$ energy splitting does not inherently result in low ISC, as in the strong coupling regime the total reorganization

energy (λ_M) of 3986 cm^{-1} possessed a pivotal contribution from Gaussian dependence. Such outcome underscores the vibronic driven nature of ISC in this complex, where shining light into the overlap of vibrational levels of S_1 and T_1 states becomes essential, which can be achieved by the Huang-Rhys factors. Under these circumstances, the symmetric and antisymmetric stretches of water displayed the highest overlap, with energies of 3519 , 3835 and 3855 cm^{-1} , followed by the torsion of the ligand scaffold of 1574 cm^{-1} . The decomposition of normal modes into local vibrational modes revealed the pronounced localised character of high-energy vibrations, which also possessed large values of λ_M as they were highly displaced.



CONCLUSIONS

Herein, we evaluated the dynamics of ISC in $[\text{Eu}(\text{TTA})_3(\text{H}_2\text{O})_2]$ complex using a novel theoretical approach. The results imply a vibronic-driven character of ISC, where further insights were harnessed by local vibrational theory, opening a pathway towards enhanced photonic compounds.

REFERENCES

- ¹ A. N. C. Neto, et al. Inorg. Chem. 2022, 61, 16333 – 16346.
² F. Neese, Wires Comp. Mol. Sci. 2022, e1606.

ACKNOWLEDGMENTS

FAPESP No. 2023/05718-9, GridUNESP.

Determinação da Importância do Alumínio Extra-rede na Protólise σC-C e σC-H do Isobutano Catalisada por HY e HUSY: Uma Abordagem DFT.

Fábio Jr. F. S. Henrique (PQ),^{1*} Marcelo M. Pereira (PQ)¹ e Pierre M. Esteves (PQ).¹

fabiojrhenrique@pos.iq.ufrj.br

¹Centro de Tecnologia, Instituto de Química, Cidade Universitária, Universidade Federal do Rio de Janeiro, Rio de Janeiro 21949-900 RJ, Brasil.

Palavras Chave: Catálise, Zeólita, Faujasita, Isobutano, DFT.

INTRODUÇÃO

A zeólita USY, com topologia faujasita (FAU), é um dos componentes ativos mais importantes presente no catalisador de craqueamento catalítico fluido (FCC), para converter gasóleo em produtos valiosos.¹ Acredita-se, que os catalisadores ácidos sólidos, como a zeólita USY, apresentem dois tipos de sítios ácidos: Brønsted e Lewis, relacionados com os grupos hidroxila em ponte na estrutura zeolítica e os alumínios extra-rede (EFAL), respectivamente.² Aqui, via modelagem molecular, buscamos compreender a influência do EFAL, no mecanismo de ativação do isobutano como molécula modelo em zeólitas FAU ácidas, nomeadamente HY e HUSY.



Figura 1. Proposta dos sítios ácidos ativos para a ativação de isobutano na HUSY.

MÉTODOS

Foram realizados estudos teóricos por meio do software Quantum Espresso®, utilizando a abordagem da Teoria do Funcional da Densidade (DFT) em condições periódicas de contorno. As coordenadas atômicas, foram otimizadas por meio de aproximações de gradiente generalizado (GGA) com o funcional de Perdew-Burke-Ernzerhof, empregando pseudopotenciais Ultrasoft de Vanderbilt. As interações de Van der Waals foram computadas por meio do método de correção de dispersão de Grimme (DFT-D3). As zeólitas HY e HUSY foram representadas por suas células unitárias primitivas. Os deslocamentos químicos teóricos de ressonância magnética nuclear (δ) foram calculados utilizando o software GIPAW, conforme a fórmula $\delta = -(\sigma - \sigma_{\text{ref}})$, tendo o hidrato $\text{Al}(\text{OH})_3$ como referência para o alumínio. Foram propostos sete modelos de sítios ácidos de Brønsted envolvendo o EFAL.

RESULTADOS

Resultados teóricos indicaram que a espécie $[\text{Al}(\text{H}_2\text{O})_2]^{3+}$, coordenada ao anel de sodalita de 6 membros, correspondia de maneira mais precisa à ressonância magnética nuclear (RMN) experimental da HUSY. As barreiras energéticas para a protólise das ligações $\sigma\text{C-H}$ do isobutano eram de 44,0 kcal/mol e 30,2 kcal/mol nas zeólitas HY e USY, respectivamente. O catalisador HUSY exibiu uma barreira mais baixa devido à menor obstrução estérica no sítio ácido, permitindo uma aproximação mais eficaz do hidrogênio no carbono terciário do isobutano. Na desprotonação do carbônio terc-butil e na formação da olefina isobuteno, ambas as zeólitas apresentaram baixas barreiras energéticas (2,9 kcal/mol para HY e 0 kcal/mol para HUSY), graças à estabilização do carbocátion terciário por interações de Van der Waals na estrutura zeolítica. A protólise da ligação $\sigma\text{C-C}$ do isobutano resultou em barreiras energéticas de 37,8 kcal/mol para HY e 31,8 kcal/mol para HUSY. No caso do HUSY, uma barreira energética menor foi observada devido ao maior acesso ao sítio ácido. No entanto, a formação do carbocátion sec-propil revelou uma quimissão significativa entre os oxigênios na estrutura de ambas as zeólitas, com valores registrados de 23,5 kcal/mol e 15,1 kcal/mol para HY e USY, respectivamente.

CONCLUSÕES

Estudos teóricos nos permitiram construir um modelo de EFAL para o HUSY por meio de cálculos teóricos de RMN de ^{27}Al , confirmados por dados experimentais. Além disso, observamos que o HUSY apresentou barreiras de energia mais baixas para a protólise das ligações $\sigma\text{C-H}$ e $\sigma\text{C-C}$ devido a possuir maior acidez e sítios ácidos mais acessíveis para possíveis reações.

REFERÊNCIAS

1. Garcia-Martinez, J.; Li, K.; Krishnaiah, G. Chem. Commun. 2012, 48, 11841–11843.
3. Corma, A.; Fornés, V.; Rey, F. Appl.Catal. 1990, 59, 267–274.

AGRADECIMENTOS

Os autores agradecem à CAPES, CNPq, PGQU e Petrobras pelo seu apoio.

Predicting Pt-195 NMR chemical shift in Pt(II) complexes using the new NMR-ZORA basis sets

Joyce H. C. e Silva (PG),¹ Diego F. S. Paschoal (PQ)^{1*}

diegopaschoal01@gmail.com

¹Núcleo de Química Teórica e Computacional de Macaé, Polo Ajuda, Instituto Multidisciplinar de Química, Centro Multidisciplinar UFRJ-Macaé, Universidade Federal do Rio de Janeiro, Macaé, RJ, Brazil.

Keywords: Cancer, Pt(II) complexes, NMR, Relativistic effects.

INTRODUCTION

Nuclear Magnetic Resonance (NMR) spectroscopy has been widely used in characterization, reactivity and QSAR studies of Pt(II) complexes with anticancer potential^{1,2}. The theoretical prediction of the Pt-195 NMR chemical shift ($\delta^{195}\text{Pt}$) is a complicated task, since computational aspects such as electronic correlation, basis sets, solvent and relativistic effects must be well described². In the present study, a computational protocol for predicting the $\delta^{195}\text{Pt}$ in Pt(II) complexes with a new NMR-ZORA basis sets were proposed.

METHODS

Initially, the NMR-DKH basis sets² were recontracted as NMR-ZORA for H-He, Li-Ne, Na-Ar, and Pt atoms, with the contraction coefficients through the coefficients of atomic orbitals calculated at HF-SC-ZORA level. The structures of Pt(II) complexes studied were optimized and characterized as a minimum point on the potential energy surface (PES) at B3LYP/LANL2TZ(f)/def2-SVP/C-PCM level. The $\delta^{195}\text{Pt}$ was calculated according to equation: $\delta^{195}\text{Pt}_{\text{calc}} = \sigma_{\text{ref}} - \sigma_{\text{calc}}$, where σ_{ref} is the calculated shielding constant for internal reference $[\text{PtCl}_6]^{2-}$ in D_2O .² The Pt(II) complexes cisplatin and carboplatin were considered in the construction of the protocol, with $\sigma^{195}\text{Pt}$ calculated at GIAO-DFT-Functional-SC-ZORA/NMR-ZORA/C-PCM level, considering 39 functionals. The role of the relativistic effects and the basis sets was also evaluated. The best protocol was applied in 30 Pt(II) complexes. All these calculations were carried out in ORCA 5.0.3 program. Besides, 4-components calculations considering 6 DFT functionals and 3 basis sets were also performed in ReSpect 5.1.0 program.

RESULTS

Considering the calculated results for cisplatin and carboplatin with the 39 functionals at GIAO-DFT-Functional-SC-ZORA/NMR-ZORA/C-PCM level, the GGA functionals presented the smallest relative deviations (RD), with the BP86 and OPBE functionals presenting a mean relative deviation (MRD) of only 0.3% in relation to the experimental values. Table 1 presents an evaluation of the role

of relativistic effects, considering the BP86/NMR-ZORA/CPCM (Model 0) and BP86-SC-ZORA/NMR-ZORA/CPCM (Model 1) protocols, and of the basis sets, considering the BP86-SC-ZORA/SARC-TZVPP-ZORA/ZORA-def2-TZVPP/CPCM (Model 2) and BP86-SC-ZORA/jorge-TZP-ZORA/CPCM (Model 3) protocols in predicting $\delta^{195}\text{Pt}$. Furthermore, the best result obtained in the calculations of 4-components, 4c-KT2/dyall.vqz (Model 4) are also presented.

Table 1. Calculated $\delta^{195}\text{Pt}$ (in ppm) for cisplatin and carboplatin with distinct protocols.

Protocols	cisplatin	carboplatin
Model 0	-895	-399
Model 1	-2094	-1707
Model 2	-2348	-1874
Model 3	-1294	-861
Model 4	-2147	-1853
Expt.	-2097	-1714

The Model 1 was applied in 30 Pt(II) complexes, presenting a MRD of only 4.5%, with a coefficient of determination (R^2) of 0.9853 (Fig. 1).

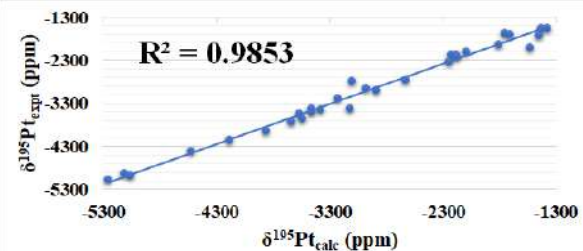


Fig. 1. Linear regression between calculated (Model 1) and experimental $\delta^{195}\text{Pt}$ for the set of 30 Pt(II) complexes studied.

CONCLUSIONS

The protocol BP86-SC-ZORA/NMR-ZORA/CPCM //B3LYP/LANL2TZ(f)/def2-SVP/CPCM, named as Model 1, presented itself as an excellent alternative for the study of $\delta^{195}\text{Pt}$ in Pt(II) complexes, showing the quality of NMR-ZORA basis sets.

REFERENCES

¹A.C. Tsipis, I.N. Karapetsas, *Magn. Reson. Chem.* **2017**, 55, 662.

²D. Paschoal et al., *J. Comput. Chem.* **2016**, 37, 2360.

ACKNOWLEDGMENTS

The authors would like to thank the Brazilian agency FAPERJ (E-26/201.336/2022 – BOLSA and E-26/210.070/2022) and CAPES (Finance Code 001) for the financial support.



Simulação computacional do processo de adsorção do peptídeo difenilalanina no fagrafeno prístico e com a presença de defeito

Brena Maria Freire de Sousa (PG),¹ Tarciso Silva de Andrade Filho (PQ).^{1*}

brenafreire@unifesspa.edu.br; tarcisofilho@unifesspa.edu.br

¹Programa de Pós-Graduação em Química, Universidade Federal do Sul e Sudeste do Pará, Marabá-PÁ, Brazil;

²Faculdade de Física, Universidade Federal do Sul e Sudeste do Pará, Marabá-PÁ, Brazil.

Palavras Chave: Peptídeos; Difenilalanina; Fagrafeno; Adsorção; DFT.

INTRODUÇÃO

Estudos experimentais e teóricos estão sendo realizados tendo como base o aminoácido difenilalanina (FF)¹. Estes estudos são motivados por esta molécula ser um dipeptídeo extraído do polipeptídeo β-amiloíde, principal componente presente nas placas amiloides em pacientes com Alzheimer e Parkinson, somada a sua capacidade de formar estruturas secundárias². Além disso, a FF possui uma boa interação com superfícies metálicas. Essa interação expande caminhos para a investigação da produção de novos materiais conjugados baseados no grafite para a construção de dispositivos biológicos³.

Diante do exposto, este trabalho se objetivou em compreender por meio de cálculos teóricos a interação em nanoescala do dipeptídeo FF com a estrutura do fagrafeno prístico e com a presença de defeitos. Alguns dos passos galgados para chegar lá foram: verificar o tipo de adsorção entre a FF e o fagraneno (PG – *Phagraphene*), descrever se os sistemas funcionam como bons sensores biológicos, bem como, analisar a transferência de carga e verificar o tipo de dopagem no sistema mais estável.

MÉTODOS

Os cálculos relacionados aos processos de interação da FF no PG foram realizados no pacote de simulação Quantum Espresso, o qual é um conjunto integrado de códigos computacionais para cálculos de estruturas eletrônicas e modelagem de materiais com base na DFT⁴.

RESULTADOS

Para iniciar a simulação envolvendo o processo de adsorção, consideramos sete possíveis configurações formadas entre o adsorvente e o adsorvato sob investigação. O conjunto de dados, energia de adsorção, distância e pós processamento, mostram que todas as configurações no PG prístico e com a presença de defeito são estáveis, a FF interagiu com PG, preferencialmente, via empilhamento π-π deslocado.

Nossos resultados também evidenciaram que a presença de defeito na estrutura do PG aumentou a reatividade dos sistemas, mas não alterou de forma significativa a transferência de carga dos complexos, mostrando

que os mesmos são estáveis quando se trata da presença desta interferência. A ligação de Van der Waals é a interação mais forte formada entre a molécula FF e a nanocamada de PG. A superfície do PG possui capacidade de adsorção moderada revelando ser um possível sensor do peptídeo FF.

O estudo da adsorção da FF no PG nos permitiu evidenciar a fisssão que ocorre no sistema, uma análise mais detalhada nos complexos de interesse possibilitou verificar como estava ocorrendo a interação entre a superfície e a molécula. As curvas TDOS e PDOS possibilitaram avaliar a dopagem extrínseca tipo-p na configuração mais estável. A presença de defeitos na estrutura do PG proporcionou um aumento na reatividade de alguns dos sistemas.

CONCLUSÕES

Os cálculos teóricos aqui realizados possibilitaram descrever que o PG funciona como um excelente sensor do peptídeo FF. Os resultados obtidos aqui podem prover como um guia útil para a exploração de novos materiais híbridos orgânicos/inorgânicos em diversas aplicações biomédicas. Até onde sabemos este é o primeiro estudo teórico sobre as interações que envolvem a FF e o PG para futuras aplicações biomédicas.

REFERÊNCIAS

¹ YAN, X.; ZHU, P.; LI, J. Self-assembly and application of diphenylalanine-based nanostructures. *Chem. Soc. Rev.*, 2010, vol. 39, p. 1877.

² BASAVALINGAPPA, V. et al. Diphenylalanine-Derivative Peptide Assemblies with Increased Aromaticity Exhibit Metal-like Rigidity and High Piezoelectricity. *ACS Nano*, 2020, v. 14, p. 7025–7037.

³ TOMBA, G. et al. Structure and Energetics of Diphenylalanine Self-Assembling on Cu (110). *J. Phys. Chem. A*. 2007, v. 111, p. 12740–12748.

⁴ GIANNONI, P. et al. QUANTUM ESPRESSO: a modular and open-source software project for quantum simulations of materials. *J. Phys Condens*, 2009, v. 21, p. 395502.

AGRADECIMENTOS

CNPq e UNIFESSPA

STUDY OF THE CORRELATION BETWEEN HAMMETT CONSTANTS AND NITROBENZENES SENSITIVITY (h_{50})

Roberta Siqueira Soldaini de Oliveira (PG),¹ Itamar Borges Jr.(PQ).^{1*}

roberta.siqueira@ime.eb.br; itamar@ime.eb.br

¹ Departamento de Química, Instituto Militar de Engenharia (IME), Rio de Janeiro, RJ, 22290-270, Brazil.

Keywords: Nitrobenzenics; Hammett's theory; Substituent effects..

INTRODUCTION

Nitrobenzenic explosives are energetic materials usually displaying high performance combined with low initiation sensitivity. For these reasons, they have been the most used type of explosives in warlike devices¹. Their sensitivity can be usually measured by the parameter h_{50} which is the height measured by dropping a weight of a given mass over a small amount of explosive that results in 50% of the drops triggering the explosive material². Our group has been seeking a precise correlation between structure and property for several types of compounds using accurate methods of characterizing the electronic structure of molecules, such as atomic charge and electronic density. This methodology has been especially useful in studying the sensitivity of explosives using the specific property of h_{50} .³⁻⁶ In this work, we seek the structure–property correlation through the constants proposed in Hammett's theory⁷⁻⁹ trying to verify if the experimental results of h_{50} observed for a family of nitrobenzenes can be related to such constants.

METHODS

Forty-two nitrobenzenic molecules of practical interest as energetic materials were investigated. DFT-M06-2X/TZVP single point calculations of the molecules employing the Gaussian 03 software were carried out employing published geometries determined at the same level. We used our machine-Learning (ML)-based σ constants.⁸⁻⁹ Experimental h_{50} values were directly confronted with the calculated values of Hammett's constants for the chosen nitrobenzene substituents and a possible correlation between these magnitudes was sought.

RESULTS

The h_{50} values when plotted versus the sigma values... generated the following graphical results shown in figure 1.

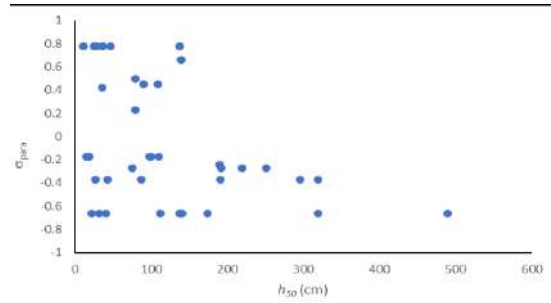
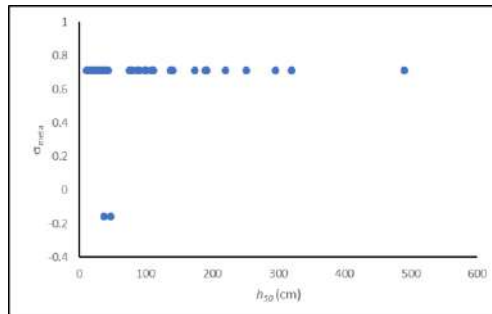


Figure 1. Best correlations h_{50} and calculated Hammett's constants.

It is noticed that there is not a good correlation between the quantities considered.

This may be related to the fact that our group of nitrobenzenic molecules are not disubstituted structures. Because they are polysubstituted, it was necessary to take a fragment of them in common as a reference and then visualize different possibilities of substitution in meta and para positions.

CONCLUSIONS

Hammett's theory is based on disubstituted molecules. Directing its possible application in rings with multiple ligands showed that a more efficient deepening of the methodology to be used is necessary. It is in this direction that the next steps of this research will be directed.

REFERENCES

- 1 D. M. Badgjar, M. B. Talawar, S. N. Asthana, P. P. Mahulikar, Advances in Science and Technology of Modern Energetic Materials: An Overview, *J. Hazard. Mater.* 2008, 151, 289-305.
- 2 (D. Mathieu, Toward a Physically Based Quantitative Modeling of Impact Sensitivities, *J. Phys. Chem. A* 2013, 117, 2253-2259; [b] D. Mathieu, T. Alaimo, Impact Sensitivities of Energetic Materials: Exploring the Limitations of a Model Based Only on Structural Formulas, *J. Mol. Graph.* 2015, 62, 81-86.
- 3 G. Anders, I. Borges, Topological Analysis of the Molecular Charge Density and Impact Sensitivity Models of Energetic Molecules, *J. Phys. Chem. A* 2011, 115, 9055-9068
- 4 R. S. S. De Oliveira, I. Borges, Correlation between Molecular Charge Densities and Sensitivity of Nitrogen-Rich Heterocyclic Nitroazole Derivative Explosives, *J. Mol. Model.* 2019, 25, 314; [b] M. a. S. Oliveira, I. Borges, On the Molecular Origin of the Sensitivity to Impact of Cyclic Nitramines, *International Journal of Quantum Chemistry* 2019, 119, 14.
- 5 R. S. S. De Oliveira, I. Borges, Correlation Between Molecular Charge Properties And Impact Sensitivity Of Explosives: Nitrobenzene Derivatives; Propellants, Explosives, Pyrotechnics, Vol.46, pags309-321
- 6 (a) L. P. Hammett, *Chem. Rev.*, 1935, 17, 125-136; (b) L. P. Hammett, *J. Chem. Phys.*, 1937, 4, 613-617.
- 7 G. Monteiro-de-Castro, J. C. Duarte, I. Borges Jr., *J. Org. Chem.*, 2023, DOI: 10.1021/acs.joc.3c00410.
- 8 G. Monteiro-de-Castro, J. C. Duarte, I. Borges Jr., *J. Comp. Chem.*, 2023, DOI:10.1002/jcc.27195

ACKNOWLEDGMENTS

CNPq, FAPERJ, and CAPES.

Assessment of a computational protocol to predict the standard reduction potential of Fe(III) complexes

Rayane M. Cavalcante (IC),^{1*} Letícia S. Amorim (PG),¹ Diego F. S. Paschoal (PQ)¹

rayanemeloc@gmail.com; diegopaschoal01@gmail.com

¹Núcleo de Química Teórica e Computacional de Macaé, Polo Ajuda, Instituto Multidisciplinar de Química, Centro Multidisciplinar UFRJ-Macaé, Universidade Federal do Rio de Janeiro, Macaé, RJ, Brazil.

Keywords: Cancer, Iron complexes, Reduction potential, Basis sets, DFT.

INTRODUCTION

Iron complexes have demonstrated activity against resistant cancer cells and selective cytotoxicity. These complexes act, in general, as prodrugs, with redox reactions as the main biotransformation. The computational study of Fe complexes is an important tool to help in the search of new complexes with antineoplastic potential.¹ So, the present study presents the construction of a computational protocol for predicting the standard reduction potential (ϵ^0) of Fe(III) complexes.

METHODS

The $[\text{Fe}(\text{bipy})_3]^{+3/+2}$ system, whose experimental data of ϵ^0 is available (1.030 V),² was selected as a model for the development of the computational protocol. The experimental data was obtained by cyclic voltammetry in aqueous solution, with the normal hydrogen electrode (NHE) as reference. In this work, ϵ^0 was calculated based on the half-reaction of the electrochemical cell in relation to the NHE. The ϵ^0 was obtained according to equation:

$$\epsilon^0 (\text{V}) = 27.2114 \times (\text{G}_{\text{ox}} - \text{G}_{\text{red}}) - \epsilon_{\text{abs}}^0 (\text{NHE})$$

with the ΔG values obtained from the construction of a thermodynamic cycle, with the optimized structures and thermal corrections obtained in the gas phase. The implicit SMD model, with the dielectric constant set for water, was used for including the solvent effects. For the construction of the computational protocol, the role of the DFT functional (32 functionals), iron basis set (FEBS = 15 basis sets), ligands basis sets (LBS = 06 basis sets), and relativistic effects (DKH2) was assessed in predicting the ϵ^0 . The calculations were performed in ORCA 5.0.3 program.

RESULTS

First, the role of the DFT functional was evaluated at DFT-Functional/def2-SVP level (Fig. 1). The results suggest the choice of functionals from different classes to evaluate the role of FEBS, with the hybrid meta-GGA M06-2X and the GGA PWP, that presented absolute deviations (AD) of 34mV and 113mV, respectively, being selected. Regarding the role of the FEBS (Fig. 2), the results show a compromise between the DFT functional and the FEBS, with the PWP/LANL2DZ/def2-SVP

presenting an AD of only 29mV, and the M06-2X/def2-SVP/def2-SVP presenting an AD of only 34mV. Recently, Orjuela et al.³ obtained an AD of 330 mV in the direct calculation of ϵ^0 for the $[\text{Fe}(\text{bipy})_3]^{+3/+2}$ system, that is, the results of the present study show a better agreement with the experiment. Besides, a total of 9 protocols presented AD below 100mV, being selected for further application in the study of ϵ^0 of other Fe(III) complexes.

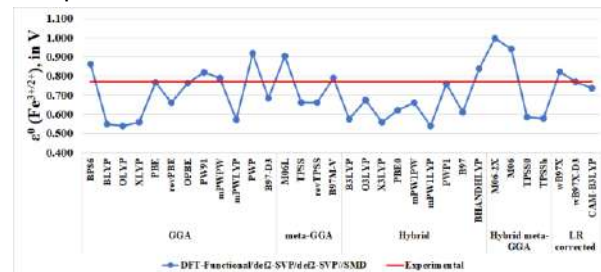


Fig. 1. Calculated ϵ^0 at DFT-functional/def2-SVP level.

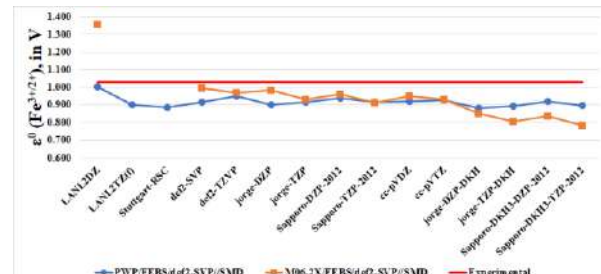


Fig. 2. Calculated ϵ^0 at PWP/FEBS/def2-SVP/SMD and M06-2X/FEBS/def2-SVP/SMD levels.

CONCLUSIONS

The computational protocols obtained in the study show an excellent agreement with the experimental value of ϵ^0 for the $[\text{Fe}(\text{bipy})_3]^{+3/+2}$ system. The role of LBS is also being analyzed, as well as the application of the protocols in a set of 10 Fe(III) complexes.

REFERENCES

- ¹BASU, U. et al. *Coord. Chem. Rev.* **2020**, v. 417, p. 21339.
- ²RULÍSEK, L. *J. Phys. Chem. C* **2013**, v. 117 p. 16871–16877.
- ³ORJUELA, A. L. et al. *RSC Adv.* **2022**, v. 12, p. 24077.

ACKNOWLEDGMENTS

The authors would like to thank the Brazilian agency FAPERJ (E-26/201.336/2022 – BOLSA and E-26/210.070/2022) and CAPES (Finance Code 001) for the financial support.



PROPOSITION OF CANDIDATES FOR SARS-CoV-2 M^{pro} INHIBITORS BASED ON MOLECULAR MODELING OF THIAZOLES

Mariana S. Gomes (PG),^{1*} Vinicius S. P. Nunes (PQ),¹ Diego F. S. Paschoal (PQ)¹

gomesmarianna997@gmail.com; diegopaschoal01@gmail.com

¹NQTCM: Núcleo de Química Teórica e Computacional de Macaé, Polo Ajuda, Instituto Multidisciplinar de Química, Centro Multidisciplinar UFRJ-Macaé, Universidade Federal do Rio de Janeiro, Macaé, RJ, Brazil.

Keywords: SARS-CoV-2, thiazoles, bioinformatics, molecular docking, ADMET

INTRODUCTION

SARS-CoV-2 is formed by non-structural and structural proteins. An important molecular target of this virus is nsp5, also called main protease, M^{pro} or 3CL^{pro}, which is a non-structural protein, being a cysteine protease involved in virus replication inside the host cell¹.

In studies that aim to reposition known drugs for the treatment of COVID-19, nitazoxanide (NTZ) is a thiazole with some prominence. This pro-drug has shown great potential in inhibiting replication *in vitro* of MERS-CoV and other coronaviruses. In the context of COVID-19, *in vitro* studies showed that nitazoxanide had an EC₅₀ of 2.12 µM for SARS-CoV-2, similar to the EC₅₀ value of 2.99 µM for MERS-CoV^{3,4}.

The present study searches for potential M^{pro} inhibitors of SARS-CoV-2 through the molecular modeling of thiazoles and the search in databases available in the literature.

METHODS

Initially, the NTZ and a set of 87 NTZ-like thiazoles, with biological activity described in the literature, were selected. The structure of these ligands were optimized and characterized as a minimum point on the potential energy surface through harmonic frequency calculations using the semiempirical PM3 level in the gas phase. These calculations were performed with the ORCA 5.0.1 program.

The structure of M^{pro} (PDB 6W63) was obtained from the Protein Data Bank (PDB). Molecular docking studies were performed with the Autodock Vina 1.1.2 software. Besides, we carried out an evaluation of the pharmacokinetic and toxicological (ADMET) profile *in silico*, through the following servers: pkCSM pharmacokinetics⁵, OSIRIS Property Explorer⁶ and StopTOX². In addition, an analysis of ligand-protein interactions was performed using the 2D interaction map of the Discovery program, in order to understand the types of interactions that occur between thiazoles and the active site of M^{pro}.

RESULTS

From the molecular docking studies of the NTZ and 87 selected thiazoles with the M^{pro} protein, those ligands that showed binding affinity (BA),

higher than the NTZ (BA = 6.4 kcal mol⁻¹) were discarded for the other steps of the analysis, since they showed a lower interaction with the M^{pro}, when compared with NTZ. With analysis of the interaction map of NTZ with the active site of M^{pro}, two strong interactions of hydrogen bonds with residues of His41 and Ser144 can be highlighted, as well as a Pi-Sulfur interaction with Cys145. It is important to highlight that the residues Cys145 and His41 represent the catalytic dyad of M^{pro} and are responsible for its activity of cleaving other proteins. In the next step, the ADMET profile of compounds was analyzed on the servers pkCSM, OSIRIS, and StopTOX. The compounds that showed disadvantageous properties for a possible drug against SARS-CoV-2, such as hepatotoxicity, acute oral toxicity, mutagenicity, tumorigenicity and irritant effects, were discarded. Finally, an analysis of the interaction maps of thiazoles selected in the ADMET step with M^{pro} was carried out, and those that presented interactions with the catalytic dyad of the enzyme in a similar way that NTZ interacted were selected as promising, being the compounds of ID 78 and 79.

CONCLUSIONS

The present work carried out an *in silico* evaluation of the interaction of NTZ and 87 thiazoles with the M^{pro} protein of the SARS-CoV-2. From the molecular docking studies, ADMET profile of the compounds and the analysis of the profile of the 2D interaction maps with the active site of the target, a set of 2 thiazoles, named compounds 78 and 79, were selected for the next step of the work, where molecular dynamics simulations are being performed for an evaluation under thermodynamic conditions.

REFERENCES

- R. ARYA et al. *J. Mol. Biol.* **2021**, 433, 2, 166725.
- J.V.B. BORBA et al. *Environ. Health Perspect.* **2022**, 130, 2.
- Y.A. HELMY et al. *J. Clin. Med.* **2020**, 9, 4, 1225.
- G.M. NITUDESCU et al. *Int. J. Mol. Med.* **2020**, 46, 467-488.
- D.E.V. PIRES et al. *J. Med. Chem.* **2015**, 58, 9, 4066–4072.
- T. SANDER et al. *J. Chem. Inf. Model.* **2009**, 49, 2, 232–246.

ACKNOWLEDGMENTS

The authors would like to thank the Brazilian agency FAPERJ (E-26/203.818/2021 – BOLSA, E-26/210.070/2022 and E-26/201.336/2022 – BOLSA) and CAPES (Finance Code 001) for the financial support.

Computational Studies of Coffee Extracts as Carbon Steel Corrosion Inhibitors

Giuliana Pineschi Braun (IC),¹ Cintia Braune Guerra (PG)², Lilian Ferreira de Senna (PQ)³, Dalva Cristina Baptista do Lago (PQ)⁴ Maurício Tavares de Macedo (PQ).^{1*}

gbbraun467@gmail.com; cruzmtmr@gmail.com

Universidade do Estado do Rio de Janeiro (UERJ)

Palavras Chave: *Coffee extracts, Corrosion inhibitors, DFTB, DFT, Molecular modelling*

INTRODUÇÃO

It is known that corrosion inhibitors act at the interface between the metal and the acidic solution through adsorption processes that stops the dissolution of the metal surface. Recent studies have shown that extracts of coffee could be an interesting “green” alternative for the corrosion protection of carbon steel. Studies suggest that the kind of phenolic compound present in the coffee extracts affects their inhibitory efficiency. This present work intends to add relevant information about energetic, geometric and electronic properties, obtained with a computational model that mimics the molecular adsorption of a set of coffee compounds on the carbon steel, due to the numerous experimental studies on anticorrosive properties of coffee extracts.

MÉTODOS

A nanostructured iron model containing 127 atoms (Fe_{127}) was built keeping Fe–Fe distances according to the experimental values of the metal bulk (2.486 Å and 2.870 Å). The **caffeine**, **querceutina**, **catechin**, **kaempferol**, **ferulic acid**, **caffeoic acid** and **syringic acid** (Figure 1) were relaxed on plane 110 of Fe_{127} . The adsorption process was firstly performed in Tight-Binding approximation (DFTB). Single point calculations in DFT level, using B3LYP/LANL2DZ/6-31G(d,p) methodology, were performed, removing the iron atoms located at edges, decreasing the cluster size to Fe_{56} . The preferential electron spin state was determined, and the adsorption energies were corrected with the counterpoise method. All calculations were performed using the G09W program suite and the structures and orbitals were visualized in Gaussview 5.0.

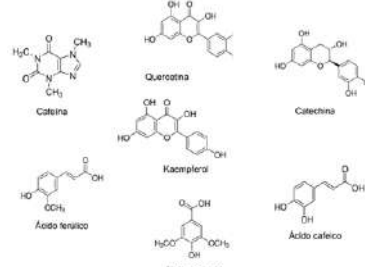


Figure 1. Coffee compounds tested individually.

RESULTADOS

PAA	Anchorage (NA)	Sites (natureza)	Σ Carga Ferro (e)	Energia adsorção (kcal/mol)
Cafeína (I)	1	Ar	-0,214	-44,70
Quercetina (II)	1	Ar	-0,190	-71,10
Catequina (III)	1	Ar	-0,039	-82,18
Ác. Ferúlico (IV)	2	D, Ar	+0,262	-107,08
Kaempferol (V)	2	O _{ch} , Ar	-0,132	-116,71
Ác. Caffeico (VI)	3	O _{ch} , D, Ar	+0,074	-122,78
Ác. Siringico (VII)	4	O _{ch} , OH _{ch} , C _{ch} , Ar	+0,094	-133,37

Table 1. Anchoring number, adsorption site, Fe charge density and adsorption energy, for compounds adsorbed on iron.

Caffeine is the compound with the weakest adsorption on Fe agglomerate (Tab. 1). On the other hand, it is the one that most transfers electronic density to the metal (-0.214 e). Among all tested compounds, the chlorogenic acids have higher adsorption energies, especially the syringic acid (-133.37 kcal mol⁻¹). However, unlike caffeine and flavonoids, these compounds decrease the electron density in the iron cluster.

CONCLUSÕES

The order of adsorption strength is followed by the growth of the number of anchor points. Chlorogenic acids, despite adsorbing more strongly, do not tend to transfer charge to iron. Among the flavonoids, kaempferol showed adsorption close to those observed for chlorogenic acids, but with good charge transfer to the iron model. The species that transfers the most charge density to iron is caffeine, which in the literature presents excellent results as a corrosion inhibitor.

REFERÊNCIAS

- FOUDA, A.E.A.S., EL-ASKALANY, A.H., MOLOUK, A.F.S. *et al.* *Sci Rep* 11, 21672, 2021.
 COSTA, M. A. J. L.; DE GOIS, J. S.; TOALDO, I. M., BAUERFELDT, A. C. F., BATISTA, D. B., BORDIGNON-LUIZ, M., LAGO, D. C. B., LUNA, A. S., SENNA, L. F. *Materials Research*, v. 23, n. 5, 2020.
 RAMOS, S. A. F.; SENNA, L. F. D.; LAGO, D. C. B. D. *Materials Research*, v. 22, 2019

AGRADECIMENTOS

CAPES, Universidade do Estado do Rio de Janeiro (UERJ)

Complexo de inclusão Cânfora@ β -Ciclodextrina: Um estudo computacional

Ismael de Alencar Pessoa (IC), Igor José Gomes da Silva (PQ), João Miller de Melo Henrique (PQ), Iran da Luz Sousa (PQ). *

ismael.alencar@aluno.ifsertao-pe.edu.br; iran.sousa@ifsertao-pe.edu.br

¹ Instituto Federal de Educação, Ciência e Tecnologia do Sertão Pernambucano, 56200-000 Ouricuri-PE, Brazil

Palavras Chave: (Cânfora, β -Ciclodextrina, Complexo de Inclusão).

INTRODUÇÃO

As ciclodextrinas (CDs) apresentam uma estrutura espacial cônica cuja a conformação assumida confere a esta molécula importantes propriedades físico-químicas, como a capacidade de encapsular diferentes tipos de espécies apolares no interior da sua cavidade hidrofóbica, formando complexos de inclusão - estruturas do tipo hóspede-hospedeiro - com diferentes compostos orgânicos, inorgânicos e biológicos sem ligação covalente. [1]

O presente trabalho tem como objetivo estudar teoricamente os efeitos do confinamento na estrutura eletrônica da cânfora encapsulada na β -Ciclodextrina, focando nos fatores envolvidos na energia de complexação e nas mudanças conformacionais.

MÉTODOS

Neste trabalho, foi realizada uma varredura energética via método semi-empírico PM6 de forma a obter as energias de complexação entre a cânfora e a β -CD. A aproximação Cânfora-Ciclodextrina foi definida através da coordenada de varredura (d), sendo a distância entre o átomo de oxigênio da cânfora e o centro da β -CD. A energia de complexação (Eq. 1). O esquema de inclusão da cânfora, ao longo da distância (d), com intervalos de -6 a 6 angstrom (\AA), com variações de 1 \AA em cada passo foi considerado.

$$\text{E}_{\text{complexação}} = E_{\beta\text{-CD}} + E_{\text{Cânfora}} - E_{\text{Cânfora}@\beta\text{-CD}} \quad (1)$$

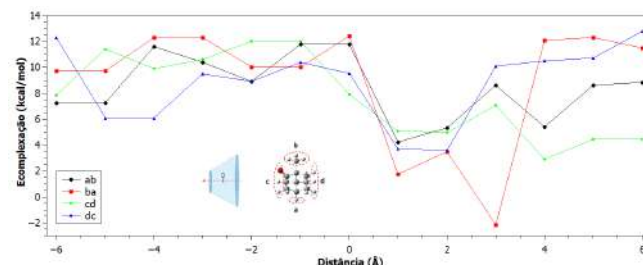
Foram considerados diferentes modos de orientações para a cânfora para o processo de inclusão, conforme esquema reportado por Celebioglu *et al* [2] (Fig. 1). Todos os cálculos foram realizados no Gaussian 09 (Rev. A02). [3]

RESULTADO

Os resultados derivados da análise energética do processo de inclusão do complexo Cânfora@ β -CD revelaram que as maiores energias de complexação encontram-se na orientação dc, a uma distância de 6 \AA [Estrutura 6-dc] (Fig. 1). Esta geometria molecular apresenta energia de complexação igual a -12,8 kcal.mol⁻¹. Entretanto, é interessante notar que a estrutura correspondente à orientação ab e distância de 0 \AA

[estrutura 0-ab] exibe uma energia relativamente próxima, registrando 12,4 kcal.mol⁻¹.

Figura 1. Energia de complexação para o processo de inclusão da cânfora na β -CD.



Para a estrutura 6-dc, verifica-se que cânfora apresenta-se praticamente na parte externa da β -CD. Entretanto, verifica-se uma possível ligação de hidrogênio no complexo formado e isso pode ter favorecido a estabilização do sistema. Já para o complexo 0-ab verifica-se que a molécula hóspede encontra no interior na cavidade da Ciclodextrina, e verifica-se também possíveis pontos de estabilização via ligação de hidrogênio. Essas possíveis interações intermoleculares serão investigadas posteriormente. No pôster, iremos mostrar as estruturas otimizadas.

CONCLUSÕES

No processo de inclusão é verificado que várias estruturas apresentam altas energias de complexação, em torno 12 kcal/mol. As estruturas com maiores energias de complexação são estabilizadas por ligação de hidrogênio. O trabalho encontra-se em andamento e no pôster iremos mostrar os resultados das nossas investigações utilizando a ferramenta NBO.

REFERÊNCIAS

¹Araújo, M, V, G. et al. Molecular and Biomolecular Spectroscopy, 2009, 1, 165.

²Celebioglu, A., Aytac, Z., Kilic, M.E. et al. J Mater Sci, 2018, 53, 5436.

³www.gaussian.com

AGRADECIMENTOS

Ao CENAPAD-UFC (Centro Nacional de Processamento de Alto Desempenho – Universidade Federal do Ceará) pela infraestrutura computacional. Ao IFsertãoPE/Ouricuri pelo apoio financeiro e institucional.

Reinforcement Learning for Adsorbate–Substrate Modeling in *Silico* – the Genesis of RLMaterial software

Maicon P. Lourenço^{1*}(PQ), Jiří Hostaš²(PQ), Colin Bellinger³(PQ), Alain Tchagang³(PQ) and Dennis R. Salahub²(PQ)

*maiconpl01@gmail.com

¹Departamento de Química e Física, UFES; ²Department of Chemistry, University of Calgary; ³National Research Council of Canada.

Keywords: Reinforcement learning; deep neural network, chemical adsorption, host-guest, DFT and DFTB.

INTRODUCTION

Modeling functional materials for new discovery requires understanding the substrate@adsorbate interactions. However, in most cases, assembling the adsorbate@substrate manually can result in structures far from the global minimum. In this work, an artificial intelligence method based on reinforcement learning (RL)¹ for adsorbate@substrate structural determination was developed and implemented in the *RL Software for Material Design and Discovery (RLMaterial)*. The code was used to study the glycine interactions with boron nitride (BN) and phenylboronic acid in cyclodextrin (Fig. 1). Transfer learning (TL) between different systems and methods is also reported.

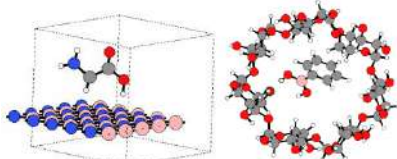


Figure 1. The optimum structures of glycine@BN and phenylboronic acid@cyclodextrin found by RL.

METHODS

In RL¹ an agent interacts with the environment (e.g.: DFTB calculator and a structure generator) to maximize long-term sum of rewards, Fig. 2. This results in Bellman equation², $Q(s_i, a_j)$, which is used to build a Q-matrix. The next actions, a' (translations and rotations), are obtained from a policy, $\pi^*(s_i)$, and are applied in the current state, s_i , resulting in a new state: s_{i+m} . A machine learning model can be used to estimate the $Q(s_i, a_j)$ values. The DFTB method was used to build the energy landscape for the systems in Fig. 1.

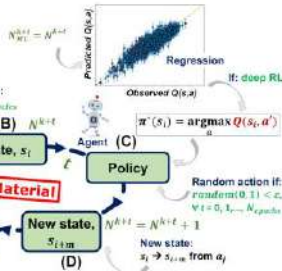


Figure 2. The RL method workflow as implemented in the RLMaterial. An adsorbate@substrate configuration defines a state, s_i . TL uses the Q-table from previous RL independent runs as an initial guess (step A) to the next run.

RESULTS

RL results for glycine@BN (top) and phenylboronic acid@cyclodextrin (down) are shown in Fig. 3.

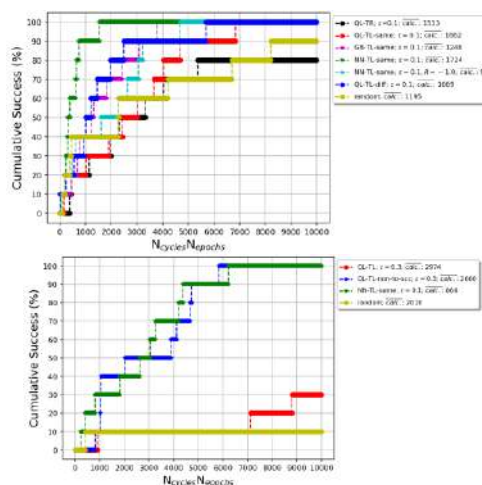


Figure 3. Cumulative success in finding the optimum glycine@BN (top) and phenylboronic acid@cyclodextrin (down) structures (within 10^{-4} Ha.) as a function of the number of RL iterations: $N_{cycles} \times N_{epochs}$. N_{cycles} is number of times a random state is obtained to initialize the RL epochs (N_{epochs}). QL: Q-learning. TL: transfer learning. TR: tabula rasa, where TL is not used. ϵ -greedy: controls exploration. NN and GB: artificial neural network and gradient boosting regressors, respectively. “Same” and “Diff” (top): the initial Q-table guess comes from the same and different chemical systems, respectively. “Same” and “non-to-scc” (down): the initial Q-table comes from the SCC and from non-SCC DFTB levels, respectively. R: reward. Random: random actions. “calc.”: the average number of states evaluated in ten RL independent runs.

CONCLUSIONS

RLMaterial was developed for the structural determination of interfaces. TL between systems and methods in the RL framework has been explored and investigations involving different functionals, VWN to PBE to PBE0, are in progress. The results highlights the potential of the RL method in finding optimum structures.

REFERENCES

- ¹Bellman; *on the theory of dynamic programming*; PNAS, 38 (8), 1952. ²Watkins et al.; *Q-learning*; ML, 8, 1992.

ACKNOWLEDGMENTS

FAPES, CNPq, CAPES, NRC.

Investigação estrutural da Magadiita a partir de cálculos DFT.

Bruna Nádia N. Silva (PQ),^{*1,2} Heloise O. Pastore (PQ),² Alexandre A. Leitão (PQ).¹
*brunaneves@ice.ufjf.br

¹Departamento de Química, Universidade Federal de Juiz de Fora, Juiz de Fora, MG, 36036-330, Brasil

²Instituto de Química, Universidade Estadual de Campinas, Campinas, SP, 13083-876, Brasil

Palavras Chave: *Magadiita, cálculo DFT, elucidação estrutural, calcinação, troca iônica.*

INTRODUÇÃO

A Na-Magadiita ($\text{Na}_2\text{Si}_{14}\text{O}_{28}(\text{OH})_2 \cdot 8\text{H}_2\text{O}$) é um silicato lamelar da mesma família da kanemita, makatita, etc. Este sólido é amplamente conhecido na literatura por fornecer materiais funcionalizados promissores na adsorção de gases, retenção de metais tóxicos e catálise heterogênea.^[1a-c] Embora com larga aplicação experimental, a magadiita passou por décadas sem elucidação estrutural na literatura. Com isso, este trabalho forneceu a participação dos cálculos DFT na resolução estrutural recente da Na-magadiita. Cálculos eletrônicos, espectroscópicos e termodinâmicos corroboraram com a proposta inicial do refinamento de Rietveld, auxiliando nas descrições experimentais deste material.

MÉTODOS

Todos os cálculos DFT foram executados no pacote QUANTUM ESPRESSO, usando bases de onda planas e condições de contorno periódicas. O funcional escolhido foi do tipo PBE-GGA e os pseudopotenciais do tipo Vanderbilt Ultrasoft. Energias de corte de 55 Ry e malha de pontos k $2 \times 2 \times 1$ foram obtidas por testes de convergência. Os parâmetros de RMNES dos núcleos de ^{29}Si , ^{23}Na e ^1H foram obtidos através do método GIPAW. As funções termodinâmicas para as reações de decomposição térmica e troca iônica foram calculadas através dos fônons obtidos no ponto Γ , de acordo com a DFPT.^[2a-e]

RESULTADOS

O modelo inicial do refinamento de Rietveld da Na-magadiita foi otimizado (Figura 1a) e a comparação do DRX confirmou a preservação dos principais picos (Figura 1b). Os sinais de RMNES simulados também corroboraram com os dados experimentais (Figura 1c-e), validando a estrutura obtida.^[3a] Análises termodinâmicas de decomposição térmica identificaram duas etapas de desidratação e uma de calcinação do material (Figura 2) em bom acordo com a TG.^[3b] Quanto à troca catiônica, os modelos K-, Ca- e Mg-magadiitas apresentaram esferas de hidratação semelhantes à forma sódica (Figura 3a-g), cuja as ligações de hidrogênio variaram conforme a força de interação cátion-água-lamela de cada espécie (Figura 3h-k).^[3c]

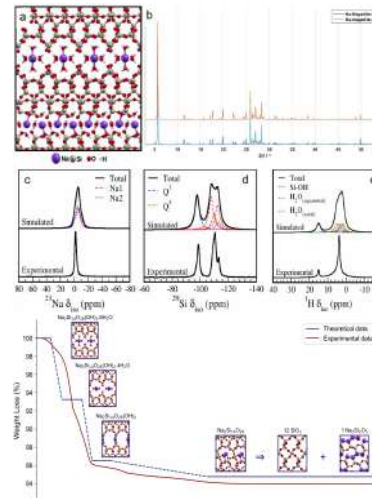


Figura 1 – (a) Modelo otimizado da Na-magadiita, (b) DRX, e espectros de RMNES dos núcleos (c) ^{23}Na , (d) ^{29}Si e (e) ^1H .

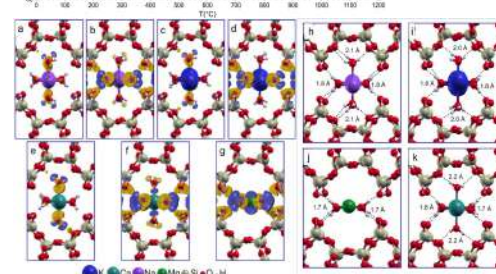


Figura 2 – Análise de TG experimental e simulada da Na-magadiita.

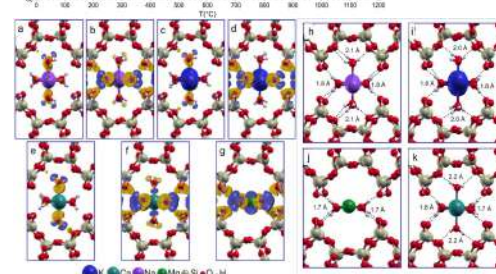


Figura 3 – Diferença de densidade de carga da (a,b) Na-, (c,d) K-, (e,f) Ca-, (g) Mg-magadiitas e ligações de hidrogênio da (h) Na-, (i) K-, (j) Mg- e (k) Ca-magadiitas.

CONCLUSÕES

Após otimizações, DRX e RMNES simulados validaram o modelo experimental. Análises termodinâmicas identificaram três etapas de calcinação deste sólido. Investigações das K-, Ca- e Mg-magadiitas mostraram semelhanças estruturais às Na-magadiita. Em três publicações, as simulações DFT forneceram descrições deste silicato desconhecidas até então.

REFERÊNCIAS

- (a) G.L. Paz, et al., *J. Mol. Catal. A: Chem.*, 2016, 422, 1–8; (b) G.P. Campos, et al., *New J. Chem.*, 2020, 44, 9998; (c) R. K. Almeida, et al., *Microporous and Mesoporous Mater.*, 2019, 284, 1–9.
- (a) P. Giannozzi, et al., *J. Phys.: Condens. Matter.*, 2009, 21, 395502; (b) P. Hohenberg, W. Kohn, *Phys. Rev.*, 1964, 136, B864–B871; (c) J. P. Perdew, et al., *Phys. Rev. Lett.*, 1996, 77, 3865–3868; (d) C. J. Pickard, F. Mauri, *Phys. Rev. B.*, 2001, 63, 245101; (e) S. Baroni, et al., *Rev. Mod. Phys.*, 2001, 73, 515.
- (a) Y. Krysiak, et al., *Chem. Mater.*, 2021, 33, 3207–3219; (b) B. N. N. Silva, et al., *Phys. Chem. Chem. Phys.*, 2022, 24, 14416–14423; (c) B. N. N. Silva, et al., *Appl. Clay Sci.*, 2023, 231, 106749.

AGRADECIMENTOS

Os autores agradecem à CNPq, à FAPESP, à FAPEMIG e ao CENAPAD-SP.

Neural network force fields for liquid water

Luana S. Pedroza (R)^{1*}

l.pedroza@ufabc.edu.br

¹Centro de Ciências Naturais e Humanas, Universidade Federal do ABC, Santo André, SP, Brazil

Keywords: water, neural network, DFT

INTRODUCTION

Water is the most important liquid on Earth. However, there are still some of its properties that are not yet fully understood. Atomistic simulations have shown to be an important tool, providing one way to improve our comprehension of water. In particular, quantum mechanical simulations seem to be the most appropriate choice, since they have, by construction, an accurate predictive potential. Recent developments in density functional theory (DFT), *i.e.* new functionals and better description of van der Waals interactions, have made it possible to describe water with reasonable accuracy, and good cost/accuracy compromise. Yet, even with DFT it is difficult to perform simulations on large systems at long time scales. Artificial Neural Networks (ANN) force fields have been shown to be able to yield accurate (on par with the method they were fitted to) results with low cost. In this work we employ ANNs to represent the water potential surface with DFT-quality, and compare ANNs trained at different methods in describing macroscopic properties of water under different conditions including nuclear quantum effects.

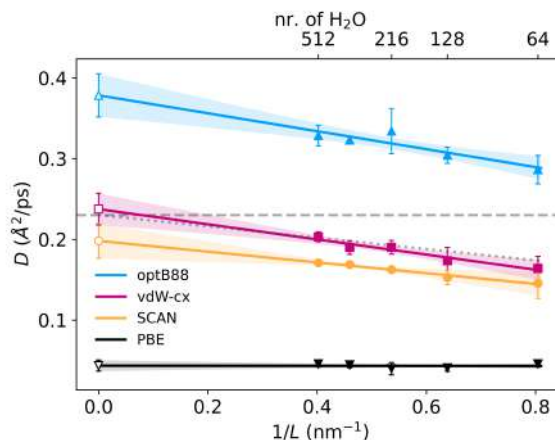
METHODS

Density functional theory calculations were performed upon 18 thousand sampled configurations for each of the following xc-functionals: PBE, two functionals with van der Waals (vdW) interactions: vdW-cx, and optB88-vdW, and the meta-GGA SCAN. Neural networks (NN) were trained to reproduce the energies and forces of each xc-functional using a modified version of the DeepMD-kit code¹. A different NN was obtained for each functional. The NNs have 4 fully connected hidden layers with 320, 160, 32, 16 neurons each, respectively. After training the NN for each xc-functional, we performed molecular dynamics (hereafter labeled NN-MD) for different system sizes: 64, 128, 216, 512 and 1728 water molecules

RESULTS

Our NN-trained force fields reproduce the pair distribution functions of water with DFT-like precision. It also clearly shows that static properties quickly converge in terms of timescales and system size.² To extend the analysis of our NN model, we have also performed NN-MD simulations including Nuclear Quantum Effects via

Partially Adiabatic Centroid Molecular Dynamics (PACMD) for all functionals. We have also obtained the diffusion coefficient, as illustrated in the plot below:



CONCLUSIONS

We performed simulations for different xc-functionals and verified that the quality of the approximation is essential. We also show that structural properties are less dependent on the size of the training data-set compared to dynamical ones (such as the diffusion coefficient), and a good sampling (selecting data reference for training process) can lead to a small sample with good precision.³

REFERENCES

- H. Wang, L. Zhang, J. Han, E. Weinan, *JCPC*, 2018, **228**, 178.
- A. Torres, L. S. Pedroza, M. V. Fernandez-Serra, A. R. Rocha, *JPCB*, 2021, **125**, 10772
- M. S. Gomes-Filho, A. Torres, A. R. Rocha, L. S. Pedroza, *JPCB*, 2023, **127**, 1422

ACKNOWLEDGMENTS

The authors acknowledge financial support from FAPESP (Grant # FAPESP 2017/10292-0, 2020/09011-9, 2017/02317-2 and 2016/01343-7). This work used the computational resources from the Centro Nacional de Processamento de Alto Desempenho em São Paulo (CENAPAD-SP) and GRID-UNESP. The authors acknowledge the National Laboratory for Scientific Computing (LNCC/MCTI, Brazil) for providing HPC resources of the SDumont supercomputer, which have contributed to the research results reported within this paper.